Nucleic Acids and Molecular Biology 31

Kazuhiko Nakatani
Yitzhak Tor *Editors*

Modified Nucleic Acids

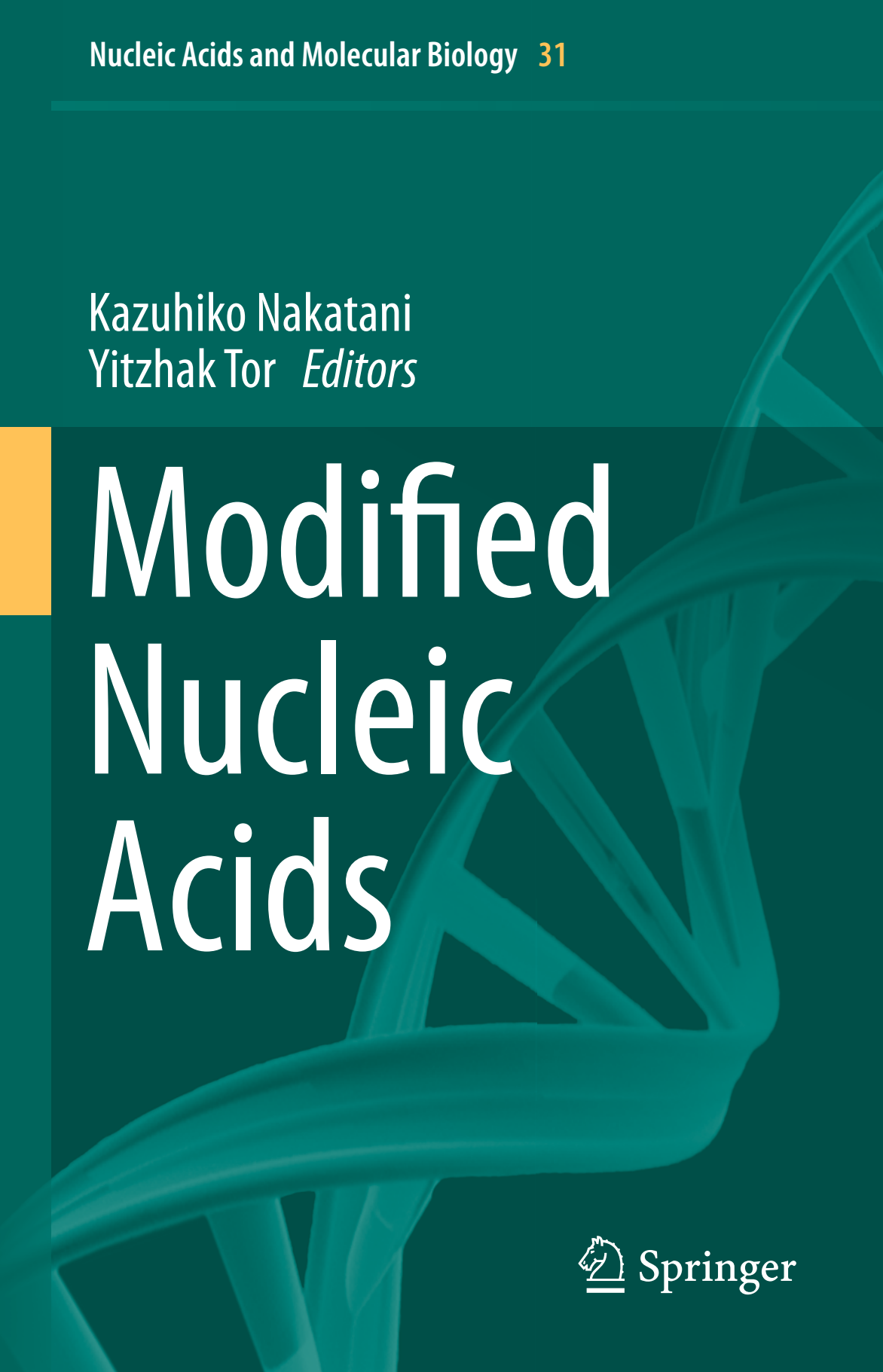

Springer

Nucleic Acids and Molecular Biology

Volume 31

Series editor
Janusz M. Bujnicki
International Institute of Molecular
and Cell Biology
Laboratory of Bioinformatics and
Protein Engineering
Trojdena 4
02-109 Warsaw
Poland

More information about this series at http://www.springer.com/series/881

Kazuhiko Nakatani • Yitzhak Tor
Editors

Modified Nucleic Acids

Springer

Editors
Kazuhiko Nakatani
The Institute of Scientific and Industrial Research
Osaka University
Ibaraki, Osaka
Japan

Yitzhak Tor
University of California, San Diego
La Jolla
California
USA

ISSN 0933-1891 ISSN 1869-2486 (electronic)
Nucleic Acids and Molecular Biology
ISBN 978-3-319-27109-5 ISBN 978-3-319-27111-8 (eBook)
DOI 10.1007/978-3-319-27111-8

Library of Congress Control Number: 2015960936

Printed on acid-free paper

This Springer imprint is published by Springer Nature
The registered company is Springer International Publishing AG Switzerland

Preface

Modified nucleosides, nucleotides, and oligonucleotides have become a mainstay of modern science. Used as biochemical and biophysical tools, as well as actual drugs and key component of discovery assays, one cannot but appreciate the impact such synthetic analogs have had on chemistry, biology, and medicine over the past several decades. With this backdrop in mind, we have put together this edited volume to honor Professor Isao Saito and celebrate his recent retirement, which also provided us with the opportunity to share some of his contributions with the community.

For those of us who operate in the exciting field of modified nucleic acids, Professor Saito needs no introduction. For the benefit of the younger readers, we very briefly highlight some of his interests. Trained as a synthetic chemist, Professor Saito turned his attention to biological problems early in his career, as the field focusing on the chemical biology of nucleic acids started emerging. While on the faculty at Kyoto University, he has made numerous contributions to the development of photochemical transformations, including a light-mediated cross-linking reaction of DNA. As his interests in electron transfer reactions, photophysics, and photobiology evolved, he combined his synthetic skills to develop new modified nucleosides as probes. Most notable for the community interested in developing fluorescent analogs of biomolecular building blocks, his work on base-discriminating fluorescent (BDF) nucleosides, which has been advanced while on the faculty at Nihon University over the past dozen years, stands out as it has served as inspiration for research groups around the world.

Appropriately, the first chapter in our collection, by Tor discusses the synthesis and properties of emissive 5-modified uridine analogs, an area extensively explored by the Saito group. Perhaps complementary to this pyrimidine-centric discussion, the following chapter by Saito presents emissive fluorescent purine analogs. Various modifications are discussed, with attention to historically important contributions. Staying within the general area of fluorescent oligonucleotides, Okamoto then discusses the utility on thiazole orange, when tethered to nucleic acid, as a probe for monitoring nucleic acid-based processes both in vitro and in vivo. Along

related themes, Wagenknecht elaborates on his approaches to emissive nucleic acids, labeled with cyanine-styryl fluorophores. In particular, the chapter highlights his "DNA/RNA Traffic Lights," where the combination of thiazole orange and thiazole red facilitates the development of novel multicolor probes. In a similar fashion and relying on the double helical architecture to dictate the interactions between chromophores, Yamana discusses his multichromophore assemblies. Particularly intriguing are the unique photophysical features emerging and the significant differences observed between DNA and RNA duplexes.

Enzymatic approaches to the preparation of modified nucleic acid are discussed by Hocek. In particular, effective approaches for the synthesis of modified triphosphates are highlighted. When recognized by polymerases, such a building block can provide an effective pathway for assembling modified nucleic acids. Once incorporated, modified nucleosides and nucleoside surrogates can serve diverse purposes. In the following chapter, Fujimoto discusses the utility of cross-linking reactions. The formation of stable adducts can then be exploited for chemical, biological, as well as nanotechnological applications.

While the majority of chapters in this book discuss photochemical and photophysical processes in nucleic acids, Sigurdsson takes a unique approach and exploits the utility of electron paramagnetic resonance (EPR) spectroscopy to study nucleic acid structure and dynamics. While the readout tool is clearly distinct, this approach also relies on the incorporation of modified nucleosides into oligonucleotides, albeit decorated with spin labels rather than with photoactive or emissive chromophores. The chapter provides an excellent introduction to EPR spectroscopy and highlights a wide spectrum of stable free-radical-containing nucleoside analogs.

Yet another distinct approach is taken by Nakatani, who relies on noncovalent binding of low MW ligands to a DNA scaffold to endow the resulting assemblies with novel properties. Specifically, ligands with high affinity to mismatched or unpaired sites (coined MBL), containing a 1,8-naphthyridine core, are shown to be versatile building blocks for diverse applications, ranging from nanostructure assembly to monitoring processes such as PCR. Another approach for the noncovalent assembly of higher structures is presented by Obika, who utilizes synthetic triplex-forming oligonucleotides (TFO). Restricting the ribose conformation by covalently bridging the 2′ and 4′ positions is shown to be a promising solution to some of the long-standing limitations which have impacted this field.

Keeping with the theme of modified nucleosides and their utility, Sasaki discusses several useful approaches for nucleic acid modification and for sensing damaged nucleotides. Specifically, modified nucleosides capable of forming sequence-specific cross-links are presented, and examples for their utility in the context of both double-stranded and other folds (e.g., triplexes, i-motifs) are discussed. Furthermore, a method for detecting 8-oxoguanosine, a damaged nucleoside, which serves as a biomarker for cellular oxidative stress, is presented. Finally, Hirao discusses his elegant approach for the design of unnatural base pairs, which are orthogonal to the native Watson–Crick ones. Such expanded genetic alphabets, which can be replicated and transcribed with high fidelity,

have found intriguing biotechnological applications, including the generation of modified aptamers for targeting specific proteins and cells.

It has been our pleasure editing these contributions and assembling this volume in honor of Professor Saito. We wish him joy in pursuing his diverse passions as he retires from academia. His special take on bioorganic chemistry and chemical biology will certainly last, as the individuals he had trained are now populating illustrious academic institutions and pursuing their own independent investigations, undoubtedly inspired by his pioneering work. We hope the reader, including students and young investigators, also find inspiration in learning about the contributions made by more established investigators and feel motivated to be bold and creatively explore their own unique multidisciplinary directions.

Osaka, Japan — Kazuhiko Nakatani
La Jolla, CA — Yitzhak Tor
August 2015

Contents

Chapter 1
Emissive 5-Substituted Uridine Analogues

Andrea Fin, Alexander R. Rovira, Patrycja A. Hopkins, and Yitzhak Tor

Abstract Chemical biology and medicinal chemistry applications require new nucleoside analogues with well-defined photophysical properties in order to visualize, monitor, and advance the understanding of nucleic acids. To impart favorable photophysical properties upon the native nucleosides and decipher structure–property relationships, robust and flexible synthetic procedures are required. Modification at the 5-position of uridine likely comprises the largest number of chemical variations investigated to enhance and tune the photophysical properties of this practically non-emissive nucleoside. The chapter discusses the design, synthesis, and characterization of diverse emissive uridine analogues.

1.1 Introduction

Our ability to understand the structure and dynamics of biological systems is coupled to our capabilities to accurately visualize signals coming from biologically relevant molecules with time and space resolution. Due to its sensitivity and time scale, fluorescent spectroscopy plays a predominant role among noninvasive techniques used for illuminating biological processes. Among biomolecules and their building blocks, nucleosides and oligonucleotides are practically non-emissive, a feature stemming from the extremely fast non-radiative decay of the excited state of the native nucleobases (which results in subpicosecond excited state lifetimes and low fluorescence quantum yield in water) [1]. This "unfortunate" situation complicates the biophysical analysis of native nucleic acids, as only a limited number of rare naturally occurring nucleosides display useful photophysical features [2–5].

To overcome these obstacles, chemists have modified the pyrimidine and purine heterocycles in an attempt to alter and tune the photophysical properties of these biologically relevant building blocks. To maintain bio-compatibility and bio-functionality, the majority of the chemical modifications were introduced at

A. Fin • A.R. Rovira • P.A. Hopkins • Y. Tor (✉)
Department of Chemistry and Biochemistry, University of California San Diego, 9500 Gilman Drive, La Jolla, CA 92093-0358, USA
e-mail: ytor@ucsd.edu

K. Nakatani, Y. Tor (eds.), *Modified Nucleic Acids*, Nucleic Acids and Molecular Biology 31, DOI 10.1007/978-3-319-27111-8_1

the purines' 7-position and the pyrimidines' 5-position [6]. Since a systematic and comprehensive description of the implemented chemical modifications would be lengthy, this book chapter focuses on modifications at the 5-position of the uridine core, an area actively pursued by Professor Saito. We first provide a brief overview of the most common synthetic pathways for the functionalization of the 5-position of uridine. This is followed by a review of emissive uridine analogues, where the most recently reported fluorophores are discussed. Finally, the concept of isomorphicity and some recent examples of functionalized isomorphic emissive uridine analogues are described, focusing on their photophysical properties and potential applications.

1.2 Synthesis of 5-Substituted Uridines: A Brief Overview

For both structural reasons and synthetic considerations, substitution at carbon-5 is most commonly seen in modified uridine analogues. C-5 modifications are accessible through a large number of simple and selective methods, but are most commonly synthesized from the halide precursors **1a** (Fig. 1.1). In evaluating the overall strategies, one needs, however, to distinguish between reactions performed on the nucleoside itself versus reactions carried out on the nucleobase, which are then followed by glycosylation reactions. Many of the reactions listed below can be applied to both. While each method has its own merit, the direct modification of the nucleoside, when feasible, typically prevents complicating issues of anomeric ambiguity.

The 5-halo uridines are commonly subjected to transition metal-catalyzed cross-coupling reactions, most notably palladium-based reactions. Common reactive pathways include coupling with aryl boronic acids **2a** [7], organostannanes **2b** [8], alkynes **2c** [9], and alkenes **2d** [10] (Fig. 1.2). The use of organostannanes is often found when coupling heterocycles directly to the C-5 position of uridine. Using this approach, a wide variety of heterocycles have been attached [8]. In certain cases, the products of these reactions are subjected to additional transformations (see below).

It is worth noting that such cross-coupling methods can frequently be applied to the nucleobases themselves as well as to both ribose and deoxyribose nucleosides. As an example for the former approach, a protected uracil may be subjected to halogenation followed by glycosylation and coupling reactions as seen in Saito's synthesis of α-5-cyanovinyldeoxyuridine **3**. This makes use of standard glycosylation conditions followed by a Heck-type coupling to form the desired carbon–carbon bond at the 5-position [11] (Fig. 1.3).

Historically, 5-substituted uridine derivatives were often synthesized through standard Vorbrüggen condensation conditions of a 5-substituted uracil with a protected sugar [12] (Fig. 1.4). Following this, the use of 5-organomercury uridine salts such as **1b** became one of the first instances of making use of palladium coupling to install alkylated substrates [10] (Fig. 1.5).

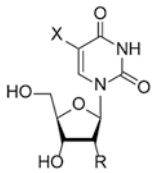

Fig. 1.1 Common 5-substituted uridine precursors

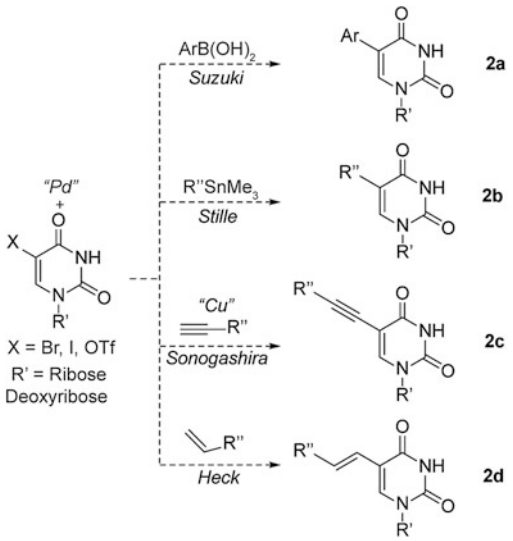

Fig. 1.2 Schematic representation of most common palladium-catalyzed reactions for the functionalization of uridine

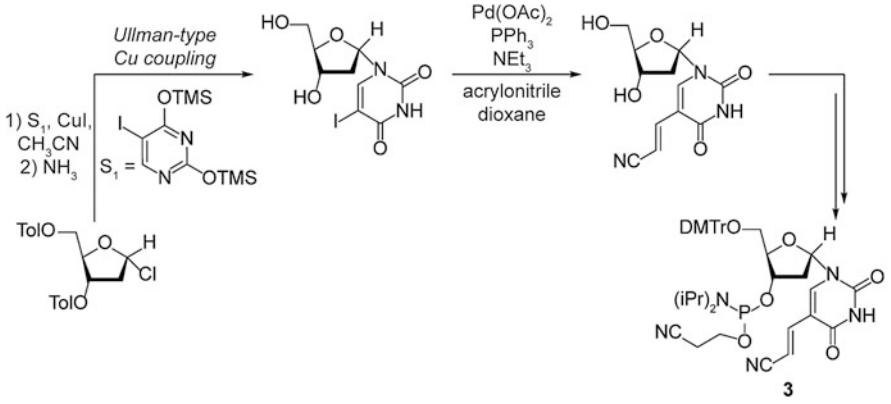

Fig. 1.3 Schematic representation of α-5-cyanovinyldeoxyuridine synthetic pathway

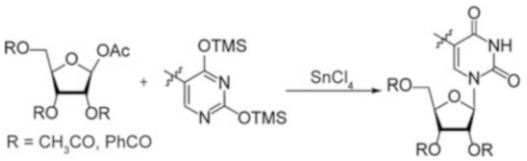

Fig. 1.4 Classical Vorbrüggen condensation of uridine derivatives

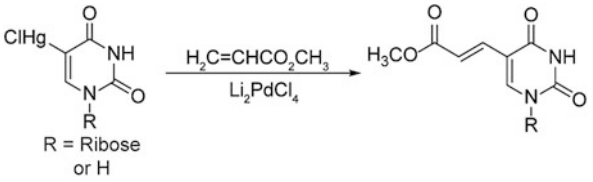

Fig. 1.5 Schematic representation of palladium coupling via organomercurate

The use of palladium chemistry facilitated mild reaction conditions that were tolerated by a wide variety of functional groups. As described in the synthesis of 2′-deoxyuridine derivatives, these substrates were commonly difficult to synthesize and purify before the use of transition metal catalysis [13]. This is often attributed to the hydrolysis-prone glycosidic C–N bond found in most naturally occurring nucleosides (Fig. 1.5).

A less common approach to the synthesis of 5-substituted uridines (e.g., **4**) was employed by Miyasaka and coworkers [14]. Through the use of both specifically bulky sugar protecting groups (e.g., *O-tert*-butyl-dimethylsilyl) and organolithium reagents known to form coordination complexes, electrophiles were selectively added to C-5. This is suggested to occur through an intermediate in which the sugar is locked in a complex that hinders the hydrogen located at C-6 (Fig. 1.6).

Separate from the traditional 5-substituted pyrimidines are the fused analogues **5** such as those synthesized by Tor [15]. When preparing such 5-N4-fused derivatives, the syntheses frequently start from a protected 5-halogenated uridine. In the case of **5**, the thiophene-substituted uridine is ultimately transformed into a fused pyrrolo-2′-deoxycytidine analogues via an amination reaction followed by a Cu(I)-catalyzed cyclization (Fig. 1.7).

Substituted quinazolines, which can be viewed as 5,6-benzo-fused uridines (e.g., **6**), have also been synthesized to act as uridine surrogates [16]. The synthesis of these analogues relies on known chemistry traditionally employed in the construction of pyrimidine rings, schematically shown in Fig. 1.8. Starting from substituted anthranilic acids, acid-catalyzed cyclization with potassium cyanate provides the desired uridine face. A similar compound employing a fused thieno [3,2-*d*]pyrimidine heterocycle makes use of a similar synthesis [17].

Other compounds of interest within the further-modified 5-substituted-uridine derivatives are the 6-aza-uridines **7a** and **7b** [18]. The synthesis of these derivatives starts with a pre-functionalized thiophene glyoxylic acid, which thermally cyclizes under basic conditions. This nucleoside synthesis employs glycosylation of the post-modified 5-substituted 6-aza-uridine through a Vorbrüggen condensation of the activated nucleobase with the benzoyl-protected, acetylated sugar (Fig. 1.9).

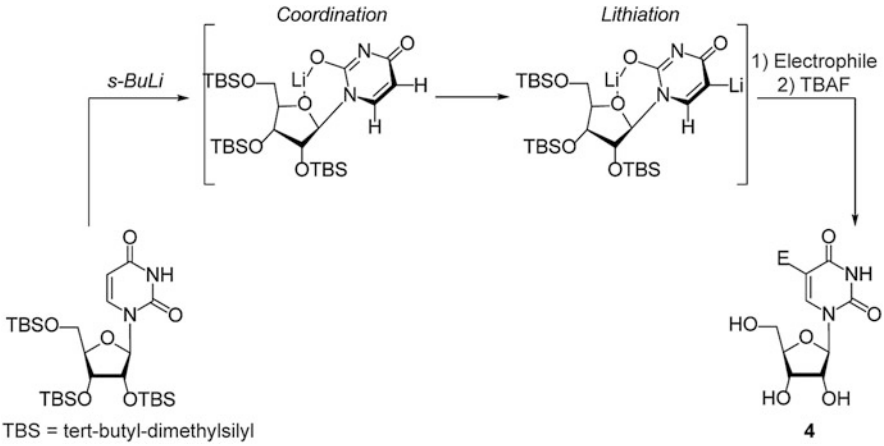

Fig. 1.6 Alkyl-lithium synthesis of 5-substituted uridines

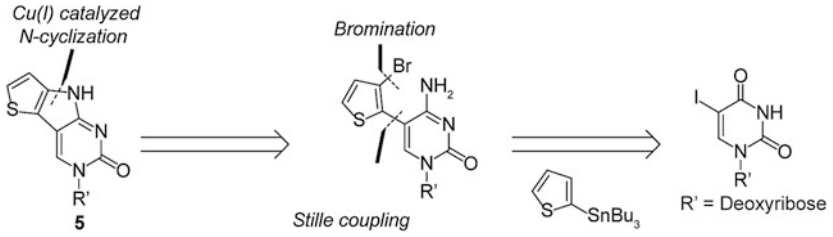

Fig. 1.7 Retrosynthesis of fused pyrrolo-2′-deoxycytidine analogues

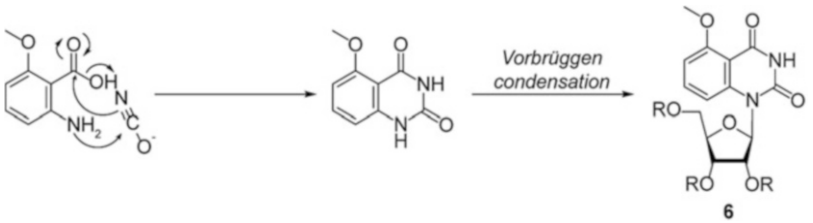

Fig. 1.8 Schematic representation of the synthesis of the fused benzalkoxy uridine surrogate

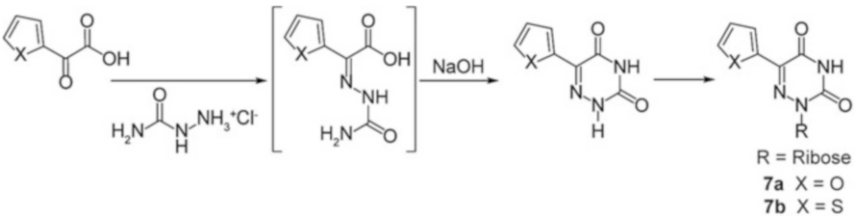

Fig. 1.9 Schematic representation of the 5-substituted-6-aza-uridine synthesis

1.3 Extended Uridine Analogues: Photophysical Properties and Applications

Extended emissive uridine analogues can be classified according to the linkage between the uridine moiety and the fluorophore. A flexible, non-conjugating linker can be used to connect a chromophore to the nucleobase, yielding nucleoside analogues characterized by the photophysical properties of the linked chromophore (Fig. 1.10). Emissive uridine analogues labeled with established fluorophores can also be obtained by clicking uridine surrogates, already incorporated into oligonucleotides, to properly modified fluorescent probes bearing complementary reactive functional groups (Figs. 1.11 and 1.12). Finally, the uridine core may be connected to a chromophore through an electronically conjugating bridge thus altering both aromatic systems. These emissive analogues are generally characterized by unique and frequently unpredictable photophysical properties (Figs. 1.13, 1.14, 1.15, 1.16, 1.17, 1.18, and 1.19).

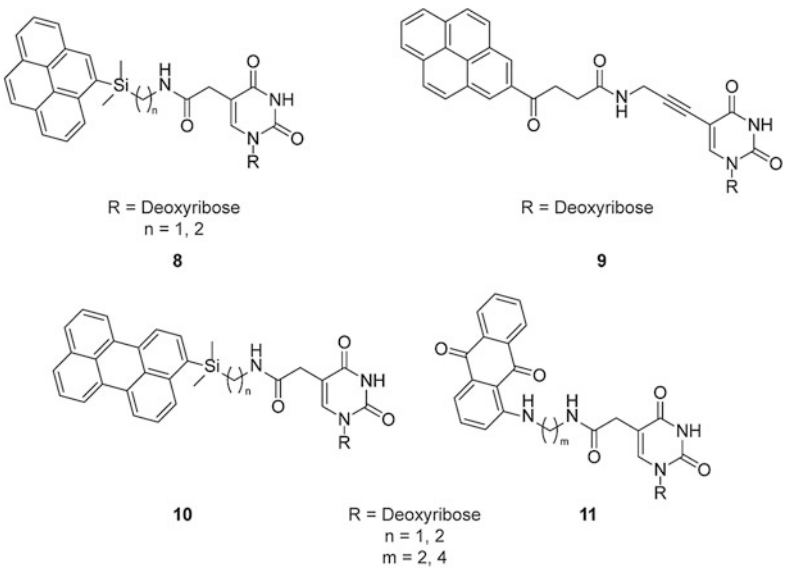

Fig. 1.10 Example of extended non-conjugated uridine analogues

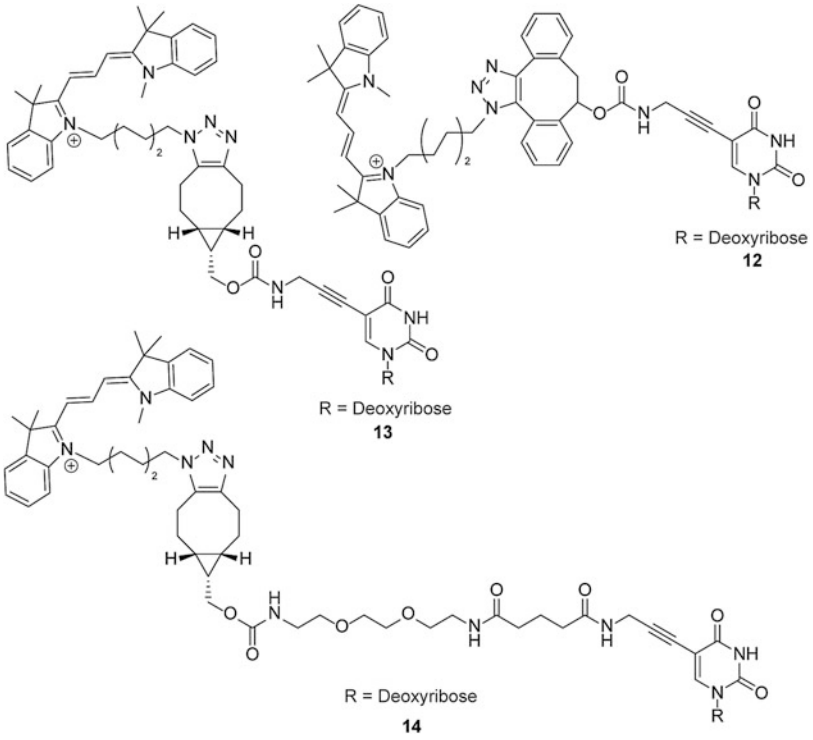

Fig. 1.11 Example of extended non-conjugated uridine analogues bearing Cy3 dye

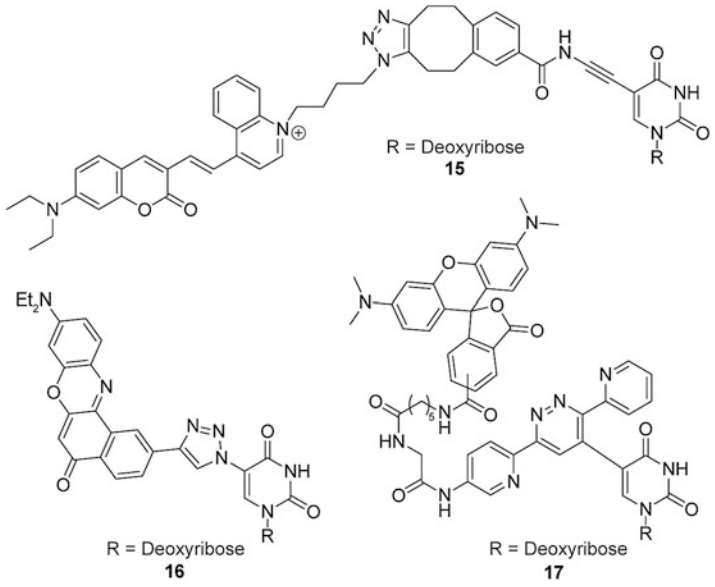

Fig. 1.12 Example of extended non-conjugated uridine analogues bearing different fluorophores

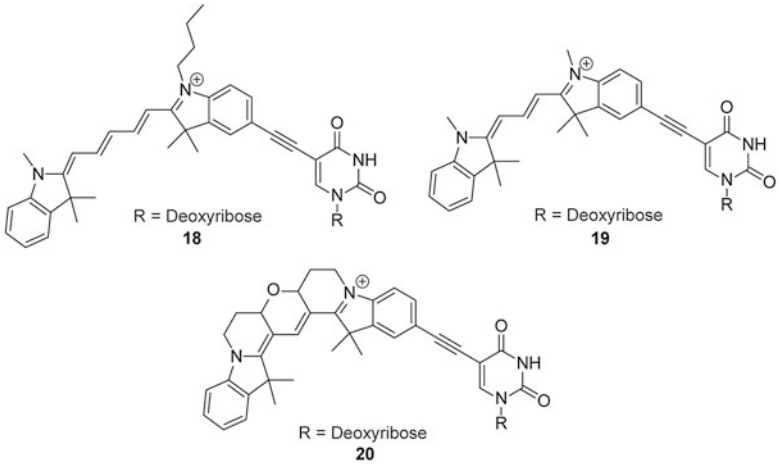

Fig. 1.13 Example of extended conjugated deoxyuridine analogues bearing Cy3, Cy5, and locked Cy3 dyes

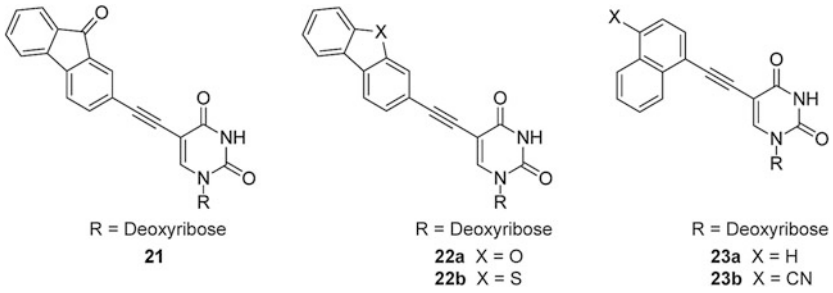

Fig. 1.14 Example of extended conjugated deoxyuridine analogues bearing various fluorophores

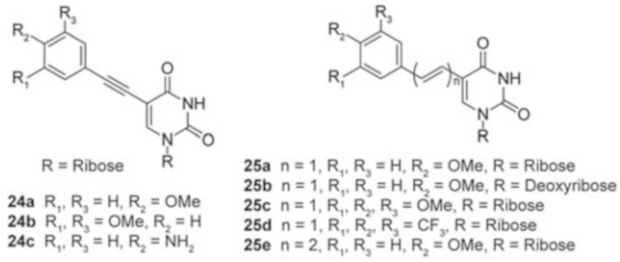

Fig. 1.15 Collection of emissive uridine analogues bearing a rigid or flexible conjugating connection

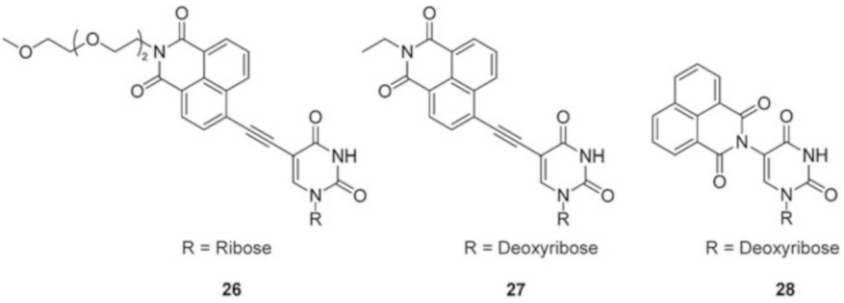

Fig. 1.16 Structure of Lucifer chromophore and naphthalene monoimide bearing uridine derivatives

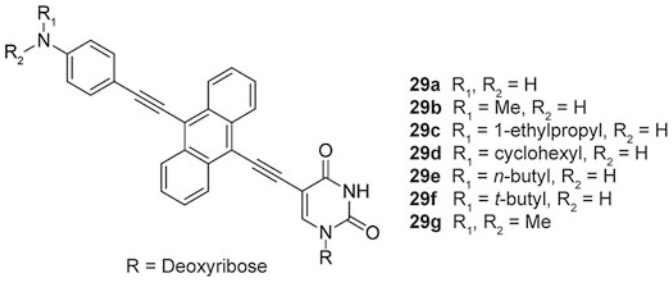

Fig. 1.17 Structure of the pH-responsive deoxyuridines **29a–g**

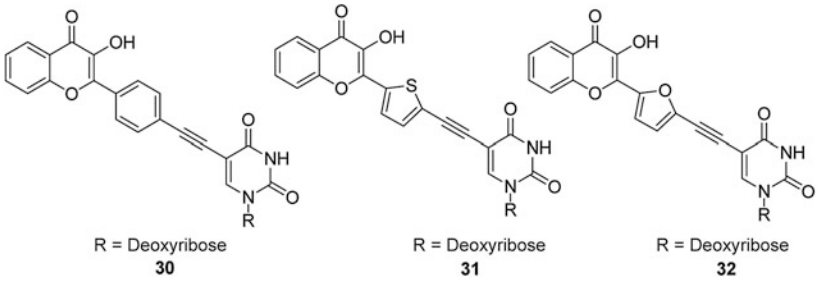

Fig. 1.18 Structure of the dual emissive environmental sensitive deoxyuridines

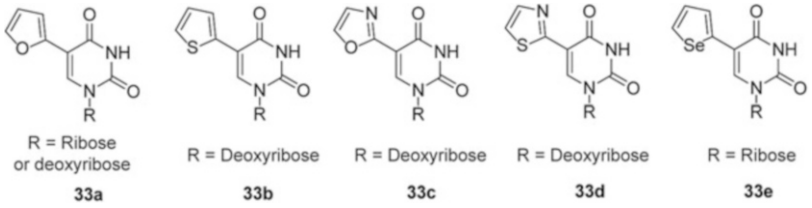

Fig. 1.19 Structure isomorphic 5-substituted uridine with single aromatic 5-member ring

1.3.1 Non-conjugated Fluorophores

The extended, non-conjugated emissive uridine analogues are generally synthesized by linking well-known fluorophores to a uridine moiety through a flexible bridge (Fig. 1.10). A recent example of this strategy is the preparation of **8** in which an aminomethyl or ethyl silylated pyrene was condensed with carboxymethyl uridine. The silicon-based moiety was introduced to enhance the photophysical properties. This modification caused an increase in fluorescence quantum yield and bathochromic shift of the emission maximum. Once incorporated into a single strand oligonucleotide in two adjacent positions, the neighboring pyrene moieties give rise to an excimer emission at 480 nm that disappears upon duplex formation with a complementary single strand of DNA. Due to the distinct fluorescence fingerprints of the pyrene and the excimer emissions, this probe was capable of discriminating single base mismatch in duplexes [19, 20].

A similar pyrene bearing nucleoside **9** showed remarkable sensitivity to environmental polarity for both the absorption (345–355 nm) and emission (396–467 nm) spectra. The emission of **9** was strongly quenched in DNA probes by a neighboring guanosine while enhanced by a matched adenosine. Doubly modified single strand ODN showed unique emission spectra patterns depending on the number of adenosine residues on the complementary strand, making this nucleoside analogue useful for the detection of adenosine-rich sequences [21].

The perylene- (**10**) and anthraquinone-based (**11**) deoxyuridine nucleoside analogues complete the series of recently synthesized uridine analogues bearing bulky polyaromatic chromophores. Nucleosides **10** and **11** were developed together to function as a molecular beacon (MB) in oligonucleotides. The MB's stem–loop places the emitter **10** and quencher **11** in close proximity, causing 98 % quenching of **10**. Upon hybridization to the complementary ODN, a 49-fold increase of the perylene emission was seen with a perfect matched sequence and around 23-fold enhancement with the single base mismatched sequences [22]. The same experimental design yielded similar results when **11** was used as quencher of a perylene moiety attached to a 5′-phosphate group of adenosine residue [23].

1.3.2 Click Chemistry for Labeling of ODN

Emissive nucleoside analogues bearing well-known fluorophores not only have to show remarkable photochemical properties but must also be chemically compatible with established solid-state or enzymatic protocols for their incorporation into oligonucleotides. In some cases, the overall dimension or the presence of acid or base sensitive groups on the fluorophore prevents a straightforward incorporation into ODNs. To overcome this limitation, nucleosides bearing functional reactive groups are synthesized, incorporated into ODN, and then clicked to bright fluorophores functionalized with complementary moieties. Such "post-

incorporation labeling" of ODNs with fluorophores under physiological conditions has been largely facilitated by click chemistry and related protocols [24, 25].

One of the most common click reactions used in nucleic acid chemistry is the copper-catalyzed azide–alkyne 3 + 2 cycloaddition. The stability of these functional groups in aqueous media and the negligible reactivity with other functional groups in nucleic acids (bio-orthogonality) are the main advantages of this synthetic approach. However, such a protocol cannot be applied in vivo due to the cytotoxicity of copper (I). To avoid this limitation, highly activated alkynes were introduced, providing a copper-free ring strain-promoted azide–alkyne cycloaddition reactions [26]. A recent example of this strategy was reported for the preparation of ODNs incorporating deoxyuridine labeled with cyanine dye **12**, **13**, and **14** (Fig. 1.11). 5-aminopropargyl-2′-deoxyuridine-5′-triphosphates linked to dibenzocyclooctyne or bicylo [6.1.0] non-4-yne were prepared and enzymatically incorporated into ODNs by primer extension and polymerase chain reactions. Once incorporated, the alkyne group of the nucleoside was clicked with the Cy3 dye functionalized with an azide moiety [27].

A similar strategy was applied for the preparation of **15**, a modified deoxyuridine bearing a quinolinium-styryl-coumarin azide dye with far-red emission maxima (720 nm). Upon conjugation of the dye to the ODN, the fluorescence intensity was enhanced 130-fold. The remarkable increase of the emission signal and the fast reaction kinetics of the click reaction make this analogue potentially suitable for in vitro investigations due to the off/on emission properties of the probe before and after the cycloaddition, respectively [28].

The post-insertion labeling strategy can also be applied to the preparation of extended conjugated nucleotides as seen for **16**. DNA containing 5-iodo-2′-deoxyuridine was subjected to two-step reactions for the in-situ formation of the azide moiety and the subsequent click reaction with the ethynyl-functionalized nile red chromophore. The labeled DNA was easily detected by UV–Vis spectroscopy, showing absorption maxima at 610 nm and was characterized by emission maxima at 658 nm. The DNA showed a good fluorescence quantum yield of 29 % for the single and 31 % for the double strand [29].

An alternative bio-orthogonal chemical labeling protocol used in chemical biology is based on the inverse electron demand Diels–Alder reaction between an electron-rich dienophile and an electron-deficient tetrazine [30–32]. This methodology was implemented for in vitro labeling of ODNs and proteins by the use of strained dienophiles such as cyclopropene, trans-cyclooctene, and norbornene [33–35]. Nevertheless, nucleosides linked to these functional molecules were showing inhibition of their cellular metabolism [36]. Recently, Luedtke and coworkers have introduced the smallest possible dienophile bearing nucleoside, 5-vinyl-2′-deoxyuridine, as a potential metabolic label for cellular nucleic acids [37]. 5-vinyl-2′-deoxyuridine was incorporated into DNA by endogenous enzymes in HeLa cells and, subsequently, stained with a TAMTRA–tetrazine conjugate to provide **17** as cellular labeling DNA probe. It is worth noting that the inverse electron demand Diels–Alder reaction was shown to be orthogonal to the 3 + 2 azide–alkyne cycloaddition and displayed similar fast kinetic.

1.3.3 Conjugated Fluorophores

Extending the uridine π-system by electronically conjugating it to additional aromatic moieties can affect the physical–organic properties of the nucleobase (e.g., pK_a values, tautomeric equilibria) and of the fluorophore (e.g., absorption and emission spectra), generating a new entity with unique and valuable, but often unpredictable, properties.

Brown and coworkers have optimized the synthesis of deoxyuridine phosphoramidites bearing Cy5 (**18**), Cy3 (**19**), and locked Cy3 (**20**) fluorophores allowing the multiple incorporation of these bright dyes into oligonucleotides through solid-phase synthesis (Fig. 1.13). The locked cyanine nucleoside analogue **20** has shown superior fluorescence properties relative to **18** and **19** since the photoinduced cis/trans isomerization of the polymethine linker is eliminated [38]. Moreover, fluorescence quenching due to dye–dye and dye–DNA interaction was reduced through a locked conformation due to the rigid linker between the chromophore and nucleoside [39]. Such nucleoside analogues were successfully used in detecting mutations by Scorpion and HyBeacons probes.

The same strategy was applied for the conjugation of a 9-fluorenone moiety at the 5-position of deoxyuridine, resulting in nucleoside **21**. Despite its low quantum yield, nucleoside **21** showed polarity sensitive emission (536–550 nm) (Fig. 1.14). Upon incorporation into ODN, **21** displayed good emission sensitivity toward detecting nucleotide polymorphism with pyrimidines as flanking bases [40]. Similar desirable photophysical properties were achieved upon replacing the fluorenone moiety with dibenzofuran **22a** and dibenzothiophene **22b**, creating a new type of quencher-free linear beacon probes. This facilitated the discrimination amongst flanking bases and base mismatches [41].

A minimalist design connecting a deoxyuridine to a 1-naphthalenylethynyl or 4-cyano-1-naphtalenylethynyl group, **23a** and **23b**, provided interesting photophysical properties of the doubly labeled ODN probes. Fluorescence quenching, due to photoinduced electron transfer, was observed when the DNA was labeled with **23a** at two consecutive or interstrand neighboring positions. On the other hand, the emission of the duplex containing **23a** and **23b** in adjacent positions was red-shifted by 85 nm and significantly quenched. It was hypothesized that this might be due to exciplex formation between the two different naphthalene units located in the DNA major groove [42].

A library of substituted uracil-based nucleoside derivatives was introduced by Fischer and coworkers, varying the substituents position on the chromophore and linking them to the pyrimidine by a rigid ethynyl (**24a–c**) or a mono or divinylene moiety (**25a–e**) (Fig. 1.15). The latter group of nucleoside analogues **25a–e** exhibited the longest absorption and emission wavelengths together with the highest emission quantum yields [7]. Among these nucleosides, **25b** displayed the best properties in terms of emission red-shift to 478 nm and quantum yield (12 %). The nucleoside was incorporated into an oligonucleotide for the detection of cyclin

D1 mRNA in total RNA cell extract from cancerous human cells, following variations in the emission intensity [43].

One of the limitations of emissive nucleosides bearing small chromophores is typically their UV excitation maxima and low fluorescence quantum yields once incorporated into oligonucleotides. To overcome these challenges, a bright Lucifer chromophore was introduced at the C-5 position of uridine **26** (Fig. 1.16). The extended conjugation of this analogue provided remarkable fluorescence properties such as sensitivity to environmental polarity (480–528 nm) and good to high quantum yields (11 % in water and 87 % in dioxane). The presence of the 1,8-naphthalimide was shown to be compatible with the preparation of the corresponding nucleoside triphosphate and phosphoramidite for the enzymatic and solid state incorporation in ODN, respectively. Once incorporated into oligonucleotides, the emission of **26** was responsive to flanking base variations and base-pair substitution [44]. Independently, Zhou and coworkers have reported the copper-free functionalization of 5-iodo-2′-deoxyuridine in aqueous media for the preparation of **27**, which showed comparable photophysical properties to **26** [45].

A Lucifer-like chromophore was also conjugated through the imide moiety to deoxyuridine to provide the emissive nucleoside **28**. In comparison to the classical connection through the naphthalene core in **26** and **27**, the linkage to the imide nitrogen generated an hypsochromic shift of the emission maximum to 415 nm for **28** once incorporated into a single strand oligonucleotide. Nevertheless, the fluorescence of the nucleoside analogue was sensitive to single nucleotide polymorphism upon hybridization into DNA duplexes [46].

A distinct family of emissive uridine derivatives **29a**–**g**, sensitive to changes in pH, was recently introduced by Saito and coworkers. Different substituents on the aniline nitrogen were introduced to shift the pK_a values between 3 and 6.1. In neutral or alkaline media, the emission of the modified uridine are quenched due to photoinduced electron transfer between the aniline and anthracene core. In acidic environments, the protonated aniline is unable to quench the anthracene emission resulting in enhanced fluorescence intensity [47].

A family of dual emission environmentally sensitive deoxyuridines, **30**–**32**, was synthetized by a convergent synthetic strategy based on the Sonogashira and the Algar–Flyn–Oyamada coupling reactions. The 3-hydroxychromones bearing uridine showed the typical dual emission pattern due to an excited state intramolecular proton transfer (ESIPT). The blue-shifted peak was assigned to the emission band of the so-called “normal form” (N*) while the other to the tautomeric form (T*). The emission properties of all three uridine analogues were sensitive to polarity, both in terms of band shift and relative ratios of the N/T peaks intensity. Moreover, these probes were characterized by good fluorescence quantum yield values in different solvents including water, which is not common for polarity sensitive dyes. Finally, the presence and the variation in the relative intensity of the two emission peaks were shown to be a useful tool for the detection of different levels of hydration of the nucleosides [48].

1.4 Isomorphic Emissive Uridine Analogues

The concept of isomorphic nucleosides was introduced to identify a class of nucleobase analogues that closely resemble their natural counterparts in terms of overall dimension (isosterism) and ability to form Watson–Crick base pairs. Accordingly, the isomorphic emissive uridine analogues are encompassing substituted uridines bearing small heteroaromatic moieties at the 5 position. This simple and small modification generally confers unique properties upon the new nucleoside analogues such as exclusive absorption bands ($\geq$300 nm), acceptable quantum yields, and red-shifted emission bands exceeding 400 nm. In most cases, such nucleoside analogues are environmentally sensitive [8, 49–53].

1.4.1 Conjugated 5-Membered Heterocycles

A family of isomorphic nucleosides **33a–d** was introduced by a simple one-step palladium-catalyzed coupling from commercially available compounds (Fig. 1.19) [54, 55]. The emission properties were shown to be sensitive to changes in environmental polarity while the absorption spectra were almost unchanged, likely indicating a significant component of charge transfer and a twisted conformation of the excited state [8, 56].

While **33c** and **33d** were characterized by emission bands at 400 and 404 nm, respectively, and low quantum yields in water, **33a** showed an intense red-shifted emission at 430 nm, decaying deeply into the visible range (>550 nm) (Table 1.1). The absorption and emission spectra remained unchanged upon single incorporation of **33a** into single strand ODN. Upon hybridization to a perfect complement, the emission was significantly quenched but easily detectable. Interestingly, the melting curve of a **33a**-containing duplex was characterized by identical T_m as compared to the unmodified duplex. When hybridized to a single strand containing an abasic site, the emission of **33a** was enhanced sevenfold compared to the perfect matched duplex. The T_m increased by 4 °C, suggesting a flip of the nucleobase and a π–π intrahelical stacking of the furan moiety, stabilizing the DNA duplex. Moreover, the emission decayed sharper above 500 nm compared to the matched duplex indicating flatter orientation of the pending furan with restricted rotational freedom. The molecular rotor character of **33a** was further supported by a remarkable emission intensity enhancement in a binary solvent mixture with increased viscosity as well as by lowering the temperature of a pure **33a** solution in glycerol. These experiments substantiated the hypothesized nucleoside flip and subsequent enhanced emission observed for **33a** in an abasic site-containing duplex [57].

The fluorescence features of **33a** were not only sensitive to environmental viscosity but also strongly affected by the polarity of the media. This property, coupled with the proximity of the furan moiety to the nucleobase and its placement in the major groove, prompted its use as a probe for the groove's micropolarity.

Table 1.1 Photophysical properties of isomorphic uridine analogues in water [8, 49–52]

	Abs (ε)	Em (Φ)		Abs (ε)	Em (Φ)
33a	316 (11.0)	431 (0.03)	**33e**	325 (9.2)	454 (0.01)
33b	314 (9.0)	434 (0.01)	**34a**	322 (16.1)	446 (0.19)
33c	296 (10.0)	400 (<0.01)	**34b**	293 (–)	484 (<0.01)
33d	316 (11.5)	404 (<0.01)	**34c**	318 (9.3)	458 (0.03)

Absorption and emission wavelengths are reported in nm; the molar extinction factor is relative to water solution and is reported in 10^3 M^{-1} cm^{-1}

Different from related investigations carried out with extended probes, **33a**, located deeper in the major groove, yielded a rather apolar environmental readout in agreement with theoretical models, suggesting a steep increase in the dialectric constant upon moving away from the groove wall toward the groove exterior [58].

The advantages of **33a** were not limited to its simple preparation or the straightforward conversion to the cytidine analogue [59], but included enzymatic compatibility and potential applications in biochemical and medicinal chemistry. The uridine derivative was converted to the corresponding 5′-triphosphate and subsequently enzymatically incorporated into ODNs by T7 RNA polymerase with an overall efficiency of 78 % compared to the natural UTP. Interestingly, T7 RNA polymerase showed a slight preference for the **33a** triphosphate in comparison to the UTP when the transcription reaction was carried out in equimolar concentrations of both triphosphates. Following the same enzymatic procedure, a bacterial A-site labeled with **33a** in close proximity of the binding site was prepared to monitor aminoglycoside antibiotics binding by monitoring fluorescence changes [60]. A similar design was used to monitor the HIV-1 TAR–Tat interaction [61].

The thiophene analogue **33b** showed similar features to that of **33a** [15, 62]. Recently, oligonucleotides containing single and multiple-labeling **33b** in alternating or neighboring positions were prepared by solid-state incorporation to investigate its effect on duplex stability and the fluorescence response to the duplex formation or dissociation. Multiple incorporations of **33b** did not affect the stability or the conformation of the DNA duplexes. Interestingly, an additional Cotton effect in the duplex containing three neighboring **33b** was noticed around 320 nm, indicating a likely alignment of the adjacent thiophene units. The fluorescence intensity of the single-labeled, single stranded ODN was slightly quenched upon hybridization to the duplex as is the case for the majority of emissive nucleoside analogues. The ODN containing three alternating **33b** analogues was characterized by a similar emission intensity of the single strand while the fluorescence was dramatically increased upon duplex formation, suggesting a chromophore–chromophore quenching due to the high flexibility in the single stranded oligomer. The same quenching phenomena could also explain the overall lower emission intensity and further quenching in the oligonucleotide bearing three adjacent modified nucleosides. Such a remarkable variation of the photochemical properties upon hybridization allowed the determination of the duplex melting temperature by

monitoring the fluorescence intensity, providing results in agreement with classical T_m measurements [63].

Recently, a selenophene-based 5-substituted uridine **33e** was synthesized and shown comparable fluorescence properties and sensitivity toward environmental polarity (437–453 nm) relative to **33a**. The presence of selenium and its X-ray radiation anomalous scattering properties can facilitate the use of this nucleoside as a dual probe for combining solution-based fluorescence measurements and solid-state X-ray studies. This nucleoside was also converted to the triphosphate following standard protocol and enzymatically incorporated into oligonucleotides. Neither the emission intensity nor the helix stability was affected by the presence of **33e** as a uridine analogue along the strand. Similar to **33a**, the selenophene analogue was used to monitor the binding of aminoglycosides to an A-site RNA with comparable results [49].

The extension of the electronic conjugation by fusing a phenyl ring to the furano or thiophene moiety of **32a** and **32b** is a recent addition to this class of isomorphic uridine analogues providing probes **34a**, **34b**, and **34c** (Fig. 1.20). The larger π-conjugated system of **34a** was shown to impart a minimal red-shift of 6 nm in the absorption maximum (332 nm), while the emission maximum (451 nm) was bathochromically shifted by 15 nm compared to **32a**. Despite these unimpressive variations of the photophysical properties, the solvatochromism and the sensitivity toward viscosity were reported to be comparable to that of the furano precursor and were exploited to prove the utility of **34a** in the discrimination of flanking base and the detection of abasic sites upon incorporation into oligonucleotides [50].

The introduction of a methyl group in the β-position of the furan ring increased the molecular rotor characteristic of probe **34b**. The remarkable sensitivity toward viscosity made this probe useful for the investigation of DNA triplex formation due to its higher emission quantum yield in viscous or apolar media. A 16-fold emission enhancement was reported in response to triplex formation with hairpin duplexes. Finally, the on/off emission of **34b** upon triplex formation was applied for the detection of miRNA in conjunction with rolling-cycle amplification [51].

Similar synthetic pathways and photophysical properties were reported for **34c** in which the thiophene ring was extended by a phenyl moiety. The ability of **34c** to respond to variation in polarity and viscosity was used to follow the formation of micelles and reverse micelle in good agreement with standard methods. Moreover, the ODNs containing an enzymatically incorporated **34c**, were able to report the

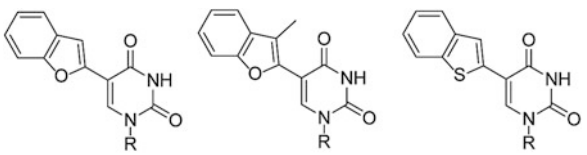

R = Deoxyribose R = Deoxyribose R = Ribose

34a **34b** **34c**

Fig. 1.20 Structure isomorphic 5-substituted uridine with extended aromatic rings

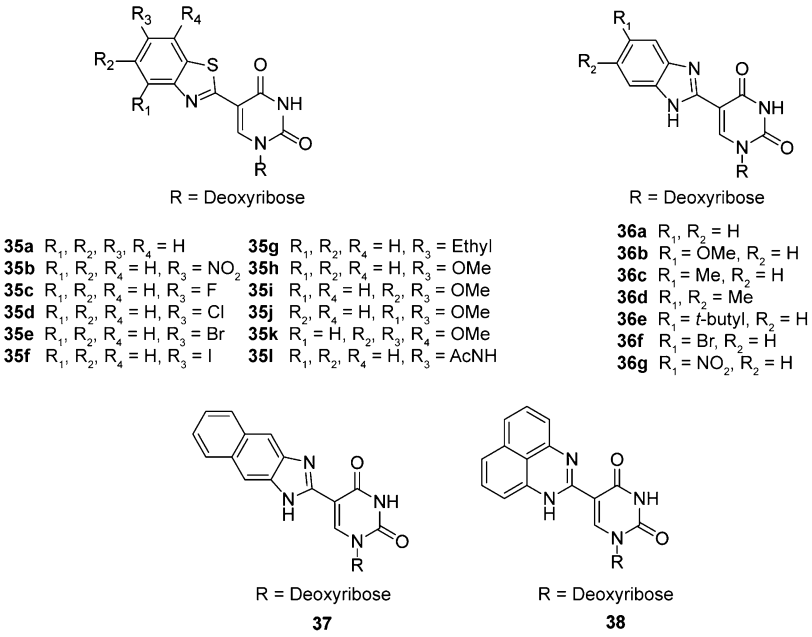

Fig. 1.21 Fluorescence deoxyuridine analogues synthesized by oxidative cyclization from 5-formyl-2′-deoxyuridine

formation and variation in the environment of micelles, showing its promise for investigating cell-like confined environments [52, 53].

A family of emissive deoxyuridines bearing substituted benzothiazoline derivatives **35a–l** was prepared by Matsuda and coworkers (Fig. 1.21). While the emission intensity in acid and neutral pH was not high, the putative deprotonation of the N3 was shown to increase the emission intensity of the uridine analogues in basic aqueous media. The dimethoxy derivative **35i** was reported to be a useful probe in SNP detection as well as chemically stable for the preparation of the corresponding 5′-triphosphate and in the subsequent incorporation by DNA polymerase [64, 65]. Moreover, the straightforward reactivity and selectivity of the non-emissive bis(4,5-dimethoxyaniline-2-yl)disulfide, the precursor of **35i**, was used to detect 5-formyl-deoxyuridine residues in oligonucleotides by premixing it with DTT and carrying out the reaction in acetate buffer at room temperature, generating **35i** within the ODN [66].

Similar strategies were implemented for the synthesis of a class of benzimidazolyl-2′-deoxyuridines **36a–g**, **37**, and **38** from substituted phenylendiamine and 5-formyl-uridine in the presence of hydrogen peroxide. Like the analogues previously described, this strategy was shown to be selective for the functionalization of 5-formyl-uridine in the presence of other nucleosides. Complementary to the benzothiazoline derivatives, the benzimidazolyl analogues have shown higher emissive quantum yield in acidic media. This likely arises from

the protonation of the imidazole nitrogen and the ability to strengthen the intramolecular hydrogen-bond-mediated coplanarization to the uridine moiety [67].

1.4.2 Conjugated 6-Membered Heterocycles

Historically, some of the isomorphic uridine derivatives were first introduced for entirely different applications and their remarkable environmentally sensitive photophysical properties were unnoticed [54]. Recently, the multisensing character of an emissive deoxyuridine derivative bearing a conjugated pyridine ring **39** was investigated in detail, reporting the ability to tune its photophysical properties in response to change in pH, viscosity, and polarity of the media (Fig. 1.22). The absorption red-shift, upon protonation of the pyridine nitrogen, was shown to be as remarkable as the emission intensity enhancement of the protonated form, likely due to an intramolecular hydrogen-bonding-mediated planarization and rigidification of the extended fluorophore. This finding was in agreement with the previously reported crystal structures for the neutral and protonated molecules containing pyridine fragment in proximity to carbonyl groups [68]. Similar locked conformation between the pyridine and the pyrimidine rings was also achieved by increasing the viscosity in a binary solvent mixture, with a tenfold emission increase between pure methanol to pure glycerol. In addition, **39** was also characterized by a high sensitivity toward solvent polarity changes depicted by a Stokes shift variation of around 3500 cm^{-1}, between dioxane (36.0 kcal mol^{-1}) and water (63.1 kcal mol^{-1}) [69].

A further extension of the π-system was recently demonstrated through connecting a naphthalene moiety to 2′-deoxy-uridine (**40**). This new nucleoside displayed emission solvatochromism (386–404 nm) and an overall red-shifted spectrum compared to an isolated naphthalene chromophore indicating an extension of the electronic conjugation to the uridine moiety [70]. Upon incorporation into oligonucleotides, the absorption spectrum of **40** was characterized by a minimal shift and a small hyperchromism when hybridized to form the fully matched duplex. The emission spectra of the perfect matched DNA showed an increased intensity and 26 nm blue-shift, suggesting that the naphthyl group was placed in a compact hydrophobic microenvironment pointing toward the duplex major groove.

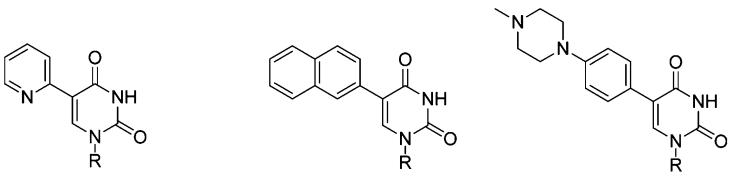

Fig. 1.22 Structure of isomorphic uridine derivatives

In a complementary manner, when duplexes with mismatched sequences or bearing an abasic site were formed with **40**, the absorption spectra were characterized by bathochromic and hypochromic effect, and the fluorescence was partially quenched [71].

A different functionalization of a phenyl group with methyl-piperazine was described in the preparation of **41**. The conjugate acid of methyl-piperazine has a pK_a value near 10 facilitating a partial neutralization of the DNA phosphate anions by protonated **41**, thus facilitating cell transfection of the modified ODN into HeLa cell without transfection agents. The fluorescent signal of **41** at 502 nm was still detectable in cells after three hours post-transfection [72].

1.4.3 Emissive 5-Substituted-6-Azauridine

The basic design of our first-generation nucleosides was based on conjugating heterocycles such as thiophene or furan to the pyrimidine core (Fig. 1.23). These probes may be classified as *isomorphic* as they closely resemble the native nucleosides with respect to their dimensions and ability to form Watson–Crick base pairs. Conjugating an electron-rich 5-membered ring at the electron-poor pyrimidine core resulted in visibly emitting nucleosides (390–443 nm), albeit with rather low quantum yields ($\Phi = 0.01$–0.035 in water). Further enhancing the polarization of this donor–acceptor system by replacing the pyrimidine with a more electron-deficient 1,2,4-triazine core (6-azapyrimidine) resulted in red-shifted absorption and emission maxima [18]. Rewardingly, significantly higher emission quantum yields were observed ($\Phi = 0.05$–0.20 in water). To achieve further bathochromic shift, "push–pull" interactions were enhanced by directly conjugating a donor group through an extended aromatic system to the electron deficient 6-azauridine [73].

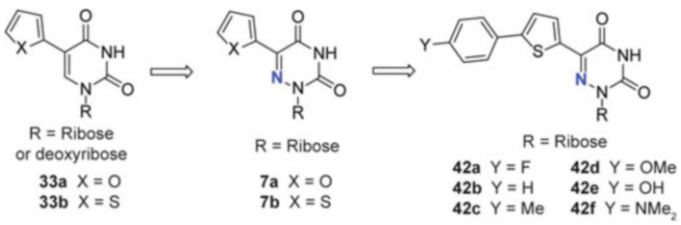

Fig. 1.23 Evolution of the design for visibly emitting nucleosides

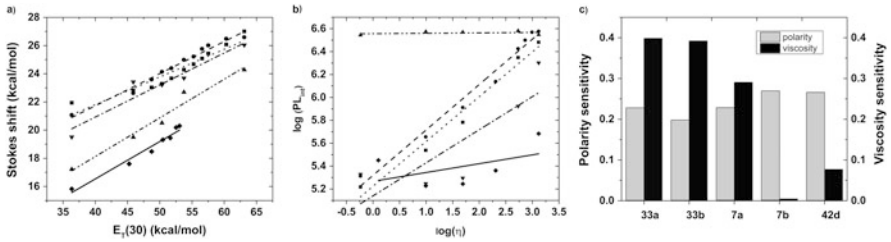

Fig. 1.24 (**a**) Correlating Stokes shift versus $E_T(30)$ values for compounds **33a** (*dash*), **33b** (*dot*), **7a** (*dash dot*), **7b** (*dash dot dot*), and **42d** (*solid line*); (**b**) correlating log emission intensities versus log viscosity for **33a–b**, **7a–b**, and **42d**. (**c**) Viscosity (*dark gray*) and polarity sensitivity (*light gray*) for compounds **32a–b**, **7a–b**, and **42d** represented by slopes from (**a**) and (**b**)

All 5-substituted uridine analogues (**33a**, **33b**, **7a**, **7b**, and **42a–f**) showed a bathochromic shift and increased emission intensity with increasing polarity (Fig. 1.24). There was little to no variations observed for the absorption spectra for **7a** and **42a–f**. To evaluate the influence of viscosity, which can hinder the formation of twisted excited states, mixtures of two solvents with very low and high viscosities but with minimal differences in polarities [methanol ($\eta_{20°C} = 0.583$ cp, $E_T(30) = 55.4$ kcal mol^{-1}) and glycerol ($\eta_{20°C} = 1317$ cp, $E_T(30) = 57.0$ kcal mol^{-1})] were used. The fluorescent intensity of **33a–b** and **7a** drastically intensifies with increasing viscosity, suggesting a molecular rotor behavior. However, **7b** and **42d** show little to no response toward viscosity suggesting that they might not adopt a twisted excited state upon excitation. Additionally, in the 6-aza motif there is a significant difference between the furanyl **7a** and thiophenyl **7b** derivatives. It is speculated that a larger heteroatom hinders free rotation around the aryl–aryl bond, impacting the relative ground state orientation of the thiophene ring with respect to the 6-aza position.

The photophysical properties of 6-azauridines are sensitive to changes in its protonation state. Titration of **7b** and **42d** between pH 2 and 12 yielded a pK_a value of 6.7 for both. This value is in close agreement to the previously observed value for 6-aza-uridine (p$K_a = 6.8$) [74], but differs significantly from that of the parent uridine (9.3–9.5) [75]. This feature makes 5-thiopheno-substituted 6-azauridines attractive probes for studying (de)protonation events on RNA.

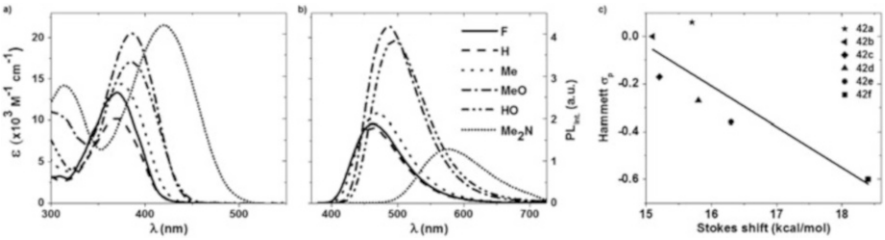

Fig. 1.25 Molar absorptivity (**a**) and emission (**b**) spectra for **42a** (*solid line*), **42b** (*dash*), **42c** (*dot*), **42d** (*dash dot*), **42e** (*dash dot dot*), and **42f** (*short dot*) in dioxane. (**c**) Calculated Stokes shift in kcal mol^{-1} for spectra taken in dioxane are correlated with Hammett σ_{para}

We hypothesized that altering the electronic character of the directly conjugated substituents would influence the charge transfer character, ideally yielding a red shift of absorption and emission maxima with increasing electron-rich character of the donor group. This was realized in the extended family **42a–f**. All extended nucleosides are visibly emitting in a wide window of 450–600 nm (Fig. 1.25). Increasing the electron-rich character of the substitution results in a bathochromic shift of the absorption and emission maxima in the following general order **42a** ≈ **42b** < **42c** < **42d** < **42e** < **42f**. Additionally, when Stokes shifts are plotted versus Hammett σ_{para} and $\sigma+_{para}$ parameters, a reliable linear trend is seen, supporting the underlying hypothesis [76].

1.5 Conclusions

As evident from the examples outlined in this chapter, emissive uridine analogues represent an intriguing family of useful fluorophores with potentially valuable applications. This heterocycle is receptive to diverse modifications where minimal or larger electronic and structural perturbations can confer useful photophysical properties. Designing such analogs, however, remains an empirical exercise. The relationship between molecular structure and photophysical properties is hard to predict and can only be experimentally validated. This issue is particularly challenging with regards to the fine tunability of photophysical properties of newly designed fluorescent nucleosides and their susceptibility to environmental perturbations.

The synthesis of such analogues has, however, advanced considerably in recent decades. General and now established synthetic pathways, such as palladium mediate catalysis, as well as newly explored routes like inverse electron demand Diels–Alder reaction have been reported for the insertion of chromophores, fluorogenic groups, or functional linkers for "post-incorporation labeling" on the uridine 5-position. The collection of emissive uridine analogues is constantly growing by the functionalization of the nucleoside with non-conjugating bright chromophores like pyrene, perylene, or cyanine-based motifs. In a complementary

manner, fluorophores such as fluorenone, Lucifer dye, 3-hydroxychromone, and many others were directly connected to uridine extending its electronic system. This approach generally conferred to the new nucleoside analogues unique photophysical sensitivity toward environmental parameters like pH, polarity, or viscosity.

Small fluorogenic heterocycles groups like furan, thiophene, or pyridine were also conjugated to uridine to provide the so-called "isomorphic" nucleoside analogues with remarkable emission properties. Recently, this family was enlarged by combining the isomorphicity of the original family with a single atom "mutagenesis" to provide distinct and highly emissive 5-substituted-6-azauridine analogues. The driving force behind the continuous design and implementation of new emissive uridine analogues is provided by the need to better understand and visualize biological relevant macromolecules and processes involving nucleic acids, nucleoside, and oligonucleotides, a research topic pioneered by Professor Saito [77–79].

References

1. Peon J, Zewail AH (2001) DNA/RNA nucleotides and nucleosides: direct measurement of excited-state lifetime by femtosecond fluorescence up-conversion. Chem Phys Lett 348:255–262
2. Munninger KO, Chang SH (1972) A fluorescent nucleoside from glutamic acid tRNA of Escherichia coli K 12. Biochem Biophys Commun 46:1837–1842
3. Maelicke A, Vonderha F, Cramer F (1973) Spectroscopic properties of oligonucleotides excised from the anticodon region of phenylalanine tRNA from yeast. Biopolymers 12:27–43
4. Paszyc S, Rafalska M (1979) Photochemical properties of Y_t base in aqueous solution. Nucleic Acids Res 6:385–398
5. McCloskey JA, Crain PF, Edmonds CG, Gupta R, Hashizume T, Phillipson DW, Stetter KO (1987) Structure determination of a new fluorescent tricyclic nucleoside from archaebacterial tRNA. Nucleic Acids Res 15:683–693
6. Sinkeldam RW, Greco NJ, Tor Y (2010) Fluorescent analogs of biomolecular building blocks: design, properties, and applications. Chem Rev 110:2579–2619
7. Segal M, Fischer B (2012) Analogues of uracil nucleosides with intrinsic fluorescence (NIF-analogues): synthesis and photophysical properties. Org Biomol Chem 10:1571–1580
8. Greco NJ, Tor Y (2005) Simple fluorescent pyrimidine analogues detect the presence of DNA abasic sites. J Am Chem Soc 127:10784–10785
9. Crisp G, Flynn BL (1993) Palladium-catalyzed coupling of terminal alkynes with 5-(trifluoromethanesulfonyloxy)pyrimidine nucleosides. J Org Chem 58:6614–6619
10. Ruth JL, Bergstrom DE (1976) Synthesis of C-5 substituted pyrimidine nucleosides via organopalladium intermediates. J Am Chem Soc 98:1587–1589
11. Ogino M, Yoshimura Y, Nazakawa A, Saito I, Fujimoto K (2005) Template-directed DNA photoligation via α-5-cyanovinyldeoxyuridine. Org Lett 7:2853–2856
12. Vorbrüggen H, Krolikiewicz K, Bennua B (1981) Nucleoside synthesis with trimethylsilyl triflate and perchlorate as catalyst. Chem Ber 114:1234–1255
13. De Ornellas S, Williams TJ, Baumann CG, Fairlamb IJS (2013) Catalytic C–H/C–X bond functionalization of nucleosides, nucleotides, nucleic acids, amino acids, peptides and protein. In: Ribas X (ed) C–H/C–X bond functionalization: transition metal mediation, vol 11. RSC, Cambridge, pp 409–447

14. Hayakawa H, Tanaka H, Obi K, Itoh M, Miyasaka T (1987) A simple and general entry to 5-substituted uridines based on the regioselective lithiation controlled by a protecting group in the sugar moiety. Tetrahedron Lett 28:87–90
15. Noé MS, Ríos AC, Tor Y (2012) Design, synthesis, and spectroscopic properties of extended and fused pyrrolo-dC and pyrrolo-C analogs. Org Lett 14:3150–3153
16. Xie Y, Dix AV, Tor Y (2009) FRET enabled real time detection of RNA-small molecule binding. J Am Chem Soc 131:17605–17614
17. Tor Y, Del Valle S, Jaramillo D, Srivatsan SG, Ríos AC, Weizman H (2007) Designing new isomorphic fluorescent nucleobase analogues: the thieno[3,2-d]pyrimidine core. Tetrahedron 63:3608–3614
18. Sinkeldam RW, Hopkins PA, Tor Y (2012) Modified 6-aza uridines: highly emissive pH-sensitive fluorescent nucleosides. ChemPhysChem 13:3350–3356
19. Moriguchi T, Ichimura M, Kato M, Suzuki K, Takahashi Y, Shinozuka K (2014) Development of the excimer probe responsible for DNA target bearing the silylated pyrenes at base moiety. Bioorg Med Chem Lett 24:4372–4375
20. Gias Uddin M, Moriguchi T, Ichimura M, Shinozuka K (2012) Synthesis and properties of molecular beacon DNA probe bearing novel silylated pyrene derivative. Key Eng Mater 497:47–50
21. Sekhar Bag S, Kundu R, Matsumoto K, Saito Y, Saito I (2010) Singly and doubly labeled base-discriminating fluorescent oligonucleotide probes containing oxo-pyrene chromophore. Bioorg Med Chem Lett 20:3227–3230
22. Sato Y, Moriguchi T, Shinozuka K (2012) Termini-free molecular beacon utilizing silylated perylene and anthraquinone attached to the C-5 position of pyrimidine nucleobase. Chem Lett 41:420–422
23. Chowdhury JA, Moriguchi T, Shinozuka K (2015) Pseudo-dumbbell-type molecular beacon probes bearing modified deoxyuridine derivatives and a silylated pyrene as a fluorophore. Bull Chem Soc Jpn 88:496–502
24. Kolb HC, Finn MG, Sharpless KB (2001) Click chemistry: diverse chemical function from a few good reactions. Angew Chem Int Ed 40:2004–2021
25. Neef AB, Luedtke NW (2014) An azide-modified nucleoside for metabolic labeling of DNA. ChemBioChem 15:789–793
26. Jewett JC, Bertozzi CR (2010) Cu-free click cycloaddition reactions in chemical biology. Chem Soc Rev 39:1272–1279
27. Ren X, Gerowska M, El-Sagheer AH, Brown T (2014) Enzymatic incorporation and fluorescent labeling of cyclooctyne-modified deoxyuridine triphosphates in DNA. Bioorg Med Chem 22:4384–4390
28. Stubinitzky C, Cserép GB, Bätzner E, Kele P, Wagenknecht H-A (2014) 2′-Deoxyuridine conjugated with a reactive monobenzocyclooctyne as a DNA building block for copper-free click-type postsynthetic modification of DNA. Chem Commun 50:11218–11221
29. Beyer C, Wagenknecht H-A (2010) In situ azide formation and "click" reaction of nile red with DNA as an alternative postsynthetic route. Chem Commun 46:2230–2231
30. Lang K, Davis L, Torres-Kolbus J, Chou C, Deiters A, Chin JW (2012) Genetically encoded norbornene directs site-specific cellular protein labelling via a rapid bioorthogonal reaction. Nat Chem 4:298–304
31. Kaya E, Vrabel M, Deiml C, Prill S, Fluxa VS, Carell T (2012) A genetically encoded norbornene amino acid for the mild and selective modification of proteins in a copper-free click reaction. Angew Chem Int Ed 2012(51):4466–4469
32. Devaraj NK, Weissleder R, Hilderbrand SA (2008) Tetrazine-based cycloadditions: application to pretargeted live cell imaging. Bioconjug Chem 19:2297–2299
33. Patterson DM, Nazarova LA, Xie B, Kamber DN, Prescher JA (2012) Functionalized cyclopropenes as bioorthogonal chemical reporters. J Am Chem Soc 134:18638–18643
34. Lang K, Davis L, Wallace S, Mahesh M, Cox DJ, Blackman ML, Fox JM, Chin JW (2012) Genetic encoding of bicyclononynes and trans-cyclooctenes for site-specific protein labeling

in vitro and in live mammalian cells via rapid fluorogenic Diels–Alder reactions. J Am Chem Soc 134:10317–10320
35. Plass T, Milles S, Koehler C, Szymanski J, Mueller R, Wiessler M, Schultz C, Lemke EA (2012) Amino acids for Diels–Alder reactions in living cells. Angew Chem Int Ed 51:4166–4170
36. Verri A, Focher F, Duncombe RJ, Basnak I, Walker RT, Coe PL, de Clercq E, Andrei G, Snoeck R, Balzarini J, Spadari S (2000) Anti-(herpes simplex virus) activity of 4′-thio-2′-deoxyuridines: a biochemical investigation for viral and cellular target enzymes. Biochem J 351(Pt 2):319–326
37. Rieder U, Luedtke NW (2014) Alkene-tetrazine ligation for imaging of cellular DNA. Angew Chem Int Ed 53:9168–9172
38. Sanborn ME, Connolly BK, Gurunathan K, Levitus M (2007) Fluorescence properties and photophysics of the sulfoindocyanine Cy3 linked covalently to DNA. J Phys Chem B 111:11064–11074
39. Hall LM, Gerowska M, Brown T (2012) A highly fluorescent DNA toolkit: synthesis and properties of oligonucleotides containing new Cy3, Cy5 and Cy3B monomers. Nucleic Acids Res 40:e108
40. Ryu JH, Heo JY, Bang E-K, Hwang GT, Kim BH (2012) Quencher-free linear beacon systems containing 2-ethynylfluorenone-labeled 2′-deoxyuridine units. Tetrahedron 68:72–78
41. Lee J, Cho HY, Hwang GT (2013) Highly efficient quencher-free molecular beacon systems containing 2-ethynyldibenzofuran- and 2-ethynyldibenzothiophene-labeled 2′-deoxyuridine units. ChemBioChem 14:1353–1362
42. Tanaka M, Oguma K, Saito Y, Saito I (2012) Enhancement of fluorescence quenching and exciplex formation in DNA major groove by double incorporation of modified fluorescent deoxyuridines. Bioorg Med Chem Lett 22:4103–4105
43. Segal M, Yavin E, Kafri P, Shav-Tal Y, Fischer B (2013) Detection of mRNA of the cyclin D1 breast cancer marker by a novel duplex-DNA probe. J Med Chem 56:4860–4869
44. Tanpure AA, Srivatsan SG (2014) Synthesis, photophysical properties and incorporation of a highly emissive and environment-sensitive uridine analogue based on the Lucifer chromophore. ChemBioChem 15:1309–1316
45. Yuan L, Zhang Z, Xu X, Zhou X (2014) Chemical labeling of 5-iodo-2′-deoxyuridine with 4-ethynyl-N-ethyl-1,8-naphthalimide using copper-free Sonogashira cross-coupling in aqueous medium. Synthetic Commun 44:1007–1011
46. Gondelaa A, Kumarb TS, Walczaka K, Wengel J (2010) Synthesis and biophysical properties of oligodeoxynucleotides containing 2′-deoxy-5-(4-nitro-1H-imidazol-1-yl)-β-D-uridine and 2′-deoxy-5-(1,3-dioxo-1H-benzo[de]isoquinolin-2(3H)-yl)-β-D-uridine monomers. Chem Biodivers 7:350–362
47. Saito Y, Miyamoto S, Suzuki A, Matsumoto K, Ishihara T, Saito I (2012) Fluorescent nucleosides with ‘on–off’ switching function, pH-responsive fluorescent uridine derivatives. Bioorg Med Chem Lett 22:2753–2756
48. Barthes NPF, Karpenko IA, Dziuba D, Spadafora M, Auffret J, Demchenko AP, Mély Y, Benhida R, Michel BY, Burger A (2014) Development of environmentally sensitive fluorescent and dual emissive deoxyuridine analogues. RSC Adv 5:33536–33545
49. Pawar MG, Nuthanakanti A, Srivatsan SG (2013) Heavy atom containing fluorescent ribonucleoside analog probe for the fluorescence detection of RNA-ligand binding. Bioconjugate Chem 24:1367–1377
50. Tanpure AA, Srivatsan SG (2012) Synthesis and photophysical characterisation of a fluorescent nucleoside analogue that signals the presence of an abasic site in RNA. ChemBioChem 13:2392–2399
51. Kanamori T, Ohzeki H, Masaki Y, Ohkubo A, Takahashi M, Tsuda K, Ito T, Shirouzu M, Kuwasako K, Muto Y, Sekine M, Seio K (2015) Controlling the fluorescence of benzofuran-modified uracil residues in oligonucleotides by triple-helix formation. ChemBioChem 16:167–176

52. Pawar MG, Srivatsan SG (2011) Synthesis, photophysical characterization, and enzymatic incorporation of a microenvironment-sensitive fluorescent uridine analog. Org Lett 13:1114–1117
53. Pawar MG, Srivatsan SG (2013) Environment-responsive fluorescent nucleoside analogue probe for studying oligonucleotide dynamics in a model cell-like compartment. J Phys Chem B 117:14273–14282
54. Gutierrez AJ, Terhorst TJ, Matteucci MD, Froehler BC (1994) 5-Heteroaryl-2′-deoxyuridine analogs. Synthesis and incorporation into high-affinity oligonucleotides. J Am Chem Soc 116:5540–5544
55. Wigerinck P, Pannecouque C, Snoeck R, Claes P, De Clercq E, Herdewijn P (1991) 5-(5-Bromothien-2-yl)-2′-deoxyuridine and 5-(5-chlorothien-2-yl)-2′-deoxyuridine are equipotent to (E)-5-(2-bromovinyl)-2′-deoxyuridine in the inhibition of herpes simplex virus type I replication. J Med Chem 34:2383–2389
56. Greco NJ, Tor Y (2007) Furan decorated nucleoside analogues as fluorescent probes: synthesis, photophysical evaluation, and site-specific incorporation. Tetrahedron 63:3515–3527
57. Sinkeldam RW, Wheat AJ, Boyaci H, Tor Y (2011) Emissive nucleosides as molecular rotors. ChemPhysChem 212:567–570
58. Sinkeldam RW, Greco NJ, Tor Y (2008) Polarity of major grooves explored by using an isosteric emissive nucleoside. ChemBioChem 9:706–709
59. Greco NJ, Sinkeldam RW, Tor Y (2009) An emissive C analog distinguishes between G, 8-oxoG, and T. Org Lett 11:1115–1118
60. Srivatsan SG, Tor Y (2007) Fluorescent pyrimidine ribonucleotide: synthesis, enzymatic incorporation, and utilization. J Am Chem Soc 129:2044–2053
61. Srivatsan SG, Tor Y (2007) Using an emissive uridine analogue for assembling fluorescent HIV-1 TAR constructs. Tetrahedron 63:3601–3607
62. Lane RSK, Jones R, Sinkeldam RW, Tor Y, Magennis SW (2014) Two-photon-induced fluorescence of isomorphic nucleobase analogs. ChemPhysChem 15:867–871
63. Noé MS, Sinkeldam RW, Tor Y (2013) Oligodeoxynucleotides containing multiple thiophene-modified isomorphic fluorescent nucleosides. J Org Chem 78:8123–8128
64. Hirose W, Sato K, Matsuda A (2011) Fluorescence properties of 5-(5,6-dimethoxybenzothiazol-2-yl)-2′-deoxyuridine ($d^{bt}U$) and oligodeoxyribonucleotides containing $d^{bt}U$. Eur J Org Chem 2011:6206–6217
65. Sato K, Sasaki A, Matsuda A (2011) Highly fluorescent 5-(5,6-dimethoxybenzothiazol-2-yl)-2′-deoxyuridine 5′-triphosphate as an efficient substrate for DNA polymerases. ChemBioChem 12:2341–2346
66. Hirose W, Sato K, Matsuda A (2010) Selective detection of 5-formyl-2′-deoxyuridine, an oxidative lesion of thymidine, in DNA by a fluorogenic reagent. Angew Chem Int Ed 49:8392–8394
67. Guo P, Xu X, Qiu X, Zhou Y, Yan S, Wang C, Lu C, Ma W, Weng X, Zhang X, Zhou X (2013) Synthesis and spectroscopic properties of fluorescent 5-benzimidazolyl-2′-deoxyuridines 5-fdU probes obtained from o-phenylenediamine derivatives. Org Biomol Chem 11:1610–1613
68. Clapham KM, Batsanov AS, Greenwood RDR, Bryce MR, Smith AE, Tarbit B (2008) Functionalized heteroarylpyridazines and pyridazin-3(2H)-one derivatives via palladium-catalyzed cross-coupling methodology. J Org Chem 73:2176–2181
69. Sinkeldam RW, Marcus P, Uchenik D, Tor Y (2011) Multisensing emissive pyrimidine. ChemPhysChem 12:2260–2265
70. Wanninger-Weiß C, Wagenknecht H-A (2007) Synthesis of 5-(2-pyrenyl)-2′-deoxyuridine as a DNA modification for electron-transfer studies: the critical role of the position of the chromophore attachment. Eur J Org Chem 1:64–71
71. Sekhar Bag S, Pradhan MK, Das SK, Jana S, Bag R (2014) Wavelength shifting oligonucleotide probe for the detection of adenosine of a target DNA with enhanced fluorescence signal. Bioorg Med Chem Lett 24:4678–4681

72. Park SM, Nam S-J, Jeong HS, Kim WJ, Kim BH (2011) The effects of the 4-(4-methylpiperazine)phenyl group on nucleosides and oligonucleotides: cellular delivery, detection, and stability. Chem Asian J 6:487–492
73. Hopkins PA, Sinkeldam RW, Tor Y (2014) Visibly emissive and responsive extended 6-aza-uridines. Org Lett 16:5290–5293
74. Seela F, Chittepu P (2007) Oligonucleotides containing 6-aza-2′-deoxyuridine: synthesis, nucleobase protection, pH-dependent duplex stability, and metal-DNA formation. J Org Chem 72:4358–4366
75. Luyten I, Pankiewicz KW, Watanabe KA, Chattopadhyaya J (1998) Determination of the tautomeric equilibrium of Ψ-uridine in the basic solution. J Org Chem 63:1033–1040
76. Lakowicz JR (2006) Principles of fluorescence spectroscopy. Springer, New York
77. Okamoto A, Tainaka K, Saito I (2003) Clear distinction of purine bases on the complementary strand by a fluorescence change of a novel fluorescent nucleoside. J Am Chem Soc 125:4972–4973
78. Okamoto A, Kanatani K, Saito I (2004) Pyrene-labeled base-discriminating fluorescent DNA probes for homogeneous SNP typing. J Am Chem Soc 126:4820–4827
79. Okamoto A, Saito Y, Saito I (2005) Design of base-discriminating fluorescent nucleosides. J Photochem Photobiol C 6:108–122

Chapter 2
Fluorescent Purine Nucleosides and Their Applications

Yoshio Saito, Azusa Suzuki, and Isao Saito

Abstract Fluorescent nucleosides have been used in diverse fields as powerful reporter molecules for investigating structures, functions, and interactions of DNA and RNA, in addition to the conventional applications related to genomics such as gene detection, single nucleotide polymorphism (SNP) typing, and fluorescence imaging. In addition to the traditional fluorescent nucleosides such as 2-aminopurine (2AP), different types of fluorescent nucleosides possessing other functions such as the ability of sensing viscosity, polarity, and surrounding pH at local environments of nucleic acids have been developed. In this chapter, the design strategy of various fluorescent nucleosides, particularly purine derivatives, are described together with their photophysical characteristics. Fluorescent purine nucleosides are classified into several types depending upon their structural features. Design concept for environmentally sensitive fluorescent purine nucleosides and their applications to fluorescent DNA probes are described.

List of Abbreviations

2AP	2-Aminopurine
ATP	Adenosine triphosphate
BDF	Base-discriminating fluorescence
BRCA1	Breast cancer type 1
CD	Circular dichroism
DF	Discrimination factor
ESF	Environmentally sensitive fluorescence
GTP	Guanosine triphosphate
ICT	Intramolecular charge transfer
LE	Locally excited
MB	Molecular beacon
NTP	Nucleoside triphosphate

Y. Saito (✉) • A. Suzuki
Department of Chemical Biology and Applied Chemistry, College of Engineering, Nihon University, Koriyama, Fukushima 963-8642, Japan
e-mail: saitoy@chem.ce.nihon-u.ac.jp

I. Saito
Institute of Advanced Energy, Kyoto University, Uji, Kyoto 611-0011, Japan

K. Nakatani, Y. Tor (eds.), *Modified Nucleic Acids*, Nucleic Acids and Molecular Biology 31, DOI 10.1007/978-3-319-27111-8_2

ODN	Oligodeoxynucleotide
PEX	Primer extension
S/N	Signal to noise
SNP	Single nucleotide polymorphism

2.1 Introduction

Fluorescent molecules are widely used in diverse fields such as chemistry, biology, biotechnology, and medicine owing to their extraordinary high sensitivity, specificity, simplicity, non-invasiveness, and low cost as compared with other methods. The combination of reporter fluorescent molecules and modern fluorescent technology, including fluorescence imaging techniques, enables the visualization of complex phenomena in biological systems. As the modern fluorescence technology progress, the development of new fluorescent molecules possessing additional functions becomes more important due to the great interest in their applications. Fluorescent molecules possessing various functions have been developed and incorporated into biopolymers like proteins, lipids, polysaccharides, and nucleic acids and widely utilized as reporter molecules. For example, environmentally sensitive fluorescent amino acids that elucidate changes in the local environment by the alteration in their fluorescence wavelength and intensity have been incorporated into proteins and used to directly monitor structural changes caused by ligand binding [1, 2]. Thus, the introduction of such fluorescent molecules into targeted biomolecules provides valuable information on the structure, location, and function, as well as on the mode of molecular interactions, and greatly contributes to the elucidation of biomolecular mechanisms in vitro and in vivo.

Fluorescent nucleosides are also used as reporter molecules in the structural analysis of RNA and for the detection of various types of nucleic acids. Since the initial report of 2-aminopurine (**2AP**) in 1969 [3], numerous studies have implemented to incorporate useful photophysical features into nonemissive native nucleosides [4–6]. Many isomorphic fluorescent nucleosides have been reported whose character closely resembles to those of their corresponding natural nucleosides, including hydrogen bonding patterns with minimally perturbing oligonucleotide duplex structure. In general, the expansion of the aromatic ring system results in a favorable photophysical property such as red-shifted absorption and emission with higher quantum efficiency. Thus, size-expanded nucleosides, which extend the conjugation of the natural nucleobase by fusing aromatic rings in various ways, have also shown to be the reporter molecules and applied to fluorescent oligodeoxynucleotide (ODN) probes after the incorporation into ODNs. Other approaches, including the attachment of fluorescent aromatic or heteroaromatic chromophores via a linker or the direct attachment of fluorescent chromophores to native nucleobase, have been reported to attain fluorophore-conjugated purine nucleoside derivatives. Unlike classical fluorescent nucleosides, recently developed nucleosides have other important functions such as the ability of sensing viscosity,

polarity, and pH in addition to simple labeling function. Thus, these fluorescent nucleosides can be used as powerful reporter probes for structural studies on nucleic acids, sequencing, molecular diagnostics, and fluorometric assays of nucleic acids.

In this chapter, fluorescent nucleosides are classified into several types depending upon their structural features and emissive properties, and their applications as fluorescent markers are also described in detail. Although numerous reviews on fluorescent nucleosides and oligonucleotides have already appeared [4–6], the recent advancement of the fluorescent purine nucleosides are not well reviewed. Recent development of fluorescent purine nucleosides is described in this chapter with particular emphasis on the design concept of practically useful fluorescent purine nucleosides. In addition to the design strategy and classification, we also describe the application of ODNs containing various fluorescent purine derivatives.

2.2 Isomorphic Fluorescent Purine Nucleosides

We have classified the fluorescent purine analogs into six main categories: (1) isomorphic, (2) size-expanded, (3) fluorophore-tethered, (4) base-modified, (5) push–pull type conjugated, and (6) dual-fluorescent nucleosides. Here, each type is demonstrated with sub-categories and their applications.

2.2.1 2AP Analogs

Isomorphic fluorescent nucleosides are the emissive surrogates for natural nucleosides that minimize the structural and functional perturbation of nucleic acids when incorporated into oligonucleotides, thus making them suitable for the investigation of the structure and function of nucleic acids and their interactions with related biomolecules including proteins. The **2AP (1)** is a well-known and widely utilized isomorphic fluorescent nucleoside (Fig. 2.1a) [3]. The fluorescence quantum yield of **2AP** is quite high ($\Phi_F = 0.68$) in neutral aqueous conditions, and the red-shifted absorption spectrum permits excitation beyond the range of natural nucleobases and proteins. **2AP** forms a stable Watson–Crick base pair with thymine and maintain the normal B-DNA structure. Moreover, solid-phase oligonucleotide synthesis using phosphoramidite chemistry enables the incorporation of **2AP** in any position of both DNA and RNA strands.

There are numerous reports on **2AP**-containing oligonucleotides. The incorporation of **2AP** into ODNs provides a powerful tool to probe the structure and dynamics of the target DNA and RNA. For example, Guests et al. synthesized a series of ODN duplexes containing **2AP** (5′-d(CGG**2AP**GGC)-3′/3′-(GCCXCCG)-5′, where X = A, T, G, or C) and studied the structural dynamics of mismatched base pairs in DNA by measuring time-resolved fluorescence anisotropy decay

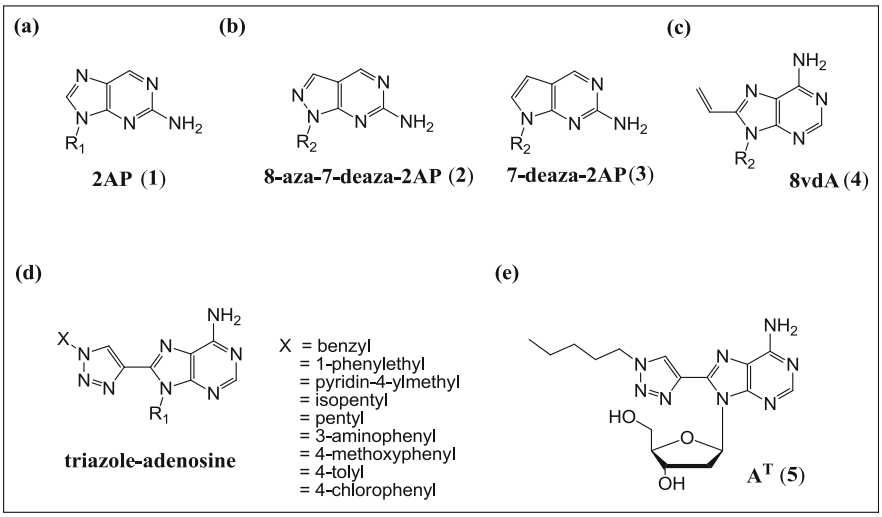

Fig. 2.1 Structures of isomorphic fluorescent aminopurines: (**a**) 2-aminopurine ribonucleoside (**1**), (**b**) 2AP derivatives (**2**) and (**3**), (**c**) 8-vinyl-2′-deoxyadenosine (**4**), (**d**) triazolyl adenosine derivatives, and (**e**) 8-(1-pentyl-1H-1,2,3-triazol-4-yl)-2′-deoxyadenosine (**5**) (R_1 = ribose; R_2 = 2′-deoxyribose)

[7]. Menger et al. studied the Mg^{2+}-dependent conformational changes in hammerhead (HH) ribozyme by fluorescence changes in **2AP** incorporated into either the substrate or the ribozyme [8]. Furthermore, Tor et al. reported the design and synthesis of internally fluorescent **2AP**-containing HH ribozymes that change fluorescence parameters, directly reflecting the progress of the ribozyme's cleavage chemistry [9]. Several examples for monitoring protein-induced conformational changes in nucleic acids using **2AP**-containing ODN probes have been demonstrated [10–12]. However, there is still a great demand for further development of isomorphic fluorescent nucleosides with stronger emissions, because the fluorescence quantum yield of **2AP** in single- or double-stranded oligonucleotides is quite low.

Seela and Becher reported emissive 8-aza-7-deazapurine-2-amine 2′-deoxyribonucleoside (8-aza-7-deaza-**2AP,** **2**) as purine-2-amine 2′-deoxyribonucleoside derivative (Fig. 2.1b) [13]. They examined the thermal stability and photophysical properties of ODNs containing 8-aza-7-deaza-**2AP** and compared the properties with those of **2AP**- and 7-deaza-**2AP**-containing ODNs. They found that ODN duplexes containing **2AP** or 8-aza-7-deaza-**2AP** are less stable than those containing natural 2′-deoxyadenosine. The fluorescence emission of these **2AP** derivatives was strongly quenched in single-stranded and duplex states owing to their stacking interactions. The residual fluorescence of ODNs is used to determine melting temperatures (T_m values) as an alternative to the UV melting analysis.

Mely et al. reported 8-vinyl-2′-deoxyadenosine (**8vdA**, **4**), a fluorescent derivative with improved photophysical properties, as an alternative to **2AP** (Fig. 2.1c) [14]. The quantum yield of the **8vdA** monomer was similar to that of **2AP** and was sensitive to solvent type and temperature but not to pH. They demonstrated that ODNs containing **8vdA** (5′-CGTTTTX**8vdA**XTTTTGC-3′, where X = A or T) form more stable duplexes than the corresponding **2AP**-containing ODNs, possibly because **8vdA** adopts an anti-conformation to maintain Watson–Crick hydrogen bonding. In addition, the fluorescence quantum yield of **8vdA** was significantly higher than that of **2AP** in single-stranded ODNs and duplexes. **8vdA** is used as a non-perturbing analog of **2AP** for same purposes.

Grotli and Wilhelmsson have developed a series of 8-(1*H*-1,2,3-triazol-4-yl)-substituted adenosine derivatives using Sonogashira cross-coupling and click chemistry (Fig. 2.1d) [15, 16]. These triazole-adenine derivatives show desirable photophysical properties, including higher quantum yield and larger brightness factor. In particular, isopentyl-substituted derivatives show a high quantum yield in both THF ($\Phi_F = 0.62$) and water ($\Phi_F > 0.50$) as a free nucleoside [16]. Thus, 2′-deoxyribo derivative of 8-(1-pentyl-1*H*-1,2,3-triazol-4-yl)adenosine (**A**$^{\mathbf{T}}$, **5**: Fig. 2.1e) was developed and incorporated into ODNs (5′-d(CGCAX**A**$^{\mathbf{T}}$XTCG)-3′, neighboring bases X = A, G, C, or T) [15]. The fluorescence quantum yield of **A**$^{\mathbf{T}}$-containing ODNs was strongly affected by the type of neighboring base. However, the fluorescence quantum yield in single strands ($\Phi_F > 0.2$, both the flanking bases X = A) and duplexes ($\Phi_F = 0.05$, both the flanking bases X = A) was lower than that recorded for **A**$^{\mathbf{T}}$ monomer in water ($\Phi_F = 0.61$), while 10–50 times higher than the corresponding values for 2AP. In addition, **A**$^{\mathbf{T}}$ exhibited only a minor destabilization of DNA duplexes as compared with 2AP, and CD data also revealed that **A**$^{\mathbf{T}}$ only causes minimal structural perturbations to normal B-DNA. When incorporated into ODN probes, the isomorphic fluorescent nucleoside **A**$^{\mathbf{T}}$ has significant potential for monitoring the microenvironment in DNA.

2.2.2 Thieno Analogs of Ribo and Deoxyribo Nucleosides

Although several isomorphic fluorescent purine nucleosides including classical **2AP** have been developed, they have several demerits such as low quantum yield when present in the oligonucleotide either in single-stranded form or duplex structure. Thus, it is necessary to develop the nucleosides that has more advantageous than the previously reported fluorescent analogs. In this regard, Tor et al. reported a highly emissive and isomorphic purine $^{\mathbf{th}}$**G** (**6**) and $^{\mathbf{th}}$**A** (**7**) and pyrimidine $^{\mathbf{th}}$**C** (**8**) and $^{\mathbf{th}}$**U** (**9**) ribonucleoside sets (Fig. 2.2a) [17–20]. These thieno analogs of ribonucleosides, which are derived from thieno[3,4-*d*]pyrimidine, show favorable photophysical features [19]. Their excitations at long-wavelength UV-absorption maxima are significantly red-shifted from those of their natural counterparts, ranging from 304 nm ($^{\mathbf{th}}$**U**) to 341 nm ($^{\mathbf{th}}$**A**) in water and yield visible

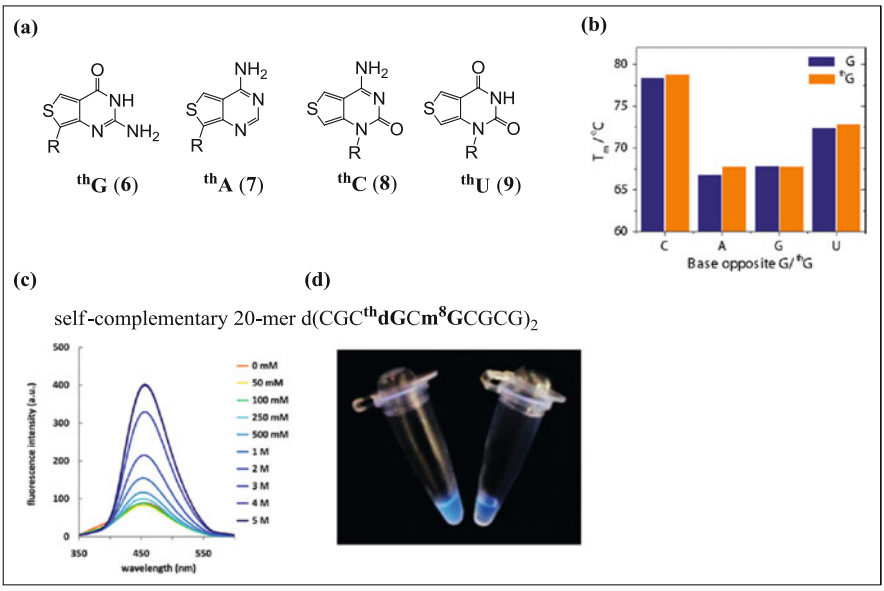

Fig. 2.2 (**a**) Structures of thieno[3,4-*d*]pyrimidine nucleoside analogs (R = ribose). (**b**) Comparison of T_m values for duplexes of th**G** and **G** with their complementary and mismatched base (reprinted with permission from Sinkeldam et al., J Am Chem Soc (2011) 133:14912–14915. Copyright 2011 American Chemical Society). (**c**) Observation of B–Z transition through changes in fluorescence intensity by adjusting $NaClO_4$ concentration. (**d**) Visual detection of B–Z transition by Zαβ interaction. 4 eq. (*left*) or 0 eq. (*right*) of Zαβ protein (reprinted with permission from Park et al., Chem Commun (2014) 50:1573–1575. Copyright 2014 The Royal Society of Chemistry)

Table 2.1 Photophysical data of thieno[3,4-*d*] pyrimidine nucleoside analogs

	λ_{abs} (ε)	λ_{em} (Φ_F)	Stokes shift
th**G**	321 (4.15)	453 (0.46)	9580
th**A**	341 (7.44)	420 (0.21)	5950
th**C**	320 (4.53)	429 (0.41)	8300
th**U**	304 (3.16)	409 (0.41)	8860

λ_{abs}, λ_{em}, ε, and Stokes shift are reported in nm, nm, 10^3 M^{-1} cm^{-1}, and cm^{-1}, respectively

emissions between 409 nm (th**U**) and 453 nm (th**A**) with a high quantum yield, as summarized in Table 2.1.

To investigate thermal stability of RNA duplexes with thieno-analogs, 17-mer th**G**-containing RNA (5′-r(GAGCGAUGXGUAGCGAG)-3′, X = th**G**) was synthesized and hybridized with complementary oligonucleotides (3′-r(CUCGCUACY-CAUCGCUC)-5′, Y = C, G, U, or A) (Fig. 2.2b). Replacing the natural G residue with th**G** increased the duplex stability slightly (ΔT_m = +1.0 °C). In addition, a similar stability trend was observed for all mismatched th**G**-containing duplexes (Y = G, U, and A), with increasing stability relative to the corresponding native

duplex, suggesting that **thG** acts as an emissive isomorphic guanine analog. **thG** maintained Watson–Crick hydrogen bonding faces and allowed minimal perturbation to duplex stability when it is present in the ODN duplexes. The fluorescence spectra of **thG**-containing RNA were measured in the absence and presence of complementary RNAs. Unlike classical **2AP**, even when an oligonucleotide containing -G**thG**G- sequence was used, quenching by flanking G residues was not observed, and a strong visible emission was observed [$\Phi_F = 0.10$ (ssRNA) and 0.08 (dsRNA)].

Tor et al. subsequently investigated the ability of T7 RNA polymerase to initiate and maintain RNA transcription using 5′-triphosphate of **thG** (**thGTP**) and compared its performance with natural GTP [21]. They determined that **thG**-modified transcripts were synthesized with a yield comparable with that of the native nucleoside, and **thGTP** is accepted as a GTP surrogate in both the initiation and elongation steps of T7 RNA polymerase. Thus, **thG** acts as a potential surrogate of guanosine and was used as an efficient fluorescent probe for RNA structural analysis.

Sugiyama et al. focused on the application of a G-mimic deoxyribonucleoside analog, 2-aminothieno[3,4-*d*]pyrimidine (**thdG**), as a versatile emissive deoxyguanosine [22]. **thdG** was incorporated into ODNs to investigate the conformational transition from B-DNA to Z-DNA. They had previously demonstrated that the B–Z transition was detected by measuring the fluorescence intensity of **2AP**. Based on these studies, 10-mer ODN containing **thdG** (5′-d(CGCGC **thdG** CGCG)-3′) was prepared, and the resulting changes in the electronic properties of DNA transitioning between B- and Z-DNA were investigated. They found that the B–Z transition became more difficult when G was replaced by **thdG**. Thus, the self-complementary 20-mer d(CGC **thdG** C**m^{8}G**CGCG)$_2$ containing 8-methylguanine (**m^{8}G**) as a Z-DNA-stabilizing base was synthesized, and its fluorescence intensity was observed at various salt concentrations. As shown in Fig. 2.2c, a dramatic change in fluorescence intensity in response to the B–Z transition was observed. A strong fluorescence enhancement caused by the disruption of charge transfer attributable to the four-base π-stacks occurred in Z-DNA, whereas the fluorescence was very weak in the B-DNA. The increase in fluorescence intensity of **thdG** was proportional to the increase in the ratio of the Z-conformation, which was achieved by adjusting $NaClO_4$ concentration. Furthermore, they succeeded in the visual detection of DNA–protein interactions. When Zαβ protein, DNA binding domain of double-stranded RNA adenosine deaminase that specifically binds to Z-DNA, is titrated into a solution containing ODN probes, the fluorescence of ODN probes containing **thdG** increased strongly in real time as the B–Z transition occurs (Fig. 2.2d). Thus, the ODN probes containing **thdG** serves as useful tools in the development of visual detection methodologies of DNA.

2.3 Size-Expanded Fluorescent Purine Nucleosides

2.3.1 1,N^6-Ethenoadenosine (εA) and Related Derivatives

The first example of an expanded fluorescent purine nucleoside was recorded by Leonard et al. in 1972 [23, 24]. They synthesized a highly fluorescent ATP analog, 1,N^6-ethenoadenosine (**εA, 10**) triphosphate, from the reaction of ATP with chloroacetaldehyde and described its fluorescence properties and its behavior in several adenine nucleotide-binding enzyme systems. The extended π-conjugation of **εA** induces red shift to the absorption spectrum and lower excitation energy relative to the natural nucleic acids and proteins, which permits selective excitation. In addition, **εA** exhibits an intense fluorescence emission in the visible region ($\lambda_{em} = 415$ nm, $\Phi_F = 0.56$ in buffer, pH 7.0) with a relatively long lifetime (20 ns) as a small chromophore. The characteristic intense emission and long lifetime of **εA** enable its application as novel probes for diagnostics, sequencing, and molecular structure recognition studies. After the study by Leonard et al., several derivatives of 1,N^6-ethenoadenosine were also reported (Fig. 2.3a) [25–29]. Tsou and Yip developed 2-aza-1,N^6-ethenoadenosine (**2-aza-εA**, **11**) and various 2-substituted 1,N^6-ethenoadenosines as fluorescent ribonucleoside derivatives [28, 29]. Seela et al. reported 7-deaza-(**7-deaza-εA**, **12**), 8-aza-7-deaza-(**8-aza-7-deaza-εA**, **13**), and 7-deaza-2,8-diaza-1,N^6-ethenoadenosine (**7-deaza-2,8-diaza-εA**, **14**) ribonucleosides with interesting photophysical properties [25–27]. The photophysical data of the etheno nucleosides listed in Table 2.2 indicates that particularly 7-deaza-2,8-diaza derivatives exhibit unique fluorescent properties as free nucleosides. 7-Deaza-2,8-diaza-**εA** shows an emission maximum at 511 nm in methanol that is red-shifted to 531 nm in aqueous buffer solution (pH 7.0).

The introduction of **εA** derivatives into oligonucleotides using solid-phase phosphoramidite chemistry was demonstrated by Srivastava et al. in 1994 [30]. 1,N^6-etheno deoxyribo and ribo-adenosines have been synthesized and introduced selectively into various DNA and RNA sequences at single or multiple sites with predetermined positions. Using solid-phase synthesis, Srivastava et al. also prepared **εA**-containing modified sequences as primers and demonstrated PCR amplification. Although multiple incorporations of or replacements by **εA** in the primer sequence around the 3′-end or the center were shown to prevent the amplification, such incorporations or replacements around the 5′-end did not prevent the amplification, which is similar to the behavior of the natural primer. Thus, the chemical synthesis of **εA**-containing ODNs using a DNA/RNA synthesizer extends the range of applications of **εA** as a fluorescent probe.

Although recent research shows that **εA** completely lacks recognition capabilities for all natural bases [31], oligonucleotide probes containing ribo/deoxyribo **εA** or various **εA** derivatives provide useful fluorescent probes for the studies of structures and functions of DNA/RNA, protein–DNA/RNA binding, and diagnostic applications. As a derivative of 1,N^6-etheno-2′-deoxyadenosine (**εA$_d$**, **10b**), 1,N^6-etheno-7-deaza-2′-deoxyadenosine (**εc^{7}A$_d$**, **12b**) was also developed by Seela

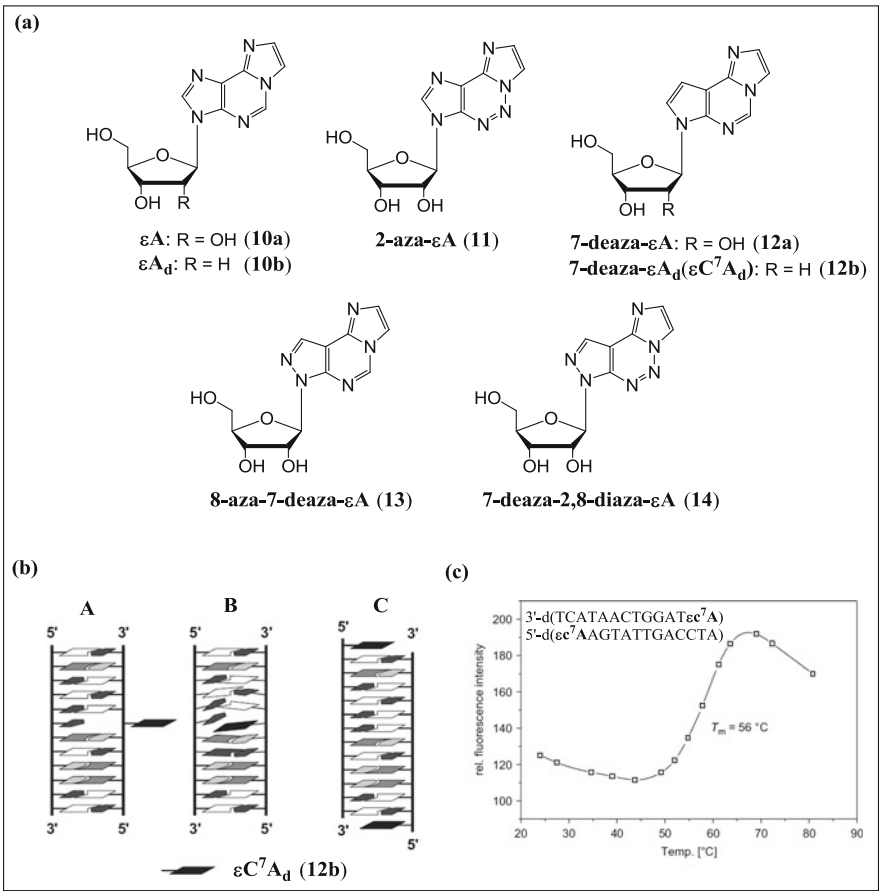

Fig. 2.3 (**a**) Structures of 1,N^6-ethenoadenosine derivatives. (**b**) Possible structures of the duplexes 5′-d(TAGGTC**εc^{7}A**ATACT) 3′-d(ATCCAGTTATGA) [**A** (unlikely) and **B**], 5′-d (**εc^{7}A**TAGGTCAATACT) 3′-d(ATCCAGTTATGA**εc^{7}A**) (**C**). (**c**) Temperature dependence of the fluorescence emission of the duplex (reprinted from Tetrahedron 63; Seela et al., 1,N^6-Etheno-2′-deoxytubercidin and pyrrolo-C: synthesis, base pairing, and fluorescence properties of 7-deazapurine nucleosides and oligonucleotides, 3471–3482 (2007), with permission from Elsevier)

et al. and introduced into oligonucleotides. **εc^{7}A$_d$** is more stable than **εA$_d$** in both acidic and alkaline conditions and exhibits a strong emission ($\Phi_F = 0.53$) with a large Stokes shift ($\Delta\lambda = 134$ nm) as a free nucleoside. As in the case for **εA$_d$**, **εc^{7}A$_d$** does not form base pairs with natural bases in oligonucleotide duplexes and therefore acts as a universal base. When **εc^{7}A$_d$** is located at the center of a duplex (e.g., 5′-d(TAGGTC**εc^{7}A$_d$**ATACT)-3′/3′-d(ATCCAGTTATGA)-5′), the neighboring base pairs might be distorted as shown in Fig. 2.3b (B). However, when this modified base is located in the overhanging position (e.g., 5′-d (**εc^{7}A$_d$**AGTATTGACCTA)-3′/3′-d(TCATAACTGGAT**εc^{7}A$_d$**)-5′), it stabilizes

Table 2.2 Fluorescence data of 1,N^6-ethenoadenosme derivatives measured in methanol at room temperature

	λ_{ex} max (nm)	λ_{em} max (nm)	Φ_F		λ_{ex} max (nm)	λ_{em} max (nm)	Φ_F
εA (10a)	298	410	0.2	**8-aza-7-deaza-εA (13)**	300	441	0.14
2-aza-εA (11)	349	481	0.05	**7-deaza-2,8-diaza-εA (14)**	367	511	0.01
7-deaza-εA$_d$ (12a)	297	409	0.14				

the preformed oligonucleotide duplex as indicated in Fig. 2.3b (C). In this case, the temperature-dependent fluorescent measurements of the oligonucleotide duplexes exhibited sigmoidal melting profiles. However, this is not the case for duplexes containing central **εc^{7}A$_d$** (Fig. 2.3c). These favorable photophysical features of **εc^{7}A$_d$** are used to investigate the interaction of nucleosides and oligonucleotides, and **εc^{7}A$_d$** is also applied to DNA probe for the purpose of monitoring DNA denaturation.

2.3.2 Benzo-Fused Nucleosides (xDNA)

In 1976, Leonard et al. developed another type of novel size-expanded fluorescent purine nucleoside, *lin*-benzoadenosine [32–34]. The structural design of this molecule involves the formal insertion of a benzene ring between the two rings of adenine and increases its size by approximately 2.4 Å. This "stretched-out" version of the adenine ribonucleoside and its triphosphate was used to probe the steric requirement of the active site of an ATP-dependent enzyme. The conversion of *lin*-benzoadenosine to the deoxyribonucleoside derivative (**dxA**) was reported in 1984. However, it was not incorporated into ODNs, because automated DNA/RNA synthesizers were not invented at that time.

The base-pairing and stacking properties of size-expanded deoxyribonucleoside in ODNs were extensively studied by Kool et al. [35, 36]. They developed a set of all four benzo-fused-expanded DNA nucleosides (**dxA**, **dxT**, **dxG**, and **dxC**) and established a stable new four-base genetic system termed as xDNA (Fig. 2.4a, b). As part of their extensive studies on this xDNA system, photophysical properties of size-expanded nucleosides in ODN were also reported. They conducted a preliminary experiment using short 12-mer ODNs 5′-d(AAGAA**xA**GAAAAG)-3′ and its complimentary strand of the sequence 5′-d(CTTTTC**xA**TTCTT)-3′). The **dxA**-containing single-stranded ODN, 5′-d(AAGAA**xA**GAAAAG)-3, exhibited an emission reduced by five times relative to that of pyrimidine ODN, 5′-d (CTTTTC**xA**TTCTT)-3′, because of the quenching by adjacent purine bases (Fig. 2.5a). As shown in Fig. 2.5b, the fluorescence intensity of **dxA**-containing

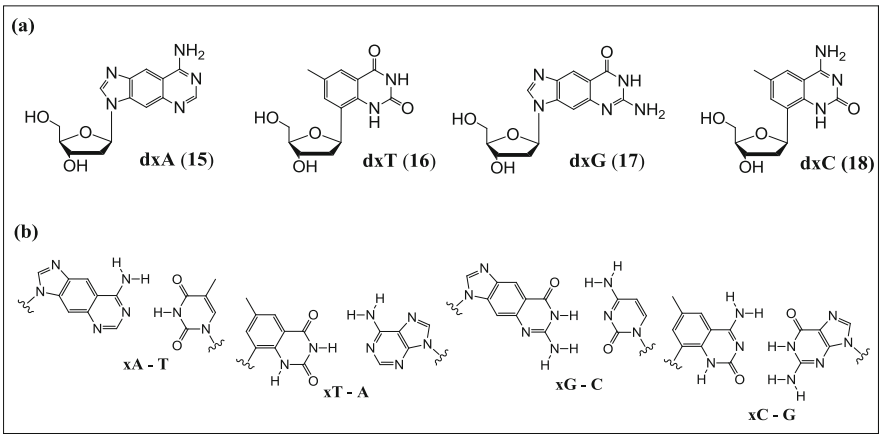

Fig. 2.4 (**a**) Structures of benzo-fused nucleosides **dxA** (**15**), **dxT** (**16**), **dxG** (**17**), and **dxC** (**18**). (**b**) Proposed structures of expanded base pairs formed between **xA**, **xT**, **xG**, or **xC** with Watson–Crick complements

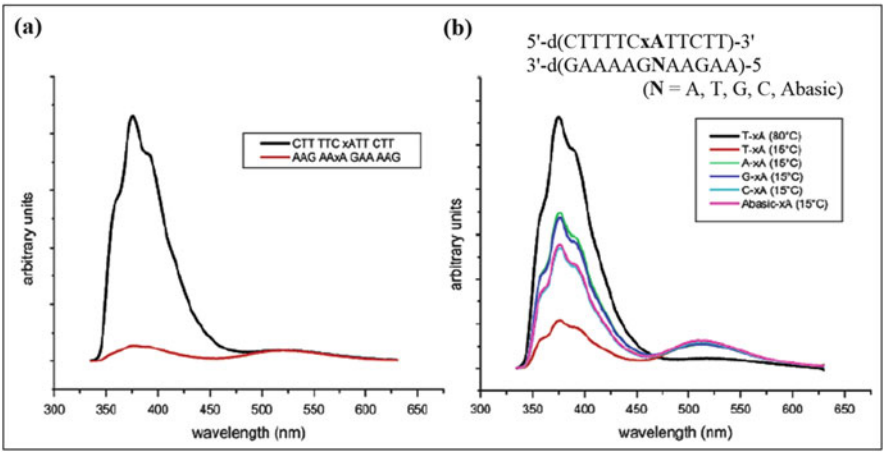

Fig. 2.5 (**a**) Fluorescence spectra of single-stranded DNA containing **xA**. (**b**) Fluorescence spectra of DNA duplexes containing **xA** (reprinted with permission from Gao et al., J Am Chem Soc (2004) 126:11826–11831. Copyright 2004 American Chemical Society)

pyrimidine ODN was dramatically decreased by duplex formation [5′-d (CTTTTC**xA**TTCTT)-3′/3′-d(GAAAAG**N**AAGAA)-5′, N = A, T, G, C, or abasic site], suggesting that intra and interstrand interactions between **dxA** and purine bases cause fluorescence quenching. When **dxA** was introduced into ODNs, a new emission was observed at a longer wavelength of approximately 520 nm (Fig. 2.5a, b). The new emission is likely caused by the electronic interaction between **dxA** and its neighboring bases. Therefore, it was inferred that benzo-fused size-expanded nucleoside **dxA** is able to respond to microenvironmental changes (e.g., local

helicity) by changing its fluorescence intensity. Thus, these size-expanded fluorescent purine nucleosides may be used in monitoring the chemical interactions of biomolecules, gene detection, diagnosis, and imaging applications.

2.3.3 *Methoxybenzodeazaadenosine (^{MD}A) and Methoxybenzodeazainosine (^{MD}I)*

Saito et al. demonstrated size-expanded purine nucleosides, methoxybenzodeazaadenosine (**19**) and methoxybenzodeazainosine (**20**), as base-discriminating fluorescent (BDF) nucleosides and used these artificial bases to detect single-nucleotide alterations in DNA [37, 38]. Fluorescent oligonucleotide probes containing $^{\mathbf{MD}}\mathbf{A}$ and $^{\mathbf{MD}}\mathbf{I}$ emit strong fluorescence only when the bases opposite to them in the complementary strand are cytosine and thymine, respectively. As shown in Fig. 2.6a, the fluorescence intensities of the single-stranded 5′-d(CGCAAT$^{\mathbf{MD}}$**A**TAACGC)-3′ and duplexes with complementary ODN 5′-d(GCGTTATATTGCG)-3′ were very weak ($\Phi_F = 0.005$ and <0.005, respectively). However, the fluorescence spectrum of duplex 5′-d(CGCAAT$^{\mathbf{MD}}$**A**TAACGC)-3′/5′-d(GCGTTACATTGCG)-3′ showed an intense fluorescence at 424 nm ($\Phi_F = 0.081$). In contrast, when ^{MD}I-containing ODN 5′-d(CGCAAT$^{\mathbf{MD}}$**I**TAACGC)-3′ was hybridized with its complementary strand 5′-d(GCGTTAAATTGCG)-3′, a strong emission was observed at 424 nm, and the intensity increased almost sixfold when compared to the duplex 5′-d(CGCAAT$^{\mathbf{MD}}$**I**TAACGC)-3′/5′-d(GCGTTACATTGCG)-3′ ($\Phi_F = 0.011$ and 0.002, respectively).

The clear change in the fluorescence of $^{\mathbf{MD}}\mathbf{A}$- or $^{\mathbf{MD}}\mathbf{I}$-containing ODNs based on the type of the base on the complementary strand is particularly useful for SNP typing and gene sequence detection. Thus, SNP detection of T/C sequence in the human breast cancer type 1 gene (BRCA1) was tested by using $^{\mathbf{MD}}\mathbf{A}$- and $^{\mathbf{MD}}\mathbf{I}$-containing BDF probes. The BDF probe, 5′-d(GGTACCA$^{\mathbf{MD}}$**A**TGAAATA)-3′ or 5′-d(GGTACCA$^{\mathbf{MD}}$**I**TGAAATA)-3′, was mixed with target ODN, 3′-d(CCATGGTTACTTTAT)-5′, 3′-d(CCATGGTCACTTTAT)-5′, or a 1:1 mixture of both ODNs (heterozygous state), and the fluorescence was read with a fluorescence imager. As shown in Fig. 2.6b, BDF probes containing $^{\mathbf{MD}}\mathbf{A}$ and $^{\mathbf{MD}}\mathbf{I}$ can clearly distinguish C and T, respectively, from other bases opposite to the BDF nucleoside. In addition, a combination of both BDF probes enables a rapid detection of the T/C SNPs of heterozygous samples.

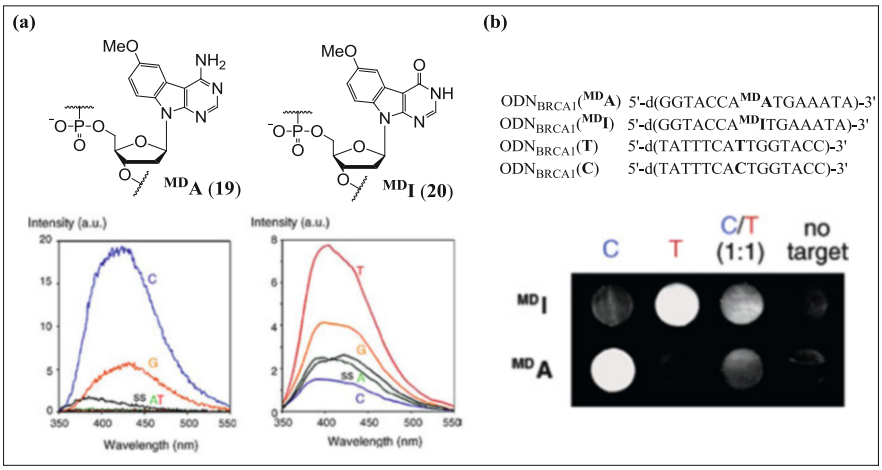

Fig. 2.6 (**a**) Structures of ^{MD}**A** (**19**) and ^{MD}**I** (**20**), and the fluorescence spectra of BDF nucleoside-containing probes hybridized with ODN possessing A, G, C, or T opposite to the BDF base; "ss" denotes a single-stranded probe. (**b**) Determination of T/C allele type of BRCA1 using fluorescence change of ODN_{BRCA1}(^{MD}**A** or ^{MD}**I**) (reprinted with permission from Okamoto et al., J Am Chem Soc (2003) 125:9296–9297. Copyright 2003 American Chemical Society)

2.4 Fluorophore-Tethered Purine Nucleosides

2.4.1 Base-Discriminating Fluorescent Purine Nucleosides

Fluorescent nucleosides that change their emission intensities in response to changes in their local environments such as polarity, viscosity, and surrounding pH are of special interest due to their various applications. Moreover, ODN probes possessing such fluorescent nucleosides are used to detect changes in the DNA microenvironment, such as those that occur during hybridization and conformational changes, and is used for SNP typing as well. In 2004, Okamoto and Saito reported conceptually new fluorescent nucleosides called BDF nucleosides that can distinctly indicate the base type opposite to the modified fluorescent nucleobase by a change in its fluorescence intensity [39]. Among BDF nucleosides, pyrene-labeled pyrimidine nucleosides, ^{Py}**U** (**21**) and ^{Py}**C** (**22**), exhibit particularly unique fluorescence properties depending on the base type of the complementary strand and can clearly identify perfectly matched adenine and guanine opposite to ^{Py}**U** and ^{Py}**C**, respectively, by a drastic change in their fluorescence intensities (Fig. 2.7).

Pyrene-1-carboxaldehyde is known to possess solvent polarity-dependent fluorescence properties. The fluorescence intensity of pyrene-1-carboxaldehyde in a polar solvent is high ($\Phi_F = 0.15$ in ethanol), whereas the intensity in nonpolar solvents like *n*-hexane is quite low ($\Phi_F < 0.001$). In nonpolar solvents, the fluorescence results from non-emissive n–π* state, whereas when the solvent polarity increases, π–π* state that lies slightly above n–π* state is shifted below n–π* state

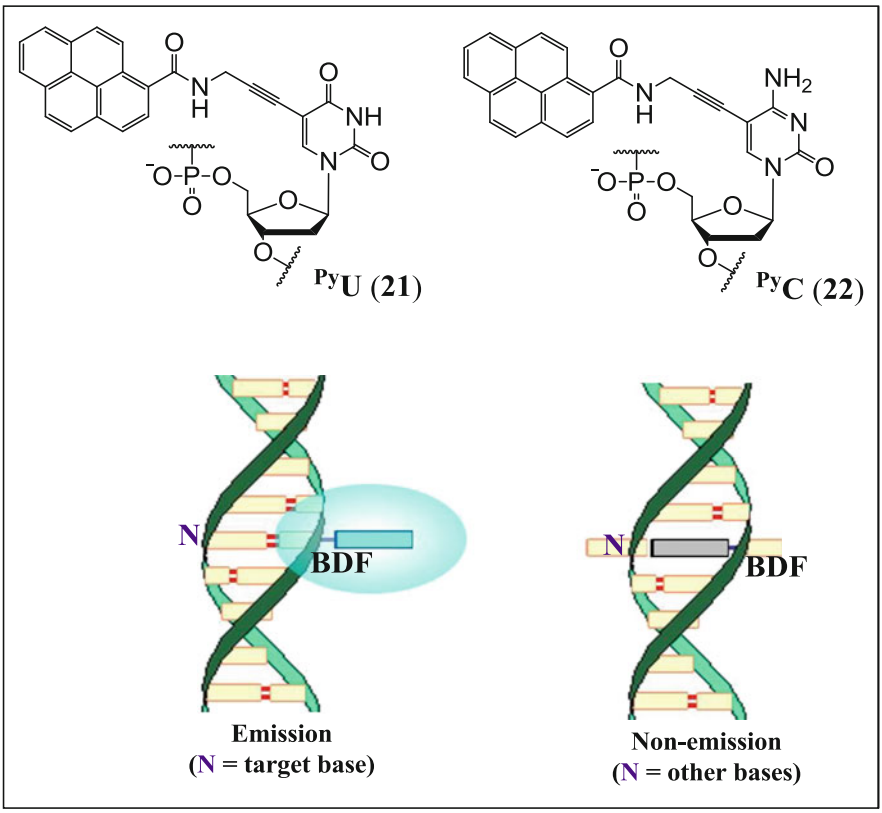

Fig. 2.7 Structures of BDF nucleosides ^{Py}**U** (**21**) and ^{Py}**C** (**22**), and schematic illustration of the ODN probes containing BDF nucleoside for SNP typing

by solvent relaxation during the lifetime of the excited state, thus becoming the emitting state to result in a strong fluorescence emission. By using these polarity-dependent fluorescence changes in pyrene carbonyl compounds, ^{Py}**U** and ^{Py}**C** are expected to discriminate matched and mismatched base types on the target DNA. When the pyrenecarboxamide fluorophore is attached at C-5 position of a pyrimidine base via a rigid linker, the fluorophore is extruded outside the DNA duplex owing to the base pairing of ^{Py}**U** and ^{Py}**C** with adenine and guanine, respectively, into a highly polar aqueous phase, resulting in a strong fluorescence. In contrast, when the pyrene is inside the duplex owing to a lack of base-pairing, i.e., in the case of mismatch, the BDF nucleoside shows no emission because the pyrene is located at a highly hydrophobic site inside the DNA duplex. In fact, an ODN probe containing ^{Py}**U** was shown to indicate matches and mismatches in the target DNA strand by significant differences in its fluorescence intensity. The fluorescence spectrum of the perfectly matched duplex (5′-d(CGCAAT^{Py}**U**TAACGC)-3′/3′-d(GCGTTAAATTGCG)-5′) showed a strong emission at 397 nm ($\Phi_F = 0.203$). In contrast, the fluorescence of the mismatched duplexes (5′-d

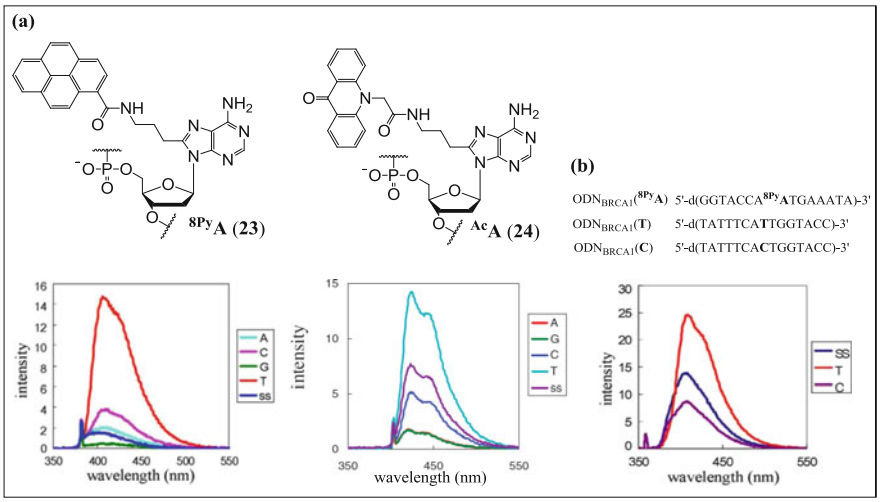

Fig. 2.8 (**a**) Structures of ^{8Py}**A** (**23**) and ^{Ac}**A** (**24**), and the fluorescence spectra of BDF purine nucleoside-containing probes hybridized with an ODN possessing A, G, C, or T opposite to the BDF purine bases; "ss" denotes a single-stranded probe. (**b**) Fluorescence spectra of **ODN$_{BRCA1}$**(^{8Py}**A**) hybridized with **ODN$_{BRCA1}$(T)** or **ODN$_{BRCA1}$(C)** and of single-stranded **ODN$_{BRCA1}$**(^{8Py}**A**)

(CGCAAT^{Py}**U**TAACGC)-3′/3′-d(GCGTTANATTGCG)-5′, N = C, G or T), and the single-stranded ODN probe showed a only weak emission (U = 0.136, 0.070, 0.045, and 0.077, respectively).

Saito et al. reported pyrene- and acridone-labeled 2′-deoxyadenosine derivatives ^{8Py}**A** and ^{Ac}**A** as BDF purine nucleoside [40, 41]. After synthesizing ^{8Py}**A**- and ^{Ac}**A**-containing ODN probes, their fluorescence properties were examined in the presence of complementary ODNs differing by a single base opposite to the BDF base. As shown in Fig. 2.8a, mismatched duplexes (ODN (^{8Py}**A** or ^{Ac}**A**)/3′-d(GCGTTANATTGCG)-5′, N = C, G, or A) and single-stranded ODN (^{8Py}**A** or ^{Ac}**A**) showed a weak emission, whereas matched duplex (ODN (^{8Py}**A** or ^{Ac}**A**)/3′-d(GCGTTA**T**ATTGCG)-5′) showed significantly enhanced fluorescence.

Since ^{8Py}**A**- and ^{Ac}**A**-containing ODN probes show a clear difference in fluorescence intensity depending on the base type opposite to them in the target strand, SNP detection of the T/C SNP sequence of the BRCA1 gene was examined by using ^{8Py}**A**-containing BDF probe. As shown in Fig. 2.8b, a strong emission was observed with ODN$_{BRCA1}$(^{8Py}**A**)/ODN$_{BRCA1}$(T) duplex. In contrast, mismatched duplex (ODN$_{BRCA1}$(^{8Py}**A**)/ODN$_{BRCA1}$(C)) and single-stranded ODN$_{BRCA1}$(^{8Py}**A**) showed a weak emission. The fluorescence quantum yield of matched duplex ($\Phi_F = 0.280$) was at least 2.3 times larger than that observed for mismatched duplexes. Therefore, BDF probes containing ^{8Py}**A** and ^{Ac}**A** are used for the identification of thymine base in a target DNA by measuring a change in fluorescence intensity.

2.4.2 *Quencher-Free Molecular Beacons Containing Aryl-Conjugated Fluorescent Purine Nucleosides*

In 2005, Kim et al. reported a new strategy for preparing modified quencher-free molecular beacons (MBs) based on fluorescence quenching by photoinduced electron transfer (Fig. 2.9a) [42]. Quencher-free MBs containing pyrene-labeled $\mathbf{A}^{\mathbf{PY}}$ (**25**) at the 5′ end of the hairpin stem were developed and applied for the detection of nucleotide alternation in the target DNA. Because of its base stacking ability and high quantum yield, pyrene was selected as the fluorophore. The MB systems employed by Kim et al. are controlled primarily by two key factors. First, the neighboring bases of $\mathbf{A}^{\mathbf{PY}}$ at the 5′ end are more important in the quenching process than those at the 3′ end, and the quenching efficiency of the neighboring bases at the 5′ end follows the order C > G > T > A, regardless of the presence of matched or mismatched neighboring base pairs. The fluorescence of pyrene is strongly

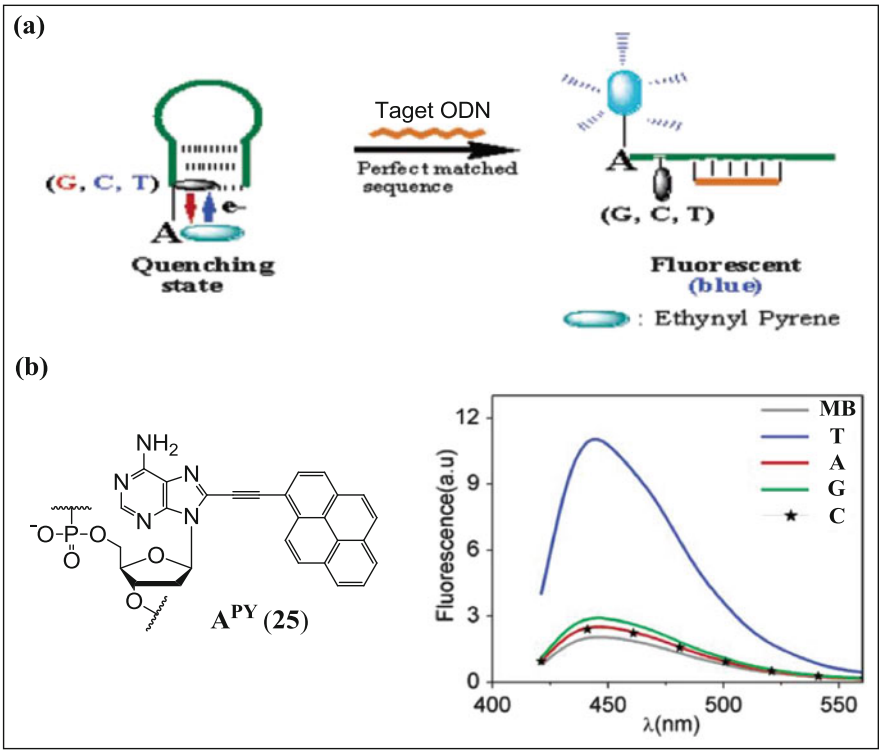

Fig. 2.9 (**a**) Schematic illustration of modified quencher-free molecular beacons (MBs) based on fluorescence quenching by photoinduced electron transfer. (**b**) Structure of 8-(1-pyrenylethynyl)-2′-deoxyadenosine $\mathbf{A}^{\mathbf{PY}}$ (**25**) and the fluorescence spectra of $\mathbf{A}^{\mathbf{PY}}$-containing MB hybridized with the perfectly matched and single-base mismatched target sequences and that of MB only (reprinted with permission from Seo et al., Org Lett (2005) 22:4931–4933. Copyright 2005 American Chemical Society)

quenched through non-covalent intermolecular stacking interactions with terminal G, C, and T but not with A in the closed hairpin form. The other key factor is the formation of stable $\mathbf{A^{PY}}$/neighboring base stacking. The discrimination factor (DF), which is defined as the ratio of the fluorescence intensities of the open and closed forms, is sensitive to the type of the neighboring base and the thermodynamic stability of the end stacking interaction in the closed form. They demonstrated that matched G-C neighboring base pairs at the 5′ end of the stem are favorable for this MB system. MBs containing $\mathbf{A^{PY}}$ at the 5′ end clearly discriminated the target sequences. As shown in Fig. 2.9, $\mathbf{A^{PY}}$-containing MB (5′-d($\mathbf{A^{PY}}$YCGAGAAGTTAGAACCTATGCTCGZ)-3′, Y = G, Z = C) showed weak fluorescence in the closed form. When the MB was hybridized with its perfectly matched target DNA (3′-d(TTCAATCTNGGATAC)-5′, N = T), a strong fluorescence emission was observed, such as that in the open form (DF = 7.1), indicating that the MB containing $\mathbf{A^{PY}}$ at the 5′ end serves as useful quencher-free MBs. Their $\mathbf{A^{PY}}$-containing MB systems are able to discriminate matched and single-base mismatched sequences (3′-d(TTCAATCNTGGATAC)-5′, N = C, A, and G) and are used for SNP detection (Fig. 2.9b).

2.4.3 *Purine Nucleoside Analogs by Click Chemistry*

The catalytic Huisgen cycloaddition of azides and alkynes is an efficient reaction that facilitates the preparation of diverse molecules under mild physiological conditions with an extremely high reaction ratio and efficiency. Using this Click reaction, Seela et al. have synthesized 7-deazapurine and 8-aza-7-deazapurine nucleosides related to 2′-deoxyadenosine and 2′-deoxyguanosine bearing 7-octadiynyl or 7-tripropargylamine side chains and the corresponding oligonucleotides [43–48]. As shown in Fig. 2.10, the ligation of fluorogenic dyes such as 9-azidomethyl anthracene, 3-azido-7-hydroxycoumarine, or 1-azidomethyl pyrene via a click reaction resulted in the formation of various fluorescent nucleoside derivatives. Among these, 8-aza-7-deazapurine-pyrene conjugates exhibited favorable photophysical properties [43]. Although abasic 1-octyne-pyrene conjugate exhibits strong fluorescence emission ($\Phi_F = 0.034$), 7-deazapurine-pyrene click conjugated with octadiynyl linker ($\mathbf{oct^7c^7A_d}$ and $\mathbf{oct^7c^7G_d}$, **26** and **27**, respectively) as a free nucleoside exhibits weaker fluorescence relative to that of 8-aza-7-deazapurine derivatives ($\mathbf{oct^7z^8c^7A_d}$ and $\mathbf{oct^7z^8c^7G_d}$, **28** and **29**, respectively) owing to the intramolecular charge transfer (ICT) quenching between the nucleobase and pyrene residue (Fig. 2.11). The fluorescence intensity of octadiynyl conjugates in methanol increases in the order, $\mathbf{oct^7c^7G_d}$ ($\Phi_F = 0.004$) < $\mathbf{oct^7c^7A_d} < \mathbf{oct^7z^8c^7A_d} < \mathbf{oct^7z^8c^7G_d}$ ($\Phi_F = 0.037$). Conversely, all the tripropargylamine double-click conjugates containing two proximal pyrenes ($\mathbf{trpa^7c^7A_d}$, $\mathbf{trpa^7c^7G_d}$, $\mathbf{trpa^7z^8c^7A_d}$, and $\mathbf{trpa^7z^8c^7G_d}$, **30**-**33**) exhibit an intense excimer emission at approximately 465 nm together with a vibronic monomer emission at 377 and 395 nm. Particularly, $\mathbf{trpa^7z^8c^7G_d}$ (excimer fluorescence, $\Phi_F = 0.059$)

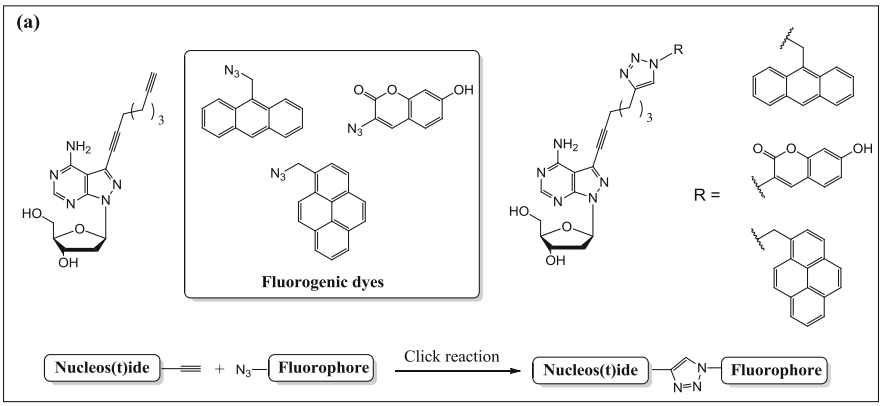

Fig. 2.10 The concept of copper(I)-catalyzed azide–alkyne cycloaddition

showed the highest excimer emission, whereas **trpa^{7}c^{7}G$_d$** (excimer fluorescence, $\Phi_F = 0.020$) showed the lowest.

Considering their application in ODN probes, the photophysical properties and thermal stability of 7-deazapurine- and 8-aza-7-deazapurine-containing oligonucleotides were investigated. Single- and double-stranded oligonucleotides containing 8-aza-7-deazapurine derivatives (**oct^{7}z^{8}c^{7}A$_d$**, **oct^{7}z^{8}c^{7}G$_d$**, **trpa^{7}z^{8}c^{7}A$_d$**, and **trpa^{7}z^{8}c^{7}G$_d$**) exhibited a more intense pyrene emission compared with that of 7-deazapurine derivatives (**oct^{7}c^{7}A$_d$**, **oct^{7}c^{7}G$_d$**, **trpa^{7}c^{7}A$_d$**, and **trpa^{7}c^{7}G$_d$**) (Fig. 2.12a, b). The low oxidation potential of 7-deazapurines, particularly 7-deazaguanine, causes strong fluorescence quenching in oligonucleotides as well. Therefore, 8-aza-7-deaza purine nucleosides are ideal purine surrogates for natural nucleobases, since pyrene is not quenched by such 8-aza-7-deazapurine derivatives because of their higher oxidation potential relative to that of 7-deazapurines. T_m experiments also revealed that replacing a single nucleoside with a pyrene conjugate substantially stabilizes the corresponding duplexes: 6–12 °C for the duplexes with a modified adenine base and 2–6 °C for those with a modified guanine base. When considering the design of fluorescent oligonucleotide probes, a modification at the C7-position of 7-deazapurine derivatives is attractive because the substituent at this position is accommodated in the major groove of the DNA and does not destabilize duplex structure.

2.4.4 Pyrene-Tethered 7-Deazaadenosine (^{Py}A) and Guanosine (^{Py}G)

We have developed fluorescent purine nucleosides **^{Py}A** (**34**) and **^{Py}G** (**35**) that identify the opposite base on a target ODN by fluorescence quenching mechanism [49, 50]. Fluorescent oligonucleotide probes containing **^{Py}A** exhibit strong

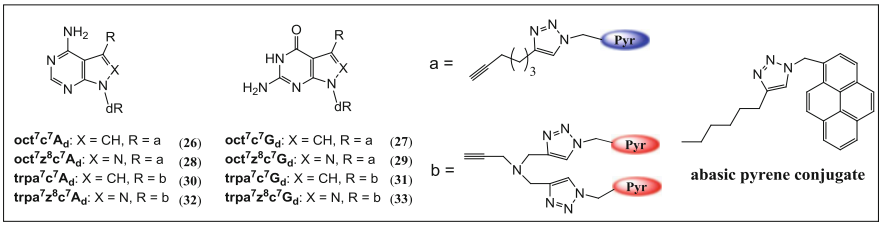

Fig. 2.11 Structures of pyrene "Click" conjugates of 7-deazapurine and 8-aza-7-deazapurine nucleosides and abasic pyrene compound (dR = 2′-deoxyribose)

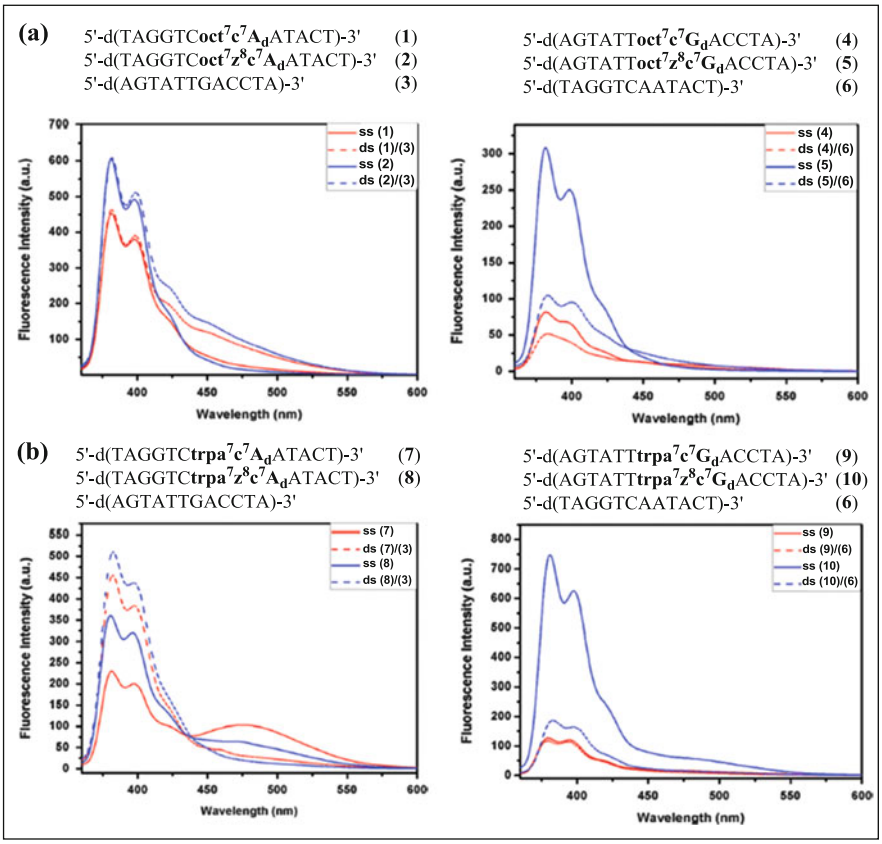

Fig. 2.12 (**a**) Fluorescence spectra of 7-deazapurine and 8-aza-7-deazapurine oligonucleotide "mono-Click" conjugates. (**b**) Fluorescence spectra of 7-deazapurine and 8-aza-7-deazapurine oligonucleotide "double-click" conjugates (reprinted with permission from Ingale et al., J Org Chem (2012) 77:188–199. Copyright 2011 American Chemical Society)

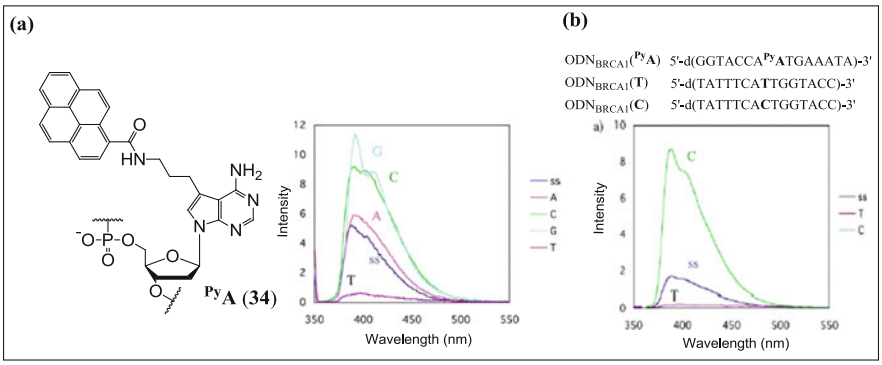

Fig. 2.13 (**a**) Structure of ^{Py}**A** (**34**) and the fluorescence spectra of ^{Py}**A**-containing ODN probe hybridized with ODN possessing A, G, C, or T base opposite to the ^{Py}**A** base; "ss" denotes a single-stranded ODN (^{Py}**A**). (**b**) Fluorescence spectra of **ODN$_{BRCA1}$**(^{Py}**A**) hybridized with **ODN$_{BRCA1}$**(**T**) or **ODN$_{BRCA1}$**(**C**) and that of single-stranded **ODN$_{BRCA1}$**(^{Py}**A**)

fluorescence quenching only when the base opposite to ^{Py}**A** in the complementary strand is a perfectly matched thymine [50]. As shown in Fig. 2.13a, fluorescence intensities of the single-stranded probe ODN 5′-d(CGCAAT^{Py}**A**TAACGC)-3′ and the duplexes with one-base mismatched complementary ODNs (5′-d(GCGTTANATTGCG)-3′, N = A, G, or C) were relatively strong ($\Phi_F = 0.054$–0.098). In contrast, the fluorescence of the perfectly matched duplex 5′-d(CGCAAT^{Py}**A**TAACGC)-3′/5′-d(GCGTTACATTGCG)-3′ was almost completely quenched ($\Phi_F = 0.006$). The decreased fluorescence emission of perfectly matched duplex is caused by the intercalation of the pyrene chromophore into the duplex. Whereas, mismatched base pair containing ^{Py}**A** shows a strong fluorescence emission because the intercalation of the pyrene unit is less favorable as compared with the case of perfectly matched duplex. As for the practical application of ^{Py}**A**, SNP detection of T/C (wild type/mutant) present in the BRCA1 gene was performed using ^{Py}**A**-containing ODN probe. As shown in Fig. 2.13b, an efficient quenching was observed with perfectly matched ODN$_{BRCA1}$(^{Py}**A**)/ODN$_{BRCA1}$(T) duplex (wild type), whereas mismatched duplex (ODN$_{BRCA1}$(^{Py}**A**)/ODN$_{BRCA1}$(C)) emitted strongly. Further, the fluorescence quantum yield of the matched duplex (^{Py}**A**/T, $\Phi_F = 0.002$) was approximately 47 times less than that of the mismatched duplex (^{Py}**A**/C, $\Phi_F = 0.094$). Thus, ^{Py}**A**-containing ODN probe facilitates the identification of thymine on a target DNA by a drastic change of fluorescence intensities.

Similar fluorescence pattern was obtained with ODNs containing ^{Py}**G** (**35**), and the fluorescence property of ^{Py}**G** was applied for the design of self-quenched MBs with free 3′- and 5′-ends (Fig. 2.14a) [49]. As shown in Fig. 2.14b, MB1 showed extremely weak fluorescence in its closed form. When MB1 was hybridized with target ODN, strong fluorescence was appeared at 400 nm as it was in open form,

indicating that the MB containing ^{Py}**G** in the duplex of the stem serves as an efficient self-quenching MB with a high signal-to-noise (S/N) ratio.

To further improve the efficiency, detection wavelength, and ends-free MBs, the same strategy was applied to the design of an excimer emissive MB containing two pyrene fluorophores separated by two bases in the middle region of the stem (MB 2; Fig. 2.14c). As shown in Fig. 2.14d, MB 2 showed only a monomer emission in its closed form, whereas in the presence of target ODN, excimer fluorescence was appeared at 535 nm together with the monomer emission. The fluorescence intensity at 535 nm was measured using a fluorescence plate reader (Fig. 2.14e). Because of its large S/N ratio (53/1) and strong emission at 535 nm, as visualized in the fluorescence imaging system, MB 2 are usable as an excellent ends-free self-quenched MB. These observations can be explained by considering that in the closed form, two pyrene rings at the site opposite to the stem cannot sterically interact with each other, and the excimer formation is prohibited by the intercalation of the pyrene rings into the stem duplex. In contrast, in the open form, two

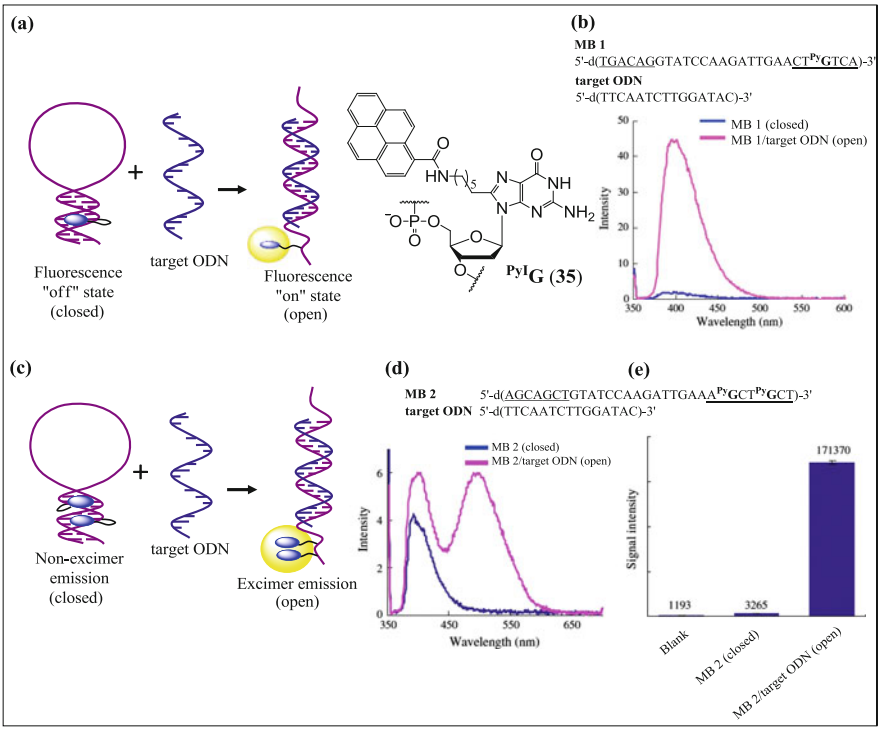

Fig. 2.14 (**a**) Concept for ends-free MB using pyrene-labeled 2′-deoxyguanosine ^{Py}**G** (**35**) and structure of ^{Py}**G**. (**b**) Fluorescence spectra of MB 1 and the duplex formed by hybridization with target ODN. (**c**) Schematic illustration of MB detectable by excimer emission. (**d**) Fluorescence spectra of MB 2 and the duplex formed by hybridization with target ODN. (**e**) Fluorescence signal intensity of MB 2 and the duplex formed by hybridization with target ODN as determined by fluorescence plate reader

pyrene rings located in a single-stranded region can easily interact with each other to result in an excimer formation.

2.5 Base-Modified Purine Nucleoside Triphosphate for Polymerase Synthesis

Another method of constructing functionalized ODN probes is the use of modified nucleoside triphosphates (dNTPs) via enzymatic reaction using polymerases. Hocek et al. recently developed a simple and efficient general methodology for the synthesis of base-modified dNTPs through Pd-catalyzed aqueous Suzuki–Miyaura or Sonogoshira cross-coupling reactions of halogenated dNTPs with arylboronic acids or acetylenes. They also combined this methodology with enzymatic DNA synthesis for the construction of functionalized ODNs [51–56]. Using this approach, the incorporation of various functional groups, such as amino acids, ferrocenes, amino and nitrophenyl groups, and labeling groups into DNA, are accomplished (Fig. 2.15a) [51–53, 56].

As an example of fluorescently labeled nucleoside, they demonstrated **dA^{R}** (**36a-d**) and **dU^{R}** (**37a-d**), and their triphosphates, **dA^{R}TP** and **dU^{R}TP** (R = BIF, BFU, BOX, and ABOX), bearing multimode fluorescent and ^{19}F NMR detectable BIF, BFU, BOX, and ABOX labeling groups by single-step aqueous cross-coupling reactions of the corresponding halogenated nucleobases with biarylboronates (Fig. 2.15b) [55]. These triphosphates, dN^{R}TPs, were good substrates for KOD XL polymerase and are incorporated into ODN probes by primer extension (PEX).

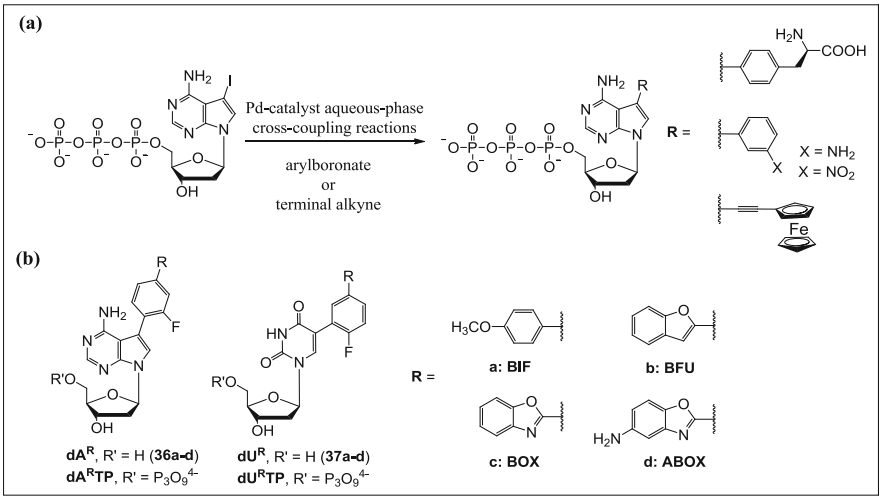

Fig. 2.15 (**a**) Synthesis of 7-substituted 7-deaza-2′-deoxyadenosine 5′-triphospates by cross-coupling reactions. (**b**) Structures of modified nucleosides and dNTPs

Table 2.3 Photophysical properties of the modified nucleosides in methanol

$\mathbf{dN^R}$	λ_{abs} (nm)	ε (L mol^{-1} cm^{-1})	λ_{em} (nm)	Φ_F
$\mathbf{dA^{BIF}}$	286	23,000	366, 386	0.73
$\mathbf{dA^{BFU}}$	323	36,000	409	0.66
$\mathbf{dA^{BOX}}$	321	26,000	475	0.10
$\mathbf{dA^{ABOX}}$	280, 327	22,400, 16,000	535	0.12
$\mathbf{dU^{BIF}}$	288	18,000		
$\mathbf{dU^{BFU}}$	318	38,000	402	0.11

Some of the base-modified nucleosides were sensitive to the environment and/or the secondary structures of DNA.

The photophysical data of the modified nucleosides were summarized in Table 2.3. Focusing on purine derivatives, the absorption and emission maxima of various modified 7-deaza-2′-deoxyadenosine derivatives ($\mathbf{dA^R}$, R = BIF, BFU, BOX, and ABOX) in methanol as free nucleosides ranging from 280 to 323 nm and from 370 to 540 nm, respectively. $\mathbf{dA^{BFU}}$ (**36b**) (λ_{em} = 409 nm) having electron-rich benzofurane and a larger π-electron system than $\mathbf{dA^{BIF}}$ (**36a**) (λ_{em} = 366 and 386 nm), emitting fluorescence at a longer wavelength. Introduction of an *N*-heteroatom ($\mathbf{dA^{BOX}}$ (**36c**) λ_{em} = 475 nm) induced a 66 nm red shift from $\mathbf{dA^{BIF}}$, and further addition of an electron-donating amino group ($\mathbf{dA^{ABOX}}$ (**36d**) λ_{em} = 535 nm) induced an additional 60 nm red shift from the parent $\mathbf{dA^{BOX}}$. Fluorescence spectra of $\mathbf{dA^{ABOX}}$ in different solvents are shown in Fig. 2.16a. Whereas the fluorescence intensities of $\mathbf{dA^{ABOX}}$ are strong in nonpolar solvents such as dioxane (λ_{em} = 480 nm, Φ_F = 0.62), very weak fluorescence was observed in polar solvents such as methanol (λ_{em} = 535 nm, Φ_F = 0.12) and water (λ_{em} = 565 nm, Φ_F = 0.009). Thus, $\mathbf{dA^{ABOX}}$ is highly solvatochromic nucleoside ($\Delta\lambda$ = 85 nm) and is used as a reporter molecule to identify structural changes such as DNA duplex formation and mismatches (Fig. 2.16b–e). These modified nucleosides were also enzymatically incorporated into ODN probes (5′-d(CATGGGCGGCATGGG$\mathbf{A^R}$GGG)-3′, R = BIF, BFU, BOX, and ABOX) by PEX using a primer ODN (5′-d(CATGGGCGGCATGGG)-3′), and their fluorescence spectra were measured in the absence and presence of complementary strand (3′-d(GTACCCGCCGTACCCNCCC)-5′, N = A, T, G, or C) after magnetose-paration. Interestingly, several 7-deaza-2′-deoxyadenosine derivatives, $\mathbf{dA^{BIF}}$ and $\mathbf{dA^{BOX}}$, exhibited base-discriminating ability in the sequence containing adjacent guanosine and were used for single-mismatch detection in electron-donating flanking sequences (Fig. 2.16b, c). They also succeeded in developing site-specific incorporation of one modification through single-nucleotide extension followed by PEX [54]; thus, their methodology for the polymerase construction of base-modified ODNs is able to apply modified ODN probes to diagnostic and chemical biology. Furthermore, $\mathbf{dA^{ABOX}}$ (**36d**) is very sensitive to acidic pH in oligonucleotides. As shown in Fig. 2.16f, $\mathbf{dA^{ABOX}}$ shows a continual blue shift of the emission maxima in an acidic environment. In particular, the emission maxima largely change in the range of pH = 7, 6, 5 (λ_{em} = 550, 535, and 499 nm, respectively).

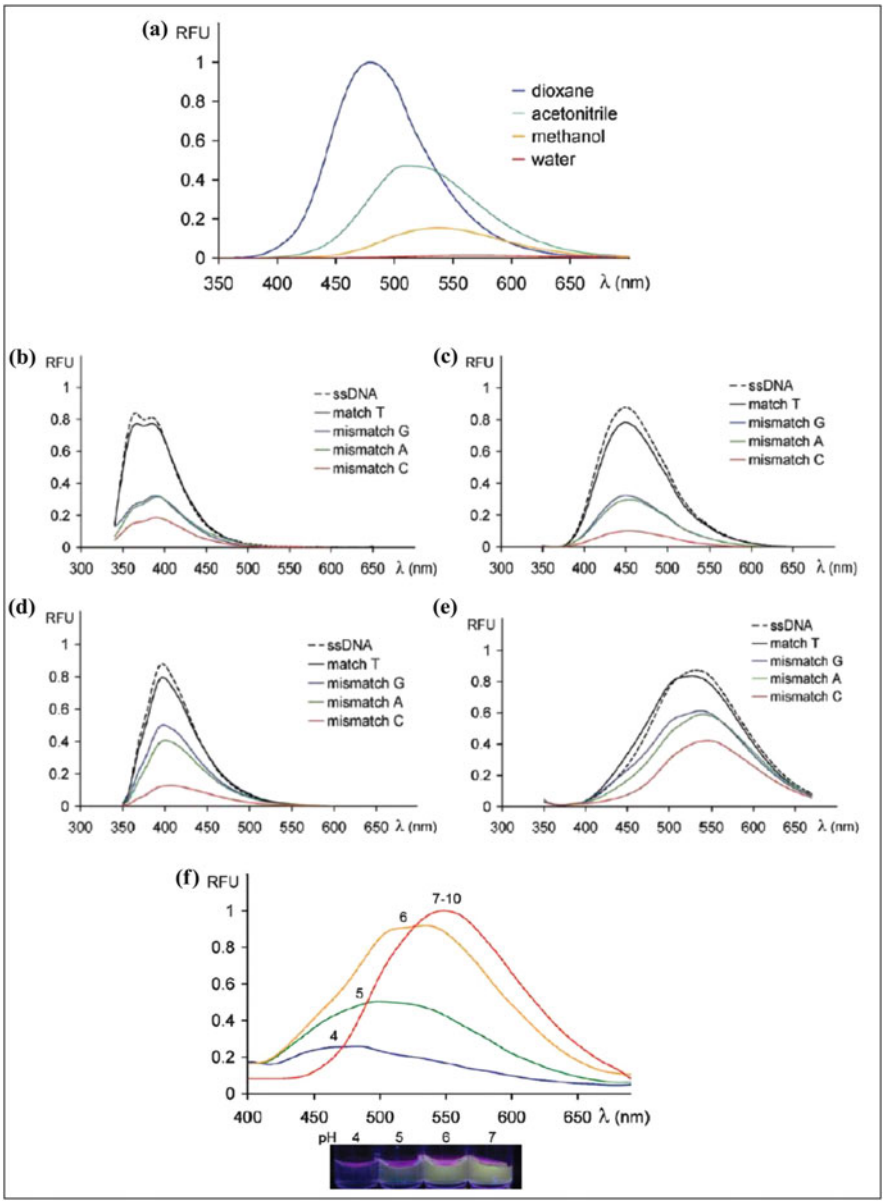

Fig. 2.16 (**a**) Fluorescence spectra of **dA**$^{\mathbf{Abox}}$ (**36d**) in different solvents. Fluorescence spectra of (**b**) **dA**$^{\mathbf{BIF}}$-, (**c**) **dA**$^{\mathbf{BOX}}$-, (**d**) **dA**$^{\mathbf{BFU}}$-, and (**e**) **dA**$^{\mathbf{ABOX}}$-labeled ODN hybridized with the complementary strand containing T, G, A, and C opposite to the modified nucleoside. (**f**) Fluorescence spectra of **dA**$^{\mathbf{ABOX}}$ (**36d**)-labeled duplex at different pHs (4–10) (reprinted with permission from Riedl et al., J Org Chem (2012) 77:1026–1044. Copyright 2011 American Chemical Society)

Thus, $\mathbf{dA}^{\mathbf{ABOX}}$ is a useful sensor nucleoside for monitoring pH in biological systems.

2.6 Push–Pull Type-Conjugated Purine Nucleosides Possessing Solvatochromicity

2.6.1 C8-Substituted Deoxypurine Nucleosides

When considering base modification, modification of purine bases is more appropriate, because purine bases have larger π-conjugated systems than pyrimidine bases, and their modification results in favorable photophysical properties such as red-shifted absorption and emission bands and higher quantum yields. In addition, the greater electron-donating ability of purine bases as compared with pyrimidines, which is the result of the lower oxidation potential of adenine and guanine, enables easy construction of the intramolecular donor–acceptor system. Generally, the insertion of an intramolecular donor–acceptor system within a molecule is a suitable approach for attaining remarkable solvatochromicity. The introduction of electron-donating substituents into purine bases provides environmentally sensitive fluorescent probes with remarkable high solvatochromicity that are useful for investigating structures and functions of nucleic acids. Fairlamb et al. demonstrated several push–pull type C8-phenylethynyl-substituted adenosines and guanosines; however, these nucleosides were not incorporated into oligonucleotides (Fig. 2.17a) [57]. We have developed various push–pull type C8-arylethynylated fluorescent 2′-deoxyadenosines and 2′-deoxyadenosines. Among the C8-substituted purine nucleosides synthesized (Fig. 2.17b) [58–63], acetyl-substituted 8-styryl-2′-deoxyguanosine derivative $^{\mathbf{AV}}\mathbf{G}$ exhibited unique photophysical features [58]. To construct an intramolecular donor–acceptor system, an electron-withdrawing aromatic ring and electron-donating guanosine are directly attached via double bonds in this molecule. As shown in Fig. 2.18a, electron-withdrawing acetyl-substituted $^{\mathbf{AV}}\mathbf{G}$ exhibited a remarkably high solvatochromicity ($\Delta\lambda = 81$ nm) suggesting that intramolecular donor–acceptor system within a molecule is indispensable for solvatofluorochromicity.

These environmentally sensitive fluorescent nucleosides are potentially useful for the structural studies of nucleic acids as well as for the detection of target DNA sequences. For instance, the 16-mer ODN probe containing $^{\mathbf{AV}}\mathbf{G}$, 5′-d(GTATCCT$^{\mathbf{AV}}$**G**AGATTGAA)-3′ was synthesized, and its photophysical properties were examined. The fluorescence spectra of $^{\mathbf{AV}}\mathbf{G}$-containing ODN probe were measured in the absence and presence of a complementary 15-mer target ODN, 3′-d(CATAGGTTCTAACTT)-5′, forming a bulge structure at $^{\mathbf{AV}}\mathbf{G}$. As shown in Fig. 2.18b, the fluorescence intensity of single-stranded ODN probe was very weak, and an emission maximum was observed at 550 nm. In contrast, the fluorescence intensity of the duplex containing the bulge structure was enhanced, and the

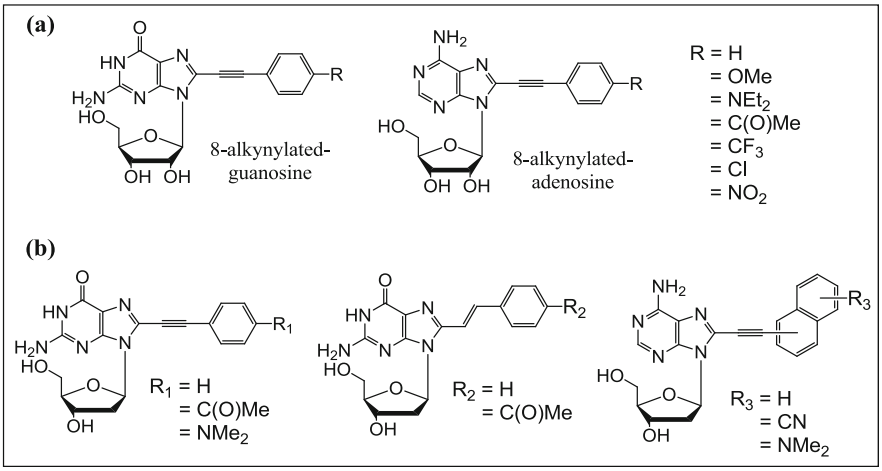

Fig. 2.17 (**a**) Structures of 8-alkynylated purine nucleosides. (**b**) Structures of various push–pull type fluorescent 2′-deoxypurine nucleosides

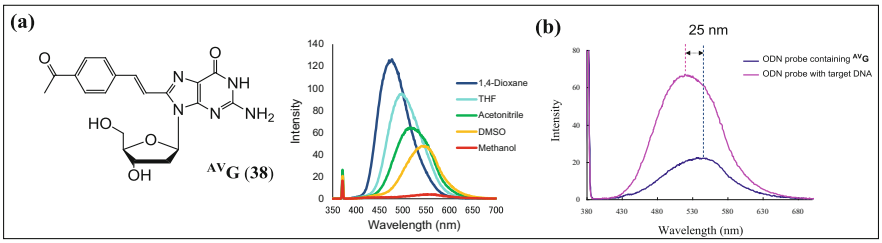

Fig. 2.18 (**a**) Structure of acetyl-substituted 8-styryl-2′-deoxyguanosine ^{AV}**G** (**38**) and the fluorescence spectra of ^{AV}**G** in various solvents. (**b**) Fluorescence spectra of ^{AV}**G**-containing ODN probe and the duplex formed by hybridization with target DNA

emission maximum was significantly blue-shifted to 526 nm ($\Delta\lambda = 24$ nm). The fluorescence color change was easily observable by naked eye under illumination with a 365 nm transilluminator. The difference in the fluorescence of the single- and double-stranded structures is due to the change in the local environment near ^{AV}**G**.

Various C8-arylated 2′-deoxyguanosine derivatives (Fig. 2.19a) were also synthesized by using Suzuki–Miyaura cross-coupling reactions for site-specific synthesis of modified ODNs [64]. The fluorescence spectra of **8-p-OHPh-G**- (**39**) and **8-(2-Bth)-G**- (**40**)-containing 11-mer ODNs were synthesized, and their fluorescent spectra were measured in the absence and presence of the complementary ODN (3′-d(GGTACGATGG)-5′). When **8-p-OHPh-G**-containing ODN probe was hybridized with its complementary ODN, the fluorescence maximum was blue-shifted by 18 nm and observed at 390 nm with the quenching in its fluorescence (Fig. 2.19b). When **8-(2-Bth)-G**-containing ODN probe was hybridized with its complementary ODN, the fluorescence of the duplex similarly blue-shifted by

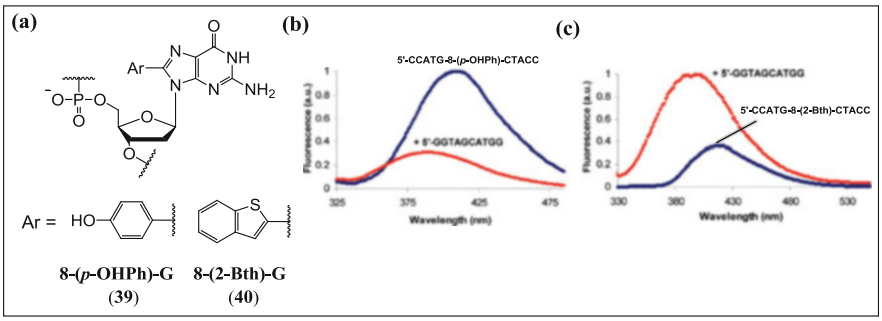

Fig. 2.19 (**a**) Structures of C8-arylated 2′-deoxyguanosines, **8-(*p*-OHPH)-G** (**39**) and **8-(2-Bth)-G** (**40**). Normalized fluorescence spectra of (**b**) **8-(*p*-OHPh)-G-**containing ODN probe (*blue*) plus complementary target strand (*red*) and (**c**) **8-(2-Bth)-G**-containing ODN probe (*blue*) plus complementary target strand (*red*) (reprinted with permission from Omumi et al., J Am Chem Soc (2011) 133:42–50. Copyright 2011 American Chemical Society)

20 nm and observed at 400 nm, but its intensity was enhanced threefold as compared with the fluorescence of single-stranded probe, indicating that C8-arylated 2′-deoxyguanosine derivatives are very sensitive to DNA microenvironments (Fig. 2.19c).

2.6.2 C7-Substituted 8-Aza-7-Deazapurine Nucleosides

C7-Substituted 8-aza-7-deaza-2′-deoxyguanosine derivative ^{na}**G** (**41**) is shown to be an excellent environmentally sensitive fluorescent (ESF) purine nucleoside that forms a stable Watson–Crick base pair and changes its fluorescence emission wavelength upon hybridization with target oligonucleotides [65]. When incorporated into DNA, this fluorescent nucleoside indicated structural changes such as single strands, perfect matches, mismatches, and deletions by significant changes in emission wavelength as well as its intensity.

Single-stranded ODN probes containing ESF nucleoside ^{na}**G** (**41**) were hybridized with complementary DNA possessing matched, mismatched, and abasic site, and their fluorescence spectra were measured (Fig. 2.20a). When the base opposite to ^{na}**G** in the complementary strand was perfectly matched cytosine in the duplex 5′-d(CGCAAT^{na}**G**TAACGC)-3′/5′-d(GCGTTACATTGCG)-3′, the fluorescence maximum was red-shifted by 29 nm and observed at 409 nm when compared to other mismatched duplexes (5′-d(CGCAAT^{na}**G**TAACGC)-3′/5′-d(GCGTTANATTGCG)-3′, N = G, A, T) and the single-stranded ODN. The fluorescence change caused by different opposite bases in the complementary strand is ascribable to the local environmental change near ESF base ^{na}**G**.

The fluorescence property of ^{na}**G** was applied to the design of MB that detects target DNA by the change in the fluorescence intensity and wavelength. ^{na}**G** was

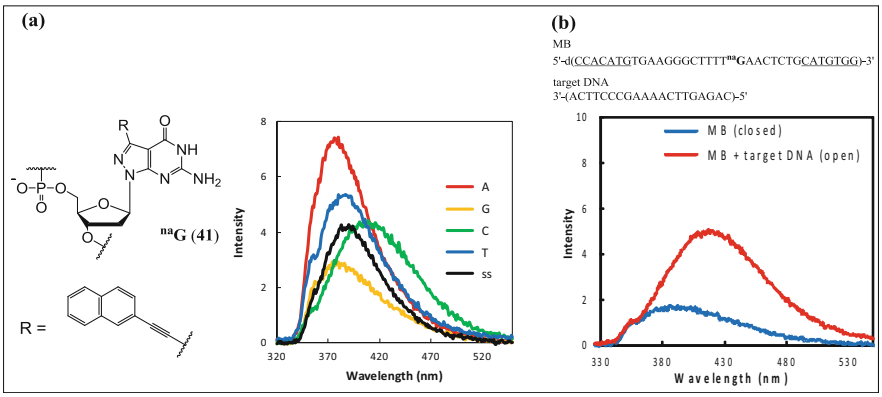

Fig. 2.20 (**a**) Structure of ^{na}**G** (**41**) and the fluorescence spectra of ^{na}**G**-containing ODN hybridized with ODN possessing A, G, C, or T base opposite to the ^{na}**G** base; "ss" denotes a single-stranded ODN. (**b**) Fluorescence spectra of hairpin MB and the duplex formed by hybridization with target DNA

incorporated into the loop region of an MB, and bcr/abl cancer gene sequence was detected by this MB. When the MB was hybridized with target DNA (ODNbcr/abl, cancer gene sequence), the fluorescence maximum was red-shifted by 30 nm as observed at 417 nm with a strong emission intensity, as in the case for open form, indicating that the MB containing ^{na}**G** in the loop region serves as a useful ends-free MB with a large red shift in the emission wavelength (Fig. 2.20b).

2.7 Dual Fluorescent Purine Nucleosides

2.7.1 C7-Substituted 8-Aza-7-Deazaadenosine Derivatives

We have developed conceptually new fluorescent purine nucleosides, ^{cna}**A** (**42**) and $^{cn\text{-}a}$**A** (**43**), that discriminate base types on a target ODN opposite to the fluorescent purine nucleosides by a dual fluorescence mechanism (Fig. 2.21a) [66–68]. The dual fluorescence resulting from ICT process in fluorophore containing internal electron donor–acceptor system are used as probes for studying microenvironmental parameters such as local polarity and structural change. On the basis of this design concept for charge transfer type molecules with internal donor and acceptor groups, we have devised novel environmentally sensitive dual fluorescent purine nucleosides ^{cna}**A** and $^{cn\text{-}a}$**A**. To increase their ICT character, an electron-withdrawing cyano group is introduced into the naphthalene chromophore of both nucleosides. These designed nucleosides showed remarkably high solvatochromicity and emitted environmentally sensitive dual fluorescence, which originates from the independent electronic transitions of coplanar and non-coplanar

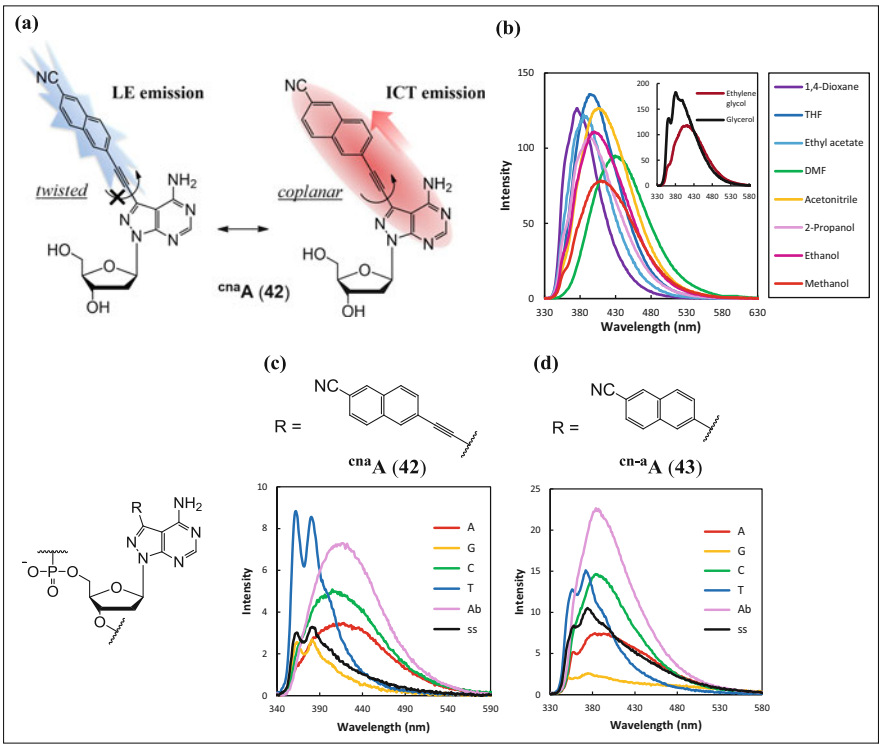

Fig. 2.21 (**a**) Structure of environmentally sensitive fluorescent dual fluorescent nucleoside ^{cna}**A** (**42**). (**b**) Fluorescence spectra of ^{cna}**A** in various solvents (*inset*: in ethylene glycol and glycerol). (**c**) Fluorescence spectra of ^{cna}**A**-containing ODN hybridized with ODN possessing A, G, C, T, or abasic site opposite to the ^{cna}**A** base; "ss" denotes a single-stranded ^{cna}**A**-containing ODN. (**d**) Fluorescence spectra of $^{cn\text{-}a}$**A**-containing ODN hybridized with ODN possessing A, G, C, T, or abasic site opposite to the $^{cn\text{-}a}$**A** base; "ss" denotes a single-stranded $^{cn\text{-}a}$**A**-containing ODN

conformers of the nucleobase and naphthalene moiety. When coplanar alignment of the nucleobase and naphthalene ring occurred, ^{cna}**A** and $^{cn\text{-}a}$**A** exhibited a broad ICT emission and can act as solvatochromic nucleosides. In contrast, when the naphthalene ring was located in a sterically restricted space or in viscous solvents and twisted, these chromophores exhibited a blue-shifted locally excited (LE) dual emission (Fig. 2.21b).

These distinct photophysical features of ^{cna}**A** and $^{cn\text{-}a}$**A** were applied to the sensing of local polarity and structure at specific site of DNA. The fluorescence spectra of ODN probes containing these modified bases in the presence and absence of complementary strands (5′-d(GCGTTANATTGCG)-3′, N = T, C, G, A, abasic site) were measured. The fluorescence emission of single-stranded ODN (5′-d(CGCAAT^{cna}**A**TAACGC)-3′) was relatively weak. When complementary strands were added, the fluorescence intensity of the duplex DNA was enhanced considerably. In particular, when added a complementary strand containing an abasic site, a

very strong broad fluorescence emission band appeared at red-shifted wavelength (417 nm). When the base of the complementary strand in duplex ODN opposite to ^{cna}**A** or $^{cn\text{-}a}$**A** was mismatched, strong broad emission bands were observed at red-shifted wavelengths. When the base was a perfectly matched thymine in the duplex 5′-d(CGCAAT^{cna}**A**TAACGC)-3′/5′-d(GCGTTATATTGCG)-3′, the fluorescence maximum was blue-shifted to two peaks at 362 and 381 nm, and an enhanced dual fluorescence emission with vibronic structures was observed (Fig. 2.21c). The microenvironmental alterations caused by changing the opposing base resulted in a considerable change in the fluorescence intensity and emission wavelength of ^{cna}**A**-containing ODN probe. A similar result was obtained with $^{cn\text{-}a}$**A**-containing ODN probes (Fig. 2.21d). These dual fluorescent nucleosides are used as a thymine selective DNA probe that discriminate the thymine base in target ODN sequence by a distinct change in emission wavelength.

2.7.2 C3-Substituted 3-Deazaadenosine Derivatives

C3-Naphthylethynylated 3-deaza-2′-deoxyadenosine ^{3nz}**A** (**44**) behaved as a solvatochromic ESF nucleoside that exhibits dual modes of fluorescence emissions arising from ICT and LE states depending on the molecular coplanarity [67]. This ESF nucleoside is unique for indicating microenvironmental change in the minor groove of DNA. To design a highly solvatochromic molecule possessing an ICT state in a coplanar configuration, 3-deazaadenine skeleton was selected. Sterically hindered 1-ethynylnaphthalene moiety was attached at the C3-position of 3-deazaadenine to enhance the fluorescence intensity and stabilize the twisted ground-state conformation. When a coplanar alignment of the nucleobase and the naphthalene ring is attained, ^{3nz}**A** shows an ICT character and exhibits a solvatochromic red-shifted fluorescence. In more stable twisted ground-state conformation, ^{3nz}**A** exhibits a blue-shifted dual emission from the naphthalene ring and 3-deazaadenine moiety. The geometrical restrictions to coplanarity between the 3-deazaadenine and naphthalene ring arising from the crowding effect in DNA minor groove are strongly correlated with these ICT and LE states.

The fluorescence spectra of the ODN probe containing ^{3nz}**A**, 5′-d(CGCAAT^{3nz}**A**TAACGC)-3′ were measured in the absence and presence of a complementary ODN, (5′-d(GCGTTANATTGCG)-3′, N = G, A, and T). The fluorescence emission of the single-stranded ODN was weak and appeared at 419 nm. After the complementary strands were added, the fluorescence intensity was enhanced. When the base opposite to ^{3nz}**A** in the complementary strand was a mismatched base, a stronger emission was observed in a blue-shifted region (363–403 nm). However, an enhanced fluorescence emission was observed when the opposite base was a perfectly matched thymine (5′-d(CGCAAT^{3nz}**A**TAACGC)-3′/5′-d(GCGTTATATTGCG)-3′), and the emission maximum was red-shifted by 54 nm from other mismatched bases (Fig. 2.22a).

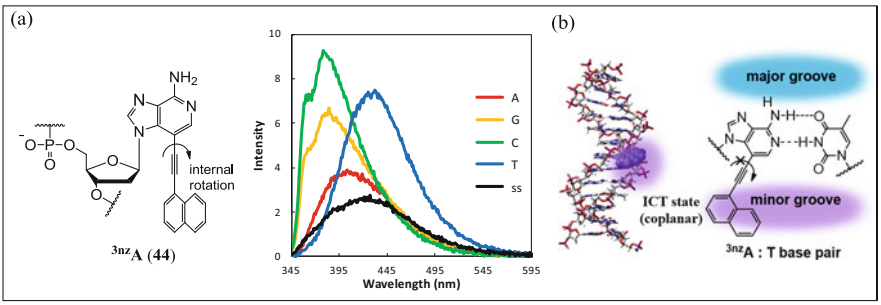

Fig. 2.22 (**a**) Structure of ESF nucleoside ^{3nz}**A** (**44**) and the fluorescence spectra of ^{3nz}**A**-containing ODN hybridized with ODN possessing A, G, C, or T base opposite to the ^{3nz}**A** base; "ss" denotes a single-stranded ODN. (**b**) An ODN probe containing ^{3nz}**A** exhibits a characteristic ICT fluorescence from coplanar structure only when the opposite base is perfectly matched thymine

When the opposing base was a perfectly matched thymine, 1-ethynylnaphthalene moiety extruded into the minor groove of the DNA duplex owing to the base-pair formation between ^{3nz}**A** and thymine (Fig. 2.22b). In this case, the rotation of the naphthalene ring around the linker axis was disturbed in the crowded narrow minor groove, and the conformation of 3-deazaadenine and the naphthalene ring becomes almost coplanar. Thus, a strong emission from the ICT state was observed at longer wavelength (432 nm). When the opposite base was mismatched, twisted ground state conformation of ^{3nz}**A** was maintained, and a strong LE emission from the naphthalene moiety was observed in a blue-shifted region.

References

1. Cohen BE, McAnaney TB, Park ES, Jan YN, Boxer SG, Jan LY (2002) Probing protein electrostatics with a synthetic fluorescent amino acid. Science 296:1700–1703
2. Lee HS, Guo J, Lemke EA, Dimla RD, Schultz PG (2009) Genetic incorporation of a small, environmentally sensitive, fluorescent probe into proteins in *Saccharomyces cerevisiae*. J Am Chem Soc 131:12921–12923
3. Ward DC, Reich E, Stryer L (1969) Fluorescence studies of nucleotides and polynucleotides: I. Formycin, 2-aminopurine riboside, 2,6-diaminopurine riboside, and their derivatives. J Biol Chem 244:1228–1237
4. Dai N, Kool ET (2011) Fluorescent DNA-based enzyme sensors. Chem Soc Rev 40:5756–5770
5. Ranasinghe RT, Brown T (2005) Fluorescence based strategies for genetic analysis. Chem Commun 5487–5502
6. Sinkeldam RW, Greco NJ, Tor Y (2010) Fluorescent analogs of biomolecular building blocks: design, properties, and applications. Chem Rev 110:2579–2619
7. Guest CR, Hochstrasser RA, Sowers LC, Millar DP (1991) Dynamics of mismatched base pairs in DNA. Biochemistry 30:3271–3279

8. Menger M, Tuschl T, Eckstein F, Porschke D (1996) Mg^{2+}-dependent conformational changes in the hammerhead ribozyme. Biochemistry 35:14710–14716
9. Kirk SR, Luedtke NW, Tor Y (2001) 2-Aminopurine as a real-time probe of enzymatic cleavage and inhibition of hammerhead ribozymes. Bioorg Med Chem 9:2295–2301
10. Holz B, Klimasauskas S, Serva S, Weinhold E (1998) 2-Aminopurine as a fluorescent probe for DNA base flipping by methyltransferases. Nucleic Acids Res 26:1076–1083
11. Lacourciere KA, Stivers JT, Marino JP (2000) Mechanism of neomycin and rev peptide binding to the Rev responsive element of HIV-1 as determined by fluorescence and NMR spectroscopy. Biochemistry 39:5630–5641
12. Raney KD, Sowers LC, Millar DP, Benkovic SJ (1994) A fluorescence-based assay for monitoring helicase activity. Proc Natl Acad Sci USA 91:6644–6648
13. Seela F, Becher G (2000) Synthesis, base pairing, and fluorescence properties of oligonucleotides containing 1*H*-pyrazolo[3,4-*d*]pyrimidin-6-amine (8-aza-7-deazapurin-2-amine) as an analogue of purin-2-amine. Helv Chim Acta 83:928–942
14. Gaied NB, Glasser N, Ramalanjaona N, Beltz H, Wolff P, Marquet R, Burger A, Mély Y (2005) 8-Vinyl-deoxyadenosine, an alternative fluorescent nucleoside analog to 2-′-deoxyribosyl-2-aminopurine with improved properties. Nucleic Acids Res 33:1031–1039
15. Dierckx A, Dinér P, El-Sagheer AH, Kumar JD, Brown T, Grøtli M, Wilhelmsson LM (2011) Characterization of photophysical and base-mimicking properties of a novel fluorescent adenine analogue in DNA. Nucleic Acids Res 39:4513–4524
16. Dyrager C, Börjesson K, Dinér P, Elf A, Albinsson B, Wilhelmsson LM, Grøtli M (2009) Synthesis and photophysical characterisation of fluorescent 8-(1*H*-1,2,3-triazol-4-yl)adenosine derivatives. Eur J Org Chem 2009:1515–1521
17. Liu W, Shin D, Tor Y, Cooperman BS (2013) Monitoring translation with modified mRNAs strategically labeled with isomorphic fluorescent guanosine mimetics. ACS Chem Biol 8:2017–2023
18. Samanta PK, Manna AK, Pati SK (2012) Thieno analogues of RNA nucleosides: a detail theoretical study. J Phys Chem B 116:7618–7626
19. Shin D, Sinkeldam RW, Tor Y (2011) Emissive RNA alphabet. J Am Chem Soc 133:14912–14915
20. Tor Y, Valle SD, Jaramillo D, Srivatsan SG, Rios A, Weizman H (2007) Designing new isomorphic fluorescent nucleobase analogues: the thieno[3,2-*d*]pyrimidine core. Tetrahedron 63:3608–3614
21. McCoy LS, Shin D, Tor Y (2014) Isomorphic emissive GTP surrogate facilitates initiation and elongation of in vitro transcription reactions. J Am Chem Soc 136:15176–15184
22. Park S, Omoto H, Zheng L, Sugiyama H (2014) Highly emissive deoxyguanosine analogue capable of direct visualization of B-Z transition. Chem Commun 50:1573–1575
23. Secrist JA III, Barrio JR, Leonard NJ, Weber G (1972) Fluorescent modification of adenosine-containing coenzymes. Biological activities and spectroscopic properties. Biochemistry 11:3499–3506
24. Secrist JA III, Barrio JR, Leonard NJ (1972) A fluorescent modification of adenosine triphosphate with activity in enzyme systems: 1, N6-ethenoadenosine triphosphate. Science 175:646–647
25. Lin W, Li H, Ming X, Seela F (2005) 1, N6-Etheno-7-deaza-2,8-diazaadenosine: synthesis, properties and conversion to 7-deaza-2,8-diazaadenosine. Org Biol Chem 3:1714–1718
26. Seela F, Schweinberger E, Xu K, Sirivolu VR, Rosemeyer H, Becker EM (2007) 1, N6-Etheno-2′-deoxytubercidin and pyrrolo-C: synthesis, base pairing, and fluorescence properties of 7-deazapurine nucleosides and oligonucleotides. Tetrahedron 63:3471–3482
27. Sugiyama T, Schweinberger E, Kazimierczuk RN, Rosemeyer H, Seela F (2000) 2-Aza-2-′-deoxyadenosine: synthesis, base-pairing selectivity, and stacking properties of oligonucleotides. Chem Eur J 6:369–378
28. Yip KF, Tsou KC (1973) Synthesis of fluorescent adenosine derivatives. Tetrahedron Lett 14:3087–3090

29. Yip KF, Tsou KC (1975) Synthesis of 2-substituted 1, N6-ethenoadenosines. J Org Chem 40:1066–1070
30. Srivastava SC, Raza SK, Misra R (1994) 1, N6-Etheno deoxy and ribo adenosine and 3, -N4-etheno deoxy and ribo cytidine phosphoramidites. Strongly fluorescent structures for selective introduction in defined sequence DNA and RNA molecules. Nucleic Acids Res 22:1296–1304
31. Calabretta A, Leumann CJ (2013) Base pairing and miscoding properties of 1, N6-ethenoadenine- and 3, N4-ethenocytosine-containing RNA oligonucleotides. Biochemistry 52:1990–1997
32. Leonard NJ, Sprecker MA, Morrice AG (1976) Defined dimensional changes in enzyme substrates and cofactors. Synthesis of lin-benzoadenosine and enzymatic evaluation of derivatives of the benzopurines. J Am Chem Soc 98:3987–3994
33. Leonard NJ, Scopes DIC, Van Der Lijn P, Barrio JR (1978) Dimensional probes of the enzyme binding sites of adenine nucleotides. Biological effects of widening the adenine ring by 2.4 Å. Biochemistry 17:3677–3685
34. Scopes DIC, Barrio JR, Leonard NJ (1977) Defined dimensional changes in enzyme cofactors: fluorescent "Stretched-out" analogs of adenine nucleotides. Science 195:296–298
35. Gao J, Liu H, Kool ET (2004) Expanded-size bases in naturally sized DNA: evaluation of steric effects in Watson-Crick pairing. J Am Chem Soc 126:11826–11831
36. Liu H, Gao J, Maynard L, Saito YD, Kool ET (2004) Toward a new genetic system with expanded dimensions: size-expanded analogues of deoxyadenosine and thymidine. J Am Chem Soc 126:1102–1109
37. Okamoto A, Tanaka K, Fukuta T, Saito I (2003) Design of base-discriminating fluorescent nucleoside and its application to T/C SNP typing. J Am Chem Soc 125:9296–9297
38. Okamoto A, Kamei T, Saito I (2006) DNA hole transport on an electrode: application to effective photoelectrochemical SNP typing. J Am Chem Soc 128:658–662
39. Okamoto A, Kanatani K, Saito I (2004) Pyrene-labeled base-discriminating fluorescent DNA probes for homogeneous SNP typing. J Am Chem Soc 126:4820–4827
40. Saito Y, Hanawa K, Motegi K, Omoto K, Okamoto A, Satio I (2005) Synthesis and properties of purine-type base-discriminating fluorescent (BDF) nucleosides: distinction of thymine by fluorescence-labeled deoxyadenosine derivatives. Tetrahedron Lett 46:7605–7608
41. Saito Y, Hanawa K, Kawasaki N, Bag SS, Saito I (2006) Acridone-labeled base-discriminating fluorescence (BDF) nucleoside: synthesis and their photophysical properties. Chem Lett 35:1182–1183
42. Seo YJ, Ryu JH, Kim BH (2005) Quencher-free, end-stacking oligonucleotides for probing single-base mismatches in DNA. Org Lett 7:4931–4933
43. Ingale SA, Pujari SS, Sirivolu VR, Ding P, Xiong H, Mei H, Seela F (2012) 7-Deazapurine and 8-aza-7-deazapurine nucleoside and oligonucleotide pyrene "click" conjugates: synthesis, nucleobase controlled fluorescence quenching, and duplex stability. J Org Chem 77:186–199
44. Ingale SA, Seela F (2014) Nucleoside and oligonucleotide pyrene conjugates with 1,2,3-triazolyl or ethynyl linkers: synthesis, duplex stability, and fluorescence changes generated by the DNA-dye connector. Tetrahedron 70:380–391
45. Mei H, Ingale SA, Seela F (2013) Pyrene and bis-pyrene DNA nucleobase conjugates: excimer and monomer fluorescence of linear and dendronized cytosine and 7-deazaguanine click adducts. Tetrahedron 69:4731–4742
46. Seela F, Xiong H, Leonard P, Budow S (2009) 8-Aza-7-deazaguanine nucleosides and oligonucleotides with octadiynyl side chains: synthesis, functionalization by the azide-alkyne "click" reaction and nucleobase specific fluorescence quenching of coumarin dye conjugates. Org Biomol Chem 7:1374–1387
47. Seela F, Pujari SS (2010) Azide-alkyne "click" conjugation of 8-aza-7-deazaadenine-DNA: synthesis, duplex stability, and fluorogenic dye labeling. Bioconjug Chem 21:1629–1641

48. Seela F, Ingale SA (2010) "Double click" reaction on 7-deazaguanine DNA: synthesis and excimer fluorescence of nucleosides and nucleotides with branched side chains decorated with proximal pyrenes. J Org Chem 75:284–295
49. Matsumoto K, Shinohara Y, Bag SS, Takeuchi Y, Morii T, Saito Y, Saito I (2009) Pyrene-labeled deoxyguanosine as a fluorescence sensor to discriminate single and double stranded DNA structures: design of ends free molecular beacons. Bioorg Med Chem Lett 19:6392–6395
50. Saito Y, Miyauchi Y, Okamoto A, Saito I (2004) Base-discriminating fluorescent (BDF) nucleoside: distinction of thymine by fluorescence quenching. Chem Commun 1704–1705
51. Brázdilová P, Vrábel M, Pohl R, Pivoňková H, Havran L, Hocek M, Fojta M (2007) Ferrocenylethynyl derivatives of nucleoside triphosphates: synthesis, incorporation, electrochemistry, and bioanalytical applications. Chem Eur J 13:9527–9533
52. Cahová H, Havran L, Brázdilová P, Pivoňková H, Pohl R, Fojta M (2008) Aminophenyl- and nitrophenyl-labeled nucleoside triphosphates: synthesis, enzymatic incorporation, and electrochemical detection. Angew Chem Int Ed 47:2059–2062
53. Čapek P, Cahová H, Pohl R, Hocek M, Gloeckner C, Marx A (2007) An efficient method for the construction of functionalized DNA bearing amino acids groups through cross-coupling reactions of nucleoside triphosphates followed by primer extension or PCR. Chem Eur J 13:6196–6203
54. Ménová P, Cahová H, Plucnara M, Havran L, Fojta M, Hocek M (2013) Polymerase synthesis of oligonucleotides containing a single chemically modified nucleobase for site-specific redox labelling. Chem Commun 49:4652–4654
55. Riedl J, Pohl R, Rulišek L, Hocek M (2012) Synthesis and photophysical properties of biaryl-substituted nucelos(t)ides. Polymerase synthesis of DNA probes bearing solvatochromic and pH-sensitive dual fluorescent and ^{19}F NMR labels. J Org Chem 77:1026–1044
56. Vrábel M, Horáková P, Pivoňková H, Kalachova L, Černocká H, Cahová H, Pohl R, Šebest P, Havran L, Hocek M, Fojta M (2009) Base-modified DNA labeled by $[Ru(bpy)_3]^{2+}$ and $[Os(bpy)_3]^{2+}$ complexes: construction by polymerase incorporation of modified nucleoside triphosphates, electrochemical and luminescent properties, and applications. Chem Eur J 15:1144–1154
57. Firth AG, Fairlamb IJS, Darley K, Baumann CG (2006) Sonogashira alkynylation of unprotected 8-brominated adenosines and guanosines: fluorescence properties of compact conjugated acetylenes containing a purine ring. Tetrahedron Lett 47:3529–3533
58. Matsumoto K, Takahashi N, Suzuki A, Morii T, Saito Y, Saito I (2011) Design and synthesis of highly solvatochromic fluorescent 2′-deoxyguanosine and 2′-deoxyadenosine analogs. Bioorg Med Chem Lett 21:1275–1278
59. Saito Y, Suzuki A, Imai K, Nemoto N, Saito I (2010) Synthesis of novel push-pull-type solvatochromic 2′-deoxyguanosine derivatives with longer wavelength emission. Tetrahedron Lett 51:2606–2609
60. Saito Y, Koda M, Shinohara Y, Saito I (2011) Synthesis and photophysical properties of 8-arylbutadienyl 2′-deoxyguanosines. Tetrahedron Lett 52:491–494
61. Saito Y, Kugenuma K, Tanaka M, Suzuki A, Saito I (2012) Fluorometric detection of adenine in target DNA by exciplex formation with fluorescent 8-arylethynylated deoxyguanosine. Bioorg Med Chem Lett 22:3723–3726
62. Shinohara Y, Matsumoto K, Kugenuma K, Morii T, Saito Y, Saito I (2010) Design of environmentally sensitive fluorescent 2′-deoxyguanosine containing arylethynyl moieties: distinction of thymine base by base-discriminating fluorescent (BDF) probe. Bioorg Med Chem Lett 20:2817–2820
63. Suzuki A, Takahashi N, Okada Y, Saito I, Nemoto N, Saito Y (2013) Naphthalene-based environmentally sensitive fluorescent substituted 2′-deoxyadenosines: application to DNA detection. Bioorg Med Chem Lett 23:886–892
64. Omumi A, Beach DG, Baker M, Gabryelski W, Manderville RA (2011) Postsynthetic guanine arylation of DNA by Suzuki-Miyaura cross-coupling. J Am Chem Soc 133:42–50

65. Saito Y, Suzuki A, Okada Y, Yamasaka Y, Nemoto N, Saito I (2013) An environmentally sensitive fluorescent purine nucleoside that changes emission wavelength upon hybridization. Chem Commun 49:5684–5686
66. Suzuki A, Nemoto N, Saito I, Saito Y (2014) Design of an environmentally sensitive fluorescent 8-aza-7-deaza-2′-deozyadenosine derivative with dual fluorescence for the specific detection of thymine. Org Biomol Chem 12:660–669
67. Suzuki A, Yanaba T, Saito I, Saito Y (2014) Molecular design of an environmentally sensitive fluorescent nucleoside, 3-deaza-2′-deoxyadenosine derivative: distinguishing thymine by probing the DNA minor groove. ChemBioChem 15:1638–1644
68. Saito Y, Suzuki A, Yamauchi T, Saito I (2015) Design and synthesis of 7-naphthyl-8-aza-7-deaza-2′-deoxyadenosines as environmentally sensitive fluorescent nucleosides. Tetrahedron Lett 56:3034–3038

Chapter 3
Thiazole Orange-Tethered Nucleic Acids and ECHO Probes for Fluorometric Detection of Nucleic Acids

Akimitsu Okamoto

Abstract Thiazole orange (TO) is a well-known fluorescent dye that emits strong fluorescence when it binds to nucleic acid. A number of TO-tethered nucleic acids have been developed for the fluorometric detection of nucleic acids. This chapter summarizes several TO-tethered nucleic acids and shows how the diverse range of such fluorescence-modified nucleic acids enriches the methodology available for DNA sequence typing and RNA monitoring. In addition, the chapter highlights recent advances in exciton-controlled hybridization-sensitive fluorescent oligonucleotide (ECHO) probes, which have a fluorescence-labeled nucleotide in which two TO subunits are linked covalently. ECHO probes have enabled fluorometric distinction between the probe distribution and target RNA localization in living cells. Further modifications of ECHO probes have made possible a variety of practical applications for intracellular RNA imaging, with the most recent derivatives possessing diverse abilities such as nuclease resistance, photoactivation, self-avoidance, binding to higher-ordered structures, and multicoloring.

3.1 Introduction

Nucleic acids are among most important biomolecules involved in the control of cell functions, and the observation of the behavior of nucleic acids in a cell is the best way of monitoring and understanding ongoing cell function expression. The use of artificially prepared nucleic acid fragments provides a straightforward method for the analysis and visualization of single-stranded nucleic acids, because hybridization of the synthetic nucleic acid fragments complementary to the target nucleic acid readily provides highly sequence-specific affinity. The flexible design of nucleic acid fragments can offer nucleic acid analysis when the sequence

A. Okamoto (✉)
Research Center for Advanced Science and Technology, The University of Tokyo, 4-6-1 Komaba, Meguro-ku, Tokyo 153-8904, Japan
e-mail: okamoto@chembio.t.u-tokyo.ac.jp

K. Nakatani, Y. Tor (eds.), *Modified Nucleic Acids*, Nucleic Acids and Molecular Biology 31, DOI 10.1007/978-3-319-27111-8_3

information is available. Progress in the solid-phase preparation of nucleic acids has contributed to the design of artificial nucleic acids containing a variety of functional nucleotides, including nucleotides labeled with a fluorescent dye at the desired position in the sequence.

The use of fluorescent signals is probably the most powerful way of sensing target nucleic acids. Organic dyes such as cyanines and fluoresceins, and inorganic dyes such as quantum dots, have so far been attached to the end or interior of nucleic acid fragments to monitor the behavior of the target nucleic acid in a cell. Conventional fluorescent dyes undergo fluorescence when irradiated with light containing suitable excitatory wavelengths. However, information obtained from the measurement of fluorescence intensity must be treated with caution, because the intensity simply reflects the concentration of dye molecules and does not necessarily represent the abundance of the target nucleic acid. Background fluorescent noise from dye-labeled nucleic acid fragments that are not bound to the target remains, and excess fluorescence can lead to a false-positive signal. Thus, dye-labeled nucleic acid fragments that do not participate in the detection of the target nucleic acids must be removed from the sample prior to measurement, which usually requires several difficult rinsing procedures. Background fluorescence emission is a critical issue in in vivo assays such as live cell imaging, in which it is difficult to wash out the excess fluorescent signal in a cell. Turning on the fluorescent signal only at the target binding site is the best way to diminish the background noise. Thus, the design of a latent fluorescent dye in which the fluorescence is turned off when the dye does not bind to its target site is decisive for the development of simplified nucleic acid imaging, resulting in a reliable real-time fluorescence imaging protocol.

How should fluorescence intensity be controlled in the next nucleic acid imaging? Several photochemical mechanisms, such as excimer fluorescence [1–6], photoinduced charge transfer [7–15], photoinduced electron transfer [16–22], and energy transfer [23–27], have been used in many fluorescence-switching systems. Förster resonance energy transfer (FRET) is a good way of the fluorescence emission control in a sequence-specific fashion [28–33]. *Molecular beacons*, which are representative of hybridization-sensitive fluorescent nucleic acids, are now one of the best choices for fluoroscopic nucleic acid detection. The changes in fluorescence intensity caused by changes in the distance between a fluorescent dye and a quencher dye attached to the strand ends upon duplex formation with the target nucleic acid are applied to molecular beacons [34–36]. A number of other synthetic nucleic acids containing alternative photochemical concepts are also being developed to produce the next generation of fluorescent probes for nucleic acid sensing. This chapter summarizes several synthetic nucleic acids possessing a functional fluorescent dye thiazole orange and shows how the diverse range of such compounds enriches the methodology available for nucleic acid imaging.

3.2 Thiazole Orange

Thiazole Orange (TO, 1-methyl-4-[(3-methyl-2(3*H*)-benzothiazolylidene)methyl] quinolinium *p*-tosylate) is a member of a family of asymmetric cyanines. This dye contains a benzothiazole ring covalently linked to a quinoline ring through a monomethine bridge [37] (Fig. 3.1). TO is the product of a rational design effort to develop an effective dye for reticulocyte analysis [38].

One of the important properties of TO is the enhancement of fluorescence intensity upon intercalation with a DNA duplex; that is, TO undergoes strong fluorescence in a DNA-bound state, whereas the fluorescence of unbound TO is weaker [39, 40]. In a monomeric state, TO exhibits very low fluorescence in aqueous solution (fluorescent quantum yield (Φ_f) = 0.0002) because of intramolecular twisting around the vinyl bond in the excited state [41–47]. The chromophore is cationic and has high affinity for DNA because it intercalates into DNA base pairs ($K_b = 3.3 \times 10^5$ M^{-1}). Upon intercalation and consequent restriction of rotation around the methine bond between the two heterocyclic systems of TO, the nonradiative decay channel of TO is closed and the Φ_f increases to 0.1−0.4 in the DNA duplex. There is no base-specific interaction between TO and DNA [39]. Therefore, gel electrophoresis and fluorometric titration studies indicate a linear increase in the fluorescence intensity with DNA length.

A homodimeric TO, 1,1′-(4,4,8,8-tetramethyl-4,8-diazaundecamethylene)-bis-{4-[3-methyl-2,3-dihydro(benzo-1,3-thiazole)-2-methylidene]}quinolinium tetraiodide (TOTO) [39, 48–51], binds strongly, but noncovalently, to the DNA duplex through bisintercalation from the minor groove side (Fig. 3.2). The enhancement of the Φ_f upon the binding of TOTO to DNA is more than 3000-fold. Thus, TOTO allows high-sensitivity detection of DNA by fluorescence scanners [52].

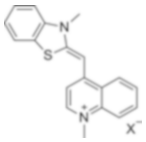

Fig. 3.1 Thiazole orange (TO); X^- is, for example, tosylate

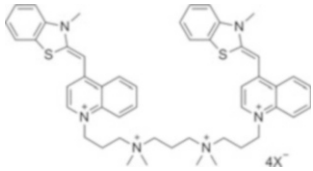

Fig. 3.2 TOTO, a homodimeric TO; X^- is, for example, iodide

3.3 A Variety of TO-Tethered Nucleic Acids

A significant amount of research has focused on linking TO dyes to artificial DNA strands or DNA analogues and on developing their applications in nucleic acid analysis [41, 53–57] (Fig. 3.3). TO has been linked covalently to the phosphodiester or to the 5′-terminus of nucleic acid fragments. In addition, TO was added through propyl spacers or incorporated as a base surrogate into peptide nucleic acid (PNA) to detect single-nucleotide polymorphisms (SNPs).

A DNA fragment labeled with oxazole yellow (YO), which is a derivative of TO in which the sulfur atom is replaced with oxygen, was tested at first [58]. The YO–DNA conjugate showed enhanced fluorescence upon hybridization with a complementary nucleic acid. The hybridization-sensitive fluorescence enhancement was applied to real-time monitoring of the in vitro transcription process of a plasmid DNA construct containing the 5′-end noncoded region of hepatitis C virus RNA. The fluorescence from the mixture exhibited a time-dependent linear increase corresponding to production of the target RNA.

The Krull group modified TO dyes with ethylene glycol linkers and covalently linked them to the 5′-end of DNA strands after solid-phase DNA synthesis [53, 59–61]. The TO-tethered DNA strands exhibited enhancement of fluorescence intensity upon hybridization with the complementary DNA strands at the surfaces of optical fibers.

Asseline et al. also developed αT_{20}–TO conjugates as hybridization-sensitive fluorescent probes for mRNA in living cells [54, 62–64]. The TO-labeled α-DNA was applied to the in situ time-resolved detection of mRNA in adherent fibroblasts, resulting in a high intensity of fluorescent signals.

The Kubista group constructed another hybridization-sensitive fluorescent probe in which TO is tethered to a peptide nucleic acid (PNA) strand [41, 65]. The probe

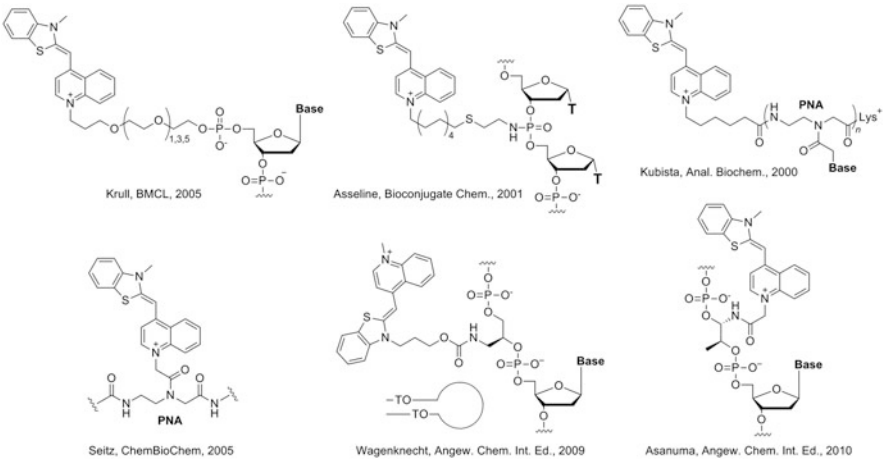

Fig. 3.3 A variety of TO-tethered nucleic acids

contained both the excellent hybridization properties of PNA and the large fluorescence enhancement of TO upon binding to DNA. Free probes showed low fluorescence. The fluorescence of probes increased almost 50-fold upon hybridization to the complementary DNA.

Seitz and co-workers have energetically researched forced intercalation (FIT) probes. FIT probes possess TO as a fluorescent base in a PNA strand for homogeneous SNP detection [42, 43, 55, 66–70]. TO in the probes has the characteristics of a universal base while maintaining duplex stability. The emission of FIT probes is attenuated when they are forced to intercalate next to a mismatched base pair. FIT probes were used to distinguish the target DNA strand from its SNP mutant under nonstringent hybridization conditions.

The Wagenknecht group developed an excimer-type TO probe [56, 71, 72]. In this approach, a single TO dye shows typical green emission when used as an artificial DNA base, whereas the interstrand TO dimer exhibits an orange excimer-type emission inside the DNA duplex. The photophysical interaction of two TO chromophores results in a large Stokes shift of nearly 100 nm with a brightness that is comparable to that of a single TO label in DNA. Such a characteristic change to the fluorescence profile makes the TO pair a powerful fluorescent label for applications in molecular diagnostics and for imaging in chemical cell biology.

Asanuma et al. have recently developed a highly sensitive in-stem molecular beacon (ISMB) by combining TO with a second dye [57, 73]. For example, the interaction between TO and Cy3 was utilized to design ISMB probes in which both a fluorophore and a quencher on D-threoninols are incorporated as a pseudo base pair. Minimization of the difference between the λ_{max} of the fluorophore and quencher in ISMB probes is critical for maximizing the efficiency of quenching before hybridization with the target nucleic acid.

3.4 ECHO Probes

3.4.1 Principle

The TO-tethered nucleic acids show strong fluorescence emission upon hybridization with the target nucleic acid sequences. However, a more specific design of fluorescent DNA derivatives, based on the characteristic photochemical properties of TO, would enable effective nucleic acid sensing with lower background fluorescence.

TO dyes show little emission by the exciton coupling effect [74–78] when they arrange in parallel (H-aggregation) [79–84]. Interaction between TO dyes has been explained in terms of exciton coupling theory, in which the excited state of the TO dimer splits into two energy levels [85–88]. The transition to the upper excitonic state is allowed for the H-aggregates, which then rapidly deactivate to a lower state. Emission from the lower state is theoretically forbidden, and thus the singlet excited

state of the aggregate becomes trapped in a nonemissive state. If two TO dyes linked covalently to a DNA strand are positioned parallel to each other, the emission from the TO aggregate formed in the DNA strand can be suppressed strongly by the excitonic interaction between dyes. By contrast, strong emission will be observed when the DNA strand binds to the complementary nucleic acid, because the aggregate is dissolved and each dye independently intercalates into the nascent duplex structure.

According to the principle described above, a DNA strand containing a fluorescence-labeled nucleotide in which two TO subunits are linked covalently was designed (Fig. 3.4). The synthesis of the TO subunit of the fluorescent nucleotide was attained through a conventional dye synthetic protocol [40, 89, 90]. A synthetic nucleoside with two amino linkers was prepared from a uridine derivative through the addition of an acrylate group at C5 [91] and subsequent extension of a branched linker with tris(2-aminoethyl)amine [89] (Scheme 3.1). The nucleotide precursor was incorporated into DNA strands through a conventional phosphoramidite method using a DNA autosynthesizer to give a diamino-modified DNA strand. Finally, mixing a diamino-modified DNA strand with activated TO dyes gave a DNA strand containing a doubly TO-labeled nucleotide. This labeled nucleotide was named D_{514} because the maximum of the absorption band of the

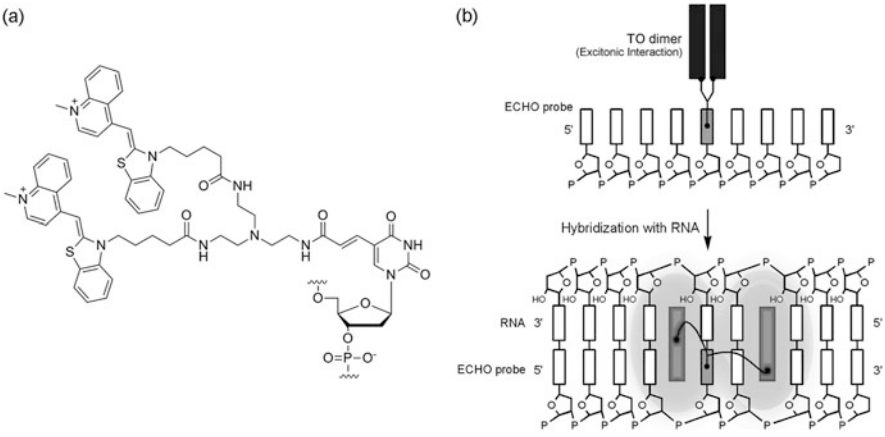

Fig. 3.4 ECHO probe containing a D_{514} nucleotide. (**a**) Structure. (**b**) Schematic representation of the binding of an ECHO probe to the target RNA

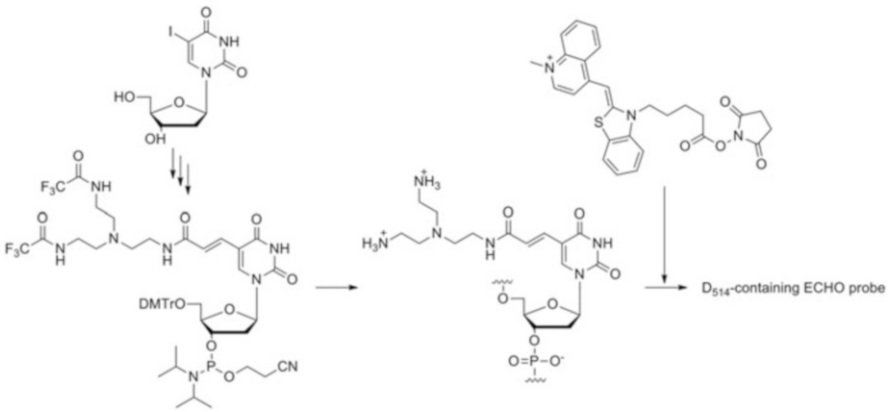

Scheme 3.1 Outline of the synthesis of a D_{514}-containing ECHO probe

D_{514}-containing DNA strand after hybridization with the complementary DNA was approximately 514 nm.

2′-Deoxycytidine was also modified by two TO dyes to get the cytosine derivative of D_{514}. The preparation was attained through the di(*n*-butyl)formamidine protection of the cytosine 4-NH_2 group [92–94].

The D_{514}-containing DNA strands showed characteristic absorption, excitation, and emission spectra before and after hybridization with the complementary nucleic acids [89]. An intense absorption band at approximately 480 nm appeared when the D_{514}-containing DNA strand was in an unhybridized state, whereas an absorption band at approximately 510 nm became predominant when the D_{514}-containing DNA strand was hybridized with the complementary nucleic acid. The blueshift of the absorption band in the unhybridized state indicates excitation of the aggregated form of the dye in D_{514} to an upper excitonic state. The emission spectra were observed at approximately 530 nm as a single broad band. When the D_{514}-containing DNA strand hybridized with the complementary DNA strand, strong emission was observed, whereas the emission intensity was strongly suppressed before hybridization. The excitation spectra displayed a single broad peak at 510 nm regardless of the structural state. This wavelength correlates with the absorption band at longer wavelength, suggesting that the absorption wavelength leading to the fluorescence emission is only from the band observed at 510 nm. The new fluorescent DNA, in which the fluorescence emission is controlled by such interdye excitonic interaction, was named an ECHO (exciton-controlled hybridization-sensitive fluorescent oligonucleotide) probe [95, 96].

The DNA strands containing a monomeric TO (M_{514}) showed different photochemical behavior from their D_{514} counterparts [89]. The lack of an exciton coupling effect in M_{514} resulted in no spectral shift (510 nm) between the single- and double-stranded states. In addition, the quenching efficiency was compromised. The exciton control of D_{514} is the most important key of the quenching mechanism in ECHO probes.

The thermodynamics of ECHO/DNA duplexes was reported by the Hayashizaki group [97]. The thermodynamic parameters were obtained from the melting curves of 64 ECHO/DNA duplexes measured by fluorescence, and the results exhibited a substantial increase in duplex stability compared with DNA/DNA duplexes of the same sequence ($\Delta\Delta G^{\circ}_{37} = -2.6 \pm 0.7$ kcal mol^{-1}). In order to predict the thermodynamic parameters for duplex stability, a nearest-neighbor model was constructed. Evaluation of the parameters by cross-validation tests showed high predictive reliability for the fluorescence-based parameters. A tool for predicting the thermodynamics of formation of ECHO/DNA duplexes is now available at http://genome.gsc.riken.jp/echo/thermodynamics/.

3.4.2 Fluorescent In Situ Hybridization

Fluorescent in situ hybridization (FISH) is a useful tool for gene expression analysis. However, conventional FISH is a cumbersome and time-consuming method containing repetitive washing processes. Because of the superior signal-to-noise ratio of ECHO probes compared with conventional fluorescence-labeled nucleic acid probes, a high-resolution FISH has become possible by adapting ECHO probes (ECHO–FISH) [98]. The ECHO–FISH technology included no stringent washing steps, giving a 25 min procedure, from fixation to mounting, and made clear fluorescence detection of the intracellular RNA possible.

ECHO–FISH exhibited the following detection specificity: (1) single mismatches in D_{514} probes diminish FISH signals; (2) sense control probes reveal only background FISH signals; (3) the cellular distribution pattern of FISH signals is consistent with the immunostaining pattern of the target protein; and (4) discrete localization patterns of poly(A) RNA in nuclear speckles, telomeres, minor satellite DNA, and major satellite DNA on chromosomes are consistent with previous reports. The small size of D_{514} probes (13–50 nt) makes it possible to apply ECHO–FISH to detect isoforms that differ in only small regions of the genes.

For example, 5′-$T_6D_{514}T_6$-3′, which was designed for the detection of poly(A)$^+$ RNA, exhibited the localization of RNA with this sequence in areas such as intranuclear speckles in both HeLa cells and in dissociated hippocampal cultures. The shape, size, and number of puncta per cell varied among cells. CaMKIIα-, Tubb2b-, and Nr4a1-specific probes revealed predominantly cytoplasmic distribution of the target RNA. The use of the ECHO–FISH technique with a 5′-$T_6D_{514}T_6$-3′ probe also revealed poly(A) RNA inside neuronal processes labeled by fluorescent phalloidin and at postsynaptic contacting sites opposite to synaptophysin-positive clusters. The cytoplasmic FISH signals detected by CaMKIIα-specific probes extended into the distal dendrites, which is consistent with previous findings that CaMKIIα mRNA is transported into dendrites and translated locally.

3.4.3 *Live Cell RNA Imaging*

To monitor RNA effectively in a living cell and to avoid background fluorescence and washing processes, high hybridization sensitivity of the fluorescent emission of a probe is essential. The way that the fluorescence of ECHO probes is quenched in the unhybridized state makes them suitable for this purpose. In addition, the fluorescence of ECHO probes increases immediately after mixing with the target RNA [99]. ECHO probes can be applied to living HeLa cells by using manipulator-assisted microinjection or transfection to visualize intracellular mRNA localization. For example, immediately after the injection of 5′-$T_6D_{514}T_6$-3′ into the nucleus of a living HeLa cell, fluorescence was observed from the nucleus; the fluorescence spectrum data obtained from a multichannel detector on excitation at 488 nm identified the origin of the emission to be from the 5′-$T_6D_{514}T_6$-3′ hybridized probe. Images from cells into which nontarget probes were injected exhibited negligible fluorescence emission, and these probes exhibited little background fluorescence or nonspecific emission originating from binding to other cell components.

The Cy5-conjugated ECHO probe, which can hybridize with poly(A)$^+$ RNA, was also prepared to establish the difference between the distribution of the probe and the localization of the target RNA in a living cell [100]. The fluorescence images from D_{514} and Cy5 of the Cy5-conjugated ECHO probe in the cells were clearly different (Fig. 3.5). Cy5 fluorescence, which indicates cellular distribution of the probe, was strong and uniform throughout the nuclei except for the nucleoli. By contrast, D_{514} fluorescence, which indicates the localization of poly(A)$^+$ RNA through probe hybridization, was mainly observed in the nuclei as clear puncta. The fluorescence profile suggests that the cell nucleus was filled with the Cy5-conjugated ECHO probe and that the D_{514} probe fluorescence showed the localization of probe-hybridized poly(A)$^+$ RNA.

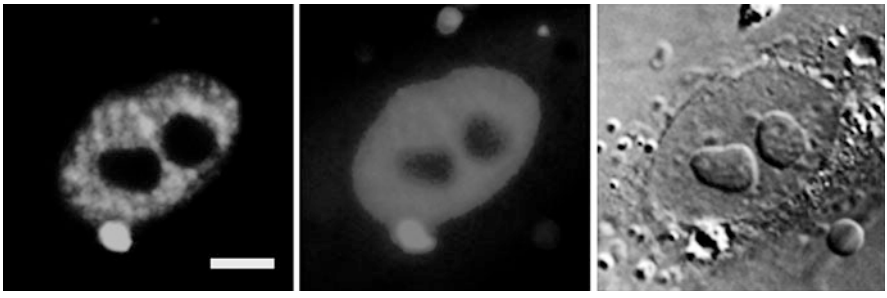

Fig. 3.5 Difference between the localization of the probe-hybridized poly(A)$^+$ RNA and the distribution of the probe in a living MDCK cell using Cy5-conjugated ECHO probe. *Left*, the fluorescence derived from D_{514}; *center*, the fluorescence derived from Cy5; *right*, differential interference contrast. *Bar*: 10 μm

3.5 Modified ECHO Probes

3.5.1 Modification of Dyes (1): A Variety of Fluorescent Colors

In efforts to understand temporal correlations between gene expression and the interaction of nucleic acids, a series of new fluorescent nucleotides were designed in which the TO moiety was substituted by its derivatives. These novel probes, which were also based on excitonic interaction chemistry, had on/off performance levels as high as those of ECHO probes [101, 102]. Thus, a series of derivatives have been developed with at least 15 emission wavelengths in ECHO probes, from blue to the near-infrared region. A list of D_{nnn} nucleotides is shown in Fig. 3.6. However, care must be taken over inefficient exciton control, which is observed in a few nucleotides in hybridization with RNA strands (D_{539}, D_{570}, and D_{590}). The appropriate control of dye aggregation in the unhybridized state is a key point that determines the functionality and usefulness of a particular ECHO probe.

A model experiment with simultaneous live-cell RNA imaging using different wavelengths was performed [101]. The emission spectrum obtained using a multichannel detector confirmed that the fluorescence in the cells arose from emission from the dyes of the probes. Three ECHO probes with different emission wavelengths (D_{514}, D_{543}, and D_{640}) were prepared for three different miRNA sequences, and a mixture of the three probes was microinjected into the nuclei of artificially miRNA-enriched HeLa cells. The ECHO probe recognized the target miRNA in the cell and emitted fluorescence with a miRNA-specific emission wavelength. The fluorescence emission with three different wavelengths was observed simultaneously in cells containing the three miRNA strands.

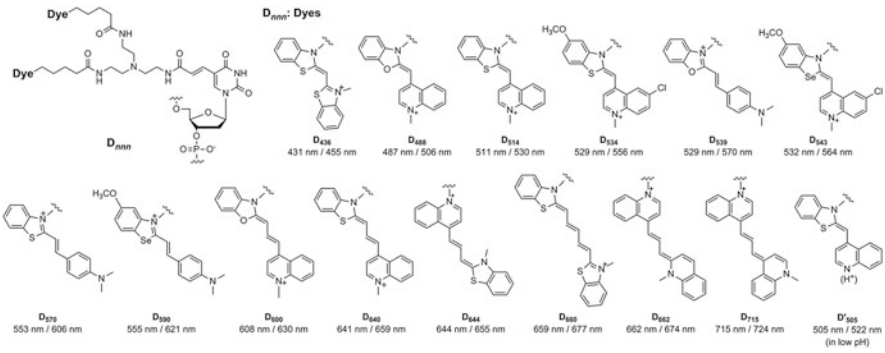

Fig. 3.6 A series of D_{nnn} ECHO probes

3.5.2 *Modification of Dyes (2): Desmethyl TO*

Although the use of a diverse range of fluorescent wavelengths has expanded the ECHO probe series, the simultaneous incorporation of suitable dyes into one probe molecule is complex, because postsynthetic incorporation of dyes is used for probe synthesis (Scheme 3.1). The positive charge on the dyes used in ECHO probes makes such compounds insoluble in organic solvents, meaning that the dyes must be incorporated after DNA autosynthesis. The key to solving this problem is to design a dye-tethering nucleoside unit that is soluble in several organic solvents, thus providing an alternative method of incorporating the dye into the probe.

The desmethyl TO dye unit was tethered to the thymidine derivative to give a nucleoside that was doubly modified with a dye that was suitable for excitation at 505 nm (D'_{505}; Fig. 3.6) [103]. The use of uncharged desmethyl TO made the preparation of the nucleoside unit and the reactions in the cycles of DNA synthesis more efficient, because both the dye and the dye-tethering nucleoside are soluble in the organic solvents used in the synthetic processes. The synthesized D'_{505}-containing oligonucleotides were used for RNA imaging after purification, without the further modifications typically required in conventional ECHO probes.

Desmethyl TO, which is used for dyes of D'_{505}, is inherently weakly emissive [40]. Nevertheless, dyes of D'_{505}-containing oligonucleotide were protonated at pH 7, and the oligonucleotide exhibited hybridization-sensitive fluorescence emission through control of excitonic interactions of the dyes of D'_{505}. The emission behavior is the same as that of conventional ECHO probes.

Measurements at pH 5–7 showed on/off switching of fluorescence and a shift of absorption depending on the addition of a complementary RNA strand, which is similar to the behavior of conventional ECHO probes. Because acidic pH is important for the protonation and emission of D'_{505}, the fluorescence from a D'_{505}-containing oligonucleotide at higher pH (pH 8–10) was weak even in the presence of the complementary RNA strand.

The greatest advantage of the incorporation into the ECHO probes of a "ready-made" fluorescent nucleotide with the function of hybridization-sensitive fluorescence switching is to make it possible to incorporate a further, different fluorescence color in combination with the conventional ECHO probe procedure. For example, a D'_{505}–D_{600}-double-colored ECHO probe exhibited on/off switching of fluorescence at the emission wavelengths of either D'_{505} or D_{600} depending on the addition of the complementary RNA strand. The partially hybridized D'_{505}–D_{600} probe emitted fluorescence corresponding to the hybridized region.

FRET between D'_{505} and D_{600} was also observed when the distance between the two nucleotides was short. The FRET system of a multicolored ECHO probe is applicable to RNA imaging and may provide a way to simplify the monitoring of specific cells and specifically the task of locating RNA in a cell through acceptor bleaching assays [104, 105]. A poly(A)$^+$ RNA-targeting D'_{505}–D_{600} probe emitted strong fluorescence from D_{600} when excited with a 488 nm laser after transfection into living HeLa cells because the FRET process was active, whereas the

fluorescence from D'_{505} was weak. After one of the strongly emitting cells was irradiated repeatedly with a 561 nm laser, the fluorescence from D_{600} was reduced to 16 % only in the irradiated cell. Upon the photobleaching of D_{600} dyes, the strong fluorescence of the FRET donor D_{514} was recovered (490 % before photobleaching).

3.5.3 *Modification of Backbones (1): 2′-O-Methyl RNA*

ECHO probes with a DNA backbone are digested by cellular nucleases. Thus, the usefulness of the probe may be limited to in vitro or short-term cell observation. In order to add nuclease resistance to ECHO probes for the long-term intracellular RNA observation, the DNA backbone of ECHO probes was replaced by a 2′-*O*-Methyl RNA (2′-*O*-MeRNA) backbone [106] (Fig. 3.7). 2′-*O*-MeRNA is known to have higher affinity for RNA targets and higher resistance ability against nucleases than the corresponding DNA [107–109]. Investigation of the nuclease resistance of probes showed that S1 endonuclease degraded about 90 % of DNA probes within 12 h, whereas about 95 % of 2′-*O*-MeRNA probes remained undigested after 12 h of incubation. Exonuclease I also digested the DNA probes rapidly, whereas the digestion of 2′-*O*-MeRNA probes was suppressed. Damage to the probe-hybridizing RNA by RNase H degrades the original function of RNA as well as reducing the probe fluorescence. The DNA probe and RNA strand hybrids showed a gradual decrease in fluorescence to about 65 % of the initial value within 1 h. By contrast, when 2′-*O*-MeRNA probes were used, no significant decrease of fluorescence was observed, even in the presence of RNase H.

The high nuclease resistance of 2′-*O*-MeRNA probes makes long-term intracellular RNA imaging possible. Intracellular mRNA behavior during cell life events, such as migration and division, was observed through long-term monitoring of $5'\text{-}^{OMe}U_6D_{514}{}^{OMe}U_6\text{-}3'$-transfected cells. The fluorescence in the mother cells was evenly distributed to their two daughter cells after cell division.

3.5.4 *Modification of Backbones (2): Locked Nucleic Acid*

Accessing RNA sequences that form higher-order structures and distinguishing the target RNA sequence from SNP mutants are often thermodynamically difficult for

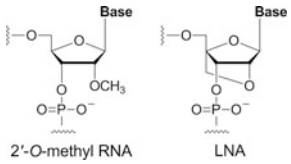

Fig. 3.7 Modification of backbones

fluorescent nucleic acid probes. Incorporation of locked nucleic acid (LNA) nucleotide units into hybridization-sensitive probes solved such problems [110–114] (Fig. 3.7). Chimeric probes, having selected positions modified with LNA nucleotides, enhanced duplex stability. In addition, incorporation of LNA trinucleotides into ECHO probes enhanced the thermostability of duplexes formed with complementary sequences, whereas the duplex stability with mismatched sequences was much lower [115]. For example, insertion of LNA nucleotides into ECHO probes facilitated analysis of the higher-order structures of HIV-1 TAR RNA, which is the transactivation response element located at the 5′-end of HIV-1 mRNA [115, 116]. A 16-mer ECHO–LNA conjugate (5′-GC$\underline{T}$C$\underline{^{m}C\,C}\underline{A}$GGCD$_{514}CAG\underline{A}$T-3′; where $\underline{X}$ is an LNA nucleotide) was designed for the TAR RNA stem–loop structure, and it provided high binding affinity to TAR RNA. However, it is important to ensure that during LNA nucleotide incorporation into ECHO probes, the LNA nucleotides are at least three nucleotides apart from D_{514} so that the strong fluorescence of the hybrid by LNA incorporation is retained. The rigid LNA structure prevents intercalation of the TO unit of D_{514} when a LNA nucleotide lies adjacent to the D_{514} nucleotide, resulting in lower fluorescence intensity.

Combination of an ECHO probe and an SNP-recognizing LNA trinucleotide was effective for mix-and-read fluorescent SNP typing [117]. LNA-incorporating ECHO probes can be designed for the fluorescent SNP detection of placenta-specific 4 (PLAC4) rs130833, which is an SNP located in the transcribed regions of placental-expressed mRNA in maternal plasma [118, 119]. ECHO–LNA conjugate probes, 5′-AGD$_{514}$TAG$\underline{A^{m}CG}$A-3′ and 5′-AGD$_{514}$TAG$\underline{ATG}$A-3′, exhibited a much larger gap between the T_m values of the hybrids of the matched and mismatched LNA-containing ECHO probes and PLAC4 RNA compared with DNA probes. As a result, fluorescence emission that was selective for matched PLAC4 RNA hybrids was observed under appropriate temperature control.

3.5.5 *Modification of Nucleobases (1): Inosine and* N*-Ethylcytidine*

Hybridization-sensitive fluorescent probes have an inherent disadvantage. The self-dimerization of the probes results in strong background fluorescence emission. Incorporation of an ability to avoid dimerization into the structure of ECHO probes would be required to improve the function of fluorometric nucleic acid analysis. The key point is to weaken the interaction between probes, and in particular to weaken the relatively strong guanine–cytosine hydrogen bonds, while maintaining sufficient hydrogen-bonding ability to hybridize with the target nucleic acid. This concept, which involves control of thermostability, utilizes a base pair formed by 2′-deoxyinosine (I) as a surrogate of 2′-deoxyguanosine and N^4-ethyl-2′-deoxycytidine (E) as a surrogate of 2′-deoxycytidine. The I–E base pair is unstable, but I and E bases can form more stable base pairs with cytosine and

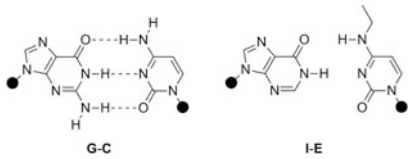

Fig. 3.8 Base pair formed by inosine (I) and N^4-ethylcytidine (E)

guanine, respectively [120–122]. The I and E bases were incorporated into an ECHO probe [123] (Fig. 3.8). An original ECHO probe, 5′-CGCAAGD$_{514}$GAACGC-3′, exhibited insufficient suppression of fluorescence intensity before the addition of the complementary nucleic acid (55 % suppression). By contrast, the emission intensity of the I–E-substituted probe 5′-EIEAAID$_{514}$IAAEIE-3′ was well suppressed before hybridization (96 % suppression).

The sequence of I–E-substituted probes has to be designed carefully. It should be ensured that E is not placed next to either of the bases adjacent to D$_{514}$. A significant reduction in the fluorescence intensity has been observed for several such I–E probes in spite of the addition of the complementary nucleic acid. The N^4-ethyl group of E, which protrudes into the major groove of the duplex structure of the hybrid, sterically hinders the approach of the TO dye from the major groove side for intercalation.

The I–E-substituted ECHO probe contributes to the design of long probe sequences for mRNA imaging. For example, a 50 nt I–E-substituted probe was prepared for the detection of β-actin mRNA, and the fluorescence appeared at the β-actin mRNA-localized cytoplasmic area after microinjection of the probes.

3.5.6 Modification of Nucleobases (2): Caged ECHO Probes

Caging technologies have been used in many biological applications to activate substances in a spatiotemporal manner. In order to obtain a caged ECHO probe for spatiotemporal monitoring of intracellular RNA, a photolabile nitrobenzyl (NB) unit, α-methyl-2-nitro-4,5-dimethoxybenzyl alcohol, was tethered to the N3 of D$_{nnn}$ nucleotides (^{NB}D$_{nnn}$, $nnn = 514$, 600, and 715) [124] (Fig. 3.9). The photolabile NB unit suppressed the function of the probes by decreasing the hybridization ability of probes. Synthetic T$_6$^{NB}D$_{514}$T$_6$ showed little fluorescence emission even in the presence of A$_{13}$.

In order to uncage protected ECHO (^{NB}ECHO) probes, a brief irradiation using a laser at 360 or 405 nm is sufficient to remove the NB group from ^{NB}D$_{nnn}$. After photolysis, the probes have the property of hybridization-sensitive fluorescence emission. Area-specific uncaging of the ^{NB}ECHO probe in a living cell using a blue laser was applicable to visualization of subnuclear mRNA diffusion. The ^{NB}ECHO probe offers an alternative to the most popular area-specific photocontrolled

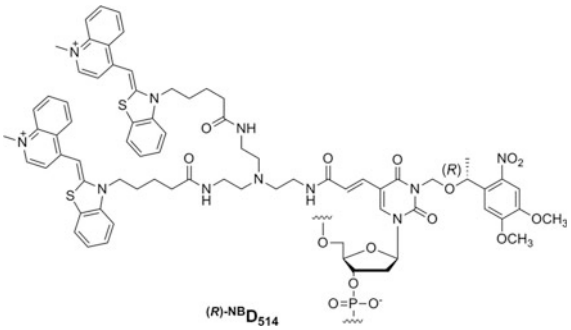

Fig. 3.9 A caged ECHO probe

fluorescence recovery after photobleaching (FRAP) assay [125–129] or fluorescence loss in photobleaching (FLIP) assay [130–132].

3.6 Conclusion

TO exhibits strong fluorescence property when it binds to nucleic acid duplex, and many TO-tethered nucleic acids have been developed for the detection of the target nucleic acids in a huge amount of nucleic acid mixture. The ECHO probe technology, one of TO probes, made possible to detect the target nucleic acid and to analyze both the spatial and temporal dimensions of the diverse RNA dynamics in a living cell. Further expansion of the diversity of TO-tethered nucleic acids should lead to further improvements in the methodology of nucleic acid imaging.

Acknowledgements The author thanks the members of the Okamoto Laboratory for helpful discussions. The research on ECHO probes in Okamoto Laboratory was supported by the Funding Program for Next Generation World-Leading Researchers, Japan (LR036).

References

1. Aoki I, Kawabata H, Nakashima K, Shinkai SJ (1991) Chem Soc Chem Commun 1771–1773
2. Paris PL, Langenhan JM, Kool ET (1998) Nucleic Acids Res 26:3789–3793
3. Nishizawa S, Kato Y, Teramae N (1999) J Am Chem Soc 121:9463–9464
4. Yamana K, Iwai T, Ohtani Y, Sato S, Nakamura M, Nakano H (2002) Bioconjugate Chem 13:1266–1273
5. Okamoto A, Ichiba T, Saito I (2004) J Am Chem Soc 126:8364–8365
6. Lee HN, Xu Z, Kim SK, Swamy KMK, Kim Y, Kim S-J, Yoon J (2007) J Am Chem Soc 129:3828–3829
7. Weber G, Farris FJ (1979) Biochemistry 18:3075–3078
8. Grynkiewicz G, Poenie M, Tsien RY (1985) J Biol Chem 260:3440–3450
9. Macgregor RB, Weber G (1986) Nature 319:70–73
10. Pierce DW, Boxer SG (1992) J Phys Chem 96:5560–5566

11. Martin MM, Plaza P, Meyer YH, Badaoui F, Bourson J, Lefèvre JP, Valeur B (1996) J Phys Chem 100:6879–6888
12. Cohen BE, McAnaney TB, Park ES, Jan YN, Boxer SG, Jan LY (2002) Science 296:1700–1703
13. Okamoto A, Tainaka K, Nishiza K, Saito I (2005) J Am Chem Soc 127:13128–13129
14. Okamoto A, Tainaka K, Unzai T, Saito I (2007) Tetrahedron 63:3465–3470
15. Tainaka K, Tanaka K, Ikeda S, Nishiza K, Unzai T, Fujiwara Y, Saito I, Okamoto A (2007) J Am Chem Soc 129:4776–4784
16. Fages F, Desvergne JP, Bouas-Laurent H, Marsau P, Lehn JM, Kotzyba-Hibert F, Albrecht-Gary AM, Al-Joubbeh M (1989) J Am Chem Soc 111:8672–8680
17. Bissell RA, de Silva AP, Gunaratne HQN, Lynch PLM, Maguire GEM, McCoy CP, Sandanayake KRAS (1993) Top Curr Chem 168:223–264
18. James TD, Sandanayake KRAS, Iguchi R, Shinkai S (1995) J Am Chem Soc 117:8982–8987
19. Bergonzi R, Fabbrizzi L, Lichelli M, Mangano C (1998) Coord Chem Rev 170:31–46
20. Walkup GK, Burdette SC, Lippard SL, Tsien RY (2000) J Am Chem Soc 122:5644–5645
21. Miura T, Urano Y, Tanaka K, Nagano T, Ohkubo K, Fukuzumi S (2003) J Am Chem Soc 125:8666–8671
22. Urano Y, Kamiya M, Kanda K, Ueno T, Hirose K, Nagano T (2005) J Am Chem Soc 127:4888–4894
23. Wu P, Rice KG, Brand L, Lee YC (1991) Proc Natl Acad Sci USA 88:9355–9359
24. Mergny J-L, Boutorine AS, Garestier T, Belloc F, Rougée M, Bulychev NV, Koshkin AA, Bourson J, Lebedev AV, Valeur B, Thuong NT, Hélène C (1994) Nucleic Acids Res 22:920–928
25. Wu P, Brand L (1994) Anal Biochem 218:1–13
26. Hillisch A, Lorenz M, Diekmann S (2001) Curr Opin Struct Biol 11:201–207
27. Klostermeier D, Millar DP (2002) Biopolymers 67:159–179
28. Valeur B (2002) Molecular fluorescence: principles and applications. Wiley-VCH, Weinheim
29. van der Meer BW, Coker G III, Chen S-YS (1994) Resonance energy transfer: theory and data. VCH, New York
30. Fang X, Li JJ, Perlette J, Tan W, Wang K (2000) Anal Chem 72:747A–753A
31. Broude NE (2002) Trends Biotechnol 20:249–256
32. Okamoto A, Tanabe K, Inasaki T, Saito I (2003) Angew Chem Int Ed 42:2502–2504
33. Tan W, Wang K, Drake TJ (2004) Curr Opin Chem Biol 8:547–553
34. Tyagi S, Kramer FR (1996) Nat Biotechnol 14:303–308
35. Tyagi S, Btaru DP, Kramer FR (1998) Nat Biotechnol 16:49–53
36. Piatek AS, Tyagi S, Pol AC, Telenti A, Miller LP, Kramer FR, Alland D (1998) Nat Biotechnol 16:359–363
37. Nygren J, Svanvik N, Kubista M (1998) Biopolymers 46:39–51
38. Lee LG, Chen C-H, Chiu LA (1986) Cytometry 7:508–517
39. Rye HS, Yue S, Wemmer DE, Quesada MA, Haugland RP, Mathies RA, Glazer AN (1992) Nucleic Acids Res 20:2803–2812
40. Ikeda S, Okamoto A (2007) Photochem Photobiol Sci 6:1197–1201
41. Svanvik N, Westman G, Wang D, Kubista M (2000) Anal Biochem 281:26–35
42. Kummer S, Knoll A, Socher E, Bethge L, Herrmann A, Seitz O (2012) Bioconjugate Chem 23:2051–2060
43. Karunakaran V, Lustres JLP, Zhao L, Ernsting NP, Seitz O (2006) J Am Chem Soc 128:2954–2962
44. Silva GL, Ediz V, Yaron D, Armitage BA (2007) J Am Chem Soc 129:5710–5718
45. Carlsson C, Larsson A, Jonsson M, Albinsson B, Norden B (1994) J Phys Chem 98:10313–10321
46. Ghasemi J, Ahmadi S, Ahmad AI, Ghobadi S (2008) Appl Biochem Biotechnol 149:9–22
47. Netzel TL, Nafisi K, Ziao M, Lenhard JR, Johnson I (1995) J Phys Chem 99:17936–17947
48. Benson SC, Mathies RA, Glazer AN (1993) Nucleic Acids Res 21:5720–5726

49. Benson SC, Singh P, Glazer AN (1993) Nucleic Acids Res 21:5727–5735
50. Hirons GT, Fawcett JJ, Crissman HA (1994) Cytometry 15:129–140
51. Jacobsen JP, Pedersen JB, Hansen LF, Wemmer DE (1995) Nucleic Acids Res 23:753–760
52. Hansen LF, Jensen LK, Jacobsen JP (1996) Nucleic Acids Res 24:859–867
53. Wang X, Krull UJ (2005) Bioorg Med Chem Lett 15:1725–1729
54. Privat E, Asseline U (2001) Bioconjugate Chem 12:757–769
55. Köhler O, Jarikote DV, Seitz O (2005) ChemBioChem 6:69–77
56. Berndl S, Wagenknecht H-A (2009) Angew Chem Int Ed 48:2418–2421
57. Hara Y, Fujii T, Kashida H, Sekiguchi K, Liang X, Niwa K, Takase T, Yoshida Y, Asanuma H (2010) Angew Chem Int Ed 49:5502–5506
58. Ishiguro T, Saitoh J, Yawata H, Otsuka M, Inoue T, Sugiura Y (1996) Nucleic Acids Res 24:4992–4997
59. Hanafi-Bagby D, Piunno PAE, Wust CC, Krull UJ (2000) Anal Chim Acta 411:19–30
60. Wang X, Krull UJ (2002) Anal Chim Acta 470:57–70
61. Algar WR, Massey M, Krull UJ (2006) J Fluoresc 16:555–567
62. Asseline U, Chassignol M, Aubert Y, Roig V (2006) Org Biomol Chem 4:1949–1957
63. Lartia R, Asseline U (2006) Chem Eur J 12:2270–2281
64. Privat E, Melvin T, Asseline U, Vigny P (2001) Photochem Photobiol 74:532–541
65. Svanvik N, Nygren J, Westman G, Kubista M (2001) J Am Chem Soc 123:803–809
66. Jarikote DV, Krebs N, Tannert S, Röder B, Seitz O (2007) Chem Eur J 13:300–310
67. Socher E, Jarikote DV, Knoll A, Röglin L, Burmeister J, Seitz O (2008) Anal Biochem 375:318–330
68. Köhler O, Seitz O (2003) Chem Commun 2938–2939
69. Köhler O, Jarikote DV, Seitz O (2004) Chem Commun 2674–2675
70. Jarikote DV, Köhler O, Socher E, Seitz O (2005) Eur J Org Chem 2005:3187–3195
71. Serndl S, Wagenknecht H-A (2009) Angew Chem Int Ed 48:2418–2421
72. Menacher F, Rubner M, Berndl S, Wagenknecht H-A (2008) J Org Chem 73:4263–4266
73. Kamiya Y, Ito A, Ito H, Urushihara M, Takai J, Fujii T, Liang X, Kashida H, Asanuma H (2013) Chem Sci 4:4016–4021
74. Khairutdinov RF, Serpone N (1997) J Phys Chem B 101:2602–2610
75. Simon LD, Abramo KH, Sell JK, McGown LB (1998) Biospectroscopy 4:17–25
76. Cosa G, Focsaneanu K-S, McLean JRN, McNamee JP, Scaiano JC (2001) Photochem Photobiol 73:585–599
77. Sagawa T, Tobata H, Ihara H (2004) Chem Commun 2–4
78. Fürstenberg A, Julliard MD, Deligeorgiev TG, Gadjev NI, Vasilev AA, Vauthey E (2006) J Am Chem Soc 128:7661–7669
79. West W, Pearce S (1965) J Phys Chem 69:1894–1903
80. Czikkely V, Forsterling HD, Kuhn H (1970) Chem Phys Lett 6:207–210
81. Harrison WJ, Mateer DL, Tiddy G-J Jr (1996) J Phys Chem 100:2310–2321
82. Zeena S, Thomas KG (2001) J Am Chem Soc 123:7859–7865
83. Hannah KC, Armitage BA (2004) Acc Chem Res 37:845–853
84. Rösch U, Yao S, Wortmann R, Würthner F (2006) Angew Chem Int Ed 45:7026–7030
85. Kasha M (1963) Radiat Res 20:55–70
86. Kasha M, Rawls HR, El-Bayoumi MA (1965) Pure Appl Chem 11:371–392
87. Levinson GL, Simpson WT, Curtis W (1957) J Am Chem Soc 79:4314–4320
88. McRae EG, Kasha M (1958) J Chem Phys 28:721–722
89. Ikeda S, Okamoto A (2008) Chem Asian J 3:958–968
90. Okamoto A (2010) Chem Rec 10:188–196
91. Ashwell M, Jones AS, Kumar A, Sayers JR, Walker RT, Sakuma T, de Clercq E (1987) Tetrahedron 43:4601–4608
92. Ikeda S, Yuki M, Yanagisawa H, Okamoto A (2009) Tetrahedron Lett 50:7191–7195
93. Switzer CY, Moroney SE, Benner SA (1993) Biochemistry 32:10489–10496
94. Froehler BC, Matteucci MD (1983) Nucleic Acids Res 11:8031–8036

95. Wang DO, Okamoto A (2012) J Photochem Photobiol C 13:112–123
96. Okamoto A (2011) Chem Soc Rev 40:5815–5828
97. Kimura Y, Hanami T, Tanaka Y, de Hoon MJL, Soma T, Harbers M, Lezhava A, Hayashizaki Y, Usui K (2012) Biochemistry 51:6056–6067
98. Wang DO, Matsuno H, Ikeda S, Nakamura A, Yanagisawa H, Hayashi Y, Okamoto A (2012) RNA 18:166–175
99. Kubota T, Ikeda S, Okamoto A (2009) Bull Chem Soc Jpn 82:110–117
100. Kubota T, Ikeda S, Yanagisawa H, Yuki M, Okamoto A (2011) Bioconjugate Chem 22:1625–1630
101. Ikeda S, Kubota T, Yuki M, Okamoto A (2009) Angew Chem Int Ed 48:6480–6484
102. Ikeda S, Yanagisawa H, Nakamura A, Wang DO, Yuki M, Okamoto A (2011) Org Biomol Chem 9:4199–4204
103. Okamoto A, Sugizaki K, Yuki M, Yanagisawa H, Ikeda S, Sueoka T, Hayashi G, Wang DO (2013) Org Biomol Chem 11:362–371
104. Miyawaki A (2003) Dev Cell 4:295–305
105. Ikeda S, Kubota T, Wang DO, Yanagisawa H, Yuki M, Okamoto A (2011) Org Biomol Chem 9:6598–6603
106. Kubota T, Ikeda S, Yanagisawa H, Yuki M, Okamoto A (2009) Bioconjugate Chem 20:1256–1261
107. Freier SM, Altmann KH (1997) Nucleic Acids Res 25:4429–4443
108. Lesnik EA, Freier SM (1998) Biochemistry 37:6991–6997
109. Cramer H, Pfleiderer W (2000) Nucleosides Nucleotides Nucleic Acids 19:1765–1777
110. Petersen M, Wengel J (2003) Trends Biotechnol 21:74–81
111. Koshkin AA, Singh SK, Nielsen P, Rajwanshi VK, Kumar R, Meldgaard M, Olsen CE, Wengel J (1998) Tetrahedron 54:3607–3630
112. Chou L-S, Meadows C, Wittwer CT, Lyon E (2005) BioTechniques 39:644–647
113. Tolstrup N, Nielsen PS, Kolberg JG, Frankel AM, Vissing H, Kauppinen S (2003) Nucleic Acids Res 31:3758–3762
114. Simeonov A, Nikiforov TT (2002) Nucleic Acids Res 30:e91
115. Sugizaki K, Okamoto A (2010) Bioconjugate Chem 21:2276–2281
116. Dingwall C, Ernberg I, Gait MJ, Green SM, Heaphy S, Karn J, Lowe AD, Singh M, Skinner MA (1990) EMBO J 9:4145–4153
117. You Y, Moreira BG, Behlke MA, Owczarzy R (2006) Nucleic Acids Res 34:e60
118. Lo YMD, Tsui NBY, Chiu RWK, Lau TK, Leung TN, Heung MMS, Gerovassili A, Jin Y, Nicolaides KH, Cantor CR, Ding C (2007) Nat Med 13:218–223
119. Go ATJI, Visser A, Mulders MAM, Blankenstein MA, van Vugt JMG, Oudejans CBM (2007) Clin Chem 53:2223–2224
120. Woo J, Meyer RB, Gamper HB (1996) Nucleic Acids Res 24:2470–2475
121. Lahoud G, Timoshchuk V, Lebedev A, de Vega M, Salas M, Arar K, Hou Y-M, Gamper H (2008) Nucleic Acids Res 36:3409–3419
122. Hoshina S, Chen F, Leal NA, Benner SA (2008) Nucleic Acids Symp Ser 52:129–130
123. Ikeda S, Kubota T, Yuki M, Yanagisawa H, Tsuruma S, Okamoto A (2010) Org Biomol Chem 8:546–551
124. Ikeda S, Kubota T, Wang DO, Yanagisawa H, Umemoto T, Okamoto A (2011) ChemBioChem 12:2871–2880
125. Bancaud A, Huet S, Rabut G, Ellenberg J (2010) In: Goldman RD, Swedlow JR, Spector DL (eds) Live cell imaging: a laboratory manual, 2nd edn. Cold Spring Harbor Laboratory Press, New York, pp 67–94
126. Lippincott-Schwartz J, Snappl E, Kenworthy A (2001) Nat Rev Mol Cell Biol 2:444–456
127. Klonis N, Rug M, Harper I, Wickham M, Cowman A, Tilley L (2002) Eur Biophys J 31:36–51
128. Ellenberg J, Siggia ED, Moreira JE, Smith CL, Presley JF, Worman HJ, Lippincott-Schwartz J (1997) J Cell Biol 138:1193–1206

129. Handwerger KE, Murphy C, Gall JG (2003) J Cell Biol 160:495–504
130. Cole NB, Smith CL, Sciaky N, Terasaki M, Edidin M, Lippincott-Schwartz J (1996) Science 273:797–801
131. Belgareh N, Rabut G, Bai SW, van Overbeek M, Beaudouin J, Daigle N, Zatsepina OV, Pasteau F, Labas V, Fromont-Racine M, Ellengerg J, Doye V (2001) J Cell Biol 154:1147–1160
132. Phair RD, Misteli T (2000) Nature 404:604–609

Chapter 4
Synthetic Wavelength-Shifting Fluorescent Probes of Nucleic Acids

Christian Schwechheimer, Marcus Merkel, Peggy R. Bohländer, and Hans-Achim Wagenknecht

Abstract Visualizing of nucleic acids represents not only an important task for molecular imaging but also for chemical biology in general. Fluorescent labels can be incorporated either synthetically into nucleic acids by their corresponding building blocks (both phosphoramidites and nucleoside triphosphates) or postsynthetically by one of the recent sophisticating "click"-type reacting building blocks. Herein, we focus on the development of new photostable cyanine-styryl dyes and on wavelength-shifting fluorescent probes as promising tools for molecular imaging. The double helical architecture around two fluorophores is crucial for efficient photophysical interactions that range from excitonic and excimer-type to energy transfer interactions. This is equally important for fluorescent labels as isosteric and non-isosteric DNA base replacements. Especially, the latter ones yield fluorescent DNA and RNA systems with dual emission color readout as wavelength-shifting probes. Our DNA and RNA "traffic light" combines the green emission of TO with the red emission of TR. The concept can be transferred to a DNA system that is synthetically easier to access since the dyes were attached postsynthetically as 2′-modifications. Using newly synthesized dyes of the cyanine-styryl type, new nucleic acid probes were realized with high quantum yields and excellent photostability. Combined as energy transfer pairs not only wavelength-shifting DNA probes with red-green-transfer emission color change but also yellow-blue pairs were realized. All of them show good emission color contrasts due to very efficient energy transfer. These wavelength-shifting probes have a significant potential to be applied on the RNA level for molecular imaging of living cells.

C. Schwechheimer • M. Merkel • P.R. Bohländer • H.-A. Wagenknecht (✉)
Institute of Organic Chemistry, Karlsruhe Institute of Technology (KIT), Fritz-Haber-Weg 6, 76131 Karlsruhe, Germany
e-mail: Wagenknecht@kit.edu

K. Nakatani, Y. Tor (eds.), *Modified Nucleic Acids*, Nucleic Acids and Molecular Biology 31, DOI 10.1007/978-3-319-27111-8_4

4.1 Introduction

Fluorescent imaging, nowadays called "molecular imaging," represents a growing research field since it allows the direct visualization of biomolecules as they function in their natural cellular environment [1]. Moreover, fluorescent imaging has been significantly pushed forward by the sophisticating high resolution techniques, like PALM [2] and STED [3], that representatively are mentioned here. Currently, the key challenge for molecular imaging is the design and synthesis of tailor-made and photostable fluorescent probes and their conjugation to biologically relevant molecules. For imaging of proteins that comprise the largest fraction of biomolecules of interest inside the cells, a complete toolbox for fluorescent tagging of proteins has evolved since the pioneering work of Nobel laureates Shimomura [4], Chalfie [5], and Tsien [6], which nowadays enables ready analysis of protein location and function by fusion with the green fluorescent protein (and its many differently colored variants) to chimeric proteins. Although proteins play decisive roles in a lot of biological functions inside cells, non-proteinaceous biomolecules are not less important, and fluorescent labeling of those cellular components, including mainly nucleic acids and small molecules, has remained challenging [1]. Hence, visualizing of nucleic acids represents not only an important task for molecular imaging but also for chemical biology in general. From the preparative and organic–chemical viewpoint, fluorescent modification of nucleic acids, both DNA and RNA, is accessible by the phosphoramidite chemistry as building block chemistry. Fluorescent labels can be incorporated either synthetically into nucleic acids by their corresponding building blocks [7, 8] or postsynthetically by one of the recent sophisticating "click"-type reacting building blocks [9–12]. Biochemical preparation of longer pieces of fluorescently labeled DNA can be achieved by PCR amplification using modified nucleoside triphosphates [13, 14].

Herein, we summarize our work over the last decade to label nucleic acids chemically with fluorophores. Especially, we focused on the development of new photostable new cyanine-styryl dyes and on wavelength-shifting fluorescent probes ("DNA/RNA traffic lights") as promising tools for molecular imaging. The most important parameters that were pursued are excitation beyond 450 nm (to avoid cellular autofluorescence), brightness (defined as $\varepsilon \times \Phi_F$), photostability, energy transfer, selectivity, and sensitivity.

4.2 Isosteric and Non-isosteric Base Substitutions

In general, fluorophores can be conjugated directly to the heteroaromatic systems of DNA/RNA bases, conjugated to the ribofuranoside moieties of these nucleosides or incorporated into the base stack as DNA/RNA base replacements. Based on the expectation that the DNA architecture will play a major role for fluorophore interactions (*vide infra*), we chose primarily the DNA/RNA base replacement

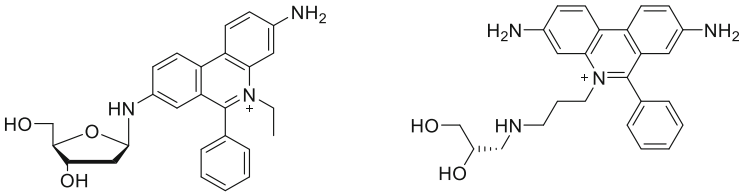

Fig. 4.1 Ethidium as non-isosteric DNA base replacements, either as nucleoside (*left*) or as nucleoside analog (*right*)

approach. Thereby, expanded conjugated systems of known staining agents like ethidium bromide and thiazole orange (for the latter one see Chap. 2) could be covalently attached to oligonucleotides such that they are able to intercalate into the base stack. The intercalating properties of ethidium bromide between two adjacent base pairs was first proposed by Lerman et al. [15] As an artificial DNA base, ethidium was firstly covalently attached directly to 2′-desoxyribofuranose (Fig. 4.1) [16]. Unfortunately, but also expectedly, this nucleoside bears hydrolytic instability especially under basic conditions. Thus, the sugar moiety was replaced by (*S*)-2-amino-1,3-propanediol as acyclic linker to achieve a better stability and to avoid degradation during solid phase DNA synthesis [17]. Incorporated into nucleic acids, UV/vis absorption shows the intercalation of the phenanthridinium group by a bathochromic shift and fluorescence by a hypsochromic shift, similar to the non-covalently bound ethidium.

However, large π-systems, such as those of ethidium bromide, obviously do not fit into B-DNA and hence are expected to disturb the natural DNA helix, which is reflected by melting temperature measurements. Hence, it is highly desirable to substitute natural bases by isosteric fluorophores. However, this is a challenge since small chromophore units do not exhibit fluorescence, and, if at all, are not excitable in the visible absorption range. One prominent and widely used example is 2-aminopurine [18]. Compared to adenosine, this constitutional isomer exhibits fluorescence and is able to form base pairs with thymidine (DNA) or uridine (RNA) (Fig. 4.2) [19]. The absorption of 2-aminopurine allows excitation separately and outside the DNA absorption range, but the emission is still in the UV-A range, quenched and significantly quenched in double-stranded DNA due to charge-transfer processes. A promising fluorophore in this regard is 4-aminophthalimide (API) [20]. The highly fluorescent and solvatochromic properties of this dye were exploited in many applications [21–24]. The shape and size fit to that of natural bases, especially purines, and the imide functionality allows base pairing to a specific counter base with a suitable hydrogen bonding pattern (Fig. 4.2). The C-nucleosides of API and 2,4-diaminopyrimidine (DAP) were incorporated into oligonucleotides as a new artificial, orthogonal, and fluorescent base pair [23]. UV/vis absorption and steady-state fluorescence spectroscopy showed that the glycosidic modification of the fluorophore does not affect its optical properties. If the API-modified DNA1 is hybridized with the complementary counter strands (carrying the natural nucleosides opposite to API), the double strand is strongly

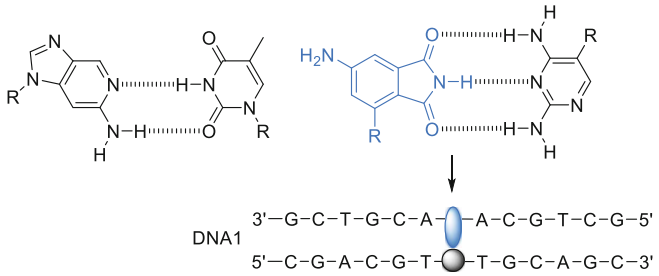

Fig. 4.2 Unnatural base pairs of 2-aminopurine nucleoside with thymidine (*left*) and 4-aminophthalimide (API) with 2,4-diaminopyrimidine (DAP), both as nucleosides (*right*) in DNA1; R = 2′-desoxyribose

destabilized compared to the non-modified duplexes. This results from poor stacking properties of the chromophore inside the DNA and the nonspecific hydrogen bonding pattern to the natural nucleobases. The similar effect is observed with DAP as counter base though it was desired to be complementarity to API. At higher temperatures (30–40 °C), the base pair between API and DAP closes and that shows that base stacking plays an important role in duplex stabilization even if the base pair does not significantly exceed the size of natural ones.

In single- and double-stranded DNA the API modification shows an absorption maximum that allows excitation at the border to the visible range and separated from the absorption of nucleic acids. Due to excimer forming between API and solvent molecules (especially protic solvents) the quantum yield of the chromophore in water is very low [25]. Incorporated into DNA the fluorescence represents a 2.7-fold increase compared to the "free" API. In the DNA double strand the fluorescence intensity is even doubled which indicates the intercalation of the chromophore into the rather nonpolar environment of DNA and the prevention of the excimer formation. The comparison of the API nucleoside to the other base surrogates (ethidium bromide, 2-aminopurine) shows its potential as a new artificial fluorescent DNA base. Especially the Stokes' shift of 140 nm for API in DNA is much better usable than the corresponding one for ethidium bromide (~105 nm).

4.3 Fluorescence Shifts with Thiazole Orange and Thiazole Red: From TO Dimers to "Traffic Lights"

As biological media and live cells show intrinsic background fluorescence, it is not only of importance to design molecular probes with excitation beyond 450 nm but also with a large wavelength shift between excitation and emission to separate them from each other. Alternatively to energy transfer processes (*vide infra*), excimer formation between two identical chromophores potentially yields significant shifts of the emission wavelength. DNA with interstrand and intrastrand dimers of pyrene

exhibit strong excimer-type fluorescence [26–32], also in molecular beacons [33–35]. However, the emission intensity of such fluorophore arrangements along DNA is potentially limited by aggregation of the dyes which typically results in self-quenching of the fluorescence. The excimer-type fluorescence of perylene diimides in DNA shifts the maximum from ~560 to ~660 nm, which can be used to detect and quantify single base variations [36, 37]. However, the low fluorescence quantum yields that are observed for perylene diimides in DNA represent a significant disadvantage for nucleic acid probing and imaging [38]. Among the brightly emitting and broadly applied cyanine dyes [39], thiazole orange (TO) represents a promising alternative to pyrene and PDI. TO exhibits an oxidation potential ($TO^+/TO^{\bullet 2+}$) of +1.4 V (vs. NHE) [40]. Together with $E_{00} = 2.4$ V for TO, the excitation is not sufficient for the photooxidation of DNA. This stands clearly in contrast to perylene diimide and pyrene. TO was extensively used as a non-covalently binding staining agent for nucleic acids [41]. This dye was linked covalently to the phosphodiester bridges [42–44] or to the 5′-terminus [45–47] of oligonucleotides. There are several reports about the synthesis of TO as DNA base surrogates using the nucleoside approach [48] or the approach to substitute the 2′-deoxyribofuranoside by serinol [49] or (S)-aminopropanediol [20, 50] as an acyclic linker (DNA2). In order to develop excimer-based DNA probes, two TO fluorophores were combined as interstrand chromophore pairs [51]. Both dyes were incorporated as DNA base substitutions using (S)-aminopropanediol and are forced in close proximity to each other by the surrounding double helical architecture (Fig. 4.3). Remarkably, the fluorescence of such duplexes bearing the interstrand TO dimer (DNA3) is shifted to a broad structureless band with a maximum around ~580 nm that corresponds to an orange-colored emission. We have shown that concomitantly with the cooperative thermal dehybridization of the whole duplex, the orange fluorescence of the TO dimer in the DNA double strand shifts back to the TO-typical green color in the single strands. That shows that the intact helical duplex is required as a structural framework for the bathochromic fluorescence shift. In contrast to the excimer-type fluorescence of DNA3, the emission of intrastrand TO dimers in DNA4 is not shifted but quenched significantly. In principal, the latter result is expected when cyanine dyes are excitonically coupled with each other in aggregates. We transferred this approach also to RNA. The interstrand TO dimer could be used for imaging of CHO cells transfected by TO-labeled RNA. In principal, the yellow-colored emission of the RNA double strand was distinguishable from the green TO emission of the RNA single strands by confocal microscopy [52].

Since the two fluorescence colors (green and orange/yellow) overlay, the TO dimer has an intrinsic disadvantage with respect to nucleic acid imaging. In order to tune the fluorescence wavelength shift, one TO dye was replaced by thiazole red (TR). The only difference between the two dyes is the slightly longer methine bridge (two carbons more) shifting the emission to longer wavelengths. Both dyes, TO and TR, as DNA base surrogates can be combined to an interstrand energy transfer pair (Fig. 4.4) [53].

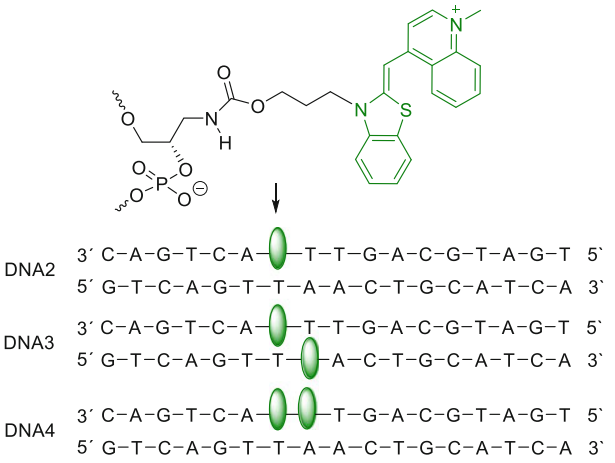

Fig. 4.3 Thiazole orange (TO) as DNA/RNA base replacement in DNA2–DNA4

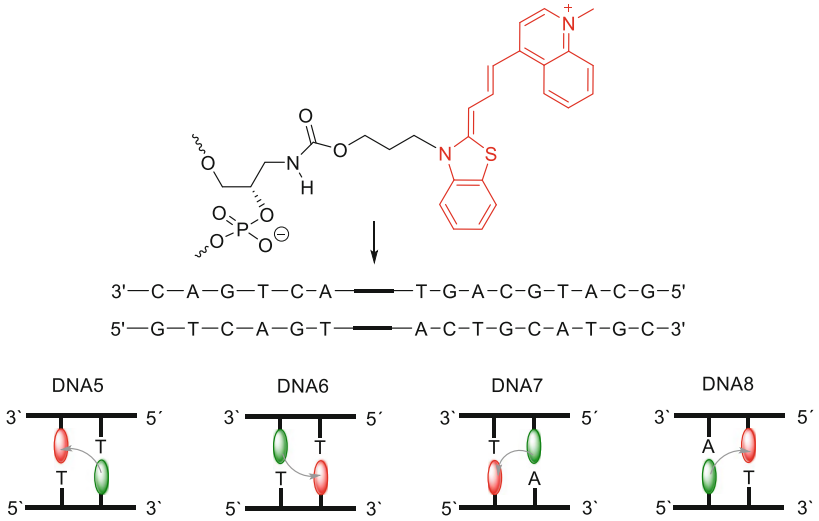

Fig. 4.4 Energy transfer between TO (*green*, for structure see Fig. 4.3) and TO as DNA/RNA base replacements in DNA5–DNA8

Remarkably, the melting temperature (T_m) of such TO/TR-labeled DNA double strands is reduced by less than 2 °C in comparison to natural A-T base pairs. The sequence complementarity of the neighboring sequence is not altered. In the initial orientation (**DNA5**), the fluorescence color ratio red/green (R/G) in vitro was 6 and could be also observed when DNA was microinjected in CHO-K1 cells and imaged in vivo [53]. The variation of all four possible 3′/5′-orientations (**DNA6–DNA8**) improved the R/G ratio to 20 just for one case [54]. The melting temperature analysis revealed the opposite effect; the double strands with good fluorescence

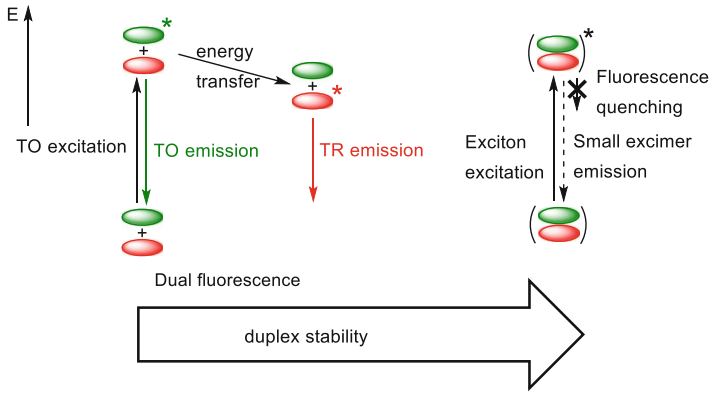

Fig. 4.5 Excitonic interactions between TO (*green*) and TR (*red*, for structures see Figs. 4.3 and 4.4) interfere with efficient energy transfer in duplexes with high stability

color ratios exhibited the lowest melting temperature and vice versa. Hence, the energy transfer efficiencies vary due to different excitonic interactions that interfere with the energy transfer. It became clear that the fluorescent readout which is based on an efficient energy transfer between TO and TR depends on the surrounding RNA or DNA double helical architecture and its stability. In particular, excitonic interactions between the two dyes potentially are responsible for a significant drop of the energy transfer efficiency (Fig. 4.5). If ground state dimers were excited, they cannot undergo energy transfer, since energy transfer requires the selective excitation of an energy donor (TO) and the proximity of an unexcited acceptor (TR). In order to elucidate this influence more systematically, we studied DNA hairpins that bear TO and TR in the stem region and allow the alteration of the duplex stability by variation of the loop construction [55].

So far, both dyes (TO and TR) were incorporated synthetically into oligonucleotides by using the two corresponding phosphoramidites as DNA building blocks. Our first attempt towards synthetically easier accessible wavelength-shifting DNA probes was that one of the dyes has been inserted postsynthetically via the Huisgen–Sharpless–Meldal cycloaddition. The first advantage is that this "click"-type chemistry is well established for oligonucleotide modification and makes possibly complicated and time-consuming syntheses of DNA building blocks unnecessary [10, 11]. Secondly, this approach offers the possibility that different dye combinations can be tested rapidly [56]. This was shown representatively with our very photostable cyanine–indole–quinolinium (CyIQ) dye in DNA9–DNA12 (Fig. 4.6). According to the optical-spectroscopic results, the uridine–adenosine base pair at the site of modification could block undesired excitonic (ground state) interactions between TO and TR that were observed in the past in certain TO/TR orientations and interfered with efficient energy transfer [57]. Consequently, the different diagonal orientations of the dyes do not show significant differences in the optical properties.

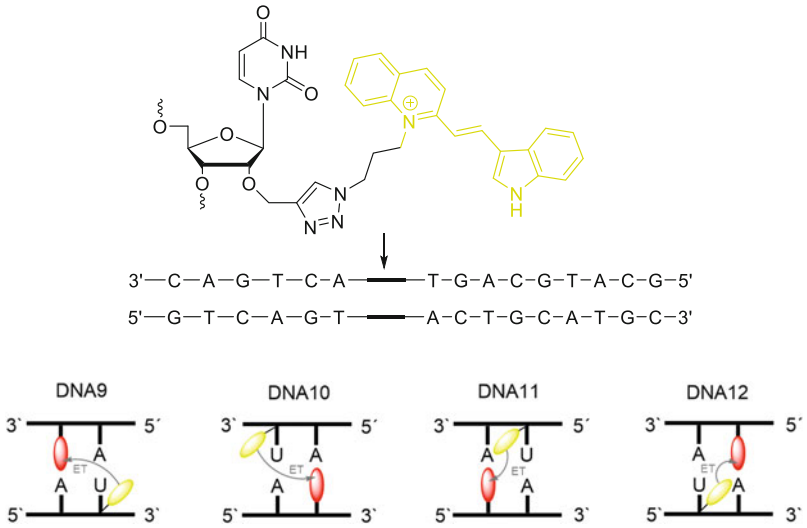

Fig. 4.6 Energy transfer between CyIQ (*yellow*) as 2′-modification and TR as DNA base replacement in DNA9–DNA12 (*red*, for structure see Fig. 4.4)

4.4 Photostable Cyanine-Styryl Dyes and Combinations as Pairs of 2′-Modification

Powerful nucleic acid probes are characterized by high quantum yields and brightness. Moreover, a large Stokes' shift, an excitation beyond $\lambda = 400$ nm, and a good photostability are beneficial. Our concept of "DNA traffic lights" initially used the fluorescent dyes TO and TR as base replacements together with (*S*)-2-amino-1,3-propanediol that mimics the sugar in common nucleosides [7]. The dyes were linked to the amino group via a propyl carbamate linker. As described above, the corresponding wavelength-shifting nucleic acid probes exhibit a good color contrast [58–61]. Additionally, the synthesis of the corresponding phosphoramidites—as well as the DNA synthesis using those—was time-consuming. Alternatively, the commercially available 2′-propargyluridine was inserted and subsequently modified by advanced fluorophores using the copper(I)-catalyzed azide-alkyne-"click" reaction [62]. The resulting triazole linkage is stable for many applications [10, 11, 63]. Accordingly, the conceptual approach of "DNA traffic lights" was transferred to a DNA system that can be prepared by "clicking" of azides for both dyes. Another goal was to enhance the photostability of the applied dyes (*vide infra*). Combining both efforts yielded a new powerful interstrand chromophore pair of cyanide-modified thiazole red (TR-CN) and cyanine indole pyridinium dye (CyIP) with better optical properties than the TO/TR combination (Fig. 4.7) [64]. In fact, by comparing the fluorescence loss during continuous irradiation, TR-CN with a half-life time of 66 min is more stable than TR (7 min). Moreover, the newly synthesized green fluorescent donor dye CyIP exhibited a strongly extended half-

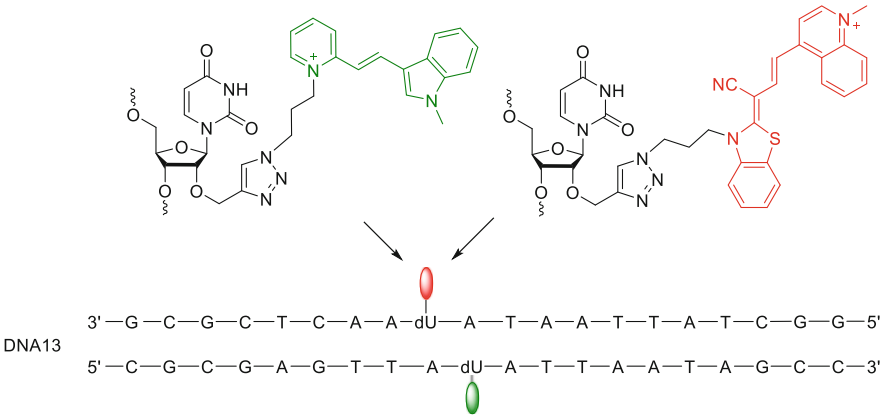

Fig. 4.7 Energy transfer between CyIP (*green*) and TR-CN (*red*) as 2′-modification in DNA13

life time of 636 min, compared to TOs (32 min) [64]. The melting temperatures of the TO/TR-modified double strands like DNA5–DNA8 show a slight destabilization through the incorporation of the base replacement in comparison to a completely unmodified double strand [53]. In contrast, duplexes like DNA13 are stabilized by ~2 °C in comparison to the unmodified double strand, which probably can be attributed to dye–DNA and dye–dye interactions [64]. The red-to-green color contrast of DNA13 with ratio of 77:1 is much better than TO/TR combination (20:1). This comparison shows clearly the great potential of the postsynthetic modification of nucleic acids compared to the elaborate synthesis and subsequent incorporation of modified phosphoramidites for each dye separately.

In addition to the improved synthetically accessibility of modified nucleic acid probes, the photostability of the used fluorophores plays an important role. A high photostability enables long-term observations and also reduces the phototoxicity of the respective dye, which has a special meaning for observations within living cells [65, 66]. Cyanines, in general, exhibit a high increase in fluorescence in the presence of nucleic acids, and hence they are suitable probes [67]. The main degradation pathway of the cyanine-styryl dyes takes place via formation of singlet oxygen (Fig. 4.8) [70]. This occurs when the dye molecule is in the triplet state. By triplet–triplet energy transfer—while the singlet–triplet energy gap of the dye must be greater than the energy gap between $^3O_2$ and $^1O_2$—very reactive singlet oxygen is formed and the dye molecule relaxes into the singlet ground state [58]. Further singlet oxygen leads to formation of reactive oxygen species (ROS) which make an additional contribution to the photodegradation of the dye [65, 66]. In addition to the relaxation of triplet state and simultaneous generation of singlet oxygen, it is also possible to form radical cations or anions, which are not fluorescent (blinking) and probably quite reactive. The photodegradation of dyes occurs consequently from both the excited triplet and radical states [59].

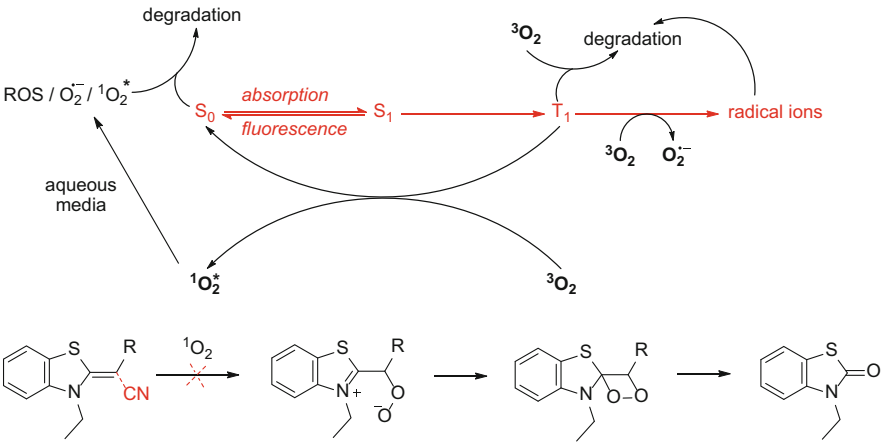

Fig. 4.8 General pathways of oxygen-dependent photodegradation of dyes (*red*) and example of photodegradation process of cyanine dyes according to Hahn et al. A cyanide substituents in α-position of the benzothiazole prevents this [68, 69]

In particular, the cyano substituent positioned at the monomethine bridge of TR-CN increases the photostability by a factor of 9 [64]. This tracks well with observations by Hahn et al. that singlet oxygen attacks the α-positioned carbon atom of the benzothiazole unit of corresponding cyanine dyes. In the further course of the reaction, the 1,2-dioxetanes and finally the benzothiazolones are formed through cycloreversion. According to results by Armitage et al., the cyanine dyes that are substituted in α-position of the benzothiazole part by cyanide do not show reactivity towards singlet oxygen; thus, the photostability is increased [68]. Armitage et al. published the synthesis of the corresponding TO derivative (TO-CN). The assumption that TO-CN cannot planarize by binding to DNA due to the cyano substituent was confirmed by the X-ray analysis [69]. Despite the superior photostability, we expected from TO-CN that there is no benefit for usage of this probe for nucleic acids. Since the quantum yield of TO-CN is very small, it can be assumed that the chromophore mainly relaxes to the ground state via vibrational relaxation and an internal conversion process.

By today, a broad set of cyanine-styryl dyes could be realized, and very efficient energy transfer pairs are expected to come out of this. Nearly all of our cyanine-styryl dyes developed by our group show outstanding optical behavior combined with better photostability compared to the initial lead structure CyIQ (Fig. 4.9) [64, 71–74]. Especially the quantum yields show a very significant increase in the presence of double-stranded DNA (Table 4.1) which makes these dyes suitable "light-up" probes for nucleic acids in general.

Further investigations of the photodegradation processes of selected cyanine-styryl dyes revealed interesting substituent effects and enabled us to get first hints for a structure–activity relationship (Fig. 4.10) [74]. CyIQ (**1**), **5**, and **8** were

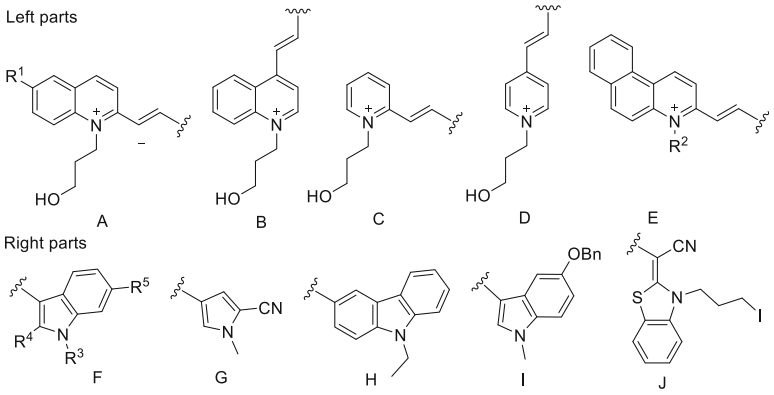

Dye	Left part	Substituents	Right part	Substituents
1 (CyIQ)	A	R^1=H	F	R^3=R^4=R^5=H
3	A	R^1=H	F	R^3=CH_3, R^4=R^5=H
4	A	R^1=F	F	R^3=R^4=R^5=H
5	A	R^1=OCH_3	F	R^3=R^4=R^5=H
6	A	R^1=OCH_3	F	R^3=CH_3, R^4=R^5=H
7	A	R^1=H	H	
8	B		F	R^3=R^4=R^5=H
9	B		F	R^3=CH_3, R^4=R^5=H
10	B		F	R^3=R^4=H, R^5=*i*Pr
11	B		F	R^3=CH_3, R^4=R^5=*i*Pr
12	B		F	R^3=H, R^4=Ph, R^5=H
13	B		F	R^3=CH_3, R^4=Ph, R^5=H
14	B		H	
15	B		I	
16	C		F	R^3=R^4=R^5=H
2 (CyIP)	C		F	R^3=CH_3, R^4=R^5=H
17	C		F	R^3=H, R^4=Ph, R^5=H
18	C		F	R^3=CH_3, R^4=Ph, R^5=H
19	D		F	R^3=R^4=R^5=H
20	D		F	R^3=CH_3, R^4=R^5=H
21	D		F	R^3=H, R^4=Ph, R^5=H
22	D		F	R^3=CH_3, R^4=Ph, R^5=H
23	D		G	
24	E	R^1=$(CH_2)_3$-OH	F	R^3=R^4=R^5=H
25	E	R^1=CH_3	J	

Fig. 4.9 Structures of our cyanine-styryl dyes **1**–**25**

irradiated and the photodegradation products were analyzed by nano ESI-MS. The primary photodegradation product of **1** is oxidized at the 4-position of the quinolinium part and at the 2-position of the indole part. The electron density is increased at the 2-position by methylation of the indole nitrogen, and in this case an attack by singlet oxygen and other ROS is significantly reduced. Thus, a mechanism for the photooxidation of the indole part could be proposed. While maintaining the CyIQ-backbone, the methoxylation at position 6 of the quinolinium part increases the electron density at the 4-position and leads to an enhanced photostability. The only observable photooxidation of dye **5** occurs at position 6 via a proposed demethylating mechanism, which increases the photostability a lot

Table 4.1 Quantum yields of dyes non-covalently bound to double-stranded (ds)DNA, as covalent modification in single-stranded (ds) DNA, as covalent modification in dsDNA and half-lifetime of fluorescence during continuous irradiation

Dye	Φ_F (non-covalent)[a] (%)	Φ_F (ssDNA)[b] (%)	Φ_F (dsDNA)[b] (%)	$t_{1/2}$[c] (min)
TO [20, 72]	16.5	16.8	–	32
TR [20, 72]	11.6	26.2	–	7
TR-CN [64]	32.9	59.9	66.8	66
CyIQ(**1**) [71, 72]	4.4	25.5	10.9	90
CyIP(**2**) [64]	2.4	9.8	9.4	225
3 [71]	6.6	40.4	20.4	205
4 [71]	1.5	–	–	50
5 [71]	5.7	–	–	264
6 [71]	5.8	47.1	21.2	425
7 [71]	6.1	–	–	130
8 [71]	12.8	–	–	186
9 [71]	17.6	51.2	33.2	441
10 [71]	12.7	–	–	67
11 [71]	15.3	43.7	26.1	241
12 [71]	5.2	–	–	101
13 [73, 74]	18.8	39.0	31.9	317
14 [71]	12.5	57.2	35.8	134
15	3.6	–	–	269
16 [74]	1.2	–	–	187
17 [74]	2.3	–	–	146
18 [74]	4.1	10.2	8.9	78
19 [74]	1.9	–	–	636
20 [60]	4.6	36.2	28.3	293
21 [74]	5.8	–	–	162
22 [74]	13.7	–	–	49
23 [60]	1.0	5.2	4.6	658
24 [71]	17.0	–	–	13
25 [74]	35.5	–	–	11

[a]10 μM dye + 4 equiv. unmodified dsDNA(17mer)
[b]2.5 μM ss or dsDNA
[c]Photostability, 10 μM dye, 2.5 μM unmodified dsDNA, 75 W Xenon lamp equipped with a 305 nm cutoff filter. All measurements were recorded in 10 mM NaP_i (pH 7) and 250 mM NaCl in 5 % ethanol

[71]. Furthermore, the displacement of the dimethine bridge from the 2- to the 4-position on the quinolinium part leads to increased photostability. The combination of methylation of the indole nitrogen and methoxylation of the quinoline part at the 6-position results in an outstanding fluorophore with a very long half-life time and very good optical properties for fluorescent imaging [71].

Selected dyes with promising optical properties and photostability were incorporated as 2′-modifications into oligonucleotides via “click” chemistry. In general, those singly modified DNA single strands and double strands show significantly

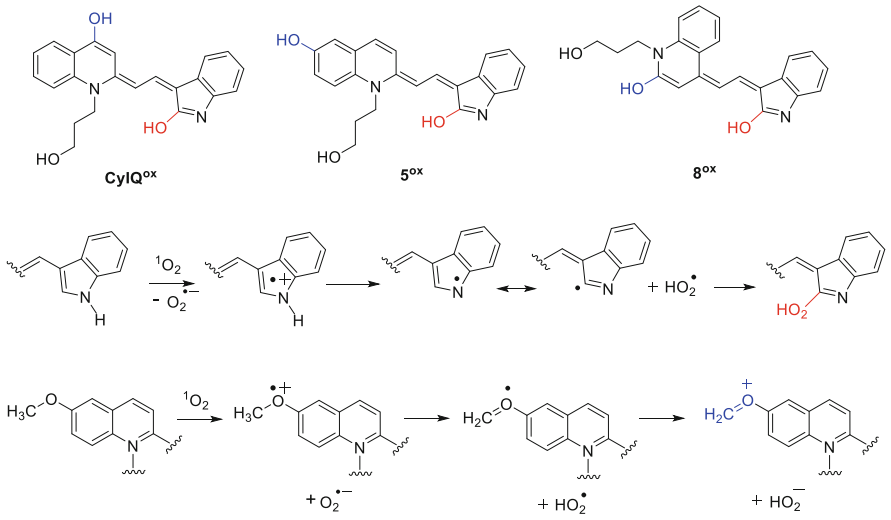

Fig. 4.10 Main photodegradation products of CyIQ (**1**), **5**, and **8**, and the proposed photooxidation processes

Table 4.2 Excitation/emission wavelength (λ_{exc}, λ_{em}), apparent Stokes' shifts ($\lambda_{app.Stokes}$), energy transfer efficiencies and contrast (corrected values via $I_{F,acceptor}/I_{F,donor}$)

Donor dye	Acceptor dye	λ_{exc} (nm)	λ_{em} (nm)	$\lambda_{app.Stokes}$ (nm)	Energy transfer efficiency[a] (%)	Color contrast[b]	T_m[c] (°C)
16	**13**	435	616	181	92.1	104	66.9
20	**13**	435	613	178	85.6	72	66.2
18	TR-CN	430	613	183	85.4	102	66.5
	13	435	613	178	88.9	133	66.7
23	TR-CN	389	607	218	85.2	131	66.7
	14	389	637	248	92.8	32	66.1
	9	389	609	220	95.4	67	64.9
	13	389	615	226	92.1	74	65.6
	3	391	572	181	90.2	69	65.3
	6	391	566	175	86.5	66	65.3

[a]Determined via fluorescence lifetimes
[b]Determined by the fluorescence intensity at the corresponding fluorescence maxima
[c]Compared to a completely unmodified double strand with $T_m = 64.5$ °C. All measurements were recorded with 2.5 μM dsDNA in 10 mM NaP_i (pH 7) and 250 mM NaCl

better quantum yields than the corresponding dyes non-covalently bound double-stranded DNA (Table 4.1). Based on these results, it looked reasonable to combine selected dyes as covalent 2′-modifications to energy transfer pairs similar to the approach already described for the CyIP/TR-CN pair (see Fig. 4.7). All of these dye combinations represents excellent wavelength-shifting DNA probes since they show very efficient energy transfer (86–95 %) and high emission color contrasts (up to 133, Table 4.2). In addition to the pairs with red-green-transfer emission

color change also yellow-blue-pair were realized, based on the blue fluorescent donor dye **23** with a half-life time of 658 min (which among the highest photostability of all presented dyes herein). The determination of the melting temperatures revealed the stabilization of the double-modified strands compared to the unmodified double strand presumably by enforced dye–dye and dye–nucleic acid interactions.

4.5 Summary

The double helical architecture around two fluorophores is crucial for efficient photophysical interactions that range from excitonic and excimer-type to energy transfer interactions. This is equally important for fluorescent labels as isosteric and non-isosteric DNA base replacements. Especially, the latter one yield fluorescent DNA and RNA systems with dual emission color readout as wavelength-shifting probes. Especially, our DNA and RNA "traffic light" that combine the green emission of TO with the red emission of TR represented an important tool for fluorescent probing since it was applied as molecular beacons [61], as aptasensors [54] and as probes to monitor the siRNA delivery into cells [75]. The concept can be transferred to a DNA system that is synthetically easily accessible since the dyes were attached postsynthetically as 2′-modifications. Using newly synthesized dyes of the cyanine-styryl type new nucleic acid probes were realized with high quantum yields and excellent photostability. Combined as energy transfer pairs not only wavelength-shifting DNA probes with red-green-transfer emission color change but also yellow-blue pairs were realized. All of them show good emission color contrasts due to very efficient energy transfer. These wavelength-shifting probes have a significant potential to be applied on the RNA level for molecular imaging of living cells.

Acknowledgements This research is supported by the DFG (Grant Nos. Wa 1386/9, Wa1386/13, Wa 1386/17, and GRK 2039).

References

1. Chang PV, Bertozzi CR (2012) Imaging beyond the proteome. Chem Commun 48:8864–8879
2. Betzig E, Patterson GH, Sougrat R, Lindwasser OW, Olenych S, Bonifacino JS, Davidson MW, Schwartz JL, Hess HF (2006) Imaging intracellular fluorescent proteins at nanometer resolution. Science 313:1642–1645
3. Klar TA, Jakobs S, Dyba M, Egner A, Hell SW (2000) Fluorescence microscopy with diffraction resolution barrier broken by stimulated emission. Proc Natl Acad Sci U S A 97:8206–8210
4. Shimomura O (2009) Discovery of green fluorescent protein (GFP) (Nobel lecture). Angew Chem Int Ed 48:5590–5602

5. Chalfie M (2009) GFP: lighting up life (Nobel lecture). Angew Chem Int Ed 48:5603–5611
6. Tsien RY (2009) Constructing and exploiting the fluorescent protein paintbox (Nobel lecture). Angew Chem Int Ed 48:5612–5626
7. Schmucker W, Wagenknecht H-A (2012) Organic chemistry of DNA functionalization; chromophores as DNA base substitutes versus DNA base/2′-modifications. Synlett 23:2435–2448
8. Sinkeldam RW, Greco NJ, Tor Y (2010) Fluorescent analogs of biomolecular building blocks: design, properties, and applications. Chem Rev 110:2579–2619
9. Weisbrod SH, Marx A (2008) Novel strategies for the site-specific labelling of nucleic acids. Chem Commun 44:5675–5685
10. El-Sagheer AH, Brown T (2010) Click chemistry with DNA. Chem Soc Rev 39:1388–1405
11. Gramlich PM, Wirges CT, Manetto A, Carell T (2008) Postsynthetic DNA modification through the copper-catalyzed azide-alkyne cycloaddition reaction. Angew Chem Int Ed 47:8350–8358
12. Merkel M, Peewasan K, Arndt S, Ploschik D, Wagenknecht H-A (2015) Copper-free postsynthetic labeling of nucleic acids by means of bioorthogonal reactions. ChemBioChem 16:1541–1553
13. Hocek M, Fojta M (2011) Nucleobase modification as redox DNA labelling for electrochemical detection. Chem Soc Rev 40:5802–5814
14. Hocek M (2014) Synthesis of base-modified 2′-deoxyribonucleoside triphosphates and their use in enzymatic synthesis of modified DNA for applications in bioanalysis and chemical biology. J Am Chem Soc 79:9914–9921
15. Lerman LS (1961) Structural considerations in the interaction of DNA and acridines. J Mol Biol 3:18–30
16. Huber R, Amann N, Wagenknecht H-A (2004) Synthesis of DNA with phenanthridinium as an artificial DNA base. J Org Chem 69:744–751
17. Valis L, Wagenknecht H-A (2007) Phenanthridinium as an artificial DNA base: comparison of two alternative acylic 2′-deoxyribose substitutes. Synlett 13:2111–2115
18. O'Neill MA, Barton JK (2002) 2-aminopurine: a probe of structural dynamics and charge transfer in DNA and DNA:RNA hybrids. J Am Chem Soc 124:13053–13066
19. Dallmann A, Dehnel L, Peters T, Mügge C, Griesinger C, Tuma J, Ernsting NP (2010) 2-aminopurine incorporation perturbs the dynamics and structure of DNA. Angew Chem Int Ed 49:5989–5992
20. Holzhauser C, Berndl S, Menacher F, Breunig M, Göpferich A, Wagenknechr H-A (2010) Synthesis and optical properties of cyanine dyes as fluorescent DNA base substitutions for live cell imaging. The journal Eur J Org Chem 1239–1248
21. Vazquez ME, Rothman DM, Imperiali B (2004) A new environment-sensitive fluorescent amino acid for Fmoc-based solid phase peptide synthesis. Org Biomol Chem 2:1965–1966
22. Sharma V, Lawrence DS (2009) Über-responsive peptide-based sensors of signaling proteins. Angew Chem Int Ed 48:7290–7293
23. Fiebig T (2009) Exciting DNA. J Phys Chem B 113:9348–9349
24. Soujanya T, Krishna TSR, Samanta A (1992) The nature of 4-aminophthalimide-cyclodextrin inclusion complexes. J Phys Chem 96:8544–8548
25. Wenge U, Wagenknecht H-A (2011) Synthetic GFP chromophore and control of excited-state proton transfer in DNA. Synthesis 3:502–508
26. Kashida H, Asanuma H, Komiyama M (2006) Insertion of two pyrene moieties into oligodeoxyribonucleotides for the efficient detection of deletion polymorphisms. The journal Chem. Commun. 2768–2770
27. Trkulja I, Haener R (2007) Monomeric and heterodimeric triple helical DNA mimics. J Am Chem Soc 129(25):7982–7989
28. Malinovskii VL, Samain F, Haener R (2007) Helical arrangement of interstrand stacked pyrenes in a DNA framework. Angew Chem Int Ed 46(24):4464–4467

29. Balakin KV, Korshun VA, Mikhalev II, Maleev GV, Malakhov AD, Prokhorenko IA, Berlin YA (1998) Conjugates of oligonucleotides with polyaromatic fluorophores as promising DNA probes. Biosens Bioelectron 13:771–778
30. Yamana K, Iwai T, Ohtani Y, Sato S, Nakamura M, Nakano H (2002) Bis-pyrene-labeled oligonucleotides: sequence specificity of excimer and monomer fluorescence changes upon hybridization with DNA. Bioconjug Chem 13(6):1266–1273
31. Yamana K, Fukunaga Y, Ohtani Y, Sato S, Nakamura M, Kim WJ, Akaike T, Maruyama A (2005) DNA mismatch detection using a pyrene-excimer-forming probe. The journal Chem. Commun. 2509–2511
32. Seio K, Mizuta M, Tasaki K, Tamaki K, Ohkubo A, Sekine M (2008) Hybridization-dependent fluorescence of oligodeoxynucleotides incorporating new pyrene-modified adenosine residues. Bioorg Med Chem 16(17):8287–8293
33. Fujimoto K, Shimizu H, Inouye M (2004) Unambiguous detection of target-DNAs by excimer-monomer switching molecular beacons. J Org Chem 69:3271–3275
34. Chen Y, Yang CJ, Wu Y, Conlon P, Kim Y, Lin H, Tan W (2008) Light-switching excimer beacon assays for ribonuclease H kinetic study. ChemBioChem 9(3):355–359
35. Conlon P, Yang CJ, Wu Y, Chen Y, Martinez K, Kim Y, Stevens N, Marti AA, Jockusch S, Turro NJ, Tan W (2008) Pyrene excimer signaling molecular beacons for probing nucleic acids. J Am Chem Soc 130(1):336–342
36. Wagner C, Wagenknecht H-A (2006) Perylene-3,4:9,10-tetracarboxylic acid bisimide dye as an artificial DNA base surrogate. Org Lett 8:4191–4194
37. Baumstark D, Wagenknecht H-A (2008) Perylene bisimide dimers as fluorescent glue for DNA and for base mismatch detection. Angew Chem Int Ed 47:2652–2654
38. Zeidan TA, Carmieli R, Kelley RF, Wilson TM, Lewis FD, Wasielewski MR (2008) Charge-transfer in DNA in hairpin conjugates with perylenediimide as a base-pair surrogate. J Am Chem Soc 130:13945–13955
39. Mishra A, Behera RK, Mishra BK, Behera GB (2000) Cyanines during the 1990s. A Review. Chem Rev 100:1973–2011
40. Hosoi K, Hirano A, Tani T (2001) Dynamics of photocreated positive holes in silver bromide microcrystals with adsorbed cyanine dyes. J Appl Phys 90:6197–6204
41. Glazer AN, Rye HS (1992) Stable dye-DNA intercalation complexes as reagents for high-sensitivity fluorescence detection. Nature 359:859–861
42. Lartia R, Asseline U (2006) New cyanine-oligonucleotide conjugates: relationships between chemical structures and properties. Chem Eur J 12:2270–2281
43. Privat E, Asseline U (2001) Synthesis and binding properties of oligo-2′-deoxyribonucleotides covalently linked to a thiazole orange derivative. Bioconjug Chem 12:757–769
44. Privat E, Melvin T, Asseline U, Vigny P (2001) Oligonucleotide-conjugated thiazole orange probes as "light-up" probes for messenger ribonucleic acid molecules in living cells. Photochem Photobiol 74:532–541
45. Algar WR, Massey M, Krull UJ (2006) Fluorescence resonance energy transfer and complex formation between thiazole orange and various dye-DNA conjugates: implications in signaling nucleic acid hybridization. J Fluoresc 16:555–567
46. Asseline U, Chassignol M, Aubert Y, Roig V (2006) Detection of terminal mismatches on DNA duplexes with fluorescent oligonucleotides. Org Biomol Chem 4:1949–1957
47. Wang X, Krull UJ (2005) Synthesis and fluorescence studies of thiazole orange tethered onto oligonucleotide: development of a self-contained DNA biosensor on a fiber optic surface. Bioorg Med Chem Lett 15:1725–1729
48. Hövelmann F, Bethge L, Seitz O, Single Labeled DNA (2012) FIT probes for avoiding false-positive signaling in the detection of DNA/RNA in qPCR or cell media. ChemBioChem 13:2072–2081
49. Bethge L, Singh I, Seitz O (2010) Designed thiazole orange nucleotides for the synthesis of single labelled oligonucleotides that fluoresce upon matched hybridization. Org Biomol Chem 8:2439–2448

50. Menacher F, Rubner M, Berndl S, Wagenknecht H-A (2008) Thiazole orange and Cy3: improvement of fluorescent DNA probes using short range electron transfer. J Org Chem 73:4263–4266
51. Berndl S, Wagenknecht H-A (2009) Fluorescent color readout of DNA hybridization with thiazole orange as an artificial DNA base. Angew Chem Int Ed 48:2418–2421
52. Berndl S, Breunig M, Gopferich A, Wagenknecht HA (2010) Imaging of RNA delivery to cells by thiazole orange as a fluorescent RNA base substitution. Org Biomol Chem 8(5):997–999
53. Yoon TP, Ischay MA, Du J (2010) Visible light photocatalysis as a greener approach to photochemical synthesis. Nat Chem 2:527–532
54. Holzhauser C, Wagenknecht HA (2012) "DNA traffic lights": concept of wavelength-shifting DNA probes and application in an aptasensor. ChemBioChem 13(8):1136–1138
55. Barrois S, Wörner S, Wagenknecht H-A (2014) The role of duplex stability for wavelength-shifting fluorescent DNA probes: energy transfer vs. exciton interactions in DNA "traffic lights". Photochem Photobiol Sci 13:1126–1129
56. Berndl S, Herzig N, Kele P, Lachmann D, Li X, Wolfbeis OS, Wagenknecht H-A (2009) Comparison of a nucleosidic vs. a non-nucleosidic postsynthetic "click" modification of DNA with base-labile fluorescent probes. Bioconjug Chem 20:558–564
57. Holzhauser C, Rubner MM, Wagenknecht H-A (2013) Energy transfer-based wavelength-shifting DNA probes with "clickable" cyanine dyes. Photochem Photobiol Sci 12:722–724
58. Wilkinson F, Abdel-Shafi AA (1997) Mechanism of quenching of triplet states by oxygen: biphenyl derivatives in acetonitrile. J Phys Chem A 101:5509–5516
59. Zheng Q, Juette MF, Jockusch S, Wasserman MR, Zhou Z, Altman RB, Blanchard SC (2014) Ultra-stable organic fluorophores for single-molecule research. Chem Soc Rev 43:1044–1056
60. Bohländer PR, Vilaivan T, Wagenknecht H-A (2015) Strand displacement and duplex invasion into double-stranded DNA by pyrrolidinyl peptide nucleic acids. Org Biomol Chem 13 (35):9223–9230
61. Holzhauser C, Wagenknecht H-A (2011) In-stem labeled molecular beacons for distinct fluorescent colort readout. Angew Chem Int Ed 50:7268–7272
62. Huisgen R (1962) 1,3-Dipolar cycloaddition. Past and future. Angew Chem Int Ed 2:565–598
63. Grotli M, Douglas M, Eritja R, Sproat BS (1998) 2′-*O*-propargyl oligoribonucleotides: synthesis and hybridisation. Tetrahedron 54:5899–5914
64. Bohländer PR, Wagenknecht H-A (2014) Synthesis of a photostable energy-transfer pair for "DNA traffic lights". The journal Eur. J. Org. Chem. 7547–7551
65. Kassab K (2002) Photophysical and photosensitizing properties of selected cyanines. J Photochem Photobiol B 68:15–22
66. Davies MJ (2004) Reactive species formed on proteins exposed to singlet oxygen. Photochem Photobiol Sci 3:17–25
67. Armitage BA (2005) Cyanine dye-DNA interactions: intercalation, groove binding, and aggregation. Top Curr Chem 253:55–76
68. Toutchkine A, Nguyen D-V, Hahn KM (2007) Merocyanine dyes with improved photostability. Org Lett 9:2775–2777
69. Shank NI, Pham HH, Waggoner AS, Armitage BA (2013) Twisted cyanines: a non-planar fluorogenic dye with superior photostability and its use in a protein-based fluoromodule. J Am Chem Soc 135:242–251
70. Toutchkine A, Kraynov V, Hahn K (2004) Solvent-sensitive dyes to report protein conformational changes in living cells. J Am Chem Soc 125:4132–4145
71. Bohländer P, Wagenknecht H-A (2013) Synthesis and evaluation of cyanine-styryl dyes with enhanced photostability for fluorescent DNA staining. Org Biomol Chem 11:7458–7462
72. Rubner M, Holzhauser C, Bohländer P, Wagenknecht H-A (2012) A "clickable" styryl dye for fluorescent DNA labeling by excitonic and energy transfer interactions. Chem Eur J 18:1299–1302
73. Walter H-K, Bohländer PR (2015) Development of a wavelength-shifting fluorescent module for the adenosine aptamer using photostable cyanine dyes. ChemistryOpen 4:92–96

74. Bohländer PR, Wagenknecht H-A (2015) Bright and photostable cyanine-styryl chromophores with green and red fluorescence color for DNA staining. Methods Appl Fluores 3:044003
75. Holzhauser C, Liebl R, Göpferich A, Wagenknecht H-A, Breunig M (2013) RNA "traffic lights": an analytical tool to monitor siRNA integrity. ACS Chem Biol 3:6331–6333

Chapter 5
DNA-Assisted Multichromophore Assembly

Tadao Takada, Mitsunobu Nakamura, and Kazushige Yamana

Abstract Chromophores in a π-stacked system show unique photophysical properties, such as energy and charge transfer through the strong electronic coupling interaction between the chromophores. A variety of supramolecular structures to realize efficient light-harvesting and charge conduction properties have been designed and prepared. DNA and RNA are a useful building block and a platform to incorporate functional molecules at defined positions through chemical modification of DNA. Therefore, we can construct a one-dimensional or helical array of multichromophores in DNA or along RNA duplexes. This chapter deals with our recent approaches to DNA-assisted multichromophore assembly that involves the synthesis of pyrene π-stack array on RNA, perylene π-stack array in DNA, charge transfer complex formed in DNA, and multi-organic-dyes assembly based on the interaction between Zn(II)-cyclen and thymine base in DNA.

Nucleic acids and their analogues can be used as scaffolds or templates in a bottom-up approach to arrange molecules in nanoarchitectures [1, 2]. Among nucleic acid-based nanoobjects, spatially arranged π-aromatic chromophores are currently of interest because they provide an efficient medium for excitation energy and electron migration, which would be usable in functional nanomaterials [2, 3]. For instance, pyrene or perylene chromophores can stack on one another with substantial overlap in their π-orbitals, allowing one-dimensional transport of charge carriers [3–12]. These columnar structures have potential applications in optical and molecular electronic devices, such as organic field effect transistors and solar cells [13–20].

There are many advantages in multichromophore systems over single chromophores. One is the high absorption that is particularly useful in light-harvesting applications [21–23]. The other is the photophysical properties that are different from the monomeric components. For examples, interactions between chromophores in the ground state and excited state give new complexes such as excimers and exciplexes that exhibit unique fluorescence at the different wavelength from the monomeric component [24–26]. Multichromophore systems have another

T. Takada • M. Nakamura • K. Yamana (✉)
Department of Applied Chemistry, Graduate School of Engineering, University of Hyogo, 2167 Shosha, Himeji, Hyogo 671-2280, Japan
e-mail: yamana@eng.u-hyogo.ac.jp

K. Nakatani, Y. Tor (eds.), *Modified Nucleic Acids*, Nucleic Acids and Molecular Biology 31, DOI 10.1007/978-3-319-27111-8_5

advantage that the photophysical properties can be controlled through arrangement of chromophores in geometrical and directional manners [27].

DNA- or RNA-assisted assembly of multichromophores has been accomplished using either covalent or noncovalent approaches [28]. The recent advances in chemical and biochemical methods for DNA/RNA synthesis and modification permit us to prepare the covalent assembly of multichromophores with well-defined structures [24]. Although the covalent approach is common and reliable, it faces the problem that the synthesis of DNA–chromophore conjugates is tedious and time-consuming. On contrary, noncovalent interactions between chromophores and DNA structures could be used in an easy and convenient way to drive the formation of supramolecular multichromophoric system [29–34]. However, there are limited numbers of methods for placing diverse dyes at precise locations in DNA.

Over the recent several years, we have been interested in development of methods for the synthesis of DNA/RNA-mutichromophore systems. The purpose of this chapter is to overview our methods to assemble multichromophores on DNA and RNA. Some potential applications of these systems to biosensors and electronic devices will be discussed.

5.1 Pyrene π-Stack Array on RNA

Pyrene shows a structured fluorescence of the monomeric excited state (monomer) and a broad and structureless fluorescence of the excited dimer (excimer). Over the many years, because of the sensitivity of pyrene fluorescence to its environment, pyrene and its derivatives have been frequently utilized as a fluorescence probe for the detection of the dynamics or structural properties of synthetic polymers [35, 36], phospholipids [37–40], polypeptides [41–43], and DNA [44–48]. Recently, pyrene and its π-stack assembly have attracted much interest in applications as organic semiconductors [49]. Organized pyrene π-stacks are important to control their electronic properties, such as the energy gap and charge carrier mobility in the development of electronic and optoelectronic devices.

The assembly of pyrene molecules in an aqueous solution presents a significant challenge. Biomolecules such as peptides and nucleic acids are a powerful tool for not only the construction of nanoarchitectures [50–55], but also the integration of molecules [56–67] and nanomaterials [68–73] in a defined space with a defined distance, because of their programmable self-assembling properties. Hence, we can utilize biomolecules for pyrene assembly. For examples, Sisido and co-workers showed a one-dimensional pyrene helical arrangement using the poly(L-1-pyrenylalanine) backbone [74, 75]. The pyrene-stacked nanostructures constructed in the cavity of a tobacco mosaic virus rod was reported by Endo, Majima, and co-workers [76]. Kool and co-workers demonstrated the pyrene π-stack arrays on a DNA-like backbone using pyrene-substituted C-nucleoside [77]. Wagenknecht and co-workers proved the formation of a pyrene π-stacked array in multiple 5-(pyren-1-yl)-2-deoxyuridines incorporating DNAs [4]. Asanuma and co-workers

developed pyrene-tethered threoninol linkers and constructed pyrene arrays inside the DNA duplexes [78]. Häner and co-workers showed the DNA-assisted formation of π-stacked arrays using oligopyrenotides [3]. Kim and co-workers demonstrated that interstrand pyrene stacking occurred in DNA duplexes having 8-ethynylpyrene-substituted deoxyadenosines [79].

We have disclosed that a pyrene, which was covalently attached via one carbon linker to the 2′-*O*-sugar residue of uridine, was located outside of the A-form RNA duplexes. The attachment of a pyrene in a similar way to the B-form DNA duplexes resulted in pyrene intercalation. Thus pyrene-modified RNA duplex exhibits strong fluorescence, while pyrene-modified DNA duplex shows very weak emission (Fig. 5.1) [80]. The observed weak fluorescence is resulted from emission quenching that occurs efficiently by virtue of the stacking interactions between the pyrene ring and the base pairs in DNA. In the RNA duplex, the efficient quenching does not occur because of the outside location that leads to the strong emission. By incorporation of nitrobenzene as an electron accepter into the RNA duplex, the efficient charge transfer was observed from photo-excited pyrene to the accepter over a long distance [81, 82]. This observation indicates that RNA duplex is an attractive medium for charge migration.

The consecutive incorporation of the pyrene-modified uridine into an RNA strand exhibited excimer fluorescence upon hybridization with a RNA complement but not with a DNA complement. In addition, the binding of a pyrene-modified RNA sequence to a mismatch containing RNA complement does not afford the excimer fluorescence [83, 84]. Therefore, the pyrene-modified RNA oligonucleotide can be used as a fluorescence probe for RNA sequences. When more pyrenes

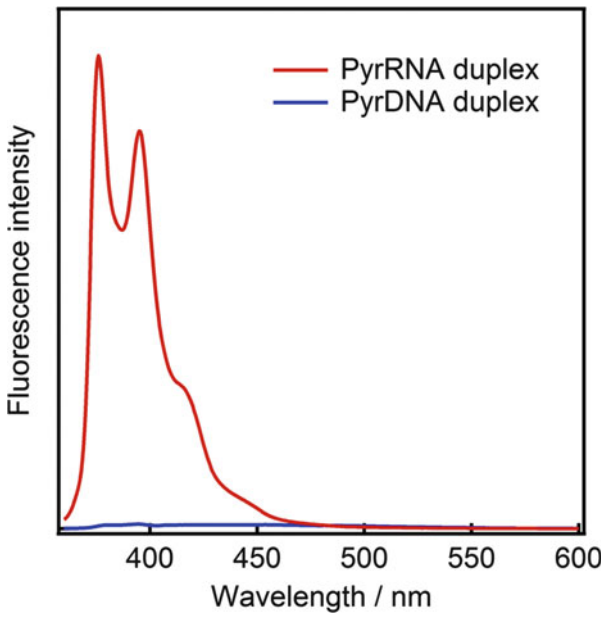

Fig. 5.1 Fluorescence spectra of pyrene–RNA duplex and pyrene–DNA duplex

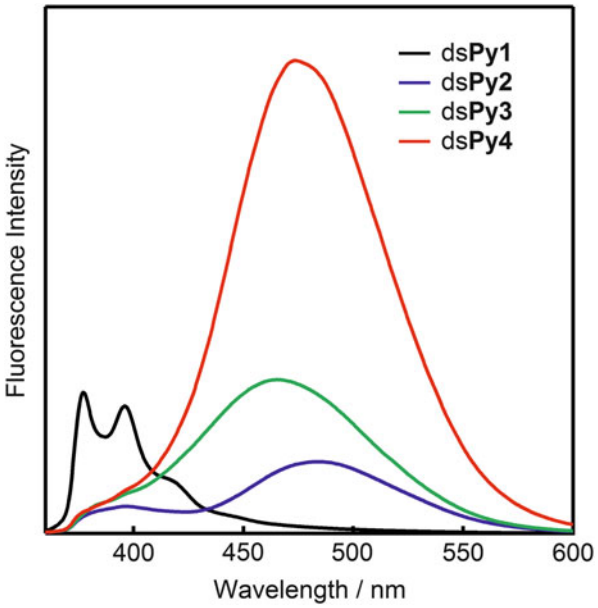

Fig. 5.2 Fluorescence spectra of multiple pyrene-modified RNA duplexes

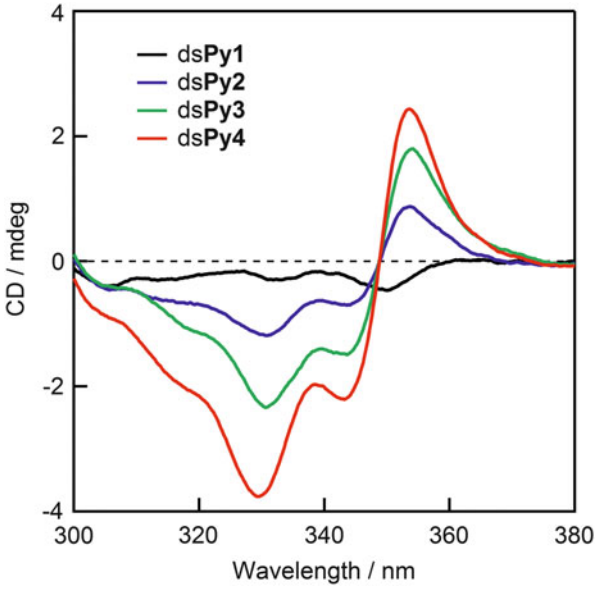

Fig. 5.3 CD spectra of multiple pyrene-modified RNA duplexes

were incorporated into an RNA strand, the excimer fluorescence in the RNA duplexes became larger, and the intense circular dichroism signals due to the exciton coupling among the pyrenes were observed (Figs. 5.2 and 5.3) [85–

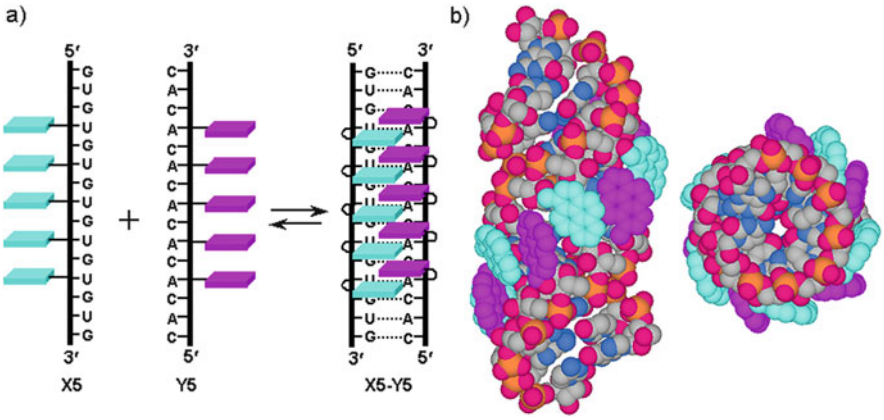

Fig. 5.4 Schematic representation (**a**) of duplex formation between multi-pyrene-modified RNA sequences (**X5-Y5**). *Side view* and *top view* (**b**) of duplex structure of **X5-Y5**

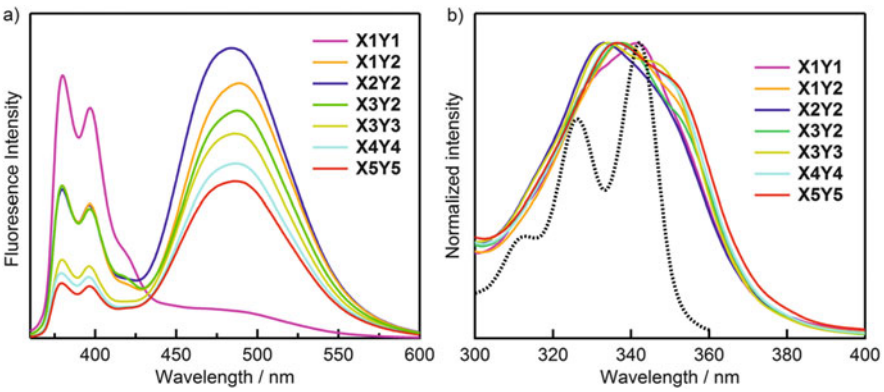

Fig. 5.5 (**a**) Fluorescence spectra of **XnYn**s ($\lambda_{ex} = 350$ nm) and (**b**) excitation spectra of **XnYn**s monitored at 490 nm. *Dotted line* is the excitation spectrum of **X1Y0** monitored at 376 nm

87]. Recently, we have reported that complementary 15-mer RNAs having five 2′-*O*-pyrene-modified nucleosides, which are separated by one nucleoside from each other, could form a duplex without any loss of thermal stability [88]. In the RNA duplex, the ten pyrenes can be assembled like a zipper in a helical manner along the duplex (Fig. 5.4). The important finding is that the pyrene arrays exhibiting strong excimer fluorescence are characterized by a broad and structureless excitation spectrum (Fig. 5.5) [89]. Hence, the excimer is a static excimer due to the direct excitation of the associated pyrenes in the ground state.

5.2 Perylene π-Stack Array in DNA

Among many aromatic chromophores, perylenediimide and its derivatives have attracted much research interest, because they can be used as a strong electron acceptor in organic semiconductor devices [90–93]. Moreover, owing to their tendency to form π-stacked structures, perylenediimides can be used to create several functional supramolecular materials [94]. It has been reported that covalent modification of DNA by perylenes gave some conjugates displaying unique photophysical properties [95–100]. The terminal modification of DNA by a perylenediimide has been shown to be useful to connect two different DNA duplexes [95, 97–101]. It has also been shown that cationic perylenediimides can bind to duplex, triplex, and quadruplex DNA structures [102–107].

DNA as well as RNA is a promising material as a template for assembling some functional molecules on a nanoscale. Developments of methods to generate molecular arrays on DNA are important because of their applications in DNA-based nanomaterials and nanodevices [8, 108–113]. DNA has several advantages that defined sequence and length DNA can be synthesized by an easier way than RNA, and arrangement of chromophores on DNA can be controlled via sequence-specific self-assembling property [2]. In addition to these properties, DNA itself is known to act as a charge transporting material [8]. Many DNA-mediated charge transport studies afford much knowledge about the charge transfer and successive charge separation that occur on DNA, which should lead to development of DNA-based electronic devices [7–12, 17–20]. A number of artificial DNAs have been used to generate molecular array along the helix axis. As described earlier, there have been two approaches to realize such molecular arrays. One is a covalent approach that uses DNAs attached to functional molecules at the defined positions. The other approach involves a non-covalent method to organize molecules in designed DNA sequences [114].

The later approach is superior when DNA, whose structures and sequences are suitable for tight binding to aromatic chromophores, is available either by a chemical or biochemical method. We hypothesized that an artificial cavity or a pocket created inside DNA might be used to capture a planar aromatic molecule such as a perylene by help with hydrophobic and π–π interactions (Fig. 5.6). The cavity can be introduced into DNA by replacing of a nucleoside with a deoxyribospacer or an abasic analog. The pocket size in DNA can be predetermined by a number of deoxyribospacer that are incorporated into a DNA sequence. We anticipated that multiperylenedimides might be assembled in a pocket-size-dependent manner. Our approach has proven to be useful to prepare the DNA–pyrylene complexes in which the perylene chromophores were bound to the pocket as a monomer or cofacially stacked as a dimer, a trimer, and upto a hexamer (Fig. 5.6) [115]. The DNA–perylene complexes were found to be more stable than DNA duplex with all natural bases. The important feature of this approach is that the DNA–perylene complexes can be synthesized by a simple mixing of pocket-

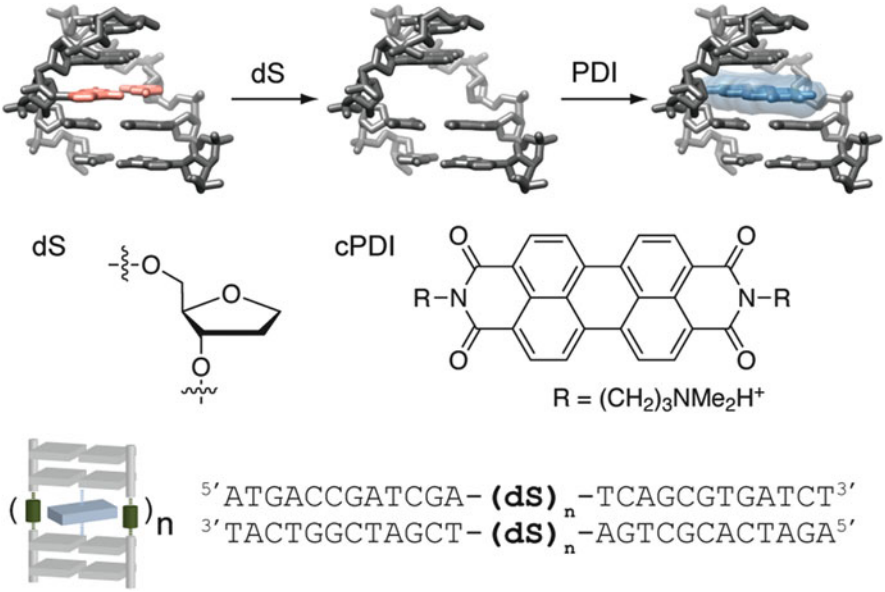

Fig. 5.6 Illustration of the specific binding of PDI to a hydrophobic pocket created within DNA by replacing nucleosides with a basic site analogs. Chemical structures of a deoxyribose spacer (**dS**) and a perylenediimide (**cPDI**) and sequences of DNA with the different size of the pocket ($\mathbf{dS}_n$, $n = 0$–6)

containing DNA duplex with cationic perylenediimide derivative in an aqueous buffer solution.

We investigated the photophysical properties of DNA/perylene monomer (**P1**), DNA/perylene dimer (**P2**), and DNA/perylene trimer complexes (**P3**) [116]. All three complexes showed a prompt on/off photocurrent response upon irradiation of visible light. The photocurrent intensity was found to be strongly dependent upon the number of perylenes in the complex. The perylenedimide dimer and the trimer showed nearly fourfold and eightfold enhanced photocurrents compared to the monomer, respectively (Fig. 5.7). The results implied that the stacked form of the perylene chromophores generated the charge-separated state different from the monomer and led to an efficient conversion of the photon to the photocurrent signal. Time-resolved transient absorption measurement revealed that the long-lived intermediates derived from the charge delocalization of the π-electron over the stacked perylenediimide chromophores are yielded in the dimer and the trimer complexes (Fig. 5.8). Little or no charge separation occurred on the perylene-diimides randomly bound to DNA that gave no photocurrent under the irradiation. Consequently, these results support the idea that the cofacial arrangement of functional chromophores in the π-stacked array is essential for the hole/electron transfer pathway and generation of the long-lived charge-separated state.

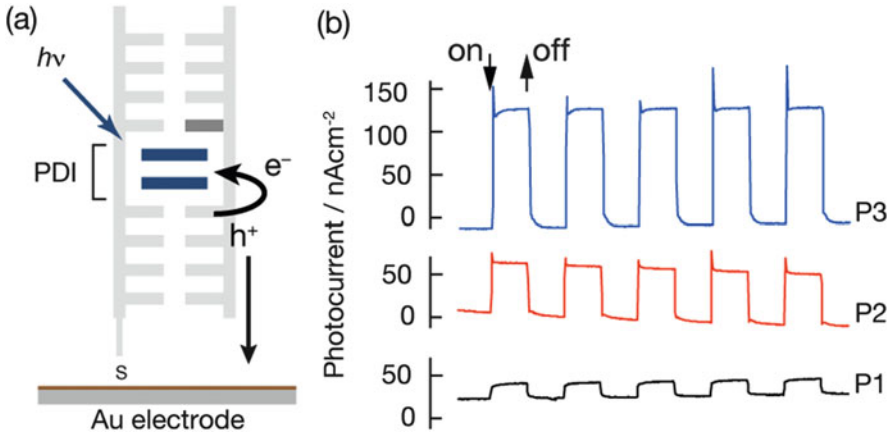

Fig. 5.7 (**a**) Photocurrent generation of gold electrodes modified with **Pn** (**n**: 1–3) complexes. Photocurrent is generated through charge separation and charge transfer initiated by the excitation of PDI chromophores inside DNA. (**b**) Photocurrent response observed upon irradiation at 540 nm for the **Pn** complexes

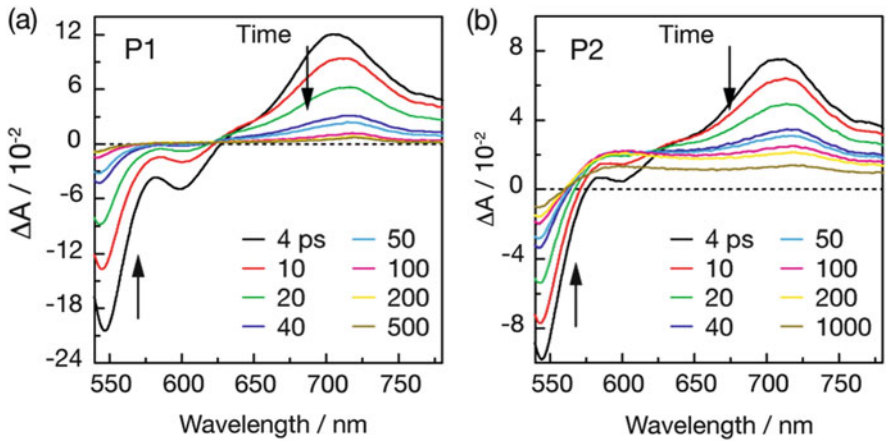

Fig. 5.8 Transient absorption spectra for (**a**) **P1**, (**b**) **P2** after excitation with a 540-nm laser pulse (150 fs)

5.3 Fluorescent DNA–Perylene Complex

In our previous studies, it have been shown that perylenediimides possessing dimethylaminopropyl groups at imide functions exhibit unique properties in non-covalent binding to a hydrophobic pocket such as abasic site as well as a

mismatch base pair in DNA [117]. However, the perylene chromophore used in these studies showed weak fluorescence due to the fluorescence quenching by the electron transfer between the excited perylene and the neighboring purine bases in DNA [118, 119]. To develop a useful fluorescent probe for DNA/RNA by utilizing perylene derivatives, it is crucial to overcome the limitation of their fluorescence quenching properties. We therefore focused our attention to perylenediimide derivatives possessing electron-donating groups such as alkoxy groups at bay positions. It has been reported that the substitution of perylene by an electron-donating group can modulate the electronic state, the electron transferability, and the emission properties [105, 120, 121].

We investigated the binding of the alkoxy-substituted perylene chromophores (PO) to the hydrophobic pocket created inside DNA and their emission behavior in the pocket (Fig. 5.9). It is shown that the fluorescence intensity of PO was enhanced by a factor of more than 100 upon binding of PO to the DNA pocket. A simple binary complex composed of a stem–loop DNA probe, and PO was designed to exploit the fluorescence change of PO. We found that PO acts as a light-up fluorescent probe for the detection of DNA as well as RNA sequences at nanomolar concentration (Fig. 5.10). This study provides the first example of a perylene-based fluorescent DNA/RNA probe that does not require dye modification of probe-oligonucleotide sequences.

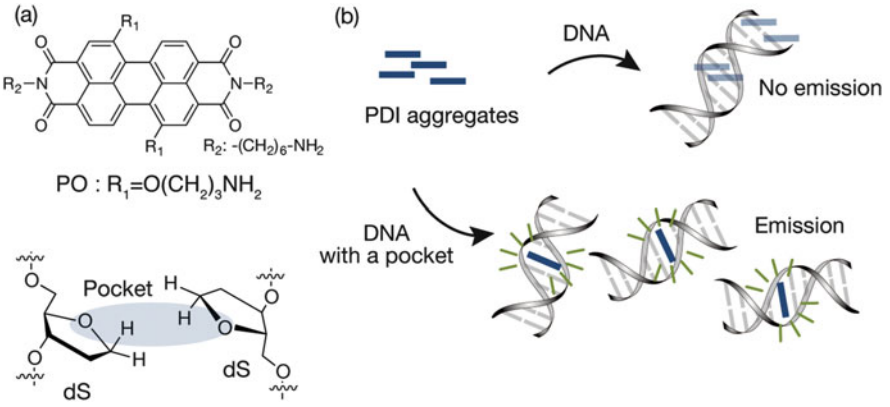

Fig. 5.9 (**a**) Chemical structures of perylenediimide (PDI) derivatives (**PO**) and a pocket created by deoxyribospacer pairs (**dS/dS**). (**b**) Schematic illustration of binding of PDI to DNA with or without a pocket, leading to a change in the emissive state of PDI

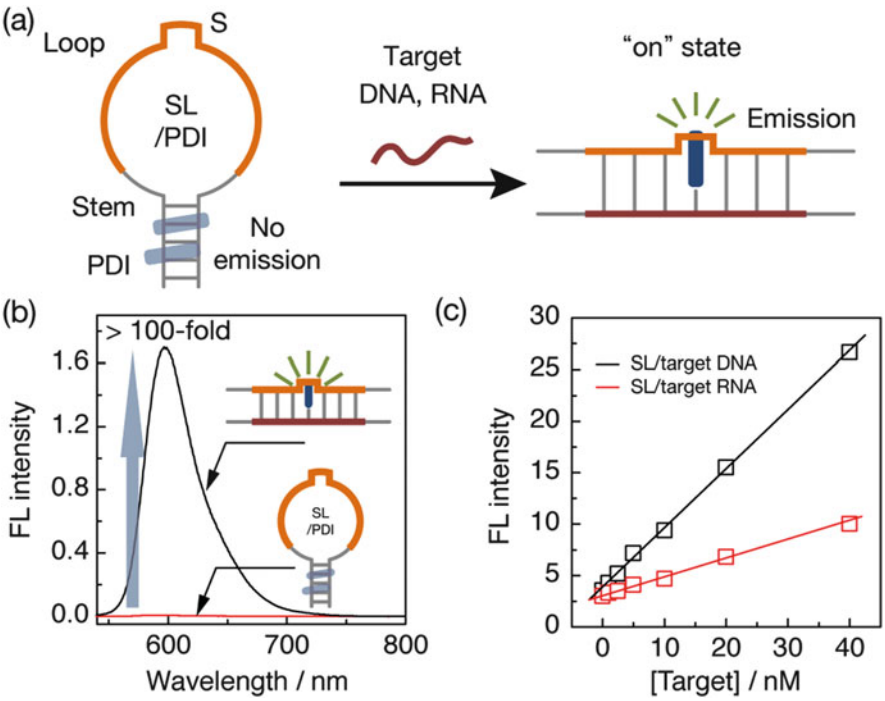

Fig. 5.10 (**a**) Light-up fluorescent sensor composed of a PO/SL binary complex responding to the hybridization event. (**b**) Fluorescence response of the **PO/SL** probe before and after hybridization with complementary DNA. (**c**) Concentration dependence of **PO/SL** probe emission in the range of 1–40 nM target DNA (*black*) or RNA (*red*)

5.4 Charge Transfer Complex in DNA

Charge Transfer (CT) interactions between donor and acceptor molecules have been used as a driving force to create specific molecular structures, because they are suitable for alternate placement of the two different aromatic molecules [122–124]. Among many molecules for the CT, a pair of naphthaldiimide as a donor and dialkoxynaphthalene as an acceptor is a most frequently used example for such structures. It has been reported that the synthetic oligomer possessing two different naphthalene molecules can form face-centered folded structure [125–127]. The polarized substituents on the aromatic rings, namely, alkoxy groups and diimide carbonyl groups, are a key element to facilitate the face-centered stacking structure.

We examined that DNA duplex having a hydrophobic pocket with an appropriate size might be used to construct a CT complex in the DNA pocket (Fig. 5.11). We have chosen a pair of naphthaldiimide (NDI) and dialkoxynaphthalene (DAN) having cationic amino groups in the side chains in order to increase their water solubility and affinity to DNA. It has been shown that the hydrophobic pocket created by insertion of two deoxyribospacers into the middle of 24-mer DNA

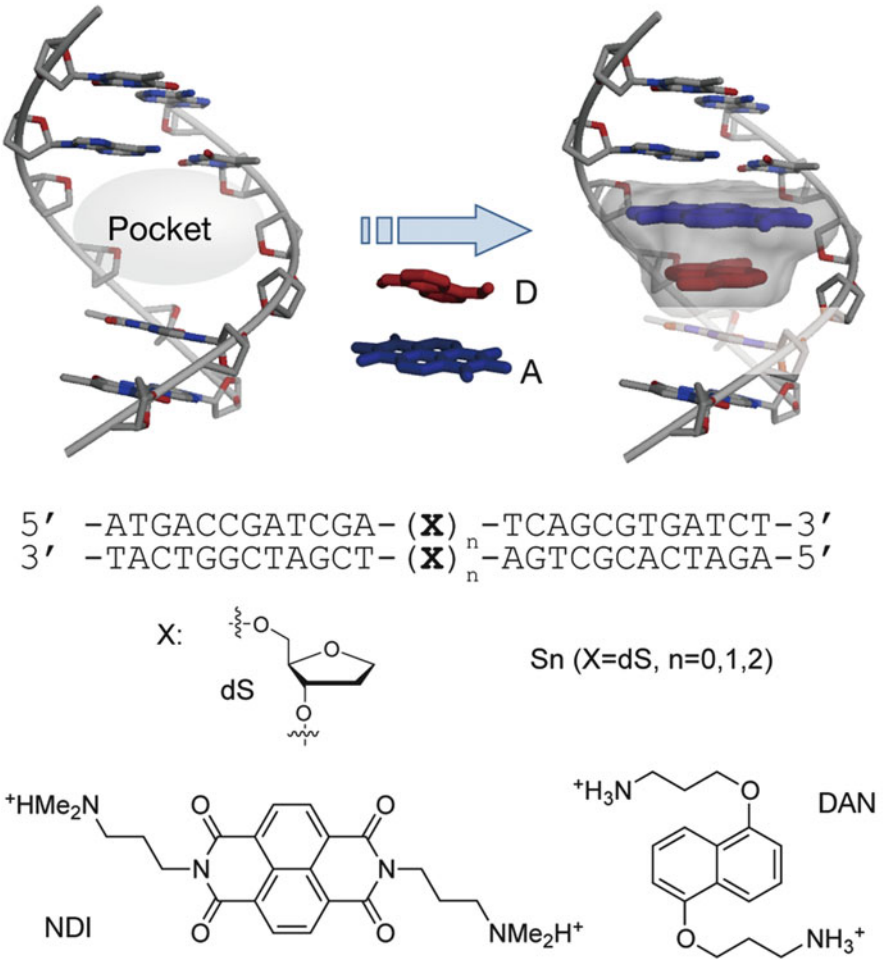

Fig. 5.11 Schematic illustration of the formation of a charge transfer (CT) complex composed of donor (D) and acceptor (A) within the hydrophobic cavity of DNA. The naphthaldiimide (**NDI**) and dialkoxynaphthalene (**DAN**) derivatives were used as electron acceptor and donor molecules, respectively

duplex indeed acts as a scaffold to form the CT between NDI and DAN in a specific manner [128].

5.5 Aromatic π-Stack Assembly Using Interaction Between Zn(II)-Cyclen and Thymine in DNA

Because highly ordered chromophore aggregates especially in one-dimensional systems exhibit unique energy transfer, electron transfer, and electroconductive properties, they have recently attracted considerable attention for applications in

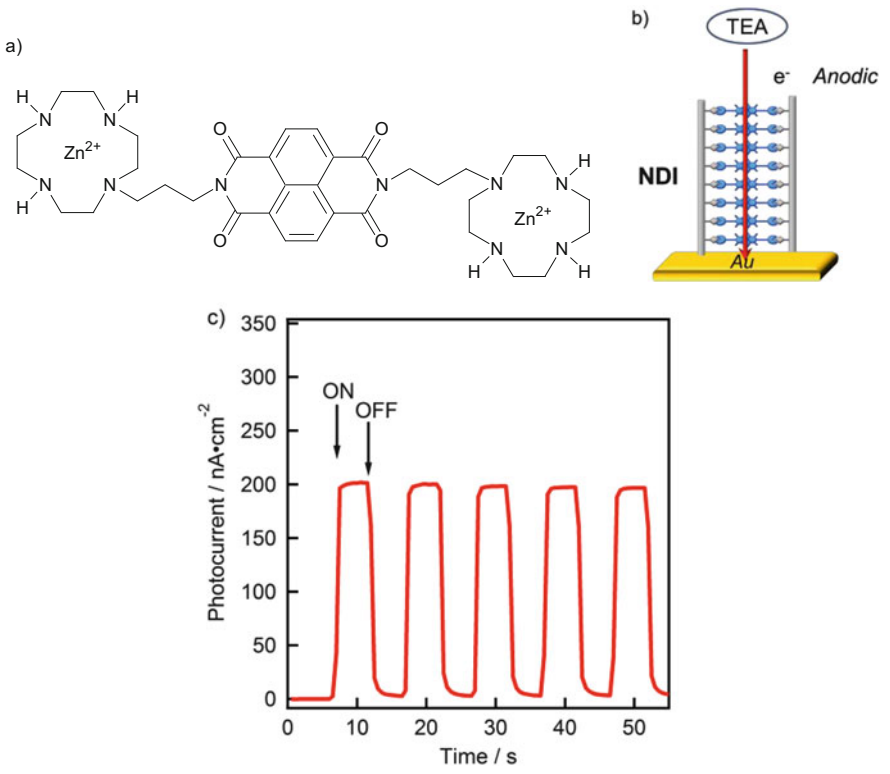

Fig. 5.12 (**a**) Structure of NDI derivative having two Zn(II)-cylcens. (**b**) Schematic illustration of DNA-NDI-stacks immobilized on Au electrode. (**c**) Anodic photocurrent responses of DNA-NDI-stacks immobilized on Au electrode

light-harvesting systems [129–132], organic field effect transistors [133, 134], and photovoltaic cells [135–137]. By using oligo-DNA, we can arrange finite chromophores in defined spaces or distances and can also control the arrangement structures on the basis of DNA self-assembling properties that can build duplexes, triplexes, quadruplexes, and multidimensional structures.

It is known that Zn(II)-cyclen selectively binds to thymine base in DNA via the coordination of the Zn(II) center with the deprotonated imide nitrogen and the hydrogen bonds between the carbonyl group of thymine and the NH group of Zn (II)-cyclen [138, 139]. Moreover, it has the advantage that the functionalization with hydrophilic Zn(II)-cyclen enhances the solubility of hydrophobic chromophores in aqueous media. We utilized Zn(II)-cyclen as a receptor unit of chromophore building blocks. We have shown that naphthalenediimide (NDI) derivative having two Zn(II)-cylcens formed highly ordered NDI-stacks with dTn-DNAs and that the DNA-NDI-stacks immobilized on Au electrode generated strong photocurrent under the UV-Vis irradiation (Fig. 5.12) [140].

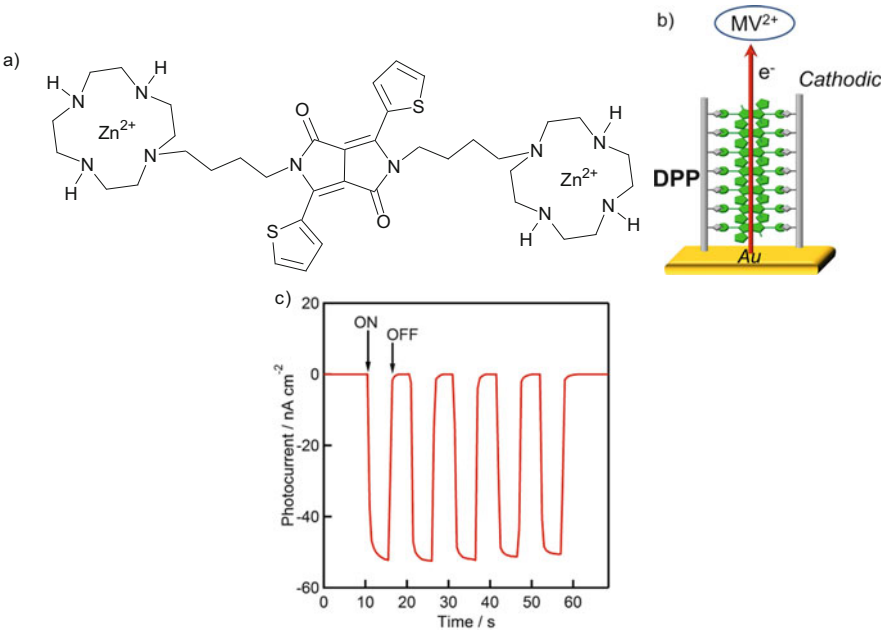

Fig. 5.13 (**a**) Structure of DPP derivative having two Zn(II)-cylcens. (**b**) Schematic illustration of DNA-DPP-stacks immobilized on Au electrode. (**c**) Cathodic photocurrent responses of DNA-DPP-stacks immobilized on Au electrode

To expand the concept of the DNA-templated chromophore assembly by the Zn (II)-cyclen approach, the applicability to other chromophores must be confirmed. We have been interested in diketopyrrolopyrrole (DPP) derivatives, which are widely used as materials for optoelectronic devices such as photovoltaic cells and field effect transistors, because they have ease of synthesis and modification, absorb visible light, and behave as a donor chromophore against NDI derivatives. We synthesized bis(2-thienyl)-DPP derivative having two Zn(II)-cylcens. The J-type DPP assembly exhibiting unique photoelectronic properties can be formed by self-organization of the DPP-Zn(II) cyclens with dT_n-DNAs (Fig. 5.13) [141]. We showed that the selective binding of Zn(II)-cyclen to thymine base is a useful way for the construction of multichromophore assembly on DNA.

5.6 Summary and Outlook

This chapter deals with our recent researches that focus on DNA or RNA as a nanomaterial for a useful building block to assemble functional chromophores at defined positions and directions on DNA. Through development of methods for the attachment of chromophores via a covalent or a noncovalent way into DNA or

RNA, we have constructed a one-dimensional or a helical array of multichromophores in DNA duplexes or along RNA duplexes. In particular, we showed that the multiperylene–DNA systems exhibit a unique light-harvesting property due to the long-lived charge separation in the face-to-face perylenes stacking occurring in DNA duplex. The photocurrent would be used as a sensing signal for DNA and RNA detection. The other topic is the multi-organic-dye arrays that can be built by interaction between a specific ligand and a nucleic acid base. By this way, we can construct a designated number of organic-dyes array by using oligoDNA with defined length. The organic-dye array–DNA may be used as a nanowire to conduct charge migration. Our results therefore should open an important step toward developments of new types of biosensors and electronic devices. Further studies along this line are now underway in our group.

References

1. Hoeben FJM, Jonkheijm P, Meijer EW, Schenning APHJ (2005) About supramolecular assemblies of π-conjugated systems. Chem Rev 105(4):1491–1546. doi:10.1021/cr030070z
2. Malinovskii VL, Wenger D, Häner R (2010) Nucleic acid-guided assembly of aromatic chromophores. Chem Soc Rev 39(2):410–422. doi:10.1039/b910030j
3. Malinovskii VL, Samain F, Häner R (2007) Helical arrangement of interstrand stacked pyrenes in a DNA framework. Angew Chem Int Ed 46(24):4464–4467
4. Mayer-Enthart E, Wagenknecht H-A (2006) Structure-sensitive and self-assembled helical pyrene array based on DNA architecture. Angew Chem Int Ed 45(20):3372–3375. doi:10.1002/anie.200504210
5. Häner R, Samain F, Malinovskii VL (2009) DNA-assisted self-assembly of pyrene foldamers. Chem Eur J 15(23):5701–5708. doi:10.1002/chem.200900369
6. Bittermann H, Siegemund D, Malinovskii VL, Häner R (2008) Dialkynylpyrenes: strongly fluorescent, environment-sensitive DNA building blocks. J Am Chem Soc 130 (46):15285–15287. doi:10.1021/ja806747h
7. Lewis FD, Letsinger RL, Wasielewski MR (2001) Dynamics of photoinduced charge transfer and hole transport in synthetic DNA hairpins. Acc Chem Res 34(2):159–170. doi:10.1021/ar0000197
8. Genereux JC, Barton JK (2010) Mechanisms for DNA charge transport. Chem Rev 110 (3):1642–1662. doi:10.1021/cr900228f
9. Giese B (2000) Long-distance charge transport in DNA: the hopping mechanism. Acc Chem Res 33(9):631–636. doi:10.1021/ar990040b
10. Kawai K, Majima T (2013) Hole transfer kinetics of DNA. Acc Chem Res 46 (11):2616–2625. doi:10.1021/ar400079s
11. Valis L, Wang Q, Raytchev M, Buchvarov I, Wagenknecht H-A, Fiebig T (2006) Base pair motions control the rates and distance dependencies of reductive and oxidative DNA charge transfer. Proc Natl Acad Sci USA 103(27):10192
12. Kanvah S, Joseph J, Schuster GB, Barnett RN, Cleveland CL, Landman U (2010) Oxidation of DNA: damage to nucleobases. Acc Chem Res 43(2):280–287. doi:10.1021/ar900175a
13. Bhosale R, Míšek J, Sakai N, Matile S (2010) Supramolecular n/p-heterojunction photosystems with oriented multicolored antiparallel redox gradients (OMARG-SHJs). Chem Soc Rev 39(1):138–149. doi:10.1039/b906115k

14. Acuna GP, Moller FM, Holzmeister P, Beater S, Lalkens B, Tinnefeld P (2012) Fluorescence enhancement at docking sites of DNA-directed self-assembled nanoantennas. Science 338 (6106):506–510. doi:10.1126/science.1228638
15. Liu S, Clever GH, Takezawa Y, Kaneko M, Tanaka K, Guo X, Shionoya M (2011) Direct conductance measurement of individual metallo-DNA duplexes within single-molecule break junctions. Angew Chem Int Ed 50(38):8886–8890. doi:10.1002/anie.201102980
16. Guo X, Gorodetsky AA, Hone J, Barton JK, Nuckolls C (2008) Conductivity of a single DNA duplex bridging a carbon nanotube gap. Nat Nanotechnol 3(3):163–167. doi:10.1038/nnano.2008.4
17. Kawai K, Kodera H, Osakada Y, Majima T (2009) Sequence-independent and rapid long-range charge transfer through DNA. Nat Chem 1(2):156–159. doi:10.1038/nchem.171
18. Willner I, Patolsky F, Wasserman J (2001) Photoelectrochemistry with controlled DNA-cross-linked CdS nanoparticle arrays this research is supported by the U.S.-Israel Binational Science Foundation. The Max Planck Research Award for International Cooperation (I.W.) is gratefully acknowledged. Angew Chem Int Ed 40(10):1861–1864
19. Okamoto A, Kamei T, Saito I (2006) DNA hole transport on an electrode: application to effective photoelectrochemical SNP typing. J Am Chem Soc 128(2):658–662. doi:10.1021/ja057040t
20. Zhang H, Baker BA, Cha T-G, Sauffer MD, Wu Y, Hinkson N, Bork MA, McShane CM, Choi K-S, McMillin DR, Choi JH (2012) DNA oligonucleotide templated nanohybrids using electronic type sorted carbon nanotubes for light harvesting. Adv Mater 24(40):5447–5451. doi:10.1002/adma.201201628
21. Schenning APHJ, von Herrikhuyzen J, Jonkheijm P, Chen Z, Würthner F, Meijer EW (2002) Photoinduced electron transfer in hydrogen-bonded oligo(p-phenylene vinylene)—perylene bisimide chiral assemblies. J Am Chem Soc 124(35):10252–10253. doi:10.1021/ja020378s
22. Garo F, Häner R (2012) A DNA-based light-harvesting antenna. Angew Chem Int Ed 51 (4):916–919. doi:10.1002/anie.201103295
23. Sakai N, Bhosale R, Emery D, Mareda J, Matile S (2010) Supramolecular n/p-heterojunction photosystems with antiparallel redox gradients in electron- and hole-transporting pathways. J Am Chem Soc 132(20):6923–6925. doi:10.1021/ja101944r
24. Teo YN, Kool ET (2012) DNA-multichromophore systems. Chem Rev 112(7):4221–4245. doi:10.1021/cr100351g
25. Kashida H, Takatsu T, Sekiguchi K, Asanuma H (2010) An efficient fluorescence resonance energy transfer (FRET) between pyrene and perylene assembled in a DNA duplex and its potential for discriminating single-base changes. Chem Eur J 16(8):2479–2486. doi:10.1002/chem.200902078
26. Ono T, Wang S, Koo C-K, Engstrom L, David SS, Kool ET (2012) Direct fluorescence monitoring of DNA base excision repair. Angew Chem Int Ed 51(7):1689–1692. doi:10.1002/anie.201108135
27. Teo YN, Wilson JN, Kool ET (2009) Polyfluorophores on a DNA backbone: a multicolor set of labels excited at one wavelength. J Am Chem Soc 131(11):3923–3933. doi:10.1021/ja805502k
28. Khakshoor O, Kool ET (2011) Chemistry of nucleic acids: impacts in multiple fields. Chem Commun 47(25):7018–7024. doi:10.1039/C1CC11021G
29. Sargsyan G, Schatz AA, Kubelka J, Balaz M (2013) Formation and helicity control of ssDNA templated porphyrin nanoassemblies. Chem Commun 49(10):1020–1022. doi:10.1039/c2cc38150h
30. Sezi S, Wagenknecht H-A (2013) DNA-templated formation of fluorescent self-assembly of ethynyl pyrenes. Chem Commun 49(81):9257–9259. doi:10.1039/c3cc44733b
31. Narayanaswamy N, Suresh G, Priyakumar UD, Govindaraju T (2014) Double zipper helical assembly of deoxyoligonucleotides: mutual templating and chiral imprinting to form hybrid DNA ensembles. Chem Commun. doi:10.1039/c4cc06759b

32. Sargsyan G, Leonard BM, Kubelka J, Balaz M (2014) Supramolecular ssDNA templated porphyrin and metalloporphyrin nanoassemblies with tunable helicity. Chem Eur J 20 (7):1878–1892. doi:10.1002/chem.201304153
33. Janssen PGA, Ruiz-Carretero A, González-Rodríguez D, Meijer EW, Schenning APHJ (2009) pH-Switchable helicity of DNA-templated assemblies. Angew Chem Int Ed 48 (43):8103–8106. doi:10.1002/anie.200903507
34. Benvin AL, Creeger Y, Fisher GW, Ballou B, Waggoner AS, Armitage BA (2007) Fluorescent DNA nanotags: supramolecular fluorescent labels based on intercalating dye arrays assembled on nanostructured DNA templates. J Am Chem Soc 129(7):2025–2034. doi:10.1021/ja066354t
35. Duhamel J (2012) New insights in the study of pyrene excimer fluorescence to characterize macromolecules and their supramolecular assemblies in solution. Langmuir 28 (16):6527–6538
36. Winnik FM (1993) Photophysics of preassociated pyrenes in aqueous polymer solutions and in other organized media. Chem Rev 93(2):587–614
37. Choi J, Konno T, Takai M, Ishihara K (2009) Controlled drug release from multilayered phospholipid polymer hydrogel on titanium alloy surface. Biomaterials 30(28):5201–5208
38. Garai K, Baban B, Frieden C (2011) Dissociation of apolipoprotein E oligomers to monomer is required for high-affinity binding to phospholipid vesicles. Biochemistry 50 (13):2550–2558
39. You L, Gokel GW (2008) Fluorescent, synthetic amphiphilic heptapeptide anion transporters: evidence for self-assembly and membrane localization in liposomes. Chem Eur J 14 (19):5861–5870
40. Hong H, Blois TM, Cao Z, Bowie JU (2010) Method to measure strong protein-protein interactions in lipid bilayers using a steric trap. Proc Natl Acad Sci USA 107 (46):19802–19807. doi:10.1073/pnas.1010348107
41. Okada K, Bartolini F, Deaconescu AM, Moseley JB, Dogic Z, Grigorieff N, Gundersen GG, Goode BL (2010) Adenomatous polyposis coli protein nucleates actin assembly and synergizes with the formin mDia1. J Cell Biol 189(7):1087–1096. doi:10.1083/jcb.201001016
42. Oh KJ, Cash KJ, Plaxco KW (2006) Excimer-based peptide beacons: a convenient experimental approach for monitoring polypeptide-protein and polypeptide-oligonucleotide interactions. J Am Chem Soc 128(43):14018–14019
43. Bains G, Patel AB, Narayanaswami V (2011) Pyrene: a probe to study protein conformation and conformational changes. Molecules 16(9):7909–7935
44. Ono T, Wang S, Koo C-K, Engstrom L, David SS, Kool ET (2012) Direct fluorescence monitoring of DNA base excision repair. Angew Chem Int Ed 51(7):1689–1692
45. Sezi S, Varghese R, Vilaivan T, Wagenknecht H-A (2012) Conformational control of dual emission by pyrrolidinyl PNA–DNA hybrids. ChemistryOpen 1(4):173–176
46. Zhu H, Lewis FD (2007) Pyrene excimer fluorescence as a probe for parallel G-quadruplex formation. Bioconjug Chem 18(4):1213–1217
47. Nagatoishi S, Nojima T, Juskowiak B, Takenaka S (2005) A pyrene-labeled G-quadruplex oligonucleotide as a fluorescent probe for potassium ion detection in biological applications. Angew Chem Int Ed 44(32):5067–5070. doi:10.1002/anie.200501506
48. Okamoto A, Ichiba T, Saito I (2004) Pyrene-labeled oligodeoxynucleotide probe for detecting base insertion by excimer fluorescence emission. J Am Chem Soc 126 (27):8364–8365. doi:10.1021/ja049061d
49. Figueira-Duarte TM, Müllen K (2011) Pyrene-based materials for organic electronics. Chem Rev 111(11):7260–7314. doi:10.1021/cr100428a
50. Xu X, Yuan H, Chang J, He B, Gu Z (2012) Cooperative hierarchical self-assembly of peptide dendrimers and linear polypeptides into nanoarchitectures mimicking viral capsids. Angew Chem Int Ed 51(13):3130–3133

51. Lim Y-B, Moon K-S, Lee M (2009) Recent advances in functional supramolecular nanostructures assembled from bioactive building blocks. Chem Soc Rev 38(4):925–934
52. Wei B, Dai M, Yin P (2012) Complex shapes self-assembled from single-stranded DNA tiles. Nature 485(7400):623–626. doi:10.1038/nature11075
53. Wang T, Sha R, Dreyfus R, Leunissen ME, Maass C, Pine DJ, Chaikin PM, Seeman NC (2012) Self-replication of information-bearing nanoscale patterns. Nature 478 (7368):225–228
54. Gu H, Chao J, Xiao S-J, Seeman NC (2010) A proximity-based programmable DNA nanoscale assembly line. Nature 465(7295):202–205
55. Ackermann D, Jester S-S, Famulok M (2012) Design strategy for DNA rotaxanes with a mechanically reinforced PX100 axle. Angew Chem Int Ed 51(27):6771–6775
56. Verbiest T, Samyn C, Boutton C, Houbrechts S, Kauranen M, Persoons A (1996) Second-order nonlinear optical properties of a chromophore-functionalized polypeptide. Adv Mater 8 (9):756–759
57. Parkash J, Robblee JH, Agnew J, Gibbs E, Collings P, Pasternack RF, de Paula JC (1998) Depolarized resonance light scattering by porphyrin and chlorophyll a aggregates. Biophys J 74(4):2089–2099
58. Pieroni O, Fissi A, Angelini N, Lenci F (2001) Photoresponsive polypeptides. Acc Chem Res 34(1):9–17
59. Jones G, Vullev VI (2002) Photoinduced electron transfer between non-native donor-acceptor moieties incorporated in synthetic polypeptide aggregates. Org Lett 4(23):4001–4004
60. Channon KJ, Devlin GL, MacPhee CE (2009) Efficient energy transfer within self-assembling peptide fibers: a route to light-harvesting nanomaterials. J Am Chem Soc 131 (35):12520–12521
61. Rao KV, Datta KKR, Eswaramoorthy M, George SJ (2012) Light-harvesting hybrid assemblies. Chem Eur J 18(8):2184–2194
62. Hainke S, Seitz O (2009) Binaphthyl-DNA: stacking and fluorescence of a nonplanar aromatic base surrogate in DNA. Angew Chem Int Ed 48(44):8250–8253. doi:10.1002/anie.200903194
63. Brotschi C, Leumann CJ (2003) DNA with hydrophobic base substitutes: a stable, zipperlike recognition motif based on interstrand-stacking interactions. Angew Chem Int Ed 42 (14):1655–1658
64. Kashida H, Asanuma H, Komiyama M (2004) Alternating hetero H aggregation of different dyes by interstrand stacking from two DNA–dye conjugates. Angew Chem Int Ed 43 (47):6522–6525
65. Asanuma H, Shirasuka K, Takarada T, Kashida H, Komiyama M (2003) DNA-dye conjugates for controllable H* aggregation. J Am Chem Soc 125(8):2217–2223
66. Baumstark D, Wagenknecht H-A (2008) Fluorescent hydrophobic zippers inside duplex DNA: interstrand stacking of perylene-3,4:9,10-tetracarboxylic acid bisimides as artificial DNA base dyes. Chem Eur J 14(22):6640–6645
67. Wilson TM, Zeidan TA, Hariharan M, Lewis FD, Wasielewski MR (2010) Electron hopping among cofacially stacked perylenediimides assembled by using DNA hairpins. Angew Chem Int Ed 49(13):2385–2388
68. Sharma N, Top A, Kiick KL, Pochan DJ (2009) One-dimensional gold nanoparticle arrays by electrostatically directed organization using polypeptide self-assembly. Angew Chem Int Ed 48(38):7078–7082
69. Kuzyk A, Schreiber R, Fan Z, Pardatscher G, Roller E-M, Hogele A, Simmel FC, Govorov AO, Liedl T (2012) DNA-based self-assembly of chiral plasmonic nanostructures with tailored optical response. Nature 483(7389):311–314
70. Sharma J, Chhabra R, Cheng A, Brownell J, Liu Y, Yan H (2009) Control of self-assembly of DNA tubules through integration of gold nanoparticles. Science 323(5910):112–116. doi:10.1126/science.1165831

71. Rajendran A, Endo M, Sugiyama H (2012) Single-molecule analysis using DNA origami. Angew Chem Int Ed 51(4):874–890
72. Nakata E, Liew FF, Uwatoko C, Kiyonaka S, Mori Y, Katsuda Y, Endo M, Sugiyama H, Morii T (2012) Zinc-finger proteins for site-specific protein positioning on DNA-origami structures. Angew Chem Int Ed 51(10):2421–2424
73. Tanaka K, Clever GH, Takezawa Y, Yamada Y, Kaul C, Shionoya M, Carell T (2006) Programmable self-assembly of metal ions inside artificial DNA duplexes. Nat Nanotechnol 1(3):190–194
74. Egusa S, Sisido M, Imanishi Y (1985) One-dimensional aromatic crystals in solution. 4. Ground- and excited-state interactions of poly(L-1-pyrenylalanine) studied by chiroptical spectroscopy including circularly polarized fluorescence and fluorescence-detected circular dichroism. Macromolecules 18(5):882–889
75. Sisido M, Imanishi Y (1985) One-dimensional aromatic crystals in solution. 5. Empirical energy and theoretical circular dichroism calculations on helical poly(L-1-pyrenylalanine). Macromolecules 18(5):890–894
76. Endo M, Wang H, Fujitsuka M, Majima T (2006) Pyrene-stacked nanostructures constructed in the recombinant tobacco mosaic virus rod scaffold. Chem Eur J 12(14):3735–3740
77. Wilson JN, Teo YN, Kool ET (2007) Efficient quenching of oligomeric fluorophores on a DNA backbone. J Am Chem Soc 129(50):15426–15427
78. Kashida H, Sekiguchi K, Liang X, Asanuma H (2010) Accumulation of fluorophores into DNA duplexes to mimic the properties of quantum dots. J Am Chem Soc 132 (17):6223–6230. doi:10.1021/ja101007d
79. Seo YJ, Rhee H, Joo T, Kim BH (2007) Self-duplex formation of an APy-substituted oligodeoxyadenylate and its unique fluorescence. J Am Chem Soc 129(16):5244–5247
80. Nakamura M, Fukunaga Y, Sasa K, Ohtoshi Y, Kanaori K, Hayashi H, Nakano H, Yamana K (2005) Pyrene is highly emissive when attached to the RNA duplex but not to the DNA duplex: the structural basis of this difference. Nucleic Acids Res 33(18):5887–5895. doi:10.1093/nar/gki889
81. Maie K, Miyagi K, Takada T, Nakamura M, Yamana K (2009) RNA-mediated electron transfer: double exponential distance dependence. J Am Chem Soc 131(37):13188–13189. doi:10.1021/ja902647j
82. Fukuda M, Nakamura M, Takada T, Yamana K (2010) Syntheses and fluorescence of RNA conjugates having pyrene-modified adenosine and nitrobenzene-modified uridine base pairs. Tetrahedron Lett 51(13):1732–1735. doi:10.1016/j.tetlet.2010.01.081
83. Yamana K, Zako H, Asazuma K, Iwase R, Nakano H, Murakami A (2001) Fluorescence detection of specific RNA sequences using 2′-pyrene-modified oligoribonucleotides. Angew Chem Int Ed 40(6):1104–1106. doi:10.1002/1521-3773(20010316)40:6<1104::AID-ANIE11040>3.0.CO;2-2
84. Mahara A, Iwase R, Sakamoto T, Yamana K, Yamaoka T, Murakami A (2002) Bispyrene-conjugated 2′-O-methyloligonucleotide as a highly specific RNA-recognition probe. Angew Chem Int Ed 41(19):3648–3650. doi:10.1002/1521-3773(20021004)41:19<3648::AID-ANIE3648>3.0.CO;2-Y
85. Nakamura M, Ohtoshi Y, Yamana K (2005) Helical pyrene-array along the outside of duplex RNA. Chem Commun 41:5163. doi:10.1039/b507808c
86. Nakamura M, Shimomura Y, Ohtoshi Y, Sasa K, Hayashi H, Nakano H, Yamana K (2007) Pyrene aromatic arrays on RNA duplexes as helical templates. Org Biomol Chem 5 (12):1945–1951. doi:10.1039/B705933G
87. Maie K, Nakamura M, Takada T, Yamana K (2009) Fluorescence quenching properties of multiple pyrene-modified RNAs. Bioorg Med Chem 17(14):4996–5000. doi:10.1016/j.bmc.2009.05.074
88. Nakamura M, Murakami Y, Sasa K, Hayashi H, Yamana K (2008) Pyrene-zipper array assembled via RNA duplex formation. J Am Chem Soc 130(22):6904–6905. doi:10.1021/ja801054t

89. Nakamura M, Fukuda M, Takada T, Yamana K (2012) Highly ordered pyrene [small pi]-stacks on an RNA duplex display static excimer fluorescence. Org Biomol Chem 10 (48):9620–9626. doi:10.1039/C2OB26773J
90. Görl D, Zhang X, Würthner F (2012) Molecular assemblies of perylene bisimide dyes in water. Angew Chem Int Ed 51(26):6328–6348. doi:10.1002/anie.201108690
91. Xie Z, Stepanenko V, Radacki K, Würthner F (2012) Chiral J-aggregates of atropo-enantiomeric perylene bisimides and their self-sorting behavior. Chem Eur J 18 (23):7060–7070. doi:10.1002/chem.201200089
92. Shao C, Stolte M, Würthner F (2013) Quadruple π stack of two perylene bisimide tweezers: a bimolecular complex with kinetic stability. Angew Chem Int Ed 52(29):7482–7486. doi:10.1002/anie.201302479
93. Marty R, Nigon R, Leite D, Frauenrath H (2014) Two-fold odd-even effect in self-assembled nanowires from oligopeptide-polymer-substituted perylene bisimides. J Am Chem Soc 136 (10):3919–3927. doi:10.1021/ja412384p
94. Würthner F (2004) Perylene bisimide dyes as versatile building blocks for functional supramolecular architectures. Chem Commun 14:1564. doi:10.1039/b401630k
95. Bevers S, Schutte S, McLaughlin LW (2000) Naphthalene- and perylene-based linkers for the stabilization of hairpin triplexes. J Am Chem Soc 122(25):5905–5915. doi:10.1021/ja0001714
96. Rahe N, Rinn C, Carell T (2003) Development of donor? Acceptor modified DNA hairpins for the investigation of charge hopping kinetics in DNA. Chem Commun 17:2120. doi:10.1039/b307395e
97. Neelakandan PP, Pan Z, Hariharan M, Zheng Y, Weissman H, Rybtchinski B, Lewis FD (2010) Hydrophobic self-assembly of a perylenediimide-linked DNA dumbbell into supramolecular polymers. J Am Chem Soc 132(44):15808–15813. doi:10.1021/ja1076525
98. Menacher F, Stepanenko V, Würthner F, Wagenknecht H-A (2011) Assembly of DNA triangles mediated by perylene bisimide caps. Chem Eur J 17(24):6683–6688. doi:10.1002/chem.201100141
99. Baumstark D, Wagenknecht H-A (2008) Perylene bisimide dimers as fluorescent “glue” for DNA and for base-mismatch detection. Angew Chem Int Ed 47(14):2612–2614. doi:10.1002/anie.200705237
100. Wagner C, Wagenknecht H-A (2006) Perylene-3,4:9,10-tetracarboxylic acid bisimide dye as an artificial DNA base surrogate. Org Lett 8(19):4191–4194. doi:10.1021/ol061246x
101. Abdalla MA, Bayer J, Rädler JO, Müllen K (2004) Synthesis and self-assembly of perylenediimide–oligonucleotide conjugates. Angew Chem Int Ed 43(30):3967–3970. doi:10.1002/anie.200353621
102. Liu ZR, Rill RL (1996) N,N′-bis[3,3′-(dimethylamino)propylamine]-3,4,9,10-perylenetetracarboxylic diimide, a dicationic perylene dye for rapid precipitation and quantitation of trace amounts of DNA. Anal Biochem 236(1):139–145. doi:10.1006/abio.1996.0142
103. Takada T, Yamaguchi K, Tsukamoto S, Nakamura M, Yamana K (2014) Light-up fluorescent probes utilizing binding behavior of perylenediimide derivatives to a hydrophobic pocket within DNA. Analyst 139(16):4016–4021. doi:10.1039/c4an00493k
104. Tuntiwechapikul W, Lee JT, Salazar M (2001) Design and synthesis of the G-quadruplex-specific cleaving reagent perylene-EDTA·iron(II). J Am Chem Soc 123(23):5606–5607. doi:10.1021/ja0156439
105. Szelke H, Schübel S, Harenberg J, Krämer R (2010) Interaction of heparin with cationic molecular probes: probe charge is a major determinant of binding stoichiometry and affinity. Bioorg Med Chem Lett 20(4):1445–1447. doi:10.1016/j.bmcl.2009.12.105
106. Samudrala R, Zhang X, Wadkins RM, Mattern DL (2007) Synthesis of a non-cationic, water-soluble perylenetetracarboxylic diimide and its interactions with G-quadruplex-forming DNA. Bioorg Med Chem 15(1):186–193. doi:10.1016/j.bmc.2006.09.075

107. Kern JT, Thomas PW, Kerwin SM (2002) The relationship between ligand aggregation and G-quadruplex DNA selectivity in a series of 3,4,9,10-perylenetetracarboxylic acid diimides †. Biochemistry 41(38):11379–11389. doi:10.1021/bi0263107
108. Furst A, Landefeld S, Hill MG, Barton JK (2013) Electrochemical patterning and detection of DNA arrays on a two-electrode platform. J Am Chem Soc 135(51):19099–19102. doi:10.1021/ja410902j
109. Genereux JC, Barton JK (2009) Molecular electronics: DNA charges ahead. Nat Chem 1 (2):106–107. doi:10.1038/nchem.188
110. Gill R, Patolsky F, Katz E, Willner I (2005) Electrochemical control of the photocurrent direction in intercalated DNA/CdS nanoparticle systems. Angew Chem Int Ed 44 (29):4554–4557. doi:10.1002/anie.200500830
111. Lu C-H, Willner B, Willner I (2013) DNA nanotechnology: from sensing and DNA machines to drug-delivery systems. ACS Nano 7(10):8320–8332. doi:10.1021/nn404613v
112. Woller JG, Hannestad JK, Albinsson B (2013) Self-assembled nanoscale DNA-porphyrin complex for artificial light harvesting. J Am Chem Soc 135(7):2759–2768. doi:10.1021/ja311828v
113. Stein IH, Steinhauer C, Tinnefeld P (2011) Single-molecule four-color FRET visualizes energy-transfer paths on DNA origami. J Am Chem Soc 133(12):4193–4195. doi:10.1021/ja1105464
114. Ruiz-Carretero A, Janssen PGA, Kaeser A, Schenning APHJ (2011) DNA-templated assembly of dyes and extended π-conjugated systems. Chem Commun 47(15):4340. doi:10.1039/c0cc05155a
115. Takada T, Otsuka Y, Nakamura M, Yamana K (2012) Molecular arrangement and assembly guided by hydrophobic cavities inside DNA. Chem Eur J 18(30):9300–9304. doi:10.1002/chem.201201469
116. Takada T, Ashida A, Nakamura M, Fujitsuka M, Majima T, Yamana K (2014) Photocurrent generation enhanced by charge delocalization over stacked perylenediimide chromophores assembled within DNA. J Am Chem Soc 136(19):6814–6817. doi:10.1021/ja501535z
117. Takada T, Ashida A, Nakamura M, Yamana K (2013) Cationic perylenediimide as a specific fluorescent binder to mismatch containing DNA. Bioorg Med Chem 21(19):6011–6014. doi:10.1016/j.bmc.2013.07.040
118. Zheng Y, Long H, Schatz GC, Lewis FD (2005) Duplex and hairpin dimer structures for perylene diimide-oligonucleotide conjugates. Chem Commun 38:4795–4797. doi:10.1039/b509754a
119. Zeidan TA, Carmieli R, Kelley RF, Wilson TM, Lewis FD, Wasielewski MR (2008) Charge-transfer and spin dynamics in DNA hairpin conjugates with perylenediimide as a base-pair surrogate. J Am Chem Soc 130(42):13945–13955. doi:10.1021/ja803765r
120. Krausharp S, Lysetska M, Würthner F (2005) DNA-binding fourfold spermine functionalized perylene bisimide dye. Lett Org Chem 2(4):349–353
121. Menacher F, Wagenknecht H-A (2011) Synthesis of DNA with green perylene bisimides as DNA base substitutions. Eur J Org Chem 2011(24):4564–4570. doi:10.1002/ejoc.201100519
122. Das A, Molla MR, Maity B, Koley D, Ghosh S (2012) Hydrogen-bonding induced alternate stacking of donor (D) and acceptor (A) chromophores and their supramolecular switching to segregated states. Chem Eur J 18(32):9849–9859. doi:10.1002/chem.201201140
123. Au-Yeung HY, Dan Pantoş G, Sanders JKM (2009) Amplifying different [2]catenanes in an aqueous donor−acceptor dynamic combinatorial library. J Am Chem Soc 131 (44):16030–16032. doi:10.1021/ja906634h
124. Ghosh S, Ramakrishnan S (2005) Small-molecule-induced folding of a synthetic polymer. Angew Chem Int Ed 44(34):5441–5447. doi:10.1002/anie.200501448
125. Gabriel GJ, Iverson BL (2002) Aromatic oligomers that form hetero duplexes in aqueous solution. J Am Chem Soc 124(51):15174–15175. doi:10.1021/ja0275358
126. Peebles C, Piland R, Iverson BL (2013) More than meets the eye: conformational switching of a stacked dialkoxynaphthalene-naphthalenetetracarboxylic diimide (DAN-NDI) foldamer

to an NDI-NDI fibril aggregate. Chem Eur J 19(35):11598–11602. doi:10.1002/chem.201302009
127. Bradford VJ, Iverson BL (2008) Amyloid-like behavior in abiotic, amphiphilic foldamers. J Am Chem Soc 130(4):1517–1524. doi:10.1021/ja0780840
128. Takada T, Otsuka Y, Nakamura M, Yamana K (2014) Formation of a charge transfer complex within a hydrophobic cavity in DNA. RSC Adv 4(103):59440–59443. doi:10.1039/C4RA11761A
129. Bhosale R, Misek J, Sakai N, Matile S (2010) Supramolecular n/p-heterojunction photosystems with oriented multicolored antiparallel redox gradients (OMARG-SHJs). Chem Soc Rev 39(1):138–149
130. Chen C-H, Liu K-Y, Sudhakar S, Lim T-S, Fann W, Hsu C-P, Luh T-Y (2005) Efficient light harvesting and energy transfer in organic-inorganic hybrid multichromophoric materials. J Phys Chem B 109(38):17887–17891
131. Peng K-Y, Chen S-A, Fann W-S (2001) Efficient light harvesting by sequential energy transfer across aggregates in polymers of finite conjugational segments with short aliphatic linkages. J Am Chem Soc 123(46):11388–11397
132. Fleming CN, Maxwell KA, DeSimone JM, Meyer TJ, Papanikolas JM (2001) Ultrafast excited-state energy migration dynamics in an efficient light-harvesting antenna polymer based on Ru(II) and Os(II) polypyridyl complexes. J Am Chem Soc 123(42):10336–10347
133. Zang L, Che Y, Moore JS (2008) One-dimensional self-assembly of planar pi-conjugated molecules: adaptable building blocks for organic nanodevices. Acc Chem Res 41(12):1596–1608
134. Hide F, Díaz-García MA, Schwartz BJ, Heeger AJ (1997) New developments in the photonic applications of conjugated polymers. Acc Chem Res 30(10):430–436
135. Greyson EC, Stepp BR, Chen X, Schwerin AF, Paci I, Smith MB, Akdag A, Johnson JC, Nozik AJ, Michl J, Ratner MA (2010) Singlet exciton fission for solar cell applications: energy aspects of interchromophore coupling. J Phys Chem B 114(45):14223–14232
136. Hardin BE, Hoke ET, Armstrong PB, Yum J-H, Comte P, Torres T, Frechet JMJ, Nazeeruddin MK, Gratzel M, McGehee MD (2009) Increased light harvesting in dye-sensitized solar cells with energy relay dyes. Nat Photon 3(7):406–411
137. Coakley KM, McGehee MD (2004) Conjugated polymer photovoltaic cells. Chem Mater 16(23):4533–4542
138. Shionoya M, Kimura E, Shiro M (1993) A new ternary zinc(II) complex with [12]aneN4 (=1,4,7,10-tetraazacyclododecane) and AZT (=3′-azido-3′-deoxythymidine). Highly selective recognition of thymidine and its related nucleosides by a zinc(II) macrocyclic tetraamine complex with novel complementary associations. J Am Chem Soc 115(15):6730–6737
139. Kikuta E, Murata M, Katsube N, Koike T, Kimura E (1999) Novel recognition of thymine base in double-stranded DNA by zinc(II)-macrocyclic tetraamine complexes appended with aromatic groups. J Am Chem Soc 121(23):5426–5436
140. Nakamura M, Okaue T, Takada T, Yamana K (2012) DNA-templated assembly of naphthalenediimide arrays. Chem Eur J 18(1):196–201
141. Tsuto K, Nakamura M, Takada T, Yamana K (2014) Diketopyrrolopyrrole J-aggregates formed by self-organization with DNA. Chem Asian J 9:1618–1622. doi:10.1002/asia.201402063

Chapter 6
Polymerase Synthesis of Base-Modified DNA

Jitka Dadová, Hana Cahová, and Michal Hocek

Abstract Enzymatic synthesis of base-modified DNA by polymerase incorporation of modified nucleotides is discussed. Modified 2′-deoxyribonucleoside triphosphates (dNTPs) are key substrates for polymerases and can be prepared either by triphosphorylation of modified nucleosides or by direct aqueous cross-coupling reactions of halogenated dNTPs with alkynes, arylboronic acids, or alkenes. The methods of polymerase synthesis include primer extension, PCR, nicking enzyme amplifications, and other methods which enable the synthesis of diverse types of long or short and double-stranded DNA or single-stranded oligonucleotides. The applications include labeling in diagnostics (labeling or coding of DNA bases) and chemical biology (bioconjugations, modulation of protein binding, etc.).

6.1 Introduction

DNA containing functionalized nucleobases have attracted interest of many researchers in the past decades. They have high potential for applications in chemical biology, nanotechnology, material science, as well as bioanalysis [1–4]. Oligonucleotides (ON) up to 100–200 nucleotides are nowadays routinely synthesized on the solid support using phosphoramidite building blocks [5]. Diverse types of base-modified ONs or DNA have been prepared by this method [6–10], but

J. Dadová • H. Cahová
Gilead Sciences & IOCB Research Center, Institute of Organic Chemistry and Biochemistry, Academy of Sciences of the Czech Republic, Flemingovo nam. 2, 16610 Prague 6, Czech Republic

M. Hocek (✉)
Gilead Sciences & IOCB Research Center, Institute of Organic Chemistry and Biochemistry, Academy of Sciences of the Czech Republic, Flemingovo nam. 2, 16610 Prague 6, Czech Republic

Department of Organic Chemistry, Faculty of Science, Charles University in Prague, Hlavova 8, 12843 Prague 2, Czech Republic
e-mail: hocek@uochb.cas.cz

K. Nakatani, Y. Tor (eds.), *Modified Nucleic Acids*, Nucleic Acids and Molecular Biology 31, DOI 10.1007/978-3-319-27111-8_6

this approach has certain limitations. Major problem is that the additional functional groups are often not compatible with the phosphoramidite synthesis protocol. In particular, any strongly electrophilic or nucleophilic groups, as well as any oxidizable functions, must be orthogonally protected. On the other hand, DNA can be modified also post-synthetically, mostly by CuAAC click reactions of alkyne-modified ONs [11–13].

Base-modified DNA can be also prepared enzymatically by polymerase incorporation of functionalized nucleotides using 2′-deoxynucleoside triphosphates (dNTPs) as substrates. This approach was pioneered by Langer et al. in 1981 [14], and since then many functionalized dNTPs (**dN^{X}TP**s) were used as substrates for various DNA polymerases [15–17]. In this chapter, we focus on the synthesis and polymerase incorporation of nucleotide derivatives modified/labeled at the major-groove edge of the nucleobase with intact Watson–Crick base-pairing properties (typically 5-substituted pyrimidine and 7-substituted 7-deazapurine nucleotides). It does not cover the field of unnatural base pairs and expansion of the genetic alphabet which has been reviewed elsewhere [18].

6.2 Synthesis of Base-Modified 2-′Deoxynucleoside 5′-*O*-Triphosphates

Base-functionalized dNTPs containing a functional group or a label at the major-groove edge of the nucleobase are the key starting compounds needed as potential substrates for polymerases. The substituent is linked to the nucleobase typically through a stable C–C bond, which can be easily formed by Pd-catalyzed cross-coupling reactions. Then, the modified dNTPs can be prepared in two principal approaches. In the classical approach, functionalized dNTPs is obtained by cross-coupling of a halogenated 2′-deoxynucleoside (**dN^{I}**) followed by triphosphorylation of the resulting modified nucleoside (**dN^{X}**) to obtain target **dN^{X}TP**s (Scheme 6.1a). The second (more straightforward) approach is a direct aqueous cross-coupling reaction of a halogenated dNTP (**dN^{I}TP**s, Scheme 6.1b) [19].

6.2.1 5′-O-Triphosphorylation of 2′-Deoxynucleosides

Several methods have been developed (Scheme 6.2) for the conversion of base-functionalized or halogenated 2′-deoxynucleosides (**dN^{X}**) to their 5′-*O*-triphosphates (**dN^{X}TP**s) [20]. However, so far there is no universal, high-yielding phosphorylation protocol applicable to any nucleoside. The protocols and conditions for the triphosphorylation as well as for the purification need to be optimized case by

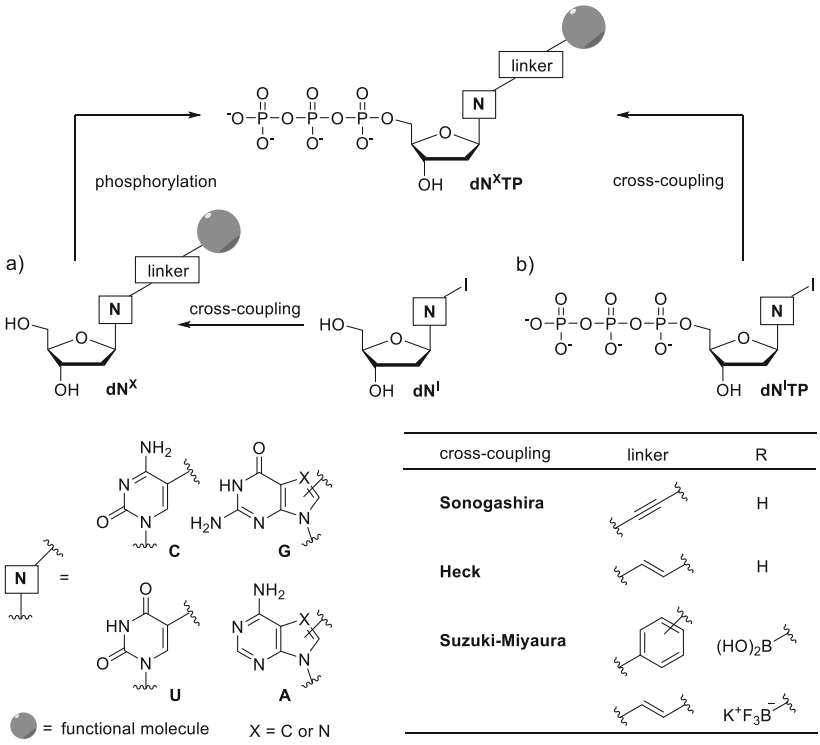

Scheme 6.1 General strategy for the synthesis of base-modified dNTPs by (**a**) modification of the corresponding nucleoside followed by triphosphorylation and (**b**) direct cross-coupling reaction

case for the synthesis of each desired **dN^{X}TP** depending on the type of nucleobase and on the substituent.

Yoshikawa described the first method for the synthesis of dNTPs (Scheme 6.2a) [21, 22]. The procedure involves selective 5′-mono-phosphorylation of an unprotected nucleoside with phosphorous oxychloride yielding 5′-phosphorodichloridate intermediate. This intermediate is in situ treated with tributylammonium pyrophosphate to yield a cyclic triphosphate, which is subsequently hydrolyzed to the desired dNTP. This method is simple, (in most cases) selective, and no protection of the initial nucleoside is required. A broad palette of **dN^{X}TP**s prepared by this protocol has been reported (Fig. 6.1), bearing amino [23–28] and thiol groups [29], boronic acids (**1**) [30], perfluoroalkylated chains (**2**) [31], diamondoids (**3**) [32], amphiphilic chains (**4**) [33], fluorescent molecular rotors (**5**) [34], organic polymers [35], vinyl group [36], amino acids [37], or even oligonucleotides (**6**) [38, 39].

Another very popular protocol for the 5′-*O*-triphosphorylation of 2′-deoxynucleosides was reported by Ludwig and Eckstein using salicyl chlorophosphite in the first step (Scheme 6.2b) [40]. In this method, 3′-*O*-protected 2′-deoxynucleoside is reacted with salicyl chlorophosphite yielding activated phosphite intermediate which is in situ treated with tributylammonium pyrophosphate.

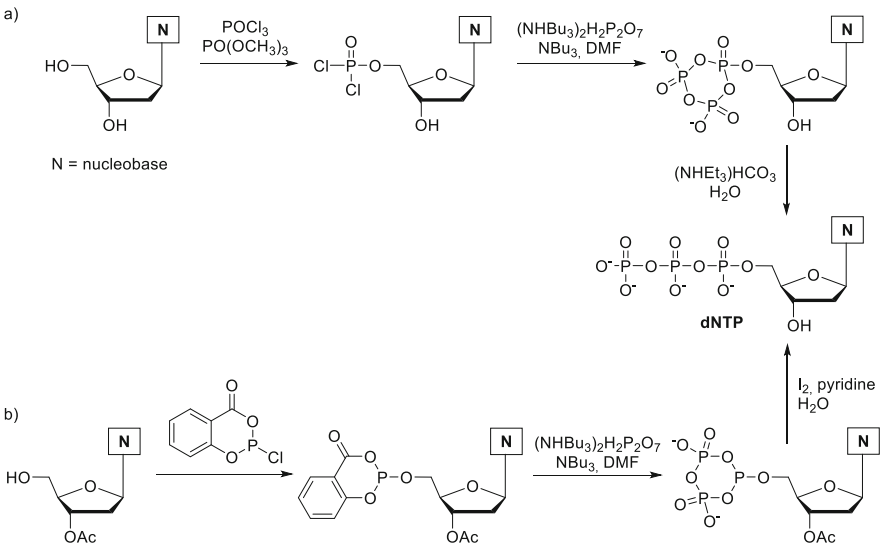

Scheme 6.2 Methods for the synthesis of dNTPs. (**a**) Yoshikawa; (**b**) Ludwig–Eckstein protocol

The resulting cyclic intermediate is subsequently oxidized by iodine and hydrolyzed to the desired dNTP. An advantage of this approach is higher specificity (lower formation of undesired side products, e.g., mono-, di-, and oligophosphates) compared to the Yoshikawa method [41]. However, the use of protected nucleoside is necessary, which results in additional steps of protecting group manipulation. The Ludwig–Eckstein protocol has been applied for the synthesis of **dN^{X}TP**s (Fig. 6.1) containing metal complexes [42], histamine (**7**) [43] or residues applicable in organocatalysis (**8**) [44] and spin-labeling (**9**) [45].

6.2.2 Cross-Coupling Reactions for the Direct Synthesis of dN^{X}TPs

The second approach is the direct synthesis of **dN^{X}TP**s by aqueous cross-coupling reactions of dN^{I}TP. It overcomes the traditional multistep procedures involving protecting group manipulation. Cross-coupling reactions are in general very tolerant to most of reactive functional groups. The expansion of this methodology was allowed by the development of water soluble phosphine ligands [46, 47]. Shaughnessy and co-workers tested several of these ligands in aqueous Suzuki–Miyaura arylation of unprotected 5-iodo-2′-deoxyuridine and 7-iodo-7-deaza-2′-deoxyadenosine with arylboronic acids in a mixture of water and acetonitrile [48]. They found that the best catalytic system is $Pd(OAc)_2$ in combination with commercially available triphenylphosphine-3,3′,3″-trisulfonic acid trisodium salt (TPPTS) in the presence of inorganic base (i.e., Na_2CO_3). This palladium

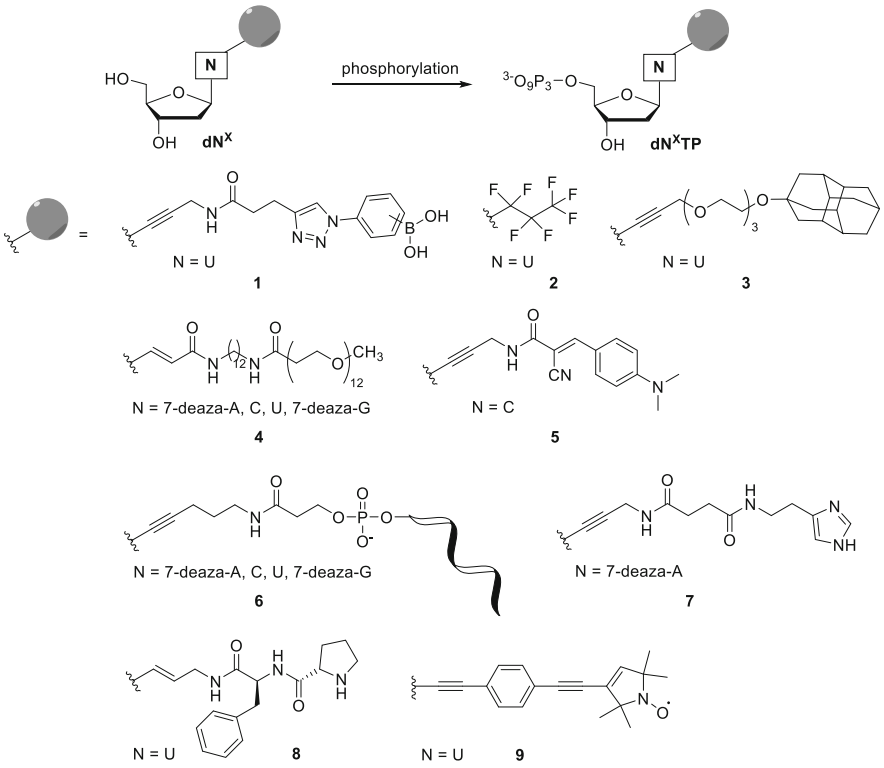

Fig. 6.1 Selected examples of **dN^{X}TP**s synthesized using triphosphorylation of **dN^X**

complex has been later used for the synthesis of many functionalized **dN^{X}TP**s either by Sonogashira or Suzuki–Miyaura cross-coupling reactions.

The main general drawback of direct modification of **dN^{I}TP**s via cross-coupling reactions is the sensitivity of triphosphates towards hydrolysis under elevated temperature. Therefore, it is important to optimize the reaction to be completed within 30–60 min. Fortunately, the bases required for coupling (either, e.g., K_2CO_3 for Suzuki or triethylamine for Sonogashira and Heck) stabilize the triphosphates. Nevertheless, efficient purification of the desired **dN^{X}TP**s by reverse-phase HPLC must be performed to separate hydrolytic byproducts.

Sonogashira coupling

The first direct aqueous cross-coupling reaction of an iodinated dNTP was performed by Thoresen et al. in 2003 [49]. They used the Sonogashira reaction for the attachment of rigid fluorescein moieties to 5-I-dUTP (Fig. 6.2, entry 1). A high $Pd(OAc)_2$ catalyst loading (20 mol%) in the presence of TPPTS (5 equiv to Pd) and triethylamine (36 equiv) as a base was necessary and the reaction proceeded at 25 °C in phosphate buffer (pH 7.2) with a long reaction time (17 h). The final triphosphate **10** was isolated in moderate yield (41 %).

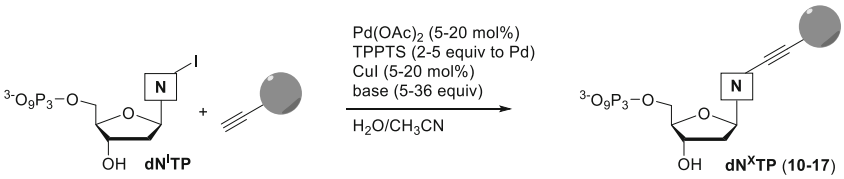

Entry	dN^ITP		dN^XTP	Conditions	Yield (%)
1	5-I-dUTP	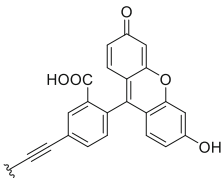	**10**	phosphate buffer (pH 7.2) 25 °C, 17 h	41
2	5-I-dUTP	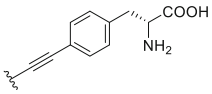	**11a**	60 °C, 30-45 min	66
3	7-I-7deaza-dATP		**11b**		67
4	5-I-dCTP	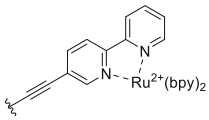	**12**	70 °C, 1 h	35
5	7-I-7deaza-dATP	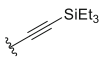	**13**	80 °C, 30 min	11
6	5-I-dCTP	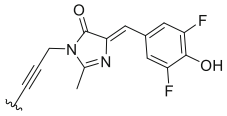	**14**	55 °C, 45 min	28
7	5-I-dCTP	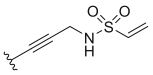	**15**	75 °C, 45 min	23
8	7-I-7deaza-dATP	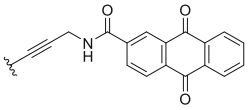	**16**	75 °C, 1 h	80
9	7-I-7deaza-dATP	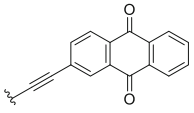	**17**	$[Pd(PPh_3)_2Cl_2]$ (5 mol%) CuI (10 mol%) $i Pr_2EtN$ (10 equiv) H_2O/DMF (1:4) 75 °C, 1 h	30

Fig. 6.2 Selected examples of **dN^XTPs** syntheses using direct Sonogashira cross-coupling

Later on, Hocek and co-workers modified conditions for the Sonogashira reaction of **dN^{I}TP**s (elevated temperatures and short times), and they extended the reaction scope to the functionalization of purine nucleotides (entries 2 and 3) [50]. Base-modified nucleoside triphosphates **11a**,**b** containing phenylalanine moiety were prepared through aqueous-phase arylation using lower amount of Pd $(OAc)_2$ (10 mol%) with the same Pd to TPPTS ratio (1:5). The solvent was changed to water/acetonitrile mixture (2:1), and the reaction was performed at higher temperature (60 °C) for significantly shorter time (30–45 min). The yields of both pyrimidine (**11a**) and purine (**11b**) (d) NTPs were comparable (ca. 66 %). The reaction conditions were further utilized for the synthesis of **dN^{X}TP**s bearing metal complexes (**12**; entry 4) [51] or triethylsilylethynyl group (**13**) (entry 5) [52]. TMS-acetylene-linked triphosphate **13** was isolated in poor yield of 11 % after direct Sonogashira reaction due to poor solubility of TMS-acetylene in water, and therefore classical triphosphorylation of substituted nucleoside was performed giving a higher yield (47 %).

Later on, the Sonogashira reaction was also used to prepare **dN^{X}TP**s in which conjugate ethynyl linker was changed to non-conjugate propargyl tether (entries 6 and 7). Fluorescent derivative **14** (entry 6) [53] and highly reactive Michael acceptor **15** (entry 7) [54] were isolated in the yields of about 25 %. Balintová et al. synthesized **dN^{X}TP**s **16** and **17** bearing redox active anthraquinone (entries 8 and 9) [55]. Derivative **16** in which anthraquinone is attached to 7-deaza-dATP via propargyl linker was isolated in good yield (80 %) under the above-mentioned conditions. But no conversion to **17** was observed when anthraquinone was conjugated with ethynyl linker. Therefore, in that case, it was necessary to change the solvent to a mixture water/DMF (1:4). Complex $[Pd(PPh_3)_2Cl_2]$ (5 mol%) was used as a catalyst, and the triphosphate **17** was obtained in satisfactory yield of 30 %.

In general, the Sonogashira cross-coupling reaction can be used to prepare **dN^{X}TP**s directly from their **dN^{I}TP**s precursors in one step. The catalytic system of choice is mostly $Pd(OAc)_2$/TPPTS (1:1 to 1:5), and 5–20 mol% of palladium is sufficient to perform the reaction. Reaction time is maximum 1 h at 50–80 °C, and the products are usually isolated by reverse-phase HPLC. The yields of **dN^{X}TP**s depend strongly on the type of dN^{I}TP and structure of the modification to be introduced, and they may vary from 10 to 80 %.

Suzuki–Miyaura coupling

Aqueous Suzuki–Miyaura cross-coupling reaction has been extensively used for arylation of various halogenated nucleosides and nucleotides [56]. Recently, it was even applied to direct post-synthetic modification of halogenated oligonucleotides [57–59].

The first Suzuki reaction of iodinated dNTP with aryl boronic acid was published by Hocek and co-workers in 2006 (Fig. 6.3, entry 1) [60]. In this work, various reaction conditions were tested for the introduction of phenylalanine moiety to the position 8 of dATP yielding triphosphate **18**. The best catalytic system was Pd $(OAc)_2$ (10 mol% with 5 equiv of TPPTS), and an excess of Cs_2CO_3 (36 equiv) was

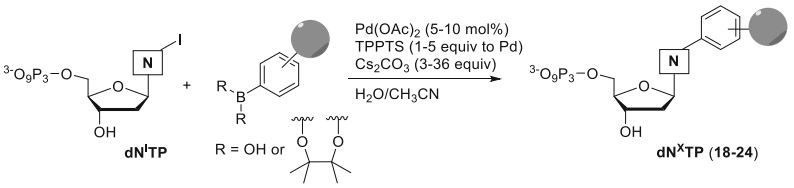

Entry	$dN^{I}TP$		$dN^{X}TP$	Conditions	Yield (%)
1	8-Br-dATP	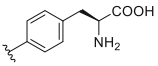	**18**	125 °C, 20 min	55
2	8-Br-dGTP		**19**	Na_2PdCl_4 (2.5 mol%) TPPTS (2.5 equiv to Pd) K_2CO_3 (1.5 equiv) H_2O 80 °C, 1 h	85
3	7-I-7deaza-dATP	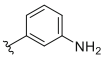	**20a**	120 °C, 30 min [a]	40
4	5-I-dCTP		**20b**		43
5	5-I-dUTP		**20c**		43
6	7-I-7deaza-dGTP		**20d**	100 °C, 30 min [b]	32
7	5-I-dCTP		**21**	100 °C, 1 h	65
8[c]	7-I-7deaza-dATP	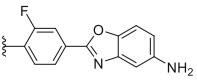	**22**	90 °C, 45 min	26
9	7-I-7deaza-dATP	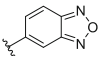	**23a**	75 °C, 45 min	22
10	5-I-dCTP		**23b**		10
11[d]	5-I-dUTP		**24**	80 °C, 50 min	56

[a] Mixture H_2O/CH_3CN (2:1). [b] Mixture H_2O/CH_3CN (1:2). [c] Aryl pinacolatoboronate was used. [d] Vinyl trifluoroborate potassium salt was used instead of boronic acid.

Fig. 6.3 Selected examples of base-modified **$dN^{X}TP$**s synthesis by direct Suzuki–Miyaura arylation reaction

used as a base. The reaction was conducted in the mixture water/acetonitrile (2:1) at 125 °C for 20 min, and the desired product **18** was isolated in good yield (55 %).

In the same year, Wagner published synthesis of 8-phenyl-dGTP **19** (entry 2) via Suzuki reaction [61]. In this case, water was used as a sole solvent and Na_2PdCl_4/TPPTS as a source of palladium which was able to overcome the generally reduced reactivity of guanine nucleos(t)ides in Pd-catalyzed reactions. Guanine moiety has

an acidic proton, which may be deprotonated in high pH and high temperature used for Suzuki reaction. The resulting anion can coordinate to palladium [62].

Conditions for the direct Suzuki reaction on 7-I-7-deaza-dGTP were optimized also by Hocek group (entries 3–6). When preparing a series of all four aminophenyl-modified **dN^{X}TP**s, adenosine (**20a**), cytidine (**20b**), and thymidine (**20c**) derivatives were isolated in good yields (40–43 %) [63] using the general procedure developed previously [60]. However, 7-deazaguanosine derivative **19d** was obtained in very low yield, and the product contained a high proportion of the corresponding diphosphate [64]. Later on, an improved synthesis of **20d** with higher yield and lower diphosphate content has been published [65]. Lower reaction temperature (100 °C) and higher acetonitrile content (2:1 mixture acetonitrile/water) together with a higher excess of the boronic acid led to the desired triphosphate **20d** in 32 % yield.

The Suzuki cross-coupling was then used for the preparation of various functionalized **dN^{X}TP**s bearing reactive aldehyde moiety (e.g., compound **21**, entry 7) [66], fluorescent biaryl derivatives (e.g., 2-phenyl-5-aminobenzoxazole **22**, entry 8) [67] and redox active benzofurazane (e.g., compound **23**, entries 9 and 10) [68].

Very recently, Suzuki cross-coupling was also used for the direct synthesis of vinyl-modified dNTPs (entry 11) [69]. The reaction proceeded smoothly with Pd(OAc)$_2$/TPPTS in the ratio 1:1, and for instance, the target-modified uridine triphosphate **24** was obtained in good yield (56 %).

To conclude, **dN^{X}TP**s can be efficiently prepared from their dN^{I}TPs precursors using Suzuki–Miyaura arylation with the system Pd(OAc)$_2$/TPPTS (1:1 to 1:5; 5–10 mol% of palladium) as a catalyst. Reaction time (30 min to 1 h) and temperature (75–125 °C) depend strongly on the type of dN^{I}TP and the structure of the modification to be introduced. The products are usually isolated by reverse-phase HPLC in the yields varying from 10 to 70 %.

Heck reaction

The Heck reaction is another extensively applied cross-coupling which is very useful in attachment of alkenyl groups [70, 71]. It has been used for functionalization of pyrimidine nucleosides [72]. On the other hand, its application for modifications of purine nucleosides was problematic [73]. In Famulok group, methyl acrylate-modified 2′-deoxyuridine triphosphate was prepared by Heck coupling of 5-I-dU with methyl acrylate in DMF followed by classical triphosphorylation [26]. The first direct aqueous-phase alkenylation of 5-I-dUTP was described by Shanmugasundaram in 2012 [74]. (*E*)-5-Aminoallyl dUTP was synthesized by the reaction of 5-I-dUTP with allylamine in the presence of K_2PdCl_4 and sodium acetate at room temperature. The product was isolated in good yield (74 %), but its further incorporation into DNA or any other application has never been described.

Hocek group has studied reactivity of iodinated nucleotides in aqueous Heck reaction with *n*-butyl acrylate and compared it with the triphosphorylation of acrylate-modified nucleosides (Fig. 6.4) [75]. For those cross-couplings, it was

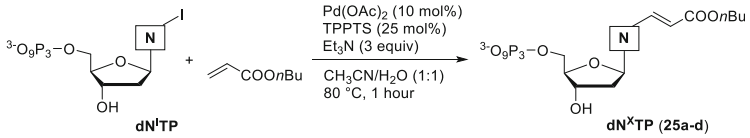

Entry	$dN^{I}TP$	Product	Yield of Heck coupling (%)	Yield of phosphorylation (%)[a]
1	7-I-7deaza-dATP	**25a**	43	28
2	7-I-7deaza-dGTP	**25b**	44	25
3	5-I-dUTP	**25c**	4[b]	40
4	5-I-dCTP	**25d**	-	19

[a] Conditions: 1. $\mathbf{dN^{BA}}$, $POCl_3$, $PO(OMe)_3$, 0 °C; 2. $(NHBu_3)_2H_2P_2O_7$, Bu_3N, DMF, 0 °C; 3. 2M TEAB.
[b] The yield of **25c** increased to 14 % when DMF was used as a solvent.

Fig. 6.4 Synthesis of acrylate-modified dNTPs by direct aqueous Heck reaction

necessary to use large excess of *n*-butylacrylate (10 equiv to $\mathbf{dN^{I}TP}$s), $Pd(OAc)_2$ (10 mol%), and TPPTS (2.5 equiv to Pd). The mixture water/acetonitrile (1:1) was used as solvent, and the reaction was stopped after 1 h at 80 °C in order to minimize hydrolysis of the triphosphates.

The developed method is suitable for the synthesis of alkenylated 7-deazapurine nucleotides (**25a**, **b**; entries 1 and 2), for which the direct aqueous coupling procedure is more efficient than phosphorylation of modified nucleosides. However, only traces of modified uridine triphosphate **25c** and no cytidine triphosphate **25d** at all (entries 3 and 4) were isolated from the Heck reaction of 5-iodopyrimidine dNTPs. Therefore, the phosphorylation approach is necessary for the synthesis of these compounds. It means that the aqueous Heck cross-coupling is far less general than the Suzuki and Sonogashira reactions, and further optimization of alkene-modified dNTPs synthesis is highly desirable.

6.3 Enzymatic Synthesis of Base-Modified DNA

Incorporation of base-modified nucleotides by DNA polymerases

Base-modified dNTPs have been broadly utilized in enzymatic synthesis of modified DNA. In order to preserve the Watson–Crick pairing and minor-groove interactions which are needed for efficient and specific incorporation, the modifications must be attached to positions which point out to the major groove (Fig. 6.5). In pyrimidines, the modification can be linked at position 5. However, it was shown that a bulky group bound in position 8 of purines (dA or dG) could initiate or even stabilize DNA in Z form. The reason is steric hindrance between sugar hydrogens

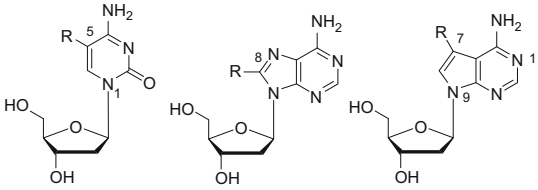

Fig. 6.5 The types of base-modified nucleosides

and group in position 8 in classic anti-conformation. This is also explanation for poor acceptance of 8-modified dATP by various DNA polymerases [50, 76]. Only small modifications such as bromine, methyl [76], or vinyl [77] were well tolerated by DNA polymerases. Also 8-oxo-dGTP was shown to be a poor substrate for DNA polymerase and reverse transcriptase [78, 79]. Incorporation of 8-NH_2-dGTP proceeded more easily [80]. Perrin et al. synthesized series of modified dATP bearing imidazolyl group bound via various linkers in position 8, but incorporation of just two of them was partially successful using Dpo4 DNA polymerase from Y family [81]. They also claimed synthesis of DNAzymes containing these bases using Sequenase DNA polymerase, but products were not sufficiently characterized to prove the identity of the ON products [82, 83]. Therefore, purines are replaced by 7-deazapurines, and the substituent is linked to the position 7. These dNTPs analogues are excellent substrates for polymerases, and these modifications do not disrupt the structure of DNA duplexes.

DNA polymerases

The DNA polymerases are divided into seven main DNA polymerase families (A, B, C, D, X, Y, and RT—reverse transcriptase) [84, 85]. The classification is based on amino acid sequence comparisons and crystal structure analysis. Independent of their detailed domain structures, all polymerases share common architectural feature—shape of the right hand consisting of "thumb," "palm," and "fingers" domains. The palm domain catalyzes the phosphoryl transfer reaction, finger domain mediates interactions with the incoming dNTP and template base to which it is paired, and thumb plays role in positioning of the duplex DNA and translocation [86]. Most commonly used DNA polymerases in molecular biology are polymerases from families A (Klenow fragment of *Escherichia coli*, Taq of *Thermus aquaticus*, Sequenase genetically engineered form T7 DNA polymerase, and Bst of *Bacillus stearothermophilus*) or B (KOD Dash of *Pyrococcus kodakaraensis*, Vent of *Thermococcus litoralis*, Pwo of *Pyrococcus woesei*, Phusion—*Pyrococcus*-like enzyme fused with a processivity-enhancing domain, 9°N from the extremely thermophilic marine archaea *Thermococcus* species 9°N-7, Deep Vent from *Pyrococcus* species GB-D, and Therminator a genetically engineered form of 9°N). The (exo−) variants of Klenow fragment and Vent DNA polymerases or Sequenase, 9°N, and KOD XL without $3' \rightarrow 5'$ exonuclease activity are also broadly employed for synthesis of the base-modified DNA. While the PEX reaction in presence of the DNA polymerases with the exonuclease activity may lead to products of various length as DNA polymerase cleaves from the 3′end already incorporated nucleotides. The (exo−) DNA polymerases produce the

dsDNA with uniform length, and the analysis of the product is not complicated by the presence of shorter fragments. Some polymerases (especially KOD XL) produce $n+1$ products resulting from non-templated incorporation of another nucleotide (usually dA) at the 3′-end. Beside commercially available DNA polymerases, the attempts to develop engineered DNA polymerase with enhanced efficiency for modified dNTPs were made. Holliger group prepared DNA polymerase capable of synthesis of 1 kb DNA decorated with cyanine dyes [87]. Marx et al. Generated new Therminator pol variant able to polymerize sugar as well as base-modified nucleotides [88]. Many base-modified dNTPs might be enzymatically incorporated to DNA by several DNA polymerases. However, the KOD XL proved to be the most robust for enzymatic synthesis of modified DNA and became the polymerase of the first choice.

Methods for polymerase synthesis of ONs and DNA

The very basic reaction leading to dsDNA modified in one strand is primer extension (PEX). The reaction takes place at isothermal conditions suitable for particular DNA polymerase. The reaction mixture contains a template DNA, primer, modified dNTP (one or more), and the remaining natural dNTPs (Fig. 6.6a). The PEX is suitable for synthesis of middle-sized dsDNA (15–100 bp) with modification in one strand. The analysis of PEX is usually performed by polyacrylamide gel electrophoresis. The primer is labeled at 5′-end by radioactive ^{32}P phosphate or by fluorescent tag. The employment of fluorescent tags allows avoiding the fastidious work with radioactivity but provides lower sensitivity and lower signal/noise ratio. To get reliable information on incorporation of modified dNTP into DNA, the parallel "positive" and "negative" experiments must be performed. The experiment with natural dNTPs must lead to fully

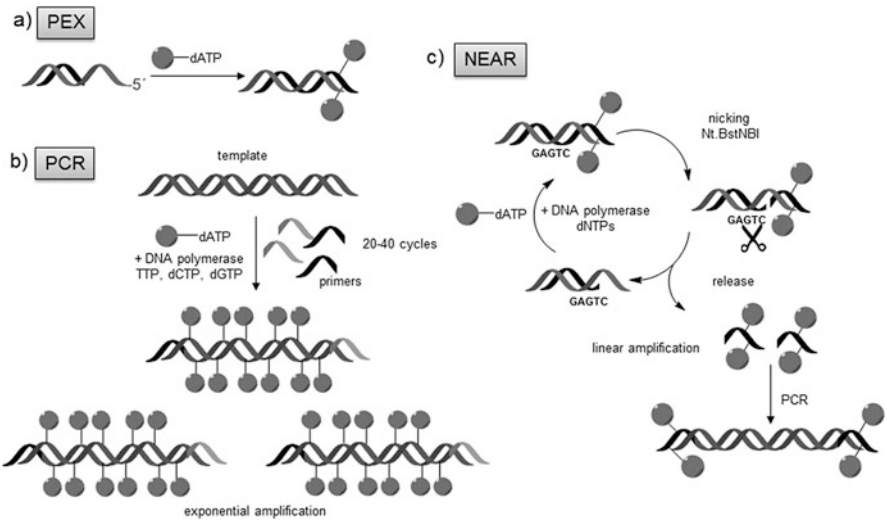

Fig. 6.6 Methods of enzymatic synthesis of base-modified DNA

prolonged product contrary to negative control where the modified dNTP is missing as well as its natural derivative, and the product must not be prolonged, i.e., DNA polymerase has high fidelity and experimental conditions do not force it to implement instead of missing dNTP one of the remaining dNTPs (e.g., instead modified dATP the incorporation of TTP, dCTP, or dGTP does not take place). The PEX can also serve for preparation of modified ssDNA. In such case, the product is after reaction captured to magnetic streptavidin beads via biotin attached to 5′end of template. The ssDNA product is released by thermal denaturation into solution [89].

Polymerase chain reaction (PCR) is a method for preparation of longer DNA (100–1000 bp) with higher density of modifications in both strands (Fig. 6.6b). The reaction mixture contains template DNA, a pair of primers, heat-stable DNA polymerase, and modified dNTP (one or more) and the rest of natural dNTPs. The reaction is usually performed in 20–40 PCR cycles of repeated denaturation, annealing, and extension of primers. The temperatures and times of individual steps depend on sequence, length, and sequence of primers, DNA polymerase, and modifications of dNTPs. It seems that every modification demands optimization of conditions. The analysis of products is usually performed by agarose gel electrophoresis, and the products are visualized by interaction with fluorescent intercalation reagents (ethidium bromide, SYBR green, GelRed, etc.). In certain cases such as DNA containing derivatives of 2′-deoxy-7-deazaguanosine, the fluorescent visualization is not possible as DNA product quenches the fluorescence of DNA intercalators [90–92]. In such case, the radioactive labeling is necessary. Since the PCR requires that not only the modified dNTPs are perfect substrates for the polymerase but also the polymerase must be able to read through modified template, the PCR reaction often fails for dNTPs modified by bulkier groups.

A complementary technique for the synthesis of short modified ssONs was recently developed by using nicking enzyme amplification reaction (NEAR) [93]. The method is isothermal DNA amplification of short oligonucleotides (10–20 nt) employing DNA polymerase, Nt.Bst.NBI nicking endonuclease, and modified dNTPs (Fig. 6.6c). The principle is that short oligonucleotides cannot form stable DNA duplex at higher temperature and dissociate under these conditions. But primer is long enough to hybridize with template and initiate the PEX in the presence of DNA polymerase, modified, and natural dNTPs. Afterwards, the nicking enzyme cleaves the dsDNA in the recognition sequence, and the shorter oligonucleotide is released to solution. The template sequence is again available to hybridization with new primer and reaction repeats. The reaction was scaled up to nanomolar amounts and was proved to be suitable source of short-labeled primers for PCR or functionalized aptamers [94]. The method has been already used for synthesis of DNA bearing fluorescent molecular rotors [34] or fluorescent Bodipy-labeled DNA [95].

All of aforementioned methods lead to DNA modified along all the newly synthesized stretches. In case the site-specific single labeling of internal parts of the DNA sequence is demanded, there is also general methodology for enzymatic

synthesis of single-stranded oligonucleotides bearing a single base modification in the internal part of the sequence. A single nucleotide incorporation (SNI) procedure is applicable to all sequences when the modification is followed by another nucleobase. If the modification needs to be incorporated into a homonucleobase stretch, a biotinylated template one-nucleotide longer than the primer is employed for the SNI, and after the magnetoseparation, the extended primer is subjected to another PEX with a full-length template [65]. Another enzymatic method for incorporation of various tags to 3′-end employs terminal deoxynucleotidyl transferase. Unlike classical PEX or PCR, the method does not require template strand and therefore is virtually applicable to any DNA [64].

Competitive incorporation of modified dNTPs in the presence of natural nucleotides

Common enzymatic methods for the synthesis of the modified DNA employ functionalized dNTPs in the absence of its natural counterpart to ensure the incorporation of modified dNTP by the DNA polymerase. It is even possible to synthesize the DNA decorated by modifications on every base by PEX or PCR in the presence of only modified dNTPs [25, 26, 96]. But the data on the incorporation of modified dNTP in competition with natural one were very scarce, presumably because it was believed that the modified dNTPs must be much worse substrates for DNA polymerases. Nevertheless, any in vivo application of modified dNTPs requires the incorporation of functionalized dNTPs in the competition with their natural counterparts.

Only recently, a specific method for studying the outcome of competitive incorporation of modified nucleotide in the presence of the corresponding natural dNTP was developed (Fig. 6.7). This method is based on selective cleavage of sequence containing incorporated modified or natural nucleotide by restriction endonucleases. Certain restriction endonucleases are not capable to cleave DNA containing the modification in recognition sequence. This study brought surprising discovery that certain aromatic derivatives of 7-deaza dATP can be better substrates for the DNA polymerases and can be incorporated into DNA with priority whereas most dCTPs are slightly worse substrates. The kinetic study and semi-empirical calculations explain this phenomenon by increased affinity of the 7-aryl dATPs to

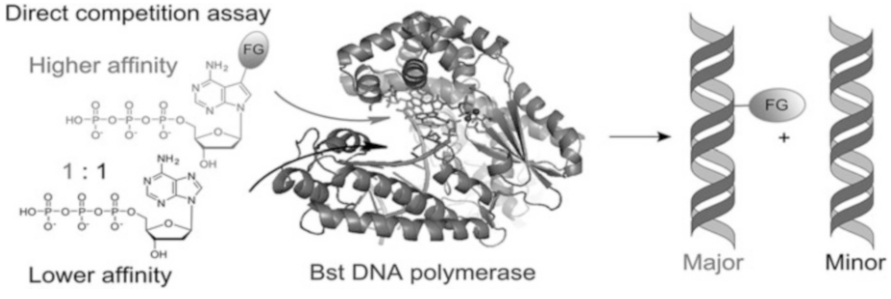

Fig. 6.7 Competitive incorporation of base-modified dATP versus dATP [94]

the active site of the polymerase complex with the primer and template because of increased stacking [97].

Applications

Base-functionalized DNA have been utilized in a wide range of applications from bioanalysis to chemical biology or material science. The enzymatic synthesis of base-modified DNA is suitable for labeling of DNA by fluorescent [98, 99], redox [100], or spin tags [45]. Hocek and Fojta groups developed a broad range of dNTPs bearing oxidizable and reducible functional group and their enzymatic incorporation into DNA. They reported preparation of the DNA modified by ferrocene [89], amino- and nitrophenyl [63, 101], ruthenium and osmium complexes [51], anthraquinones [55], benzofurazanes [68], and many others. There is necessity of development of full set of four orthogonal labels, readable in the presence of all others. So far, they have identified two orthogonal labels (nitrophenyl group and benzofurazane).

The fluorescently labeled nucleic acids are used in Sanger sequencing [102], and many dNTPs bearing fluorescent tags are known [23, 49, 103] and have been already commercially available. Recently, the environment sensitive labels for study of the DNA–protein interaction [104] or for the detection of changes in the secondary DNA structures [67] were developed. The GFP fluorophore as an example of a molecular rotor lighting-up due to steric hindrance was attached to dNTP, incorporated to DNA, and used for protein-binding assays and time-resolved study of PEX [53].

DNA bearing diverse reactive groups is also suitable for post-synthetic bioconjugations. DNA with attached ethynyl and octadiynyl derivatives was used for the Cu-catalyzed click reactions with various azido-modified functional groups [7, 11, 105, 106]. Azido-modified oligonucleotides were developed to be post-synthetically modified by Staudinger ligation [107, 108]. Oligonucleotides bearing dienes were used in Diels–Alder (DA) cycloadditions [109, 110] and DNA with attached vinyl in inverse DA reaction [13, 36]. Cu-catalyzed click reactions and inverse DA reaction were shown to be orthogonal, and both post-synthetic reactions can be performed on one molecule of DNA [111]. Direct Suzuki–Miyaura cross-coupling on oligonucleotides allowed insertion of aryl or alkenyl groups [59]. A new type of photoswitchable DNA was also prepared by Suzuki reaction under modified conditions [58]. Recently, the maleimide-modified fluorescent dyes were attached to DNA via new “photoclick” reaction of diaryltetrazole group [10]. The DNA decorated with aldehyde can be stained by hydrazone formation [66] and used in synthesis of peptide-oligonucleotide conjugates via reductive amination with lysine [112]. Vinylsulfonamide, as an excellent Michael acceptor for selective reaction with cysteine, attached to DNA cross-links with p53 protein [54].

The base-modified DNA found several applications in modern chemical biology. For example, Williams [27, 113] or Hollenstein [44] use base-modified dNTPs for in-vitro selection of DNAzymes. Base-modified dNTPs were also used in preparation of DNA aptamers to improve their performance, activity, or biostability [15, 114].

Hocek group studied the influence of various modifications in major groove to interaction with restriction endonucleases type II. They have detected quite high tolerance of RE to base-modified A or T, whereas C and G modifications were not tolerated and such DNA was poor substrate for RE [69, 115, 116, 117]. The in-depth knowledge on tolerance of RE to various modifications led to development of the transient protection of the DNA sequence from the RE cleavage. The DNA bearing (triethylsilyl)ethynyl group in position 7 of 7-deaza-A is protected from cleavage of certain RE till the moment the silyl group is cleaved by ammonia. Such DNA with attached ethynyl group is then good substrate for RE and can be easily cleaved in recognition sequence [52]. Also photocaging can serve for transient protection of DNA from RE cleavage. Photocleavable 5-[(2-nitrobenzyl)oxymethyl]uracil dNTP was used for enzymatic synthesis of DNA resistamt to cleavage by REs. Irradiation by UV (365 nm) causes photocleavage and releases 5-hydroxymethyluracil DNA which is cleavable by most RE [118].

6.4 Conclusion and Outlook

Many diverse base-modified dNTPs are easily available by triphosphorylation of modified nucleosides or by aqueous cross-coupling reactions of halogenated dNTPs with terminal alkynes or arylboronic acids. There are several polymerase-catalyzed procedures suitable for the synthesis of different long or short ssONs or dsDNA containing one, several, or many modifications. They already found many applications in bioanalysis and chemical biology. Major drawback of the polymerase synthesis of modified ONs is the relatively high cost and limited potential for scale-up where the most important problem is an efficient separation of the ON products from dNTPs and enzymes on larger scale. We assume that some smart application of solid-supported enzymatic reactions and/or affinity-based purifications should be feasible to solve this problem. Further there is a lot of space for further development of new useful labels and for many practical applications in chemical biology.

References

1. Wilner OI, Wilner I (2012) Functionalized DNA nanostructures. Chem Rev 112:2528–2556. doi:10.1021/cr200104q
2. Clever GH, Kaul C, Carell T (2007) DNA-metal base pairs. Angew Chem Int Ed 46:6226–6236. doi:10.1002/anie.200701185
3. Famulok M, Hartig JS, Mayer G (2007) Functional aptamers and aptazymes in biotechnology, diagnostics, and therapy. Chem Rev 107:3715–3743. doi:10.1021/cr0306743
4. Torring T, Voigt NV, Nangreave J et al (2011) DNA origami: a quantum leap for self-assembly of complex structures. Chem Soc Rev 40:5636–5646. doi:10.1039/c1cs15057j

5. Caruthers MH (2013) The chemical synthesis of DNA/RNA: our gift to science. J Biol Chem 288:1420–1427. doi:10.1074/jbc.X112.442855
6. Gierlich J, Burley GA, Gramlich PME et al (2006) Click chemistry as a reliable method for the high-density postsynthetic functionalization of alkyne-modified DNA. Org Lett 8:3639–3642. doi:10.1021/ol0610946
7. Seela F, Sirivolu VR, Chittepu P (2008) Modification of DNA with octadiynyl side chains: synthesis, base pairing, and formation of fluorescent coumarin dye conjugates of four nucleobases by the alkyne-azide "click" reaction. Bioconjugate Chem 19:211–224. doi:10.1021/bc700300f
8. Shibata T, Glynn N, McMurry TBH et al (2006) Novel synthesis of O6-alkylguanine containing oligodeoxyribonucleotides as substrates for the human DNA repair protein, O6-methylguanine DNA methyltransferase (MGMT). Nucleic Acids Res 34:1884–1891. doi:10.1093/nar/gkl117
9. Hentschel S, Alzeer J, Angelov T et al (2012) Synthesis of DNA interstrand cross-links using a photocaged nucleobase. Angew Chem Int Ed 51:3466–3469. doi:10.1002/anie.201108018
10. Arndt S, Wagenknecht H (2014) "Photoclick" postsynthetic modification of DNA. Angew Chem 53:14580–14582. doi:10.1002/anie.201407874
11. Gramlich PME, Wirges CT, Manetto A, Carell T (2008) Postsynthetic DNA modification through the copper-catalyzed azide-alkyne cycloaddition reaction. Angew Chem Int Ed 47:8350–8358. doi:10.1002/anie.200802077
12. El-Sagheer AH, Brown T (2010) Click chemistry with DNA. Chem Soc Rev 39:1388–1405. doi:10.1039/b901971p
13. Rieder U, Luedtke NW (2014) Alkene-tetrazine ligation for imaging cellular DNA. Angew Chem Int Ed 53:9168–9172. doi:10.1002/anie.201403580
14. Langer PR, Waldrop AA, Ward DC (1981) Enzymatic synthesis of biotin labeled polynucleotides: novel nucleic acid affinity probes. Proc Natl Acad Sci U S A 78:6633–6637
15. Kuwahara M, Sugimoto N (2010) Molecular evolution of functional nucleic acids with chemical modifications. Molecules 15:5423–5444. doi:10.3390/molecules15085423
16. Hollenstein M (2012) Nucleoside triphosphates-building blocks for the modification of nucleic acids. Molecules 17:13569–13591. doi:10.3390/molecules171113569
17. Hocek M (2014) Synthesis of base-modified 2′-deoxyribonucleoside triphosphates and their use in enzymatic synthesis of modified DNA for applications in bioanalysis and chemical biology. J Org Chem 79:9914–9921. doi:10.1021/jo5020799
18. Hirao I, Kimoto M (2012) Unnatural base pair systems toward the expansion of the genetic alphabet in the central dogma. Proc Jpn Acad Ser B 88:345–367. doi:10.2183/pjab.88.345
19. Hocek M, Fojta M (2008) Cross-coupling reactions of nucleoside triphosphates followed by polymerase incorporation. Construction and applications of base-functionalized nucleic acids. Org Biomol Chem 6:2233–2241. doi:10.1039/b803664k
20. Burgess K, Cook D (2000) Syntheses of nucleoside triphosphates. Chem Rev 100:2047–2059. doi:10.1021/cr990045m
21. Yoshikawa M, Kato T, Takenishi T (1967) A novel method for phosphorylation of nucleosides to 5′-nucleotides. Tetrahedron Lett 8:5065–5068
22. Gillerman I, Fischer B (2010) An improved one-pot synthesis of nucleoside 5′-triphosphate analogues. Nucleosides Nucleotides Nucleic Acids 29:245–256. doi:10.1080/15257771003709569
23. Kuwahara M, Nagashima JI, Hasegawa M et al (2006) Systematic characterization of 2-′-deoxynucleoside-5′-triphosphate analogs as substrates for DNA polymerases by polymerase chain reaction and kinetic studies on enzymatic production of modified DNA. Nucleic Acids Res 34:5383–5394. doi:10.1093/nar/gkl637
24. Sakthivel K, Barbas CF (1998) Expanding the potential of DNA for binding and catalysis: highly functionalized dUTP derivatives that are substrates for thermostable DNA polymerases. Angew Chem Int Ed 37:2872–2875

25. Thum O, Jäger S, Famulok M (2001) Functionalized DNA: a new replicable biopolymer. Angew Chem Int Ed 40:3990–3993
26. Jäger S, Rasched G, Kornreich-Leshem H et al (2005) A versatile toolbox for variable DNA functionalization at high density. J Am Chem Soc 127:15071–15082. doi:10.1021/ja051725b
27. Lee SE, Sidorov A, Gourlain T et al (2001) Enhancing the catalytic repertoire of nucleic acids: a systematic study of linker length and rigidity by two modified triphosphates during PCR. Nucleic Acids Res 29:1565–1573
28. Seela F, Feiling E, Gross J et al (2001) Fluorescent DNA: the development of 7-deazapurine nucleoside triphosphates applicable for sequencing at the single molecule level. J Biotechnol 86:269–279. doi:10.1016/S0168-1656(00)00418-1
29. Roychowdhury A, Illangkoon H, Hendrickson CL, Benner SA (2004) 2′-deoxycytidines carrying amino and thiol functionality: synthesis and incorporation by vent (exo-) polymerase. Org Lett 6:489–492. doi:10.1021/ol0360290
30. Cheng Y, Dai C, Peng H et al (2011) Design, synthesis, and polymerase-catalyzed incorporation of click-modified boronic acid-TTP analogues. Chem Asian J 6:2747–2752. doi:10.1002/asia.201100229
31. Holzberger B, Marx A (2009) Enzymatic synthesis of perfluoroalkylated DNA. Bioorg Med Chem 17:3653–3658. doi:10.1016/j.bmc.2009.03.063
32. Wang Y, Tkachenko BA, Schreiner PR, Marx A (2011) Diamondoid-modified DNA. Org Biomol Chem 9:7482. doi:10.1039/c1ob05929g
33. Fujita H, Nakajima K, Kasahara Y et al (2015) Polymerase-mediated high-density incorporation of amphiphilic functionalities into DNA: enhancement of nuclease resistance and stability in human serum. Bioorg Med Chem Lett 25:333–336. doi:10.1016/j.bmcl.2014.11.037
34. Dziuba D, Pohl R, Hocek M (2015) Polymerase synthesis of DNA labelled with benzylidene cyanoacetamide-based fluorescent molecular rotors: fluorescent light-up probes for DNA-binding proteins. Chem Commun 51:4880–4882. doi:10.1039/c5cc00530b
35. Baccaro A, Marx A (2010) Enzymatic synthesis of organic-polymer-grafted DNA. Chem Eur J 16:218–226. doi:10.1002/chem.200902296
36. Bußkamp H, Batroff E (2014) Efficient labelling of enzymatically synthesized vinyl-modified DNA by an inverse-electron-demand Diels–Alder reaction. Chem Commun 50:10827–10829. doi:10.1039/c4cc04332d
37. Kuwahara M, Hanawa K, Ohsawa K et al (2006) Direct PCR amplification of various modified DNAs having amino acids: convenient preparation of DNA libraries with high-potential activities for in vitro selection. Bioorg Med Chem 14:2518–2526. doi:10.1016/j.bmc.2005.11.030
38. Baccaro A, Steck AL, Marx A (2012) Barcoded nucleotides. Angew Chem Int Ed 51:254–257. doi:10.1002/anie.201105717
39. Verga D, Welter M, Steck AL, Marx A (2015) DNA polymerase-catalyzed incorporation of nucleotides modified with a G-quadruplex-derived DNAzyme. Chem Commun 51:7379–7381. doi:10.1039/c5cc01387a
40. Ludwig J, Eckstein F (1989) Rapid and efficient synthesis of nucleoside 5′-*O*-(1-thiotriphosphates), 5′-triphosphates and 2′,3′-cyclophosphorothioates using 2-chloro-4H-1,3,2-benzodioxaphosphorin-4-one. J Org Chem 54:631–635. doi:10.1021/jo00264a024
41. Caton-Williams J, Lin L, Smith M, Huang Z (2011) Convenient synthesis of nucleoside 5′-triphosphates for RNA transcription. Chem Commun 47:8142–8144. doi:10.1039/c1cc12201k
42. Weizman H, Tor Y (2002) Redox-active metal-containing nucleotides: synthesis, tunability, and enzymatic incorporation into DNA. J Am Chem Soc 124:1568–1569. doi:10.1021/ja017193q
43. Hollenstein M (2013) Deoxynucleoside triphosphates bearing histamine, carboxylic acid, and hydroxyl residues—synthesis and biochemical characterization. Org Biomol Chem 11:5162–5172. doi:10.1039/c3ob40842f

44. Hollenstein M (2012) Synthesis of deoxynucleoside triphosphates that include proline, urea, or sulfonamide groups and their polymerase incorporation into DNA. Chem Eur J 18:13320–13330. doi:10.1002/chem.201201662
45. Obeid S, Yulikov M, Jeschke G, Marx A (2008) Enzymatic synthesis of multiple spin-labeled DNA. Angew Chem Int Ed 47:6782–6785. doi:10.1002/anie.200802314
46. Genet JP, Savignac M (1999) Recent developments of palladium(0) catalyzed reactions in aqueous medium. J Organomet Chem 576:305–317
47. Shaughnessy KH (2009) Hydrophilic ligands and their application in aqueous-phase metal-catalyzed reactions. Chem Rev 109:643–710. doi:10.1021/cr800403r
48. Western EC, Daft JR, Johnson EM et al (2003) Efficient one-step Suzuki arylation of unprotected halonucleosides, using water-soluble palladium catalysts. J Org Chem 68:6767–6774. doi:10.1021/jo034289p
49. Thoresen LH, Jiao G-S, Haaland WC et al (2003) Rigid, conjugated, fluoresceinated thymidine triphosphates: syntheses and polymerase mediated incorporation into DNA analogues. Chem Eur J 9:4603–4610. doi:10.1002/chem.200304944
50. Čapek P, Cahová H, Pohl R et al (2007) An efficient method for the construction of functionalized DNA bearing amino acid groups through cross-coupling reactions of nucleoside triphosphates followed by primer extension or PCR. Chem Eur J 13:6196–6203. doi:10.1002/chem.200700220
51. Vrábel M, Horáková P, Pivoňková H et al (2009) Base-modified DNA labeled by $[Ru(bpy)_3]^{2+}$ and $[Os(bpy)_3]^{2+}$ complexes: construction by polymerase incorporation of modified nucleoside triphosphates, electrochemical and luminescent properties, and applications. Chem Eur J 15:1144–1154. doi:10.1002/chem.200801538
52. Kielkowski P, Macíčková-Cahová H, Pohl R, Hocek M (2011) Transient and switchable (triethylsilyl)ethynyl protection of DNA against cleavage by restriction endonucleases. Angew Chem Int Ed 50:8727–8730. doi:10.1002/anie.201102898
53. Riedl J, Ménová P, Pohl R et al (2012) GFP-like fluorophores as DNA labels for studying DNA-protein interactions. J Org Chem 77:8287–8293. doi:10.1021/jo301684b
54. Dadová J, Orság P, Pohl R et al (2013) Vinylsulfonamide and acrylamide modification of DNA for cross-linking with proteins. Angew Chem Int Ed 52:10515–10518. doi:10.1002/anie.201303577
55. Balintová J, Pohl R, Horáková P et al (2011) Anthraquinone as a redox label for DNA: synthesis, enzymatic incorporation, and electrochemistry of anthraquinone-modified nucleosides, nucleotides, and DNA. Chem Eur J 17:14063–14073. doi:10.1002/chem.201101883
56. Hervé G, Sartori G, Enderlin G et al (2014) Palladium-catalyzed Suzuki reaction in aqueous solvents applied to unprotected nucleosides and nucleotides. RSC Adv 4:18558–18594. doi:10.1039/c3ra47911k
57. Omumi A, Beach DG, Baker M et al (2011) Postsynthetic guanine arylation of DNA by Suzuki-Miyaura cross-coupling. J Am Chem Soc 133:42–50. doi:10.1021/ja106158b
58. Cahová H, Jäschke A (2013) Nucleoside-based diarylethene photoswitches and their facile incorporation into photoswitchable DNA. Angew Chem Int Ed 52:3186–3190. doi:10.1002/anie.201209943
59. Lercher L, McGouran JF, Kessler BM et al (2013) DNA modification under mild conditions by Suzuki-Miyaura cross-coupling for the generation of functional probes. Angew Chem Int Ed 52:10553–10558. doi:10.1002/ange.201304038
60. Čapek P, Pohl R, Hocek M (2006) Cross-coupling reactions of unprotected halopurine bases, nucleosides, nucleotides and nucleoside triphosphates with 4-borono-phenylalanine in water. Synthesis of (purin-8-yl)- and (purin-6-yl)phenylalanines. Org Biomol Chem 4:2278–2284. doi:10.1039/b604010a
61. Collier A, Wagner G (2006) A facile two-step synthesis of 8-arylated guanosine mono- and triphosphates (8-aryl GXPs). Org Biomol Chem 4:4526–4532. doi:10.1039/b614477b
62. Western EC, Shaughnessy KH (2005) Inhibitory effects of the guanine moiety on Suzuki couplings of unprotected halonucleosides in aqueous media. J Org Chem 70:6378–6388. doi:10.1021/jo0508321

63. Cahová H, Havran L, Brázdilová P et al (2008) Aminophenyl- and nitrophenyl-labeled nucleoside triphosphates: synthesis, enzymatic incorporation, and electrochemical detection. Angew Chem Int Ed 47:2059–2062. doi:10.1002/anie.200705088
64. Horáková P, Macíčková-Cahová H, Pivoňková H et al (2011) Tail-labelling of DNA probes using modified deoxynucleotide triphosphates and terminal deoxynucleotidyl tranferase. Application in electrochemical DNA hybridization and protein-DNA binding assays. Org Biomol Chem 9:1366–1371. doi:10.1039/c3cc41438h
65. Ménová P, Cahová H, Plucnara M et al (2013) Polymerase synthesis of oligonucleotides containing a single chemically modified nucleobase for site-specific redox labelling. Chem Commun 49:4652–4654. doi:10.1039/c3cc41438h
66. Raindlová V, Pohl R, Sanda M, Hocek M (2010) Direct polymerase synthesis of reactive aldehyde-functionalized DNA and its conjugation and staining with hydrazines. Angew Chem Int Ed 49:1064–1066. doi:10.1002/anie.200905556
67. Riedl J, Pohl R, Rulíšek L, Hocek M (2012) Synthesis and photophysical properties of biaryl-substituted nucleos(t)ides. Polymerase synthesis of DNA probes bearing solvatochromic and pH-sensitive dual fluorescent and ^{19}F NMR labels. J Org Chem 77:1026–1044. doi:10.1021/jo202321g
68. Balintová J, Plucnara M, Vidláková P et al (2013) Benzofurazane as a new redox label for electrochemical detection of DNA: towards multipotential redox coding of DNA bases. Chem Eur J 19:12720–12731. doi:10.1002/chem.201301868
69. Mačková M, Pohl R, Hocek M (2014) Polymerase synthesis of DNAs bearing vinyl groups in the major groove and their cleavage by restriction endonucleases. ChemBioChem 15:2306–2312. doi:10.1002/cbic.201402319
70. Heck RF (1979) Palladium-catalyzed reactions of organic halides with olefins. Acc Chem Res 12:146–151
71. Beletskaya IP, Cheprakov AV (2000) The Heck reaction as a sharpening stone of palladium catalysis. Chem Rev 100:3009–3066. doi:10.1021/cr9903048
72. Agrofoglio LA, Gillaizeau I, Saito Y (2003) Palladium-assisted routes to nucleosides. Chem Rev 103:1875–1916. doi:10.1021/cr010374q
73. Tobrman T, Dvořák D (2008) Heck reactions of 6- and 2-halopurines. Eur J Org Chem 17:2923–2928. doi:10.1002/ejoc.200800091
74. Kore AR, Shanmugasundaram M (2012) Highly stereoselective palladium-catalyzed Heck coupling of 5-iodouridine-5′-triphosphates with allylamine: a new efficient method for the synthesis of (E)-5-aminoallyl-uridine-5′-triphosphates. Tetrahedron Lett 53:2530–2532. doi:10.1016/j.tetlet.2012.03.018
75. Dadova J, Pohl R, Fojta M, Hocek M (2013) Aqueous Heck cross-coupling preparation of acrylate-modified nucleotides and nucleoside triphosphates for polymerase synthesis of acrylate-labeled DNA. J Org Chem 78:9627–9637. doi:10.1021/jo4011574
76. Cahová H, Pohl R, Bednárová L, Nováková K (2008) Synthesis of 8-bromo-, 8-methyl-and 8-phenyl-dATP and their polymerase incorporation into DNA. Org Biomol Chem 6:3657–3660. doi:10.1039/B811935J
77. Siegmund V, Diederichsen U, Marx A (2012) Enzymatic synthesis of 8-vinyl-and 8-styryl-2′-deoxyguanosine modified DNA—novel fluorescent molecular probes. Bioorg Med Chem Lett 22:3136–3139. doi:10.1016/j.bmcl.2012.03.056
78. Pavlov YI, Minnick DT, Izuta S, Kunkel TA (1994) DNA replication fidelity with 8-oxodeoxyguanosine triphosphate. Biochemistry 33:4695–4701. doi:10.1021/bi00181a029
79. Morgues S, Trzcionka J, Vasseur JJ, Pratviel G, Meunier B (2008) Incorporation of oxidized guanine nucleoside 5′-triphosphates in DNA with DNA polymerases and preparation of single-lesion carrying DNA. Biochemistry 47:4788–4799. doi:10.1021/bi7022199
80. Kamath-Loeb AS, Hizi A, Kasai H, Loeb LA (1997) Incorporation of the guanosine triphosphate analogs 8-oxo-dGTP and 8-NH_2-dGTP by reverse transcriptases and mammalian DNA polymerases. J Biol Chem 47:4788–4799. doi:10.1074/jbc.272.9.5892
81. Lam C, Hipolito C, Perrin DM (2008) Synthesis and enzymatic incorporation of modified deoxyadenosine triphosphates. Eur J Org Chem 4915–4923. doi:10.1002/ejoc.200800381

82. Hollenstein M, Hipolito CJ, Lam CH (2009) A self-cleaving DNA enzyme modified with amines, guanidines and imidazoles operates independently of divalent metal cations (M^{2+}). Nucleic Acids Res 5:1638–1649. doi:10.1093/nar/gkn1070
83. Hipolito CJ, Hollenstein M, Lam CH (2011) Protein-inspired modified DNAzymes: dramatic effects of shortening side-chain length of 8-imidazolyl modified deoxyadenosines in selecting RNaseA mimicking DNAzymes. Org Biomol Chem 9:2266–2273. doi:10.1039/c1ob05359k
84. Ito J, Braithwaite DK (1991) Compilation and alignment of DNA polymerase sequences. Nucleic Acids Res 19:4045–4049. doi:10.1093/nar/19.15.4045
85. Filée J, Forterre P, Sen-Lin T, Laurent J (2002) Evolution of DNA polymerase families: evidences for multiple gene exchange between cellular and viral proteins. J Mol Evol 54:763–773. doi:10.1007/s00239-001-0078-x
86. Steitz TA (1999) DNA polymerases: structural diversity and common mechanisms. J Biol Chem 274:17395–17398. doi:10.1074/jbc.274.25.17395
87. Ramsay N, Jemth A-S, Brown A et al (2010) CyDNA: synthesis and replication of highly Cy-dye substituted DNA by an evolved polymerase. J Am Chem Soc 132:5096–5104. doi:10.1021/ja909180c
88. Staiger N, Marx A (2010) A DNA polymerase with increased reactivity for ribonucleotides and C5-modified deoxyribonucleotides. ChemBioChem 11:1963–1966. doi:10.1002/cbic.201000384
89. Brázdilová P, Vrábel M, Pohl R, Pivoňková H et al (2007) Ferrocenylethynyl derivatives of nucleoside triphosphates: synthesis, incorporation, electrochemistry, and bioanalytical applications. Chem Eur J 13:9527–9533. doi:10.1002/chem.200701249
90. Li H, Peng X, Seela F (2004) Fluorescence quenching of parallel-stranded DNA bound ethidium bromide: the effect of 7-deaza-2′-deoxyisoguanosine and 7-halogenated derivatives. Bioorg Med Chem Lett 14:6031–6034. doi:10.1016/j.bmcl.2004.09.071
91. Seela F, Sirivolu VR, Chittepu P (2007) Modification of DNA with octadiynyl side chains: synthesis, base pairing, and formation of fluorescent coumarin dye conjugates of four nucleobases by the alkyne-azide "click" reaction. Bioconjugate Chem 19:211–224. doi:10.1021/bc700300f
92. Ménová P, Dziuba D, Güixens-Gallardo P et al (2015) Fluorescence quenching in oligonucleotides containing 7-substituted 7-deazaguanine bases prepared by the nicking enzyme amplification reaction. Bioconjugate Chem 26:361–366. doi:10.1021/acs.bioconjchem.5b00006
93. Ménová P, Hocek M (2012) Preparation of short cytosine-modified oligonucleotides by nicking enzyme amplification reaction. Chem Commun 48:6921–6923. doi:10.1039/C2CC32930A
94. Ménová P, Raindlová V, Hocek M (2013) Scope and limitations of the nicking enzyme amplification reaction for the synthesis of base-modified oligonucleotides and primers for PCR. Bioconjugate Chem 24:1081–1093. doi:10.1021/bc400149q
95. Dziuba D, Pohl R, Hocek M (2014) Bodipy-labeled nucleoside triphosphates for polymerase synthesis of fluorescent DNA. Bioconjugate Chem 25:1984–1995. doi:10.1021/bc5003554
96. Jäger S, Famulok M (2004) Generation and enzymatic amplification of high-density functionalized DNA double strands. Angew Chem Int Ed 43:3337–3340. doi:10.1002/anie.200453926
97. Kielkowski P, Fanfrlík J, Hocek M (2014) 7-Aryl-7-deazaadenine 2′-deoxyribonucleoside triphosphates (dNTPs): better substrates for DNA polymerases than dATP in competitive incorporations. Angew Chem Int Ed 53:7552–7555. doi:10.1002/anie.201404742
98. Sinkeldam RW, Greco NJ, Tor Y (2010) Fluorescent analogs of biomolecular building blocks: design, properties, and applications. Chem Rev 110:2579–2619. doi:10.1021/cr900301e
99. Tanpure AA, Pawar MG, Srivatsan SG (2013) Fluorescent nucleoside analogs: probes for investigating nucleic acid structure and function. Isr J Chem 53:366–378. doi:10.1002/ijch.201300010

100. Palecek E, Bartosik M (2012) Electrochemistry of nucleic acids. Chem Rev 112:3427–3481. doi:10.1021/cr200303p
101. Balintová J, Špaček J, Pohl R, Brázdová M et al (2015) Azidophenyl as a click-transformable redox label of DNA suitable for electrochemical detection of DNA–protein interactions. Chem Sci 6:575–587. doi:10.1039/C4SC01906G
102. Prober JM, Trainor GL, Dam RJ, Hobbs FW et al (1987) A system for rapid DNA sequencing with fluorescent chain-terminating dideoxynucleotides. Science 238:336–341. doi:10.1126/science.2443975
103. Turcatti G, Romieu A, Fedurco M, Tairi AP (2008) A new class of cleavable fluorescent nucleotides: synthesis and optimization as reversible terminators for DNA sequencing by synthesis. Nucleic Acids Res 36:e25. doi:10.1093/nar/gkn021
104. Riedl J, Pohl R, Ernsting NP et al (2012) Labelling of nucleosides and oligonucleotides by solvatochromic 4-aminophthalimide fluorophore for studying DNA–protein interactions. Chem Sci 3:2797–2806. doi:10.1039/C2SC20404E
105. Gramlich P, Warncke S, Gierlich J, Carell T (2008) Click–click–click: single to triple modification of DNA. Angew Chem Int Ed 47:3442–3444. doi:10.1002/anie.200705664
106. Seela F, Sirivolu VR (2008) Pyrrolo-dC oligonucleotides bearing alkynyl side chains with terminal triple bonds: synthesis, base pairing and fluorescent dye conjugates prepared by the azide–alkyne "click" reaction. Org Biomol Chem 6:1674–1687. doi:10.1039/b719459e
107. Weisbrod SH, Marx A (2007) A nucleoside triphosphate for site-specific labelling of DNA by the Staudinger ligation. Chem Commun 1828–1830. doi:10.1039/b809528k
108. Baccaro A, Weisbrod SH, Marx A (2007) DNA conjugation by the Staudinger Ligation: new thymidine analogues. Synthesis 1949–1954. doi:10.1055/s-2007-983728
109. Borsenberger V, Howorka S (2009) Diene-modified nucleotides for the Diels–Alder-mediated functional tagging of DNA. Nucleic Acids Res 37:1477–1485. doi:10.1093/nar/gkn1066
110. Schoch J, Wiessler M, Jäschke A (2010) Post-synthetic modification of DNA by inverse-electron-demand Diels–Alder reaction. J Am Chem Soc 132:8846–8847. doi:10.1021/ja102871p
111. Schoch J, Staudt M, Samanta A, Wiessler M, Jäschke A (2012) Site-specific one-pot dual labeling of DNA by orthogonal cycloaddition chemistry. Bioconjugate Chem 23:1382–1385. doi:10.1021/bc300181n
112. Raindlová V, Pohl R, Hocek M (2012) Synthesis of aldehyde-linked nucleotides and DNA and their bioconjugations with lysine and peptides through reductive amination. Chem Eur J 18:4080–4087. doi:10.1002/chem.201103270
113. Gourlain T, Sidorov A, Mignet N, Thorpe SJ et al (2001) Enhancing the catalytic repertoire of nucleic acids. II. Simultaneous incorporation of amino and imidazolyl functionalities by two modified triphosphates during PCR. Nucleic Acids Res 29:1898–1905. doi:10.1093/nar/29.9.1898
114. Imaizumi Y, Kasahara Y, Fujita H, Kitadume S et al (2013) Efficacy of base-modification on target binding of small molecule DNA aptamers. J Am Chem Soc 135:9412–9419. doi:10.1021/ja4012222
115. Macíčková-Cahová H, Hocek M (2009) Cleavage of adenine-modified functionalized DNA by type II restriction endonucleases. Nucleic Acids Res 37:7612–7622. doi:10.1093/nar/gkp845
116. Macíčková-Cahová H, Pohl R, Hocek M (2011) Cleavage of functionalized DNA containing 5-modified pyrimidines by type II restriction endonucleases. ChemBioChem 12:431–438. doi:10.1002/cbic.201000644
117. Mačková M, Boháčová S, Perlíková P et al (2015) Polymerase synthesis and restriction enzyme cleavage of DNA containing 7-substituted 7-deazaguanine. ChemBioChem 16:2225–2236. doi:10.1002/cbic.201500315
118. Vaníková Z, Hocek M (2014) Polymerase synthesis of photocaged DNA resistant against cleavage by restriction endonucleases. Angew Chem Int Ed 53:6734–6737. doi:10.1002/anie.201402370

Chapter 7
Photo-Cross-Linking Reaction in Nucleic Acids: Chemistry and Applications

Takashi Sakamoto and Kenzo Fujimoto

Abstract DNA/RNA photo-cross-linking reactions have great potential for regulating the functions, structures, and characters of nucleic acids. The photo-responsive manner of the reactions are expected to enable spatiotemporal control of the behavior of nucleic acids, and the thermal irreversibility of the photo-cross-linked product is expected to enable construction of thermally stable nanostructured DNA.

Therefore, various artificial nucleic acids that can photo-cross-link to complementary DNA or RNA have been developed. This chapter focuses on the chemistry of these artificial nucleic acids and their application for molecular, cellular, and chemical biology, and also DNA nanotechnology, which is an interesting field for the construction of nanomaterials in a bottom-up manner, such as DNA origami.

7.1 Introduction

The photoreaction in DNA is one of the most important phenomena in the basic study of photodamage in genomic DNA. Since the first report about photo-induced pyrimidine dimer formation in double-stranded DNA by Setlow [1], many researchers have made huge efforts to understand the mechanism of the phenomenon [2–6] and the mechanism of DNA damage repair [7–11]. In this phenomenon, the cyclobutane ring formation through [2 + 2] photocycloaddition between C5 and C6 carbons on adjacent pyrimidine bases in a DNA strand is induced by UVB irradiation, and the photoproduct causes genomic damage and cell death.

Psoralen derivatives, which can photo-cross-link with C5–C6 carbons on a pyrimidine base in a DNA strand in the same manner of pyrimidine dimer formation by UVA irradiation; contrary to the case of pyrimidine dimer formation caused by UVB irradiation [12], are key compounds in the history of the development of photo-functionalized nucleic acids. Based on the findings of psoralen derivatives,

T. Sakamoto • K. Fujimoto (✉)
School of Materials Science, Japan Advanced Institute of Science and Technology, Ishikawa, Japan
e-mail: kenzo@jaist.ac.jp

K. Nakatani, Y. Tor (eds.), *Modified Nucleic Acids*, Nucleic Acids and Molecular Biology 31, DOI 10.1007/978-3-319-27111-8_7

until now, various artificial nucleic acids that can photo-cross-link with DNA or RNA with a sequence specific manner have been developed.

In this chapter, the mechanism of the photo-cross-linking reaction in nucleic acids including psoralen and other artificial DNA photo-cross-linkers is described. The application of the photo-cross-linking reaction on gene regulation, genome analysis, and DNA-based nanotechnology is also described.

7.2 Psoralen: A Natural DNA Photo-Cross-Linker

Naturally occurring plant furocoumarins, e.g., psoralen, methoxsalen, and trioxsalen (Fig. 7.1a), that can photoreact with a DNA double strand, have been used for the treatment of various skin disorders such as Atopic dermatitis, vitiligo, eczema, and cutaneous T-cell lymphoma. Psoralen derivatives effectively intercalate to the AT region of genomic DNA, and the fran ring and pyrone ring of psoralen derivative form cyclobutane ring with C5–C6 carbon on the thymine bases possessed at different two DNA strands with UVA irradiation (Fig. 7.1b). Thus, the two DNA strands can be bound covalently via a photo-cross-linked product consisting of a psoralen derivative and two thymine bases [12]. This induces cytotoxicity only at the photoirradiated area. Since the psoralen derivatives can be activated with UVA irradiation, treatment of skin disorders can be performed without significant photodamage of genomic DNA caused by UVB-induced pyrimidine dimer formation.

The photoreaction including psoralen derivative also occurs in AU regions in double-stranded RNA. Using this reaction, the secondary structures of RNAs were successfully explored [13–16].

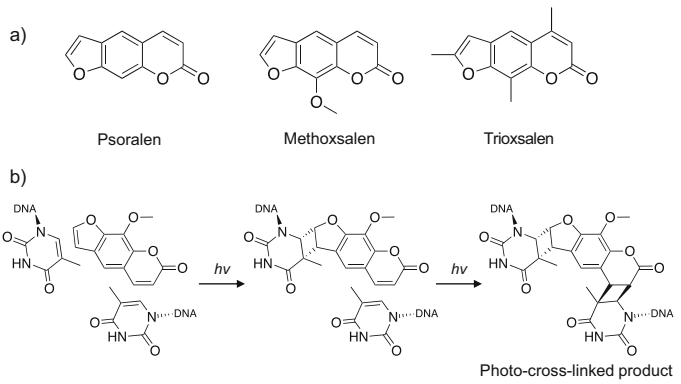

Fig. 7.1 Structure of naturally occurring plant furocoumarins (**a**) and the interstrand photo-cross-linking reaction of methoxsalen in double-stranded DNA (**b**)

7.3 Psoralen-Modified Artificial Nucleic Acids

With the development of the methodology for organic synthesis and modification of nucleic acids, psoralen derivatives have been conjugated with various synthetic oligonucleotides to give sequence specificity for the photo-cross-linking reaction of psoralen derivatives. Miller and co-workers conducted one of the most pioneering studies in this field. They introduced trioxsalen at the 5′ end of synthetic oligodeoxyribonucleotide (ODN(s)) (Fig. 7.2, Compound 1) and clearly demonstrated that the trioxsalen-modified ODN photo-cross-linked to complementary single-stranded DNA [17–19] and double-stranded DNA [20] with UVA (365 nm) irradiation. Furthermore, they also demonstrated that the trioxsalen-modified ODN having an antisense sequence for rabbit globin mRNA effectively inhibits the translation of rabbit globin mRNA in a photo-responsive manner [21]. Their findings opened the door for the development of photo-functionalized synthetic oligonucleotides. Indeed, in the early 1990s, various groups reported antisense ODN [22, 23] and triplex-forming ODN (TFO) modified with psolaren derivative [24–30]. In particular, oligonucleotide having 2′-trioxsalen-modified adenosine (Fig. 7.2, Compound 2) has the highest photoreactivity toward thymine or uracil base in a complementary DNA or RNA strand [31, 32]. Recently, coumarin-modified nucleic acid having photo-cross-linking ability to complementary DNA was reported (Fig.7.2, Compound 4 [33]). They successfully modified thymidine with coumarin using a Cu(I)-catalyzed click reaction. This is the first example of interstrand photo-cross-linking reaction by a modified pyrimidine nucleoside.

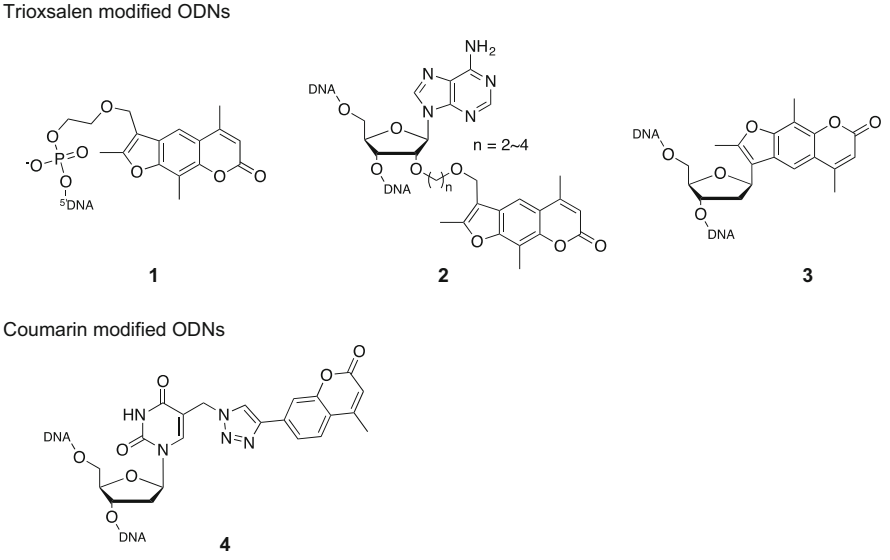

Fig. 7.2 Trioxsalen- or coumarin-modified artificial nucleic acids for DNA/RNA interstrand photo-cross-linking

7.4 3-Cyanovinylcarbazole-Modified Artificial Nucleic Acids

Owing to its photoreactivity and the ease with which it is obtained from natural plants, psoralen derivative is widely used for photo-functionalization of synthetic ODNs; however, the UVA irradiation required for the photoreaction itself sometimes causes unexpected cytotoxicity to cells. Therefore, a more highly reactive photo-cross-linker that can photo-cross-link to nucleic acids with shorter irradiation time than psoralen derivatives was required. In 2008, as a DNA photo-cross-linker having higher photoreactivity compared to psoralen derivatives, 3-cyanovinylcarbazole-modified nucleoside (^{CNV}K) was reported by Fujimoto and co-workers ([34, 35]; Fig. 7.3, Compound 1). Similar to the case of psoralen derivatives, the photo-cross-linking reaction of ^{CNV}K occurs through a [2 + 2] photocycloaddition reaction between the vinyl moiety of ^{CNV}K and C5–C6 double bond of the pyrimidine base with 365 nm irradiation. As the photoreactivity of ODN having ^{CNV}K is at least tenfold greater than that of psoralen-modified ODNs, ^{CNV}K is the most reactive DNA photo-cross-linker at that time. Since ODN having ^{CNV}K photo-cross-link with complementary DNA or RNA [36–38], and also double-stranded DNA [39], the same as the case of psoralen derivatives, they are expected to be a powerful tool for regulating the functions of nucleic acids, the same as psoralen-modified ODNs. Most recently, a novel DNA photo-cross-linker consisting of 3-cyanovinylcarbazole and D-threoninol (^{CNV}D) has been reported ([40]; Fig. 7.3, Compound 2). As the photoreactivity of ^{CNV}D is 1.8–8-fold higher than that of ^{CNV}K, this is the most highly reactive DNA photo-cross-linker reported. Furthermore, recent research by Fujimoto's group of JAIST revealed that the complementary base of the pyrimidine base that will be cross-linked with ^{CNV}K greatly affects the photoreactivity of ^{CNV}K in double-stranded DNA [41]. Particularly, in the case of cytosine as the target of ^{CNV}K, the decrease of the hydrogen bonds between the cytosine and its complementary base by the substitution of canonical guanine with a noncanonical complementary base, such as inosine and 2-aminopurine, drastically accelerates the photoreactivity 3.6–7.7-fold. These findings suggest that the local stability and/or flexibility of the photo-cross-linking site is an important factor for

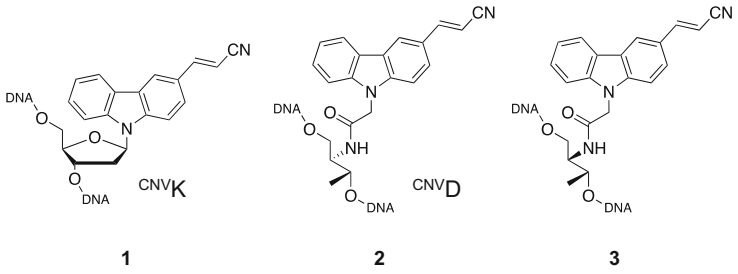

Fig. 7.3 3-Cyanovinylcarbazole-modified artificial nucleic acids for DNA/RNA interstrand photo-cross-linking

governing the photoreaction. In general, the reaction rate of the photo-cross-linking toward the cytosine base through [2 + 2] photocycloaddition is lower than that toward thymine or uracil [12, 34]. There is huge potential for improving photoreactivity toward cytosine by regulating the local stability and/or flexibility of the photo-cross-linking site with the substitution of a complementary base of cytosine.

7.5 Other Artificial Nucleic Acids

He and co-workers reported another class of DNA photo-cross-linker having a different mechanism from that of psoralen and 3-cyanovinylcarbazole derivatives: diazirine-modified nucleic acid analogue ([42]; Fig. 7.4, Compound 1). The diazirine group forms a carbene intermediate upon UVA-induced N2 elimination and cross-links to multiple nearby bases in the complementary strand. Contrary to the case of photo-cross-linking via [2 + 2] photocycloaddition, this type of photo-cross-linker can react with four kinds of nucleobases in the complementary DNA and RNA strand ([43]; Fig. 7.4, Compound 2 and 3).

As another class of the DNA photo-cross-linking reaction, recently, Asanuma's group of Nagoya University reported stilbene-modified artificial nucleic acids (Fig. 7.5 [44]). They successfully demonstrated that two complementary synthetic ODNs having stilbene moiety can photo-cross-link each other with the 340 nm irradiation through [2 + 2] photodimerization of two stilbene moieties in the double-

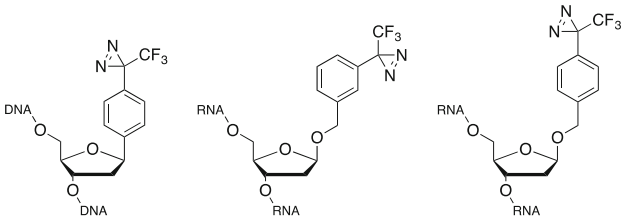

Fig. 7.4 Diazirine-modified artificial nucleic acids for DNA/RNA interstrand photo-cross-linking

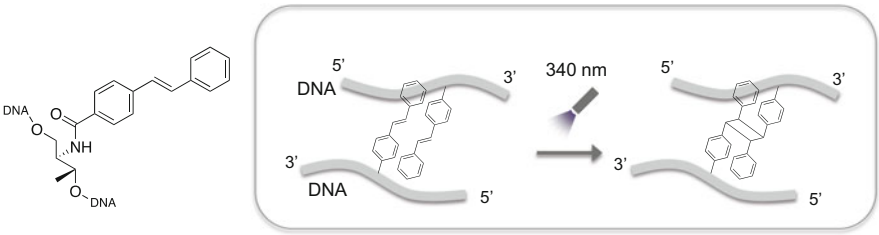

Fig. 7.5 Stilbene-modified artificial nucleic acids for DNA interstrand photo-cross-linking

stranded DNA. Contrary to the case of psoralen or 3-cyanovinylcarbazole-modified nucleic acids, it is unclear whether the reaction occurs toward native nucleic acid bases; however, the combination of the photodimerization pair can be selected freely, in their case. Therefore, the strategy has far-reaching potential for improving the photoreactivity and for regulating the irradiation wavelength required for activating the photoreaction.

7.6 Applications of Photo-Cross-Linking Reaction in Nucleic Acids

The sequence specific photo-cross-linking reaction using various photo-cross-linkers mentioned above is applicable for regulating biological events including nucleic acid, such as replication, transcription, translation, and DNA damage repair, and also DNA nanostructures (Fig. 7.6). As the timing and area of photoirradiation can be regulated completely, the spatiotemporal regulation of the biological events or nanostructures mentioned above is expected to be regulated freely with photoirradiation.

7.6.1 Photoregulation of Gene Expression

The photodynamic antisense strategy (Fig. 7.7a) is a successful example of regulating gene expression in cells. In this strategy, photo-responsive ODNs having complementary sequence of target mRNA specifically cross-link and form irreversible photoadduct with target mRNA. Therefore, the translation of target mRNA is

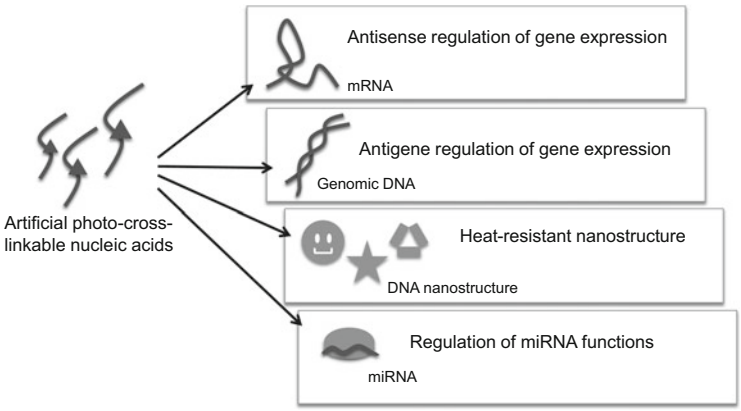

Fig. 7.6 Possible applications of sequence-specific photo-cross-linking reactions using photo-functionalized ODNs

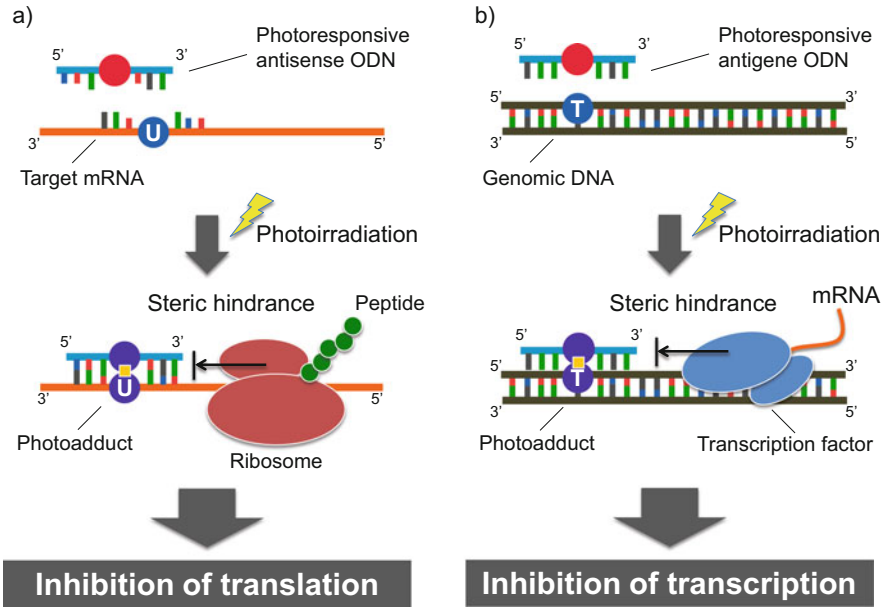

Fig. 7.7 Schematic drawings of photoregulation of gene expression based on (**a**) antisense or (**b**) antigene strategy

selectively inhibited by steric hindrance. The main concept of the photodynamic antisense strategy was advocated by Millar and co-workers as mentioned above [21]. They successfully demonstrated that trioxsalen-modified antisense ODN effectively downregulates rabbit globin gene expression in an in vitro translation system in a photo-responsive manner. In an early report of the cellular application of trioxsalen-modified antisense ODN, Chang et al. and Lin et al. successfully photo-regulated the translation of point-mutated ras protein in 453 cells [22] and collagenase I in dermal fibroblast [23], respectively. Murakami's group of KIT energetically worked in this area [45, 46], and they successfully demonstrated that trioxsalen-modified antisense ODN effectively regulates the gene expression of HPV E6 and E7 mRNA and suppresses the proliferation of HPV positive SiHa cells with nanomolar treatment of trioxsalen-modified antisense ODN and UVA irradiation. Recently, the temporal regulation of constitutive GFP gene expression has been demonstrated by the use of ^{CNV}K-modified antisense ODNs [47]. The high photoreactivity of ^{CNV}K enables quick regulation of gene expression in cells with 10 s of UVA irradiation.

As another strategy for regulating gene expression in a photo-responsive manner, the photodynamic antigene strategy (Fig. 7.7b) has been reported by several researchers. Psoralen-modified triplex forming ODNs is one of the successful examples of this strategy. The ODNs are effective for regulating gene expression with sequence specific photo-cross-linking reaction between the psoralen moiety tethered with ODN and double-stranded genomic DNA. Based on this strategy, the

downregulation of interleukin 2 receptor [27], human rhodopsin [48], and β-globin [49] genes in cells has been reported.

7.6.2 *Photo-Cross-Linking Reaction for Nucleic Acids Analysis*

Because of the highly thermal stability of the photo-cross-linked duplexes, photoreactive synthetic ODNs are applicable for highly sensitive detection of nucleic acids or as a nucleic acid capture probe.

The reactivity of the photo-cross-linking reaction through [2 + 2] photocycloaddition is quite different among pyrimidine bases. Using this character, 5-methyl modification of cytosine in the DNA strand was clearly discriminated with unmodified cytosine by the use of psoralen- or ^{CNV}K-modified ODN probes (Fig. 7.8 [50, 51]). Based on this selective photo-cross-linking reaction, the methodology for analyzing epigenetic modification of DNA can be further developed.

7.6.3 *Photo-Cross-Linking Reaction for Nanotechnology*

DNA-based nanotechnologies, such as DNA nanocrystal and DNA origami, are cutting-edge areas in nanotechnology and supramolecular science. The bottom-up manner of this technology, which relies on the simple hybridization property of DNA strands, is expected to lead to the construction of various nanostructures and functions induced by finely designed nanostructures. DNA photo-cross-linking is applicable also in this area. The thermally stable double-stranded DNA caused by the interstrand photo-cross-linking reaction of psoralen gives thermally stable

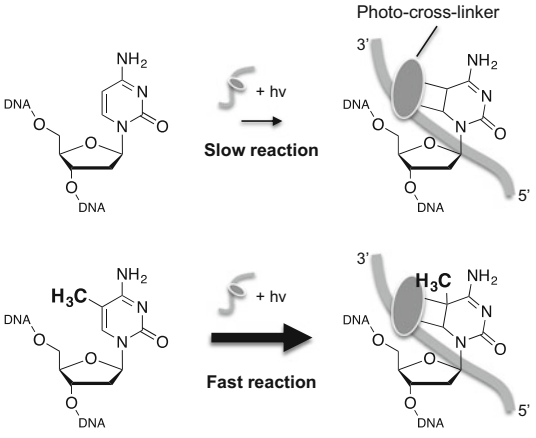

Fig. 7.8 Selective photo-cross-linking of psoralen or ^{CNV}K-modified ODN with 5-methylcytosine

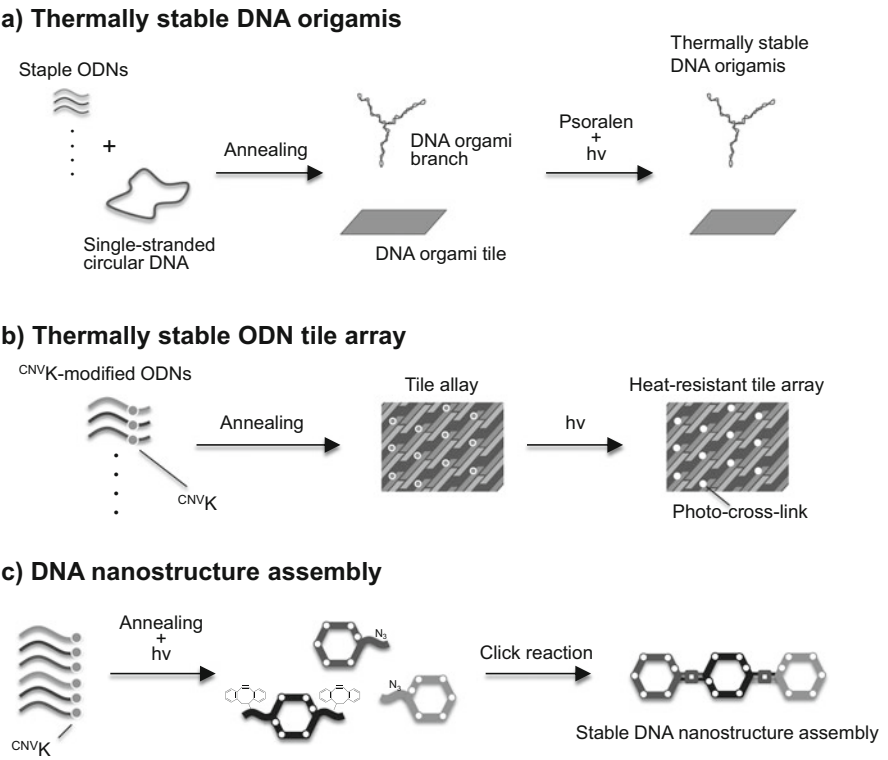

Fig. 7.9 Schematic drawings of thermally stable nanostructure with DNA photo-cross-linking reaction. (**a**) Thermally stable DNA origamis. (**b**) Thermally stable ODN tile array. (**c**) DNA nanostructure assembly

nanostructured DNA (Fig. 7.9a), such as DNA origami tiles [52], DNA origami branches [53], and branched oligonucleotide networks [54]. The ability to use these nanostructures at higher temperature enables various applications such as the creation of nanoscale electronic devices and higher-temperature assembly of functional molecules on nanostructured DNA. ^{CNV}K-modified ODNs are also applicable for constructing thermally stable DNA nanostructures. Tagawa et al. and Nakamura et al. reported that the DNA double-crossover AB-staggered tiles having ^{CNV}K and DNA 2D array including ^{CNV}K, respectively, could be stabilized by UVA irradiation (Fig. 7.9b [55, 56]). Furthermore, Gerrard et al. successfully developed a method of integrating nanostructured DNA using thermally stable nanostructured DNA modules and orthogonal copper-free click chemistry (Fig. 7.9c [57]). Since the thermal stability of nanostructured DNA is an important issue for constructing higher-ordered DNA nanostructures, the photo-cross-linking strategies mentioned above are expected to contribute to the further development of DNA-based nanotechnology.

Most recently, Kanaras's group of the University of Southampton successfully demonstrated that the assembly of nanoparticles is finely and reversibly regulated

by the irradiation of UV light [58]. They used 15 nm two gold particles modified with only one DNA strand, one has ^{CNV}K and one has a thymine base as the photo-cross-linking site, and clearly demonstrated that the dimer assembly and dis-assembly were completely regulated by 365 and 312 nm irradiation, respectively. Since the triangle and tetrahedron structure, which has gold nanoparticles at its vertexes and photo-cross-linked duplexes at its sides, is also assembled by using a similar strategy, this new technique will be of particular applicability in several research fields using nanoparticle assemblies such as catalysis, photonics, and biosensors.

7.7 Conclusion and Prospects

Functionalized ODNs having photo-cross-linking ability possess great potential for regulating functions and structures of nucleic acids because of their sequence selectivity, thermally irreversibleness, and photo-responsive manner.

However, problems still remain with the clinical application of photo-cross-linking ODNs, e.g., the cytotoxicity of photoreactive moieties, unexpected photodamage caused by UVA [59], and low transparency of UVA in bio-organs. Further development of photoreactive groups having photo-cross-linking ability with longer wavelengths and low cytotoxicity is required and also a combination with advanced light sources such as femtosecond pulse lasers that can activate molecules by two or three photons with longer wavelengths.

References

1. Setlow RB (1966) Cyclobutane-type pyrimidine dimers in polynucleotides. Science 153 (3734):379–386
2. Kao JL, Nadji S, Taylor JS (1993) Identification and structure determination of a third cyclobutane photodimer of thymidylyl-(3′-->5′)-thymidine: the trans-syn-II product. Chem Res Toxicol 6(4):561–567
3. Koning MG, van Soest JJ, Kaptein R (1991) NMR studies of bipyrimidine cyclobutane photodimers. Eur J Biochem 195(1):29–40
4. Rao SN, Keepers JW, Kollman P (1984) The structure of d(CGCGAAT[]TCGCG). d (CGCGAATTCGCG); the incorporation of a thymine photodimer into a B-DNA helix. Nucleic Acids Res 12(11):4789–4807
5. Schreier WJ, Schrader TE, Koller FO, Gilch P, Crespo-Hernández CE, Swaminathan VN, Carell T, Zinth W, Kohler B (2007) Thymine dimerization in DNA is an ultrafast photoreaction. Science 315(5812):625–629
6. Su DG, Kao JL, Gross ML, Taylor JS (2008) Structure determination of an interstrand-type cis-anti cyclobutane thymine dimer produced in high yield by UVB light in an oligodeoxynucleotide at acidic pH. J Am Chem Soc 130(34):11328–11337
7. Jiang N, Taylor JS (1993) In vivo evidence that UV-induced C-->T mutations at dipyrimidine sites could result from the replicative bypass of cis-syn cyclobutane dimers or their deamination products. Biochemistry 32(2):472–481

8. Kim ST, Sancar A (1991) Effect of base, pentose, and phosphodiester backbone structures on binding and repair of pyrimidine dimers by Escherichia coli DNA photolyase. Biochemistry 30 (35):8623–8630
9. Niggli HJ, Cerutti PA (1983) Cyclobutane-type pyrimidine photodimer formation and excision in human skin fibroblasts after irradiation with 313-nm ultraviolet light. Biochemistry 22 (6):1390–1395
10. Niggli HJ (1993) Aphidicolin inhibits excision repair of UV-induced pyrimidine photodimers in low serum cultures of mitotic and mitomycin C-induced postmitotic human skin fibroblasts. Mutat Res 295(3):125–133
11. Shwartz H, Shavitt O, Livneh Z (1988) The role of exonucleolytic processing and polymerase-DNA association in bypass of lesions during replication in vitro. Significance for SOS-targeted mutagenesis. J Biol Chem 263(34):18277–18285
12. Song P-S, Tapley KJ Jr (1979) Photochemistry and photobiology of psoralen. Photochem Photobiol 29:1177–1197
13. Calvet JP, Pederson T (1979) Photochemical cross-linking of secondary structure in HeLa cell heterogeneous nuclear RNA in situ. Nucleic Acids Res 6(5):1993–2001
14. Cantor CR, Wollenzien PL, Hearst JE (1980) Structure and topology of 16S ribosomal RNA. An analysis of the pattern of psoralen crosslinking. Nucleic Acids Res 8(8):1855–1872
15. Rabin D, Crothers DM (1979) Analysis of RNA secondary structure by photochemical reversal of psoralen crosslinks. Nucleic Acids Res 7(3):689–703
16. Wollenzien PL, Youvan DC, Hearst JE (1978) Structure of psoralen-crosslinked ribosomal RNA from Drosophila melanogaster. Proc Natl Acad Sci USA 75(4):1642–1646
17. Bhan P, Miller PS (1990) Photo-cross-linking of psoralen-derivatized oligonucleoside methylphosphonates to single-stranded DNA. Bioconjug Chem 1(1):82–88
18. Lee BL, Murakami A, Blake KR, Lin SB, Miller PS (1988) Interaction of psoralen-derivatized oligodeoxyribonucleoside methylphosphonates with single-stranded DNA. Biochemistry 27 (9):3197–3203
19. Pieles U, Englisch U (1989) Psoralen covalently linked to oligodeoxyribonucleotides: synthesis, sequence specific recognition of DNA and photo-cross-linking to pyrimidine residues of DNA. Nucleic Acids Res 17(1):285–299
20. Lee BL, Blake KR, Miller PS (1988) Interaction of psoralen-derivatized oligodeoxyribonucleoside methylphosphonates with synthetic DNA containing a promoter for T7 RNA polymerase. Nucleic Acids Res 16(22):10681–10697
21. Kean JM, Murakami A, Blake KR, Cushman CD, Miller PS (1988) Photochemical cross-linking of psoralen-derivatized oligonucleoside methylphosphonates to rabbit globin messenger RNA. Biochemistry 27(26):9113–9121
22. Chang EH, Miller PS, Cushman C, Devadas K, Pirollo KF, Ts'o PO, Yu ZP (1991) Antisense inhibition of ras p21 expression that is sensitive to a point mutation. Biochemistry 30 (34):8283–8286
23. Lin M, Hultquist KL, Oh DH, Bauer EA, Hoeffler WK (1995) Inhibition of collagenase type I expression by psoralen antisense oligonucleotides in dermal fibroblasts. FASEB J 9 (13):1371–1377
24. Giovannangéli C, Thuong NT, Hélène C (1992) Oligodeoxynucleotide-directed photo-induced cross-linking of HIV proviral DNA via triple-helix formation. Nucleic Acids Res 20 (16):4275–4281
25. Takasugi M, Guendouz A, Chassignol M, Decout JL, Lhomme J, Thuong NT, Hélène C (1991) Sequence-specific photo-induced cross-linking of the two strands of double-helical DNA by a psoralen covalently linked to a triple helix-forming oligonucleotide. Proc Natl Acad Sci USA 88(13):5602–5606
26. Cassidy RA, Kondo NS, Miller PS (2000) Triplex formation by psoralen-conjugated chimeric oligonucleoside methylphosphonates. Biochemistry 39(29):8683–8691

27. Grigoriev M, Praseuth D, Guieysse AL, Robin P, Thuong NT, Hélène C, Harel-Bellan A (1993) Inhibition of gene expression by triple helix-directed DNA cross-linking at specific sites. Proc Natl Acad Sci USA 90(8):3501–3505
28. Miller PS, Bi G, Kipp SA, Fok V, DeLong RK (1996) Triplex formation by a psoralen-conjugated oligodeoxyribonucleotide containing the base analog 8-oxo-adenine. Nucleic Acids Res 24(4):730–736
29. Miller PS, Kipp SA, McGill C (1999) A psoralen-conjugated triplex-forming oligodeoxyribonucleotide containing alternating methylphosphonate-phosphodiester linkages: synthesis and interactions with DNA. Bioconjug Chem 10(4):572–577
30. Wang G, Glazer PM (1995) Altered repair of targeted psoralen photoadducts in the context of an oligonucleotide-mediated triple helix. J Biol Chem 270(38):22595–22601
31. Higuchi M, Yamayoshi A, Yamaguchi T, Iwase R, Yamaoka T, Kobori A, Murakami A (2007) Selective photo-cross-linking of 2′-O-psoralen-conjugated oligonucleotide with RNAs having point mutations. Nucleosides Nucleotides Nucleic Acids 26(3):277–290
32. Higuchi M, Kobori A, Yamayoshi A, Murakami A (2009) Synthesis of antisense oligonucleotides containing 2′-O-psoralenylmethoxyalkyl adenosine for photodynamic regulation of point mutations in RNA. Bioorg Med Chem 17(2):475–483
33. Haque MM, Sun H, Liu S, Wang Y, Peng X (2014) Photo switchable formation of a DNA interstrand cross-link by a coumarin-modified nucleotide. Angew Chem Int Ed 53 (27):7001–7005
34. Yoshimura Y, Fujimoto K (2008) Ultrafast reversible photo-cross-linking reaction: toward in situ DNA manipulation. Org Lett 10(15):3227–3230
35. Fujimoto K, Yamada A, Yoshimura Y, Tsukaguchi T, Sakamoto T (2013) Details of the ultrafast DNA photo-cross-linking reaction of 3-cyanovinylcarbazole nucleoside: cis-trans isomeric effect and the application for SNP-based genotyping. J Am Chem Soc 135 (43):16161–16167
36. Fujimoto K, Konishi-Hiratsuka K, Sakamoto T, Yoshimura Y (2010) Site-specific photochemical RNA editing. Chem Commun (Camb) 46(40):7545–7547
37. Yoshimura Y, Ohtake T, Okada H, Fujimoto K (2009) A new approach for reversible RNA photocrosslinking reaction: application to sequence-specific RNA selection. ChemBioChem 10(9):1473–1476
38. Fujimoto K, Kishi S, Sakamoto T (2013) Geometric effect on the photocrosslinking reaction between 3-cyanovinylcarbazole nucleoside and pyrimidine base in DNA/RNA heteroduplex. Photochem Photobiol 89(5):1095–1099
39. Fujimoto K, Yoshinaga H, Yoshio Y, Sakamoto T (2013) Quick and reversible photocrosslinking reaction of 3-cyanovinylcarbazole nucleoside in a DNA triplex. Org Biomol Chem 11 (31):5065–5068
40. Sakamoto T, Tanaka Y, Fujimoto K (2015) DNA photo-cross-linking using 3-cyanovinylcarbazole modified oligonucleotide with threoninol linker. Org Lett 17 (4):936–939
41. Sakamoto T, Ooe M, Fujimoto K (2015) Critical effect of base pairing of target pyrimidine on the interstrand photo-cross-linking of DNA via 3-cyanovinylcarbazole nucleoside. Bioconjugate Chem 26(8):1475–1478. doi:10.1021/acs.bioconjchem.5b00352
42. Qiu Z, Lu L, Jian X, He C (2008) A diazirine-based nucleoside analogue for efficient DNA interstrand photocross-linking. J Am Chem Soc 130(44):14398–14399
43. Nakamoto K, Ueno Y (2014) Diazirine-containing RNA photo-cross-linking probes for capturing microRNA targets. J Org Chem 79:2463–2472
44. Doi T, Kashida H, Asanuma H (2015) Efficiency of [2+2] photodimerization of various stilbene derivatives within the DNA duplex scaffold. Org Biomol Chem 13:4430–4437
45. Murakami A, Yamayoshi A, Iwase R, Nishida J, Yamaoka T, Wake N (2001) Photodynamic antisense regulation of human cervical carcinoma cell growth using psoralen-conjugated oligo (nucleoside phosphorothioate). Eur J Pharm Sci 13(1):25–34

46. Yamayoshi A, Iwase R, Yamaoka T, Murakami A (2003) Psoralen-conjugated oligonucleotide with hairpin structure as a novel photo-sensitive antisense molecule. Chem Commun 12:1370–1371
47. Sakamoto T, Shigeno A, Ohtaki Y, Fujimoto K (2014) Photo-regulation of constitutive gene expression in living cells by using ultrafast photo-cross-linking oligonucleotides. Biomater Sci 2:1154–1157
48. Intody Z, Perkins BD, Wilson JH, Wensel TG (2000) Blocking transcription of the human rhodopsin gene by triplex-mediated DNA photocrosslinking. Nucleic Acids Res 28 (21):4283–4290
49. Shahid KA, Majumdar A, Alam R, Liu ST, Kuan JY, Sui X, Cuenoud B, Glazer PM, Miller PS, Seidman MM (2006) Targeted cross-linking of the human beta-globin gene in living cells mediated by a triple helix forming oligonucleotide. Biochemistry 45(6):1970–1978
50. Yamayoshi A, Matsuyama Y, Kushida M, Kobori A, Murakami A (2014) Novel photodynamic effect of a psoralen-conjugated oligonucleotide for the discrimination of the methylation of cytosine in DNA. Photochem Photobiol 90(3):716–722
51. Fujimoto K, Konishi-Hiratsuka K, Sakamoto T (2013) Quick, selective and reversible photocrosslinking reaction between 5-methylcytosine and 3-cyanovinylcarbazole in DNA double strand. Int J Mol Sci 14(3):5765–5774
52. Rajendran A, Endo M, Katsuda Y, Hidaka K, Sugiyama H (2011) Photo-cross-linking-assisted thermal stability of DNA origami structures and its application for higher-temperature self-assembly. J Am Chem Soc 133(37):14488–14491
53. Liu J, Geng Y, Pound E, Gyawali S, Ashton JR, Hickey J, Woolley AT, Harb JN (2011) Metallization of branched DNA origami for nanoelectronic circuit fabrication. ACS Nano 5 (3):2240–2247
54. Hartman MR, Yang D, Tran TN, Lee K, Kahn JS, Kiatwuthinon P, Yancey KG, Trotsenko O, Minko S, Luo D (2013) Thermostable branched DNA nanostructures as modular primers for polymerase chain reaction. Angew Chem Int Ed 52(33):8699–8702
55. Nakamura S, Fujimoto K (2013) Creation of DNA array structure equipped with heat resistance by ultrafast photocrosslinking. J Chem Technol Biotechnol 89:1086–1090
56. Tagawa M, Shohda K, Fujimoto K, Suyama A (2011) Stabilization of DNA nanostructures by photo-cross-linking. Soft Matter 7:10931–10934
57. Gerrard SR, Hardiman C, Shelbourne M, Nandhakumar I, Nordén B, Brown T (2012) A new modular approach to nanoassembly: stable and addressable DNA nanoconstructs via orthogonal click chemistries. ACS Nano 6(10):9221–9228
58. Harimech PK, Gerrard SR, El-Sagheer AH, Brown T, Kanaras AG (2015) Reversible ligation of programmed DNA-gold nanoparticle assemblies. J Am Chem Soc 137(29):9242–9245
59. Tadokoro T, Kobayashi N, Zmudzka BZ, Ito S, Wakamatsu K, Yamaguchi Y, Korossy KS, Miller SA, Beer JZ, Hearing VJ (2003) UV-induced DNA damage and melanin content in human skin differing in racial/ethnic origin. FASEB J 17(9):1177–1179

Chapter 8
Site-Directed Spin Labeling for EPR Studies of Nucleic Acids

Sandip A. Shelke and Snorri Th. Sigurdsson

Abstract Electron paramagnetic resonance (EPR) spectroscopy has emerged as a valuable technique to study the structure and dynamics of nucleic acids and their complexes with other biomolecules. EPR studies require incorporation of stable free radicals (spin labels), usually aminoxyl radicals (nitroxides), at specific sites in the nucleic acids using site-directed spin labeling (SDSL). In addition to the advancement of EPR instrumentation and pulsed EPR techniques, new strategies for SDSL have emerged, in particular, use of click chemistry, biopolymer catalysis, and noncovalent labeling. Furthermore, tailor-made spin labels with improved stability and spectroscopic properties have evolved, such as rigid spin labels that allow determination of accurate distances in addition to orientations between two spin labels. This chapter gives an overview of nucleic acids spin labeling using the three main strategies of SDSL, namely spin labeling during oligonucleotide synthesis, post-synthetic-, and noncovalent labeling. The spin-labeling methods have been categorized according to the labeling site.

8.1 Introduction

Nucleic acids are the reservoir of genetic information for all living organisms. DNA carries the genetic blueprint, which is transmitted to the ribosome through RNAs via transcription and translation. A subtle structural difference between DNA and RNA, namely the presence of a 2′-hydroxyl group on the sugar moieties of the latter, leads to much more diverse structural and chemical properties of RNA. RNA is not only a carrier of genetic information, it also carries out a wide range of other cellular functions central to the life, such as catalysis of chemical reactions by

S.A. Shelke
Department of Biochemistry and Molecular Biology, University of Chicago, Chicago, IL 60637, USA

S.T. Sigurdsson (✉)
Department of Chemistry, Science Institute, University of Iceland, Dunhaga 3, 107 Reykjavik, Iceland
e-mail: snorrisi@hi.is

K. Nakatani, Y. Tor (eds.), *Modified Nucleic Acids*, Nucleic Acids and Molecular Biology 31, DOI 10.1007/978-3-319-27111-8_8

ribozymes [1–3] that are found in the catalytic core of both ribosomes [4] and spliceosomes [5], regulation of gene expression by small interfering RNAs [6], metabolite-responsive regulatory control by riboswitches [7, 8], protein recognition, and cellular signaling [9]. These wide ranges of functions are attributed to their flexibility and ability to fold into complex three-dimensional structures. During the last few decades, a variety of biochemical and biophysical methods has been utilized to investigate the structural basis of the functions of these biomolecules.

X-ray crystallography and nuclear magnetic resonance (NMR) spectroscopy are high-resolution techniques that give precise information about three-dimensional arrangements of atoms in space. Although NMR spectroscopy is useful for studying structure and dynamics of biomolecules under biologically relevant conditions, it is still limited by the molecular weight of biopolymers, of up to approximately 50 kDa [10, 11]. Moreover, the range of distances between atoms that can be deduced by NMR, and are used to generate a three-dimensional structure, are limited to only a ca. 20 Å, although residual dipolar coupling (RDC) has been used to get information about the orientation of helical domains [12]. X-ray crystallography also suffers from technical challenges. For example, it remains difficult to obtain crystals of biomolecules that diffract well. This is especially true for RNAs due to their tendency to misfold, oligomerize and, in general, accommodate conformational heterogeneity. Additionally, a crystallized form may not represent a biologically active conformation.

Lower-resolution spectroscopic techniques, such as Förster resonance energy transfer (FRET) [13–15] and electron paramagnetic resonance (EPR) [16–24], have proven to be valuable for the study of structure and dynamics of biopolymers and are complementary to NMR and X-ray crystallography. Both FRET and EPR are highly sensitive and thus require small amounts of material. They can be used to map distances of up to 100 Å, enabling observation of long-range conformational changes that are triggered by a change in conditions or upon binding to other biomolecules [25, 26]. Both techniques require incorporation of reporter groups for distance measurements. In the case of FRET, two different fluorophores are required; a donor and an acceptor that are usually connected with a flexible tether, that yield moderate-to-large distance distributions. Another potential complication for FRET is that the efficiency of the fluorescence transfer depends on the relative orientation of the two fluorophores. An important feature of FRET is that it can be used for single-molecule studies [27, 28]. There are also a few other low-resolution techniques, such as small angle X-ray scattering (SAXS) [29] and circular dichroism (CD) spectroscopy [30], that have been used for probing the global shape and conformational folding of nucleic acids.

EPR spectroscopy, also called electron spin resonance (ESR), was first reported by Zavoisky in 1945 [31]. EPR is a highly sensitive and useful technique to probe the local environment of paramagnetic centers. As such, it can probe polarity and solvent accessibility. In addition, the reporter groups (spin labels) that are commonly used for EPR studies are relatively small, compared to other exogenous tags (such as fluorophores), which makes them less perturbing to the native structure of

biopolymers. Like NMR, EPR is based on the principles of magnetic resonance, interrogating spins of unpaired electrons, such as those present in free radicals. EPR detects transitions of electron spins from a lower to a higher energy level, induced by absorption of electromagnetic (microwave) radiation in the presence of an applied external magnetic field. The magnetic moment of an unpaired electron can also interact with neighboring nuclei, usually referred to as hyperfine coupling, and split each electronic spin state into $2I + 1$ levels, where I is the spin quantum number of the nuclei. The energy levels of an electron can also be affected by the presence of other electron spins through both exchange- and dipolar coupling.

The mobility of a radical is reflected in the shape of its continuous wave (CW) EPR spectrum. Figure 8.1 shows the EPR spectra of an aminoxyl radical (usually called a nitroxide, Fig. 8.1) in the fast, intermediate, and slow motion regime. The EPR spectrum of a nitroxide has three lines, due to the hyperfine coupling to the nitrogen atom ($I = 1$). As the motion of the nitroxide slows down, the spectrum becomes broader. The mobility of a spin label attached to a biopolymer is a combination of motions of the linker used to attach the spin label as well as the local and global motions of the biopolymer itself. This feature can be used to indirectly extract structural information about the dynamics of the biopolymer, sometimes referred to as structure-dependent dynamics [32–34].

Most structural studies of biopolymers with EPR are based on distance measurements between spin labels, made possible through dipolar coupling. CW-EPR can be used for measuring intermediate distances, lower than 25 Å [35, 36]. However, when the distances between the spin labels are larger, the dipolar couplings become smaller than the inhomogeneous broadening of the EPR spectrum, caused by unresolved surrounding hyperfine couplings. In order to resolve these long-range dipolar couplings from the inhomogeneous line broadening, pulsed EPR techniques are required. The most widely used pulsed EPR technique, pulsed electron–electron double resonance (PELDOR), also called double electron–electron resonance (DEER), can yield accurate distances in the range of 15–100 Å [20, 21, 37–39]. In this technique, short (5–30 ns long) but intense microwave pulses (in kW) are used, usually applying the four-pulse method [40, 41]. EPR can also yield information about relative orientations between two interacting spin centers, which can provide additional constrains to build more accurate structural models [42–

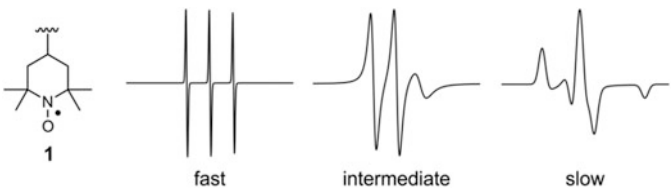

Fig. 8.1 Structure of 2,2,6,6-tetramethylpiperidine-1-oxyl (TEMPO) radical (**1**) and its CW-EPR spectra in the fast, intermediate, and slow motion regime, respectively, showing the effect of its mobility on the spectral line shapes

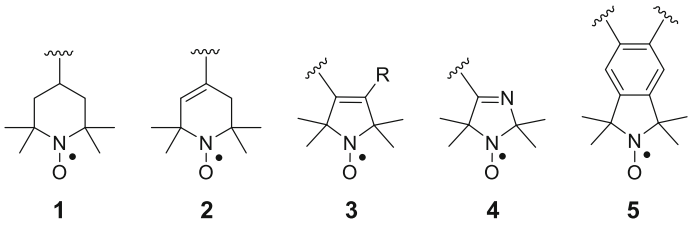

Fig. 8.2 Structures of the most commonly used nitroxide radicals for spin labeling

45]. This requires the use of rigid spin labels [46, 47], which have also enabled determination of the internal dynamics of nucleic acids [25, 48].

Although some biopolymers contain intrinsic paramagnetic centers, such as metal ions [23], most are diamagnetic and require incorporation of spin labels for EPR studies. Nitroxides are the most commonly used spin labels due to their persistent nature and relatively small size [49, 50]. Three factors contribute to the stability of nitroxide spin labels, delocalization of the unpaired electron between the oxygen and nitrogen atoms, electron donating effects of the alkyl groups on the carbon atoms adjacent to the nitroxide, and the steric shielding by the alkyl groups. Figure 8.2 shows the structures of the nitroxide moieties most commonly used for spin labeling, classified into three groups according to the size of the nitroxide-bearing ring: six-membered piperidines (**1**, **2**), five-membered pyrrolines (**3**, **4**), and isoindolines (**5**). The size of the nitroxide-bearing ring and the nature of its substituents affect the stability of the nitroxides, especially under reducing conditions [51–56]. Nitroxides are almost exclusively the spin labels of choice for EPR studies, although carbon-centered trityl radicals have recently been reported [57–59] as well as paramagnetic metal ions, such as Gd^{3+} [60].

This chapter gives an overview of site-directed spin labeling (SDSL), starting with strategies used for nucleic acids, followed by a fairly comprehensive description of nucleic acid spin labeling. The structures of the spin-labeled nucleotides will be shown, and the spin-labeling methods will be narrated. The organization of the material describing covalent labeling is by the labeling sites and will begin with nucleobase labeling, followed by labeling of the sugar moiety and the phosphate backbone. After that, noncovalent labeling will be covered, and the chapter concludes with a short perspective.

8.2 Nucleic Acid Spin Labeling

In 1965, McConnell introduced the concept of biopolymer spin labeling using nitroxide radicals [61, 62], which was initially applied to proteins [16, 18, 63] and subsequently to nucleic acids [22, 64]. During the early days of spin labeling, when automated chemical synthesis of nucleic acids was not available, spin labeling was performed by alkylation reviewed in [65]. However, due to the presence of

several reactive functional groups on the nucleic acid, this approach lacked specificity. This chapter will focus on spin labeling at selected sites.

While choosing the spin labels, a few criteria must be considered. First, the spin label has to be compatible with the synthetic methods used to prepare the spin-labeled biopolymers [47, 66]. Second, the label should be stable enough to allow EPR measurements under biologically relevant conditions [51, 67–69]. Third, the spin label must be non-perturbing to the native structure of the nucleic acid and its function, which is usually evaluated by thermal denaturation of nucleic acid helices and functional assays with and without the spin labels. Fourth, the structure of the linker for attachment of the spin labels to the nucleic acid must be carefully chosen. As mentioned earlier, the shape of an EPR spectrum is sensitive to the motion of the spin label. If the spin label is attached to the nucleic acid with a long and flexible linker, the EPR spectrum will be dominated by the motion of the spin label and has, therefore, limited use for studies of dynamics. Also, such labels will give a larger distance distribution, which reduces the accuracy of the distance measurements. In contrast, spin labels that are attached with a rigid linker that does not move independently of the biopolymer will report the actual dynamics of the site to which they are attached [70] and also yield accurate distances between two such labels [45, 48]. In some instances, a semi-flexible linker can be advantageous for studying conformational changes [71, 72] and binding interactions with other molecules [69, 73]. Although these labels yield less accurate distances, compared to the rigid spin labels, they show less orientational effects in PELDOR measurements, which can simplify the EPR measurements and data processing [74].

Another key aspect to be considered for SDSL is the spin-labeling method. There are three main strategies used for incorporation of spin labels at chosen sites (Scheme 8.1). The first two approaches rely on covalent attachment of the spin label, while the third approach takes an advantage of noncovalent interactions. The first approach utilizes incorporation of the spin labels during the chemical synthesis of nucleic acids by employing spin-labeled phosphoramidite building blocks (Scheme 8.1a). Due to advancement of automated chemical synthesis of nucleic acids, tailor-made and structurally complex labels can be incorporated at specific sites using this approach [24, 64, 75]. However, synthesis of the spin-labeled phosphoramidite building blocks is sometimes laborious and challenging. Furthermore, spin labels can be partially reduced upon exposure to the chemicals involved in oligonucleotide synthesis [47, 66].

The second SDSL approach is incorporation of spin labels into the nucleic acid after synthesis of the oligonucleotide, referred to as post-synthetic spin labeling (Scheme 8.1b). In this method, modified nucleotide(s) containing a uniquely reactive functional group, such as 4-thio-uridine [76, 77], a 2′-amino nucleoside [32, 35, 78], a phosphorothioate [79], an alkyne [80, 81], or a 2′-azido nucleoside [82], are incorporated at specific site(s) using either chemical or enzymatic synthesis. The modified oligonucleotides are subsequently reacted with a spin-labeling reagent containing the appropriate functional group; examples of functionalized spin labels for post-synthetic labeling are shown in Fig. 8.3. Post-synthetic labeling has the advantage of minimizing possible decomposition of the nitroxide during the

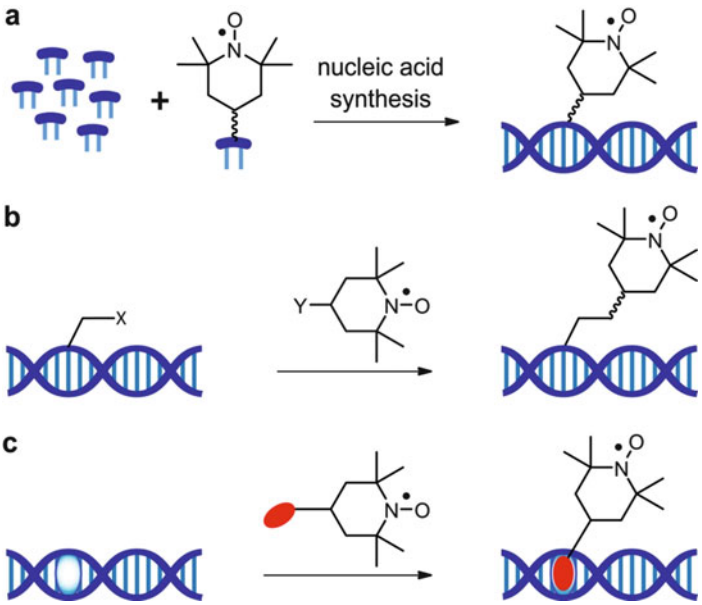

Scheme 8.1 A general scheme of the three main strategies used for site-directed spin labeling of nucleic acids, using TEMPO as a representative nitroxide. (**a**) Labeling during nucleic acid synthesis. (**b**) Post-synthetic labeling, where X and Y represent functional groups that undergo reaction to form a covalent bond between the spin label and oligonucleotide. (**c**) Noncovalent spin labeling

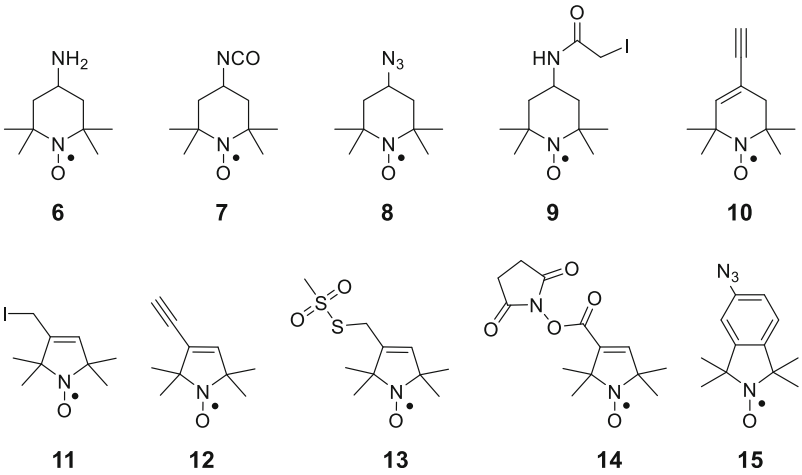

Fig. 8.3 Structures of nitroxide reagents commonly used in post-synthetic spin labeling of nucleic acids

oligonucleotide synthesis. It is also less labor intensive and often utilizes modified oligonucleotides and reagents obtained from commercial sources. Disadvantages of the post-synthetic method include incomplete labeling and possible side reactions of the spin-labeling reagent with innate functional groups of nucleic acids, such as the exocyclic amino groups of the nucleobases.

The third SDSL approach is based on ligand–receptor interactions, where a spin-labeled ligand binds through noncovalent interactions such as hydrogen bonding, ionic-, and Van der Waals interactions (Scheme 8.1c). Although there are only a few examples of using this approach for nucleic acids, there are several examples in protein spin labeling, where an active site of an enzyme or cofactor binding site has been utilized for site-specific binding of spin-labeled derivatives of their natural ligands (reviewed in [65]). The spin label ligand binding can be easily monitored by EPR spectroscopy as bound and free ligands have very different rotational correlation times [83]. Although this noncovalent strategy circumvents challenges associated with both of the aforementioned SDSL approaches that utilize covalent bonding, it requires binding sites that have a relatively high affinity for their spin-labeled ligands in order to get enough labeling for EPR studies.

8.2.1 Base Labeling

Nucleobases are the most common sites for incorporation of spin labels into nucleic acids, due to the availability of various attachment sites and functional groups that can be readily modified using a variety of different organic synthetic methods. Another advantage of nucleobase labeling is that the attached spin labels can readily be accommodated in one of the grooves, in particularly the major groove and thereby cause minimal structural perturbation. In addition to modification of the exocyclic amino groups, spin labels have been incorporated into the *C2*, *C*4, and *C*5 positions of pyrimidines. In particular, the *C*5 position is the most frequently used because of the availability of relatively simple conjugation methods, such as transition-metal-catalyzed coupling to *C*5-halogenated nucleobases and copper-catalyzed cycloaddition reactions between *C*5-alkynes and azido-nitroxides. Purine nucleobases are spin-labeled at the *C*2, *C*6, and *C*7 positions, where *C*7 is labeled by using 7-deaza nucleobase analogues. The following section contains a brief description of nucleobase spin labeling, starting with labeling of exocyclic amino groups, followed by pyrimidine and purine spin labeling through C–C bond formation. The last section describes rigid spin labels.

8.2.1.1 Exocyclic Amino Groups of Pyrimidines and Purines

The exocyclic amino groups of cytosine (*N*4), guanine (*N*2), and adenine (*N*6) nucleobases have all been modified with a spin label. Although amino groups of nucleobases are involved in base pairing and structural integrity of nucleic acid

helices, a single substitution on an amino group still allows one proton to participate in hydrogen bonding to its complementary base. Bannwarth and Schmidt demonstrated the synthesis of spin-labeled phosphoramidites of the *N*4-TEMPO-modified 2′-deoxycytidine (**16**) (Fig. 8.4a) and 5-methyl-2′-deoxycytidine (**17**) and their incorporation into DNA oligonucleotides [84]. Subsequently, Giordano and

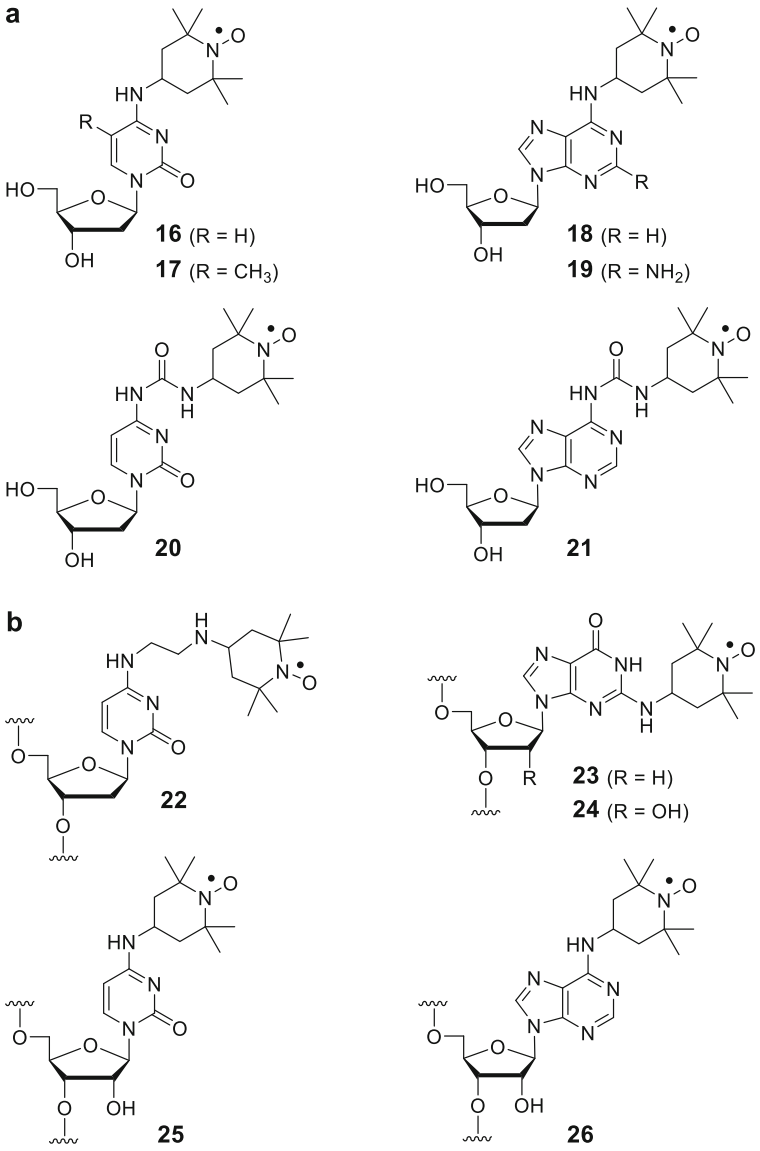

Fig. 8.4 TEMPO-labeled exocyclic amino groups of nucleosides/nucleotides using the phosphoramidite approach (**a**) and the post-synthetic convertible nucleoside approach (**b**)

coworkers reported improved yield of these phosphoramidites, along with the synthesis and incorporation of spin-labeled 2′-deoxyadenosine (**18**) and 2-amino-2′-deoxyadenosine (**19**) into DNA [85]. Since the nitroxides in these labels are directly connected to the nucleobases, their motion is sensitive to the microenvironment of the amino group, in particular, hydrogen bonding. This feature has been utilized to demonstrate that spin label **16** can not only detect mismatches but also identify its base-pairing partner in duplex DNA [86]. The spin-labeled nucleosides **20** and **21** (Fig. 8.4a), where TEMPO is connected to the exocyclic amino groups of C and A through a semi-flexible urea linkage, have also been incorporated into DNA oligomers using the phosphoramidite approach [87].

The exocyclic amino groups have also been modified by a post-synthetic modification through the convertible nucleoside approach, developed by Macmillan and Verdine [88]. In this method, a leaving group is displaced by an amine at the end of the chemical synthesis, which also deprotects the oligonucleotide and cleaves it from resin. The flexible spin label **22** (Fig. 8.4b) has been incorporated into DNA using this strategy and was used for studying dynamics as well as DNA–protein interactions by high-field EPR [89, 90]. A similar approach has been used to label the exocyclic amino group of guanine by treating 2-fluorohypoxanthine-containing oligonucleotides with 4-amino TEMPO to afford nucleotide **23**, used for studying DNA hybridization and folding of G-rich DNA sequences into G-quadruplex [91]. This spin label (**23**) has also been used to probe conformational transitions between duplex DNA [92] and structural changes induced by lesions in DNA duplexes using pulsed EPR spectroscopy [93]. Spin labels have also been installed on the exocyclic amino groups of RNA nucleobases guanine (**24**), cytosine (**25**), and adenine (**26**) (Fig. 8.4b) with good yields by Höbartner and coworkers and used for mapping secondary structures of RNAs by pulsed EPR spectroscopy [94]. More recently, the same group reported a strategy for SDSL of long RNAs that are beyond the limit of solid-phase oligonucleotide synthesis, which entailed a ligation of short spin-labeled RNA oligonucleotides to an in vitro transcribed RNA, catalyzed by a deoxyribozyme. This method was used to synthesize the *S*-adenosylmethionine-I (SAM-I) riboswitch containing **24** [95].

8.2.1.2 C5 of Pyrimidines

Conjugation of spin labels through amino groups has been reported for the 5-position of uridines, such as nucleosides **27** and **28**, which were incorporated into oligonucleotides using phosphotriester-based synthesis (Fig. 8.5a) [96, 97]. However, the first spin-labeled phosphoramidite for the incorporation of spin labels into DNA by automated chemical synthesis was reported by Hopkins and coworkers [98]. A spin-labeled uridine (**29**) and a cytosine (**30**) were prepared by a palladium-catalyzed Sonogashira cross-coupling reaction between their corresponding 5-iodo analogues and the nitroxide 2,2,5,5-tetramethylpyrrolin-1-yloxy-3-acetylene (TPA) [98, 99]. Later, Prisner and coworkers developed an on-column version of this method, where the coupling was performed during the

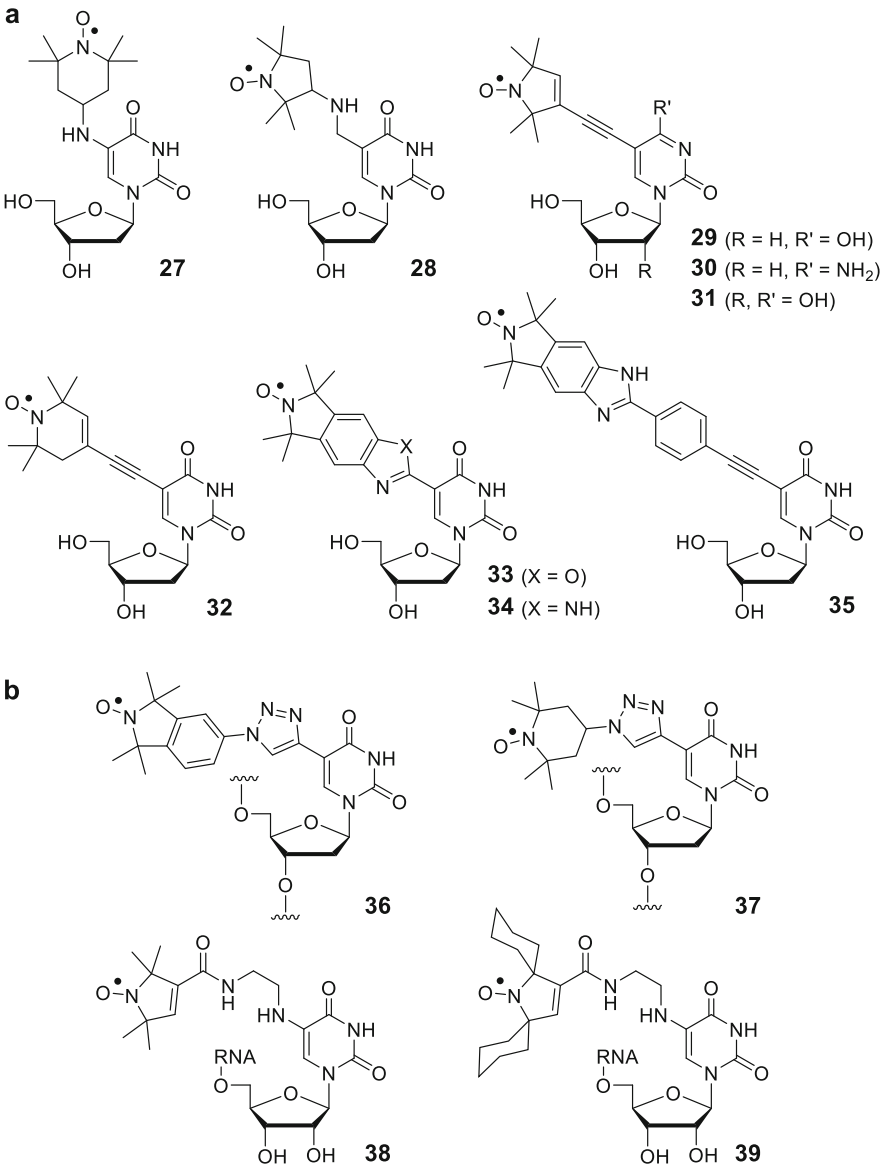

Fig. 8.5 *C*5-labeled pyrimidines. (**a**) Spin labels incorporated by the phosphoramidite method. (**b**) Spin labels incorporated post-synthetically

solid-phase synthesis of both DNA (**29**) [100, 101] and RNA (**31**) [66]. The TPA label is connected to the nucleobase by a short linker that has only rotation around the single bonds flanking the acetylene and has been a useful probe for measuring accurate long-range distances in nucleic acids by PELDOR [66, 69, 73, 100,

101]. Spin label **32** is of similar design as the TPA label and has relatively short synthesis compared to the TPA [102] and has been used to investigate G-quadruplex formation in human telomeric DNA by DEER [103].

Recently, we have reported the synthesis and incorporation of the isoindoline-derived spin labels **33** and **34** (Fig. 8.5a) into DNA oligonucleotides. These labels showed limited mobility in duplex DNA, especially **34**, where an intramolecular hydrogen bond between the *N*–H of the imidazole and *O*4 of the uracil restricted rotation around the bond connecting the spin label to the base [104]. A structurally similar but more flexible spin label (**35**) was also incorporated into DNA by the phosphoramidite approach [74]. Spin labels **32**–**35** are advantageous for distance measurements as the *N*–O bond of the nitroxide lies on the same axis as the rotatable single bonds linking the label to the nucleobase, thereby causing limited displacement of the nitroxide, relative to the nucleobase, upon bond rotation [74].

C5-labeled pyrimidines have also been incorporated into nucleic acids using post-synthetic labeling. The Cu(I)-catalyzed Huisgen–Meldal–Sharpless [3 + 2] cycloaddition reaction (click reaction) has been used to incorporate an isoindoline-derived spin label by an on-column reaction of an azido-nitroxide (**15**, Fig. 8.3) with a DNA oligomer containing 5-ethynyl-2′-deoxyuridine to produce **36** (Fig. 8.5b), which was used for probing local structural lesions in duplex DNA, such as abasic sites and mismatches [81]. Subsequently, Seela and coworkers used a similar click chemistry approach for incorporation of spin label **37,** which was used for distance measurements in DNA oligonucleotides and for studying DNA structure and DNA–protein interactions [105]. Spin labels **38** and **39** have also been incorporated into RNA oligonucleotides using post-synthetic labeling. Spin label **39** with the improved stability toward nitroxide reduction and longer relaxation time was used for distance measurements using Q-band DEER [106].

8.2.1.3 Other Pyrimidine Modifications

During early 1970s, thio-modified nucleotides, which are generally found in tRNAs, were used for SDSL of nucleic acids. For example, 4-thiouridine found in tRNAs of *E. coli* was selectively spin-labeled by alkylation under mild reaction conditions to afford spin-labeled tRNA (**40**) (Fig. 8.6) without affecting their activity [107]. Similarly, 2-thiocytidine has been used for spin labeling of tRNA, which can be enzymatically incorporated into tRNAs using tRNA nucleotidyl transferase and alkylated to yield spin-labeled nucleotide **41** [108]. Dugas and coworkers reported site-specific spin labeling of *E. coli* tRNA using the rare base 2-thio-5-(*N*-methylaminomethyl)-uridine, present in the anticodon region of Glu-tRNA, by acylation to yield nucleotide **42** [109].

After the development of phosphoramidite chemistry and solid-phase synthesis of oligonucleotides, 4-thiouridine has been site-specifically incorporated into RNA oligonucleotides and used for SDSL of RNAs by reacting it with thio-specific spin-labeling reagents to yield spin-labeled nucleotides, such as **40** [77, 110] and **43**–**45** (Fig. 8.6) [76, 110]. Spin-labeled nucleotides **44** and **45** were shown to have

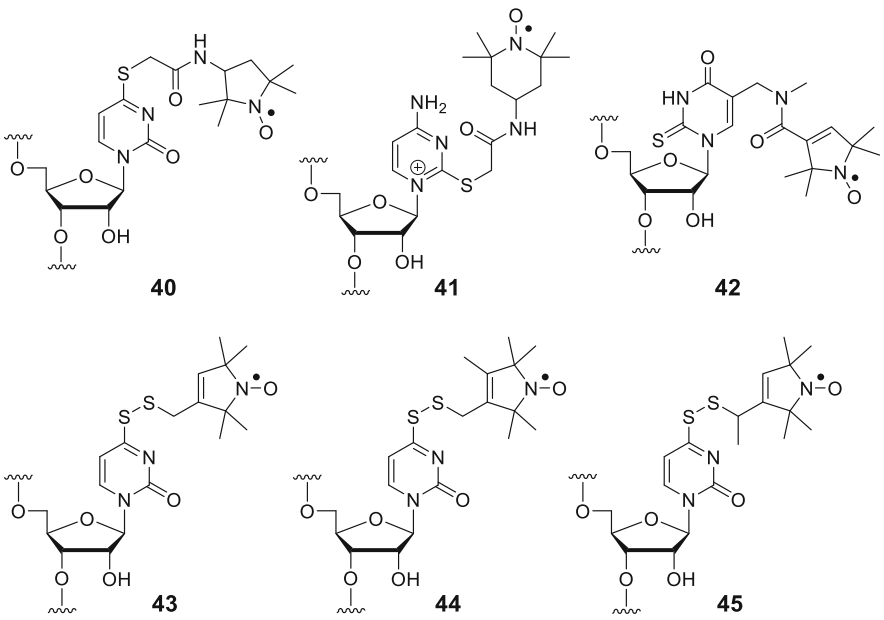

Fig. 8.6 Spin-labeled thiouridines and cytosine in RNA, from post-synthetic labeling

restricted internal motion, relative to the nitroxide **43**, due to the presence of an extra methyl group. These spin labels have been used for studying conformational changes and dynamics of RNA duplexes [76, 111, 112] as well as a synthetic tetracycline RNA aptamer upon ligand binding using pulsed EPR spectroscopy [113].

8.2.1.4 Other Purine Modifications

As described above, purines have mostly been spin-labeled at their exocyclic amino groups (**18**, **19**, **21**, **23**, **24**, and **26**, Fig. 8.4) as shown in the aforementioned section; however, there are a few examples where purines have been spin-labeled by carbon–carbon bond formation. Spin-labeled nucleotide **46** (Fig. 8.7) was prepared by a post-synthetic Diels–Alder [4 + 2] cycloaddition reaction of a nitroxide-functionalized maleimide with 7-vinyl-7-deaza-2′-deoxyguanosine [114]. Spin label **47** was incorporated into RNA using an on-column Sonogashira cross-coupling reaction between 2-iodo adenine and an alkyne-functionalized nitroxide (**12**, Fig. 8.3), during the chemical synthesis of the oligomers [66]. The spin-labeled 7-deazaadenosine analogue **48** was prepared by a post-synthetic click reaction with an alkyne-modified DNA for distance measurements by PELDOR [80]. Spin label **49** has recently been incorporated post-synthetically into RNA oligonucleotides by using a previously reported strategy [115], in which a linker containing an aliphatic amino group was delivered to a chosen RNA nucleobase (guanosine in this case)

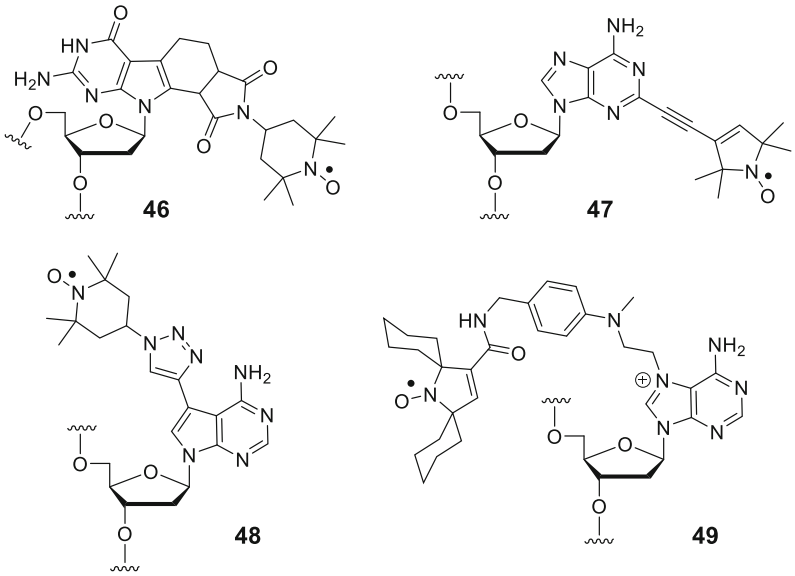

Fig. 8.7 Miscellaneous spin-labeled purine nucleotides

using a complementary DNA reagent and subsequently acylated with a spin-labeling reagent [106]. Kieffer and coworkers have used a DNA-splint-mediated ligation strategy to incorporate 6-thioguanosine at internal sites of long RNA followed by alkylation with a nitroxide to yield spin-labeled RNAs [116].

8.2.1.5 Rigid Labels

The spin labels described thus far have been attached through either flexible or semi-flexible linkers. As mentioned earlier, such labels cannot accurately report the actual dynamics of the nucleic acids, and the distance measurements by EPR using these labels result in wider distance distributions. Therefore, the ideal spin label does not move independently of the nucleic acid to which it is attached. Such spin labels are here referred to as rigid spin labels, although there are examples in the literature where spin labels that have some mobility have been called rigid, when they should more appropriately have been called semi-rigid.

Hopkins and coworkers reported the synthesis and incorporation of the first rigid spin label (**Q**, Fig. 8.8) into DNA oligonucleotides using solid-phase chemical synthesis [117, 118]. The rigid spin label **Q** is a C-nucleoside and has been used for studying sequence-dependent dynamics of duplex DNAs [119–121]. However, **Q** has a lengthy synthesis and also requires the nonnatural base-pairing partner 2-aminopurine (**2AP**), which hampered its further use for EPR studies of nucleic acids. We have synthesized the rigid spin label **Ç** ("C-spin") (Fig. 8.8) and incorporated it into DNA oligonucleotides using solid-phase synthesis [46]. In **Ç**,

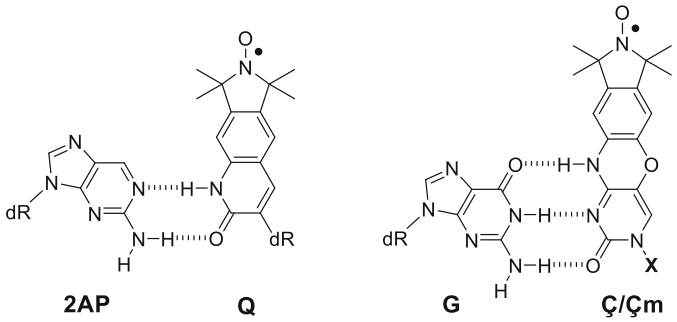

Fig. 8.8 Structures and base-pairing schemes of rigid spin label nucleosides **Q** and **Ç/Çm**, where X indicates either 2′-deoxyribose (in **Ç**) or 2′-methoxyribose (in **Çm**)

a nitroxide-bearing isoindoline ring has been fused to cytosine (C) through an oxazine linkage. The rigid spin label **Ç** can form a stable and structurally non-perturbing base pair with guanine (G), as observed in the crystal structure of a **Ç**-labeled DNA duplex [122].

Spin label **Ç** has enabled accurate distance measurements in DNA duplexes, as well as determination of the relative orientations between two such labels using pulsed EPR spectroscopy [45, 123]. Furthermore, **Ç** has been used to study the dynamics and conformations of DNA hairpin loops and bulges [47, 124] as well as motion associated with substrate recognition in a group I ribozyme [70] by CW-EPR. Spin label **Ç**, in conjunction with PELDOR, has also been used to obtain insights into internal mobility of duplex DNAs [48]. An interesting feature of **Ç** is that reduction of the nitroxide functional group yields a fluorescent probe, which has been used for both detecting single-base mismatches and to identify its base-pairing partner in duplex DNA [125–127]. The bifunctional nature of **Ç** also allowed for the study of the cocaine aptamer folding by both fluorescence and EPR spectroscopies [128]. A ribo-analogue of the rigid spin label **Ç** (**Çm**), which contains a methoxy group at 2′-position, has also been prepared and incorporated into different RNA oligonucleotides by solid-phase chemical synthesis [129] and used for distance determinations as well as orientation selections in RNA oligonucleotides by PELDOR [130].

8.2.2 Sugar Labeling

The sugar moieties of both DNA and RNA nucleotides have been used for conjugation of spin labels. However, the 2′-position is the only readily available site for labeling at internal positions of nucleic acids, which projects the label into the minor groove. In contrast, labeling of the 5′- and 3′-positions is restricted to the oligonucleotide termini. Post-synthetic modification is generally the method of choice to label the sugars. One such high-yielding spin-labeling method for RNA

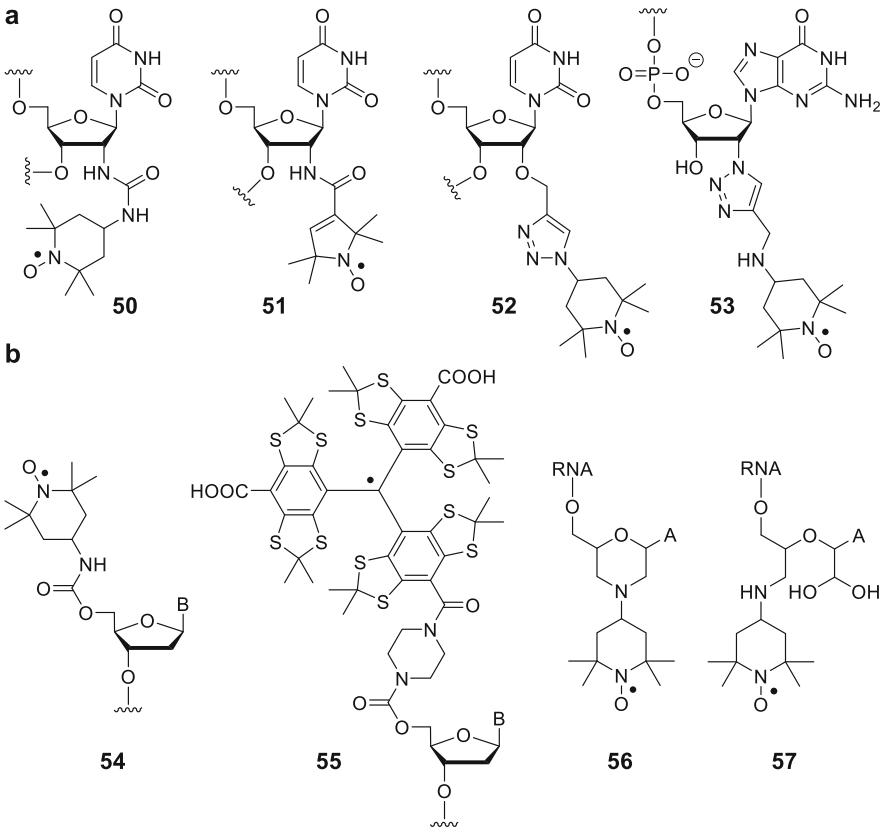

Fig. 8.9 Spin-labeled sugars. (**a**) Spin labels for incorporation at the internal positions through conjugation to the 2′-position of sugars. (**b**) Spin labels for incorporation at the 5′- and 3′-ends of nucleic acids. A stands for adenine and B for nucleobase

is the reaction of readily available 2′-amino-modified oligonucleotides with the commercially available 4-isocyanato-TEMPO (**7**, Fig. 8.3) to afford an urea-linked 2′-spin-labeled nucleotide (**50**, Fig. 8.9a) [32, 78]. Spin label **50** has been used for studying structure-dependent dynamics of the trans-activation-responsive (TAR) RNA [71, 119, 131] and metal-ion-induced folding of hammerhead ribozyme by EPR spectroscopy [132–134]. It has also been used for studying ligand-induced folding of the tetracycline aptamer [113] and for distance measurements in nucleic acids by pulsed EPR [133, 135, 136]. DeRose and coworkers have conjugated a nitroxide to the 2′-amino group through a short amide linker (**51**); however, it was found to have a destabilizing effect on RNA helices [35].

Spin labels have also been incorporated post-synthetically at 2′-positions of sugars using click-chemistry, such as the spin label nucleotide **52** [137]. This label has been used for distance measurements in DNA using DEER; however, large distance distributions were obtained due to the flexibility of the linker. Recently,

Höbartner and coworkers reported an elegant, deoxyribozyme-mediated approach for site-specific labeling of internal 2′-hydroxyls of in vitro transcribed long RNAs [82]. In this method, a 2′-labeled guanosine triphosphate (GTP) is used as a substrate for a Tb^{3+}-deoxyribozyme to install a spin label, such as **53**, on the 2′-hydroxyl group of any chosen internal adenine nucleotide through a 2′, 5′-phosphodiester linkage.

Examples of 5′-labels include TEMPO-derived spin label **54** [138] and a carbon-centered triarylmethyl (trityl or TAM) spin label (**55**) (Fig. 8.9b). The trityl labels were incorporated into short DNA oligonucleotides by coupling a trityl acid chloride with 5′-piperazine-activated short DNA oligonucleotides and used for distance measurements at physiological temperature on immobilized duplex DNA [58]. Trityl radicals have emerged as a new class of spin labels for distance measurements [57, 59, 139] and offer certain advantages over nitroxide radicals, such as a narrow spectral width, stability in reducing environment [52, 140], and a long transverse relaxation time (T_M) in the liquid state at room temperature [141]. However, trityl radicals are considerably larger than nitroxides, which limits where they can be incorporated without causing structural perturbations.

Caron and Dugas developed a 3′-end labeling strategy for tRNA using periodate oxidation of the *cis*-geminal diol of the sugar moiety at the 3′-end to make the corresponding dialdehyde, which on reductive amination with 4-amino TEMPO and sodium borohydride afforded morpholino spin label **56** [142]. A milder reducing agent, sodium cyanoborohydride, yielded spin label **57**, which showed more motional freedom than spin label **56** [143]. These labels have been used for studying 3′-end conformations and aggregations of tRNAs [143, 144].

8.2.3 Phosphate Labeling

The phosphate group of the sugar-phosphate backbone of nucleic acids is another useful site for spin labeling. Spin labels have been conjugated to the phosphorous atoms at both terminal and internal positions by replacement of one of the non-bridging oxygen atoms with the label. Advantages of phosphate labeling include the availability of post-synthetic methods using commercially available materials and the fact that phosphodiesters can be labeled independent of the nucleotide sequence and without having to prepare specifically modified nucleosides or nucleotides. Furthermore, spin labels attached to phosphorous generally interfere less with the duplex formation since they are placed at the edges of the helices. However, labeling of the phosphodiester group yields a mixture of two diastereomers, which may lead to ambiguous structural information, although the isomers of short oligonucleotides can be separated by HPLC [145, 146]. In case of an RNA phosphate labeling, the 2′-OH group adjacent to the labeled phosphodiester needs to be either replaced with a hydrogen or a 2′-OMe group, because the 2′-OH group leads to strand cleavage through 2′,3′-transesterification [147].

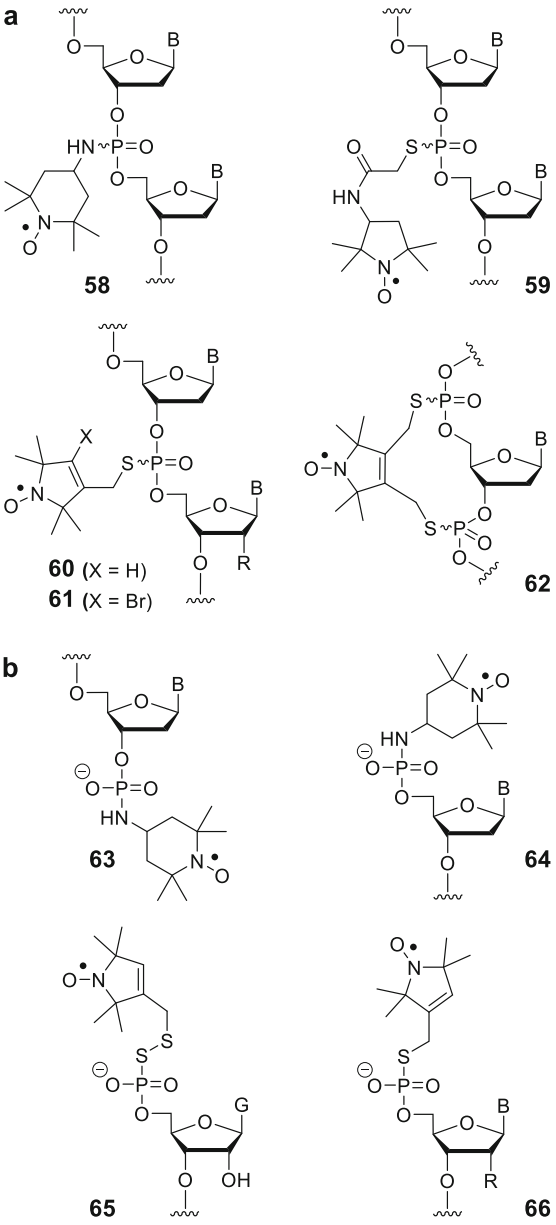

Fig. 8.10 Spin labels attached to internal phosphodiesters (**a**) and terminal phosphate groups (**b**). R stands for OH or H, and B represents a nucleobase

Phosphorous atoms of internal phosphodiesters have been spin labeled using H-phosphonate chemistry, where a hydrogen-phosphonate internucleotide linkage is introduced at a specific site during the oligonucleotide synthesis and oxidized in the presence of 4-amino TEMPO to yield phosphoramidate **58** (Fig. 8.10a) [148] or derivatives with different linkers [138]. One of the non-bridging oxygen atoms of a

phosphodiester can be replaced with sulfur by using a sulfurizing agent instead of an oxidizing agent during the chemical oligonucleotides synthesis [149]. The resulting phosphorothioate can be specifically alkylated to afford a spin-labeled nucleotide, such as **59** [150]. Similarly, RNA oligonucleotides have been spin-labeled to afford spin label **60** [79], designated as R5, which has been used for studying GNRA tetraloop–receptor interactions in RNAs [151], for dynamics [152, 153], for distance measurements [79, 154], and for studying protein–nucleic acid complexes using PELDOR [155].

Subsequently, Qin and coworkers reported a 4-bromo-substituted analogue of **60** (**61**), which has been used to study dynamics of the substrate-recognition RNA element in the group I intron ribozyme by CW-EPR spectroscopy [156], in addition to studying structure and dynamics of DNA [145, 146, 157]. Linking adjacent phosphorothioates with a nitroxide-containing bifunctional alkylating agent resulted in the conformationally restrained spin label **62** [158], similar to what has been reported for spin labeling of two cysteines in proteins [159, 160].

Due to their higher nucleophilicity, terminal phosphates are easier to modify than phosphodiesters. Dzuba and coworkers labeled both 3′- and 5′-terminal phosphates with 4-amino TEMPO to afford phosphoramidates **63** and **64** (Fig. 8.10b), respectively, and used the spin-labeled DNA to study conformational changes induced by non-nucleotide inserts in duplex DNAs by PELDOR [161]. A phosphoramidite derivative of 4-hydroxy TEMPO has been prepared and used to incorporate spin labels into the 5′-end of RNA hairpins [162]. Oligonucleotides containing terminal phosphorothioates have also been prepared by incorporation of 5′-guanosine monophosphorothioate (GMPS) during in vitro transcription of RNA using T7 RNA polymerase, which was subsequently spin labeled to afford **65** [36]. Similarly, a phosphorothioate group has been enzymatically incorporated at the 5′-position of either DNA or RNA using T4-polynucleotide kinase, followed by alkylation to yield spin-labeled nucleotide **66** [163].

8.2.4 Noncovalent Labeling

Nucleic acids have been spin-labeled noncovalently by using intercalators (reviewed in [64]). However, spin-labeled intercalating agents have limited use, because they lack sequence specificity and since multiple ligands can bind to the same nucleic acid. Lhomme and coworkers reported the first example of a noncovalent SDSL (NC-SDSL) of nucleic acids, in which a spin-labeled acridine intercalator–adenine conjugate (**67,** Fig. 8.11) was bound to an abasic site in a duplex DNA [164, 165]. The abasic site can readily be incorporated at specific sites in DNA by nucleic acid synthesis using commercially available phosphoramidites. Nakatani and coworkers prepared naphthyridine carbamate dimer (NCD, **68**) that bound specifically to G–G mismatches and used it for site-specific programmable assembly of spin probes on one- and two-dimensional DNA tiles [166–169].

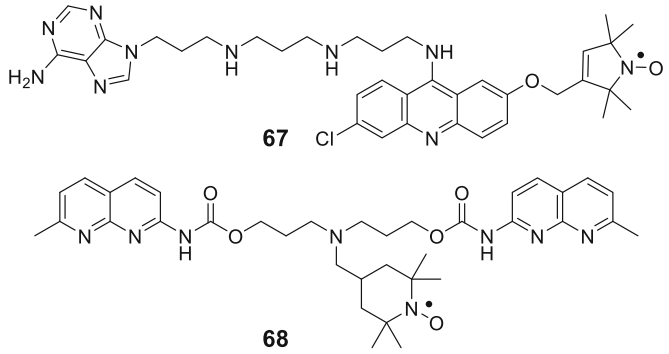

Fig. 8.11 Spin-labeled intercalator (**67**) and nitroxide-conjugated G–G mismatch-binder NCD (**68**) used for noncovalent spin labeling of nucleic acids

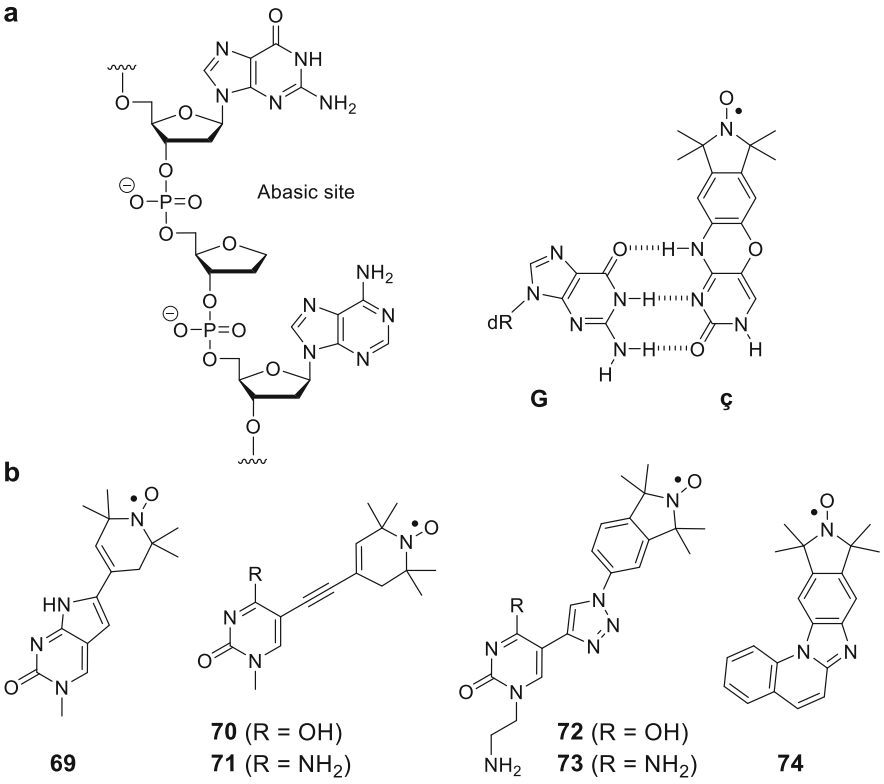

Fig. 8.12 Structure of an abasic site in DNA (**a**, *left*) and spin label **ç** base paired with G (**a**, *right*) used in NC-SDSL. (**b**) Structures of spin-labeled ligands for NC-SDSL

Our group has reported NC-SDSL of nucleic acids in which an abasic site in a duplex DNA served as a receptor for the spin-labeled ligand **ç** (Fig. 8.12a) [170]. The modified nucleobase **ç** is derived from the rigid spin label nucleoside

Ç, an analogue of the nucleobase cytosine (C). The spin label **ç** binds to the abasic site by forming hydrogen bonds with an orphan guanine base on the opposite strand and π-stacking interactions with base pairs immediately flanking the abasic site. The spin label **ç** has been used for distance measurements in duplex DNA and for studying protein-induced DNA bending using pulsed EPR [26]. A structure–function relationship study of **ç** showed that its binding is primarily governed by the identity of the base-pairing nucleotide (the orphan base) and flanking nucleotide sequence [171]. Several other derivatives of **ç** for NC-SDSL have also been reported [172].

More recently, several pyrimidine-derived spin-labeled ligands (**69–73**, Fig. 8.12b) have been screened for binding to abasic sites in nucleic acid duplexes. However, most of the labels showed lower binding affinity than **ç**, except **72**, which binds fully to abasic sites in both DNA and RNA [173]. Masters and coworkers recently reported a new class of profluorescent nitroxides, for example, spin label **74** for NC-SDSL of both DNA and RNA [174].

NC-SDSL provides a simple approach to direct spin labels to specific sites of nucleic acids and has several advantages over the other two spin-labeling strategies, the phosphoramidite- and the post-synthetic method. For example, syntheses of the spin label ligands are simpler than the spin-labeled phosphoramidites, they are relatively more stable and can be stored for extended periods of time. Furthermore, spin labeling can be performed simply by mixing the spin label ligand with the nucleic acid containing abasic sites. However, this strategy requires a binding site that has high enough affinity for the spin label ligand to ensure complete and specific binding. The NC-SDSL utilizing abasic sites is also restricted to base-pairing regions in nucleic acids.

8.3 Conclusions and Future Prospects

This chapter highlights advances in the development of site-specific spin-labeling strategies of nucleic acids. Coupled with recent advances in EPR techniques, such as pulsed EPR methods, SDSL strategies have enabled routine interrogations of the structure and dynamics of nucleic acids that give insights into their folding and functions. This includes recent examples of long RNAs, where spin labels were incorporated using either protein- or DNA catalysis. Several of the SDSL techniques are straightforward to carry out using readily available materials, which has given researchers an easy access to spin-labeled nucleic acids for EPR studies. This includes noncovalent labeling, where the label is simply mixed with a binding site for the spin label. Tailor-made spin labels with improved spectroscopic properties have evolved, for example, the rigid spin label **Ç**, which has allowed determination of relative orientations of two spin labels, in addition to accurate distance measurements in nucleic acids. The rigidity of **Ç** has also allowed the internal dynamics of DNA duplexes to be investigated by EPR spectroscopy. Carbon-centered trityl radicals have enabled distance measurements at physiological temperatures using

pulsed EPR. Trityl radicals have thus emerged as an exciting class of spin labels for EPR spectroscopy that are relatively stable under reducing conditions, which is a prerequisite for in-cell studies. While a number of spin labels have been described in the last few years, there is still a need for readily accessible spin labels with improved spectroscopic properties and stability. This will further the use of EPR spectroscopy to study nucleic acids, which has shown a great promise as a stand-alone technique or, more recently in combination with NMR spectroscopy [175] to obtain high-resolution solution structures of nucleic acids and their complexes with other biomolecules.

Acknowledgments We thank members of the Sigurdsson research group for critical reading of the manuscript and valuable comments.

References

1. Cech TR (1990) Self-splicing of group I introns. Annu Rev Biochem 59:543–568
2. Doherty EA, Doudna JA (2000) Ribozyme structures and mechanisms. Annu Rev Biochem 69:597–615
3. Fedor MJ, Williamson JR (2005) The catalytic diversity of RNAs. Nat Rev Mol Cell Biol 6(5):399–412
4. Steitz TA (2008) A structural understanding of the dynamic ribosome machine. Nat Rev Mol Cell Biol 9(3):242–253
5. Fica SM, Tuttle N, Novak T, Li NS, Lu J, Koodathingal P, Dai Q, Staley JP, Piccirilli JA (2013) RNA catalyses nuclear pre-mRNA splicing. Nature 503(7475):229–234
6. Meister G, Tuschl T (2004) Mechanisms of gene silencing by double-stranded RNA. Nature 431(7006):343–349
7. Montange RK, Batey RT (2008) Riboswitches: emerging themes in RNA structure and function. Annu Rev Biophys 37:117–133
8. Serganov A, Nudler E (2013) A decade of riboswitches. Cell 152(1-2):17–24
9. Geiss G, Jin G, Guo J, Bumgarner R, Katze MG, Sen GC (2001) A comprehensive view of regulation of gene expression by double-stranded RNA-mediated cell signaling. J Biol Chem 276(32):30178–30182
10. Dominguez C, Schubert M, Duss O, Ravindranathan S, Allain FH (2011) Structure determination and dynamics of protein-RNA complexes by NMR spectroscopy. Prog Nucl Magn Reson Spectrosc 58(1-2):1–61
11. Duss O, Yulikov M, Jeschke G, Allain FH (2014) EPR-aided approach for solution structure determination of large RNAs or protein-RNA complexes. Nat Commun 5:3669
12. Getz M, Sun X, Casiano-Negroni A, Zhang Q, Al-Hashimi HM (2007) NMR studies of RNA dynamics and structural plasticity using NMR residual dipolar couplings. Biopolymers 86(5-6):384–402
13. Preus S, Wilhelmsson LM (2012) Advances in quantitative FRET-based methods for studying nucleic acids. ChemBioChem 13(14):1990–2001
14. Roy R, Hohng S, Ha T (2008) A practical guide to single-molecule FRET. Nat Methods 5(6):507–516
15. Sahoo H (2011) Förster resonance energy transfer—a spectroscopic nanoruler: principle and applications. J Photochem Photobiol C Photochem Rev 12(1):20–30
16. Hubbell WL, Gross A, Langen R, Lietzow MA (1998) Recent advances in site-directed spin labeling of proteins. Curr Opin Struct Biol 8(5):649–656

17. Hubbell WL, Lopez CJ, Altenbach C, Yang Z (2013) Technological advances in site-directed spin labeling of proteins. Curr Opin Struct Biol 23(5):725–733
18. Hustedt EJ, Beth AH (1999) Nitroxide spin-spin interactions: applications to protein structure and dynamics. Annu Rev Biophys Biomol Struct 28:129–153
19. Prisner T, Rohrer M, MacMillan F (2001) Pulsed EPR spectroscopy: biological applications. Annu Rev Phys Chem 52:279–313
20. Schiemann O, Prisner TF (2007) Long-range distance determinations in biomacromolecules by EPR spectroscopy. Q Rev Biophys 40(1):1–53
21. Schiemann O, Reginsson GW (2011) Studying bimolecular complexes with pulsed electron-electron double resonance spectroscopy. Biochem Soc Trans 39:128–139
22. Sowa GZ, Qin PZ (2008) Site-directed spin labeling studies on nucleic acid structure and dynamics. Prog Nucleic Acid Res Mol Biol 82:147–197
23. Ubbink M, Worrall J, Canters G, Groenen E, Huber M (2002) Paramagnetic resonance of biological metal centers. Annu Rev Biophys Biomol Struct 31:393–422
24. Zhang XJ, Cekan P, Sigurdsson ST, Qin PZ (2009) Studying RNA using site-directed spin-labeling and continuous-wave electron paramagnetic resonance spectroscopy. Methods Enzymol 469:303–328
25. Prisner TF, Marko A, Sigurdsson ST (2015) Conformational dynamics of nucleic acid molecules studied by PELDOR spectroscopy with rigid spin labels. J Magn Reson 252: 187–198
26. Reginsson GW, Shelke SA, Rouillon C, White MF, Sigurdsson ST, Schiemann O (2013) Protein-induced changes in DNA structure and dynamics observed with noncovalent site-directed spin labeling and PELDOR. Nucleic Acids Res 41(1):e11
27. Blanchard SC (2009) Single-molecule observations of ribosome function. Curr Opin Struct Biol 19(1):103–109
28. Wozniak AK, Schroder GF, Grubmuller H, Seidel CA, Oesterhelt F (2008) Single-molecule FRET measures bends and kinks in DNA. Proc Natl Acad Sci U S A 105(47):18337–18342
29. Hura GL, Menon AL, Hammel M, Rambo RP, Poole FL 2nd, Tsutakawa SE, Jenney FE Jr, Classen S, Frankel KA, Hopkins RC, Yang SJ, Scott JW, Dillard BD, Adams MW, Tainer JA (2009) Robust, high-throughput solution structural analyses by small angle X-ray scattering (SAXS). Nat Methods 6(8):606–612
30. Ranjbar B, Gill P (2009) Circular dichroism techniques: biomolecular and nanostructural analyses—a review. Chem Biol Drug Des 74(2):101–120
31. Zavoisky EK (1945) Spin-magnetic resonance in paramagnetics. J Phys Acad Sci USSR 9: 211–245
32. Edwards TE, Okonogi TM, Robinson BH, Sigurdsson ST (2001) Site-specific incorporation of nitroxide spin-labels into internal sites of the TAR RNA; structure-dependent dynamics of RNA by EPR spectroscopy. J Am Chem Soc 123(7):1527–1528
33. Jeschke G (2013) Conformational dynamics and distribution of nitroxide spin labels. Prog Nucl Magn Reson Spectrosc 72:42–60
34. Spaltenstein A, Robinson BH, Hopkins PB (1989) Sequence-dependent and structure-dependent DNA-base dynamics—synthesis, structure, and dynamics of site and sequence specifically spin-labeled DNA. Biochemistry 28(24):9484–9495
35. Kim NK, Murali A, DeRose VJ (2004) A distance ruler for RNA using EPR and site-directed spin labeling. Chem Biol 11(7):939–948
36. Macosko JC, Pio MS, Tinoco I Jr, Shin YK (1999) A novel 5 displacement spin-labeling technique for electron paramagnetic resonance spectroscopy of RNA. RNA 5(9):1158–1166
37. Freed JH (2000) New technologies in electron spin resonance. Annu Rev Phys Chem 51: 655–689
38. Jeschke G (2002) Determination of the nanostructure of polymer materials by electron paramagnetic resonance spectroscopy. Macromol Rapid Commun 23(4):227–246
39. Jeschke G (2012) DEER distance measurements on proteins. Annu Rev Phys Chem 63: 419–446

40. Fedorova OS, Tsvetkov YD (2013) Pulsed electron double resonance in structural studies of spin-labeled nucleic acids. Acta Naturae 5(1):9–32
41. Martin RE, Pannier M, Diederich F, Gramlich V, Hubrich M, Spiess HW (1998) Determination of end-to-end distances in a series of TEMPO diradicals of up to 2.8 nm length with a new four-pulse double electron electron resonance experiment. Angew Chem Int Ed Engl 37(20):2833–2837
42. Bowen AM, Tait CE, Timmel CR, Harmer JR (2013) Orientation-selective DEER using rigid spin labels, cofactors, metals, and clusters. In: Timmel CR, Harmer JR (eds) Structural information from spin-labels and intrinsic paramagnetic centres in the biosciences. Springer, Berlin, pp 283–327
43. Denysenkov V, Prisner T, Stubbe J, Bennati M (2006) High-field pulsed electron–electron double resonance spectroscopy to determine the orientation of the tyrosyl radicals in ribonucleotide reductase. Proc Natl Acad Sci U S A 103(36):13386–13390
44. Hustedt EJ, Smirnov AI, Laub CF, Cobb CE, Beth AH (1997) Molecular distances from dipolar coupled spin-labels: the global analysis of multifrequency continuous wave electron paramagnetic resonance data. Biophys J 72(4):1861
45. Schiemann O, Cekan P, Margraf D, Prisner TF, Sigurdsson ST (2009) Relative orientation of rigid nitroxides by PELDOR: beyond distance measurements in nucleic acids. Angew Chem Int Ed Engl 48(18):3292–3295
46. Barhate N, Cekan P, Massey AP, Sigurdsson ST (2007) A nucleoside that contains a rigid nitroxide spin label: a fluorophore in disguise. Angew Chem Int Ed Engl 46(15):2655–2658
47. Cekan P, Smith AL, Barhate N, Robinson BH, Sigurdsson ST (2008) Rigid spin-labeled nucleoside Ç: a nonperturbing EPR probe of nucleic acid conformation. Nucleic Acids Res 36(18):5946–5954
48. Marko A, Denysenkov V, Margraf D, Cekan P, Schiemann O, Sigurdsson ST, Prisner TF (2011) Conformational flexibility of DNA. J Am Chem Soc 133(34):13375–13379
49. Kinoshita Y, Yamada KI, Yamasaki T, Sadasue H, Sakai K, Utsumi H (2009) Development of novel nitroxyl radicals for controlling reactivity with ascorbic acid. Free Radic Res 43(6): 565–571
50. Yamasaki T, Mito F, Ito Y, Pandian S, Kinoshita Y, Nakano K, Murugesan R, Sakai K, Utsumi H, Yamada K (2011) Structure-reactivity relationship of piperidine nitroxide: electrochemical, ESR and computational studies. J Org Chem 76(2):435–440
51. Azarkh M, Okle O, Eyring P, Dietrich DR, Drescher M (2011) Evaluation of spin labels for in-cell EPR by analysis of nitroxide reduction in cell extract of *Xenopus laevis* oocytes. J Magn Reson 212(2):450–454
52. Jagtap AP, Krstic I, Kunjir NC, Hansel R, Prisner TF, Sigurdsson ST (2015) Sterically shielded spin labels for in-cell EPR spectroscopy: analysis of stability in reducing environment. Free Radic Res 49(1):78–85
53. Kinoshita Y, Yamada K, Yamasaki T, Mito F, Yamato M, Kosem N, Deguchi H, Shirahama C, Ito Y, Kitagawa K, Okukado N, Sakai K, Utsumi H (2010) In vivo evaluation of novel nitroxyl radicals with reduction stability. Free Radic Biol Med 49(11):1703–1709
54. Kirilyuk IA, Polienko YF, Krumkacheva OA, Strizhakov RK, Gatilov YV, Grigor'ev IA, Bagryanskaya EG (2012) Synthesis of 2,5-bis(spirocyclohexane)-substituted nitroxides of pyrroline and pyrrolidine series, including thiol-specific spin label: an analogue of MTSSL with long relaxation time. J Org Chem 77(18):8016–8027
55. Okazaki S, Mannan MA, Sawai K, Masumizu T, Miura Y, Takeshita K (2007) Enzymatic reduction-resistant nitroxyl spin probes with spirocyclohexyl rings. Free Radic Res 41(10): 1069–1077
56. Paletta JT, Pink M, Foley B, Rajca S, Rajca A (2012) Synthesis and reduction kinetics of sterically shielded pyrrolidine nitroxides. Org Lett 14(20):5322–5325
57. Reginsson GW, Kunjir NC, Sigurdsson ST, Schiemann O (2012) Trityl radicals: spin labels for nanometer-distance measurements. Chem Eur J 18(43):13580–13584

58. Shevelev GY, Krumkacheva OA, Lomzov AA, Kuzhelev AA, Rogozhnikova OY, Trukhin DV, Troitskaya TI, Tormyshev VM, Fedin MV, Pyshnyi DV, Bagryanskaya EG (2014) Physiological-temperature distance measurement in nucleic acid using triarylmethyl-based spin labels and pulsed dipolar EPR spectroscopy. J Am Chem Soc 136(28):9874–9877
59. Yang Z, Liu Y, Borbat P, Zweier JL, Freed JH, Hubbell WL (2012) Pulsed ESR dipolar spectroscopy for distance measurements in immobilized spin labeled proteins in liquid solution. J Am Chem Soc 134(24):9950–9952
60. Matalon E, Huber T, Hagelueken G, Graham B, Frydman V, Feintuch A, Otting G, Goldfarb D (2013) Gadolinium (III) spin labels for high-sensitivity distance measurements in transmembrane helices. Angew Chem Int Ed Engl 125(45):12047–12050
61. Ohnishi SI, McConnell HM (1965) Interaction of the radical ion of chlorpromazine with deoxyribonucleic acid. J Am Chem Soc 87:2293
62. Stone TJ, Buckman T, Nordio PL, McConnell HM (1965) Spin-labeled biomolecules. Proc Natl Acad Sci U S A 54(4):1010–1017
63. Borbat P, Costa-Filho A, Earle K, Moscicki J, Freed J (2001) Electron spin resonance in studies of membranes and proteins. Science 291(5502):266–269
64. Shelke SA, Sigurdsson ST (2012) Site-directed spin labelling of nucleic acids. Eur J Org Chem 12:2291–2301
65. Shelke SA, Sigurdsson ST (2013) Site-directed nitroxide spin labeling of biopolymers. In: Timmel CR, Harmer JR (eds) Structural information from spin-labels and intrinsic paramagnetic centres in the biosciences. Springer, Berlin, pp 121–162
66. Piton N, Mu YG, Stock G, Prisner TF, Schiemann O, Engels JW (2007) Base-specific spin-labeling of RNA for structure determination. Nucleic Acids Res 35(9):3128–3143
67. Hänsel R, Luh LM, Corbeski I, Trantirek L, Doetsch V (2014) In-cell NMR and EPR spectroscopy of biomacromolecules. Angew Chem Int Ed Engl 53(39):10300–10314
68. Igarashi R, Sakai T, Hara H, Tenno T, Tanaka T, Tochio H, Shirakawa M (2010) Distance determination in proteins inside Xenopus laevis oocytes by double electron−electron resonance experiments. J Am Chem Soc 132(24):8228–8229
69. Krstić I, Hänsel R, Romainczyk O, Engels JW, Dötsch V, Prisner TF (2011) Long-range distance measurements on nucleic acids in cells by pulsed EPR spectroscopy. Angew Chem Int Ed Engl 50(22):5070–5074
70. Nguyen P, Shi X, Sigurdsson ST, Herschlag D, Qin PZ (2013) A single-stranded junction modulates nanosecond motional ordering of the substrate recognition duplex of a group I ribozyme. ChemBioChem 14(14):1720–1723
71. Edwards TE, Robinson BH, Sigurdsson ST (2005) Identification of amino acids that promote specific and rigid TAR RNA-tat protein complex formation. Chem Biol 12(3):329–337
72. Zhang X, Lee SW, Zhao L, Xia T, Qin PZ (2010) Conformational distributions at the N-peptide/boxB RNA interface studied using site-directed spin labeling. RNA 16(12): 2474–2483
73. Krstić I, Frolow O, Sezer D, Endeward B, Weigand JE, Suess B, Engels JW, Prisner TF (2010) PELDOR spectroscopy reveals preorganization of the neomycin-responsive riboswitch tertiary structure. J Am Chem Soc 132(5):1454–1455
74. Gophane DB, Endeward B, Prisner TF, Sigurdsson ST (2014) Conformationally restricted isoindoline-derived spin labels in duplex DNA: distances and rotational flexibility by pulsed electron–electron double resonance spectroscopy. Chem Eur J 20(48):15913–15919
75. Engels JW, Grünewald C, Wicke L (2014) Site-directed spin labeling of RNA for distance measurements by EPR. In: Erdmann VA, Markiewicz WT, Barciszewski J (eds) Chemical biology of nucleic acids. Springer, Berlin, pp 385–407
76. Qin PZ, Hideg K, Feigon J, Hubbell WL (2003) Monitoring RNA base structure and dynamics using site-directed spin labeling. Biochemistry 42(22):6772–6783
77. Ramos A, Varani G (1998) A new method to detect long-range protein-RNA contacts: NMR detection of electron-proton relaxation induced by nitroxide spin-labeled RNA. J Am Chem Soc 120(42):10992–10993

78. Edwards TE, Sigurdsson ST (2007) Site-specific incorporation of nitroxide spin-labels into 2′-positions of nucleic acids. Nat Protoc 2(8):1954–1962
79. Qin PZ, Haworth IS, Cai Q, Kusnetzow AK, Grant GP, Price EA, Sowa GZ, Popova A, Herreros B, He H (2007) Measuring nanometer distances in nucleic acids using a sequence-independent nitroxide probe. Nat Protoc 2(10):2354–2365
80. Ding P, Wunnicke D, Steinhoff HJ, Seela F (2010) Site-directed spin-labeling of DNA by the azide-alkyne 'Click' reaction: nanometer distance measurements on 7-deaza-2-′-deoxyadenosine and 2′-deoxyuridine nitroxide conjugates spatially separated or linked to a 'dA-dT' base pair. Chem Eur J 16(48):14385–14396
81. Jakobsen U, Shelke SA, Vogel S, Sigurdsson ST (2010) Site-directed spin-labeling of nucleic acids by click chemistry: detection of abasic sites in duplex DNA by EPR spectroscopy. J Am Chem Soc 132(30):10424–10428
82. Büttner L, Javadi-Zarnaghi F, Höbartner C (2014) Site-specific labeling of RNA at internal ribose hydroxyl groups: terbium-assisted deoxyribozymes at work. J Am Chem Soc 136(22): 8131–8137
83. McCalley R, Shimshick E, McConnell H (1972) The effect of slow rotational motion on paramagnetic resonance spectra. Chem Phys Lett 13(2):115–119
84. Bannwarth W, Schmidt D (1994) Oligonucleotides containing spin-labeled 2′-deoxycytidine and 5-methyl-2′-deoxycytidine as probes for structural motifs of DNA. Bioorg Med Chem Lett 4(8):977–980
85. Giordano C, Fratini F, Attanasio D, Cellai L (2001) Preparation of spin-labeled 2-amino-dA, dA, dC and 5-methyl-dC phosphoramidites for the automatic synthesis of EPR active oligonucleotides. Synthesis 4:565–572
86. Cekan P, Sigurdsson ST (2009) Identification of single-base mismatches in duplex DNA by EPR spectroscopy. J Am Chem Soc 131(50):18054–18056
87. Gophane DB, Sigurdsson ST (2015) TEMPO-derived spin labels linked to the nucleobases adenine and cytosine for probing local structural perturbations in DNA by EPR spectroscopy. Beilstein J Org Chem 11(1):219–227
88. Macmillan AM, Verdine GL (1990) Synthesis of functionally tethered oligodeoxynucleotides by the convertible nucleoside approach. J Org Chem 55(24):5931–5933
89. Budil DE, Kolaczkowski SV, Perry A, Varaprasad C, Johnson F, Strauss PR (2000) Dynamics and ordering in a spin-labeled oligonucleotide observed by 220 GHz electron paramagnetic resonance. Biophys J 78(1):430–438
90. Kolaczkowski SV, Perry A, Mckenzie A, Johnson F, Budil DE, Strauss PR (2001) A spin-labeled abasic DNA substrate for AP endonuclease. Biochem Biophys Res Commun 288(3): 722–726
91. Okamoto A, Inasaki T, Saito I (2004) Nitroxide-labeled guanine as an ESR spin probe for structural study of DNA. Bioorg Med Chem Lett 14(13):3415–3418
92. Sicoli G, Mathis G, Delalande O, Boulard Y, Gasparutto D, Gambarelli S (2008) Double electron-electron resonance (DEER): a convenient method to probe DNA conformational changes. Angew Chem Int Ed Engl 47(4):735–737
93. Sicoli G, Mathis G, Aci-Seche S, Saint-Pierre C, Boulard Y, Gasparutto D, Gambarelli S (2009) Lesion-induced DNA weak structural changes detected by pulsed EPR spectroscopy combined with site-directed spin labelling. Nucleic Acids Res 37(10):3165–3176
94. Sicoli G, Wachowius F, Bennati M, Hobartner C (2010) Probing secondary structures of spin-labeled RNA by pulsed EPR spectroscopy. Angew Chem Int Ed Engl 49(36):6443–6447
95. Büttner L, Seikowski J, Wawrzyniak K, Ochmann A, Höbartner C (2013) Synthesis of spin-labeled riboswitch RNAs using convertible nucleosides and DNA-catalyzed RNA ligation. Bioorg Med Chem 21(20):6171–6180
96. Duh JL, Bobst AM (1991) Sequence-specific spin labeling of oligothymidylates by phosphotriester chemistry. Helv Chim Acta 74(4):739–747
97. Strobel OK, Kryak DD, Bobst EV, Bobst AM (1991) Preparation and characterization of spin-labeled oligonucleotides for DNA hybridization. Bioconjug Chem 2(2):89–95

98. Spaltenstein A, Robinson BH, Hopkins PB (1988) A rigid and nonperturbing probe for duplex DNA motion. J Am Chem Soc 110(4):1299–1301
99. Fischhaber PL, Reese AW, Nguyen T, Kirchner JJ, Hustedt EJ, Robinson BH, Hopkins PB (1997) Synthesis of duplex DNA containing a spin labeled analog of 2′-deoxycytidine. Nucleos Nucleot 16(4):365–377
100. Schiemann O, Piton N, Mu YG, Stock G, Engels JW, Prisner TF (2004) A PELDOR-based nanometer distance ruler for oligonucleotides. J Am Chem Soc 126(18):5722–5729
101. Schiemann O, Piton N, Plackmeyer J, Bode BE, Prisner TF, Engels JW (2007) Spin labeling of oligonucleotides with the nitroxide TPA and use of PELDOR, a pulse EPR method, to measure intramolecular distances. Nat Protoc 2(4):904–923
102. Gannett PM, Darian E, Powell J, Johnson EM 2nd, Mundoma C, Greenbaum NL, Ramsey CM, Dalal NS, Budil DE (2002) Probing triplex formation by EPR spectroscopy using a newly synthesized spin label for oligonucleotides. Nucleic Acids Res 30(23):5328–5337
103. Singh V, Azarkh M, Exner TE, Hartig JS, Drescher M (2009) Human telomeric quadruplex conformations studied by pulsed EPR. Angew Chem Int Ed Engl 48(51):9728–9730
104. Gophane DB, Sigurdsson ST (2013) Hydrogen-bonding controlled rigidity of an isoindoline-derived nitroxide spin label for nucleic acids. Chem Commun 49(10):999–1001
105. Flaender M, Sicoli G, Aci-Seche S, Reignier T, Maurel V, Saint-Pierre C, Boulard Y, Gambarelli S, Gasparutto D (2011) A triple spin-labeling strategy coupled with DEER analysis to detect DNA modifications and enzymatic repair. ChemBioChem 12(17):2560–2563
106. Babaylova ES, Ivanov AV, Malygin AA, Vorobjeva MA, Venyaminova AG, Polienko YF, Kirilyuk IA, Krumkacheva OA, Fedin MV, Karpova GG, Bagryanskaya EG (2014) A versatile approach for site-directed spin labeling and structural EPR studies of RNAs. Org Biomol Chem 12(19):3129–3136
107. Hara H, Horiuchi T, Saneyosh M, Nishimur S (1970) 4-Thiouridine-specific spin-labeling of E-Coli transfer RNA. Biochem Biophys Res Commun 38(2):305–311
108. Sprinzl M, Kramer E, Stehlik D (1974) Structure of phenylalanine transfer-RNA from yeast—spin-label studies. Eur J Biochem 49(3):595–605
109. McIntosh AR, Caron M, Dugas H (1973) Specific spin labeling of anticodon of Escherichia-Coli transfer-RNA Glu. Biochem Biophys Res Commun 55(4):1356–1363
110. Rublack N, Nguyen H, Appel B, Springstubbe D, Strohbach D, Muller S (2011) Synthesis of specifically modified oligonucleotides for application in structural and functional analysis of RNA. J Nucleic Acids 2011:805253
111. Qin PZ, Feigon J, Hubbell WL (2005) Site-directed spin labeling studies reveal solution conformational changes in a GAAA tetraloop receptor upon Mg^{2+} -dependent docking of a GAAA tetraloop. J Mol Biol 351(1):1–8
112. Qin PZ, Iseri J, Oki A (2006) A model system for investigating lineshape/structure correlations in RNA site-directed spin labeling. Biochem Biophys Res Commun 343(1):117–124
113. Wunnicke D, Strohbach D, Weigand JE, Appel B, Feresin E, Suess B, Muller S, Steinhoff HJ (2011) Ligand-induced conformational capture of a synthetic tetracycline riboswitch revealed by pulse EPR. RNA 17(1):182–188
114. Okamoto A, Taiji T, Tainaka K, Saito I (2002) Oligonucleotides containing 7-vinyl-7-deazaguanine as a facile strategy for expanding the functional diversity of DNA. Bioorg Med Chem Lett 12(15):1895–1896
115. Belikova A, Zarytova V, Grineva N (1967) Synthesis of ribonucleosides and diribonucleoside phosphates containing 2-chloro-ethylamine and nitrogen mustard residues. Tetrahedron Lett 8(37):3557–3562
116. Lebars I, Vileno B, Bourbigot S, Turek P, Wolff P, Kieffer B (2014) A fully enzymatic method for site-directed spin labeling of long RNA. Nucleic Acids Res 42(15):e117
117. Miller TR, Alley SC, Reese AW, Solomon MS, Mccallister WV, Mailer C, Robinson BH, Hopkins PB (1995) A probe for sequence-dependent nucleic-acid dynamics. J Am Chem Soc 117(36):9377–9378

118. Miller TR, Hopkins PB (1994) Toward the synthesis of a 2nd-generation nitroxide spin-probe for DNA dynamics studies. Bioorg Med Chem Lett 4(8):981–986
119. Edwards TE, Okonogi TM, Sigurdsson ST (2002) Investigation of RNA-protein and RNA-metal ion interactions by electron paramagnetic resonance spectroscopy. The HIV TAR-Tat motif. Chem Biol 9(6):699–706
120. Okonogi T, Reese AW, Alley SC, Hopkins PB, Robinson BH (1999) Flexibility of duplex DNA on the submicrosecond timescale. Biophys J 77(6):3256–3276
121. Okonogi TM, Alley SC, Reese AW, Hopkins PB, Robinson BH (2000) Sequence-dependent dynamics in duplex DNA. Biophys J 78(5):2560–2571
122. Edwards TE, Cekan P, Reginsson GW, Shelke SA, Ferre-D'Amare AR, Schiemann O, Sigurdsson ST (2011) Crystal structure of a DNA containing the planar, phenoxazine-derived bi-functional spectroscopic probe Ç. Nucleic Acids Res 39(10):4419–4426
123. Marko A, Margraf D, Cekan P, Sigurdsson ST, Schiemann O, Prisner TF (2010) Analytical method to determine the orientation of rigid spin labels in DNA. Phys Rev E 81(2): 21911–21919
124. Cekan P, Sigurdsson ST (2012) Conformation and dynamics of nucleotides in bulges and symmetric internal loops in duplex DNA studied by EPR and fluorescence spectroscopies. Biochem Biophys Res Commun 420(3):656–661
125. Cekan P, Sigurdsson ST (2008) Single base interrogation by a fluorescent nucleotide: each of the four DNA bases identified by fluorescence spectroscopy. Chem Commun 29:3393–3395
126. Gardarsson H, Kale AS, Sigurdsson ST (2011) Structure–function relationships of phenoxazine nucleosides for identification of mismatches in duplex DNA by fluorescence spectroscopy. ChemBioChem 12(4):567–575
127. Gardarsson H, Sigurdsson ST (2010) Large flanking sequence effects in single nucleotide mismatch detection using fluorescent nucleoside $Ç^{f}$. Bioorg Med Chem 18(16):6121–6126
128. Cekan P, Jonsson EO, Sigurdsson ST (2009) Folding of the cocaine aptamer studied by EPR and fluorescence spectroscopies using the bifunctional spectroscopic probe Ç. Nucleic Acids Res 37(12):3990–3995
129. Höbartner C, Sicoli G, Wachowius F, Gophane DB, Sigurdsson ST (2012) Synthesis and characterization of RNA containing a rigid and nonperturbing cytidine-derived spin label. J Org Chem 77(17):7749–7754
130. Tkach I, Pornsuwan S, Höbartner C, Wachowius F, Sigurdsson ST, Baranova TY, Diederichsen U, Sicoli G, Bennati M (2013) Orientation selection in distance measurements between nitroxide spin labels at 94 GHz EPR with variable dual frequency irradiation. Phys Chem Chem Phys 15(10):3433–3437
131. Edwards TE, Sigurdsson ST (2002) Electron paramagnetic resonance dynamic signatures of TAR RNA-small molecule complexes provide insight into RNA structure and recognition. Biochemistry 41(50):14843–14847
132. Edwards TE, Sigurdsson ST (2005) EPR spectroscopic analysis of U7 hammerhead ribozyme dynamics during metal ion induced folding. Biochemistry 44(38):12870–12878
133. Kim NK, Bowman MK, DeRose VJ (2010) Precise mapping of RNA tertiary structure via nanometer distance measurements with double electron-electron resonance spectroscopy. J Am Chem Soc 132(26):8882–8884
134. Kim NK, Murali A, DeRose VJ (2005) Separate metal requirements for loop interactions and catalysis in the extended hammerhead ribozyme. J Am Chem Soc 127(41):14134–14135
135. Schiemann O, Weber A, Edwards TE, Prisner TF, Sigurdsson ST (2003) Nanometer distance measurements on RNA using PELDOR. J Am Chem Soc 125(12):3434–3435
136. Ward R, Keeble DJ, El-Mkami H, Norman DG (2007) Distance determination in heterogeneous DNA model systems by pulsed EPR. ChemBioChem 8(16):1957–1964
137. Flaender M, Sicoli G, Fontecave T, Mathis G, Saint-Pierre C, Boulard Y, Gambarelli S, Gasparutto D (2008) Site-specific insertion of nitroxide-spin labels into DNA probes by click chemistry for structural analyses by ELDOR spectroscopy. Nucleic Acids Symp Ser (Oxf) 52:147–148

138. Murakami A, Mukae M, Nagahara S, Konishi Y, Ide H, Makino K (1993) Oligonucleotides site-specifically spin-labeled at 5′-terminal or internucleotide linkage and their use in gene analyses. Free Radic Res Commun 19(Suppl 1):S117–S128
139. Kunjir NC, Reginsson GW, Schiemann O, Sigurdsson ST (2013) Measurements of short distances between trityl spin labels with CW EPR, DQC and PELDOR. Phys Chem Chem Phys 15(45):19673–19685
140. Bobko AA, Dhimitruka I, Zweier JL, Khramtsov VV (2007) Trityl radicals as persistent dual function pH and oxygen probes for in vivo electron paramagnetic resonance spectroscopy and imaging: concept and experiment. J Am Chem Soc 129(23):7240–7241
141. Owenius R, Eaton GR, Eaton SS (2005) Frequency (250MHz to 9.2 GHz) and viscosity dependence of electron spin relaxation of triarylmethyl radicals at room temperature. J Magn Reson 172(1):168–175
142. Caron M, Dugas H (1976) Specific spin-labeling of transfer ribonucleic acid molecules. Nucleic Acids Res 3(1):19–34
143. Pscheidt RH, Wells BD (1986) Different conformations of the 3′ termini of initiator and elongator transfer ribonucleic acids an EPR study. J Biol Chem 261(16):7253–7256
144. Luoma GA, Herring FG, Marshall AG (1982) Flexibility of end-labeled polymers from electron-spin resonance line-shape analysis—3′ terminus of transfer ribonucleic-acid and 5s ribonucleic-acid. Biochemistry 21(25):6591–6598
145. Grant GPG, Popova A, Qin PZ (2008) Diastereomer characterizations of nitroxide-labeled nucleic acids. Biochem Biophys Res Commun 371(3):451–455
146. Popova AM, Qin PZ (2010) A nucleotide-independent nitroxide probe reports on site-specific stereomeric environment in DNA. Biophys J 99(7):2180–2189
147. Gish G, Eckstein F (1988) DNA and RNA sequence determination based on phosphorothioate chemistry. Science 240(4858):1520–1522
148. Makino K, Murakami A, Nagahara S, Nakatsuji Y, Takeuchi T (1989) A study on spin-labeled oligonucleotide synthesis and its electron-spin resonance behavior in solution. Free Radic Res Commun 6(5):311–316
149. Burgers PMJ, Eckstein F (1979) Diastereomers of 5′-O-adenosyl 3′-O-uridyl phosphorothioate—chemical synthesis and enzymatic properties. Biochemistry 18(4):592–596
150. Fidanza JA, Mclaughlin LW (1989) Introduction of reporter groups at specific sites in DNA containing phosphorothioate diesters. J Am Chem Soc 111(25):9117–9119
151. Qin PZ, Butcher SE, Feigon J, Hubbell WL (2001) Quantitative analysis of the isolated GAAA tetraloop/receptor interaction in solution: a site-directed spin labeling study. Biochemistry 40(23):6929–6936
152. Esquiaqui JM, Sherman EM, Ionescu SA, Ye J-D, Fanucci GE (2014) Characterizing the dynamics of the leader–linker interaction in the glycine riboswitch with site-directed spin labeling. Biochemistry 53(22):3526–3528
153. Popova AM, Kalai T, Hideg K, Qin PZ (2009) Site-specific DNA structural and dynamic features revealed by nucleotide-independent nitroxide probes. Biochemistry 48(36): 8540–8550
154. Zhang X, Tung CS, Sowa GZ, Hatmal MM, Haworth IS, Qin PZ (2012) Global structure of a three-way junction in a phi29 packaging RNA dimer determined using site-directed spin labeling. J Am Chem Soc 134(5):2644–2652
155. Zhang X, Dantas Machado AC, Ding Y, Chen Y, Lu Y, Duan Y, Tham KW, Chen L, Rohs R, Qin PZ (2014) Conformations of p53 response elements in solution deduced using site-directed spin labeling and Monte Carlo sampling. Nucleic Acids Res 42(4):2789–2797
156. Grant GPG, Boyd N, Herschlag D, Qin PZ (2009) Motions of the substrate recognition duplex in a group I intron assessed by site-directed spin labeling. J Am Chem Soc 131(9):3136–3137
157. Ding Y, Zhang X, Tham KW, Qin PZ (2014) Experimental mapping of DNA duplex shape enabled by global lineshape analyses of a nucleotide-independent nitroxide probe. Nucleic Acids Res 42(18):e140

158. Nguyen PH, Popova AM, Hideg K, Qin PZ (2015) A nucleotide-independent cyclic nitroxide label for monitoring segmental motions in nucleic acids. BMC Biophys 8(1):6
159. Fleissner MR, Bridges MD, Brooks EK, Cascio D, Kalai T, Hideg K, Hubbell WL (2011) Structure and dynamics of a conformationally constrained nitroxide side chain and applications in EPR spectroscopy. Proc Natl Acad Sci U S A 108(39):16241–16246
160. Rayes RF, Kalai T, Hideg K, Geeves MA, Fajer PG (2011) Dynamics of tropomyosin in muscle fibers as monitored by saturation transfer EPR of bi-functional probe. PLoS One 6(6): e21277
161. Kuznetsov NA, Milov AD, Koval VV, Samoilova RI, Grishin YA, Knorre DG, Tsvetkov YD, Fedorova OS, Dzuba SA (2009) PELDOR study of conformations of double-spin-labeled single- and double-stranded DNA with non-nucleotide inserts. Phys Chem Chem Phys 11(31):6826–6832
162. Wunderlich CH, Huber RG, Spitzer R, Liedl KR, Kloiber K, Kreutz C (2013) A novel paramagnetic relaxation enhancement tag for nucleic acids: a tool to study structure and dynamics of RNA. ACS Chem Biol 8(12):2697–2706
163. Grant GP, Qin PZ (2007) A facile method for attaching nitroxide spin labels at the 5′ terminus of nucleic acids. Nucleic Acids Res 35(10):e77
164. Belmont P, Chapelle C, Demeunynck M, Michon J, Michon P, Lhomme J (1998) Introduction of a nitroxide group on position 2 of 9-phenoxyacridine: easy access to spin labelled DNA-binding conjugates. Bioorg Med Chem Lett 8(6):669–674
165. Thomas F, Michon J, Lhomme J (1999) Interaction of a spin-labeled adenine-acridine conjugate with a DNA duplex containing an abasic site model. Biochemistry 38(6): 1930–1937
166. Atsumi H, Maekawa K, Nakazawa S, Shiomi D, Sato K, Kitagawa M, Takui T, Nakatani K (2010) Noncovalent assembly of TEMPO radicals pair-wise embedded on a DNA duplex. Chem Lett 39(6):556–557
167. Atsumi H, Maekawa K, Nakazawa S, Shiomi D, Sato K, Kitagawa M, Takui T, Nakatani K (2012) Tandem arrays of TEMPO and nitronyl nitroxide radicals with designed arrangements on DNA. Chem Eur J 18(1):178–183
168. Atsumi H, Nakazawa S, Dohno C, Sato K, Takui T, Nakatani K (2013) Ligand-induced electron spin-assembly on a DNA tile. Chem Commun 49(57):6370–6372
169. Maekawa K, Nakazawa S, Atsumi H, Shiomi D, Sato K, Kitagawa M, Takui T, Nakatani K (2010) Programmed assembly of organic radicals on DNA. Chem Commun 46(8):1247–1249
170. Shelke SA, Sigurdsson ST (2010) Noncovalent and site-directed spin labeling of nucleic acids. Angew Chem Int Ed Engl 49(43):7984–7986
171. Shelke SA, Sigurdsson ST (2012) Structural changes of an abasic site in duplex DNA affect noncovalent binding of the spin label ç. Nucleic Acids Res 40(8):3732–3740
172. Shelke SA, Sigurdsson ST (2012) Effect of N3 modifications on the affinity of spin label ç for abasic sites in duplex DNA. ChemBioChem 13(5):684–690
173. Shelke SA, Sandholt GB, Sigurdsson ST (2014) Nitroxide-labeled pyrimidines for non-covalent spin-labeling of abasic sites in DNA and RNA duplexes. Org Biomol Chem 12(37):7366–7374
174. Chalmers BA, Saha S, Nguyen T, McMurtrie J, Sigurdsson ST, Bottle SE, Masters K-S (2014) TMIO-PyrImid hybrids are profluorescent, site-directed spin labels for nucleic acids. Org Lett 16(21):5528–5531
175. Duss O, Yulikov M, Allain FH-T, Jeschke G (2015) Combining NMR and EPR to determine structures of large RNAs and protein–RNA complexes in solution. Methods Enzymol 558: 279–331

Chapter 9
Non-covalent Modification of Double-Stranded DNA at the Mismatch and Bulged Site

Chikara Dohno and Kazuhiko Nakatani

Abstract Advances in synthetic chemistry of DNA allow us to create DNAs with chemical modifications that endow unnatural properties and functions. There is another way for chemical modification: non-covalent modification with DNA-binding molecule. Instead of the covalently introduced functionalities, DNA is modified by non-covalent binding of small molecules bearing desired functionalities. We have developed synthetic ligands that selectively bind to mismatched base pair and unpaired bulge in double-stranded DNA, which is requisite for delivering the functions at a particular location of DNA. This chapter describes the non-covalent modification of target DNA by our mismatch- and bulge-binding ligands bearing various functionalities.

9.1 Introduction

The advances of chemistry on oligonucleotide synthesis enable us the unconscious use of oligonucleotides in daily experiments as they are just one of common chemicals in the laboratory. We simply order the natural DNAs and even chemically modified DNAs by sending e-mail to the oligo houses and will have them within a reasonable time frame, just like we order the synthetic reagents. We chemists, however, know that without invention of oligonucleotide synthesis on solid support, human genome sequencing could not be achieved because thousands of PCR primers used in human genome sequencing were supplied by this method. In addition, recent advanced studies on the role of functional RNAs draw significant attention on large-scale synthesis of DNA and RNA as antisense oligonucleotides and short interfering RNA. We could get more than one gram of oligonucleotides in hand by standard solid phase phosphoramidite synthesis. The almost entire this book dedicated to the recent achievements on oligonucleotide synthesis and the use in solving and/or investigating real biological issues.

C. Dohno • K. Nakatani (✉)
The Institute of Scientific and Industrial Research, Osaka University, 8-1 Mihoga-oka, Ibaraki 567-0047, Japan
e-mail: nakatani@sanken.osaka-u.ac.jp

K. Nakatani, Y. Tor (eds.), *Modified Nucleic Acids*, Nucleic Acids and Molecular Biology 31, DOI 10.1007/978-3-319-27111-8_9

There is a totally different way for chemical modification of nucleic acids, and that is a non-covalent modification using small molecules binding to nucleic acids. A number of molecules have been reported to bind to nucleic acids by electrostatic interaction, groove binding, and intercalation [1–3]. The use of these molecules as non-covalent modifying agents for nucleic acids, however, was not seriously investigated until the development of sequence-specific DNA binders. After 20 years of their continued efforts, Dervan and his colleagues successfully developed pyrrole–imidazole (Py–Im) polyamides with a recognition rule for the minor-groove floor of Watson–Crick base pairs in double-stranded DNA [1]. Concurrently, Sugiyama and his colleagues also continued their studies on minor-groove binders, eventually to reach the Py–Im polyamides [2]. The sequence specificity of Py–Im polyamides is exceptionally high and reaches to the level of competing with the transcription factors [4, 5]. The success of Py–Im polyamides is due to the high discrimination ability of the hydrogen-bonding surface in the minor groove of target double-stranded DNA (dsDNA) sequence from others in enormous numbers of nontarget dsDNA.

Another example of non-covalent modification of nucleic acids can be found for the binding to the telomere sequence [6–8]. Telomere is the repeated DNA sequence existed at the end of chromosomes. For humans, the repeat sequence would be 5′-TTAGGG-3′. The extreme end of telomere is a single strand form, which allows folding telomere region into guanine quadruplex structure. In the case of human telomere, three G-quadruplexes were stacked with each other to form a stable structure. Because G-quadruplex is different in terms of the groove structure, shape, and π-stacking surface, small molecules specifically binding to G-quadruplex but not to B-from duplex have been reported. TMPyP4 is one of the representative molecules binding to G-quadruplex, whereas telomestatin was a natural product isolated from *Streptomyces anulatus* [9]. Those molecules have much larger binding π-surface than those binding to B-form duplex DNA by intercalation.

We have focused our attention on the recognition of mismatched and bulged bases in double-stranded DNA [10]. Unlike distamycins, netropsins which are the parent molecules leading to Py–Im polyamides recognizing the hydrogen-bonding surface in the floor of the minor groove, there were no particular precedents of molecules binding to mismatched bases except mismatch repair proteins. Mismatched bases are quite different from Watson–Crick base pairs in terms of hydrogen-bonded structure, shape, and most importantly the dynamic motion. Because mismatched base pairs are less firmly hydrogen bonded, the structure near the mismatched base pair is more feasible to the binding to small molecules. We have developed for the first time to recognize guanine–guanine and adenine–adenine mismatches flanked by two C–G base pairs (Fig. 9.1) [10]. The very first mismatch-binding ligands (MBLs) were designed for a single G–G mismatch base pair. Later it became clear that MBL recognized not only the mismatched G but also flanking matched C–G base pairs as an unexpected bonus.

MBL typically consists of two base-recognizing aromatic heterocycles connected with a flexible linker having secondary amino group (Fig. 9.1). The

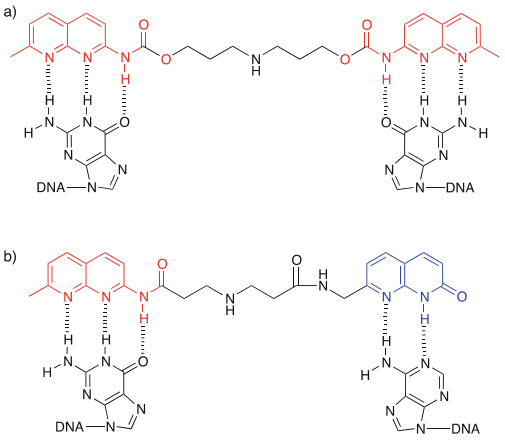

Fig. 9.1 Structure of mismatch-binding ligands (MBLs). (**a**) NCD and (**b**) NA. Acylamino-naphthyridine moiety shown in *red* recognizes guanine by three hydrogen bonds, whereas azaquinolone shown in *blue* recognizes adenine by two hydrogen bonds

linker arranges the heterocycles in appropriate positions for base recognition, and the amino group is favorable for interaction with anionic phosphate groups and sufficient solubility in water. A key base-recognition element is *N*-acyl-2-amino-1,8-naphthyridine that recognizes guanine by forming three hydrogen bonds identical to those in G–C base pair (Fig. 9.1a) [11, 12]. Thus, dimeric naphthyridine derivatives (NCD) selectively binds to G–G mismatch base pair in DNA, where two acylamino-naphthyridine moieties recognize two guanines in the mismatch by the complementary hydrogen bonding and favorable stacking interactions (Fig. 9.1a) [13, 14]. NCD particularly favors G–G mismatch flanked by C–G matched base pairs. NCD apparently recognizes the base triplets, d(CGG)/d(CGG) sequence. The similar situation was observed for naphthyridine–azaquinolone (NA, Fig. 9.1b), which was originally designed for recognition of a G–A mismatch [15]. NA indeed bound to the G–A mismatch but bound to an A–A mismatch flanked by C–G base pairs, d(CAG)/d(CAG), with much higher affinity. Origin of the unexpected selectivity was fully understood by solving structure of NA–d(CAG)/d(CAG) complex [15]. NMR solution structure verified that two NA molecules are involved in the complex (Fig. 9.2a, b), where the azaquinolone moiety recognizes an adenine in the middle A–A mismatch, and the acylamino-naphthyridine recognizes a flanking guanine. Surprisingly, cytosines that originally paired with the guanines are flipped out from the helix. NCD recognizes d(CGG)/d(CGG) sequence in the same fashion as NA (Fig. 9.2c) [16]. The unique binding mode enables the MBLs to recognize the base triplet containing a mismatch base pair.

Having developed a selective DNA binder for base triplet containing a mismatch, we have pursued the studies on non-covalent modification of DNA using the MBLs. The DNA that is going to be non-covalently modified by MBL requires a mismatch-containing base triplet in the sequence, like d(CGG)/d(CGG) and d(CAG)/d(CAG). Most part of DNA in both biological and artificial system do not include mismatch base pair, which allow us to add unnatural functions and properties specifically into the target mismatch sequence. It should be noted that MBL does not necessarily deliver the function to all target DNA. Unlike covalently

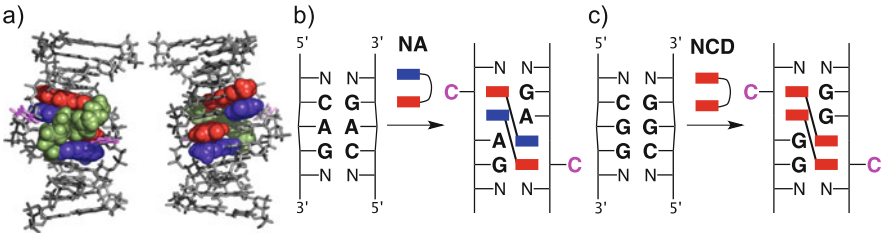

Fig. 9.2 (**a**) NMR solution structure of NA–d(CAG)/d(CAG) complex. Views from major (*left*) and minor grooves (*right*). (**b**) Schematic illustration of the NA–d(CAG)/d(CAG) complex. Naphthyridine and azaquinolone moieties are shown as *red* and *blue rectangles*, respectively. Cytosines shown in *magenta color* are flipped out. (**c**) Schematic illustration of the NCD–d(CGG)/d(CGG) complex

modified DNA, the non-covalent modification is reversible, and MBL-binding equilibrium determines the modification efficiency. The binding of MBL results in various outcomes for the target DNA depending on the MBL used. In the following section, we go into specific examples in detail of the non-covalent modification of DNA.

9.2 Enhanced Duplex Stability by MBL

Spontaneous hybridization between complementary DNA strands is a unique property essential for DNA's biological functions and a wide variety of biotechnology applications. DNA hybridization proceeds in a sequence selective manner. Hybridization with the mismatch sequence is highly unfavorable because of the thermodynamic instability of mismatch base pairs in duplex DNA. On the other hand, the larger number of matched base pairs and higher GC contents makes DNA duplex more thermodynamically stable. The feasibility and stability of DNA hybridization are determined by the sequence contexts of each DNA strands. It is useful to control duplex stability, or DNA hybridization, by external factors without changing sequence context.

DNA-binding molecules increase thermodynamic stability of DNA duplex. It has been known that classical DNA intercalators like ethidium bromide and minor-groove binder Py–Im polyamides increased the melting temperature (T_m) of DNA duplex depending on their chemical structures [17, 18]. Binding of MBL to its target sequence increases the duplex stability as well, but with additional distinctive features. First, MBL binds selectively to the target mismatch sequence and therefore stabilizes the duplex containing the target sequence. Hybridizations of other DNA sequences are not affected by the presence of MBL. Second, the MBL binding enhances the duplex stability more significantly than typical DNA binders do. The target sequence of MBL contains at least one mismatch base pair that makes DNA hybridization unfavorable. By converting the unstable mismatch-containing duplex

into the stable MBL–dsDNA complex, MBL attains drastic enhancement of duplex stability. Figure 9.2 shows how MBL recognizes and stabilizes the hybridization state of mismatch-containing sequence. NCD is a MBL for GG mismatch and consists of two acylamino-naphthyridine moieties that recognize a guanine base by a formation of three hydrogen bonds (Fig. 9.1a), affording to a pseudo complementary base pair. Two NCD molecules are consistently involved in the binding to a d(CGG)/d(CGG) (Fig. 9.2c). Upon binding of NCD, one G–G mismatch and two franking G–C base pairs in d(CGG)/d(CGG) are converted into four acylamino-naphthyridine–G base pairs, resulting in a stable complex.

It is also noteworthy that two cytosines in the complex are flipped out and, therefore, are not primarily responsible for the stability of the complex [16]. Changing the cytosine to the other bases (N), i.e., d(NGG)/d(NGG), provides a consecutive mismatch site (Fig. 9.3a). T_m of d(NGG)/d(NGG) should be much lower than that of d(CGG)/d(CGG). In contrast, T_m of complex between d(NGG)/d(NGG) and NCD should not be very different from the complex of d(CGG)/d(CGG) because supposed interactions are identical in both complexes. Consequently, drastic T_m enhancement is observed upon binding to NCD, where three mismatch base pairs (G–G mismatch franking with two G–N mismatch) are converted into four acylamino-naphthyridine–G base pairs (Fig. 9.3a).

In a particular case where two single-stranded DNAs (ssDNAs) do not spontaneously hybridize each other, NCD binding can induce transformation from the two ssDNAs to corresponding dsDNA by the stable complex formation (Fig. 9.3a), which is represented by large T_m enhancement. Figure 9.3b shows thermal melting profiles of 11-mer DNA having a d(TGG)/d(TGG) sequence that involves three contiguous mismatches (one G–G and two G–T mismatches) [19]. Clear melting transition of the DNA was not observed due to the contiguous mismatches ($T_m < 10$ °C), indicating that the DNAs exist exclusively as ssDNAs at ambient temperature. Addition of NCD increases the T_m (58.8 °C), which is sufficiently high

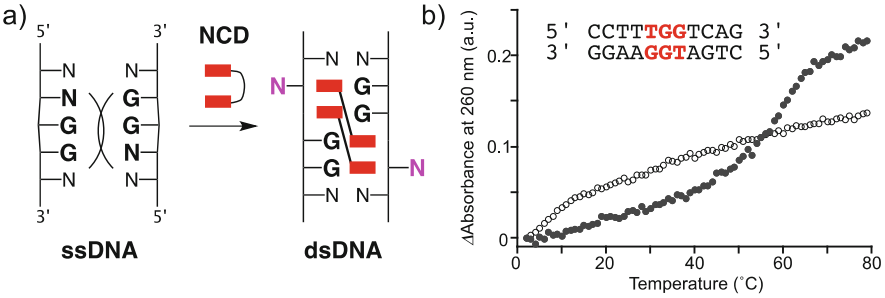

Fig. 9.3 MBL-binding induced DNA hybridization (**a**) DNA containing d(NGG)/d(NGG) (N = A, G, or T) does not spontaneously hybridize due to the presence of contiguous mismatches. The binding of NCD stabilizes the duplex by the formation of the stable NCD–d(NGG)/d(NGG) complex, resulting in hybridization of the DNA. Two Ns are flipped out in the complex and therefore do not have strong influence on the complex stability. (**b**) Thermal melting profiles of d(TGG)/d(TGG) containing DNA in the absence (*open circle*) and presence of NCD (*filled circle*)

for two ssDNAs to hybridize spontaneously under isothermal condition. Here, NCD functions as "molecular glue" for DNA that sticks the two ssDNAs together [19, 20].

9.3 DNA Nanostructure Assembly Triggered by MBL

9.3.1 Ligand-Inducible Nanostructure Formation

A number of DNAs with appropriately designed sequences can self-assemble into predetermined nanoscale objects. Recent development of DNA nanotechnologies enable us to create a variety of nanostructures with virtually any shapes [21–26]. MBL can be a building component for construction of the DNA nanostructures. DNA tetrahedron is one of the simplest 3D DNA nanostructure and has been used as a well-defined nanoscale scaffold [27]. We created a MBL-inducible DNA tetrahedron that requires MBL as the key component for complete formation of the tetrahedral structure [28].

The NCD-inducible DNA tetrahedron is made of five short DNAs (T1–T5), which were designed to produce a tetrahedral structure if all five strands are completely assembled (Fig. 9.4a) [28]. The key feature is that one of six edges in the tetrahedral structure has three d(CGG)/d(CGG) mismatch sites. In the absence of NCD, the DNA tetrahedron is at an immature state where one of the edges is not formed because the introduced mismatch sites prevent hybridization between T3 and T5 (Fig. 9.4a, tetrahedron precursor). NCD can be a last piece of the DNA tetrahedron. NCD binds to the d(CGG)/d(CGG) in the immature DNA tetrahedron and brings the unhybridized regions together to make a complete DNA tetrahedron (Fig. 9.4a, right). The NCD-induced tetrahedron formation was confirmed by AFM analysis. In the absence of NCD, planar structures with constant height of about 2 nm were observed (Fig. 9.4b), indicating formation of the tetrahedron precursor shown in Fig. 9.4a that is a flat DNA assembly with thickness corresponding to the diameter of a single dsDNA. The flat structures were almost disappeared upon addition of NCD, but instead many spots with 5.3 nm heights were observed (Fig. 9.4c), which is close to the expected height of the tetrahedron (5.6 nm). NCD is the last and key component for full construction of the three-dimensional DNA nanostructure.

9.3.2 Orderly Assembly of Electron Spin on a DNA Tile

MBL is a useful molecular tool to place an additional functionality at precise location on DNA nanostructures [29–31]. DNA nanostructures are constructed by multiple hybridization events between complementary sequences, where no

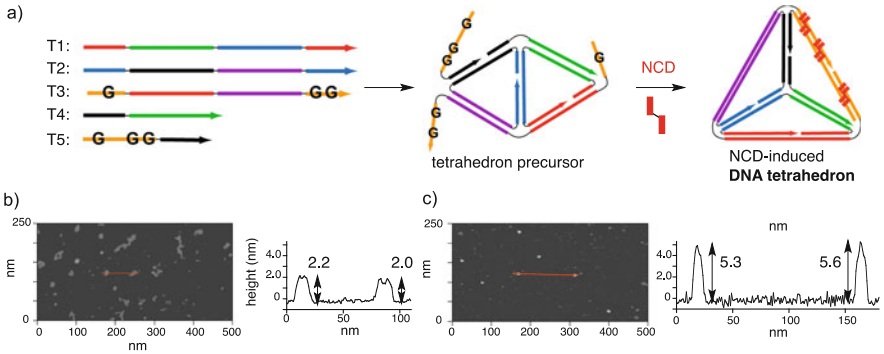

Fig. 9.4 MBL induces formation of DNA tetrahedron. (**a**) Schematic illustration of self-assembly of five ssDNAs (T1–T5) into DNA tetrahedron. In the absence of NCD, the self-assembly is incomplete because multiple GG-mismatch sites (shown as "G") prevent hybridizations between T3 and T5. Binding of NCD induces the tetrahedron formation. (**b**, **c**) AFM analysis for the tetrahedron formation. (**b**) AFM image of the five ssDNAs (T1–T5) in the absence of NCD. (**c**) AFM image of the five ssDNAs in the presence of NCD. Line-cross section analyses of the images are shown below the images

mismatch base pairs were involved. When mismatch sites are introduced into DNA nanostructures, MBL can localize at the specific position on the DNA nanostructures. In the case of the NCD-inducible tetrahedron in Fig. 9.4, six NCD molecules ideally accumulate on one edge of the DNA tetrahedron. If MBL is conjugated with a certain functionality, the MBL not only induces nanostructure formation but also delivers additional functionality on it. We have designed MBLs bearing an electron spin [31–34]. NCD-TEMPO consists of a NCD moiety covalently connected with a stable organic radical 2,2,6,6-tetramethylpiperidine *N*-oxide (TEMPO) (Fig. 9.5a). NCD-TEMPO selectively binds to a d(CGG)/d(CGG) sequence as parent NCD does and can deliver electron spins at specific locations where d(CGG)/d(CGG) sequences exist in DNA nanostructures.

We adopted a DNA tile on which NCD-TEMPO are periodically aligned (Fig. 9.5). DNA tiles are 2D-DNA nanostructures composed of two DNA tiles (DNA tiles A and B) that assemble alternately to provide a periodic and planar tiling lattice (Fig. 9.5b, c) [31]. DNA tile B has a single-stranded tail extruded from the planar surface. Another component is a helper single-stranded DNA C1, whose sequence are designed to have two d(CGG)/d(CGG) sequences when it hybridizes to the single-stranded tail on the tile B. The two ssDNAs do not hybridize spontaneously, but they can hybridize each other only when NCD-TEMPO is present (Fig. 9.5d). The MBL-induced hybridization produces a rigid duplex on the DNA tile and therefore changes surface structure of the tiling lattice. The change of nanostructured surface indicates that NCD-TEMPO induces the hybridization, and electron spins are assembled at the designated location on the DNA tile.

AFM measurements were conducted to see change of DNA nanostructure by the MBL-induced hybridization. AFM images were taken for DNA tiles A, B, and

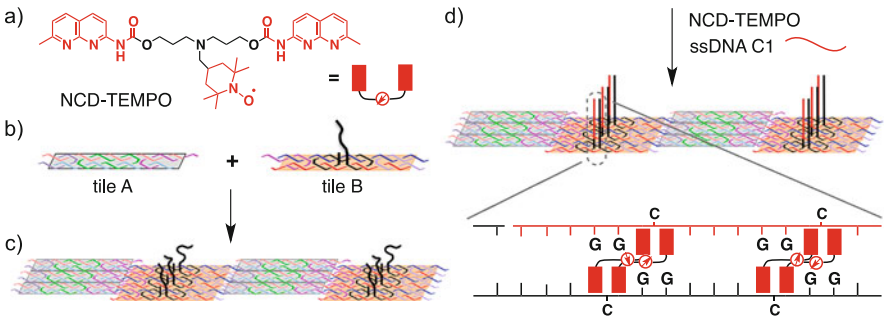

Fig. 9.5 MBL delivers electron spins on DNA tiling lattice concomitant with surface pattern changes. (**a**) Structure of NCD-TEMPO. (**b**–**d**) Schematic illustration of surface pattern change induced by NCD-TEMPO. The DNA tile is formed by self-assembly of tile A and B. The tile B has a single-stranded tail that can hybridize with a helper stand C1 (shown as a *red bar*) only in the presence of NCD-TEMPO. NCD-TEMPO-induced hybridization produces a stripe pattern with 32.6 nm periodicity on the DNA tile. The appearance of the stripe pattern indicated the assembly of electron spins on the DNA tile

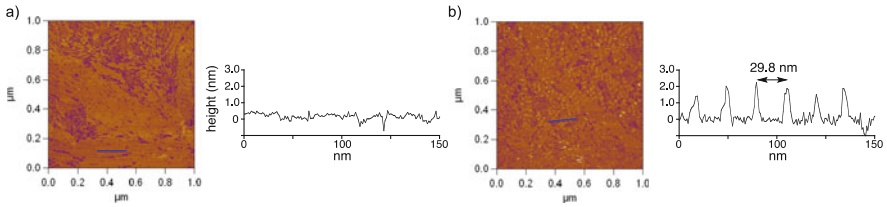

Fig. 9.6 AFM images of the DNA tile. (**a**) DNA tile (A + B) in the presence of helper ssDNA C1. (**b**) DNA tile (A + B) in the presence of ssDNA C1 and NCD-TEMPO. Line-cross section analysis along a *blue line* in each images are shown below

ssDNA C1 in the presence and absence of NCD-TEMPO (Fig. 9.6). In the absence of NCD-TEMPO, planar objects with constant height of 2 nm were observed on mica surface, indicating formation of DNA tiling lattice (Fig. 9.6a). The absence of any periodic pattern on the DNA tile indicated that ssDNA C1 did not hybridize to the single-stranded tails on DNA tile B. In the presence of NCD-TEMPO, a stripe pattern was appeared on the DNA tile (Fig. 9.6b). The stripe has a constant interval of 30 nm that are in good agreement with the distance between the single-stranded tails on assembled tile B (32.6 nm). Binding of NCD-TEMPO induced hybridization between ssDNA C1 and the single-stranded tails on tile B, and the resulting duplex extruded from the tiling lattice produced the periodic stripe. The change of nanostructured surface indicated successful assembly of electron spins on the 2D-DNA tiling lattice. We have developed a series of MBLs that have different target sequences and are conjugated with different types of electron spins. DNA is a good scaffold for placing multiple types of electron spins with well-defined

distance and orientation. Detailed review on spin labeling of DNA is given by Sigurdsson et al. in Chap. 8 [35–38].

9.4 Switching Optical Properties of Fluorescent DNA

Functional DNA that possesses fluorescent properties is one of the most studied chemically modified nucleic acids. Some of the representative fluorescent DNAs are extensively reviewed in the other chapters. Häner et al. has developed fluorescent DNAs that have non-nucleosidic chromophores as surrogates for base pairs [39]. The chromophores assemble within DNA, and the fluorescence property is sensitive to the helical structure and surrounding environments. By combination of the fluorescent DNA with MBL, we constructed a DNA-based optical switching device, where MBL functions as a one-time trigger or reversible switch for changing the optical output [40].

The chemically modified DNA, py–mis, is a light-emitting component that exhibits two distinct color emissions, blue and green, depending on the hybridization states (Fig. 9.7a, b) [39, 40]. The py–mis has a pyrene unit as a fluorophore in the middle of the sequence. In the single-stranded state, the pyrene derivative in py–mis exhibits blue fluorescence. When py–mis hybridizes to produce dsDNA, two pyrene units can interact by interstrand stacking, resulting in green fluorescence attributed to fluorescence from pyrene excimer. Because the py–mis contains two d(CGG)/d(CGG) mismatch sites that prevent py–mis from spontaneous hybridization, it emits blue fluorescence at 430 nm under ambient condition. NCD that functions as a molecular glue for DNA can be a switch of the emitting component [19, 20]. Fluorescence spectra of py–mis were markedly changed upon addition of NCD (Fig. 9.7c). The monomer fluorescence was decreased with increased concentration of NCD, while the green fluorescence at 520 nm was becoming dominant. Binding of NCD to the mismatch sites stabilized the double-stranded states of py–mis, where the pyrene units exhibit excimer fluorescence, resulting in change of optical output from blue to green.

NCD is a molecular switch for the optical output from the DNA-based system. The function of NCD is unidirectional because NCD can induce DNA hybridization but cannot induce dehybridization of duplex once formed [19, 41]. Asanuma et al. reported reversible control of DNA hybridization with chemically modified DNA containing photochromic azobenzene units [42]. In order to install reversible switching ability into NCD, we have developed NCD derivatives containing a photoresponsive unit, which allow us to control DNA hybridization reversibly by external light stimuli [20, 43]. The photoresponsive NCD, namely NCDA, consists of parent NCD molecule integrated with a photochromic azobenzene linker (Fig. 9.8a) [43–45]. The nitrogen–nitrogen double bond in azobenzene unit is in either *Z* or *E* configurations, which is interconvertible by irradiation of UV and visible light. *E*-NCDA is isomerized into *Z*-isomer by 360 nm light, while *Z*-NCDA is isomerized into *E*-isomer by 430 nm light. Another key feature is that *E*- and *Z*-

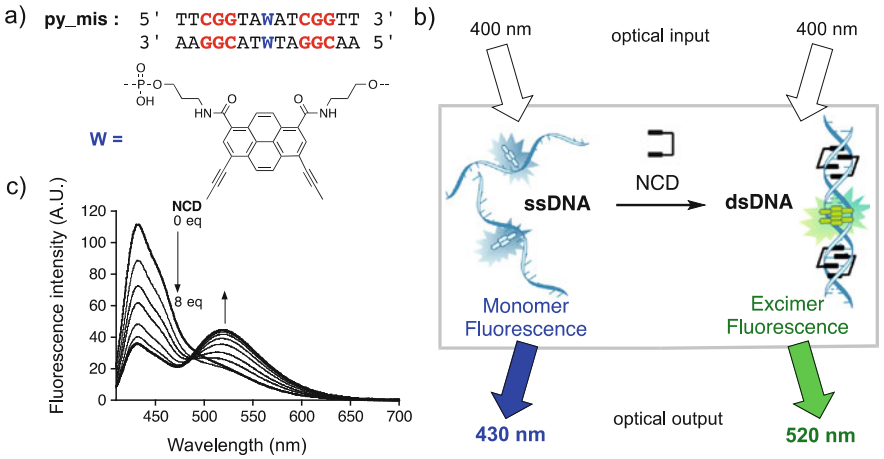

Fig. 9.7 NCD-induced unidirectional fluorescence change using the pyrene-modified fluorescent DNA. (**a**) Sequence of the DNA containing fluorescence base pair surrogate. (**b**) Schematic illustration of the NCD-induced fluorescence change in the DNA-based system. NCD changes optical output from *blue* (430 nm) to *green* (520 nm). Binding of NCD to the fluorescent DNA induces the hybridization, resulting in change of emission species from monomer to excimer. (**c**) Emission spectra of the fluorescent DNA with increasing concentration of NCD

NCDA have different abilities on stabilization of the target duplex containing a d (CGG)/d(CGG) sequence. The *Z*-NCDA induces the DNA hybridization with much higher extent than *E*-NCDA does (Fig. 9.8b). This is most likely because the folded structure of *Z*-NCDA is favorable for the binding to d(CGG)/d(CGG), while the rigid and extended nature of *E*-isomer is not. Thermal melting curve for 15 mer DNA containing two d(CGG)/d(CGG) sites showed large T_m difference between before and after 360 nm photoirradiation (Fig. 9.8c) [43]. Before photoirradiation, NCDA exists almost solely as *E*-isomer (>95 %), and the melting curve showed no clear transition because of the multiple mismatch sites. The *Z*-NCDA produced by the 360 nm photoirradiation gave apparently high T_m value ($T_m = 53$ °C). Subsequent irradiation at 430 nm again reduced the T_m value to the original level by returning to *E*-NCDA. NCDA functions as a photoswitchable molecular glue for DNA that controls the DNA hybridization containing d(CGG)/d(CGG) sequence reversibly by external light stimuli under isothermal condition.

The photoswitchable molecular glue allows a reversible light-driven switching of fluorescence from the fluorescent DNA py–mis. Here NCDA, instead of parent NCD, was used in otherwise the same system in Fig. 9.9a [40]. Fluorescence spectra of the supramolecular system were measured after iterative irradiation at 360 and 430 nm light (Fig. 9.9b). Before photoirradiation, where *E*-NCDA is predominant in the system, blue fluorescence with emission maximum at 430 nm was observed. Photoirradiation with 360 nm light increased green emission at 520 nm with concomitant decrease of the blue emission. The photoirradiation induced the isomerization from *E* to *Z*-NCDA, and the in situ generated *Z*-NCDA had the

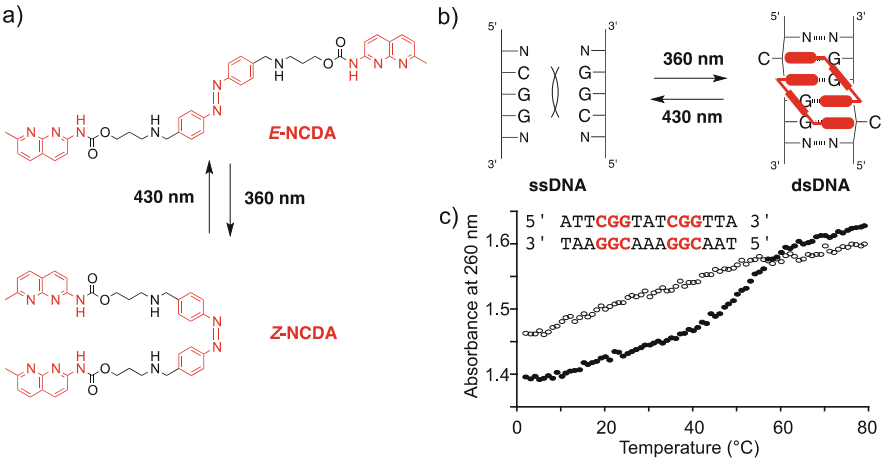

Fig. 9.8 (**a**) Structure of photoresponsive MBL, NCDA. NCDA undergoes reversible photoisomerization between *E* and *Z*-configuration. (**b**) NCDA functions as a photoswitchable molecular glue for DNA. *Z*-NCDA binds to d(CGG)/d(CGG) sequence and stabilizes the double-stranded states, while *E*-NCDA binds to the sequence much less efficiently. Two states are interchangeable by photoirradiation. (**c**) Thermal melting profiles of d(CGG)/d(CGG)-containing DNA in the presence of NCDA. Plots for the sample before photoirradiation (*open circle*) and after 360 nm photoirradiation (*filled circle*) are shown

same effect to the molecule glue NCD (Fig. 9.7). Subsequent irradiation at 430 nm completely reproduced the blue emission. By the *Z* to *E* photoisomerization, NCDA lost the ability to stabilize the hybridization of py–mis. The switching was repeatable at least five times of iterative irradiation of 360 and 430 nm (Fig. 9.9b, inset).

The supramolecular switch is operated solely by external light stimuli of different wavelengths (360 and 430 nm) that switch the optical output from blue to green emissions, and vice versa. This system is workable under isothermal condition, with no need to add chemical energy, and without accumulation of waste by-products during repeating cycles. The binding and dissociation of NCDA drives the supramolecular system consisting of the functionalized DNA assembly. NCDA is applicable for other DNA assemblies into which NCDA-binding sites, d(XGG)/d(XGG) sequence, are properly introduced. The photoswitchable molecular glue is useful to control a variety of biological and artificial events where DNA hybridization plays a key role.

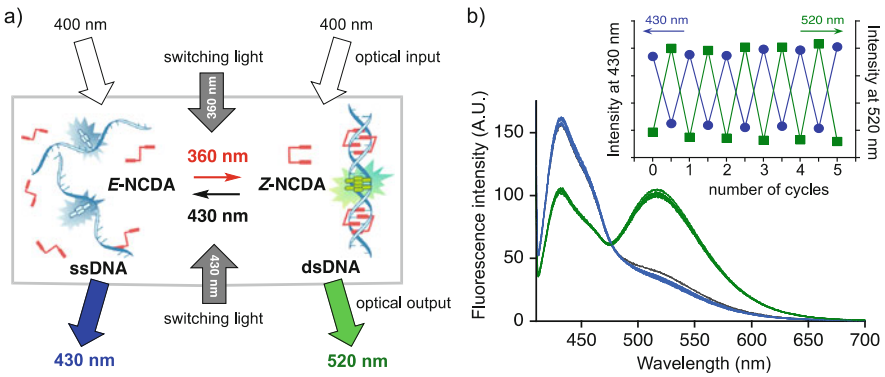

Fig. 9.9 Reversible switching of the fluorescence emissions by photoswitchable molecular glue. (**a**) Schematic illustration of the fluorescent supramolecular system. NCDA controls the hybridization of the fluorescent DNA in response to the irradiation of external light stimuli (switching lights at 360 and 430 nm), resulting in reversible control of optical output between *blue* (430 nm) and *green* (520 nm). (**b**) Emission spectra of the fluorescent DNA with iterative irradiation of two switching lights at 360 and 430 nm. The irradiation cycle was repeated for five times. Changes of fluorescence intensities at 430 and 520 nm after each cycle are also shown

9.5 Binding to Cytosine Bulge and Application to Monitor PCR Progress

9.5.1 Monitoring PCR Progress by C-Bulge-Binding Ligand (DANP)

Our mismatch-binding studies in fact started by the design of molecules binding to the bulged nucleotide [10, 11]. The bulge nucleotide has no counterpart in the duplex to form Watson–Crick base pair, thus leaving the hydrogen-bonding surface of the nucleotide largely unoccupied. We anticipated that the bulge-binding ligands can form hydrogen bonds to the bulged nucleotide and stacked by the base pairs flanking the bulged site to form a stable ligand–DNA complex. The first demonstration of recognition of the bulged nucleotide was reported for the guanine bulge with *N*-aminoacyl-2-amino-7-methyl-1,8-naphthyridine (cf. Fig. 9.1a) [11], which is a monomer of naphthyridine dimer and naphthyridine carbamate dimer as we described earlier as a binding molecule to the guanine–guanine mismatch. As an extension of the concept of bulge recognition, we discovered that *N*,*N*′-bis (3-aminopropyl)-2,7-diamino-1,8-naphthyridine (DANP) (Fig. 9.10a, b), which selectively and strongly binds to the C-bulges in duplex DNA as the protonated form $DANPH^+$ at a neutral pH to form an exclusive 1:1 stoichiometry [46]. The characteristic of DNAP is the absorption change upon binding to the C-bulge DNA. Absorption maximum of $DANPH^+$ shifts by 30 nm to a longer wavelength from that of the unbound state. Thus, the C-bulge–DANP complex can be selectively excited at 400 nm. Emission from the complex is also 30 nm longer than that of unbound

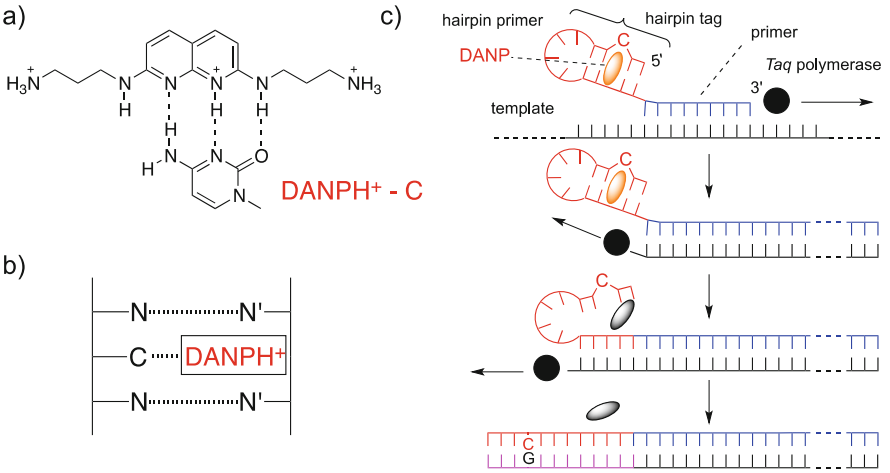

Fig. 9.10 Hydrogen-bonded structure of (**a**) protonated DANP to cytosine and (**b**) image in double-stranded DNA. (**c**) Illustration of hairpin primer PCR

DANP. With a combination of selective excitation of the DANP-bound complex and choice of appropriate wavelength for detecting the emission, the bound complex can be monitored even in the presence of excess amount of free unbound DNAP. The characteristic absorption and fluorescence properties of DANP upon binding to C-bulge DNA prompted us to use DANP for the non-covalent labeling of PCR primer in the real-time monitoring of PCR progress [47, 48].

PCR is one of the most fundamental technologies in molecular biology studies and enables the quantitative determination of the amount of nucleic acids in a sample and to identify SNPs by allele-specific PCR [49, 50]. The major challenge involved in monitoring PCR progress using fluorescently labeled primers is to translate the PCR progress into any changes occurring in the properties of fluorescent chromophores. We have addressed this issue by coupling the structural change on a hairpin DNA tag attached at the 5′ end of the primer with the fluorescence emission of a ligand selectively bound to the hairpin form. The hairpin structure containing the C-bulge site is attached at the 5′ end of the primer (Fig. 9.10c) [47]. As the PCR proceeds, the hairpin structure will be dissolved and be transformed into a duplex, resulting in the loss of the DANP-binding site and a decrease in the fluorescence at 430 nm. Our previous studies on the DANP binding and the emission from the complex suggest that C-bulge flanking two A–T base pairs (A_A/TCT) is the choice of the sequence in terms of the binding affinity of DANP and the intensity in emission spectra [46, 47]. The fluorescence profile of hairpin primer PCR as a function of the number of PCR cycles correlated very well to the PAGE analysis of amplicons, and was a mirror image of that obtained by real-time PCR using SYBR® Green as a reporting dye of amplicons, indicating that HP-PCR successfully reported the PCR progress.

9.5.2 *Monitoring PCR Progress by Covalent-Attached DANP*

One drawback of the hairpin primer PCR is that the fluorescent signal decreases with progress of PCR. We attempt to improve the hairpin primer PCR from detection of a decreasing signal to one of an increasing signal. During these studies, we noticed that the DANP emission spectra are sensitively modulated by the base pairs flanking the C-bulge. The A–T base pairs directly neighboring the C-bulge induce the emission shift toward a longer wavelength, whereas the G–C flanking base pairs effectively quench the DANP fluorescence. The affinity of DANP binding to the C-bulge flanking A–T base pairs was about 1 μM in K_d, and affinity to the fully complementary double-stranded DNA was very weak. With these information, we designed DANP-modified thymidine, where DANP was covalently anchored at the methyl group of thymine (Fig. 9.11a) and incorporated into the 5′-***T***_G-3′/5′-ACC-3′ sequence, where ***T*** is the site of DANP anchoring [51]. We hypothesized that the fluorescence of DANP would be effectively quenched when DANP bound to the C-bulge by the neighboring G–C base pair, but not when DANP was released from the C-bulge and dangling on the outside of the duplex (Fig. 9.11b). Accordingly, the increase of DANP fluorescence could be observed upon structural changes induced by the polymerase reaction from the hairpin form holding the C-bulge to a fully complementary double-stranded form.

The absorption maximum of the DANP-anchored duplexes was observed at 399 nm for 5′-***T***G-3′/3′-ACC-5′ holding the C-bulge, whereas it was observed at 377 nm for the fully matched 5′-***T***G-3′/3′-AC-5′ (Fig. 9.11c). The bathochromic shift by 22 nm suggested that the DANP anchored at the T in the 5′-***T***_G-3′/3′-ACC-5′ bound to the flanking C-bulge. As anticipated from the absorption spectra, the fluorescence change was more significant for 5′-***T***G-3′/3′-ACC-5′. Thus, the fluorescence intensity increased by fourfold due to the change from the C-bulge duplex 5′-***T***G-3′/3′-ACC-5′ to the fully matched duplex 5′-***T***G-3′/3′-AC-5′ (Fig. 9.11d), whereas only a 2.5-fold increase was observed for the change from the C-bulge duplex 5′-G_***T***-3′/3′-CCA-5′ to the fully matched duplex 5′-G***T***-3′/3′-CA-5′. This difference is due to the more pronounced fluorescence quenching

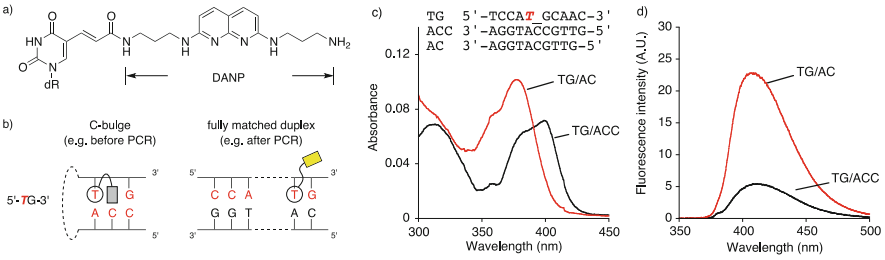

Fig. 9.11 (**a**) Structure of DANP anchored at the C5 of thymine. (**b**) Illustration of expected structures of DNAP anchored at the hairpin tag in C-bulge form (*left*, before PCR) and duplex form (*right*, after PCR). (**c**) UV and (**d**) fluorescence spectra of DANP-anchored DNA. Spectra of TG/AC and TG/ACC are shown in *red* and *black*, respectively

in the 5′-***T***_G-3′/3′-ACC-5′, also suggesting that the DANP was bound to the C-bulge. The setup of PCR experiments using the DANP-anchored primer is illustrated in Fig. 9.12a. One of the PCR primers was labeled with a hairpin tag embedded to the C-bulge and the DANP-anchored T in the 5′-***T***_G-3′/3′-ACC-5′ sequence (M13RV tag). PCR was performed with the plasmid pUC18 as a template using the M13RV-tag primer and a non-labeled M13M3 primer. The PCR products were analyzed using native polyacrylamide gel electrophoresis (PAGE) (Fig. 9.12b). The PCR product was obtained as a single band with a length of approximately 125 bp. Sequencing analysis of the PCR products revealed that adenine was incorporated opposite to the DANP-anchored T, indicating that the anchored DANP neither interfered with the DNA polymerase nor altered the nucleotide base to be incorporated during the polymerase reaction. The fluorescence intensity of the PCR solution started to increase after ten PCR cycles under the conditions using 50 pM of the template and reached a plateau after 35 cycles (Fig. 9.12c). The PCR product appeared on the PAGE gel at 15 cycles (cf. Fig. 9.12b), demonstrating consistency in the observations regarding the product formation by PAGE and fluorescence increase. With different template concentrations, the fluorescence intensity of the PCR solutions showed different threshold cycle numbers at a fluorescence intensity of 400 arbitrary units (A.U.) (Fig. 9.12d). An almost linear relationship was found between the logarithm of initial DNA

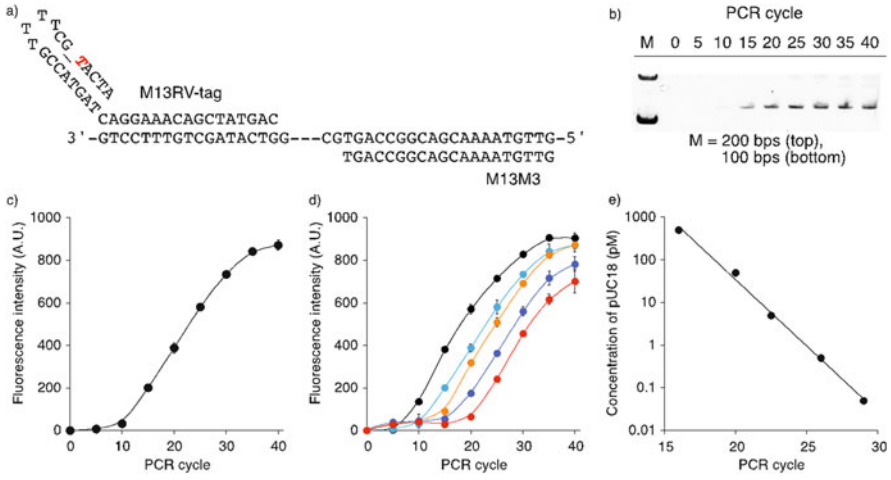

Fig. 9.12 Hairpin primer PCR with a DANP-anchored primer. (**a**) Alignment of primers on the pUC18 template. Only one template strand is shown for clarity. (**b**) PAGE analysis of PCR products. M: size marker, *top*: 200 bp, *bottom*: 100 bp. (**c**) Fluorescence intensity of PCR solutions obtained from primers M13M3 and M13RV tag using 50 pM concentrations of pUC18. The excitation wavelength was 355 nm. (**d**) Fluorescence intensity of PCR solutions obtained with primers M13M3 and M13RV tag under different concentrations of pUC18. Key: (*black*) 500 pM, (*light blue*) 50 pM, (*orange*) 5 pM, (*blue*) 0.5 pM, and (*red*) 0.05 pM. (**e**) The standard plot obtained from (**d**) at 400 A.U. as a threshold cycle number. The vertical axis is the initial DNA concentration (logarithmic) and the horizontal axis is the PCR cycle number

concentrations and the PCR cycle number (Fig. 9.12e). These results clearly showed that hairpin primer PCR with the DANP-anchored primer could be used for quantitative real-time analysis of template concentration. In separate experiments, the results of DANP-anchored hairpin primer PCR were found to be consistent with those obtained with TaqMan® probes. In addition, allele-specific PCR with the DANP-anchored hairpin primer clearly showed the discrimination of two alleles.

9.6 Conclusion

Non-covalent modification of oligonucleotides with the small molecules has broad potential not only to label the oligonucleotides with signaling functional groups but also to attribute the stability of the nano-structures of DNA and to switch the structures and functions. The scope and limitation of non-covalent labeling of nucleic acids at this moment is virtually unexplored. To achieve the specific labeling of the target DNA and DNA structures, the high sequence specificity is the important factors. In this chapter, we demonstrated the potential of mismatch-binding ligands. The bulge-binding molecule, DANP, is not a sequence-specific ligand, because DANP binds not only C-bulge but also T-bulge DNA. However, we could design the hairpin primer containing C-bulge and use it for the monitoring of the PCR progress. This is because we could design the sequence for the specific ligand, DANP, in this case. Thus, it is important for non-covalent modification of DNA to have a defined pair of small molecule and its binding DNA structure. In this regard, a small molecule–aptamer pair would be one of possible combination for the non-covalent modification of nucleic acids. For example, since a number of ligand binding to G-quadruplex has been reported, we could label DNA by a G-quadruplex forming sequence, of which presence could be detected by a binding of small molecules specifically binding to the G-quadruplex structures. These applications would significantly expand the possibility of small molecules binding to specific nucleic acid structures.

References

1. Dervan PB (2001) Molecular recognition of DNA by small molecules. Bioorg Med Chem 9:2215–2235
2. Sugiyama H, Bando T (2006) Synthesis and biological properties of sequence-specific DNA-alkylating pyrrole-imidazole polyamides. Acc Chem Res 39:935–944
3. Tse WC, Boger DL (2004) Sequence-selective DNA recognition: natural products and nature's lessons. Chem Biol 11:1607–1617
4. Mapp AK, Ansari AZ, Ptashne M, Dervan PB (2000) Activation of gene expression by small molecule transcription factors. Proc Natl Acad Sci USA 97:3930–3935

5. Kwonj Y, Arndt HD, Qian M, Choi Y, Kawazoe Y, Dervan PB, Uesugi M (2004) Small molecule transcription factor mimic. J Am Chem Soc 126:15940–15941
6. Ilyinsky NS, Varizhuk AM, Beniaminov AD, Puzanov MA, Shchyolkina AK, Kaluzhny DN (2014) G-quadruplex ligands: mechanisms of anticancer action and target binding. Mol Biol 48:778–794
7. Balasubramanian S, Hurley LH, Neidle S (2011) Targeting G-quadruplexes in gene promoters: a novel anticancer strategy? Nat Rev Drug Discov 10:261–275
8. Georgiades SN, Abd Karim NH, Suntharalingam K, Vilar R (2010) Interaction of metal complexes with G-quadruplex DNA. Angew Chem Int Ed Engl 49:4020–4034
9. Shin-Ya K, Wierzba K, Matsuo K, Ohtani T, Yamada Y, Furihata K, Hayakawa Y, Seto H (2001) Telomestatin, a novel telomerase inhibitor from Streptomyces anulatus. J Am Chem Soc 123:1262–1263
10. Nakatani K (2009) Recognition of mismatched base pairs in DNA. Bull Chem Soc Jpn 82:1055–1069
11. Nakatani K, Sando S, Saito I (2000) Recognition of a single guanine bulge by 2-acylamino-1,8-naphthyridine. J Am Chem Soc 122:2172–2177
12. Murray TJ, Zimmerman SC (1995) 7-amido-1,8-naphthyridines as hydrogen-bonding units for the complexation of guanine derivatives—the role of 2-alkoxyl groups in decreasing binding-affinity. Tetrahedron Lett 36:7627–7630
13. Nakatani K, Sando S, Saito I (2001) Scanning of guanine-guanine mismatches in DNA by synthetic ligands using surface plasmon resonance. Nat Biotechnol 19:51–55
14. Peng T, Murase T, Goto Y, Kobori A, Nakatani K (2005) A new ligand binding to G-G mismatch having improved thermal and alkaline stability. Bioorg Med Chem Lett 15:259–262
15. Nakatani K, Hagihara S, Goto Y, Kobori A, Hagihara M, Hayashi G, Kyo M, Nomura M, Mishima M, Kojima C (2005) Small-molecule ligand induces nucleotide flipping in (CAG)(n) trinucleotide repeats. Nat Chem Biol 1:39–43
16. Peng T, Nakatani K (2005) Binding of naphthyridine carbamate dimer to the (CGG)(n) repeat results in the disruption of the G-C base pairing. Angew Chem Int Ed Engl 44:7280–7283
17. Wilson WD, Ratmeyer L, Zhao M, Strekowski L, Boykin D (1993) The search for structure-specific nucleic-acid interactive drugs—effects of compound structure on Rna versus DNA interaction strength. Biochemistry 32:4098–4104
18. Pilch DS, Poklar N, Gelfand CA, Law SM, Breslauer KJ, Baird EE, Dervan PB (1996) Binding of a hairpin polyamide in the minor groove of DNA: sequence-specific enthalpic discrimination. Proc Natl Acad Sci USA 93:8306–8311
19. Peng T, Dohno C, Nakatani K (2006) Mismatch-binding ligands function as a molecular glue for DNA. Angew Chem Int Ed Engl 45:5623–5626
20. Dohno C, Nakatani K (2011) Control of DNA hybridization by photoswitchable molecular glue. Chem Soc Rev 40:5718–5729
21. Winfree E, Liu FR, Wenzler LA, Seeman NC (1998) Design and self-assembly of two-dimensional DNA crystals. Nature 394:539–544
22. Rothemund PWK (2006) Folding DNA to create nanoscale shapes and patterns. Nature 440:297–302
23. Endo M, Sugiyama H (2009) Chemical approaches to DNA nanotechnology. ChemBioChem 10:2420–2443
24. Zhang F, Nangreave J, Liu Y, Yan H (2014) Structural DNA nanotechnology: state of the art and future perspective. J Am Chem Soc 136:11198–11211
25. Linko V, Dietz H (2013) The enabled state of DNA nanotechnology. Curr Opin Biotechnol 24:555–561
26. Jones MR, Seeman NC, Mirkin CA (2015) Nanomaterials. Programmable materials and the nature of the DNA bond. Science 347:1260901
27. Goodman RP, Schaap IAT, Tardin CF, Erben CM, Berry RM, Schmidt CF, Turberfield AJ (2005) Rapid chiral assembly of rigid DNA building blocks for molecular nanofabrication. Science 310:1661–1665

28. Dohno C, Atsumi H, Nakatani K (2011) Ligand inducible assembly of a DNA tetrahedron. Chem Commun 47:3499–3501
29. Cohen JD, Sadowski JP, Dervan PB (2007) Addressing single molecules on DNA nanostructures. Angew Chem Int Ed Engl 46:7956–7959
30. Cohen JD, Sadowski JP, Dervan PB (2008) Programming multiple protein patterns on a single DNA nanostructure. J Am Chem Soc 130:402
31. Atsumi H, Nakazawa S, Dohno C, Sato K, Takui T, Nakatani K (2013) Ligand-induced electron spin-assembly on a DNA tile. Chem Commun 49:6370–6372
32. Atsumi H, Maekawa K, Nakazawa S, Shiomi D, Sato K, Kitagawa M, Takui T, Nakatani K (2010) Noncovalent assembly of TEMPO radicals pair-wise embedded on a DNA duplex. Chem Lett 39:556–557
33. Maekawa K, Nakazawa S, Atsumi H, Shiomi D, Sato K, Kitagawa M, Takui T, Nakatani K (2010) Programmed assembly of organic radicals on DNA. Chem Commun 46:1247–1249
34. Atsumi H, Maekawa K, Nakazawa S, Shiomi D, Sato K, Kitagawa M, Takui T, Nakatani K (2012) Tandem arrays of TEMPO and nitronyl nitroxide radicals with designed arrangements on DNA. Chem Eur J 18:178–183
35. Miller TR, Alley SC, Reese AW, Solomon MS, Mccallister WV, Mailer C, Robinson BH, Hopkins PB (1995) A probe for sequence-dependent nucleic-acid dynamics. J Am Chem Soc 117:9377–9378
36. Barhate N, Cekan P, Massey AP, Sigurdsson ST (2007) A nucleoside that contains a rigid nitroxide spin label: a fluorophore in disguise. Angew Chem Int Ed Engl 46:2655–2658
37. Cekan P, Smith AL, Barhate N, Robinson BH, Sigurdsson ST (2008) Rigid spin-labeled nucleoside C: a nonperturbing EPR probe of nucleic acid conformation. Nucleic Acids Res 36:5946–5954
38. Shelke SA, Sigurdsson ST (2010) Noncovalent and site-directed spin labeling of nucleic acids. Angew Chem Int Ed Engl 49:7984–7986
39. Langenegger SM, Häner R (2004) Excimer formation by interstrand stacked pyrenes. Chem Commun 2792–2793
40. Uno S, Dohno C, Bittermann H, Malinovskii VL, Häner R, Nakatani K (2009) A light-driven supramolecular optical switch. Angew Chem Int Ed Engl 48:7362–7365
41. Peng T, Dohno C, Nakatani K (2007) Bidirectional control of gold nanoparticle assembly by turning on and off DNA hybridization with thermally degradable molecular glue. ChemBioChem 8:483–485
42. Asanuma H, Ito T, Yoshida T, Liang XG, Komiyama M (1999) Photoregulation of the formation and dissociation of a DNA duplex by using the cis-trans isomerization of azobenzene. Angew Chem Int Ed Engl 38:2393–2395
43. Dohno C, Uno SN, Nakatani K (2007) Photoswitchable molecular glue for DNA. J Am Chem Soc 129:11898–11899
44. Dohno C, Uno SN, Sakai S, Oku M, Nakatani K (2009) The effect of linker length on binding affinity of a photoswitchable molecular glue for DNA. Bioorg Med Chem 17:2536–2543
45. Dohno C, Yamamoto T, Nakatani K (2009) Photoswitchable unsymmetrical ligand for DNA hetero-mismatches. Eur J Org Chem 4051–4058
46. Suda H, Kobori A, Zhang JH, Hayashi G, Nakatani K (2005) N, N′-Bis(3-aminopropyl)-2,7-diamino-1,8-naphthyridine stabilized a single pyrimidine bulge in duplex DNA. Bioorg Med Chem 13:4507–4512
47. Takei F, Igarashi M, Hagihara M, Oka Y, Soya Y, Nakatani K (2009) Secondary-structure-inducible ligand fluorescence coupled with PCR. Angew Chem Int Ed Engl 48:7822–7824
48. Takei F, Nakatani K (2013) The chemistry of PCR primers: concept and application. Isr J Chem 53:401–416
49. Erlich HA, Gelfand D, Sninsky JJ (1991) Recent advances in the polymerase chain-reaction. Science 252:1643–1651

50. Papp AC, Pinsonneault JK, Cooke G, Sadee W (2003) Single nucleotide polymorphism genotyping using allele-specific PCR and fluorescence melting curves. Biotechniques 34:1068–1072
51. Takei F, Chen X, Yu G, Shibata T, Dohno C, Nakatani K (2014) Cytosine-bulge-dependent fluorescence quenching for the real-time hairpin primer PCR. Chem Commun 50:15195–15198

Chapter 10
2′,4′-Bridged Nucleic Acids for Targeting Double-Stranded DNA

Yoshiyuki Hari and Satoshi Obika

Abstract The sequence-specific formation of triplex DNA structures comprised of double-stranded DNA (dsDNA) and an oligonucleotide, known as a triplex-forming oligonucleotide (TFO), can be widely used in the molecular biology and biochemistry fields. However, current methods have not reached a practical level of applicability because of inherent problems in natural triplex formation, including low stability and the limitations of targetable sequence. Overcoming these issues could provide for the stable and selective targeting of an arbitrary region of dsDNA by TFOs. The various approaches attempted to date include the use of 2′,4′-bridged nucleic acids to restrict the sugar conformation to C3′-*endo* via an extra bridge structure between the 2′- and 4′-positions, which showed interesting results and promising potential towards overcoming these problems. For example, the use of the 2′,4′-bridge modification in TFOs can significantly increase their ability to form triplex structures with targeted dsDNA. Thus, the combination of 2′,4′-bridge modifications and nonnatural nucleobases may have the potential to overcome this limitation of targetable sequences.

10.1 Introduction

The discovery of a 2:1 complex of polyU and polyA in 1957 initiated research involving triplex DNA technology [1, 2]. Triplex nucleic acid formation between double-stranded DNA (dsDNA) and a single-stranded oligonucleotide has attracted significant attention due to the potential applicability of genomic DNA-targeting technologies.

Triplex-forming oligonucleotides (TFOs) insert into the major groove of dsDNA to form hydrogen bonds with one strand of dsDNA, thus yielding either a parallel or

Y. Hari
Faculty of Pharmaceutical Sciences, Tokushima Bunri University, Nishihama, Yamashiro-cho, Tokushima 770-8514, Japan
e-mail: hari@ph.bunri-u.ac.jp

S. Obika (✉)
Graduate School of Pharmaceutical Sciences, Osaka University, 1-6 Yamadaoka, Suita, Osaka 565-0871, Japan
e-mail: obika@phs.osaka-u.ac.jp

K. Nakatani, Y. Tor (eds.), *Modified Nucleic Acids*, Nucleic Acids and Molecular Biology 31, DOI 10.1007/978-3-319-27111-8_10

antiparallel motif triplex. In the parallel motiftriplex, the orientation of TFO is identical to that of the target strand of dsDNA, with the T and C (protonated C; $C^{+}H$) nucleotides within the TFO generally recognizing AT and GC base pairs, respectively, in the dsDNA through Hoogsteen hydrogen bonds (Fig. 10.1a). On the other hand, TFOs in the antiparallel triplex adopt a reverse orientation from that of the target strand, with A (or T) and G forming reverse-Hoogsteen hydrogen bonds with AT and GC base pairs, respectively (Fig. 10.1b). As shown in Fig. 10.1a and b, both motifs limit the number of hydrogen bonds in a GC base pair to two, as compared to the three hydrogen bonds that form in a duplex structure; therefore, the stability of triple-helical DNA structures is significantly weaker than that of duplexed molecules.

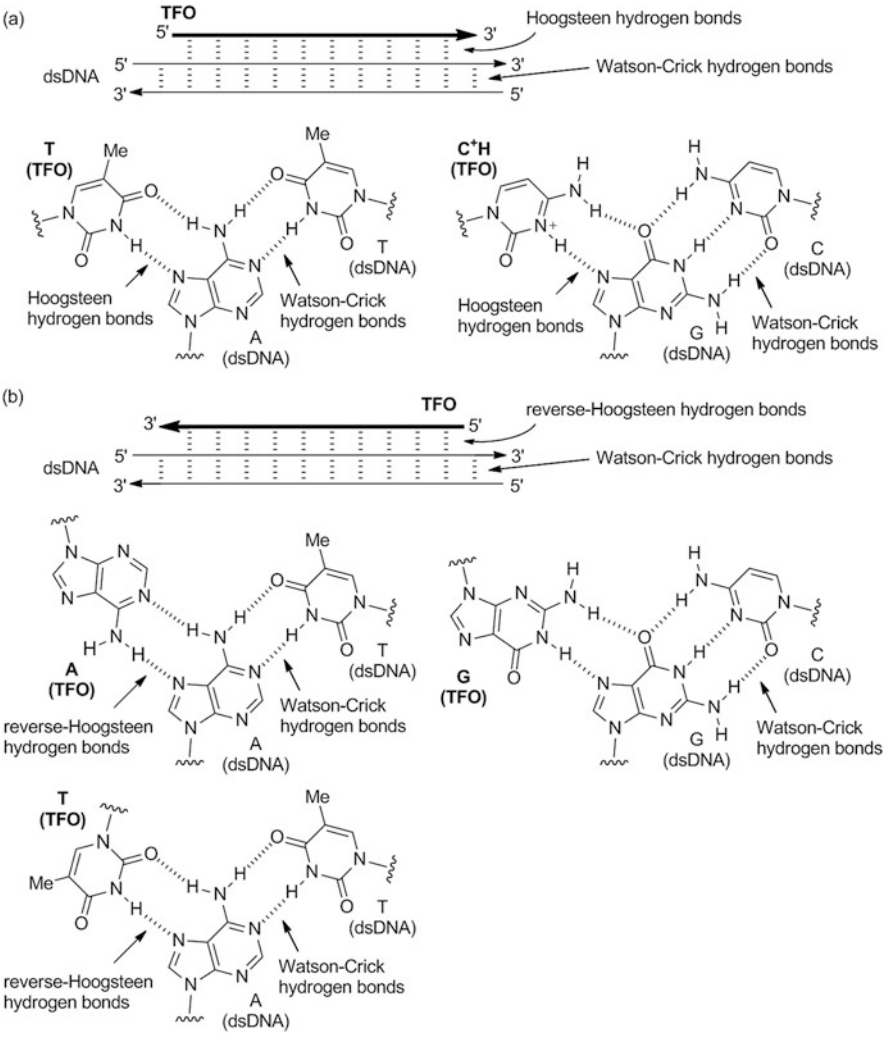

Fig. 10.1 Patterns of base triplets in triplex nucleic acids formed with dsDNA and TFO: a parallel motif triplex (**a**) and an antiparallel motif triplex (**b**)

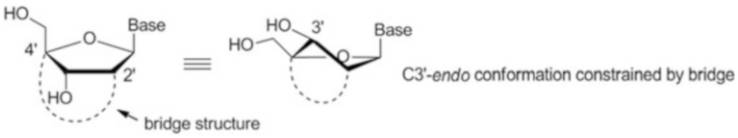

Fig. 10.2 The sugar conformation restricted to the C3′-*endo* conformation by a 2′,4′-bridge modification

Moreover, the sequence of the target strand recognized by TFOs is limited to homopurinic regions consisting of consecutive A and/or G nucleotides. These issues encompass two of the main obstacles hindering practical TFO-based gene targeting: (1) low stability of triplex structure and (2) a lack of sequences targetable by TFOs. To overcome these issues, a large number of modified nucleic acids have been developed that specifically involve the formation of parallel motifs [3–6]. There are two likely reasons for the preferential development of approaches using a parallel motif. First, when base triplets in each motif are superimposed, parallel T–AT and C^{+}H–GC base triplets are isomorphic as shown in Fig. 10.1a, whereas inconsistencies exist between antiparallel triplet pairs, which can generate structural distortion and torsion of the nucleic acid backbone in a sequence-dependent manner. The second is that the formation of antiparallel triple helices with TFOs is often difficult due to the high aggregability of purine-rich (especially G-rich) sequences.

Attempts to increase parallel triplex stability often involve sugar modifications within the TFO. Triplex structures formed from dsDNA and a single-stranded RNA molecule are more stable than DNA triplexes [7]; therefore, chemical modifications made to the sugar conformation of the nucleotide *N*-form in the TFO are expected to improve the stability of TFO:dsDNA triplex structures, particularly when altered to the C3′-*endo* conformation found in RNA molecules [8]. In fact, 2′-*O*-substituted nucleic acids preferentially adopt C3′-*endo* conformations, as 2′-*O*-methyl [9], 2′-*O*-aminopropyl [10], and 2′-*O*-guanodinoethyl derivatives [11] increase the binding affinity of TFOs to dsDNA. Among them, 2′,4′-bridged nucleic acids restricted to C3′-*endo* conformations by an extra bridge between the 2′- and 4′-positions significantly increase the binding affinity (Fig. 10.2). Thus, 2′,4′-bridged nucleic acids have a high potential for use in overcoming the problems in parallel motif triplex stability. In this chapter, we focus on the properties of 2′,4′-bridged nucleic acids and their applicability in dsDNA targeting.

10.2 Stabilization of the Triplex by 2′,4′-Bridged Nucleic Acids

Covalent bridge structures between the 2′-position and 4′-position of the sugar moiety force the nucleoside to take on a C3′-*endo* conformation suitable for triplex formation with dsDNA. Thus, 2′,4′-bridged nucleic acids shown in Fig. 10.3 have been used for modifying TFOs for dsDNA gene targeting.

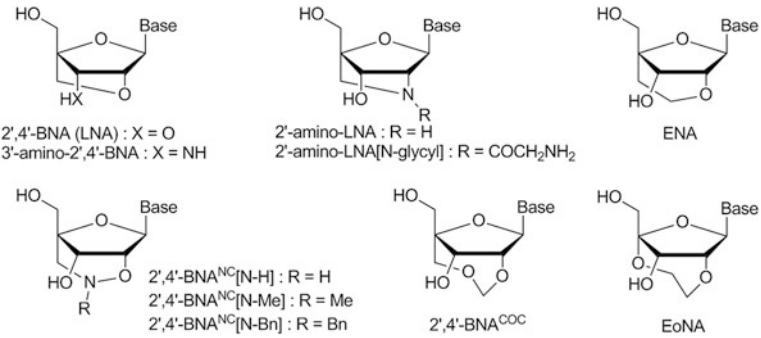

Fig. 10.3 Structures of 2′,4′-bridged nucleic acid monomers used for modifying TFOs

Modified TFOs, including the 2′-*O*,4′-*C*-methylene-bridged nucleic acid (2′,4′-BNA or LNA, Fig. 10.3) originally developed independently by us and Wengel's group [12, 13], can significantly stabilize the triplex with dsDNA in a sequence-selective fashion. Furthermore, the requirement for cysteine protonation in the formation of $C^{+}H$–GC base triplets causes pyrimidine motif triplexes to be extremely unstable at physiological neutral pH [14–16]. However, introduction of the 2′,4′-BNA modification increased the binding constant of this triplex by approximately 20-fold as shown by isothermal titration calorimetry (ITC) [16]. Kinetic analysis revealed that the 2′,4′-BNA modification leads to a reduced dissociation rate, thus improving triplex stability [16, 17]. Additionally, replacement of the cytosine nucleobase with that of 5-methylcytosine (^{m}C) enhances its recognition of a GC base pair at neutral pH [18]. Therefore, the combined use of ^{m}C and the 2′,4′-BNA modification would allow TFOs to form stable triplexes with dsDNA containing homopurinic target sequences.

While no loss of sequence-selectivity has been found in the 2′,4′-BNA-modified TFOs [19], the introduction of consecutive 2′,4′-BNA modifications can become unfavorable for triplex formation as they fail to provide the flexibility necessary to appropriately bind to dsDNA. Accordingly, fully 2′,4′-BNA-modified TFOs are entirely devoid of the ability to form a triplex with targeted dsDNA [15], whereas the inclusion of a 2′,4′-BNA monomer every 2–3 nucleotides in TFOs yielded the best combination of structural flexibility and stability [20]. Moreover, the 3′-amino analog of 2′,4′-BNA (3′-amino-2′,4′-BNA) exhibited a similar triplex-stabilizing ability along with improved nuclease resistance [21, 22]. Although triplex stabilization by 2′-amino-LNA was lower than that of 2′,4′-BNA, 2′-amino-LNA[*N*-glycyl] exceptionally stabilized the triplex among the various *N*2′-substitutions analyzed [14].

The 2′-*O*,4′-*C*-ethylene-bridged nucleic acid (ENA) developed by Koizumi's group [23] has a six-membered bridge structure, one carbon-larger bridge size than 2′,4′-BNA (Fig. 10.3). As expected, ENA also stabilized the dsDNA triplex in a comparable manner to that of 2′,4′-BNA. Notably, fully ENA-modified TFOs are

sufficient to form dsDNA triplexes despite their limited stabilizing ability per ENA modification [24].

Although 2′-*O*,4′-*C*-aminomethylene-bridged nucleic acid (2′,4′-BNA^{NC}) contains the same six-membered bridge size as ENA, substituents of the nitrogen atom in the bridge of 2′,4′-BNA^{NC} affected its triplex-stabilizing ability in the following order: unsubstituted analog (2′,4′-BNA^{NC}[N-H]) > *N*-methyl analog (2′,4′-BNA^{NC}[N-Me]) > *N*-benzyl analog (2′,4′-BNA^{NC}[N-Bn]) (Fig. 10.3). Interestingly, fully 2′,4′-BNA^{NC}[N-H]-modified TFO also bound to dsDNA and formed triplex structures [25].

Among the nucleic acid sugar modifications that have been reported to date, 2′,4′-BNA, ENA, and 2′,4′-BNA^{NC}[N-H] provide the most stable triplexes with dsDNA. For example, in UV-melting experiments using TFOs with single modifications, 2′,4′-BNA, ENA, and 2′,4′-BNA^{NC}[N-H] increased the T_m values by +11 °C, +11 °C, and +9 °C, respectively, relative to that of natural TFOs [26].

In addition to these 2′,4′-bridge modifications, there are seven-membered-bridged nucleic acids, such as 2′,4′-BNA^{COC} [27] and EoNA [28], that possess a methyleneoxymethylene or ethyleneoxy bridge between the 2′-oxygen and 4′-carbon atoms, respectively (Fig. 10.3). These modified nucleic acids are considered to provide some flexibility of the sugar conformation in the range of C3′-*endo* due to their large size. In UV-melting experiments of triplex formation with 2′,4′-BNA^{COC}- and EoNA-modified TFOs at pH 7.2, the 2′,4′-BNA^{COC} modification resulted in nearly the same or slightly higher T_ms than that of the natural triplex nucleic acid [The change in T_m per modification (ΔT_m/mod.) was up to +0.7 °C] [28]. In contrast, EoNA modifications significantly improved the stability of triplex (ΔT_m/mod was up to +3.8 °C) and likely yielded higher triplex stability as it adopted a more rigid C3′-*endo* sugar conformation than 2′,4′-BNA^{COC}due to both conformation constraints and the anomeric effect on the 4′-carbon atom.

10.3 Expansion of Targetable Sequence by 2′,4′-Bridged Nucleic Acids with Nonnatural Nucleobases

Triplex-forming DNA sequences targetable by TFOs are currently limited to homopurinic regions as shown in Fig. 10.1. This limitation could be overcome by the development of nucleic acids that stably and selectively recognize pyrimidine interruption, namely CG and TA base pairs. The combination of 2′,4′-bridged nucleic acids and nonnatural nucleobases is considered an attractive strategy to acquire the increased stability and CG or TA base pair recognition within dsDNA. A merit of this strategy is that the sugar conformation is fixed to C3′-*endo* in a N-type conformation by the 2′,4′-BNA modification, even in the case of a C–C glycosidic bonds that predominantly lead to an S-type conformation [29]. To date, 2′,4′-BNA bearing five- and six-membered heteroaromatic-based nucleobases have mainly been investigated for CG or TA base pair recognition.

10.3.1 For CG Base Pair Recognition

On the basis that a natural T can recognize a CG base pair via the single hydrogen bond between the 2-carbonyl group in T and the 4-amino group in C in a parallel triplex [30, 31], 2′,4′-BNAs (P^B and $^mP^B$) bearing 2-pyridone or 5-methyl-2-pyridone nucleobases have been developed for CG base pair recognition (Fig. 10.4). Notably, both P^B and $^mP^B$ had high and selective binding affinity for CG base pairs in dsDNA with respect to the formation of a parallel triplex [32, 33]. Moreover, a detailed analysis using ITC demonstrated that the high CG-recognition ability of P^B was attributed not only to enthalpic stabilization via hydrogen bonding and/or base stacking of the 2-pyridone nucleobase but also to entropic stabilization due to the 2′,4′-BNA modification [34]. Nevertheless, P^B and $^mP^B$ tended to have somewhat the affinity to an AT base pair though the affinity was much lower than that to the CG counterparts. The replacement of 2-pyridone by isoquinolone (Q^B, shown in Fig. 10.4) increased the nucleobase's CG base pair selectivity by decreasing its affinity to AT base pairs. In triplex UV-melting experiments under neutral conditions, P^B exhibited T_m values of 33 °C and 23 °C for CG and AT base pairs, respectively, and thus a CG-selectivity of 10 °C. Comparatively, Q^B yielded the decreased T_m value of 15 °C for an AT base pair and a CG-selectivity of 14 °C, respectively [35]. Interestingly, evaluation of 2′,4′-BNA bearing 2-pyridine (Py^B) as a basic nucleobase revealed that it has a CG-specificity greater than or equal to that of P^B [36].

A detailed structural investigation on *N*,*N*-disubstituted cytosine nucleobases to identify a nucleobase suitable for CG base pair recognition was conducted by efficiently supplying nucleic acid analogs bearing various *N*,*N*-disubstituted cytosines with a post-elongation modification method [37, 38]. This analysis revealed that 2′,4′-BNA bearing 4-[(3*S*)-3-guanidinopyrrolidino]-5-methylpyrimidin-2-one (GP^B) had a significant CG-recognition ability in a parallel motif triplex, particularly when the target CG base pair was sandwiched between AT base pairs

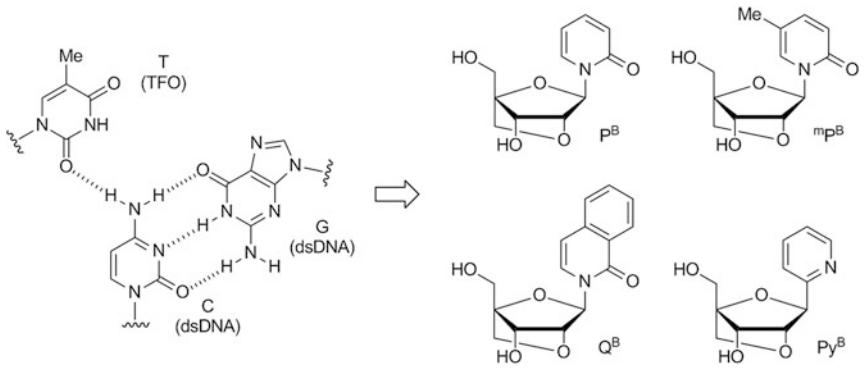

Fig. 10.4 Structures of 2′,4′-BNA monomers bearing 2-pyridone, 5-methyl-2-pyridone, isoquinolone, and 2-pyridine nucleobases

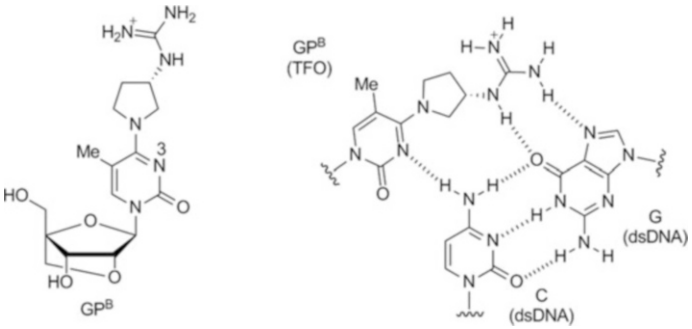

Fig. 10.5 Structure of GP^B monomer and the plausible recognition style of a CG base pair by GP^B

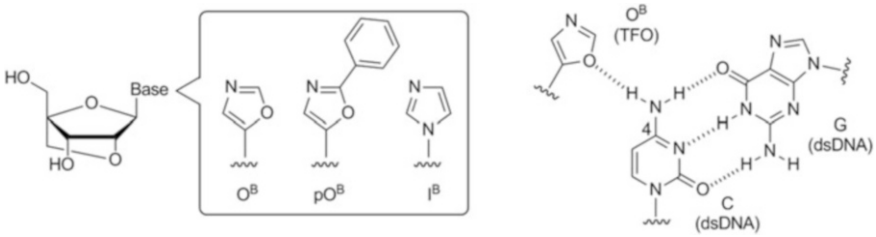

Fig. 10.6 Structures of 2′,4′-BNA monomers bearing five-membered heteroaromatics and the plausible recognition style of a CG base pair by O^B

(Fig. 10.5). In comparison, the CG affinity of GP^B was on the same level with that of a stable T–AT base triplet as shown in Fig. 10.1a. Moreover, the CG-selectivity ($\Delta T_m = 26$ °C) of GP^B as a nucleobase was superior to the AT-selectivity ($\Delta T_m = 15$ °C) of T. On the other hand, the 3-deaza analog of GP^B (N → CH at 3-position, Fig. 10.5) improved the stability and selectivity towards CG base pairs when compared to GP^B in a parallel motif triplex with dsDNA where the adjacent 3′-site was a GC base pair [39].

Several 2′,4′-BNAs bearing five-membered heteroaromatics as nucleobases have also been developed for the recognition of the 4-amino group of C in a CG base pair in triplex formation as shown in Fig. 10.6 [40, 41]. Among them, 2′,4′-BNA bearing an oxazole nucleobase (O^B) showed the highest affinity towards CG base pairs (increased T_m value by +7–8 °C compared to pO^B and I^B), although both the affinity and CG-selectivity were insufficient. The recognition of a CG base pair by O^B was speculated to occur through a hydrogen bond between the oxygen in an oxazole moiety of O^B and the 4-amino group of C [40].

10.3.2 For TA Base Pair Recognition

In general, TA base pair recognition is quite difficult, because the 5-methyl group of T in the TA base pair can disturb hydrogen bond formation with its 4-carbonyl

group. Based on T-CG (Fig. 10.4) and P^B-CG base triplets, 2′,4′-BNAs bearing 2- or 3-hydroxyphenyl nucleobases ($2H^B$ and $3H^B$, respectively) were designed with hydroxyl groups located at different positions [42]; $2H^B$ had no significant affinity ($T_m = 28$ °C) to TA base pairs, likely due to the steric repulsion between the hydroxyl group of $2H^B$ and 5-methyl group of T, whereas $2H^B$ obviously interacted with a UA base pair ($T_m = 37$ °C), which lacks a 5-methyl group (Fig. 10.7). On the contrary, $3H^B$ showed high affinity to both TA and UA base pairs with T_m values of 34 °C and 35 °C, respectively. These results may imply that a 3-hydroxyphenyl nucleobase in $3H^B$ can form a hydrogen bond with the 4-carbonyl group of T and thus avoiding steric repulsion with the 5-methyl group of T (Fig. 10.7). However, $3H^B$ has no selectivity to any base pairs (T_m values for all base pairs ranged from 33 to 35 °C), since the hydroxyl group in the nucleobase of $3H^B$ can act as both a hydrogen donor and hydrogen acceptor.

In a parallel motif triplex, 2′,4′-BNAs (bP^B and Tz^B) bearing multiple and non-fused aromatics as nucleobases had the highest affinity to a TA base pair among all four natural base pairs [43] (Fig. 10.8). Notably, the TA-recognition ability of bP^B was superior to that of Tz^B or G, a sole nucleobase capable of recognizing a TA base pair among natural nucleobases [44]. The recognition style of a TA base pair by bP^B is considered the result of the intercalation of the terminal benzene ring of bP^B between a TA base pair and the base pair of the 3′-site adjacent to the target T. 2′,4′-BNA modification of G led to no stabilization of triplex including the G-TA base triplet [43], though it was reported that sugar conformation of G in a G-TA base triple would be C3′-*endo* [45].

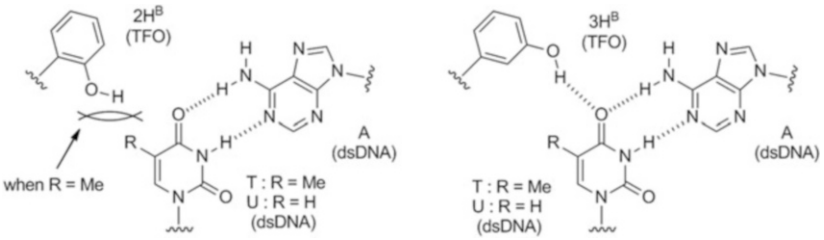

Fig. 10.7 The plausible recognition styles of TA and UA base pairs by $2H^B$ and $3H^B$

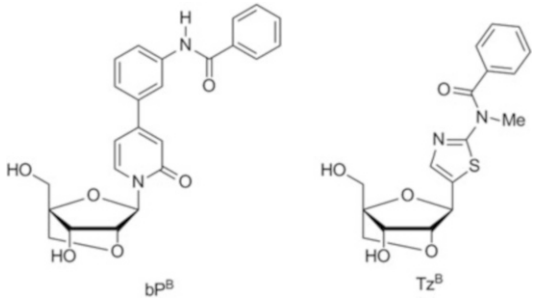

Fig. 10.8 Structures of bP^B and Tz^B monomers

10.4 Summary

In summary, this chapter details the recent progress towards gene targeting via triplex DNA formation with TFOs comprised of 2′,4′-bridged nucleic acids bearing natural and nonnatural nucleobases. In general, the use of 2′,4′-bridged nucleic acids with natural nucleobases—such as T, C, and ^{m}C—stabilized triplexes formed with dsDNA without the loss of sequence selectivity. Significantly, the stabilizing capacity of five- or six-membered-bridged nucleic acids including 2′,4′-BNA, ENA, and 2′,4′-BNA^{NC} is quite high and may achieve a practical level in terms of triplex stability. Notably, GP^{B} recognizes CG base pairs with strong affinity and high selectivity, which can lead to the extension of targetable sequences in dsDNA. Furthermore, the continued investigation on these molecules involving TA base pair binding is likely to yield promising results. In any case, 2′,4′-bridge modifications provide great promise for use in targeting arbitrary regions of dsDNA with TFOs.

References

1. Felsenfeld G, Davies DR, Rich A (1957) Formation of three-stranded polyribonucleotide molecule. J Am Chem Soc 70:2023–2024
2. Felsenfeld G, Rich A (1957) Studies on the formation of two- and three-stranded polyribonucleotides. Biochim Biophys Acta 26:457–468
3. Buchini S, Leumann CJ (2003) Recent improvements in antigene technology. Curr Opin Chem Biol 7:717–726
4. Gowers DM, Fox KR (1999) Towards mixed sequence recognition by triple helix formation. Nucleic Acids Res 27:1569–1577
5. Hari Y, Obika S, Imanishi T (2012) Towards the sequence-selective recognition of double-stranded DNA containing pyrimidine-purine interruptions by triplex-forming oligonucleotides. Eur J Org Chem 2012:2875–2887
6. Thuong NT, Hélène C (1993) Sequence-specific recognition and modification of double-helical DNA by oligonucleotides. Angew Chem Int Ed 32:666–690
7. Roberts RW, Crothers DM (1992) Stability and properties of double and triple helics: dramatic effects of RNA and DNA backbone composition. Science 258:1463–1466
8. Asensio JL, Carr R, Brown T, Lane AN (1999) Conformational and thermodynamic properties of parallel intramolecular triplex helices containing a DNA, RNA, or 2′-OMeDNA third strand. J Am Chem Soc 121:11063–11070
9. Shimizu M, Konishi A, Shimada Y, Inoue H, Otsuka E (1992) Oligo(2′-*O*-methyl)ribonucleotides. Effective probes for duplex DNA. FEBS Lett 302:155–158
10. Casset F, Cuenoud B, Hüsken D, Natt F, Altmann K-H, Wolf RM, Martin P, Moser HE (1998) Dual recognition of double-stranded DNA by 2′-aminoethoxy-modified oligonucleotides. Angew Chem Int Ed 37:1288–1291
11. Prakash TP, Püschl A, Lesnik E, Mohan V, Tereshko V, Egli M, Manoharan M (2004) 2′-*O*-[2-(guanidinium)ethyl]-modified oligonucleotides: stabilizing effect on duplex and triplex structures. Org Lett 6:1971–1974
12. Obika S, Nanbu D, Hari Y, Morio K, In Y, Ishida T, Imanishi T (1997) Synthesis of 2′-*O*,4′-*C*-methyleneuridine and -cytidine. Novel bicyclic nucleosides having a fixed $C_{3'}$-*endo* sugar puckering. Tetrahedron Lett 38:8735–8738

13. Singh SK, Koshkin AA, Wengel J, Nielsen P (1998) LNA (locked nucleic acids): synthesis and high-affinity nucleic acid recognition. Chem Commun 455–456
14. Højland T, Kumar S, Babu BR, Umemoto T, Albæk N, Sharma PK, Nielsen P, Wengel J (2007) LNA (locked nucleic acid) and analogs as triplex-forming oligonucleotides. Org Biomol Chem 5:2375–2379
15. Obika S, Uneda T, Sugimoto T, Nanbu D, Minami T, Doi T, Imanishi T (2001) 2′-*O*,4′-*C*-methylene bridged nucleic acid (2′,4′-BNA): synthesis and triplex-forming properties. Bioorg Med Chem 9:1001–1011
16. Torigoe H, Hari Y, Sekiguchi M, Obika S, Imanishi T (2001) 2′-*O*,4′-*C*-methylene bridged nucleic acid modification promotes pyrimidine motif triplex DNA formation at physiological pH: thermodynamic and kinetic studies. J Biol Chem 276:2354–2360
17. Brunet E, Alberti P, Perrouault L, Babu R, Wengel J, Giovannangeli C (2005) Exploring cellular activity of locked nucleic acid-modified triplex-forming oligonucleotides and defining its molecular basis. J Biol Chem 280:20076–20085
18. Povsic TJ, Dervan PB (1989) Triple helix formation by oligonucleotides on DNA extended to the physiological pH range. J Am Chem Soc 111:3059–3061
19. Obika S, Hari Y, Sugimoto T, Sekiguchi M, Imanishi T (2000) Triplex-forming enhancement with high sequence selectivity by single 2′-*O*,4′-*C*-methylene bridged nucleic acid (2′,4′-BNA) modification. Tetrahedron Lett 41:8923–8927
20. Sun B-W, Babu BR, Sørensen MD, Zakrzewska K, Wengel J, Sun J-S (2004) Sequence and pH effects of LNA-containing triple helix-forming oligonucleotides: physical chemistry, biochemistry, and modeling studies. Biochemistry 43:4160–4169
21. Obika S, Onoda M, Morita K, Ando J, Koizumi M, Imanishi T (2001) 3′-Amino-2′,4′-BNA: novel bridged nucleic acids having an N3′-P5′ phosphoramidate linkage. Chem Commun 1992–1993
22. Obika S, Rahman SMA, Song B, Onoda M, Koizumi M, Morita K, Imanishi T (2008) Synthesis and properties of 3′-amino-2′,4′-BNA, a bridged nucleic acid with a N3′-P5′ phosphoramidate linkage. Bioorg Med Chem 16:9230–9237
23. Morita K, Hasegawa C, Kaneko M, Tsutsumi S, Sone J, Ishikawa T, Imanishi T, Koizumi M (2002) 2′-*O*,4′-*C*-ethylene-bridged nucleic acids (ENA): highly nuclease-resistant and thermodynamically stable oligonucleotides for antisense drug. Bioorg Med Chem Lett 12:73–76
24. Koizumi M, Morita K, Daigo M, Tsutsumi S, Abe K, Obika S, Imanishi T (2003) Triplex formation with 2′-*O*,4′-*C*-ethylene-bridged nucleic acids (ENA) having C3′-*endo* conformation at physiological pH. Nucleic Acids Res 31:3267–3273
25. Rahman SMA, Seki S, Obika S, Yoshikawa H, Miyashita K, Imanishi T (2008) Design, synthesis, and properties of 2′,4′-BNA^{NC}: a bridged nucleic acid analogue. J Am Chem Soc 130:4886–4896
26. Rahman SMA, Seki S, Obika S, Haitani S, Miyashita K, Imanishi T (2007) Highly stable pyrimidine-motif triplex formation at physiological pH values by a bridged nucleic acid analogue. Angew Chem Int Ed 46:4306–4309
27. Hari Y, Obika S, Ohnishi R, Eguchi K, Osaki T, Ohishi H, Imanishi T (2006) Synthesis and properties of 2′-*O*,4′-*C*-methyleneoxymethylene bridged nucleic acid. Bioorg Med Chem 14:1029–1038
28. Hari Y, Morikawa T, Osawa T, Obika S (2013) Synthesis and properties of 2′-*O*,4′-*C*-ethyleneoxy bridged 5-methyluridine. Org Lett 15:3702–3705
29. Hari Y, Obika S, Sakaki M, Morio K, Yamagata Y, Imanishi T (2002) Effective synthesis of *C*-nucleosides with 2′,4′-modification. Tetrahedron 58:3051–3063
30. Radhakrishnan I, Patel DJ (1994) Solution structure and hydration patterns of a pyrimidine. purine.pyrimidine DNA triplex containing a novel T.CG base-triple. J Mol Biol 241:600–619
31. Yoon K, Hobbs CA, Koch J, Sardaro M, Kutny R, Weis AL (1992) Elucidation of the sequence-specific third-strand recognition of four Watson-Crick base pairs in a pyrimidine triple-helix motif: T. AT, C. GC, T. CG, and G.TA. Proc Natl Acad Sci USA 89:3840–3844

32. Obika S, Hari Y, Sekiguchi M, Imanishi T (2001) A 2′,4′-bridged nucleic acid containing 2-pyridone as a nucleobase: efficient recognition of a C·G interruption by triplex formation with a pyrimidine motif. Angew Chem Int Ed 40:2079–2081
33. Obika S, Hari Y, Sekiguchi M, Imanishi T (2002) Stable oligonucleotide-directed triplex formation at target sites with CG interruptions: strong sequence-specific recognition by 2′,4-′-bridged nucleic-acid-containing 2-pyridones under physiological conditions. Chem Eur J 8:4796–4802
34. Torigoe H, Hari Y, Obika S, Imanishi T (2003) Triplex formation involving 2′-*O*,4′-*C*-methylene bridged nucleic acid (2′,4′-BNA) with 2-pyridone base analogue: efficient and selective recognition of C:G interruption. Nucleosides Nucleotides Nucleic Acids 22:1097–1099
35. Hari Y, Obika S, Sekiguchi M, Imanishi T (2003) Selective recognition of CG interruption by 2′,4′-BNA having 1-isoquinolone as a nucleobase in a pyrimidine motif triplex formation. Tetrahedron 59:5123–5128
36. Hari Y, Matsugu S, Inohara H, Hatanaka Y, Akabane M, Imanishi T, Obika S (2010) 2′,4′-BNA bearing a 2-pyridine nucleobase for CG base pair recognition in the parallel motif triplex DNA. Org Biomol Chem 8:4176–4180
37. Hari Y, Akabane M, Hatanaka Y, Nakahara M, Obika S (2011) A 4-[(3*R*,4*R*)-dihydroxypyrrolidino]pyrimidin-2-one nucleobase for a CG base pair in triplex DNA. Chem Commun 47:4424–4426
38. Hari Y, Akabane M, Obika S (2013) 2′,4′-BNA bearing a chiral guanidinopyrrolidine-containing nucleobase with potent ability to recognize the CG base pair in a parallel-motif DNA triplex. Chem Commun 49:7421–7423
39. Akabane-Nakata M, Obika S, Hari Y (2014) Synthesis of oligonucleotides containing N, N-disubstituted 3-deazacytosine nucleobases by post-elongation modification and their triplex-forming ability with double-stranded DNA. Org Biomol Chem 12:9011–9015
40. Hari Y, Obika S, Inohara H, Ikejiri M, Une D, Imanishi T (2005) Synthesis and triplex-forming ability of 2′,4′-BNAs bearing imidazoles as a nucleobase. Chem Pharm Bull 53:843–846
41. Obika S, Hari Y, Morio K, Imanishi T (2000) Triplex formation by an oligonucleotide containing conformationally locked C-nucleoside, 5-(2-*O*,4-*C*-methylene-β-D-ribofuranosyl) oxazole. Tetrahedron Lett 41:221–224
42. Hari Y, Kashima S, Inohara H, Ijitsu S, Imanishi T, Obika S (2013) Base-pair recognition ability of hydroxyphenyl nucleobases in parallel triplex DNA. Tetrahedron 69:6381–6391
43. Obika S, Inohara H, Hari Y, Imanishi T (2008) Recognition of T·A interruption by 2′,4′-BNAs bearing heteroaromatic nucleobases through parallel motif triplex formation. Bioorg Med Chem 16:2945–2954
44. Griffin LC, Dervan PB (1989) Recognition of thymine-adenine base pairs by guanine in a pyrimidine triple helix motif. Science 245:967–971
45. Wang E, Malek S, Feigon J (1992) Structure of a G·T·A triplet in an intramolecular DNA triplex. Biochemistry 31:4838–4846

Chapter 11
Specific Recognition of Single Nucleotide by Alkylating Oligonucleotides and Sensing of 8-Oxoguanine

Shigeki Sasaki, Yosuke Taniguchi, and Fumi Nagatsugi

Abstract Gene expression is regulated by hierarchical mechanisms, for which not only the sequence but also the special structure of DNA and RNA play a vital role. This sophisticated systems also feature specific chemical modification of nucleotides as epigenetic gene regulations such as 5-methylation of cytosine. Meantime, endogenous and exogenous chemical species react with the nucleotides to have significant impact on the genetic function by causing mutations. Among mutations, a single nucleotide alteration is the most frequently found in the disease-relating genes. Therefore, for the diagnostic and therapeutic purposes, oligonucleotides are desired to discriminate a single nucleotide difference. However, because of non-covalent hybridization of the oligonucleotide with DNA and RNA, discrimination of a single nucleotide difference is not always easy. We have focused on selective alkylation as a reliable strategy for a single base recognition. Molecular design has been performed so that a non-covalent complex in a hybridized complex induces a selective reaction to the target base. On the other hand, guanine is the most susceptible base for oxidation to produce 8-oxoguanine which has a strong mutagenicity. 8-Oxoguanine formed in cells is regarded as a biomarker of oxidative stress of the cell, and a convenient sensing method is desired for diagnostic purposes. Also, determination of 8-oxo-2′-deoxyguanosine in DNA is important to reveal the oxidative damaged site in DNA. In this chapter, design concept and specific alkylating reactions will be introduced.

S. Sasaki (✉) • Y. Taniguchi
Graduate School of Pharmaceutical Sciences, Kyushu University, 3-1-1 Maidashi, Higashi-ku, Fukuoka 812-8582, Japan
e-mail: sasaki@phar.kyushu-u.ac.jp

F. Nagatsugi
Institute of Multidisciplinary Research for Advanced Materials, Tohoku University, 2-1-1 Katahira, Aoba-ku, Sendai 980-8577, Japan

K. Nakatani, Y. Tor (eds.), *Modified Nucleic Acids*, Nucleic Acids and Molecular Biology 31, DOI 10.1007/978-3-319-27111-8_11

11.1 Alkylation and Oxidation of Nucleic Acids

Nucleic acids suffer from a number of chemical reactions: hydrolysis of the phosphodiester; oxidation of ribose or 2′-deoxyribose; cleavage of *N*-glycosidic bond , alkylation, oxidation, and photoreaction of nucleobases. Epigenetic modifications of nucleic acids are highly regulated by hierarchical systems composed of nucleic acids and proteins. In contrast, chemically reactive species of both endogenous and exogenous origins react with nucleic acids randomly. Most of these randomly modified or damaged nucleic acids are repaired; however, if these are remained unrepaired, they have a strong impact on biological functions [1–3]. DNA alkylating chemotherapeutic agents, such as nitrogen mustard and mitomycin C which have two alkylating groups in a single molecule, alkylate two nucleobases to form intra-strand or interstrand cross-link of DNA to exhibit cytotoxicity [4]. Psoralen forms DNA adducts by UV irradiation with both duplex strands to form an interstrand cross-link [5, 6] Psoralen-cross-link with mRNA has been applied to enhance inhibition of translation by antisense oligodeoxynucleotides (ODNs) [7, 8]. Three-dimensional nucleic acid structures can be stabilized by cross-link formation [9–11]. Thus, a variety of cross-linking agents have also been developed for different purposes, including disulfide bonds [12], benzophenone derivatives [13], carbazoles [14], quinone methides [15, 16], phenylselenyl derivatives of pyrimidines [17], and furan derivatives [18]. A need of alkylating or cross-linking agent for biological application has lead us to develop more efficient cross-linking oligonucleotides, which will be discussed in Sect. 11.2. Section 11.3 will discuss a new technology for elective alkylation of DNA and RNA.

Oxidants are the most abundant endogenous cause for nucleobase damages [19]. 8-Oxoguanosine (8-oxoG) is a representative metabolite derived by the oxidation of guanosine (G) and induces G:C to T:A transversion mutations [20]. As the 8-oxoG level is an index of oxidative damage of cells related to some diseases and aging, there are several analytical methods such as HPLC-EC, HPLC/GC-MS, ELISA, and other methods. We have recently developed new recognition molecules for selective sensing 8-oxoG, which will be discussed in Sects. 11.4 and 11.5.

11.2 Cross-Linking Oligonucleotides

The cross-linking agent is required to furnish both stability and reactivity for efficient cross-link formation in the living system. To meet this requirement, we have designed the cross-linking agent so that high reactivity is induced after the formation of hybridized complex. This strategy for induction of reactivity has been achieved by 2-amino-6-vinylpurine derivative (**1**). This compound exhibited selective cross-linking to cytosine bases [21–26], in which the sulfide-protected derivative of 2-amino-6-vinylpurine in ODN was automatically transformed into the

active vinyl structure within the hybridized complex. This strategy was applied to inhibition of intracellular gene expression [27, 28]. The 2-amino-6-vinylpurine unit has been utilized as a platform molecule to achieve a variety of cross-linking reactions [29–34]. From a viewpoint of molecular design, a characteristic feature of this 2-amino-6-vinylpurine is that the vinyl group is directed towards the Watson–Crick base-pairing face to react with the 4-amino group of cytosine. Most of cross-linking agents are not located within the Watson–Crick base pair. In designing new cross-linking agents, we took into account that a partial base pairing and/or shape complementarity is beneficial for the proximity effect.

11.2.1 Design of Cross-Linking Agent

The 4-vinyl-(*1H*)-5-methylpyrimidine-2-one derivative (**3**: T-vinyl) was designed for cross-link formation with the 6-amino group of adenine, based on the expectation that the two bases would exhibit shape complementarity resembling a T–A base pair. A mechanism for stimulation responsive activation is built in the T-vinyl by the sulfide with 2-thiopyridine (**4**), which is activated under slightly acidic conditions (Fig. 11.1).

11.2.2 Synthesis of 2′-Deoxy-4-Vinylpyrimidine Nucleoside Analog

The 2,4,6-triisopropylbenzensulfonyl derivative of TBDMS-protected thymidine (**7**) or 2′-deoxyuridine (**8**) was treated with 2,4,6-trivinylcyclotriboroxane pyridine complex in the presence of $Pd(PPh_3)_4$, LiBr, and K_2CO_3 in H_2O–dioxane. As the

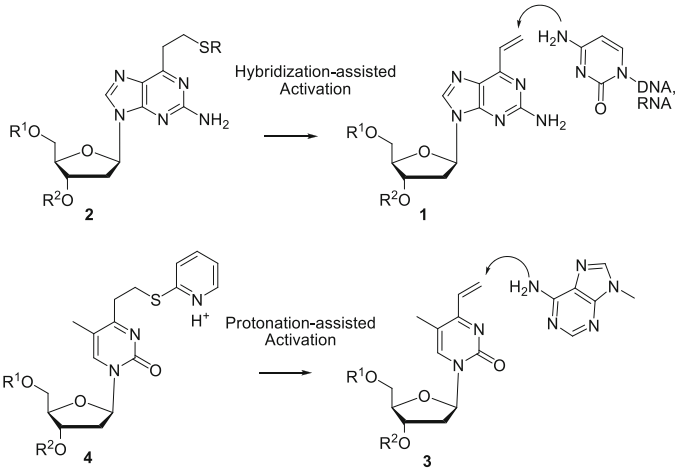

Fig. 11.1 Cross-linking agents (**1**, 2-amino-6-vinylpurine) for cytosine and (**3**, T-vinyl) for adenine

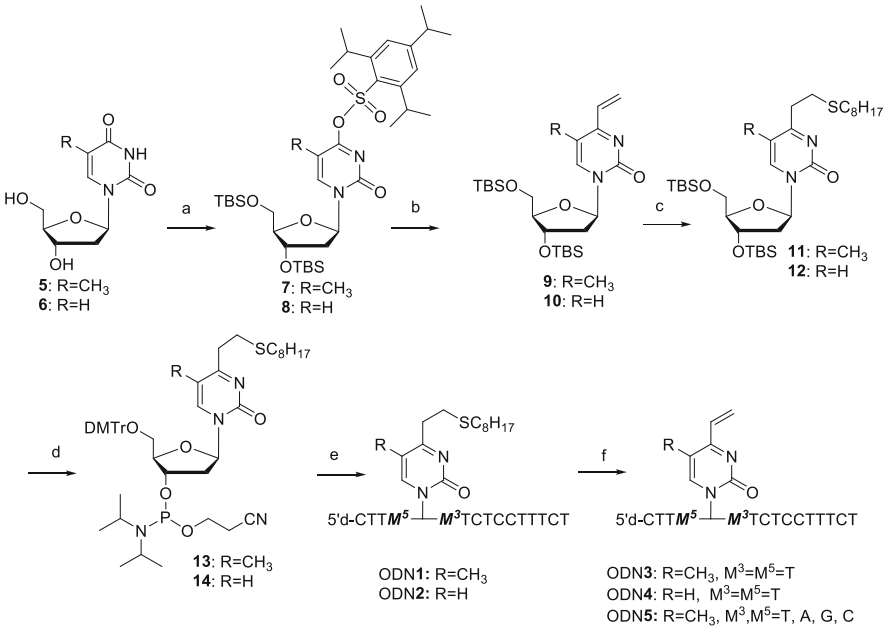

Scheme 11.1 Synthesis of the amidite precursor of T-vinyl and ODN incorporating T-Vinyl. (a) (1) TBDMSCl, imidazole, DMF, (2) 2,4,6-triisopropylbenzensulfonyl chloride, Et_3N, DMAP, CH_2Cl_2, (b) 2,4,6-trivinylcyclotriboroxane pyridine complex, $Pd(PPh_3)_4$, LiBr, K_2CO_3, H_2O:1,4-dioxane = 1:3 solution, (c) $C_8H_{17}SH$, CH_3CN, (d) (1) TBAF, THF, (2) DMTrCl, thioanisole, DIPEA, CH_2Cl_2, (3) 2-cyanoethyl *N*,*N*-diisopropylchlorophosphoramidite, DIPEA, CH_2Cl_2, (e) (1) DNA/RNA synthesizer, (2) K_2CO_3 in dry methanol in the presence of octanethiol, (3) 5 % aqueous AcOH, (f) (1) magnesium metaperoxyphthalate (MMPP) carbonate buffer, (2) 0.5 M NaOH

resulting vinylated products (**9** and **10**) were not sufficiently stable for isolation, they were protected with octanethiol (**11** and **12**) [35]. When the vinyl derivative (**9**) was protected with methanethiol, the methylsulfide protecting group was cleaved during the reaction with DMTrCl. During protection of the diol derivative with DMTrCl, thioanisole was required as a scavenger for the DMTr cation. The DMTr-protected compounds were converted to the corresponding phosphoramidite precursors (**13** and **14**) and were then utilized in a DNA/RNA automated synthesizer to produce ODN**1** and ODN**2** with various flanking bases (M^5 and M^3). Octanthiol is also needed during the cleavage of the ODNs from the resin by treatment with a dry methanol solution of K_2CO_3. The octylsulfide group was oxidized with magnesium metaperoxyphthalate (MMPP) in carbonate buffer, followed by the treatment with a NaOH solution to generate the vinyl group of the cross-linking ODN**3**–**5** (Scheme 11.1).

11.2.3 Selectivity of the Cross-Linking Oligonucleotide

The cross-linking reaction of the vinyl-ODN**3** and ODN**4** was tested using the target RNA**1** having different nucleoside residues at the complementary positions (Fig. 11.2). The cross-linking reaction of ODN**3** (R=CH_3) to the RNA**1** with U at the opposite position was completed within 15 min (Fig. 11.2a). The RNA**1** with an opposing G or A showed lower reactivity, while the RNA**1** with an opposing C did not form any cross-link product. Interestingly, ODN**4** (R=H) containing U-vinyl **3** showed much slower reaction rates while retaining the selectivity for U (Fig. 11.2b). Kinetic parameters for the cross-linking reactions have indicated that T-vinyl (**2**) is superior to U-vinyl (**3**) in terms of the smaller negative value of activation entropy. MO calculations have shown that a *syn*-conformation (**15**) is more stable than the *anti*-conformation (**16**) of T-vinyl (R=CH_3), whereas stability differences between these conformation is small in the U-vinyl (R=H). The vinyl group of the T-vinyl (R=CH_3) requires less conformational change than that of the U-vinyl (R=H) for cross-link formation to occur. The 5-methyl group on the T-vinyl (**2**) plays a role in directing the vinyl group to the Watson–Crick face by steric repulsion.

When the cross-linking reaction was monitored using HPLC, the reaction mixture at pH 7 gave two major peaks, both of which were confirmed to be the cross-linked products. Interestingly, the faster peak was an adenosine adduct; in contrast, the slower peak was a uridine adduct. Accordingly, cross-link adducts were analyzed using all 16 possible combinations of RNA**2** (N^3-U-N^5) with various 3′-, 5′-flanking nucleotide relative to U and the complementary ODN**5** (M^5-**2**-M^3) (Fig. 11.3). The cross-link formation predominantly occurred with an adenine residue at the 5′ position relative to U (Fig. 11.3a, striped columns in lanes 1–4). The adenosine residue at the 3′ position did not undergo cross-linking (lanes 5, 9,

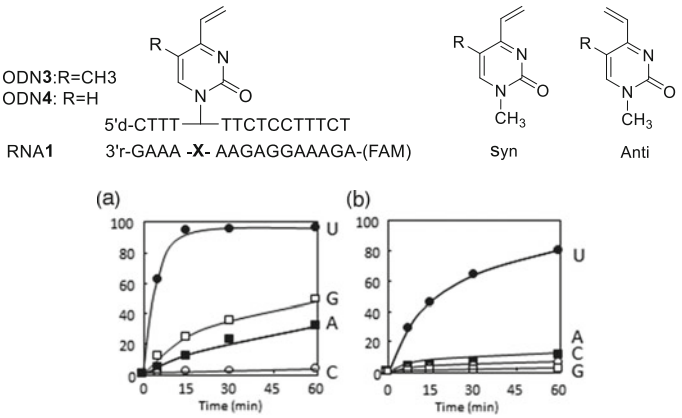

Fig. 11.2 Cross-linking reaction with ODN**3**, **4** and RNA**1**. Cross-linking conditions: [ODN]= 10 μM, RNA**1** = 1 μM, 50 mM MES buffer, 100 mM NaCl, 37 °C, pH 7.0. (**a**) Yield (%) with ODN**3**. (**b**) Yield (%) with ODN**4**

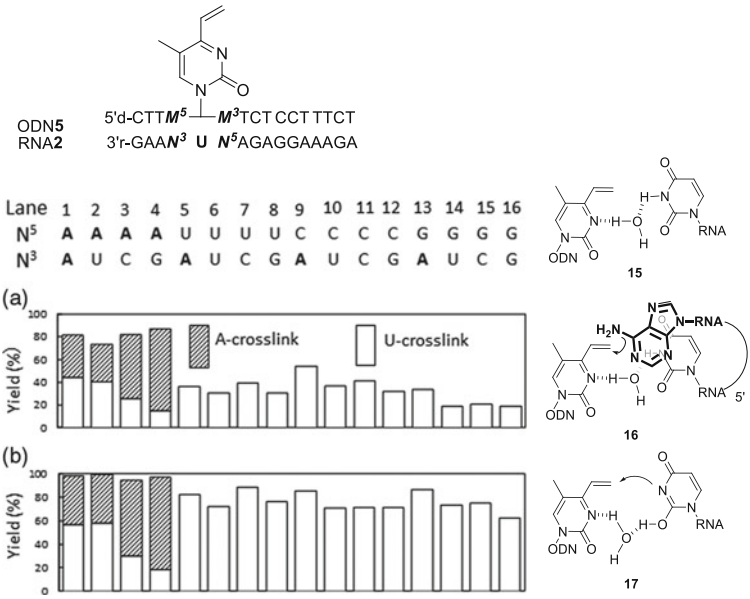

Fig. 11.3 The ratio of A- to U-cross-linking at (**a**) 5 and (**b**) 60 min. [ODN**5**] = 15 μM, [RNA**2**] = 10 μM, 50 mM MES buffer, 100 mM NaCl, pH 7.0, 37 °C. Flanking nucleosides M^3 and M^5 of ODN**5** are complementary to N^5 and N^3, respectively

and 13). Cross-link formation with the opposing U was slower than with A at the 5′-position; however, yields became higher after 60 min (Fig. 11.3b). We speculate that a bridging water molecule may participate in H-bonding interaction, as shown in **15**. Molecular modeling indicates that the 6-amino group of the adenine residue at the 5′ side is in van der Waals contact with the vinyl group of T-vinyl, as shown schematically in **16**. The RNA substrate lacking a 5′-A formed a cross-link with the N3 atom of the opposite U (Fig. 11.2b, lanes 5–16), most likely by reaction with its enol or enolate form (**17**).

11.2.4 Application of Cross-Linking for Triplex DNA

The new cross-linking agent T-vinyl was applied to triplex DNA. T-vinyl was incorporated in the homopyrimidine strand ODN**3**, which can form triplex DNA with a homopurine–homopyrimidine duplex. ODN**6** contains 5-methylcytidine (d^mC) instead of dC, which is used for triplex formation under weakly acidic conditions (**18**). The duplex was composed of DNA**1** and DNA**2**, either of which was labeled with FAM to clarify the cross-linked strand. When the reaction was performed between ODN**3** and the duplex formed with FAM-labeled DNA**1** and non-labeled DNA**2**, the cross-link was formed only in the reaction with the duplex

ODN**3**: C=dC 5'-CTTT-**2**-TTCTCC TTT CT
ODN**6**: C=d^{m}C

DNA**1** (FAM)- 5' TTTGAAA -**X**- AAGAGGAAAGA
DNA**2** 3' AAACTTT -**Y**- TTCTCCTTT CT -5' (FAM)

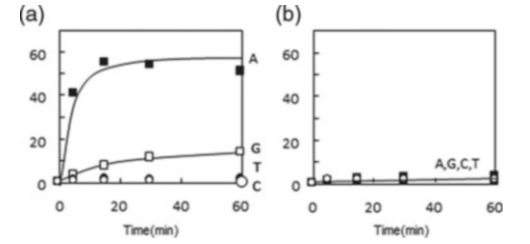

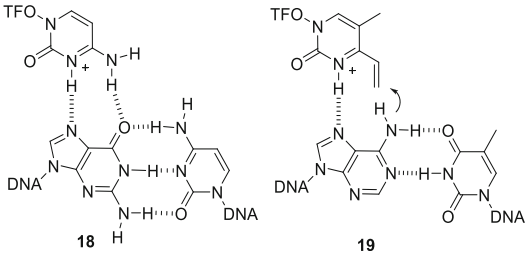

Fig. 11.4 Cross-linking reaction with T-vinyl in the triplex DNA. [ODN**3** or ODN**6**] = 25 μM, [DNA**1**/DNA**2**] = 5 μM, 50 mM MES buffer, 100 mM NaCl, 10 mM MgCl2, 25 °C, pH 5.0 (C = dC) or pH 6.1 (C = d^{m}C). The yield of the cross-linked product was obtained by monitoring FAM-labeled DNA. (**a**) Yield (%) with FAM-DNA**1** (X=). (**b**) Yield (%) with FAM-DNA**2** (Y=)

containing XY=AT (Fig. 11.4a). The duplex formed with non-labeled DNA**1** and FAM-labeled DNA**2** did not give the cross-link products (Fig. 11.4b). The cross-linked product was formed with the 6-amino group of adenine. ODN**6**, containing d^{m}C instead of dC, produced the cross-link at weakly acidic pH, whereas no adduct was formed with ODN**3** under the same conditions, indicating that cross-link formation takes place in the triplex DNA. The reactivity of the vinyl group is enhanced at acidic pH due to protonation at N3; therefore, such a protonated form might contribute to the access of the vinyl group to 6-NH_2 of the adenosine residue in the homopurine strand as depicted in **19**.

11.2.5 Intra-strand Cross-Link in i-Motif DNA

Guanine-rich single-stranded DNA can form a stable four-stranded DNA second structure, i.e., the G-quadruplex (G4-DNA) [36]. DNA sequences with the potential to form G4-DNA are frequently found in a genome [37], such as a telomere [38] and

the promoter regions [39, 40], and thought to form functionally relevant G4 DNA structures [41], C-rich DNAs are associated with G-rich DNAs as the complementary strands and also form four-stranded DNA helices [42, 43]. In this four-stranded C-rich DNA, two parallel duplexes are complexed in an antiparallel fashion by alternatively intercalating hemiprotonated cytosine–cytosine base pairs. This unique intercalated structure, called the *i*-motif, requires acidic pH for its folding due to protonation of one of the cytosines of the base pairs. The open and four-stranded form of the *i*-motif sequences are interchangeable depending on the pH [44–46] and applied in nanotechnology [47]. In the meantime, the binding ligands and chemical modification that stabilize the *i*-motifs have been investigated to reveal its intracellular existence and biological roles [48]. Nevertheless, only a few studies reported the *i*-motif folding at neutral pH [49–51]. We applied the intra-strand cross-link to the *i*-motif structure that might increase its stability in terms of both pH dependency and thermal denaturation [52].

The octylsulfide-protected amidite precursor of the T-vinyl cross-linking agent (**13**) was incorporated into the 5′-end of ODN**8**. The cross-linking reaction was performed in two ways. First, the T-vinyl unit was regenerated in ODN**8** by a general procedure including oxidation with magnesium monoperoxyphthalate followed by elimination at alkaline pH, and the mixture was then acidified at pH 5.5 and 15 °C for the cross-link formation. The structure of the cross-linked product was confirmed to be the one formed with 2′-deoxyadenosine. In the other cross-linking reaction, the T-vinyl unit of the ODN**8** was first protected with the 2-thiopyridine to form ODN**9**, and the mixture was acidified at pH 5.5 and 15 °C. In this case, the cross-link product was obtained in a better yield than the non-protected ODN**8**. Folding and unfolding of the *i*-motif were investigated by measuring the CD spectra (Fig. 11.5). Natural ODN**7** represented the folded *i*-motif, a large positive band with a peak at 286 nm and a negative band at 254 nm at pH 5.0. As the pH increased, the bands were shifted to the positive band at 274 nm and the negative band at 248 nm with an isodichroic point at 276 nm (Fig. 11.5a). [53]. These CD spectral changes reflect shift of the conformation from unfolding of the *i*-motif into a random coil structure. The CD spectra of the cross-linked product ODN**5** also showed pH-dependent unfolding of the *i*-motif into a random coil structure (Fig. 11.5b).The pH dependency of the ellipticity of ODN**1** and ODN**5** at 286 nm and 20 °C show the sigmoidal curves with the midpoints at pH 6.1 for natural ODN**7** and at pH 6.8 for the cross-linked ODN**10** (Fig. 11.5c). The midpoint of ODN**10** significantly shifted to near neutral pH. According to the thermodynamic parameters obtained at pH 5.5, the intra-strand cross-link is unfavorable for folding in terms of the enthalpy change. From the enthalpy increase, T_{10}:T_{22} and dC_1:dC_{13} base pairs in the *i*-motif were thought to be disrupted in the cross-linked structure. On the other hand, the entropy also became less negative for ODN**10**, implying that the cross-link is favorable for folding in terms of the entropy change. In other words, the intra-strand cross-linked *i*-motif is pre-organized for folding of four-stranded structure. Thus, the cross-link between the T-vinyl at the 5′-end and the internal adenine in ODN**10** produced a stabilizing effect for folding due to the favorable entropy effect over any unfavorable enthalpy effects.

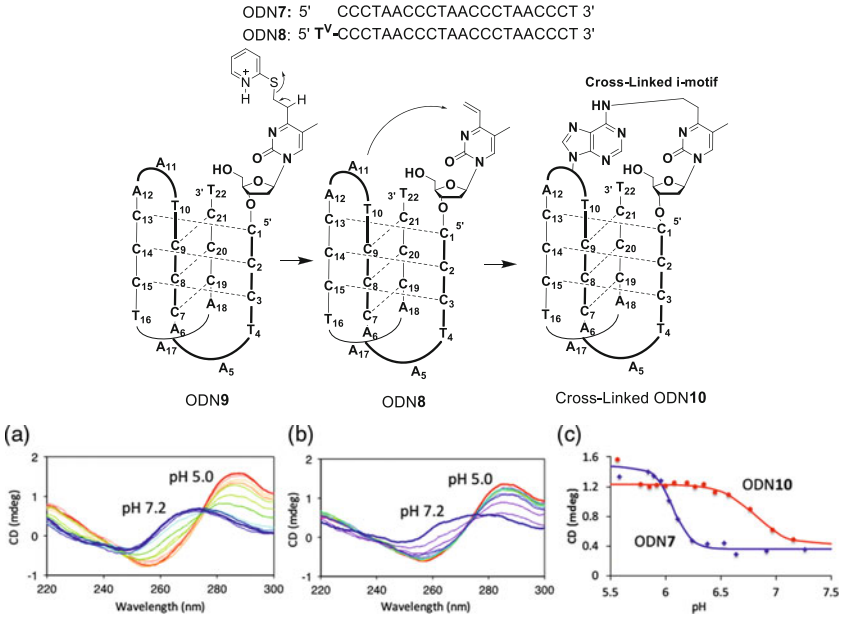

Fig. 11.5 The i-motif sequences and the expected intra-strand cross-linking. (**a**) pH-dependent CD of natural ODN**7**. (**b**) pH-Dependent CD of the cross-linked ODN**10**. (**c**) pH-dependent CD intensity at 286 nm. 2 μM ODN in 10 mM sodium cacodylate buffer containing 100 mM KCl at 20 °C

This chapter has dealt mainly with T-vinyl as the new cross-linking agent. This new molecule may find attractive applications due to its built-in mechanism for inducible reactivity. Further biological application is now ongoing in our group.

11.3 Alkylating Oligonucleotides

In the cross-linking reaction, nucleic acid strands are covalently connected. In the case where nucleic acids are modified without forming cross-link, the reaction is referred to as an alkylation. Biological alkylation such as 5-methylation of 2-′-deoxycytidine of DNA, 6*N*-methylation of adenosine of RNA, and 2′-*O*-methylation of the RNA ribose parts play significant roles in epigenetic control of gene expression. Therefore, chemical modification methods have been widely used for the study of function of structure of nucleic acids. Early works on the chemical modification methods of nucleic acids have been reviewed [54]. In this chapter, the basic strategy and recent development will be discussed [55].

11.3.1 Design and Synthesis of the Functionality-Transfer Reaction

The first example has been demonstrated by the nitrosyl group transfer from 6S of 6-thioguanine to the 4-amino group of the cytosine, leading to the site-selective deamination [56]. This strategy has been generalized as a functionality-transfer reaction for the site-specific modification of RNA. The ODN probe incorporating 2′-deoxy-6-thioguanosine (6-thio-dG) was functionalized with the 2-vinyliden-1,3-diketo moiety (**20**), and the transfer was accomplished by a sequential reaction of a Michael addition by the 4-amino group of the cytosine base followed by β-elimination of 6-thio-dG (Fig. 11.6) [57]. Subsequently, it was found that the transfer reaction with selectively enhanced for the 2-amino group of the guanine base at alkaline or neutral pH in the presence of $NiCl_2$ [58, 59]. This method was applied to the site-specific labeling of RNA [60] and O^6-methyl guanosine-containing DNA [61]. The functionality-transfer ODN probe (FT-ODN) is advantageous for RNA modification in that the driving force for promotion of the transfer is only duplex formation with the target RNA. This feature represents a contrast to other methods that use activation stimuli such as photo-irradiation or oxidation. For this strategy to be useful in the biological system, the transfer group is needed to be more stable and more reactive. Thus, we have contrived a new mechanism for induction of transfer reactivity. A pyridinyl vinyl ketone moiety was designed so that electrophilicity of the vinyl group would be enhanced through complexation with a metal cation (Fig. 11.6, **22**). The 6-thio-dG containing ODN was functionalized with (*E*)-2-idovinylpyridinylketone to produce the vinylsulfide transfer group with (*E*)-selectivity (Fig. 11.7). The use of the (*E*)-2-isomer is important, because the (*Z*)-isomer gave (*Z*)-vinylsulfide transfer group as the major isomer which did not promote the transfer reaction.

11.3.2 Selective Alkylation of Cytidine of RNA

The transfer reaction was performed at 37 °C using 5 μM of RNA**11** and 7.5 μM of ODN**11** in 50 mM HEPES buffer containing 100 mM NaCl at pH 7. The yields of modified RNA**11** obtained under different conditions are plotted against time in Fig. 11.8. In the presence of 5 μM $NiCl_2$, the transfer reaction with (*E*)-ODN**11** proceeded rapidly and was complete before 10 min to produce modified RNA**11** in approximately 90 % yield (solid line in Fig. 11.8). The transfer yield at 10 min was improved from ca 1 % to ca. 90 % compared with the previous system with the use of the diketo transfer group, meaning more than 200-fold rate acceleration. As the reactivity of (*Z*)-ODN**11** was negligible, the transfer yield of approximately 40 % yield was due to (*E*)-isomer contained in ODN**11** (dotted line in Fig. 11.8). It should also be noted that $NiCl_2$ significantly increased the reaction rate for (*E*)-ODN**11** (continuous line vs. dashed line in Fig. 11.8). The bar graph in Fig. 11.8 summarizes

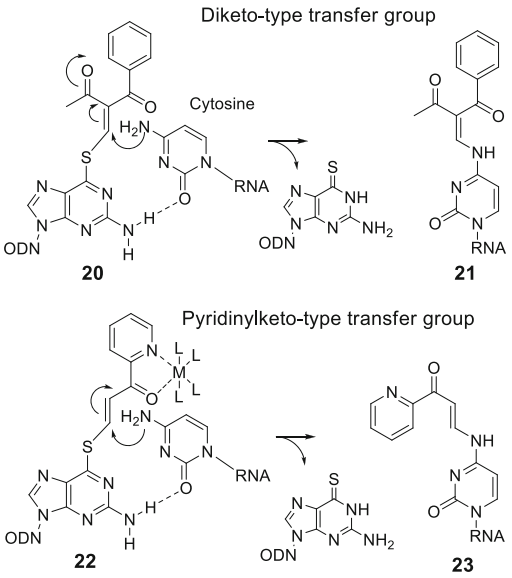

Fig. 11.6 Design of the functionality-transfer reaction to the 4-amino group of cytosine

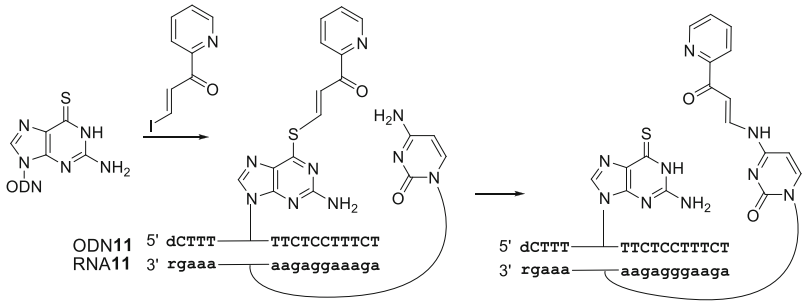

Fig. 11.7 Preparation of the functionality-transfer ODN bearing the pyridinyl keto-type transfer group and the subsequent transfer reaction to the 4-amino group of cytosine. S-functionalization: ODN**11** (50 μM) and the alkylating agent (500 μM) in 25 mM carbonate buffer at pH 10 and 0 °C for 30 min. Transfer reaction: 5 μM of RNA, 7.5 μM of ODN**11**, 50 mM HEPES, 5 μM of $NiCl_2$, and 100 mM NaCl, at pH 7

the transfer yields with (*E*)-ODN**11** at 10 min, which clearly shows a high selectivity for rC. EDTA completely inhibited the reaction by trapping metal cations in the buffer. The effect of other metal cations on activation is in the order of $Ni^{2+} > Co^{2+} > Cu^{2+}$, $Zn^{2+} > Ca^{2+}$, Mg^{2+}, Mn^{2+}, and Fe^{2+}. The maximum rate enhancement by $NiCl_2$ was reached at a concentration equimolar to the RNA substrate. Despite the fact that the transfer reaction of the pyridinyl vinyl ketone unit is activated by $NiCl_2$, the degradation half-life of (*E*)-FT-ODN**1** in the buffer

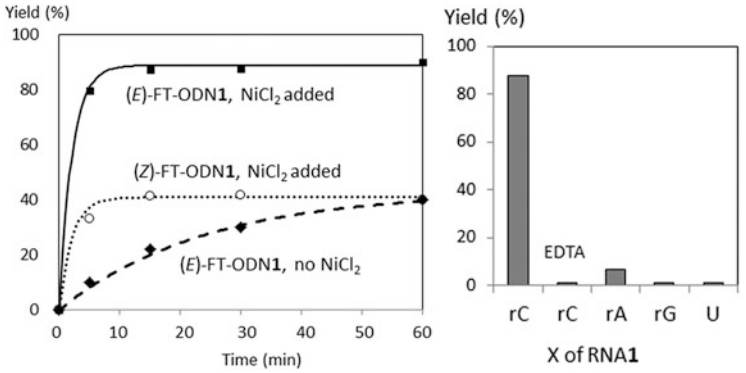

Fig. 11.8 Time course of the transfer reaction and the base selectivity. 5 μM of RNA, 7.5 μM of ODN**11**, 50 mM HEPES, 5 μM of $NiCl_2$, and 100 mM NaCl, at pH 7

(10–12 h) was not affected by $NiCl_2$. That is, the electrophilicity of (*E*)-FT-ODN**1** was not increased by $NiCl_2$.

11.3.3 Mechanism of Activation by $NiCl_2$

The transfer reaction was investigated with use of 16 different sequences with base pairs flanking the target rC, and it was clearly shown that neighboring adenine or guanine was essential for efficient transfer reaction. In particular, the reaction did not take place for the RNA substrate with 7-deazaguanosine instead of guanosine at the N5 side of rC. From the kinetic experiments, $NiCl_2$ accelerates the reaction by decreasing the entropy of activation ($-T\Delta S^{\ddagger}$). Considering that the functionality-transfer reaction proceeds through a Michael addition of the 4-NH_2 group and subsequent β-elimination of the 6-thio-dG residue (Fig. 11.9), $NiCl_2$ enhances the 1,4-addition step by forming a bridging complex between the pyridine keto unit and 7N of the purine base of the target RNA.

11.3.4 Selective Alkylation of Adenosine in RNA

For expansion of the functionality-transfer strategy, 2′-deoxy-4-thiothymidine (4-thioT) was used as a new platform to modify the 6-amino group of adenosine. The 4-thiothymidine unit in the ODN**12** was functionalized with the (*E*)-pyridinyl vinyl ketone transfer group, which was efficiently and specifically transferred to the

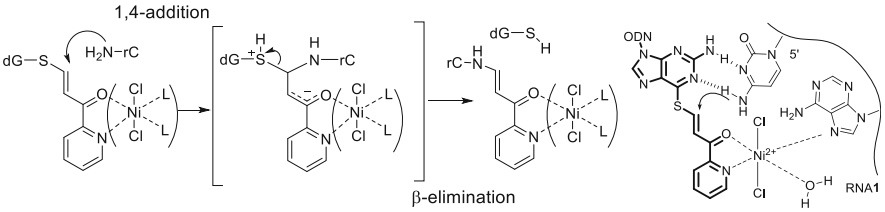

Fig. 11.9 Speculative mechanism for the activation of the transfer of the pyridinyl keto-type transfer group by $NiCl_2$

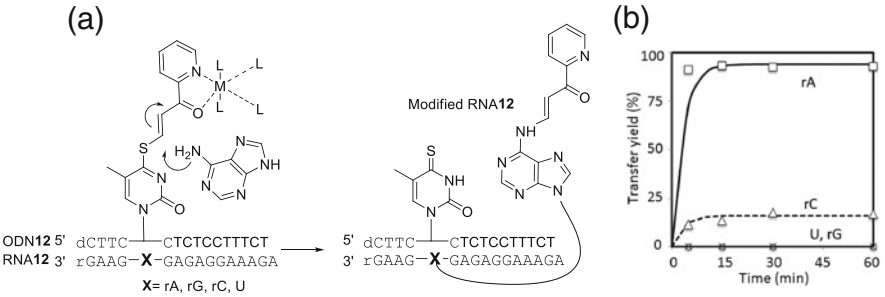

Fig. 11.10 (**a**) Design of the new functionality-transfer reaction to the 6-amino group of adenosine using 4S-functionalized 4-thiothymidine unit. (**b**) The time course of the transfer yields to rA, rC, rG, or U of RNA**12** using (*E*)-ODN**12**. The transfer reaction was performed at 37 °C using 1.0 μM RNA**12** (N^5 = rA, N^3 = rG) and 1.5 μM ODN**12** (M^5 = dC, M^3 = T) in a buffer containing 50 mM HEPES and 100 mM NaCl at pH 7.0

6-amino group of the target adenosine in RNA (Fig. 11.10). In this case, $CuCl_2$ more efficiently accelerated the reaction. This study has shown that 4-thioT is a new platform for specific modification of rA [62].

11.3.5 Application of Alkylating Oligonucleotides

The site-specific labeling of rC in RNA has been demonstrated by using an acetylene-functionalized pyridinyl keto unit (**8**) followed by Cu-catalyzed click reaction with azido derivatives (Biotin-N_3 and FAM-N_3). The diketo transfer group has been also applied to the selective modification of the 2-amino group of 2-′-deoxyguanosine. As mRNA can be specifically modified by the functionality-transfer strategy, we are now investigating the effects of the specific modification on the reverse-transcription and -translation reaction. Furthermore, this strategy is tested for specific modification of intracellular mRNA (Fig. 11.11).

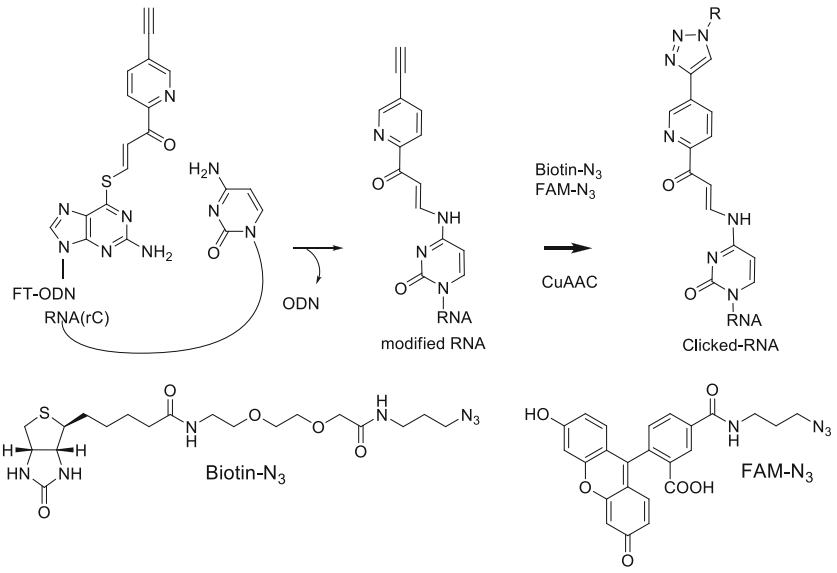

Fig. 11.11 Application of alkylating oligonucleotides for site-specific labeling of RNA

11.4 Sensing of 2′-Deoxy-8-Oxoguanosine

DNA in living organisms suffers from oxidative damage by reactive oxygen species to form a variety of oxidized nucleosides. 8-Oxo-2′-deoxyguanosine (8-oxo-dG) is a representative metabolite derived by the oxidation of 2′-deoxyguanosine (dG) and is known to induce G:C to T:A transversion mutations in DNA [20]. Several DNA repair enzymes remove 8-oxo-dG from the genome and the nucleotide pool, which is excreted from the cell. A number of studies have shown that the intracellular level of 8-oxo-dG is related to diseases and aging and that 8-oxo-dG is a biomarker for oxidative damage in cells. Currently, 8-oxo-guanine and the corresponding nucleosides (8-oxo-G and 8-oxo-dG) are typically analyzed via HPLC-ECD, HPLC-MS, etc. [63]. Nevertheless, small molecules with high specificity to 8-oxo-dG, especially those with fluorescence will find wider utility for development of sensors, biological tool, and so on. This chapter will deal with the fluorescent molecules for 8-oxo-dG in solution in the first part and those for 8-oxo-dG in DNA in the second part.

11.4.1 Design of OxoG-Clamp for Detection of 8-Oxo-dG in Solution

We have attempted to develop fluorescent small molecules for recognition of 8-oxo-dG. In a repair enzyme for 8-oxo-dG (hOGG1), 7-NH of 8-oxo-dG is

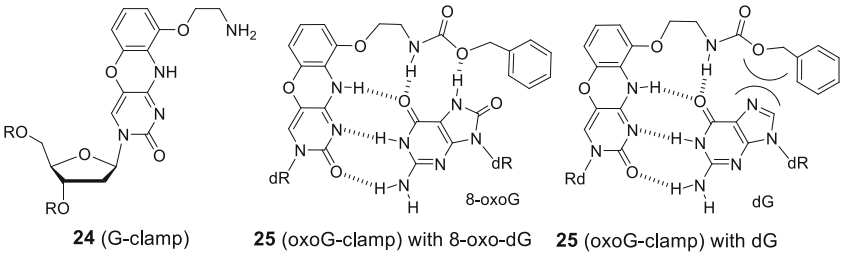

Fig. 11.12 Structure of G-clamp (**24**) and expected complex structure of oxoG-clamp (**25**) with 8-oxoG

recognized with one hydrogen bond, and no functional group is arranged to bind to the 8-oxygen atom [64]. Difficulty lies in the molecular design of small molecules to discriminate such small differences between dG and 8-oxo-dG. For designing selective molecule for 8-oxo-dG, we focused on the tricyclic cytosine derivative with selective affinity toward dG in DNA (G-clamp, **24**) [65, 66]. G-clamp is composed of phenoxazine with an aminoethoxy unit at the end (Fig. 11.12). In our approach, the derivatives were designed to have an additional functional group, benzyloxycarbonyl (**25**, Cbz) at the aminoethoxy terminal, and named "oxoG-clamp" (Fig. 11.12) [67]. It was expected that the carbamoyl group would form a hydrogen bond with 7N-H of 8-oxo-dG, whereas it would be repulsive to N7 of guanosine. Initially, the carbonyl oxygen of the Cbz group was thought to participate in hydrogen bonding. However, subsequent studies have indicated that the sp^3 oxygen of the carbamate is responsible for hydrogen bonding with 7N-H of 8-oxo-dG.

11.4.2 Sensing 8-Oxo-dG in Solution

A variety of 8-oxoG-clamp derivatives having different carbamate units and substitution of the phenoxazine part were synthesized [68, 69]. Among them, oxoG-clamp derivatives bearing benzyloxycarbonyl (**25**(Cbz),) naphthylethyloxycarbonyl (**25**(EtNaph)), and pyrenylethyloxycarbonyl (**25**(EtPyr)) exhibited high selectivity for 8-oxo-dG (Fig. 11.13). Stronger stacking interaction was postulated for the pyrene and naphthalene units. The ethyl linker may be suitable to locate the aromatic ring for staking with 8-oxo-dG (Fig. 11.14). Selectivity of the ureido derivative (NHEt) returned to dG due to hydrogen bonding with 7N of dG.

The oxoG-clamp derivatives (**25**) possess intrinsic fluorescence at about 450 nm with excitation at 365 nm. Their binding properties were investigated by titration experiments using the bis(TBDMS)protected oxoG-clamp derivatives (**25**) and 3′*O*,5′*O*-disilylated derivatives of dA, dG, dC, dT, or 8-oxo-dG (2′-deoxy-8-oxoguanosine) in a chloroform solution buffered with an organic base and acid (triethylamine–acetic acid, pH 7.0 in water). It should be noted that fluorescence of

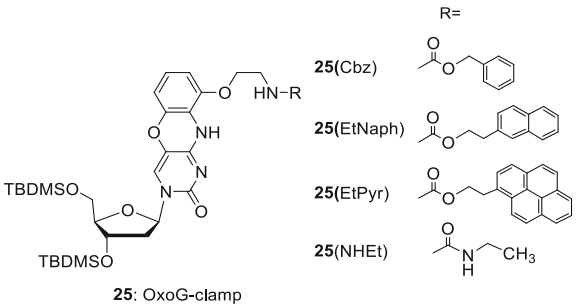

Fig. 11.13 Structure of variety of G-clamp derivatives

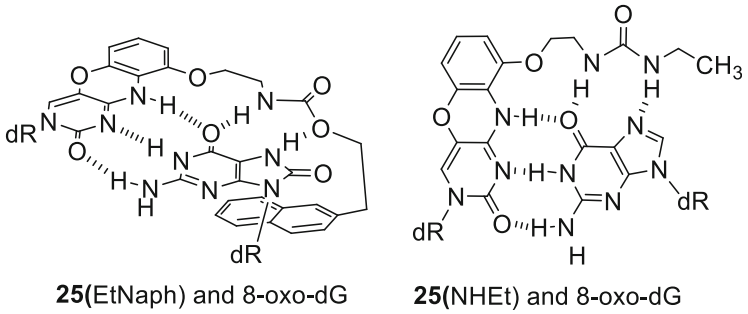

Fig. 11.14 Plausible complex structures

(Cbz) was effectively quenched by the addition of 8-oxo-dG. In a remarked contrast, almost no fluorescence quenching was observed with dG, dA, dC, or dT (Fig. 11.15). These results have clearly demonstrated high selectivity of **25**(Cbz) for 8-oxo-dG. A 1:1 ratio of the complex between **25**(Cbz) and 8-oxo-dG was confirmed by Job plot and by ESI-MS measurements, and multiple hydrogen bonds of the complex were confirmed by ^{1}H-NMR measurements. The binding constant of the complex between **25**(Cbz) and 8-oxo-dG. Among the carbamate-type 8-oxoG-clamp, the naphthalene derivative **25**(EtNaph) displayed highest affinity to 8-oxo-dG, suggesting possible involvement of a stacking interaction between the naphthalene and the 8-oxoguanosine part (Fig. 11.14). The selectivity of the urea-type oxoG-clamp (NHEt) was changed to dG, clearly demonstrating that the hydrogen bond with 7N of 8-oxo-dG or dG determines the selectivity.

Selective sensing of 8-oxo-dG by 8-oxoG-clamp is possible due to the formation of multiple hydrogen-bonded complex, in which the hydrogen bond with 7NH is significantly important for discrimination from dG. Our laboratory is now attempting to apply this sensing system for detection of intra- and extracellular 8-oxo-dG by overcoming the difficulty in forming hydrogen-bonded complex in aqueous solution.

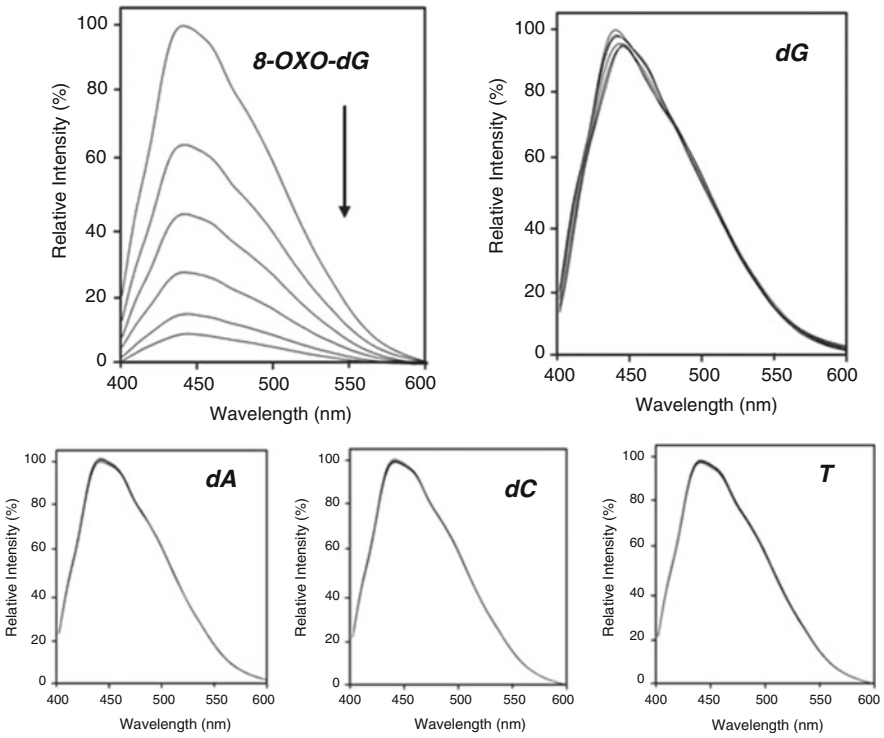

Fig. 11.15 Selective fluorescent quenching of G-clamp derivatives by 8-oxo-dG. 1 μM Cbz-8-oxoG-clamp (3′*O*,5′*O*-di-TBS), 0–10 μM target nucleoside (3′*O*,5′*O*-di-TBS) in $CHCl_3$ (10 mM TEA + 2.7 mM AcOH) at 25 °C, excitation 365 nm

11.4.3 Design of Adenosine-Diazaphenoxazine Analog for 8-Oxo-dG in DNA

Theoretical studies on the formation of 8-oxo-dG in DNA suggest a distinctive nonrandom pattern for the genome-wide distribution of 8-oxo-dG in DNA [70], along with sequence-specific DNA damage in the -GGG- context of synthesized telomeric repeat sequences [71, 72]. Sequencing of 8-oxo-dG and 8-oxo-G is important due to biological significant impact on mutation, transcription, and translation. Several methods have been developed for detecting 8-oxo-dG in DNA using antibodies [73], small molecules [74, 75], nanopore systems [76], high mass accuracy mass spectrometry [77], and engineered luciferases [78], but these methods are not suitable for analyzing the sequences of intact DNA samples. The above chapter introduced 8-oxoG-clamp as a recognition molecule for 8-oxodG in solution. The 8-oxoG-clamp in the ODN was shown to have a limitation for sensing 8-oxodG in DNA [79]. It was thought that the 8-oxoG-clamp hardly formed a selective base pair with 8-oxodG in the DNA duplex. Accordingly, we designed a new recognition molecule by focusing on the conformational isomers around the glycosidic bond of 8-oxodG in DNA [80].

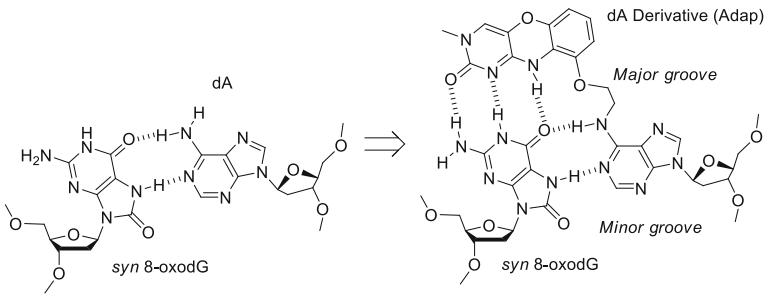

Fig. 11.16 The design of *a*denosine-*diaza*phenoxazine analog (Adap) for selective base pair formation with 8-oxo-dG in DNA

In duplex DNA, the guanine base of dG adopts the *anti*-conformation, whereas the 8-oxoguanine base of 8-oxo-dG prefers the *syn*-conformation with the Hoogsteen face forming a base pair with dA (Fig. 11.16). Accordingly, the new dA derivative was designed to connect the 1,3-diazaphenoxazine unit to the 6-amino group of dA through the ethoxy spacer. The 1,3-diazaphenoxazine skeleton might form hydrogen bonds with the Watson–Crick face of 8-oxodG in the major groove of DNA (Fig. 11.16). The new *a*denosine-*diaza*phenoxazine analog was abbreviated as Adap.

11.4.4 Synthesis of Adap

The synthesis of the key intermediate 1,3-diazaphenoxazine derivative (**30**) was started with *N*1-methyl-5-bromouracil. The substitution of the chloride of 2′*O*-, 5′*O*-diTBS-6-chloroadenosine by **30** was performed in the presence of DIPEA under reflux conditions to produce the TBDMS-protected Adap compound (**31**). After removal of the TBDMS groups of **31**, the resulting diol compound (**32**) was transformed into the amidite precursor (**33**) according to the conventional method. The Adap was incorporated into ODN with a variety of sequences by applying the amidite precursor (**33**) to the automated DNA synthesizer (Scheme 11.2).

11.4.5 The Thermal Stabilization Effects of Adap

The thermal stabilization effects of Adap were investigated using the duplex formed with ODN**13** and ODN**14** by measuring the T_m values in the buffer containing 100 mM NaCl and 10 mM sodium phosphate at pH 7.0 (Fig. 11.17). It should be noted that a selective stabilization was observed for the combination of Adap in **ODN13** and 8-oxodG in **ODN14**. The combinations of Adap with the other natural nucleobases showed lower melting temperatures; T_m (°C): 47.2 (oxodG) vs

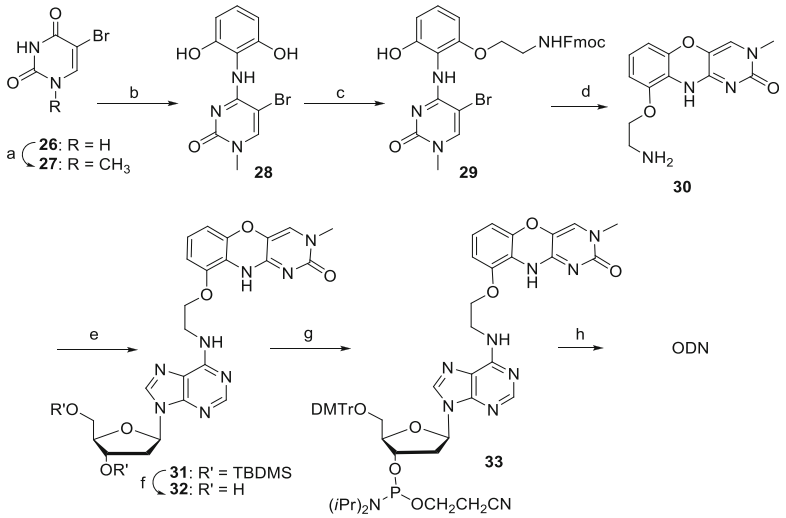

Scheme 11.2 Synthesis of Adap and its phoshporamidite. (a) (1) HMDS, reflux, and then CH_3I, MeCN, r.t. to reflux, (b) PPh_3, CCl_4, CH_2Cl_2, reflux, then 2,6-dihydroxy-aniline, DBU, (c) *N*-Fmoc-2-aminoethanol, PPh_3, DIAD, CH_2Cl_2, (d) 7 M ammonia in MeOH, (e) 2′*O*-,5′*O*-diTBS-6-chloroadenosine, DIPEA, 1-propanol, reflux, (f) TBAF, THF, (g) (1) DMTrCl, pyridine, (2) 2-Cyanoethyl-*N*,*N*′-diisopropylchlorophosphorodiamidite, DIPEA, CH_2Cl_2, (h) DNA automated synthesizer

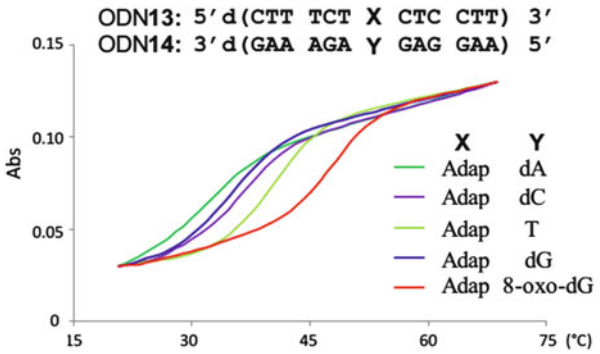

Fig. 11.17 UV-melting profiles measured using 2 μM each of the ODN strand in 100 mM NaCl and 10 mM sodium phosphate buffer at pH 7.0

31.6 (dA), 36.5 (dC), 39.6 (T), 33.9 (dG). The high selectivity is represented by significant difference in the T_m values between dG and 8-oxodG as high as 13.3 °C.

11.4.6 Sensing of 8-Oxo-dG in DNA by Adap

We next applied Adap to the fluorescent detection of 8-oxodG in DNA. The fluorescent spectra of **ODN13** containing Adap was measured in the absence and

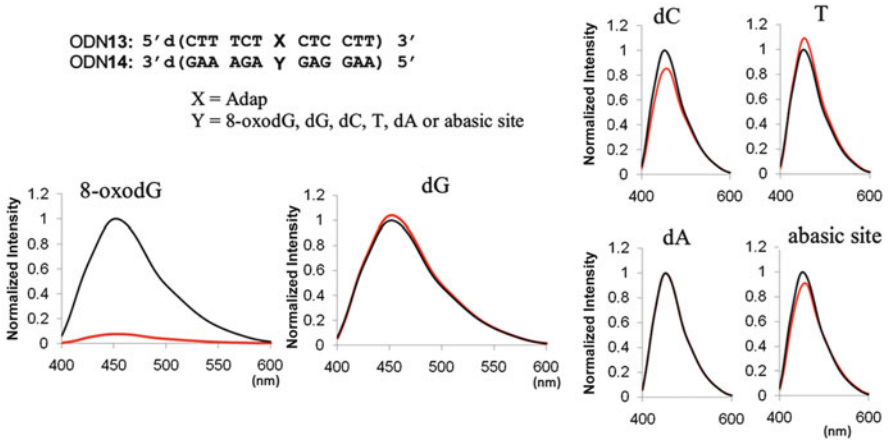

Fig. 11.18 Fluorescence quenching of Adap in **ODN13** by **ODN14**. Conditions: 100 mM NaCl and 10 mM sodium phosphate buffer at pH 7.0 and 30 °C. λ_{ex} 365 nm

the presence of **ODN14** having 8-oxodG, dG, dC, dT, dA, or dAP. The effective fluorescence quenching was observed only in the duplex formed with **ODN13** and **ODN14**(Y=8-oxodG,). No quenching was observed for dG, dC, T, dA, or dAP at Y of **ODN14** (Fig. 11.18). The quenching efficiency is high that the presence of 8-oxodG in the duplex DNA can be visually detected. The formation of a tight complex between Adap and 8-oxodG plays a key role in efficient and selective fluorescent quenching.

11.4.7 Single Nucleotide Primer Extension Using Triphosphate of Adap for Sensitive Detection of 8-Oxo-dG in DNA

The selective base pair of Adap with 8-oxo-dG can be detected by increase of fluorescence based on the FRET strategy accompanied by strand exchange reaction [81, 82]. The detection accuracy of this FRET strategy is based on the thermal stability of the duplex containing the Adap and 8-oxodG pair, and thereby requiring substantial trial and error to develop useful probes for detection of 8-oxo-dG. In the meantime, single-base extension technology is a useful tool for performing genotyping [83], and unnatural nucleosides, including universal nucleobase analogues, are being applied to the development of DNA sequencing technologies [84, 85]. Thus, we attempted to apply the Adap triphosphate (dAdapTP) to the enzymatic primer extension reaction for selective detection of 8-oxo-dG amid a large amount of dG in DNA [86] (Fig. 11.19).

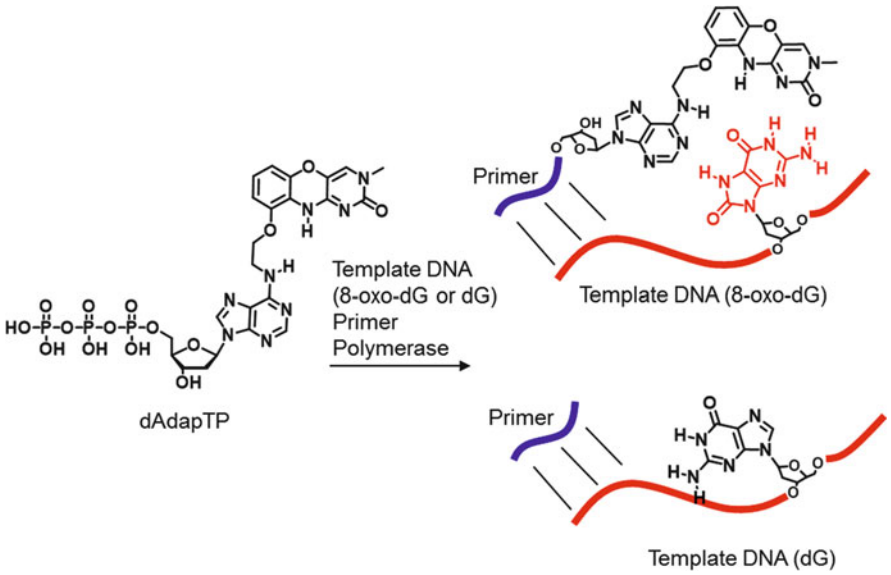

Fig. 11.19 The conceptual scheme of the application of the Adap triphosphate to the primer extension reaction for selective detection of 8-oxo-dG

The triphosphate of Adap, dAdapTP, was synthesized starting from the Adap diol, through the 3′-acetoxy Adap derivative as the intermediate. To identify the base preference of dAdapTP, single nucleotide primer extension reactions were performed using a 25-mer template, FAM-labeled 15-mer primer, and the Klenow fragment (Kf exo$^-$). Preferential extension was observed for the templates containing 8-oxo-dG or T; a somewhat lower efficiency was found for the dA template, and no significant extension occurred for the template ODNs that included dG or dC. Unfortunately, dAdapTP was incorporated opposite T even better than 8-oxo-dG because Adap has the dA skeleton. Importantly, 8-oxo-dG and dG in the template ODNs were completely discriminated.

This primer extension technology has been applied to the sequence-specific detection of 8-oxo-dG in telomeric DNA. The oxidation of dG in telomeric DNA is well known to be related to the aging, and telomeric DNA is more susceptible to oxidative base damage than non-telomeric regions in vivo. Two primers were designed for the synthetic 25-mer template ODN based on a human telomere repeat, $(TTAGGG)_4$. Template contains dG or 8-oxo-dG at X and Y position. Cy5- and Cy3 primers were designed to detect 8-oxo-dG at X and that at Y, respectively (Fig. 11.20). The Cy5 primer was extended only for template with 8-oxo-dG at X. On the other hand, the Cy3 primer was elongated only for template with 8-oxo-dG at Y. 8-Oxo-dG and dG in the human telomere sequence have been fully discriminated by the single nucleotide extension reaction using dAdapTP (Fig. 11.21).

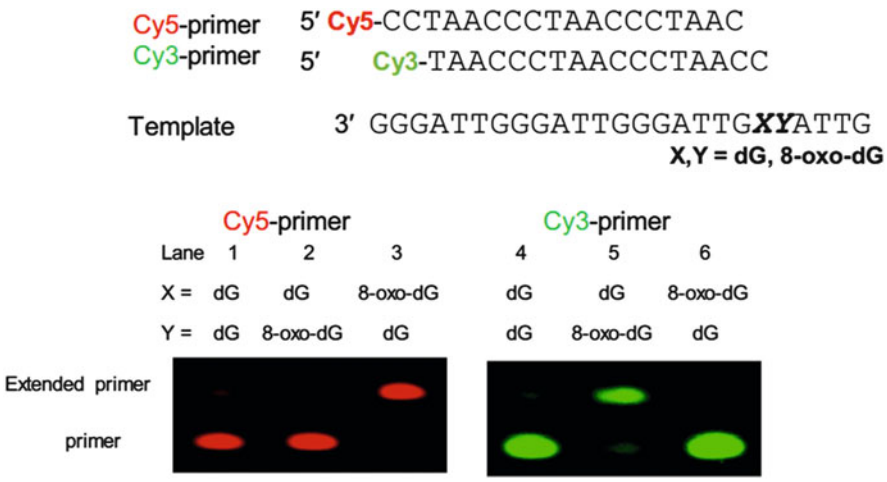

Fig. 11.20 Sequence-specific incorporation of dAdapTP for 8-oxo-dG. Cy5 primer and Cy3 primer were extended only for 8-oxo-dG at X or Y, respectively. 1.0 μM each primer and template. 0.1 unit/μL Kf(exo−), 10 mM Tris-HCl (pH 7.9), 50 mM NaCl, 10 mM $MgCl_2$, 1 mM DTT, and 62.5 μM either dAdapTP incubated at 37 °C for 10 min

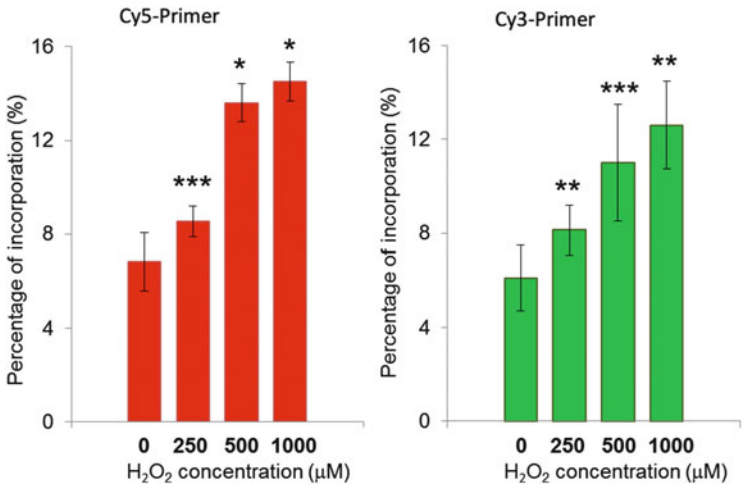

Fig. 11.21 Single nucleoside primer extension reactions in DNA (10 μg, 30 nmol in nucleotides) from HeLa cells treated with various concentrations of H_2O_2

This method has been applied to detect 8-oxo-dG in telomere DNA prepared from H_2O_2-treated HeLa. HeLa cells were cultured in medium containing H_2O_2, and DNA was extracted using an established procedure. Both Cy5- and Cy3 primers showed AdapTP extension to some extent for DNA isolated from H_2O_2-untreated HeLa DNA as a control. These results may indicate 8-oxo-dG in the telomere

formed endogenously or generated during the extraction process. The incorporation of Adap increased in a dose-dependent manner along with the concentration of H_2O_2 solution in the media. The increase rate of the Cy5-primer extension was higher than that of the Cy3 primer. As the Cy3-primer extension is strongly affected by the presence of two continuous 8-oxo-dG residues, these results likely arose from the multiple or excess oxidative sites of -GGG- sequence that might interfere with the incorporation of dAdapTP into the primer strands.

11.5 Conclusion and Perspectives

Chemical modifications of nucleic acids play a vital role of their function in living systems and regulated by highly sophisticated systems. In contrast, endogenous and exogenous randomly react with nucleic acids to cause toxicity; therefore, they are regarded as damaged nucleic acid. This chapter has dealt with alkylation and oxidation of nucleic acids. In contrast to random reactions, controlled alkylation and cross-linking of nucleic acids have potential benefits as biological tools for mechanistic study and technology of gene expression. In the first two parts, the new technologies with alkylating (functionality transfer) and cross-linking (T-vinyl) oligonucleotides have been introduced. A key feature of these reactive oligonucleotides is that highly selective reactivity is induced by activation triggered hybridization with the target sequence. The cross-linking oligonucleotides were shown in a preliminary study to exhibit efficient inhibition of gene expression with single nucleotide selectivity. The cross-linking and alkylating oligonucleotides are expected to have biological function by acting in the transcription and translation, which are now under investigation in our group.

8-Oxoguanine is a most frequently formed oxidative damage, which displays strong genotoxicity. The last part of this chapter has introduced new recognition molecules for sensing 8-oxoguanine in solution (oxo-Gclamp) as well as in DNA (Adap). Oxo-Gclamp derivatives are now being tested for devises for sensing 8-oxo-dG in blood or urine. The Adap triphosphate is potentially applicable to DNA amplification, which will broaden utility of new sensing technology for 8-oxoguanosine.

References

1. Jackson SP, Bartek J (2009) The DNA-damage response in human biology and disease. Nature 461:1071–1078. doi:10.1038/nature08467
2. Stone MP, Huang H, Brown KL, Shanmugam G (2011) Chemistry and structural biology of DNA damage and biological consequences. Chem Biodivers 8:1571–1615. doi:10.1002/cbdv.201100033
3. Jena NR (2012) DNA damage by reactive species: mechanisms, mutation and repair. J Biosci 37:503–517. doi:10.1007/s12038-012-9218-2

4. Motgomery JA (1995) Antimetabolites. In: Foye WO (ed) Cancer chemotherapeutic agents. American Chemical Society, Washington, DC, pp 111–204
5. Grillari J, Katinger H, Voglauer R (2007) Contributions of DNA interstrand cross-links to aging of cells and organisms. Nucleic Acids Res 35:7566–7576. doi:10.1093/nar/gkm1065
6. Toussaint M, Levasseur G, Tremblay M, Paquette M, Conconi A (2005) Psoralen photocrosslinking, a tool to study the chromatin structure of RNA polymerase I—transcribed ribosomal genes. Biochem Cell Biol 83:449–459. doi:10.1139/o05-141
7. Murakami A, Yamayoshi A, Iwase R, Nishida J, Yamaoka T, Wake N (2001) Photodynamic antisense regulation of human cervical carcinoma cell growth using psoralen-conjugated oligo (nucleoside phosphorothioate). Eur J Pharm Sci 13:25–34. doi:10.1016/S0928-0987(00)00204-9
8. Higuchi M, Kobori A, Yamayoshi A, Murakami A (2009) Synthesis of antisense oligonucleotides containing 2′-O-psoralenylmethoxyalkyl adenosine for photodynamic regulation of point mutations in RNA. Bioorg Med Chem 17:475–483. doi:10.1016/j.bmc.2008.12.001
9. Li Y, Tseng YD, Kwon SY, D'Espaux L, Bunch JS, McEuen PL, Luo D (2004) Controlled assembly of dendrimer-like DNA. Nat Mater 3:38–42. doi:10.1038/nmat1045
10. Tagawa M, Shohda K, Fujimoto K, Suyama A (2011) Stabilization of DNA nanostructures by photo-cross-linking. Soft Matter 7:10931. doi:10.1039/c1sm06303k
11. Rajendran A, Endo M, Katsuda Y, Hidaka K, Sugiyama H (2011) Photo-cross-linking-assisted thermal stability of DNA origami structures and its application for higher-temperature self-assembly. J Am Chem Soc 133:14488–14491. doi:10.1021/ja204546h
12. Glick GD (2003) Engineering terminal disulfide bonds into DNA. In: Beaucage SL (ed) Current protocols in nucleic acid chemistry, vol 2. Wiley, New York, pp 5.7.1–5.7.13. doi:10.1002/0471142700.nc0507s13
13. Nakatani K, Yoshida T, Saito I (2002) Photochemistry of benzophenone immobilized in a major groove of DNA: formation of thermally reversible interstrand cross-link. J Am Chem Soc 124:2118–2119. doi:10.1021/ja017611r
14. Fujimoto K, Konishi-Hiratsuka K, Sakamoto T, Yoshimura Y (2010) Site-specific photochemical RNA editing. Chem Commun (Camb) 46:7545–7547. doi:10.1039/c0cc03151h
15. Zhou Q, Rokita SE (2003) A general strategy for target-promoted alkylation in biological systems. Proc Natl Acad Sci U S A 100:15452–15457. doi:10.1073/pnas.2533112100
16. Rokita SE (ed) (2009) Quinone methides. Wiley, New York, pp 297–327
17. Peng X, In SH, Li H, Seidman MM, Greenberg MM (2008) Interstrand cross-link formation in duplex and triplex DNA by modified pyrimidines. J Am Chem Soc 130:10299–10306. doi:10.1021/ja802177u
18. Op de Beeck M, Madder A (2012) Sequence specific DNA cross-linking triggered by visible light. J Am Chem Soc 134:10737–10740. doi:10.1021/ja301901p
19. Evans MD, Dizdaroglu M, Cooke MS (2004) Oxidative DNA damage and disease: induction, repair and significance. Mutat Res Rev Mutat Res 567:1–61. doi:10.1016/j.mrrev.2003.11.001
20. Shibutani S, Takeshita M, Grollman AP (1991) Insertion of specific bases during DNA synthesis past the oxidation-damaged base 8-oxodG. Nature 349:431–434. doi:10.1038/349431a0
21. Nagatsugi F, Kawasaki T, Usui D, Maeda M, Sasaki S (1999) Highly efficient and selective cross-linking to cytidine based on a new strategy for auto-activation within a duplex. J Am Chem Soc 121:6753–6754. doi:10.1021/ja990356e
22. Nagatsugi F, Tokuda N, Maeda M, Sasaki S (2001) A new reactive nucleoside analogue for highly reactive and selective cross-linking reaction to cytidine under neutral conditions. Bioorg Med Chem Lett 11:2577–2579. doi:10.1016/S0960-894X(01)00505-4
23. Nagatsugi F, Matsuyama Y, Maeda M, Sasaki S (2002) Selective cross-linking to the adenine of the TA interrupting site within the triple helix. Bioorg Med Chem Lett 12:487–489. doi:10.1016/S0960-894X(01)00783-1

24. Kawasaki T, Nagatsugi F, Ali MM, Maeda M, Sugiyama K, Hori K, Sasaki S (2005) Hybridization-promoted and cytidine-selective activation for cross-linking with the use of 2-amino-6-vinylpurine derivatives. J Org Chem 70:14–23. doi:10.1021/jo048298p
25. Sasaki S, Nagatsugi F (2006) Application of unnatural oligonucleotides to chemical modification of gene expression. Curr Opin Chem Biol 10:615–621. doi:10.1016/j.cbpa.2006.10.006
26. Nagatsugi F, Imoto S (2011) Induced cross-linking reactions to target genes using modified oligonucleotides. Org Biomol Chem 9:2579–2585. doi:10.1039/c0ob00819b
27. Ali MM, Oishi M, Nagatsugi F, Mori K, Nagasaki Y, Kataoka K, Sasaki S (2006) Intracellular inducible alkylation system that exhibits antisense effects with greater potency and selectivity than the natural oligonucleotide. Angew Chem Int Ed 45:3136–3140. doi:10.1002/anie.200504441
28. Nagatsugi F, Sasaki S, Miller PS, Seidman MM (2003) Site-specific mutagenesis by triple helix-forming oligonucleotides containing a reactive nucleoside analog. Nucleic Acids Res 31:e31. doi:10.1093/nar/gng031
29. Taniguchi Y, Kurose Y, Nishioka T, Nagatsugi F, Sasaki S (2010) The alkyl-connected 2-amino-6-vinylpurine (AVP) crosslinking agent for improved selectivity to the cytosine base in RNA. Bioorg Med Chem 18:2894–2901. doi:10.1016/j.bmc.2010.03.008
30. Imoto S, Hori T, Hagihara S, Taniguchi Y, Sasaki S, Nagatsugi F (2010) Alteration of cross-linking selectivity with the 2′-OMe analogue of 2-amino-6-vinylpurine and evaluation of antisense effects. Bioorg Med Chem Lett 20:6121–6124. doi:10.1016/j.bmcl.2010.08.027
31. Imoto S, Chikuni T, Kansui H, Kunieda T, Nagatsugi F (2012) Fast DNA interstrand cross-linking reaction by 6-vinylpurine. Nucleosides Nucleotides Nucleic Acids 31:752–762. doi:10.1080/15257770.2012.726756
32. Hagihara S, Kusano S, Lin WC, Chao XG, Hori T, Imoto S, Nagatsugi F (2012) Production of truncated protein by the crosslink formation of mRNA with 2′-OMe oligoribonucleotide containing 2-amino-6-vinylpurine. Bioorg Med Chem Lett 22:3870–3872. doi:10.1016/j.bmcl.2012.04.123
33. Hagihara S, Lin W-C, Kusano S, Chao X, Hori T, Imoto S, Nagatsugi F (2013) The crosslink formation of 2′-OMe oligonucleotide containing 2-amino-6-vinylpurine protects mRNA from miRNA-mediated silencing. ChemBioChem 14:1427–1429. doi:10.1002/cbic.201300382
34. Kusano S, Haruyama T, Ishiyama S, Hagihara S, Nagatsugi F (2014) Development of the crosslinking reactions to RNA triggered by oxidation. Chem Commun (Camb) 50:3951–3954. doi:10.1039/c3cc49463b
35. Hattori K, Hirohama T, Imoto S, Kusano S, Nagatsugi F (2009) Formation of highly selective and efficient interstrand cross-linking to thymine without photo-irradiation. Chem Commun (Camb) (42):6463–6465. doi:10.1039/b915381k
36. Murat P, Balasubramanian S (2014) Existence and consequences of G-quadruplex structures in DNA. Curr Opin Genet Dev 25:22–29. doi:10.1016/j.gde.2013.10.012
37. Henderson A, Wu Y, Huang YC, Chavez EA, Platt J, Johnson FB, Brosh RM, Sen D, Lansdorp PM (2014) Detection of G-quadruplex DNA in mammalian cells. Nucleic Acids Res 42:860–869. doi:10.1093/nar/gkt957
38. Parkinson GN, Lee MPH, Neidle S (2002) Crystal structure of parallel quadruplexes from human telomeric DNA. Nature 417:876–880. doi:10.1038/nature755
39. Phan AT, Modi YS, Patel DJ (2004) Propeller-type parallel-stranded G-quadruplexes in the human c-myc promoter. J Am Chem Soc 126:8710–8716. doi:10.1021/ja048805k
40. Lam EYN, Beraldi D, Tannahill D, Balasubramanian S (2013) G-quadruplex structures are stable and detectable in human genomic DNA. Nat Commun 4:1796. doi:10.1038/ncomms2792
41. Brooks TA, Kendrick S, Hurley L (2010) Making sense of G-quadruplex and i-motif functions in oncogene promoters. FEBS J 277:3459–3469. doi:10.1111/j.1742-4658.2010.07759.x
42. Gehring K, Leroy JL, Guéron M (1993) A tetrameric DNA structure with protonated cytosine-cytosine base pairs. Nature 363:561–565. doi:10.1038/363561a0

43. Leroy JL, Guéron M, Mergny JL, Hélène C (1994) Intramolecular folding of a fragment of the cytosine-rich strand of telomeric DNA into an i-motif. Nucleic Acids Res 22:1600–1606. doi:10.1093/nar/22.9.1600
44. Mergny J, Lacroix L, Han X, Leroy J, Helene C (1995) Intramolecular folding of pyrimidine oligodeoxynucleotides into an i-DNA motif. J Am Chem Soc 117:8887–8898. doi:10.1021/ja00140a001
45. Zhou J, Wei C, Jia G, Wang X, Feng Z, Li C (2010) Formation of i-motif structure at neutral and slightly alkaline pH. Mol Biosyst 6:580–586. doi:10.1039/b919600e
46. Day HA, Huguin C, Waller ZAE (2013) Silver cations fold i-motif at neutral pH. Chem Commun 49:7696–7698
47. Dong Y, Yang Z, Liu D (2014) DNA nanotechnology based on i-motif structures. Acc Chem Res 47:1853–1860. doi:10.1021/ar500073a
48. Day HA, Pavlou P, Waller ZAE (2014) i-Motif DNA: structure, stability and targeting with ligands. Bioorg Med Chem 22:4407–4418. doi:10.1016/j.bmc.2014.05.047
49. Cui J, Waltman P, Le VH, Lewis EA (2013) The effect of molecular crowding on the stability of human c-MYC promoter sequence I-motif at neutral pH. Molecules 18:12751–12767. doi:10.3390/molecules181012751
50. Rajendran A, Nakano S, Sugimoto N (2010) Molecular crowding of the cosolutes induces an intramolecular i-motif structure of triplet repeat DNA oligomers at neutral pH. Chem Commun (Camb) 46:1299–1301. doi:10.1039/b922050j
51. Bhavsar-Jog YP, Van Dornshuld E, Brooks TA, Tschumper GS, Wadkins RM (2014) Epigenetic modification, dehydration, and molecular crowding effects on the thermodynamics of i-motif structure formation from C-rich DNA. Biochemistry 53:1586–1594. doi:10.1021/bi401523b
52. Kikuta K, Haishun P, Brazier J, Taniguchi Y, Onizuka K, Nagatsugi F, Sasaki S (2015) Stabilization of the i-motif structure by the intrastrand cross-link formation. Bioorg Med Chem Lett 25(16):3307–3310
53. Kaushik M, Suehl N, Marky LA (2007) Calorimetric unfolding of the bimolecular and i-motif complexes of the human telomere complementary strand, d(C(3)TA(2))(4). Biophys Chem 126:154–164. doi:10.1016/j.bpc.2006.05.031
54. Sasaki S, Onizuka K, Taniguchi Y (2011) The oligodeoxynucleotide probes for the site-specific modification of RNA. Chem Soc Rev 40:5698. doi:10.1039/c1cs15066a
55. Jitsuzaki D, Onizuka K, Nishimoto A, Oshiro I, Taniguchi Y, Sasaki S (2014) Remarkable acceleration of a DNA/RNA inter-strand functionality transfer reaction to modify a cytosine residue: the proximity effect via complexation with a metal cation. Nucleic Acids Res 42:8808–8815. doi:10.1093/nar/gku538
56. Ali M, Alam R, Kawasaki T, Nakayama S, Nagatsugi F, Sasaki S (2004) Sequence- and base-specific delivery of nitric oxide to cytidine and 5-methylcytidine leading to efficient deamination. J Am Chem Soc 126:8864–8865. doi:10.1021/ja0498888
57. Onizuka K, Taniguchi Y, Sasaki S (2009) Site-specific covalent modification of RNA guided by functionality-transfer oligodeoxynucleotides. Bioconjug Chem 20:799–803. doi:10.1021/bc900009p
58. Onizuka K, Taniguchi Y, Sasaki S (2010) A new usage of functionalized oligodeoxynucleotide probe for site-specific modification of a guanine base within RNA. Nucleic Acids Res 38:1760–1766. doi:10.1093/nar/gkp930
59. Onizuka K, Taniguchi Y, Sasaki S (2010) Activation and alteration of base selectivity by metal cations in the functionality-transfer reaction for RNA modification. Bioconjug Chem 21:1508–1512. doi:10.1021/bc100131j
60. Onizuka K, Shibata A, Taniguchi Y, Sasaki S (2011) Pin-point chemical modification of RNA with diverse molecules through the functionality transfer reaction and the copper-catalyzed azide-alkyne cycloaddition reaction. Chem Commun (Camb) 47:5004–5006. doi:10.1039/c1cc10582e

61. Onizuka K, Nishioka T, Li Z, Jitsuzaki D, Taniguchi Y, Sasaki S (2012) An efficient and simple method for site-selective modification of O6-methyl-2′-deoxyguanosine in DNA. Chem Commun 48:3969–3971
62. Oshiro I, Jitsuzaki D, Onizuka K, Nishimoto A, Taniguchi Y, Sasaki S (2015) Site-specific modification of the 6-amino group of adenosine in RNA by an interstrand functionality-transfer reaction with an S-functionalized 4-thiothymidine. ChemBioChem 16:1199–1204. doi:10.1002/cbic.201500084
63. Poulsen HE, Nadal LL, Broedbaek K, Nielsen PE, Weimann A (2014) Detection and interpretation of 8-oxodG and 8-oxoGua in urine, plasma and cerebrospinal fluid. Biochim Biophys Acta 1840:801–808. doi:10.1016/j.bbagen.2013.06.009
64. Bruner SD, Norman DP, Verdine GL (2000) Structural basis for recognition and repair of the endogenous mutagen 8-oxoguanine in DNA. Nature 403:859–866. doi:10.1038/35002510
65. Lin KY, Matteucci MD (1998) A cytosine analogue capable of clamp-like binding to a guanine in helical nucleic acids. J Am Chem Soc 120:8531–8532
66. Flanagan WM, Wolf JJ, Olson P, Grant D, Lin KY, Wagner RW, Matteucci MD (1999) A cytosine analog that confers enhanced potency to antisense oligonucleotides. Proc Natl Acad Sci U S A 96:3513–3518. doi:10.1073/pnas.96.7.3513
67. Nakagawa O, Ono S, Li Z, Tsujimoto A, Sasaki S (2007) Specific fluorescent probe for 8-oxoguanosine. Angew Chem Int Ed 46:4500–4503. doi:10.1002/anie.200700671
68. Li Z, Nakagawa O, Koga Y, Taniguchi Y, Sasaki S (2010) Synthesis of new derivatives of 8-oxoG-clamp for better understanding the recognition mode and improvement of selective affinity. Bioorg Med Chem 18:3992–3998. doi:10.1016/j.bmc.2010.04.025
69. Koga Y, Fuchi Y, Nakagawa O, Sasaki S (2011) Optimization of fluorescence property of the 8-oxodGclamp derivative for better selectivity for 8-oxo-2′-deoxyguanosine. Tetrahedron 67:6746–6752. doi:10.1016/j.tet.2011.03.111
70. Ohno M, Miura T, Furuichi M, Tominaga Y, Tsuchimoto D, Sakumi K, Nakabeppu Y (2006) A genome-wide distribution of 8-oxoguanine correlates with the preferred regions for recombination and single nucleotide polymorphism in the human genome. Genome Res 16:567–575. doi:10.1101/gr.4769606
71. Kawanishi S, Oikawa S, Murata M, Tsukitome H, Saito I (1999) Site-specific oxidation at GG and GGG sequences in double-stranded DNA by benzoyl peroxide as a tumor promoter. Biochemistry 38:16733–16739. doi:10.1021/bi990890z
72. Fleming AM, Burrows CJ (2013) G-quadruplex folds of the human telomere sequence alter the site reactivity and reaction pathway of guanine oxidation compared to duplex DNA. Chem Res Toxicol 26:593–607. doi:10.1021/tx400028y
73. Toyokuni S, Tanaka T, Hattori Y, Nishiyama Y, Yoshida A, Uchida K, Hiai H, Ochi H, Osawa T (1997) Quantitative immunohistochemical determination of 8-hydroxy-2′-deoxyguanosine by a monoclonal antibody N45.1: its application to ferric nitrilotriacetate-induced renal carcinogenesis model. Lab Invest 76:365–374
74. Zhang B, Guo LH, Greenberg MM (2012) Quantification of 8-oxodGuo lesions in double-stranded DNA using a photoelectrochemical DNA sensor. Anal Chem 84:6048–6053. doi:10.1021/ac300866u
75. Xue L, Greenberg MM (2007) Facile quantification of lesions derived from 2′-deoxyguanosine in DNA. J Am Chem Soc 129:7010–7011. doi:10.1021/ja072174n
76. An N, Fleming AM, White HS, Burrows CJ (2015) Nanopore detection of 8-oxoguanine in the human telomere repeat sequence. ACS Nano 9:4296–4307. doi:10.1021/acsnano.5b00722
77. Lim KS, Cui L, Taghizadeh K, Wishnok JS, Chan W, Demott MS, Babu IR, Tannenbaum SR, Dedon PC (2012) In situ analysis of 8-Oxo-7,8-dihydro-2′-deoxyguanosine oxidation reveals sequence- and agent-specific damage spectra. J Am Chem Soc 134:18053–18064. doi:10.1021/ja307525h
78. Furman JL, Mok PW, Badran AH, Ghosh I (2011) Turn-on DNA damage sensors for the direct detection of 8-oxoguanine and photoproducts in native DNA. J Am Chem Soc 133:12518–12527. doi:10.1021/ja1116606

79. Nasr T, Li Z, Nakagawa O, Taniguchi Y, Ono S, Sasaki S (2009) Selective fluorescence quenching of the 8-oxoG-clamp by 8-oxodeoxyguanosine in ODN. Bioorg Med Chem Lett 19:727–730. doi:10.1016/j.bmcl.2008.12.036
80. Taniguchi Y, Kawaguchi R, Sasaki S (2011) Adenosine-1,3-diazaphenoxazine derivative for selective base pair formation with 8-oxo-2′-deoxyguanosine in DNA. J Am Chem Soc 133:7272–7275. doi:10.1021/ja200327u
81. Taniguchi Y, Koga Y, Fukabori K, Kawaguchi R, Sasaki S (2012) OFF-to-ON type fluorescent probe for the detection of 8-oxo-dG in DNA by the Adap-masked ODN probe. Bioorg Med Chem Lett 22:543–546. doi:10.1016/j.bmcl.2011.10.093
82. Taniguchi Y, Fukabori K, Kikukawa Y, Koga Y, Sasaki S (2014) 2,6-diaminopurine nucleoside derivative of 9-ethyloxy-2-oxo-1,3-diazaphenoxazine (2-amino-Adap) for recognition of 8-oxo-dG in DNA. Bioorg Med Chem 22:1634–1641. doi:10.1016/j.bmc.2014.01.024
83. Steemers FJ, Chang W, Lee G, Barker DL, Shen R, Gunderson KL (2006) Whole-genome genotyping with the single-base extension assay. Nat Methods 3:31–33. doi:10.1038/nmeth842
84. Liang F, Liu Y-Z, Zhang P (2013) Universal base analogues and their applications in DNA sequencing technology. RSC Adv 3:14910. doi:10.1039/c3ra41492b
85. Loakes D (2001) Survey and summary: the applications of universal DNA base analogues. Nucleic Acids Res 29:2437–2447. doi:10.1093/nar/29.12.2437
86. Taniguchi Y, Kikukawa Y, Sasaki S (2015) Discrimination between 8-oxo-2′-deoxyguanosine and 2′-deoxyguanosine in DNA by the single nucleotide primer extension reaction with Adap triphosphate. Angew Chem Int Ed 54:5147–5151. doi:10.1002/anie.201412086

Chapter 12
Genetic Alphabet Expansion by Unnatural Base Pair Creation and Its Application to High-Affinity DNA Aptamers

Michiko Kimoto, Ken-ichiro Matsunaga, Yushi T. Redhead, and Ichiro Hirao

Abstract Half a century ago, Alexander Rich proposed a genetic alphabet expansion system by the creation of an artificial extra base pair, known as an unnatural base pair. Now, as an ultimate modification technology, the development of unnatural base pairs and their applications has rapidly advanced. Introducing new components into nucleic acids could increase their functionality and moreover create new types of functional molecules. Three types of unnatural base pairs have been shown to function as a third base pair in replication and transcription. By using the unnatural base pairs, high-affinity DNA aptamers that specifically bind to target proteins and cells have been generated. Furthermore, bacteria bearing an unnatural base pair in their plasmids have been created. Here, we introduce a series of unnatural base pairs that function in replication and transcription, as well as their application to DNA aptamer generation targeting specific proteins.

M. Kimoto
Institute of Bioengineering and Nanotechnology (IBN), 31 Biopolis Way, The Nanos, #04-01, Singapore 138669, Singapore

Center for Life Science Technologies (CLST), RIKEN, 1-7-22 Suehiro-cho, Tsurumi-ku, Yokohama, Kanagawa 230-0045, Japan

PRESTO, JST, Honcho, Kawaguchi-shi, Saitama 332-0012, Japan

K.-i. Matsunaga • I. Hirao (✉)
Institute of Bioengineering and Nanotechnology (IBN), 31 Biopolis Way, The Nanos, #04-01, Singapore 138669, Singapore

Center for Life Science Technologies (CLST), RIKEN, 1-7-22 Suehiro-cho, Tsurumi-ku, Yokohama, Kanagawa 230-0045, Japan
e-mail: ihirao@riken.go.jp

Y.T. Redhead
TagCyx Biotechnologies, 1-7-22 Suehiro-cho, Tsurumi-ku, Yokohama, Kanagawa 230-0045, Japan

K. Nakatani, Y. Tor (eds.), *Modified Nucleic Acids*, Nucleic Acids and Molecular Biology 31, DOI 10.1007/978-3-319-27111-8_12

12.1 Introduction

In cellular systems on earth, DNA molecules are replicated and transcribed to RNA by polymerase reactions, according to the fundamental rule of A–T (U) and G–C base pairings. In this biological amplification process, four kinds of nucleoside triphosphates are selectively incorporated into DNA or RNA, opposite each complementary base in DNA templates. Through the amplification process, the information in the original DNA is transferred as base sequences to the offspring DNA or RNA. Furthermore, nucleic acids (DNA and RNA) also act as functionalized molecules, such as enzymes and ligands, and thus their functionalities can be evolved within an organism naturally or in a test tube artificially, by a certain selection process combined with polymerase amplification. Thus, since the advent of the PCR amplification technique, an evolutionary engineering method has been developed to generate functional nucleic acid molecules, such as ribozymes and ligands (aptamers), from an oligonucleotide library with a randomized sequence [1–3]. The method, called in vitro selection or SELEX (Systematic Evolution of Ligands by EXponential enrichment), involves repetitive rounds of selection and amplification to enrich winning nucleic acid sequences in a library. So far, many functional oligonucleotides have been generated by this method. In particular, nucleic acid aptamers that specifically bind to target molecules show promise for diagnostics and therapeutics as next-generation antibodies [4].

However, in the last quarter century since the first SELEX reports, only one modified RNA aptamer (pegaptanib sodium, Macugen) that binds to vascular endothelial growth factor 165 (VEGF165) was approved as a treatment for age-related macular degeneration [5]. The Kd value of the anti-VEGF165 aptamer is relatively high (49–130 pM) [6], but in general, the Kd values of most conventional nucleic acid aptamers are lower (around nM orders), relative to those of antibodies. Although the affinity is not the only problem with nucleic acid aptamers [7], generating tightly binding aptamers to target molecules is the first barrier to overcome for the screening toward diagnostic and therapeutic applications. Thus, increasing nucleic acid functionality, such as aptamer affinity to targets, is an imperative challenge for widespread application of the evolutionary engineering technology.

The restricted functionality of nucleic acids is due to the use of only four kinds of nucleotide components with four bases, as compared to those of proteins, which are composed of 20 standard amino acids. As for aptamers, the high hydrophilicity of nucleic acids is a disadvantageous trait for binding to hydrophobic regions of proteins. Even the heterocycles of the nucleobases are relatively hydrophilic, due to the additional amino and/or keto groups. In accordance with this, the four kinds of nucleotides share very similar chemical and physical properties, thus reducing the diversity of nucleic acid functionality. To compensate for the limited characteristics of the components, in living organisms, various types of nucleotide modifications, especially focusing on the base moiety, exist in functional RNA molecules. In this respect, there have been many reports on artificial

oligonucleotides with modified base, sugar, or phosphate moieties, to improve nucleic acid functionality [8–12]. A successful example is slow off-rate modified DNA aptamers (SOMAmer), in which the 5-methyl groups of thymine residues are replaced with more hydrophobic groups, such as benzyl, naphthyl, or tryptamino groups. This method dramatically increased the success rate of aptamer generation by SELEX, and more than 1000 SOMAmers targeting human proteins were isolated [10, 13]. While the affinities of SOMAmers have also been improved, the Kd values of most nucleic acid aptamers are still on the average of nM orders. The strategies of these modification methods are eventually restricted by the A–T (U) and G–C base pair rules, and thus the number of components consisting of modified oligonucleotides is still limited to four.

Another strategy to improve evolutionary engineering methods is by the genetic alphabet expansion of DNA, using artificial extra base pairs (unnatural base pairs) [14–18] (Figs. 12.1 and 12.2). The creation of an unnatural base pair, functioning as a third base pair together with the natural A–T (U) and G–C base pairs in replication and/or transcription, enables not only an expansion of the genetic information density of nucleic acids but also an increase in the chemical and physical diversities of nucleic acids [19] (Figs. 12.1 and 12.2). If the created unnatural bases have different properties from those of the natural bases, then the chemical and physical diversities of oligonucleotides will be increased. Even though the creation of unnatural base pairs that can be practically used for polymerase reactions had long been a challenging task, unnatural base pairs with high fidelity in replication have recently been developed.

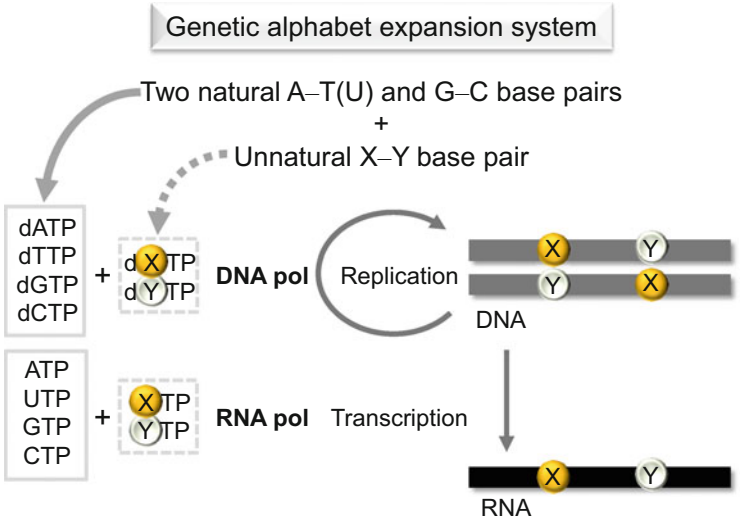

Fig. 12.1 Genetic alphabet expansion system based on the two natural base pairs and an additional, artificial third base pair (unnatural base pair, X–Y) that functions in replication and transcription. This system enables the site-specific incorporation of unnatural components into nucleic acids (DNA and RNA) through polymerase reactions mediated by unnatural base pairs

In 1989, the first experimental demonstration of unnatural base pairs was reported by Benner and co-workers [20, 21]. One of them was the iG–iC pair (Fig. 12.2b), which was proposed by Alexander Rich in 1962 [19]. Unfortunately, the fidelity of the iG–iC pair in replication is not high, because of the tautomerization of the iG base, and most of the unnatural base pair in the DNA is replaced with the A–T pair during PCR amplification. Subsequently, through extensive and consecutive efforts in many proof-of-concept experiments involving the design and physical and biological tests of different types of unnatural base pair candidates, three research groups have created unnatural base pairs with high fidelities in polymerase reactions: (1) our group for the Ds–Pa and Ds–Px pairs (Fig. 12.2c) and others [22–28] (23 is not Ds-Pa and Ds-Px papers), (2) Romesberg's group for the 5SCIS–MMO2 and 5SCIS–NaM pairs (Fig. 12.2d) [29–32] and others [33–35], and (3) Benner's group for the Z–P pair [36–38] (Fig. 12.2e). Recently, genetic alphabet expansion using these unnatural base pairs has been applied to

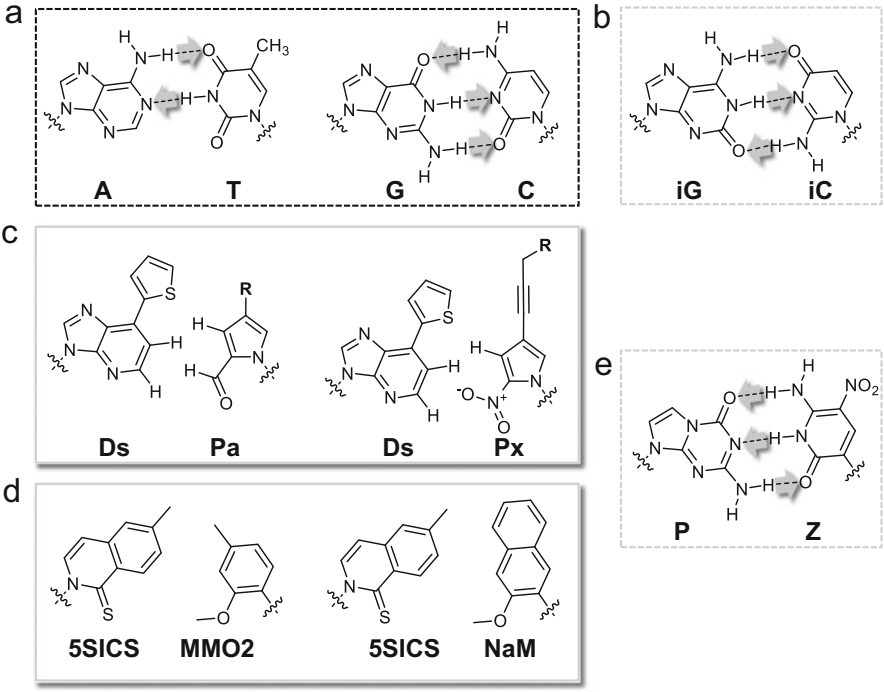

Fig. 12.2 Chemical structures of the natural and unnatural base pairs that function in polymerase reactions. The pairs with hydrogen bonding interactions between the pairing bases are enclosed in dotted lines, and those without hydrogen bonding interactions are enclosed in *solid lines*. The direction from hydrogen bond donor to acceptor is shown with *bold arrows*. (**a**) Natural A–T and G–C base pairs. (**b**) Unnatural iG–iC base pair. (**c**) Unnatural Ds–Pa and Ds–Px base pairs developed by Hirao's group. (**d**) Unnatural 5SICS–MMO2 and 5SICS–NaM base pairs developed by Romesberg's group. (**e**) Unnatural P–Z base pair developed by Benner's group. R is a functional group

generate high-affinity DNA aptamers targeting proteins by SELEX [39] and a cancer cell line by Cell-SELEX [40] and to create engineered *Escherichia coli* capable of replicating plasmid DNA containing an unnatural base pair [41].

Here, we provide an overview of the creation of unnatural base pairs by the three research groups and their applications. In Sect. 12.2, we introduce a series of unnatural base pair studies by the three independent groups, which finally succeeded in the development of unnatural base pairs that function in replication and transcription as a third base pair. Among them, the application of the hydrophobic Ds–Px pair to SELEX procedures is highlighted in Sect. 12.3. We describe the process of generating a high-affinity DNA aptamer composed of five nucleotides (A, G, C, T, and Ds) targeting VEGF165 and interferon-γ (IFNγ), including the process of the aptamer species enrichment during the selection.

12.2 Creation of Unnatural Base Pairs

12.2.1 Hirao's Base Pairs

The main design concept of our unnatural base pairs, such as Ds–Pa and Ds–Px, is to strictly refine the shape-complementarity between pairing bases, in which the ideas of steric hindrance and electrostatic repulsion are also included, to avoid mispairings (non-cognate pairings) between unnatural and natural bases. The initial idea of the shape-complementarity of pairing bases in replication was developed by Kool's group, using natural base analogues [42, 43]. We expanded this idea and developed a series of hydrogen bonded and hydrophobic unnatural base pairs that function in replication, transcription, and/or translation as a third pair [16, 17, 44].

The first generation of our unnatural base pairs includes the hydrogen-bonded pairs between a large base analogue, such as 2-amino-6-(*N*,*N*-dimethylamino) purine (x) [45, 46], 2-amino-6-(2-thienyl)purine (s) [23, 47], and 2-amino-6-(2-thiazoyl)purine (v) [48–50], and a small base analogue, such as pyridin-2-one (y) and imidazolin-2-one (z) [51] (Fig. 12.3). The x–y, s–y, and v–y pairs have two hydrogen bonds, but their donor–acceptor geometries are different from those of the natural A–T(U) and G–C pairs, like those in the iG–iC pair. Furthermore, to remove the mispairing with the natural bases, these large base analogues have sterically hindered groups at position 6. Among them, the s–y pair is useful for the site-specific incorporation of y or modified y bases into RNA, opposite s in DNA templates, by transcription using T7 RNA polymerase. The y base can be linked to desired functional groups, such as biotin and fluorescent groups, as a side chain, and these modified y substrates can also be incorporated into RNA by T7 transcription [48, 50, 52, 53].

In contrast to the y base with the six-membered ring, the five-membered z base increases the steric fitting with the s and v bases and decreases that with A. The s–z and v–z pairs are useful for the site-specific incorporation of s and v into RNA,

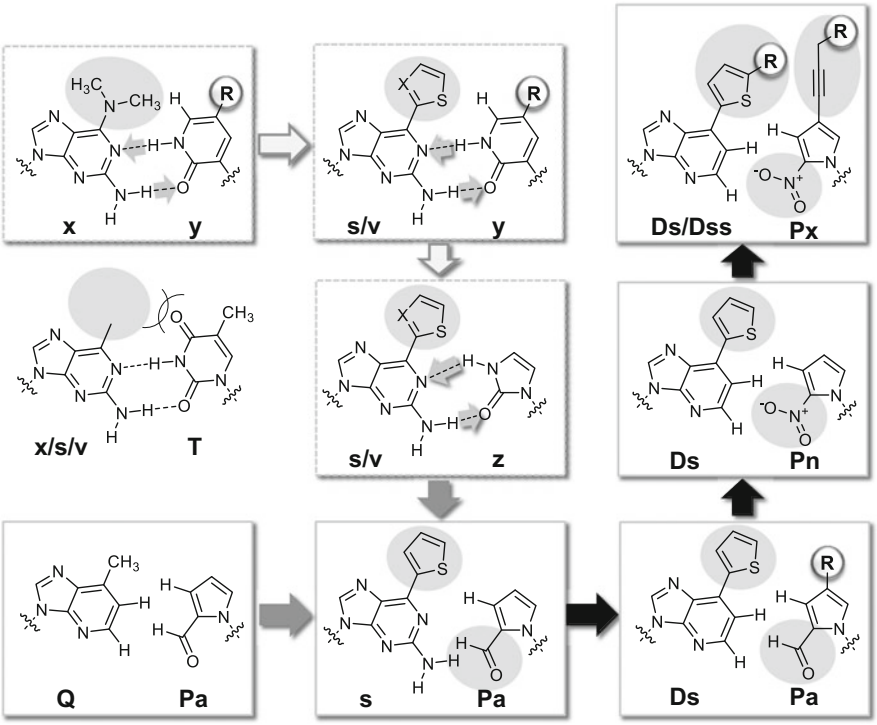

Fig. 12.3 Hirao's unnatural base pair development process: from the x–y, s/v–y, and s/v–z pairs as the first generation, to the s–Pa pair derived from the first generation and the Q–Pa pair as the second generation, followed by the hydrophobic Ds–Pa, Ds–Pn, and Ds/Dss–Px pairs as the third generation. Undesired, non-cognate pairing between the x/s/v–T pair is also shown as an example. The R enclosed in the circle represents functional groups

opposite z in templates, by T7 transcription [49, 51]. Since the s and v bases are fluorescent, the use of these s–z and v–z bases allows the site-specific fluorescent labeling of RNA molecules.

The second generation of our unnatural base pairs is between hydrophilic and hydrophobic base analogues. The unnatural base pair between s and a relatively hydrophobic base analogue, pyrrole-2-carbaldehyde (Pa), further increased the transcription efficiency and selectivity of the s incorporation into RNA opposite Pa in templates, as compared to the s–z pairing [26, 27] (Fig. 12.3). By T7 transcription using the s–Pa pair, a series of site-specific, fluorescently labeled functional RNA molecules, such as a tRNA and a ribozyme, were synthesized [54]. Since the fluorescent intensity of the s base embedded into RNA is decreased by the stacking with neighboring bases [55], the local structural changes of functional RNA molecules can be analyzed, depending on the environmental conditions [26, 27, 54].

The third generation is hydrophobic unnatural base pairs, such as the Ds–Pa, Ds–Pn, Ds–Px, Dss–Pa, Dss–Pn, and Dss–Px pairs, which function complementarily

and exhibit high fidelity in replication and transcription as third base pairs with different shape-complementarity from those of the natural base pairs [22, 24, 25, 28, 56]. By removing the hydrogen-bonding residues from both of the pairing bases, these hydrophobic base pairs can be practically used for PCR amplification. The shapes of the pairing bases snugly fit each other, and in particular, the oxygen of the nitro group in Px electrostatically clashes with the 1-nitrogen of A, reducing the non-cognate A–Px pairing. Thus, the Ds–Px pair exhibits extremely high fidelity in PCR. In replication using exonuclease-proficient Deep Vent DNA polymerase, the selectivity of the Ds–Px pairing is as high as 99.9 % per replication, and the misincorporation rate of the unnatural base substrates opposite the natural bases in templates is as low as 0.005 % per base pair per replication, corresponding to an error rate of 5×10^{-5} error per base pair. The Px base can be modified, and the selectivity of the Ds and modified Px base pairs in PCR depends on its modifications [25]. The Ds–Px pair has been applied to real-time PCR techniques [57] and SELEX for generating high-affinity Ds-containing DNA aptamers [39], as described in the next section.

The Dss base, with an additional thienyl group (R = thienyl of Ds/Dss in Fig. 12.3), is a highly fluorescent base analogue, and the nitropyrrole moiety of Pn and Px acts as a quencher [28, 58]. Thus, the Dss–Pn and Dss–Px pairs are quite unique third base pairs between a fluorophore and a quencher, and have been applied to real-time quantitative PCR and molecular beacon techniques [28, 54, 57].

12.2.2 Romesberg's Base Pairs

In the late 1990s, Romesberg's group initially reported the hydrophobic self-base pair of propynyl isocarbostyril (PICS, Fig. 12.4) [35]. Subsequently, they designed and synthesized a series of different hydrophobic base analogues, and huge combinations (~1800) of each analogue were tested in replication [59–69]. Among them, they selected the unnatural base pair between SICS and MMO2 as the prototype (Fig. 12.4) [70]. Upon further optimization, they created two hydrophobic pairs, 5SICS–MMO2 and 5SICS–NaM [30,71] (Fig. 12.4). The 5SICS–NaM pair functions in PCR using One*Taq* DNA polymerase (a mixture of DeepVent DNA polymerase and *Taq* DNA polymerase) with ~99.9 % fidelity. The 5SICS–NaM pair also functions in transcription using T7 RNA polymerase [29–32, 71]. Their continuous exploration has yielded further unnatural base pairs, such as the TPT3–NaM pair [33] (Fig. 12.4).

In 2014, by using the two unnatural base pair systems of the 5SICS–NaM and TPT3–NaM pairs, they created the first semi-synthetic living *E. coli*, in which the artificial plasmid DNA containing their unnatural base pair can be precisely amplified when supplemented with the unnatural base triphosphate substrates from the culture media [41] (Fig. 12.4). The TPT3–NaM pair was used for the PCR amplification of a plasmid bearing the unnatural base pair [34], and the 5SICS–NaM pair

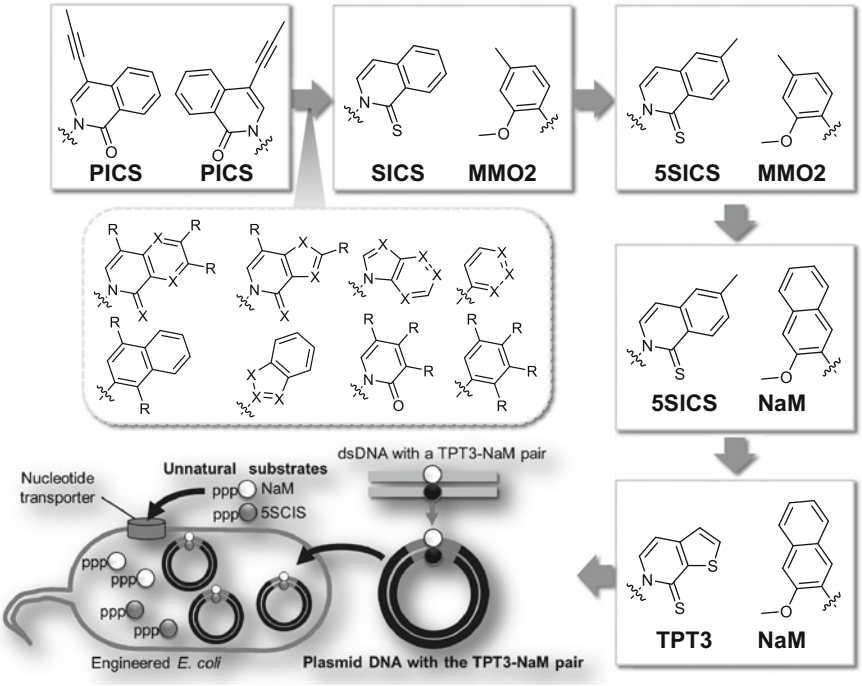

Fig. 12.4 Romesberg's hydrophobic unnatural base pairs and the introduction of the unnatural components into a plasmid, which can be replicated within an engineered *E. coli* strain. Representative nucleobase scaffolds and substitutions (X: heteroatom, R: functional group), enclosed in a *dotted square*, were used for screening of functional unnatural base pairs [70], resulting in the parent SCIS– MMO2 pair

was used for the plasmid-containing *E. coli* propagation. To supply the unnatural base triphosphates to the cells, they employed a triphosphate transporter from a microalgae. *E. coli* was transformed with two plasmids, one encoding the transporter and the other containing one unnatural TPT3–NaM pair. After approximately 24 doublings (a 15-h period of growth) with the 5SCIS and NaM triphosphates supplemented in the culture medium, the transformed *E. coli* cells maintained 86 % of the base pair in the plasmid, indicating that these unnatural nucleosides could survive in the presence of the natural DNA repair systems in the cell.

12.2.3 Benner's Base Pairs

In the late 1980s, Benner's group reported several types of unnatural base pairs with different hydrogen-bond geometries from those of the natural base pairs. One of them is the iG–iC pair (Fig. 12.2b), which was applied to transcription for the amino modification of RNA [72] and to real-time multiplex PCR (Plexor system) [73–

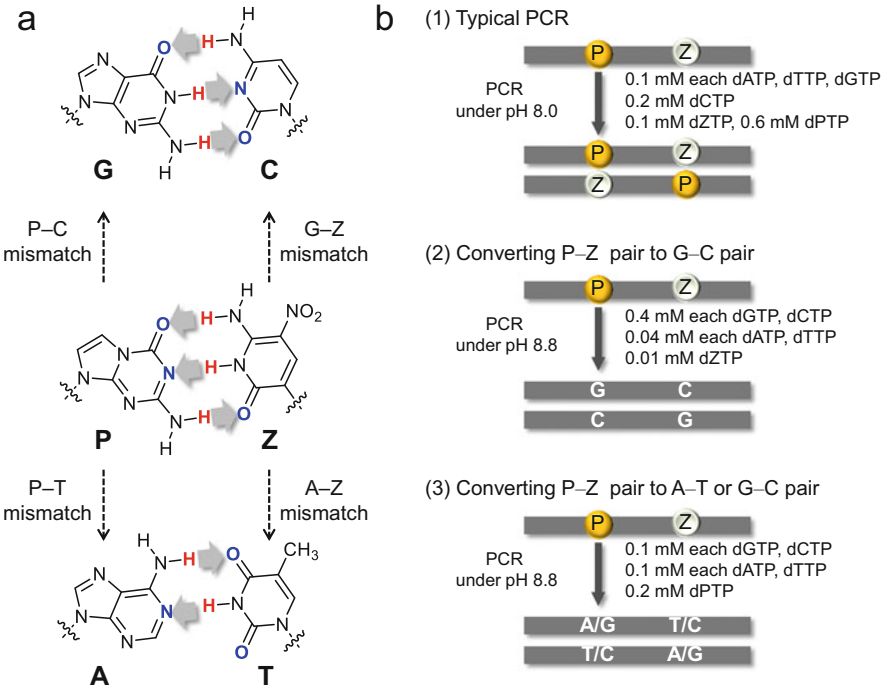

Fig. 12.5 Benner's unnatural P–Z base pair, with a different hydrogen bonding pattern from those of the natural base pairs. (**a**) Conversion of the cognate P–Z base pair to the natural G–C and A–T base pairs via possible mismatch pairing. (**b**) PCR conditions used in Benner's Cell-SELEX, for typical replication to prepare the DNA library (1), and for replacing the unnatural P–Z pairs with the natural G–C base pairs (2) or with the natural G–C and A–T base pairs (3) for sequence determination. Comparison of the replacement patterns in (2) and (3) allows the identification of the original P or Z positions in DNA

75]. They named their unnatural base pair system Artificially Expanded Genetic Information Systems (AEGIS) [20, 21, 38, 76]. To adapt AEGIS to a high-fidelity replication system, they examined several types of unnatural hydrogen-bonded base pairs [76–81]. In 2006, they created an unnatural base pair between 2-aminoimidazo[1,2-*a*]-1,3,5-triazin-4(8*H*)-one (P) and 6-amino-5-nitro-2(1*H*)-pyridone (Z) (Figs. 12.2e and 12.5a) [38], which can be used in PCR with 99.8 % fidelity [37] using *Taq* DNA polymerase and applied it to several DNA-based biotechnologies [40, 82, 83].

In 2014, they reported the generation of DNA aptamers that bind to a breast cancer cell line (MDA-MB-231) by a Cell-SELEX method involving the P–Z pair, in collaboration with Tan's group [40]. The initial DNA library for Cell-SELEX was prepared by the chemical synthesis of 52-mer DNA fragments bearing a 20-base randomized region consisting of six different bases. After 12 selection rounds, the unnatural bases in the enriched library were replaced with the natural bases by an additional PCR amplification using two different PCR conditions in the

absence of the unnatural base substrates, as shown in Fig. 12.5a, b. Since the P–Z pair was forcefully converted to the G–C pair or to the mixture of the G–C and A–T pairs [37, 40] depending on the PCR conditions, the possible P or Z positions in the randomized region can be identified by comparing the two sequence data sets. Consequently, they obtained a DNA aptamer containing both P and Z that binds to MDA-MB-231 cells with a Kd value of 30 nM.

12.3 Example of Unnatural Base DNA Aptamer Generation

As an example of applications using genetic alphabet expansion, here we describe high-affinity DNA aptamer generation using our Ds–Px pair system. Since nucleic acid aptamers are generated by an evolutionary engineering method (SELEX) composed of repeated cycles of selection and PCR amplification [1, 3], SELEX is an attractive and germane demonstration to test the ability of the replicable unnatural base pairs. We developed a genetic alphabet expansion SELEX method and generated a couple of DNA aptamers that specifically bind to target proteins, such as VEGF165 and interferon-γ, with >100-fold higher affinity than conventional DNA aptamers containing only natural bases [39]. Several ideas were adopted to improve the new SELEX method, and then we learned how to conduct the evolutionary process to isolate high-affinity DNA aptamers, via firsthand experience by performing the SELEX procedure using a randomized DNA library consisting of five different bases.

The key to the new SELEX procedure is the DNA library containing unnatural bases. We chose Ds as the fifth base and did not add Px to the library. The high hydrophobicity of the Ds base enhances the interactions with hydrophobic regions of target proteins. In addition, the absence of the pairing partner of Ds increases the structural diversity of each oligonucleotide in the library and causes the protrusion of the Ds base from the aptamer scaffolds, facilitating the interactions between the Ds base and the hydrophobic cavities of target proteins. From this perspective, we presumed that only a few Ds bases would be required to affect protein binding, and thus one to three Ds bases were introduced within a 43-base randomized region in a DNA library. This single-stranded Ds-containing DNA library can be amplified by PCR in the presence of the four natural and two unnatural base substrates by AccuPrime Pfx polymerase [25]. By PCR amplification using a primer linked with an extra tag, the Ds strands were separated from the Px strands with an extra tag on a denaturing gel, for the following selection cycles.

Currently, a major barrier is how to determine each sequence containing Ds bases from the isolated library after the SELEX procedure. In general, when using natural-base libraries, classical cloning and sequencing methods or a next-generation sequencing method can be used for DNA library sequencing. However, these conventional methods cannot be directly applied to the sequencing of the

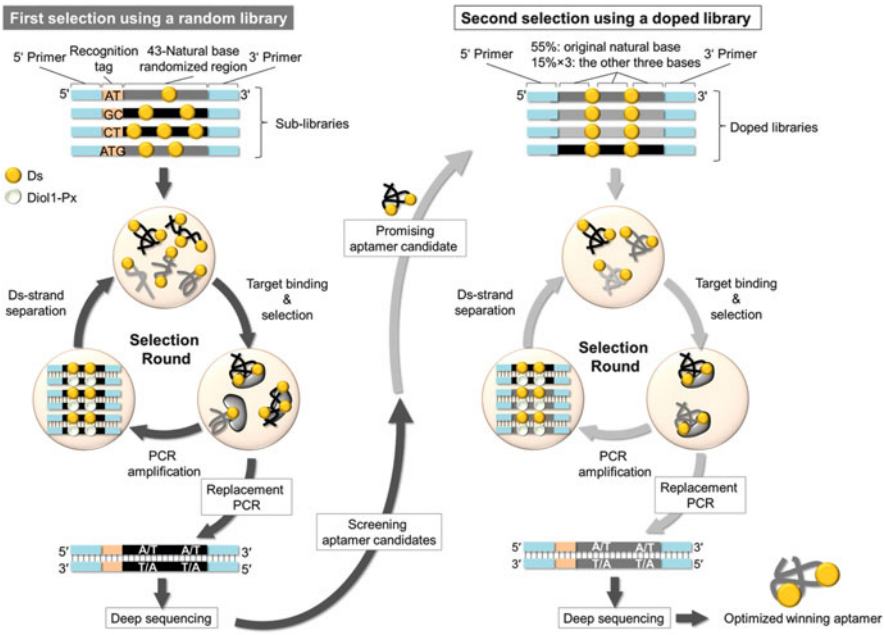

Fig. 12.6 Scheme of the SELEX procedure by Hirao's group for DNA aptamer selection using libraries containing hydrophobic Ds bases [39]. In the first selection, a mixture of 22 different chemically synthesized sub-libraries was employed as the initial library. In each selection round, target-binding DNA fragments were extracted and then amplified by PCR in the presence of dDsTP and dPxTP as unnatural substrates, together with natural dNTPs for the next round of selection. The enriched DNA library was PCR-amplified without dDsTP and dPxTP, resulting in the amplicons consisting of only natural bases, followed by sequence analysis. Details of the "replacement PCR" are described in the main text (see Sect. 12.3). After binding analyses of the obtained aptamer candidates, the most potent aptamers proceed to the second selection using a doped library. Through the doped selection and further optimization, the final "winning" aptamers were obtained

library containing unnatural bases, at present. To address this problem, we created a simple, but effective, approach using a set of Ds-containing DNA sublibraries. The sublibrary construction and the SELEX method are summarized in Fig. 12.6.

Twenty-two different sublibraries, in which one to three Ds bases were embedded at specific positions of a randomized 43-natural-base region, were chemically synthesized. Each sublibrary contained one to three Ds bases at different positions and also had a specific barcode consisting of two or three natural base sequences, as a recognition tag. By using the mixture of 22 sublibraries, we performed seven rounds of selection and amplification for VEGF165 and IFNγ. After the selection, the isolated library was again amplified by PCR in the absence of the Ds and Px substrates, but in the presence of the Pa substrates. By this process, the Ds–Px pairs in the library were efficiently replaced with the natural base pairs, mainly A–T pairs. Due to the high fidelity of the Ds–Px pair, the replacement was very difficult to conduct in PCR with only the natural base substrates, and thus we added another

unnatural base substrate, dPaTP. First, the Pa substrate was incorporated into the complementary strand opposite Ds in the library, and then the A substrate was incorporated opposite Pa, promoting the replacement of the Ds–Px pair with the A–T pair by PCR. The PCR products were sequenced by Ion Torrent deep sequencing. Using the barcode in each sequence, we could identify the initial Ds base positions. From the appearance frequency of each clone, several sequences with a high frequency were chosen from more than 90,000 sequences and were assayed for their ability to bind the target proteins. Among them, the aptamer sequence of the strongest binder was optimized by a second SELEX, using a doped library with a partially mutated sequence.

Table 12.1 shows the in vitro selection conditions used for the anti-IFNγ aptamer generation [39]. The selection pressure was gradually increased in each selection round, by reducing the concentrations of the DNA library and IFNγ, adding a competitor (the conventional DNA aptamer) [84, 85], and/or harsh washing with 3 M urea. We monitored the enrichment of the aptamer species during the selection by surface plasmon resonance (SPR) and gel-mobility shift assays of the library in each round (Fig. 12.7). After four rounds in the first SELEX, the binding species were significantly enriched (Fig. 12.7a, b). From SPR, the sequences were continuously enriched from the fourth to seventh rounds while the binding affinity increased. In the second round of SELEX, using the doped library, the binding species appeared quickly after two rounds (Fig. 12.7c).

Table 12.2 shows the theoretical copy numbers in the initial doped library used in the experiments targeting IFNγ and summarizes the data obtained after four rounds of the doped selection. The theoretical ratio of the optimized sequence in the initial library population; i.e., the number for the finally obtained optimized sequence, with one mutation at a specific position divided by that of the original

Table 12.1 Conditions of SELEX involving the Ds–Px pair, targeting human IFN-γ[a]

DNA library	Selection round	DNA		IFN-γ (nM)	Competitor (nM)	Number of washes		PCR cycles
		Pmol	(nM)			Without urea	With 3 M urea	
Random	1	300	50	25	0	5	0	22
	2	25	25	10	0	5	0	21
	3	5	5	5	0	5	0	21
	4	3	1	1	0	5	0	26
	5	3	1	1	100	5	0	20
	6	3	1	1	500	5	0	20
	7	3	1	1	500	2	3	25
Doped	1	300	50	25	0	5	0	19
	2	5	5	5	0	5	0	20
	3	3	1	1	100	5	0	17
	4	3	1	1	500	2	3	20

[a]The conditions for the first selection using a DNA library containing Ds at predetermined positions and the second selection using a doped DNA library containing three Ds bases at fixed positions of the original sequence are summarized [39]

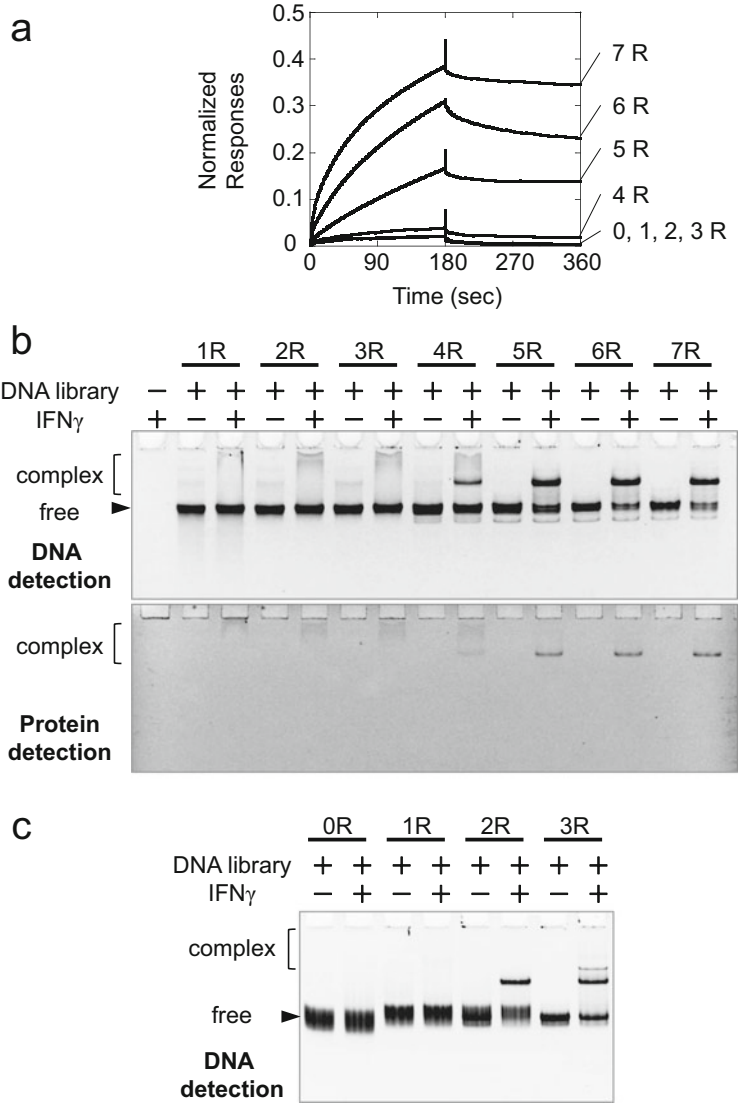

Fig. 12.7 Monitoring the enrichment process of the DNA libraries in SELEX targeting IFNγ. The conditions used in each selection round are summarized in Table 12.1. (**a**) SPR analysis of DNA libraries after each selection round in the first SELEX procedure. Each DNA library was immobilized via hybridization on a streptavidin-coated sensor chip with a biotinylated DNA probe. SPR conditions: flow rate = 30 μl/min; running buffer: PBS (305 mM NaCl) supplemented with 0.05 % Nonidet P-40, pH 7.4; injection period of 100 nM IFNγ = 180 s, dissociation period for monitoring = 180 s. (**b**) Gel-mobility shift analysis of DNA libraries after each selection round in the first SELEX procedure. Binding conditions: 100 nM DNA library, human IFNγ 200 nM, incubation at 25 °C for 30 min in PBS (155 mM NaCl) supplemented with 0.005 % Nonidet P-40. Gel electrophoresis: 10 % polyacrylamide gel containing 5 % glycerol, with 0.5× TBE as the running buffer. DNA bands were detected by SYBR Gold staining (*upper panel*), and protein bands were detected by CBB staining (*lower panel*). (**c**) Gel-mobility shift analysis of DNA libraries after each selection round in the second doped SELEX. Binding conditions: the same

Table 12.2 Ratios of enriched sequences after four rounds of the doped selection targeting human IFNγ[a]

Mutations relative to the original aptamer candidate sequence (N)	Variations of different sequences (X)[b]	Theoretical copy numbers in the initial doped library (1.8×10^{14} molecules)	After 4 rounds of the doped selection: Total extracted reads: 73,918		
			Reads	Variations	Ratio of the total reads (%)
0	1	2241	55	1	0.07
1	126	611	29,791 (29,518)[d]	3	40.30 (39.93)[d]
2	7749	167	18,980	24	25.68
3	309,960	45	10,819	57	14.64
4	9,066,330	12	4976	84	6.73
5	206,712,324	3	1776	75	2.40
6	3,824,177,994	1	1518	147	2.05

[a]Each doped position (42 sites) in the initial doped library was 55 % original and 15 % each different natural base, and 1.8×10^{14} molecules (300 pmol) were used as the initial library for the second doped selection [39]
[b]X is calculated according to the formula: $3^N \times {}_{42}C_N$
[c]The number is calculated according to the formula: $(1.8 \times 10^{14}) \times 0.55^{(42-N)} \times 0.45^N \times {}_{42}C_N/X$
[d]The top ranked, optimized sequence after the 4th round of the doped selection

sequence, is 0.27 (611/2241), and then the value reached 536.69 (29,518/55) after the doped selection, resulting in an almost 2000-fold enrichment. Doped selections allow the identification of the optimized sequence, which cannot be covered in the first selection using a random library, and also provide useful sequence information to shorten the length of the original aptamer candidate and to estimate the important secondary structure for target binding [39, 86].

Finally, we obtained an anti-VEGF165 aptamer with a 47-mer containing two Ds bases and an anti-IFNγ aptamer with a 49-mer containing three Ds bases. The secondary structures of both aptamers (Fig. 12.8) were presumed from the sequence data obtained by the second SELEX, in which the stem regions could be assigned from the co-variation mutation forming base pairs [86]. The Kd values, determined by SPR, were extremely high, 0.65 pM for the anti-VEGF165 aptamer and 38 pM for the anti-IFNγ aptamer. These binding affinities greatly surpass those of the conventional DNA aptamers consisting of only natural bases [84, 85], as well as the Ds→A mutants of the Ds aptamers, by more than 100-fold. We also confirmed that each unnatural base DNA aptamer specifically binds only to its target protein. Based on the mutant analysis, two of the three Ds bases in the anti-IFNγ aptamer

Fig. 12.7 (continued) as in (**b**) except human IFNγ 100 nM. Gel electrophoresis: the same as in (**b**) except 8 % polyacrylamide gel containing 5 % glycerol, with 0.5× TBE as the running buffer

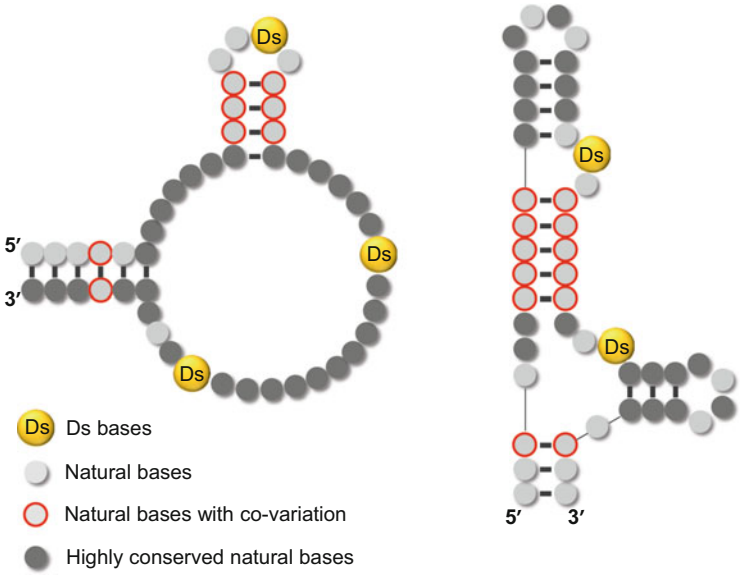

Fig. 12.8 Predicted secondary structures of the anti-IFNγ aptamer (*left*, 49-mer) and the anti-VEGF165 aptamer (*right*, 47-mer). The sequence alignment information obtained from the second doped selection is mapped on each structure. *Thick-framed circles* indicate positions where co-variations were found to form a base pair, and *dark solid circles* indicate highly conserved bases (the conservation percentage of each base in the total clone number was more than 96 %) [39]

were essential, and, thus, only two Ds bases greatly affected the tight binding to the target proteins, IFNγ and VEGF165.

12.4 Conclusion

Here, we have introduced three types of unnatural base pairs that can be used for PCR amplification. DNA aptamer generation using genetic alphabet expansion is the first demonstration to prove the importance of the introduction of new components for creating biopolymers with increased functionality. Since a bacterial strain bearing plasmids containing an unnatural base pair has been reported [41], novel bacteria producing useful pharmaceutical products or materials related to energy production could be created. Eventually, genetic alphabet expansion could be applied to the production of new peptides and proteins containing nonstandard amino acids, which would be useful for producing antibody–drug conjugates. Before that, unnatural-base DNA aptamers might contribute to the further advancement of nucleic acid pharmaceutics.

References

1. Ellington AD, Szostak JW (1990) In vitro selection of RNA molecules that bind specific ligands. Nature 346:818–822
2. Robertson DL, Joyce GF (1990) Selection in vitro of an RNA enzyme that specifically cleaves single-stranded DNA. Nature 344:467–468
3. Tuerk C, Gold L (1990) Systematic evolution of ligands by exponential enrichment: RNA ligands to bacteriophage T4 DNA polymerase. Science 249:505–510
4. Lao YH, Phua KK, Leong KW (2015) Aptamer nanomedicine for cancer therapeutics: barriers and potential for translation. ACS Nano 9:2235–2254
5. Ng EWM, Shima DT, Calias P, Cunningham ET, Guyer DR, Adamis AP (2006) Pegaptanib, a targeted anti-VEGF aptamer for ocular vascular disease. Nat Rev Drug Discov 5:123–132
6. Ruckman J, Green LS, Beeson J, Waugh S, Gillette WL, Henninger DD, Claesson-Welsh L, Janjic N (1998) 2′-Fluoropyrimidine RNA-based aptamers to the 165-amino acid form of vascular endothelial growth factor (VEGF165). Inhibition of receptor binding and VEGF-induced vascular permeability through interactions requiring the exon 7-encoded domain. J Biol Chem 273:20556–20567
7. Lakhin AV, Tarantul VZ, Gening LV (2013) Aptamers: problems, solutions and prospects. Acta Naturae 5:34–43
8. Bell NM, Micklefield J (2009) Chemical modification of oligonucleotides for therapeutic, bioanalytical and other applications. Chembiochem 10:2691–2703
9. Kuwahara M, Sugimoto N (2010) Molecular evolution of functional nucleic acids with chemical modifications. Molecules 15:5423–5444
10. Rohloff JC, Gelinas AD, Jarvis TC, Ochsner UA, Schneider DJ, Gold L, Janjic N (2014) Nucleic acid ligands with protein-like side chains: modified aptamers and their use as diagnostic and therapeutic agents. Mol Ther Nucleic Acids 3:e201
11. Taylor AI, Arangundy-Franklin S, Holliger P (2014) Towards applications of synthetic genetic polymers in diagnosis and therapy. Curr Opin Chem Biol 22:79–84
12. Wang RE, Wu H, Niu Y, Cai J (2011) Improving the stability of aptamers by chemical modification. Curr Med Chem 18:4126–4138
13. Gold L, Ayers D, Bertino J, Bock C, Bock A, Brody EN, Carter J, Dalby AB, Eaton BE, Fitzwater T, Flather D, Forbes A, Foreman T, Fowler C, Gawande B, Goss M, Gunn M, Gupta S, Halladay D, Heil J, Heilig J, Hicke B, Husar G, Janjic N, Jarvis T, Jennings S, Katilius E, Keeney TR, Kim N, Koch TH, Kraemer S, Kroiss L, Le N, Levine D, Lindsey W, Lollo B, Mayfield W, Mehan M, Mehler R, Nelson SK, Nelson M, Nieuwlandt D, Nikrad M, Ochsner U, Ostroff RM, Otis M, Parker T, Pietrasiewicz S, Resnicow DI, Rohloff J, Sanders G, Sattin S, Schneider D, Singer B, Stanton M, Sterkel A, Stewart A, Stratford S, Vaught JD, Vrkljan M, Walker JJ, Watrobka M, Waugh S, Weiss A, Wilcox SK, Wolfson A, Wolk SK, Zhang C, Zichi D (2010) Aptamer-based multiplexed proteomic technology for biomarker discovery. PLoS One 5:e15004
14. Benner SA (2012) Aesthetics in synthesis and synthetic biology. Curr Opin Chem Biol 16:581–585
15. Henry AA, Romesberg FE (2003) Beyond A, C, G and T: augmenting nature's alphabet. Curr Opin Chem Biol 7:727–733
16. Hirao I, Kimoto M (2012) Unnatural base pair systems toward the expansion of the genetic alphabet in the central dogma. Proc Jpn Acad Ser B 88:345–367
17. Hirao I, Kimoto M, Yamashige R (2012) Natural versus artificial creation of base pairs in DNA: origin of nucleobases from the perspectives of unnatural base pair studies. Acc Chem Res 45:2055–2065
18. Krueger AT, Kool ET (2009) Redesigning the architecture of the base pair: toward biochemical and biological function of new genetic sets. Chem Biol 16:242–248
19. Rich A (1962) Problems of evolution and biochemical information transfer. In: Pullman B, Kasha M (eds) Horizons in biochemistry. Academic, New York, pp 103–126

20. Piccirilli JA, Krauch T, Moroney SE, Benner SA (1990) Enzymatic incorporation of a new base pair into DNA and RNA extends the genetic alphabet [see comment]. Nature 343:33–37
21. Switzer C, Moroney SE, Benner SA (1989) Enzymatic incorporation of a new base pair into DNA and RNA. J Am Chem Soc 111:8322–8323
22. Hirao I, Kimoto M, Mitsui T, Fujiwara T, Kawai R, Sato A, Harada Y, Yokoyama S (2006) An unnatural hydrophobic base pair system: site-specific incorporation of nucleotide analogs into DNA and RNA. Nat Methods 3:729–735
23. Hirao I, Ohtsuki T, Fujiwara T, Mitsui T, Yokogawa T, Okuni T, Nakayama H, Takio K, Yabuki T, Kigawa T, Kodama K, Yokogawa T, Nishikawa K, Yokoyama S (2002) An unnatural base pair for incorporating amino acid analogs into proteins. Nat Biotechnol 20:177–182
24. Kimoto M, Kawai R, Mitsui T, Yokoyama S, Hirao I (2009) An unnatural base pair system for efficient PCR amplification and functionalization of DNA molecules. Nucleic Acids Res 37: e14
25. Yamashige R, Kimoto M, Takezawa Y, Sato A, Mitsui T, Yokoyama S, Hirao I (2012) Highly specific unnatural base pair systems as a third base pair for PCR amplification. Nucleic Acids Res 40:2793–2806
26. Hikida Y, Kimoto M, Yokoyama S, Hirao I (2010) Site-specific fluorescent probing of RNA molecules by unnatural base-pair transcription for local structural conformation analysis. Nat Protoc 5:1312–1323
27. Kimoto M, Mitsui T, Harada Y, Sato A, Yokoyama S, Hirao I (2007) Fluorescent probing for RNA molecules by an unnatural base-pair system. Nucleic Acids Res 35:5360–5369
28. Kimoto M, Mitsui T, Yamashige R, Sato A, Yokoyama S, Hirao I (2010) A new unnatural base pair system between fluorophore and quencher base analogues for nucleic acid-based imaging technology. J Am Chem Soc 132:15418–15426
29. Malyshev DA, Dhami K, Quach HT, Lavergne T, Ordoukhanian P, Torkamani A, Romesberg FE (2012) Efficient and sequence-independent replication of DNA containing a third base pair establishes a functional six-letter genetic alphabet. Proc Natl Acad Sci U S A 109:12005–12010
30. Malyshev DA, Seo YJ, Ordoukhanian P, Romesberg FE (2009) PCR with an expanded genetic alphabet. J Am Chem Soc 131:14620–14621
31. Seo YJ, Malyshev DA, Lavergne T, Ordoukhanian P, Romesberg FE (2011) Site-specific labeling of DNA and RNA using an efficiently replicated and transcribed class of unnatural base pairs. J Am Chem Soc 133:19878–19888
32. Seo YJ, Matsuda S, Romesberg FE (2009) Transcription of an expanded genetic alphabet. J Am Chem Soc 131:5046–5047
33. Dhami K, Malyshev DA, Ordoukhanian P, Kubelka T, Hocek M, Romesberg FE (2014) Systematic exploration of a class of hydrophobic unnatural base pairs yields multiple new candidates for the expansion of the genetic alphabet. Nucleic Acids Res 42:10235–10244
34. Li L, Degardin M, Lavergne T, Malyshev DA, Dhami K, Ordoukhanian P, Romesberg FE (2014) Natural-like replication of an unnatural base pair for the expansion of the genetic alphabet and biotechnology applications. J Am Chem Soc 136:826–829
35. McMinn DL, Ogawa AK, Wu Y, Liu J, Schultz PG, Romesberg FE (1999) Efforts toward expansion of the genetic alphabet: DNA polymerase recognition of a highly stable, self-pairing hydrophobic base. J Am Chem Soc 121:11585–11586
36. Chen F, Yang Z, Yan M, Alvarado JB, Wang G, Benner SA (2011) Recognition of an expanded genetic alphabet by type-II restriction endonucleases and their application to analyze polymerase fidelity. Nucleic Acids Res 39:3949–3961
37. Yang Z, Chen F, Alvarado JB, Benner SA (2011) Amplification, mutation, and sequencing of a six-letter synthetic genetic system. J Am Chem Soc 133:15105–15112
38. Yang Z, Hutter D, Sheng P, Sismour AM, Benner SA (2006) Artificially expanded genetic information system: a new base pair with an alternative hydrogen bonding pattern. Nucleic Acids Res 34:6095–6101

39. Kimoto M, Yamashige R, Matsunaga K, Yokoyama S, Hirao I (2013) Generation of high-affinity DNA aptamers using an expanded genetic alphabet. Nat Biotechnol 31:453–457
40. Sefah K, Yang Z, Bradley KM, Hoshika S, Jimenez E, Zhang L, Zhu G, Shanker S, Yu F, Turek D, Tan W, Benner SA (2014) In vitro selection with artificial expanded genetic information systems. Proc Natl Acad Sci U S A 111:1449–1454
41. Malyshev DA, Dhami K, Lavergne T, Chen T, Dai N, Foster JM, Correa IR Jr, Romesberg FE (2014) A semi-synthetic organism with an expanded genetic alphabet. Nature 509:385–388
42. Guckian KM, Krugh TR, Kool ET (1998) Solution structure of a DNA duplex containing a replicable difluorotoluene-adenine pair. Nat Struct Biol 5:954–959
43. Morales JC, Kool ET (1998) Efficient replication between non-hydrogen-bonded nucleoside shape analogs. Nat Struct Biol 5:950–954
44. Hirao I (2006) Unnatural base pair systems for DNA/RNA-based biotechnology. Curr Opin Chem Biol 10:622–627
45. Ishikawa M, Hirao I, Yokoyama S (2000) Synthesis of 3-(2-deoxy-beta-D-ribofuranosyl) pyridin-2-one and 2-amino-6-(N, N-dimethylamino)-9-(2-deoxy-beta-D-ribofuranosyl)purine derivatives for an unnatural base pair. Tetrahedron Lett 41:3931–3934
46. Ohtsuki T, Kimoto M, Ishikawa M, Mitsui T, Hirao I, Yokoyama S (2001) Unnatural base pairs for specific transcription. Proc Natl Acad Sci U S A 98:4922–4925
47. Fujiwara T, Kimoto M, Sugiyama H, Hirao I, Yokoyama S (2001) Synthesis of 6-(2-thienyl) purine nucleoside derivatives that form unnatural base pairs with pyridin-2-one nucleosides. Bioorg Med Chem Lett 11:2221–2223
48. Kawai R, Kimoto M, Ikeda S, Mitsui T, Endo M, Yokoyama S, Hirao I (2005) Site-specific fluorescent labeling of RNA molecules by specific transcription using unnatural base pairs. J Am Chem Soc 127:17286–17295
49. Mitsui T, Kimoto M, Harada Y, Yokoyama S, Hirao I (2005) An efficient unnatural base pair for a base-pair-expanded transcription system. J Am Chem Soc 127:8652–8658
50. Moriyama K, Kimoto M, Mitsui T, Yokoyama S, Hirao I (2005) Site-specific biotinylation of RNA molecules by transcription using unnatural base pairs. Nucleic Acids Res 33:e129
51. Hirao I, Harada Y, Kimoto M, Mitsui T, Fujiwara T, Yokoyama S (2004) A two-unnatural-base-pair system toward the expansion of the genetic code. J Am Chem Soc 126:13298–13305
52. Hirao I (2006) Placing extra components into RNA by specific transcription using unnatural base pair systems. Biotechniques 40:711–715
53. Kimoto M, Endo M, Mitsui T, Okuni T, Hirao I, Yokoyama S (2004) Site-specific incorporation of a photo-crosslinking component into RNA by T7 transcription mediated by unnatural base pairs. Chem Biol 11:47–55
54. Kimoto M, Hikida Y, Hirao I (2013) Site-specific functional labeling of nucleic acids by in vitro replication and transcription using unnatural base pair systems. Isr J Chem 53:450–468
55. Mitsui T, Kimoto M, Kawai R, Yokoyama S, Hirao I (2007) Characterization of fluorescent, unnatural base pairs. Tetrahedron 63:3528–3537
56. Hirao I, Mitsui T, Kimoto M, Yokoyama S (2007) An efficient unnatural base pair for PCR amplification. J Am Chem Soc 129:15549–15555
57. Yamashige R, Kimoto M, Mitsui T, Yokoyama S, Hirao I (2011) Monitoring the site-specific incorporation of dual fluorophore-quencher base analogues for target DNA detection by an unnatural base pair system. Org Biomol Chem 9:7504–7509
58. Kimoto M, Mitsui T, Yokoyama S, Hirao I (2010) A unique fluorescent base analogue for the expansion of the genetic alphabet. J Am Chem Soc 132:4988–4989
59. Berger M, Luzzi SD, Henry AA, Romesberg FE (2002) Stability and selectivity of unnatural DNA with five-membered-ring nucleobase analogues. J Am Chem Soc 124:1222–1226
60. Henry AA, Olsen AG, Matsuda S, Yu C, Geierstanger BH, Romesberg FE (2004) Efforts to expand the genetic alphabet: identification of a replicable unnatural DNA self-pair. J Am Chem Soc 126:6923–6931

61. Leconte AM, Matsuda S, Hwang GT, Romesberg FE (2006) Efforts towards expansion of the genetic alphabet: pyridone and methyl pyridone nucleobases. Angew Chem Int Ed Engl 45:4326–4329
62. Leconte AM, Matsuda S, Romesberg FE (2006) An efficiently extended class of unnatural base pairs. J Am Chem Soc 128:6780–6781
63. Matsuda S, Fillo JD, Henry AA, Rai P, Wilkens SJ, Dwyer TJ, Geierstanger BH, Wemmer DE, Schultz PG, Spraggon G, Romesberg FE (2007) Efforts toward expansion of the genetic alphabet: structure and replication of unnatural base pairs. J Am Chem Soc 129:10466–10473
64. Matsuda S, Henry AA, Romesberg FE (2006) Optimization of unnatural base pair packing for polymerase recognition. J Am Chem Soc 128:6369–6375
65. Matsuda S, Romesberg FE (2004) Optimization of interstrand hydrophobic packing interactions within unnatural DNA base pairs. J Am Chem Soc 126:14419–14427
66. Ogawa AK, Wu YQ, Berger M, Schultz PG, Romesberg FE (2000) Rational design of an unnatural base pair with increased kinetic selectivity. J Am Chem Soc 122:8803–8804
67. Ogawa AK, Wu YQ, McMinn DL, Liu JQ, Schultz PG, Romesberg FE (2000) Efforts toward the expansion of the genetic alphabet: information storage and replication with unnatural hydrophobic base pairs. J Am Chem Soc 122:3274–3287
68. Tae EL, Wu Y, Xia G, Schultz PG, Romesberg FE (2001) Efforts toward expansion of the genetic alphabet: replication of DNA with three base pairs. J Am Chem Soc 123:7439–7440
69. Wu YQ, Ogawa AK, Berger M, McMinn DL, Schultz PG, Romesberg FE (2000) Efforts toward expansion of the genetic alphabet: optimization of interbase hydrophobic interactions. J Am Chem Soc 122:7621–7632
70. Leconte AM, Hwang GT, Matsuda S, Capek P, Hari Y, Romesberg FE (2008) Discovery, characterization, and optimization of an unnatural base pair for expansion of the genetic alphabet. J Am Chem Soc 130:2336–2343
71. Seo YJ, Hwang GT, Ordoukhanian P, Romesberg FE (2009) Optimization of an unnatural base pair toward natural-like replication. J Am Chem Soc 131:3246–3252
72. Tor Y, Dervan PB (1993) Site-specific enzymatic incorporation of an unnatural base, N6-(6-aminohexyl)isoguanosine, into RNA. J Am Chem Soc 115:4461–4467
73. Lee WM, Grindle K, Pappas T, Marshall DJ, Moser MJ, Beaty EL, Shult PA, Prudent JR, Gern JE (2007) High-throughput, sensitive, and accurate multiplex PCR-microsphere flow cytometry system for large-scale comprehensive detection of respiratory viruses. J Clin Microbiol 45:2626–2634
74. Marshall DJ, Reisdorf E, Harms G, Beaty E, Moser MJ, Lee WM, Gern JE, Nolte FS, Shult P, Prudent JR (2007) Evaluation of a multiplexed PCR assay for detection of respiratory viral pathogens in a public health laboratory setting. J Clin Microbiol 45:3875–3882
75. Sherrill CB, Marshall DJ, Moser MJ, Larsen CA, Daude-Snow L, Jurczyk S, Shapiro G, Prudent JR (2004) Nucleic acid analysis using an expanded genetic alphabet to quench fluorescence. J Am Chem Soc 126:4550–4556
76. Geyer CR, Battersby TR, Benner SA (2003) Nucleobase pairing in expanded Watson-Crick-like genetic information systems. Structure 11:1485–1498
77. Hutter D, Benner SA (2003) Expanding the genetic alphabet: non-epimerizing nucleoside with the pyDDA hydrogen-bonding pattern. J Org Chem 68:9839–9842
78. Lutz MJ, Horlacher J, Benner SA (1998) Recognition of a non-standard base pair by thermostable DNA polymerases. Bioorg Med Chem Lett 8:1149–1152
79. Martinot TA, Benner SA (2004) Artificial genetic systems: exploiting the "aromaticity" formalism to improve the tautomeric ratio for isoguanosine derivatives. J Org Chem 69:3972–3975
80. Sismour AM, Benner SA (2005) The use of thymidine analogs to improve the replication of an extra DNA base pair: a synthetic biological system. Nucleic Acids Res 33:5640–5646
81. Sismour AM, Lutz S, Park JH, Lutz MJ, Boyer PL, Hughes SH, Benner SA (2004) PCR amplification of DNA containing non-standard base pairs by variants of reverse transcriptase from Human Immunodeficiency Virus-1. Nucleic Acids Res 32:728–735

82. Merritt KK, Bradley KM, Hutter D, Matsuura MF, Rowold DJ, Benner SA (2014) Autonomous assembly of synthetic oligonucleotides built from an expanded DNA alphabet. Total synthesis of a gene encoding kanamycin resistance. Beilstein J Org Chem 10:2348–2360
83. Yang Z, Durante M, Glushakova LG, Sharma N, Leal NA, Bradley KM, Chen F, Benner SA (2013) Conversion strategy using an expanded genetic alphabet to assay nucleic acids. Anal Chem 85:4705–4712
84. Potty ASR, Kourentzi K, Fang H, Jackson GW, Zhang X, Legge GB, Willson RC (2009) Biophysical characterization of DNA aptamer interactions with vascular endothelial growth factor. Biopolymers 91:145–156
85. Tam S, Huey B, Li Y, Lui GM, Hwang DG, Lantz M, Weiss TL, Hunt CA, Garovoy MR (1994) Suppression of interferon-gamma induction of MHC class II and ICAM-1 by a 26-base oligonucleotide composed of deoxyguanosine and deoxythymidine. Transpl Immunol 2:285–292
86. Hirao I, Harada Y, Nojima T, Osawa Y, Masaki H, Yokoyama S (2004) In vitro selection of RNA aptamers that bind to colicin E3 and structurally resemble the decoding site of 16S ribosomal RNA. Biochemistry 43:3214–3221

Index

K. Nakatani, Y. Tor (eds.), *Modified Nucleic Acids*, Nucleic Acids and Molecular Biology 31, DOI 10.1007/978-3-319-27111-8